A Genomic Approach to Atherosclerotic Plaque Vulnerability

The genome-wide cell-specific gene expression study of plaque rupture using laser micro-dissection and microarrays.

Kelvin Sze Yen Lee

A thesis submitted for Doctor of Philosophy

Institute of Genetic Medicine,

School of Clinical Medical Sciences,

University of Newcastle upon Tyne.

Submitted on January 2012.

I. Abstract

BACKGROUND: Macrophages in atherosclerotic plaques are believed to play a central role in plaque instability. However, the cell-specific molecular mechanisms involved are incompletely characterized. To address this, we performed genome-wide gene expression analyses using microarrays on RNA extracted from macrophage-rich regions of stable and unstable human atheromatous plaques. ***METHODS AND RESULTS:*** Plaques derived from carotid endarterectomy specimens (n=118) were designated as stable or unstable according to clinical, radiological and histopathological criteria. Macrophage-rich regions were excised from unstable and stable plaques by laser micro-dissection. Transcriptional profiling of extracted RNA was carried out using Affymetrix U133plus2 microarrays. The expression profiles were characteristic of activated macrophages. Expression profiles from stable and unstable samples clustered into distinct groups. Nine hundred and fourteen genes differentially expressed between stable and unstable sample groups were identified at a false discovery rate of 10%. The findings were confirmed by real-time PCR for eleven of the twelve genes with the highest fold expression difference ($p<0.05$). The analysis of the gene expression of the twelve highest fold expression genes by their principal components demonstrated a distribution of the samples along an axis of stability-instability in gene expression space. More specifically, components of the PPAR/Adipocytokine signalling pathway were significantly differentially expressed ($p=5.4x10^{-7}$) between stable and unstable plaques with greater expression in unstable plaques. Key components of the pathway, fatty acid binding protein 4 (FABP4) and leptin, showed nine-fold ($p=0.0086$) and five-fold ($p=0.0012$) greater expression in unstable plaques respectively. The immunohistochemistry of the protein products for FABP4 and Leptin confirmed their co-localisation with the macrophages in the plaque. ***CONCLUSION:*** Differences in gene expression signatures are present between macrophages isolated from stable and unstable human atheromatous plaques. Components of the PPAR/adipocytokine signalling pathway, specifically FABP4 and Leptin, are expressed at higher levels in macrophages from unstable plaques. These findings suggest that down-regulation of PPAR/adipocytokine signalling within plaques may have therapeutic potential.

II. Dedication

To the memory of my father,

And to my wife, for her support and encouragement.

III. Acknowledgements

I would like to acknowledge the Newcastle Neurosurgery Foundation and the Northern Brainwave Appeal. I would also like to acknowledge Prof. David Mendelow for the carotid endarterectomy specimens and Prof. Stephan Scheuler for the normal arterial specimens. I would like to acknowledge and thank Dr Danny Birchall for his supervision and training in the radiological analysis performed in this study, Janet Thompson and Dr Tuomo Polvikoski and the Department of Neuropathology, Regional Neurosurgical Centre, Newcastle General Hospital for the supervision and training in histopathology, Dr Gill Borthwick for the training in the use of the Leica Laser micro-dissection platform, Dr M Santiabanez-Koref for the supervision and training in microarray statistical analysis, Mark Scott and Dr Susan Lindsay for the training in the use of the Optical Projection Tomography equipment, and Prof. Bernard Keavney for his supervision of my PhD work.

IV. Table of Contents

I. Abstract i
II. Dedication ii
III. Acknowledgements iii
IV. Table of Contents iv
V. Lists of figures, tables and digital files xi
List of figures xi
List of tables xv
List of files in the enclosed CD xvii
Chapter 1. Introduction 1
1.1 The burden of cardiovascular disease 1
1.2 The pathobiology of atherosclerosis 2
1.2.1 Normal vessel and healthy endothelium 4
1.2.2 Initiation of atherosclerosis and early lesions 4
1.2.3 Stable advanced lesions – fibrous cap atheromata 11
1.2.4 Vulnerable advanced lesions - thin fibrous cap atheromata 13
1.2.5 Lesions with thrombi - rupture, erosion and calcific nodule 14
1.2.6 Complex lesions - healing rupture/erosions and rapid lesion growth 17
1.2.7 Advanced lesions with calcified or fibrotic modification: fibrocalcific plaque or fibroatheroma with fibrotic change 18
1.3 The clinical manifestations of atherosclerosis 19
1.3.1 The stable phenotype and stable plaque 19
1.3.2 The unstable phenotype and vulnerable plaque 20
1.3.3 The vulnerable patient 21
1.3.4 Identification and treatment of the vulnerable plaque and patient 22
1.4 Possible mechanistic processes leading to plaque rupture 23
1.4.1 Mechanical forces focus inflammatory processes 23
1.4.2 Dominant inflammatory processes increase proteolytic activity 25
1.4.3 Adaptive immune responses to auto-antigens 26
1.4.4 CD40 and CD40L interaction 28
1.4.5 Role of apoptosis 29
1.4.6 Peroxisomal proliferating activating receptors (PPARs) 31
1.4.7 Inflammatory effects of the renin-angiotensin-aldosterone axis 32
1.4.8 The effect of statins 32
1.5 Approaches to the study of plaque rupture 33
1.5.1 Athero-transcriptomics 35
1.5.2 Gene expression microarrays 36
1.6 No adequate experimental model for rupture or erosion; human studies necessary. 37

1.7 The accurate identification of the phenotype: a multi-domain assessment. 38
1.8 Heterogeneity of the plaque: a cell-specific approach. 39
1.9 Laser micro-dissection and linear amplification 40
1.10 The major cell-types in the plaque: VSMCs and Macrophages 41
1.11 Three dimensional imaging of gene expression in the plaque 42
1.12 Hypotheses 43
1.13 Aims 43
Chapter 2. Material and methods 44
2.1 Ethical approval and study execution 44
2.2 Patient recruitment, consent, clinical data collection 44
2.2.1 Carotid endarterectomy surgery 44
2.2.2 Coronary artery bypass surgery 45
2.3 Magnetic resonance imaging and angiography 46
2.3.1 Rationale 46
2.3.2 Imaging 46
2.3.3 Image Assessment 47
2.4 Transcranial doppler emboli detection 47
2.4.1 Rationale 47
2.4.2 Patient recruitment and consent 48
2.4.3 TCD recording, analysis and emboli detection 48
2.5 Specimen collection and Snap-freezing 48
2.5.1 Snap-freezing - preliminary methodological evaluation 48
2.5.2 CEA surgery and specimens 50
2.5.3 CABG surgery and radial and IMA specimens 51
2.6 Sample processing and staining for histological analysis 52
2.6.1 Formalin fixed paraffin embedded samples 52
2.6.2 Snap-frozen samples 53
2.7 Sample characterisation and selection: the three-domain analysis 55
2.7.1 Rationale 55
2.7.2 Histopathology analysis and selection 55
2.7.3 Clinical analysis and selection 55
2.7.4 Imaging analysis and selection 56
2.7.5 Correlation between groups and statistical analysis 56
2.7.6 Three-domain analysis and final sample selection 57
2.7.7 Trans-cranial doppler emboli detection 58
2.8 RNA extraction method 58
2.8.1 Rationale 58
2.8.2 RNA extraction from whole tissue 59
2.8.3 RNA extraction from Laser Micro-Dissection 59
2.8.4 The optimal RNA extraction protocol 62
2.9 RNA quantity and quality measurement 62

2.9.1 RNA evaluation by Agilent Bioanalyser RNA LabChip 62
2.9.2 RNA evaluation by Nanodrop 62
2.9.3 RNA quantification by RiboGreen 63
2.9.4 Electrophoresis and visualisation of RNA 63
2.10 Laser Micro-Dissection method 63
2.10.1 Rationale 63
2.10.1 Original Leica LMD protocols 64
2.10.2 Optimisation of the LMD process 65
2.10.3 The optimal LMD protocol 67
2.11 Validation of RNA stability and integrity from LMD 68
2.11.1 RNA stability during the LMD process 68
2.11.2 Integrity of the extracted RNA from LMD 68
2.12 LMD cryosectioning & Scout section histopathological analysis 69
2.12.1 Cryosectioning for LMD and scout sections 69
2.12.2 Immunohistochemical staining of Scout sections 70
2.12.3 Scout section histopathological analysis and identification of regions of interest for LMD 70
2.13 RNA amplification and Microarray 70
2.13.1 RNA amplification 70
2.13.2 Linear amplification 3' bias and Affymetrix microarray design 73
2.13.3 Microarray hybridization 73
2.13.4 Affymetrix Test3 microarray 73
2.13.5 Affymetrix HG-U133 plus 2.0 GeneChip microarray 74
2.14 Microarray data analysis 74
2.14.1 Microarray data analysis software 74
2.14.2 Affymetrix probeset design and transcript present/absent detection 75
2.14.3 Background correction, signal quantification, probeset summarisation and normalisation 75
2.14.4 Macrophage Expression Profile Correlation 77
2.14.5 Unsupervised exploratory clustering 77
2.14.6 Statistical analysis 79
2.14.7 Data-mining and Annotation of the Genelist 80
2.14.8 Functional bioinformatic analysis 80
2.15 Real-time PCR quantitation of target genes 81
2.15.1 Preliminary methodological optimisation 81
2.15.2 Reference gene selection and assessment 84
2.15.3 Analysis of qRTPCR data, efficiency correction, normalisation and calibration 85
2.15.4 Quantitative real-time PCR - Technical validation of microarray findings 85
2.15.5 Increasing the sample size - Biological validation by qRTPCR 86
2.16 Immunohistochemistry of target proteins 88
2.16.1 Immunohistochemistry optimisation work 88

2.16.2 Immunohistochemical work of atherosclerotic plaques 89
2.16.3 Semi-quantitative immunohistochemical analysis 90
2.16.4 Quantitative immunohistochemical analysis 90
2.17 Optical Projection Tomography of the atherosclerotic plaque 91
2.17.1 Rationale and introduction 91
2.17.2 The OPT protocol for vascular and atherosclerotic tissue 93
Chapter 3. The clinical and pathological characterisation of patients 95
3.1 Overview 95
3.2 Patient recruitment and Sample collection 95
3.2.1 Samples from patients during Carotid Endarterectomy Surgery 95
3.2.2 Samples from patients during Coronary Artery Bypass Surgery 96
3.3 Clinical Data 96
3.3.1 Clinical symptoms 96
3.3.2 Demographics 98
3.3.3 Vascular Risk Factor Profile 98
3.4 Radiological Data 100
3.4.1 Carotid plaque surface morphology and stenosis severity 100
3.4.2 Radiological evidence of cerebral infarction 100
3.5 Histopathological classification of atherosclerotic lesions: a hybrid amalgamated classification schemata 101
3.6 Histological Data 106
3.6.1 Heterogeneity of the plaque 106
3.6.2 Lesions types associated with thrombi 108
3.6.3 Stable lesions 110
3.6.4 Vulnerable lesions 111
3.7 Transcranial doppler emboli detection 115
3.8 Correlation between Clinical, Radiological and Histological Findings 117
3.8.1 Symptoms and Surface irregularity 117
3.8.2 Symptoms and Radiological evidence of infarction 118
3.8.3 Surface irregularity and Stenosis severity 119
3.8.4 Symptoms and Stenosis severity 120
3.8.5 Symptoms and histology 120
3.8.6 Surface irregularity and histology 123
3.8.7 Correlation in 3 domains: Symptoms, Surface irregularity and Histology 124
3.9 Three domain analysis, Sample usage and Selection 127
3.9.1 Selection of the unstable plaque: the ruptured thin fibrous cap atheroma 127
3.9.2 Selection of the stable plaque : the fibrous cap atheroma and fibrocalcified plaque 128
Chapter 4. The isolation and characterisation of cell-specific RNA 132
4.1 Overview 132
4.2 Evaluation of snap-freezing methods 134
4.3 Baseline evaluation of RNA quality of snap-frozen specimens 135

4.3.1 Baseline RNA extraction from whole tissue IMA specimens 135
4.3.2 Baseline RNA extraction from whole tissue CEA specimens 137
4.4 RNA extraction from small amounts of whole tissue 138
4.5 Optimisation of RNA extraction from very small amounts of LMD tissue 140
4.5.1 RNA extraction methods and DNase-I digestion 140
4.5.2 Carrier RNA 142
4.5.3 Increasing the extracted RNA yield: lysis buffer volume 143
4.5.4 Increasing the extracted RNA concentration: double elution 144
4.5.5 The optimal RNA extraction protocol 144
4.6 Preliminary Laser micro-dissection trials 145
4.6.1 LMD 145
4.6.2 RNA extraction 145
4.7 Optimisation of the LMD process 148
4.7.1 Cryosection thickness and OCT embedding media 148
4.7.2 LMD membrane slides and air-drying 148
4.7.3 Fixation and histochemical staining 149
4.7.4 Xylene clearing 150
4.7.5 Further modifications 151
4.7.6 Testing the proposed modifications 152
4.7.7 Further evaluation of LMD of VSMCs in the fibrous cap 154
4.7.8 The optimal RNA LMD protocol 154
4.8 The stability and integrity of RNA extracted from LMD 155
4.8.1 Stability of RNA of the processed LMD sections 155
4.8.2 Preservation of RNA integrity 156
4.9 LMD of the stable and ruptured atherosclerotic plaques 157
4.9.1 Scout section histological analysis and identification of VSMC and Macrophage regions for LMD 157
4.9.2 RNA extraction of VSMCs in the fibrous cap 163
4.9.3 RNA extraction of Macrophages under the fibrous cap 166
4.9.4 Regions of cellular degradation 169
4.10 RNA amplification and microarray 170
4.10.1 Batch#1: The initial 2 CEA test samples 170
4.10.2 Batch#2: The next 6 CEA samples 172
4.10.3 Batch#3: The remaining CEA samples 175
4.10.4 Hybridisation and scanning of the Affymetrix GeneChip 175
Chapter 5. The analyses of the transcriptome in plaque rupture 177
5.1 Overview 177
5.2 Background correction, signal quantification, probeset summarisation and normalisation 178
5.2.1 Box-plots: medians and distribution of global array signal intensities 178
5.2.2 MA-plots: Linearity and variance of normalised log-signal-ratios 180

5.2.3 Evaluation of probe-level processing and normalisation methods, a conclusion 182
5.3 Macrophage Expression Profile Correlation 182
5.3.1 Expression of macrophage specific genes 182
5.3.2 Macrophage gene expression signature 183
5.3.3 Gene expression profile of macrophage activation 184
5.4 Unsupervised exploratory clustering 185
5.4.1 Principal component analyses 185
5.4.2 Condition tree dendrograms 187
5.4.3 Analyses of potential confounding factors 189
5.4.4 Reclassification and inclusion of CEA14 as a stable sample 189
5.4.5 Unsupervised clustering, a conclusion 190
5.4.6 Comparison between groups (Inference statistics) 192
5.4.7 Examination of the Genelist ranked by expression fold difference 192
5.4.8 Functional bioinformatic analysis 202
5.5 Gene expression validation work 212
5.5.1 Preliminary evaluation and optimisation of RT and qRT-PCR work 212
5.5.2 Multiple reference control genes selection and assessment 218
5.5.3 Technical validation of microarray results by qRTPCR 220
5.5.4 Biological validation by qRTPCR - testing on a larger sample size 221
Chapter 6. Expression imaging in the stable and unstable plaque 224
6.1 An overview 224
6.2 Immunohistochemistry of target proteins 224
6.2.1 Preliminary antibody optimisation work 224
6.2.2 FABP4 and Leptin protein expression in the plaque 226
6.2.3 Semi-quantitative Immunohistochemistry analysis 230
6.2.4 Quantitative immunohistochemistry pilot data 231
6.3 Optical Projection Tomography of the atherosclerotic plaque 233
Chapter 7. Discussion 237
7.1 Clinical and pathological characterisation of the plaque 238
7.1.1 The PIT lesion and plaque erosion 238
7.1.2 Plaque surface morphology as an independent predictor of clinical events 239
7.1.3 Detailed plaque surface morphology using 3-dimensional MR imaging 240
7.1.4 Correlations between histology, clinical symptoms and radiographic plaque surface irregularity 241
7.1.5 Sample characterisation and selection 241
7.2 Isolation and characterisation of cell-specific RNA 243
7.2.1 The atherosclerotic plaque:unstable tissue susceptible to RNA damage ..243
7.2.2 Confounding RNA effects due to tissue ischaemia 243
7.2.3 RNA damage is inherent in the atherosclerotic plaque 244
7.2.4 Poor quality RNA extracted from VSMCs reflective of biological condition 246

7.2.5 Uniform cellular content....247
7.2.6 Optimisation of the LMD and RNA technique....248
7.2.7 Validation of RNA quality....249
7.2.8 Small sample amounts and linear amplification....249
7.3 Analyses of the transcriptome in plaque rupture....250
7.3.1 LMDed cells had expression profiles of activated macrophages....250
7.3.2 Unsupervised clustering confirmed ruptured and stable groups....251
7.3.3 Identification of genes of significant differential expression and regulated pathways....252
7.3.4 Cell signalling pathways are significantly regulated in plaque stability/instability....253
7.3.5 Activated, scavenging and phagocytic phenotype in unstable plaque macrophages....254
7.3.6 Synthetic, migratory and remodeling phenotype in stable plaque macrophages....254
7.3.7 FABP4, Leptin and the PPAR-Adipocytokine signalling pathway....256
7.3.8 Other target genes and pathways....260
7.3.9 Previous large-scale gene expression studies of atherosclerosis and plaque rupture....260
7.3.10 Microarray study design....266
7.3.11 Transcript abundance quantitation in validation....266
7.3.12 The selection of stable reference control genes....267
7.3.13 The biological validation of target genes of interest....268
7.4 Expression imaging in the stable and unstable plaque....269
7.4.1 Heterogeneity in protein expression of FABP4 and Leptin....269
7.4.2 Quantitative immunohistochemistry....270
7.4.3 Three dimensional imaging of gene and protein expression in the atherosclerotic plaque....271
7.5 Limitations of the study....272
7.6 Causality and future work....273
7.7 Conclusion....274
Conflicts of Interest and Sources of funding....275
References....276

V. Lists of figures, tables and digital files

List of figures

Figure 1. Deaths by cause in the United Kingdom in 2008 1
Figure 2. The Stary atherosclerotic lesion classification schemata 3
Figure 3. The Virmani atherosclerotic lesion classification schemata 3
Figure 4. Normal arterial vessel 4
Figure 5. Atherosclerotic lesion initiation with native LDL deposition and oxidation 5
Figure 6. Inflammation and recruitment of pro-inflammatory cells 6
Figure 7. Extensive LDL modification, foam cell formation and lipid pooling 7
Figure 8. Stary: adaptive intimal thickening, or Virmani: intimal thickening lesion 8
Figure 9. Stary I: initial lesion, or Virmani: intimal xanthoma 8
Figure 10. Stary II: Fatty streak, or Virmani: intimal xanthoma 9
Figure 11. Stary III: Intermediate lesion, or Virmani: pathological intimal thickening 9
Figure 12. Updated Stary scheme of lesion progression 10
Figure 13. Stary IV: atheroma, or Virmani: fibrous cap atheroma 11
Figure 14. Stary V: fibroatheroma, or Virmani: fibrous cap atheroma 12
Figure 15. Thin fibrous cap atheroma 13
Figure 16. Stary VI lesion 14
Figure 17. Plaque erosion 16
Figure 18. Calcified nodule 16
Figure 19. Healed rupture of a thin fibrous cap atheroma 17
Figure 20. Fibrocalcific plaque 18
Figure 21. Circumferential wall stress in the plaque 24
Figure 22. Shear stress in the plaque. 24
Figure 23. The dynamic state of the fibrous cap 25
Figure 24. Interactions of macrophages with Th1 and Th2 cells 27
Figure 25. Antigen presentation of modified lipoproteins by macrophages to the CD4 T cell via the MHC-II:peptide complex 29
Figure 26. The PPAR pathways 31
Figure 27. Liquid-nitrogen-cooled copper plate snap-freezing method 49
Figure 28. Liquid-nitrogen-cooled isopentane bath snap-freezing method. 50
Figure 29. Endarterectomised carotid atherosclerotic specimen portions for formalin-fixation and snap-freezing. 51

Figure 30. Three domain criteria of the samples for the selection of stable and unstable samples for gene expression profiling. 58
Figure 31. Overview of sample snap-frozen specimen cryosectioning, fixation, staining, processing and LMD. 65
Figure 32. The 2-cycle linear amplification reaction, cRNA fragmentation and hybridisation 72
Figure 33. 3D gene expression mapping of PAX6 in a developing embryonic human brain using optical projection tomography 92
Figure 34. Method for mounting sections on slides for histochemistry, immunohisto-chemistry or in-situ hybridisation staining for OPT....94
Figure 35. Flowchart of Carotid endarterectomy specimens collected 96
Figure 36. Histogram of all the symptomatic patients according to the time of their last clinical event 97
Figure 37. The hybrid schemata of atherosclerotic plaque progression 102
Figure 38. The complex heterogenus atherosclerotic plaque seen 107
Figure 39. Photomicrographs of Ruptured thin fibrous cap atheromas with thrombus. ..108
Figure 40. Photomicrographs of Stable thick fibrous cap atheroma 112
Figure 41. Photomicrographs of stable fibrocalcified lesions....112
Figure 42. Photomicrographs of pathological intimal thickening lesions....113
Figure 43. Photomicrographs of fibrous lesions....114
Figure 44. Photomicrographs of vulnerable thin fibrous cap atheroma. 114
Figure 45. Venn diagram of the selection of the symptomatic unstable ruptured plaque for gene expression analysis using the criteria in 3 domains. 127
Figure 46. Venn diagram of the selection of the asymptomatic stable plaque for gene expression analysis using the criteria in 3 domains. 129
Figure 47. Overview of the steps involved in sample processing leading to Microarray.133
Figure 48. H&E stained cryosections of IMA specimens using the different methods of snap-freezing 134
Figure 49. Agilent Bioanalyser electropherogram and fluorescence graphs of total RNA extracted from whole tissue IMA specimens using Trizol. 137
Figure 50. Agilent Bioanalyser Nano-chip results electropherogram and fluorescence graphs of total RNA extracted from whole tissue CEA specimens using Trizol. 138
Figure 51. Agilent Bioanalyser Pico-chip results of RNA extraction from milligrams of snap-frozen IMA tissue 139
Figure 52. Agilent Bioanalyser Pico-Chip results of RNA from LMDed VSMCs 141
Figure 53. Agilent Bioanalyser Pico-chip results with carrier RNA 143
Figure 54. IMA cryosections used for the LMD tests fixed with 95% Ethanol and without xylene clearing 146

Figure 55. Agilent Bioanalyser results of RNA extracted from the initial LMD trials of VSMCs LMDed from IMA cryosections.....147
Figure 56. The lifting artefact and 'rucking' of the section fixed in acetone.....150
Figure 57. Histochemical staining with H&E, toluidine blue and HistoGene.....150
Figure 58. Effect of xylene clearing on atherosclerotic plaque cryosections 151
Figure 59. The Bioanalyser Pico-chip results of RNA from LMD of VSMCs and Macrophages from 75% ethanol fixed, H&E stained CEA specimens using the optimised LMD protocol.....153
Figure 60. Assessment of RNA stability of the LMD sections.....155
Figure 61. Agarose gel electrophoresis of the oligo-dT primed RT-PCR of GAPDH mRNA demonstrating the preservation of the integrity of the extracted RNA 156
Figure 62. Scout and LMD cryosections of a stable thick fibrous cap atheromatous plaque. 158
Figure 63. Cryosections of CEA35 showing a ruptured thin fibrous cap atheroma with extrusion of the core contents and thrombus. 160
Figure 64. Cryosections of CEA33 showing a ruptured thin fibrous cap atheroma with very little VSMCs in the fibrous cap for LMD 161
Figure 65. Cryosections of CEA17 showing a ruptured thin fibrous cap atheroma with some VSMCs in the cap which were infiltrated with macrophages.....162
Figure 66. Agilent Bioanalyser Pico-chip results of RNA from the LMD of VSMCs in the fibrous caps of stable and ruptured plaques.....165
Figure 67. Agilent Bioanalyser Pico-chip results of RNA from the LMD of macrophages of stable and ruptured plaques 168
Figure 68. Cryosections of CEA33 demonstrating apoptotic/necrotic and healthy viable macrophage cells and the RNA isolated from these regions.....169
Figure 69. Agarose gel electrophoresis of purified and fragmented amplified cRNA 170
Figure 70. An overview of microarray data analysis. 177
Figure 71. Box-plots of the global probeset signal values of the 11 arrays 179
Figure 72. MA-plots of Log-transformed relative abundance ratios.....181
Figure 73. Condition Tree Dendrogram demonstrating the correlation of the genomic expression profiles of our study samples to other various cell/tissue samples (n=299). .183
Figure 74. Principal Components Analysis of our study samples with other samples of blood cell origin and activated/unactivated macrophages using focused subset of macrophage activation genes.....184
Figure 75. Principal component analyses of the 11 microarray samples.....186
Figure 76. Condition tree dendrograms of the 11 microarray samples.....188

Figure 77. The line-graph of relative difference in transcript expression between ruptured and stable groups of the 1,187 statistically significant probesets are represented on a logarithmic scale 194
Figure 78. A heatmap of the statistically significant differentially expressed probesets ranked by fold difference.....195
Figure 79. Gene Ontology Analysis of the statistically significant genelist 204
Figure 80. The Adipocytokine component of the PPAR/Adipocytokine Signalling Pathway with the significantly identified differentially expressed genes highlighted in red.....207
Figure 81. The PPAR component of the PPAR/Adipocytokine Signalling Pathway with the significantly identified differentially expressed genes highlighted in red. 208
Figure 82. The Wnt signalling pathway with the significantly identified differentially expressed genes highlighted in red 210
Figure 83. The TGF-beta signalling pathway with the significantly identified differentially expressed genes highlighted in red 211
Figure 84. qRTPCR amplification plots of random hexamer and oligo-dT primed RT....213
Figure 85. qRTPCR amplification plots of the 4 reverse transcriptases 213
Figure 86. Comparison matrix of the 3 different qRTPCR chemistries 214
Figure 87. Standard curve of a cDNA dilution series of the ECM2 transcript. 215
Figure 88. Pair-wise variation analysis of reference control genes.....219
Figure 89. Validation of the microarray data by Real-time quantitative PCR.....220
Figure 90. The quantitative Real-Time PCR results of the 12 top ranking statistically significant genes tested on a larger total sample number of 25.....222
Figure 91. The relative clustering and separation of the 25 samples in gene expression space using Principal Components Analysis 223
Figure 92. Frozen section immunostaining of Leptin and CD68 of a stable and unstable ruptured plaque 227
Figure 93. Paraffin-embedded immunostaining of Leptin and CD68 of an unstable ruptured thin fibrous cap atheroma 228
Figure 94. Paraffin-embedded immunostaining of Leptin and CD68 of an of a stable thick fibrous cap atheroma 229
Figure 95. Optical Projection Tomography 3D reconstructions of a whole and intact normal radial artery 235
Figure 96. Optical Projection Tomography 3D reconstructions of a whole mount atherosclerotic carotid artery removed at carotid endarterectomy.....236

List of tables

Table 1. An overview of the different approaches in the study of atherosclerosis 34
Table 2. Taqman Gene Expression Assay Probeset details.....83
Table 3. The 14 CEA samples LMDed and RNA extracted for further study.....87
Table 4. Quantitative RTPCR results of the samples with degraded and good quality RNA demonstrating the tolerance of the assay to RNA degradation 87
Table 5. CEA specimens in their clinical groups with clinical and demographic data, risk factor profile, medication, blood pressure, ECG and laboratory results.....99
Table 6. The hybrid schemata amalgamating the Virmani and Stary schemata.....104
Table 7. Breakdown of the predominant lesion types in the CAGE study to symptoms, risk factor profile, plaque stenosis and surface irregularity on MR angiography 109
Table 8. Contingency Table (3x2) comparing stable lesion types to recent symptoms. .111
Table 9. Results of trans-cranial doppler emboli detection with correlation to symptoms, angiographic stenosis and surface irregularity and plaque histology.....116
Table 10. Contingency table (3x3) comparing symptoms to the grades of plaque surface irregularity 118
Table 11. Contingency table (2x2) comparing the presence of any prior symptoms to the presence of any surface irregularity.....118
Table 12. Contingency table (2x3) comparing of presence of previous symptoms of TIA or stroke to evidence of cerebral infarction on brain imaging.....119
Table 13. Contingency table (2x4) comparing the degree of stenosis to the presence of any plaque surface irregularity.....119
Table 14. Contingency table (2x4) comparing the degree of stenosis to the presence of any prior symptoms of TIA or stroke. 120
Table 15. Contingency table (2x3) comparing histology to recent symptoms.....121
Table 16. Contingency table (3x2) comparing histology to recent symptoms, excluding the 7 PIT lesions. 121
Table 17. Contingency table (2x3) comparing histology to presence of symptoms.....122
Table 18. Contingency table (2x3) comparing histology to the presence of plaque surface irregularity detected using MR angiography. 123
Table 19. The 2-way interaction tables across the 3 conditions of clinical symptoms, angiographic plaque surface irregularity and histological lesion type 125
Table 20. The 2x2x2 cross-categorised frequency input data and the 3-way log-linear analysis of Clinical symptoms, Angiographic plaque surface irregularity and Histological lesion types 126
Table 21. Clinical, Radiological and Histological characteristics of the Ruptured Plaque samples selected for gene expression profiling 130

Table 22. Clinical, Radiological and Histological characteristics of the Stable Plaque samples selected for gene expression profiling 131
Table 23. A summary of the macro- and microscopic characteristics and RNA quality and yield using the different snap-freezing methods. 135
Table 24. Results of the RNA extraction from LMDed VSMCs using Trizol, RNeasyMicro, Picopure, NanoPrep and RNAqueousMicro 142
Table 25. Comparison of LMD slide type and air-drying 148
Table 26. Results of the different methods of fixation and histochemical staining.....149
Table 27. VSMC LMD and RNA extraction from stable and ruptured samples 164
Table 28. Macrophage LMD and RNA extraction from stable and ruptured samples.....167
Table 29. The compiled amplification and TestChip results 174
Table 30. The GeneChip Quality Control Assessment results.....176
Table 31. Comparison of the various methods of probe-level processing and global normalisation.....182
Table 32. Details of the samples taken successfully to microarray with potential confounding factors examined 191
Table 33. Table summarising the top 15 probesets of highest relative expression in ruptured samples compared to stable samples 198
Table 34. Table summarising the top 15 probesets of highest relative expression in stable samples compared to ruptured samples.....201
Table 35. The biological processes of the differentially expressed genes identified. 203
Table 36. Statistically significant KEGG Pathways identified using WebGestalt. 206
Table 37. Differentially regulated genes in PPAR/Adipocytokine Signalling Pathway....209
Table 38. R^2 correlation and calculated efficiency of qRTPCR using carrier RNA. 215
Table 39. The PCR efficiencies of the Taqman Primer Probes used and their minimum detection thresholds.....216
Table 40. qRTPCR ranging test experiment using 500pg equivalent of total RNA.....217
Table 41. Expression stability of the candidate reference genes.....219
Table 42. Demographics of patients included in unstable and stable sample groups and the corresponding significance between groups.....221
Table 43. Optimisation matrix of the antigen retrieval methods tested 225
Table 44. The semi-quantitative analysis of protein immunohistochemical staining of SMA, CD68, Leptin and FABP4 in the macrophages of stable and unstable ruptured plaques 230
Table 45. The FABP4 to CD68 and Leptin to CD68 signal intensity ratios in the 3 colour detection channels 232
Table 46. Large scale gene expression studies of human atherosclerosis 262
Table 47. Large scale human gene expression studies of plaque vulnerability.....263

List of files in the enclosed CD

StatSig1187.pdf; The statistically significant differentially expressed genelist.

StatSig1187.txt; The genelist in tab delimited format.

Movie 1.mpg; OPT 3D gene expression mapping of PAX6 in the embryonic human brain.

Movie 2.mpg; OPT 3D lateral view of radial artery.

Movie 3.mpg; OPT 3D longitudinally sectioned radial artery.

Movie 4.mpg; OPT 3D 'fly-through' of digital sections of the radial artery.

Movie 5.mpg; OPT 3D lateral view of carotid atheromatous plaque.

Movie 6.mpg; OPT 3D longitudinally sectioned carotid atheroma at the bifurcation.

Movie 7.mpg; OPT 3D transversely sectioned carotid atheroma.

Movie 8.mpg; OPT 3D 'fly-through' of digital sections of the carotid atheromatous plaque.

Chapter 1. Introduction

1.1 The burden of cardiovascular disease

In the United Kingdom, cardiovascular disease (CVD) is the leading cause of death accounting for almost 191,000 deaths a year which is a third of all deaths. The two major manifestations of CVD are coronary heart disease (CHD) and stroke. CHD by itself is the most common cause of death and accounts for about half of all CVD deaths. Stroke is the second most common cause of death (after CHD) and makes up a quarter of all CVD deaths. The relative proportions are illustrated in Figure 1[1]. CVD is one of the main causes of premature death in the UK (death before the age of 75) and accounted for 28% of premature deaths in men and 20% of premature deaths in women in the UK in 2008, causing almost 50,000 premature deaths. CHD alone is the main cause of premature death in the UK in men. One in five premature deaths in men and one in ten premature deaths in women were caused by CHD alone in the UK in 2008[1].

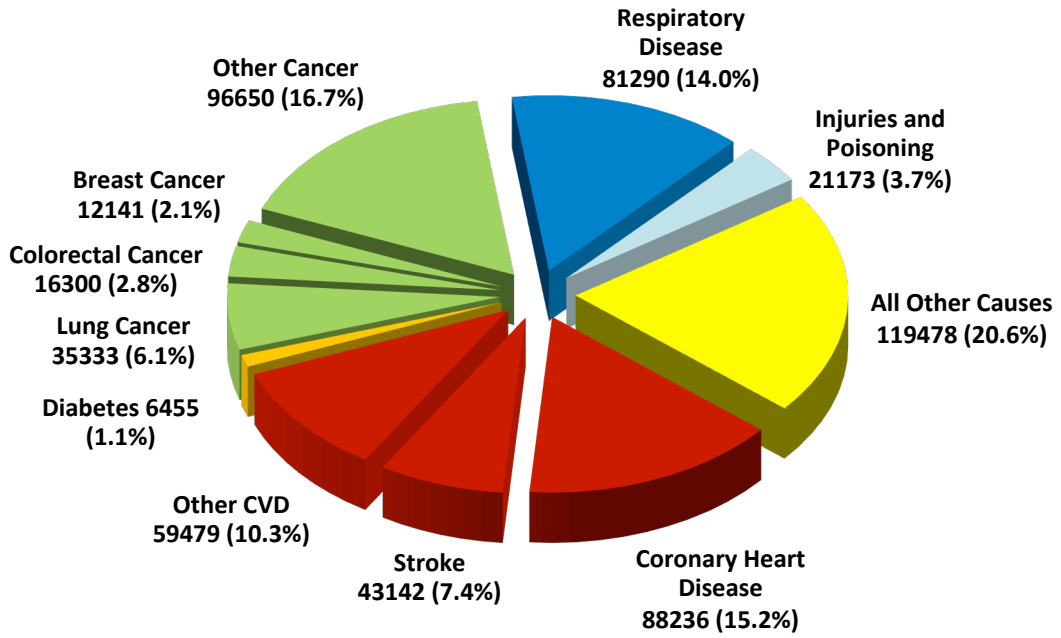

Figure 1. Deaths by cause in the United Kingdom in 2008, with number of deaths and their percentages[1].

Disease in other parts of the circulatory system accounts for a large proportion of all deaths (10%) and significant morbidity. This includes peripheral arterial disease, renovascular and mesenteric artery disease. Renovascular disease is often found in combination with atherosclerotic disease elsewhere; in up to 10% of patients with stroke

and 49% of patients with iliac and lower extremity peripheral artery disease[2], and is associated with a high mortality rate. Peripheral arterial disease is highly prevalent, affecting an estimated 12-20% of persons aged 65 years or older, and increases with age, affecting more than 35% of patients aged 70 to 82 years[3]. More than half of those affected are asymptomatic and are underdiagnosed and undertreated[3-5]. Like renovascular disease, PAD is an independent marker of advanced atherosclerotic disease in other arterial territories whether symptomatic or not[4].

1.2 The pathobiology of atherosclerosis

Athērōma, from its Latin origins, describes a 'tumour full of matter resembling gruel'; and from the Greek *Athēra* for *gruel*. The Greek word *Sklērōsis* means *hardening*[6].

Atherosclerosis is a spectrum of disease of the vasculature characterised by the deposition of lipids and cholesterol in the innermost layer of the artery (the intima) to form atheromatous plaques in medium to large sized arteries[7, 8]. In a developed advanced atherosclerotic plaque, the lipid core has necrotic debris walled off by a rim of macrophages which continually work to process the deposited lipids. The lipid core is also rich in thrombogenic antigens, most notably tissue factor. This organised necrotic lipid core is protected from the clotting factors and platelets in the circulating blood by a fibrous cap made of vascular smooth muscle cells and collagen[9].

Early anecdotal reports of atherosclerosis may have been made as early as 1799 by Caleb Hillier Parry[10], but it was only until an in-depth and systematic study in the 1850s by Rudolf Virchow of the histological characteristics of the atherosclerotic lesion in its varying stages did we begin to elucidate the pathogenesis of the disease[11]. However, there seemed to be a hiatus for nearly a century before more detailed study of the atherosclerotic plaque was initiated again. Pioneering work by Ludwig Aschoff in the 1930s and by Russell Ross and Valentin Fuster in the 70s, then by Erling Falk, Michael Davies, Peter Libby, Herbert Stary, Renu Virmani, Allard van der Wal and Prediman Shah in the later quarter of the century have unravelled the sequence of events in our understanding of atherogenesis and more recently in plaque vulnerability and rupture[7-9, 12-18].

It was the landmark work by Herbert Stary and colleagues leading to the American Heart Association Classification of Atherosclerosis in 1992 to 1995 that first described a linear sequence of events in a clear numerical order that is still favoured by many today[9, 16] (Figure 2). However, more recently an alternative scheme has been proposed by Renu Virmani and colleagues; these investigators favour a more morphologically descriptive classification system with greater flexibility in the pathways of progression of the lesions[18,

[19] (Figure 3). In the rest of this section I shall describe the plaque initiation and progression and the plaque sub-types in reference to these classification systems in detail.

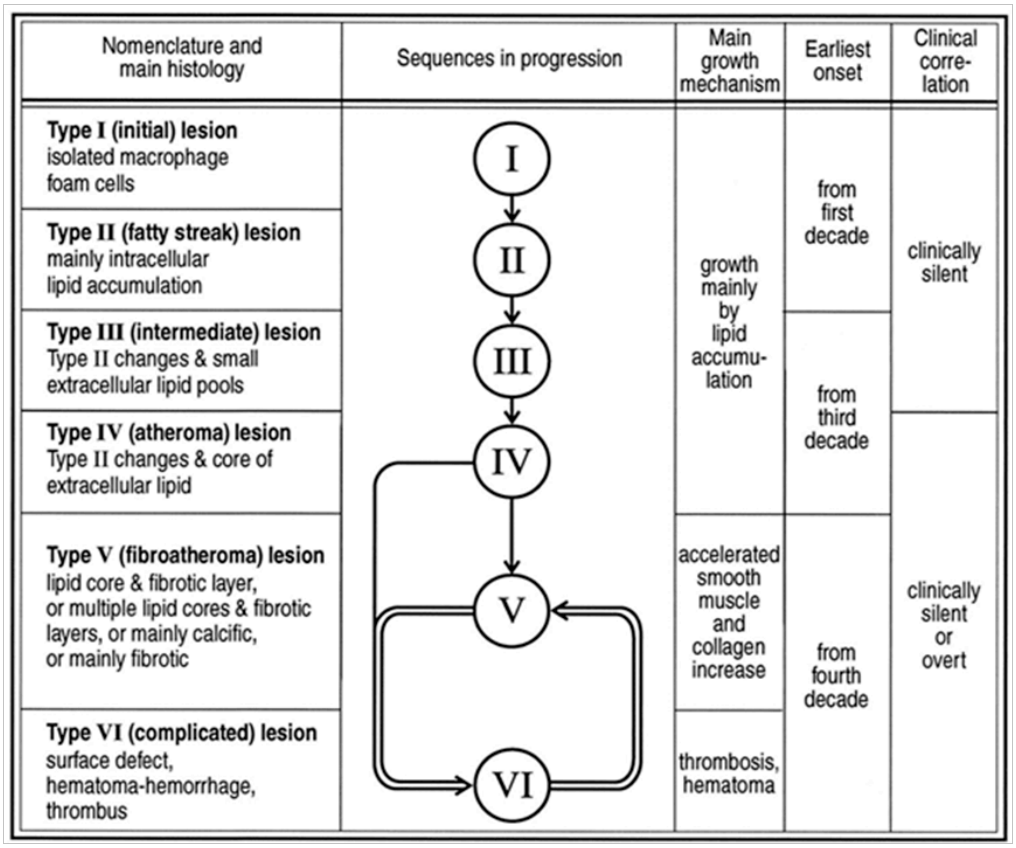

Figure 2. The Stary atherosclerotic lesion classification schemata. (Figure from Stary 1995 [9]).

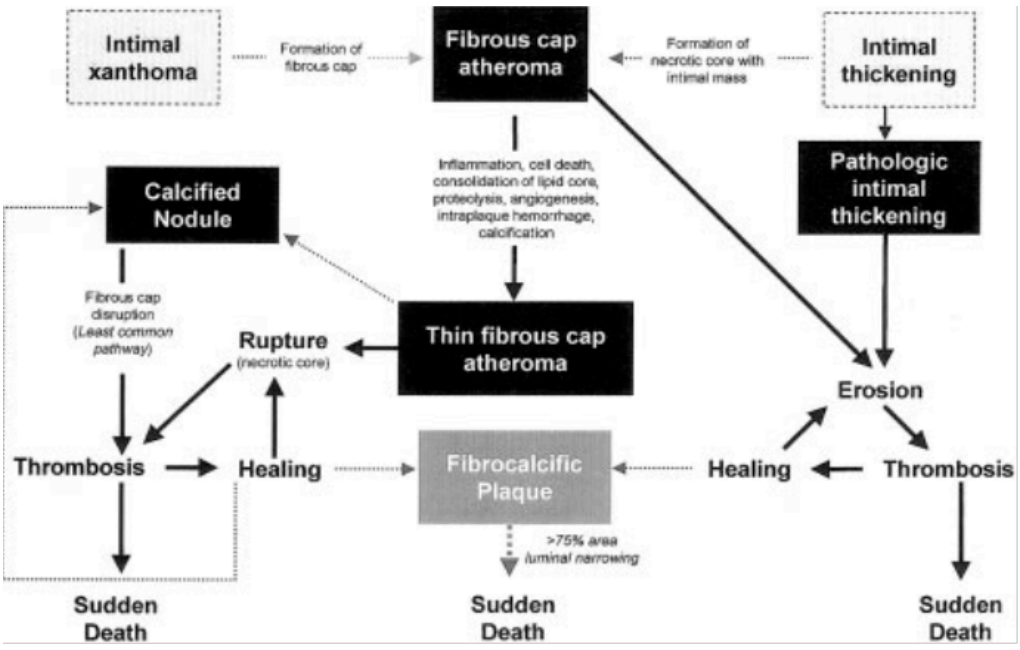

Figure 3. The Virmani atherosclerotic lesion classification schemata. (Figure from Virmani 2000[18]).

1.2.1 Normal vessel and healthy endothelium

The normal artery consists of three distinct layers; the intima, media and adventitia (Figure 4). The *tunica intima* is the innermost layer and is made of a single luminal layer of endothelial cells which is in direct contact with the circulatory blood and thus is exposed to the shear stresses from its flow. A thin layer of extracellular connective tissue matrix made up of proteoglycans and collagen lie underneath the endothelial cells with a layer of elastic fibres, the *internal elastic lamina*, at its base. The internal elastic lamina separates the intimal layer from the middle layer, the *tunica media*. The media is the muscular layer consisting of vascular smooth muscle cells (VSMCs) with elastic fibres and collagen. In medium sized arteries, there is a greater amount of smooth muscle cells giving the artery its ability to vary its muscular tone and modulate blood flow. Whereas in large arteries like the aorta, there is a greater amount of elastic fibres and collagen to impart greater arterial strength and recoil. The middle medial layer is separated to the outer *tunica adventitia* by the *external elastic lamina*. The tunica adventitia consists of collagen fibres and fibroblasts and smooth muscle cells.

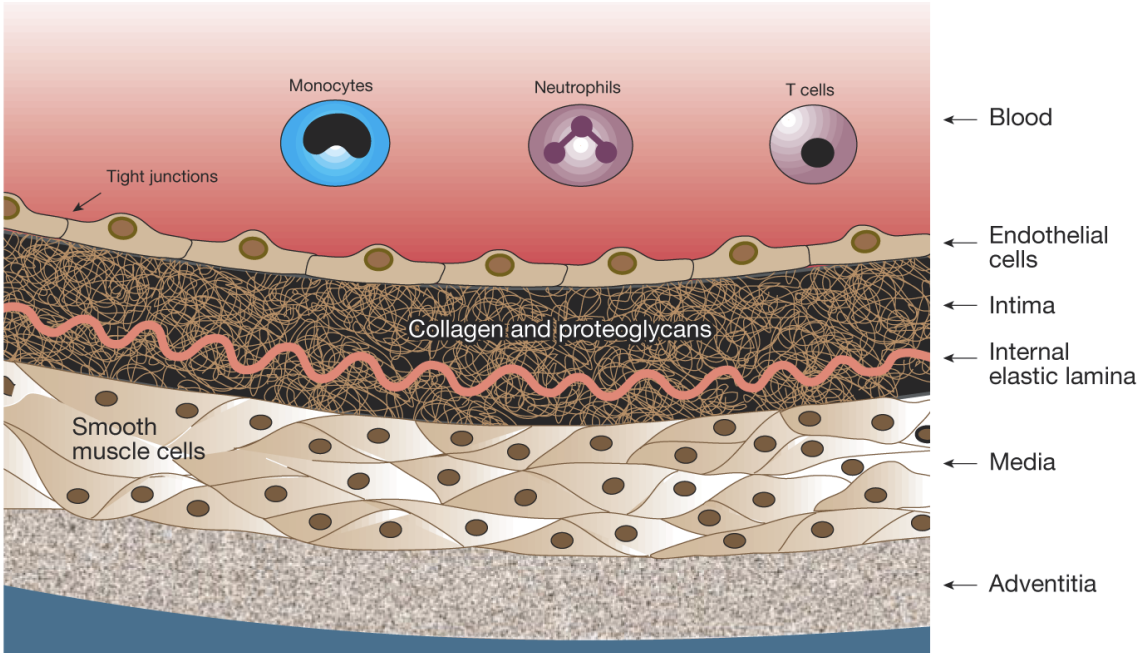

Figure 4. Normal arterial vessel. (Figure from Lusis 2000[20])

1.2.2 Initiation of atherosclerosis and early lesions

Atherosclerosis begins as subendothelial accumulation of lipid, mainly of low density lipoprotein (LDL) at sites of *endothelial dysfunction*. These atherosclerosis-prone regions occur typically at sites of arterial branching and curvature, where there is non-laminar and turbulent blood flow, resulting in temporal and spatial gradients in wall shear stresses. At

these regions, the endothelial cells are polygonal in shape and aligned randomly. The lack of laminar shear stress stimuli on these endothelial cells lead to an inability to maintain the upregulation of athero-protective genes such as eNOS (endothelial isoform of nitric oxide synthase), COX-2 (inducible isoform of cyclo-oxygenase) and Mn-SOD (manganese-dependent superoxide dismutase). The resulting dysfunctional endothelium is prone to increased permeability to macromolecules such as low density lipoprotein (LDL) as well as inflammatory cells and chemokines [21](Figure 5). In contrast, in atherosclerosis-resistant regions the artery is tubular with uniform flow of blood and the endothelial cells are tightly packed and uniformly arranged in an ellipsoidal shape in alignment to the blood flow[21].

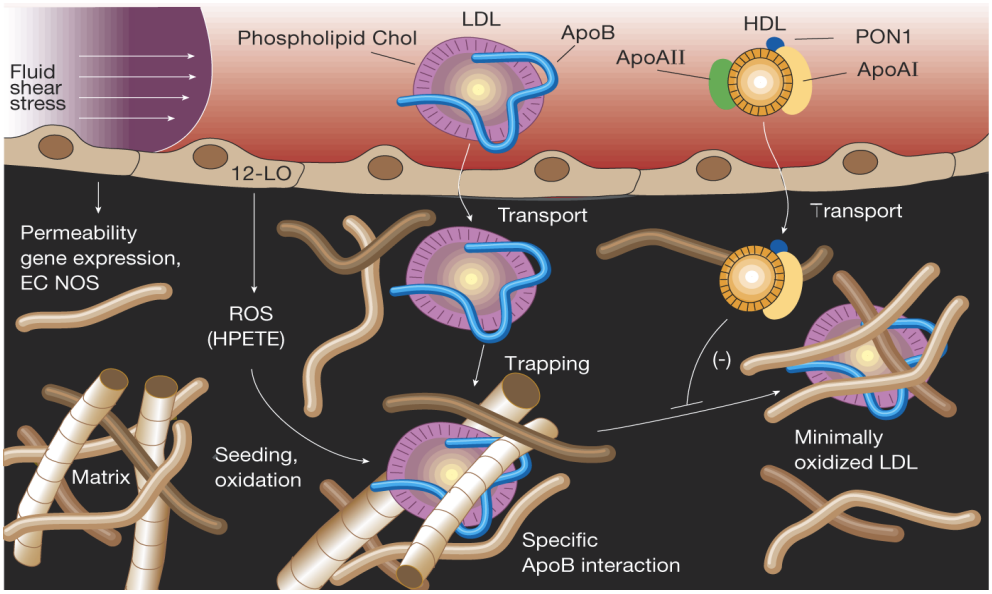

Figure 5. Atherosclerotic lesion initiation with native LDL deposition and oxidation. (Figure from Lusis 2000[20])

Native LDL passively diffuses through the tight junctions of loosely packed endothelial cells at these turbulent flow sites of low wall shear stress. Its deposition is increased with high circulating levels of LDL. It is also retained and anchored in the intima by the interaction of the LDL constituent apolipoprotein B with the intimal matrix proteoglycans[22] (Figure 5).

However, native LDL is relatively inert. It has been shown that the trapped native LDL undergoes *extensive modification* in the vessel wall; including oxidation, lipolysis, proteolysis and aggregation. It undergoes initial oxidation as a result of exposure to oxidative waste of vascular cells and lipoxygenases[23, 24]. High density lipoprotein (HDL) has a protective role by inhibiting lipoprotein oxidation (via its paraoxonase activity) as well as the removal of the excess cholesterol from peripheral tissues[25].

The resultant 'minimally oxidized LDL' stimulates the endothelial cells to produce adhesion molecules (P-selectin, E-selectin, the cell adhesion molecules ICAM-1 and VCAM-1, and others), chemotactic proteins (the monocyte chemotactic protein (MCP-1)) and growth factors (macrophage colony-stimulating factor (M-CSF))[26-31] attracting monocytes and T-cells into the subendothelial space, and the proliferation and differentiation of macrophages (Figure 6).

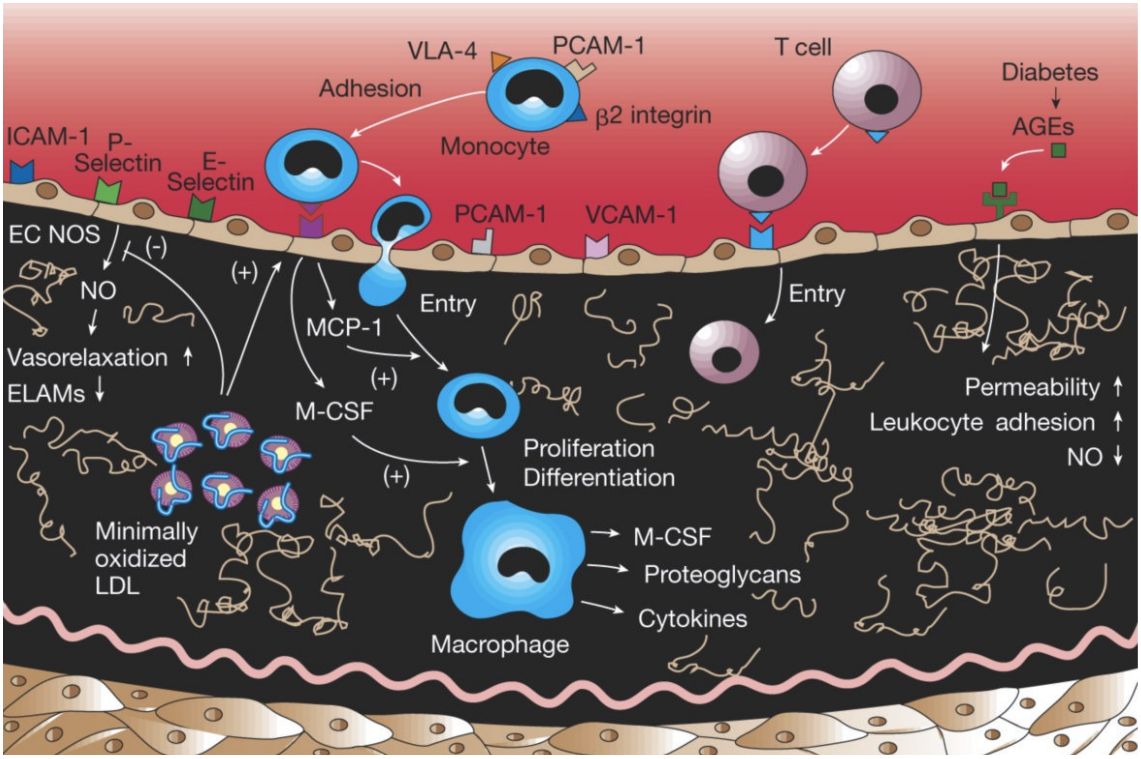

Figure 6. Inflammation and recruitment of pro-inflammatory cells. (Figure from Lusis 2000[20])

The minimally oxidised LDL is 'extensively modified' not only by the reactive oxygen species from endothelial cells and the recruited macrophages but also by the released myeloperoxidases, sphingomyelinases and secretory phospholipases in these lesions. Myeloperoxidase (MPO) generates highly reactive species which modifies LDL to avidly bind to macrophage scavenger receptors[23]. Sphingomyelinases (SMases) causes lipoprotein aggregation and increased uptake and retention in the macrophages[32]. A secretory phospholipase, the lipoprotein-associated phospholipase A2 ($sPLA_2$ or Lp-PLA2) hydrolyses oxidized phospholipids in LDL producing additional proinflammatory products; lysophosphatidylcholine and oxidised fatty acids. Transgenic mice overexpressing Lp-PLA2 show dramatically increased atherosclerosis[33] (Figure 7).

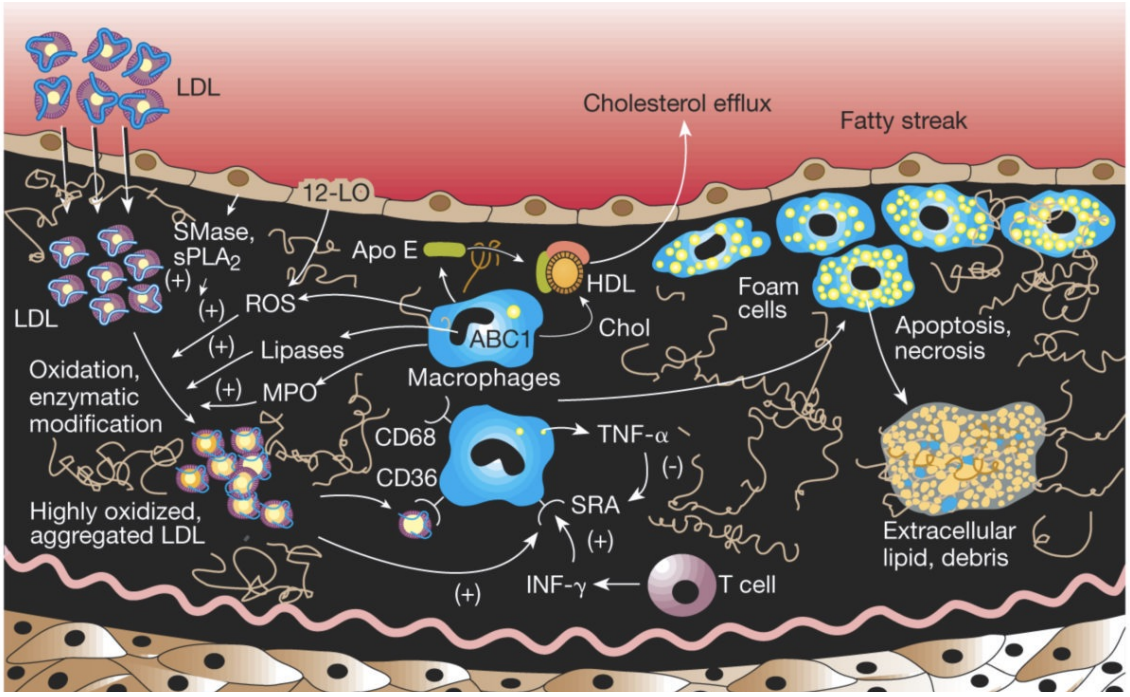

Figure 7. Extensive LDL modification, foam cell formation and extracellular lipid pooling. (Figure from Lusis 2000[20])

The resultant highly oxidised LDL is actively taken up by endocytosis into the macrophages mainly via the scavenger receptors SR-A and CD36[23, 34] to form lipid-engorged macrophages; the foam cells. Isolated pockets of foam cells form in the intima (Stary I: initial lesion or Virmani: intimal xanthoma, Figure 9). As the process of lipid deposition and modification continues more macrophages are recruited and multiple layers of foam cells are seen (Stary II: fatty streak or Virmani: intimal xanthoma, Figure 10). Eventually as the process continues, small pools of extracellular lipid are seen within an increasingly thickened intima without an evident fibrous cap (Stary III lesion: intermediate lesion or Virmani: pathological intimal thickening, Figure 11). The *early lesions (Stary I and II)* begin very early in human life and can be seen from birth onwards at various susceptible sites[18, 35].

However, these early lesions have a varying tendency to progress to adult lesions depending on where they occur. It is apparent that low or moderately susceptible sites develop intimal lesions that consist of mostly lipid and foam cells with little smooth muscle cell content (Stary I & II, Virmani intimal xanthoma) which mostly regress after childhood[36, 37] and are different in their distribution from the adult lesions seen in the third decade of life[38]. On the other hand, at highly susceptible sites where the haemodynamic turbulence and vessel wall stresses are high, the early intimal foam cell lesions occur at sites with smooth muscle cell *adaptive intimal thickening* (Stary: adaptive intimal thickening with Stary I or II features, or Virmani: intimal thickening, Figure 8) and correlate to the distribution of atherosclerotic lesions in human adults[35, 39]. This intimal thickening consists

of vascular smooth muscle cells (VSMCs) that have migrated and infiltrated into the intima and have changed from their original resting contractile phenotype to a more synthetic and replicative type[40].

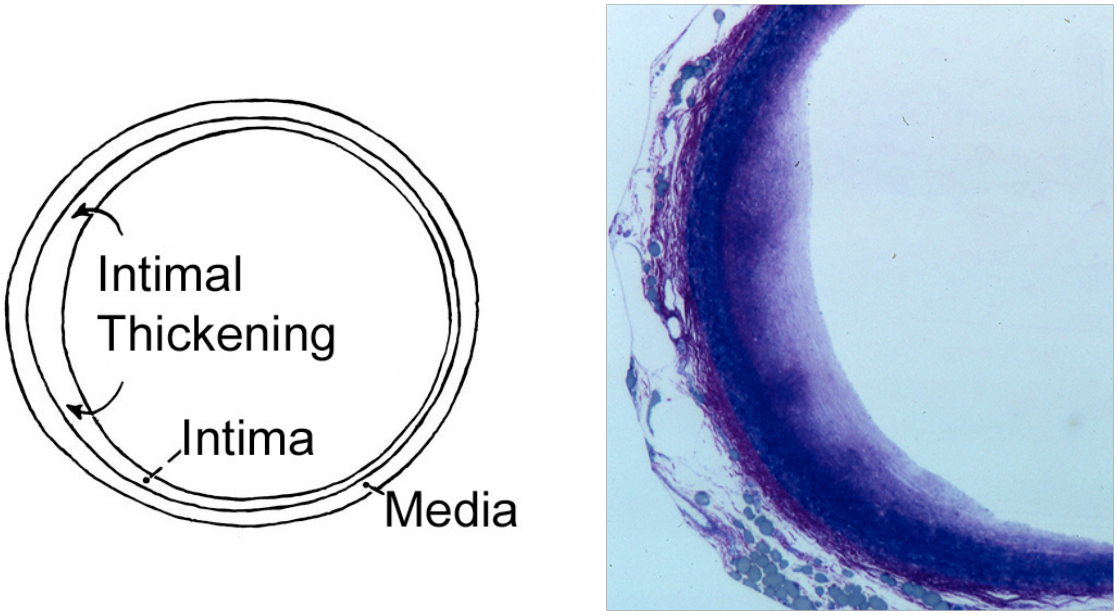

Figure 8. Stary: adaptive intimal thickening, or Virmani: intimal thickening lesion, with VSMC infiltration into the intima. (Figures from Stary[9, 41])

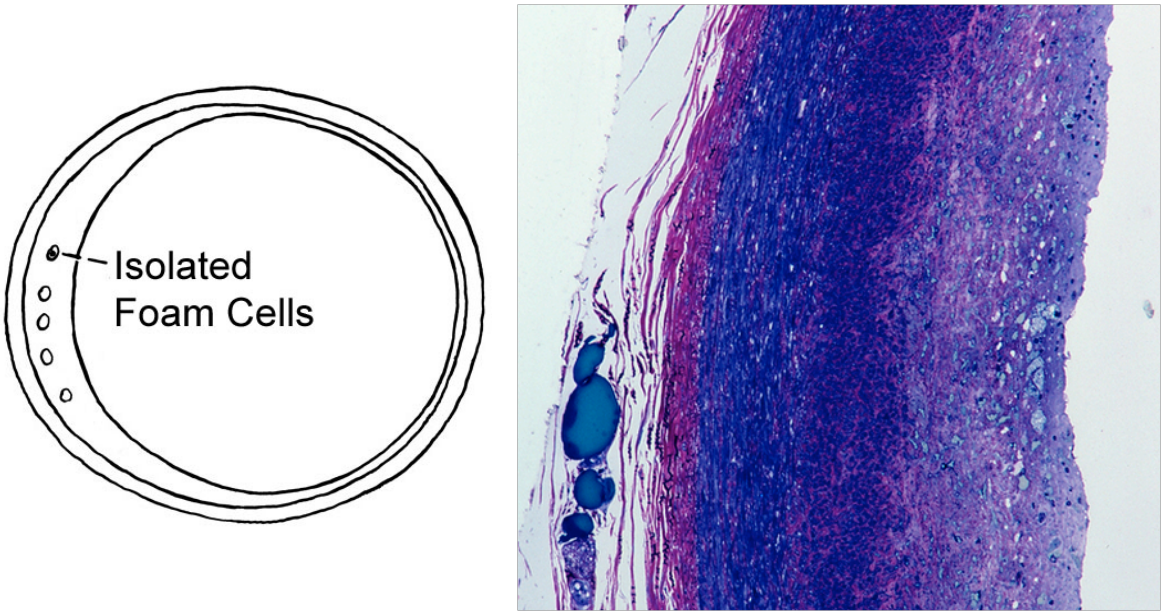

Figure 9. Stary I: initial lesion, or Virmani: intimal xanthoma. (Figures from Stary[9, 41])

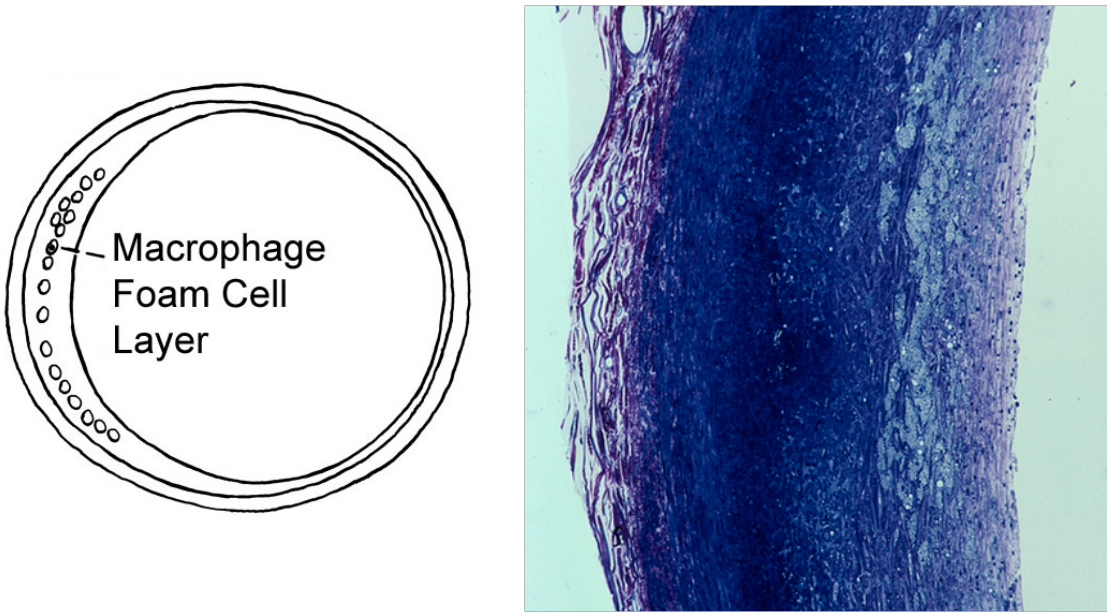

Figure 10. Stary II: Fatty streak, or Virmani: intimal xanthoma. (Figures from Stary[9, 41])

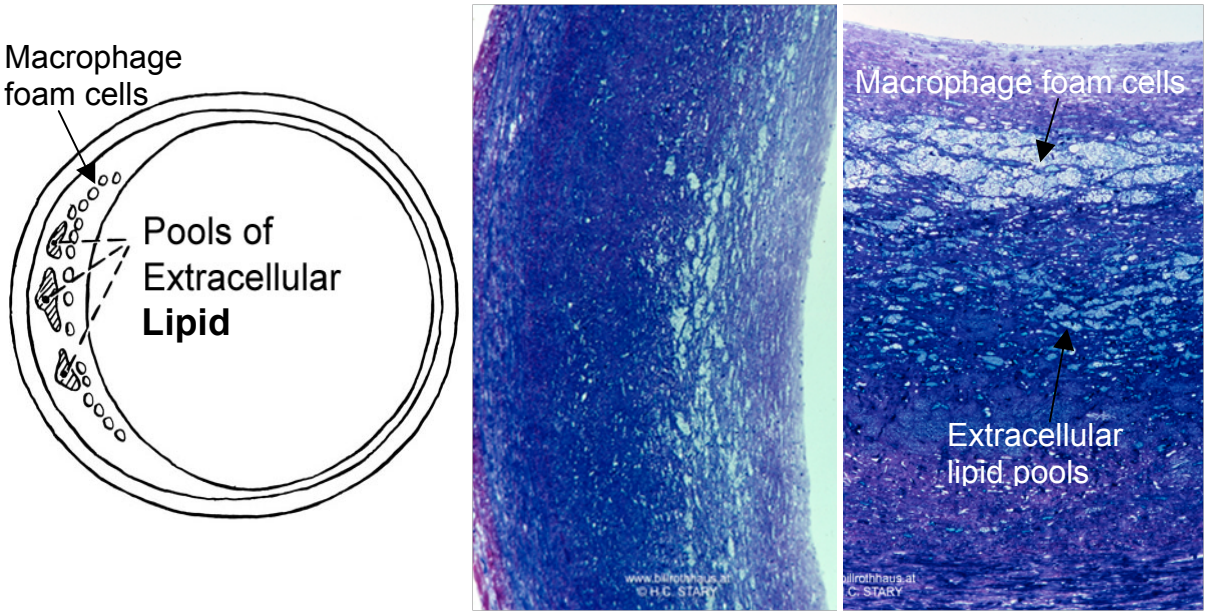

Figure 11. Stary III: Intermediate lesion, or Virmani: pathological intimal thickening. 10x magnification (middle) and 100x magnification (left). (Figures from Stary[9, 41])

The Stary classification scheme describes the progression of Stary I, II and III lesions in highly susceptible sites with adaptive intimal thickening, and thus likely to progress to adult advanced atherosclerotic lesions (highlighted by bold arrows in Figure 12) and in low to moderately susceptible sites without significant VSMC infiltration (typically occurring in youth and may regress). The Virmani scheme differs by classifying the progression prone lesions (VSMC infiltrated lipid lesions) collectively as intimal thickening and the lipid lesions which may regress (with little VSMC infiltration) as intimal xanthoma. It also proposes the classification of a putative lesion subtype called 'pathological intimal thickening' developing from intimal thickening lesions which do not progress to a fibrous cap lesion but has VSMCs in a proteoglycan-rich matrix with areas of extracellular lipid accumulation without necrosis[18]. This subtype loosely correlates with the Stary III lesion subtype. These lesions have no necrotic lipid core or fibrous cap but they are considered not to be entirely benign, being associated with endothelial erosion and thrombi[42] (described in the later section 'lesions with thrombi').

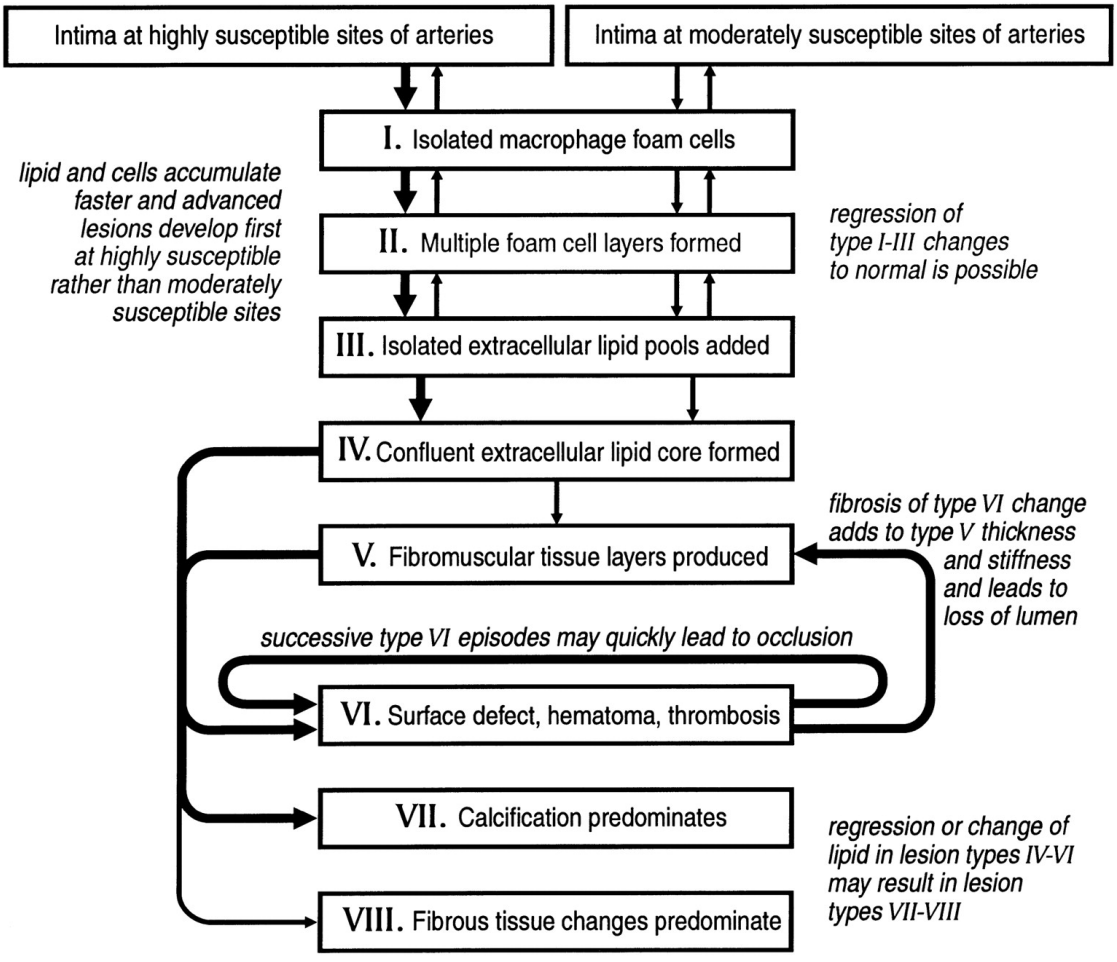

Figure 12. Updated Stary scheme of lesion progression. (Figure from Stary 2000[19])

1.2.3 Stable advanced lesions – fibrous cap atheromata

As these early lesions at highly susceptible sites with intimal thickening progressively get infiltrated with lipid and grow in size, the extracellular lipid accumulates to form the *lipid core* which is surrounded by macrophages actively taking up the modified lipid. There is gradual clonal proliferation of the migrated VSMCs in these intimal masses on the luminal side of the lesion forming a protective barrier (muscular cap) over the extracellular lipid accumulation and macrophage foam cells. There is no significant luminal narrowing seen at this stage yet as a result of medial and adventitial dilatation with the growth of the lipid lesion (Stary IV:atheroma, Virmani:fibrous cap atheroma, Figure 13). This lesion is the first advanced adult lesion seen and is commonly seen in young adults from the third decade on[9, 18].

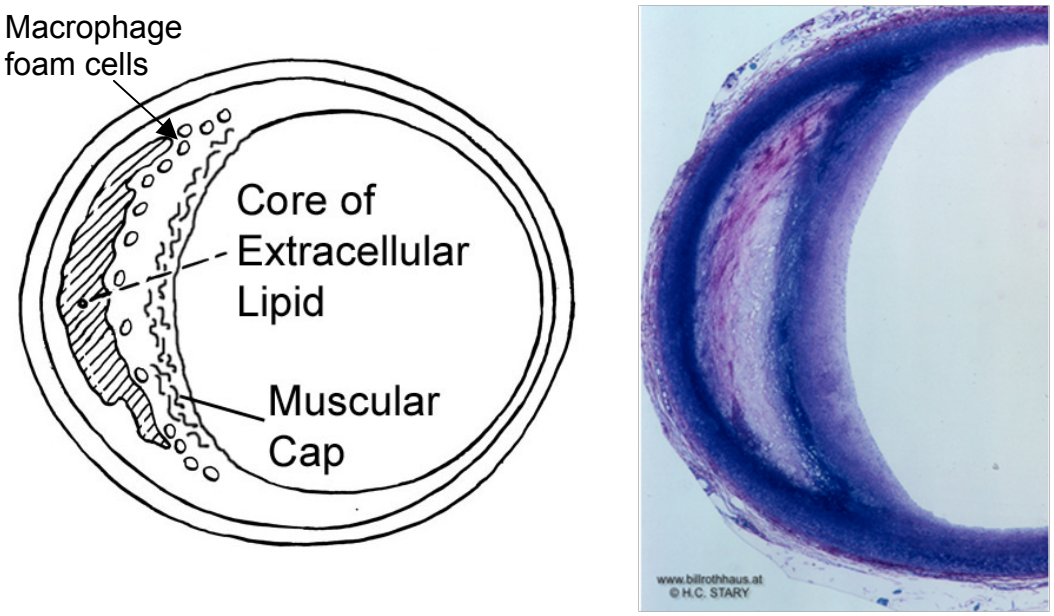

Figure 13. Stary IV: atheroma, or Virmani: fibrous cap atheroma. (Figures from Stary[9, 41])

As the lipid deposition continues and the core continues to grow in size, the centre of the core no longer remains viable, and the death of lipid-laden foam cells leave necrotic debris forming the *necrotic lipid core*. The lesion begins to protrude into the vascular lumen and stenosis of the artery begins to develop. The proliferating VSMCs over the lipid core synthesise and secrete extracellular collagen and proteoglycan forming the protective fibrous cap. Interstitial forms of fibrillar collagen types I and III arranged in triple helical coils are the principal types making up the fibrous cap[9]. This fibrous cap is a discrete layer of connective tissue that confers stability to the growing lesion; a protective wall separating the circulatory coagulation factors from the thrombogenic tissue factor found in the necrotic lipid core and its surrounding macrophages[43].

This thick fibrous cap atheroma (Stary V:fibroatheroma, or Virmani: fibrous cap atheroma, Figure 14) is the predominant stable lesion seen in middle-aged and older persons that develop significant stenosis of the vessel lumen to cause chronic stable symptoms of atherosclerosis[9, 17, 18, 42, 44, 45].

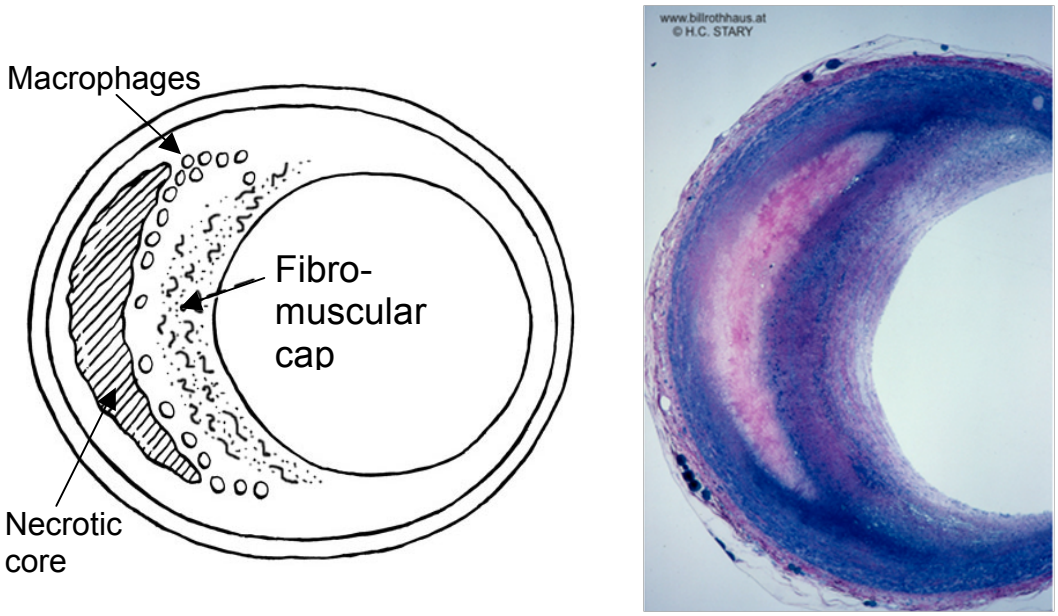

Figure 14. Stary V: fibroatheroma, or Virmani: fibrous cap atheroma. (Figures from Stary[9, 41])

The difference between Stary IV and V lesions is the formation of the collagenous fibrous cap. In conventional 5 micron thick histological sections, the muscular cap of the Stary IV lesion is indistinguishable from the fibrous cap of a Stary V lesion, and they are both indiscriminately labelled as fibrous plaque[9]. This is reflected in the Virmani scheme[18] which does not differentiate between them and collectively describes them as fibrous cap atheroma (Figure 3).

1.2.4 Vulnerable advanced lesions - thin fibrous cap atheromata

The stability of the plaque depends on the dynamic equilibrium between the maintenance and degradation of the protective fibrous cap. The extracellular matrix is synthesised and maintained by the VSMCs in the cap. This is however weakened by the release of matrix degrading, pro-apoptotic and pro-inflammatory factors by inflammatory cells, mainly the macrophages, which infiltrate and weaken the cap and diminish the VSMCs ability to synthesise cap proteins. The fibrous cap is thinned, VSMCs become reduced in number and there is inflammatory infiltrate into the vulnerable fibrous cap[18] (Figure 15). There is also evidence of intra-plaque haemorrhage, fissuring, calcification and neo-vascularisation[17, 18, 42, 44, 45].

Numerous autopsy studies of deaths due to coronary thrombosis have shown that the *thin fibrous cap atheromata (TFCA)* is the pre-requisite lesion that is most likely to rupture[18]. A thin fibrous cap is defined as one that is <65um thick with a loss of vascular smooth muscle cells and extracellular matrix with increasing inflammatory infiltrate[45]. This definition was determined from morphometric analyses of 41 ruptured plaques; where 95% of the fibrous caps measured were less than 64um thick (mean+/-SD was 23+/-19um)[19].

The thin fibrous cap atheromata is not a specific plaque type recognised in the Stary AHA classification system. Limited provision is made to describe the vulnerability of the plaque in the Stary schema (Figure 2 and Figure 12) In comparison, the Virmani schema identifies the TFCA lesion specifically as well as the modality of plaque rupture and erosion as triggering events in the acute thrombotic processes (Figure 3).

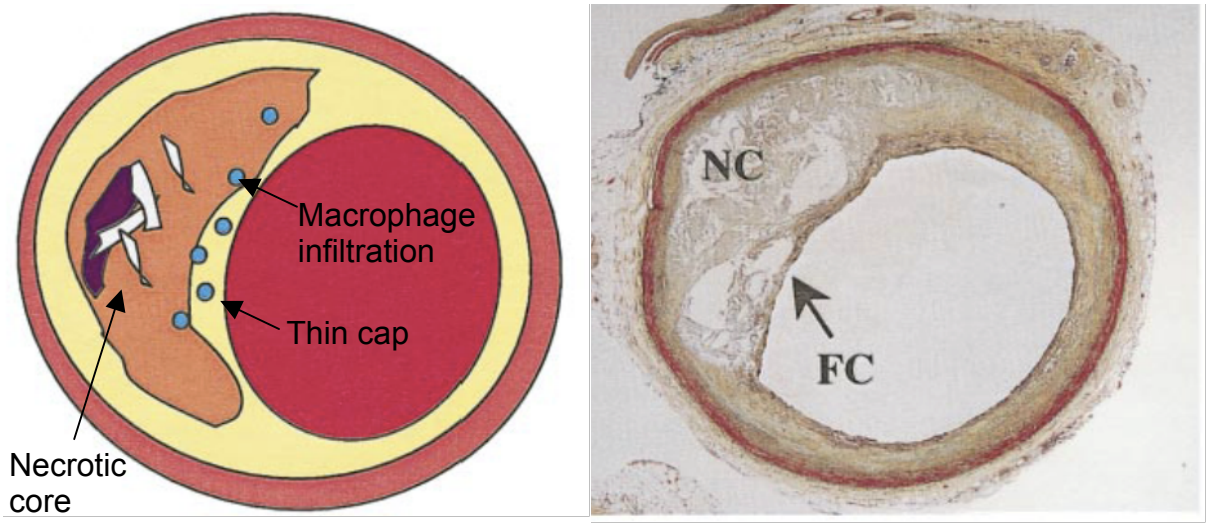

Figure 15. Thin fibrous cap atheroma. (Figures from Virmani 2000[18])

1.2.5 Lesions with thrombi - rupture, erosion and calcific nodule

Autopsy studies have revealed that the majority of acute vascular thrombotic occlusions occur as a result of plaque rupture (60-75%). The remainder are caused by erosion (25-35%) and rarely by a calcific nodule (<5%)[7, 17, 18, 42, 45, 46].

Plaque rupture

It was the original observations of autopsy tissues by Davies and colleagues which led to our current understanding that atherosclerotic cardiac deaths are mainly due to rupture of the advanced atherosclerotic plaque[7, 9, 46]. As described earlier, the thin fibrous cap atheroma is the pre-requisite lesion prone to rupture. The turbulent non-laminar blood flow sets up high gradients of mechanical shear stresses that can disrupt an already dysfunctional endothelium and weakened thin fibrous cap wall. A disruption or erosion of the weakened thin fibrous cap will result in the exposure or even extrusion of the necrotic lipid core, macrophage cells and other intra-plaque tissue, rich in tissue factor, activating platelet aggregation and thrombus formation (Stary VI: complicated lesion with surface defect, +/- haematoma, +/- thrombosis, or Virmani: ruptured thin fibrous cap atheroma, Figure 16). It is defined as an 'area of fibrous cap disruption whereby the overlying thrombus is in continuity with the underlying necrotic core'[18]. These lesions typically have a large necrotic core and a disrupted fibrous cap infiltrated by macrophages and T-lymphocytes. The VSMC content in the cap of the site of rupture may be very sparse or non-existent. There is also haemorrhage, fissuring, calcification and neo-vascularisation within the plaque. These are the hallmarks of the vulnerable ruptured lesion[18]. The mechanistic processes that influence the development of thin fibrous cap atheroma and its rupture is described later in this chapter.

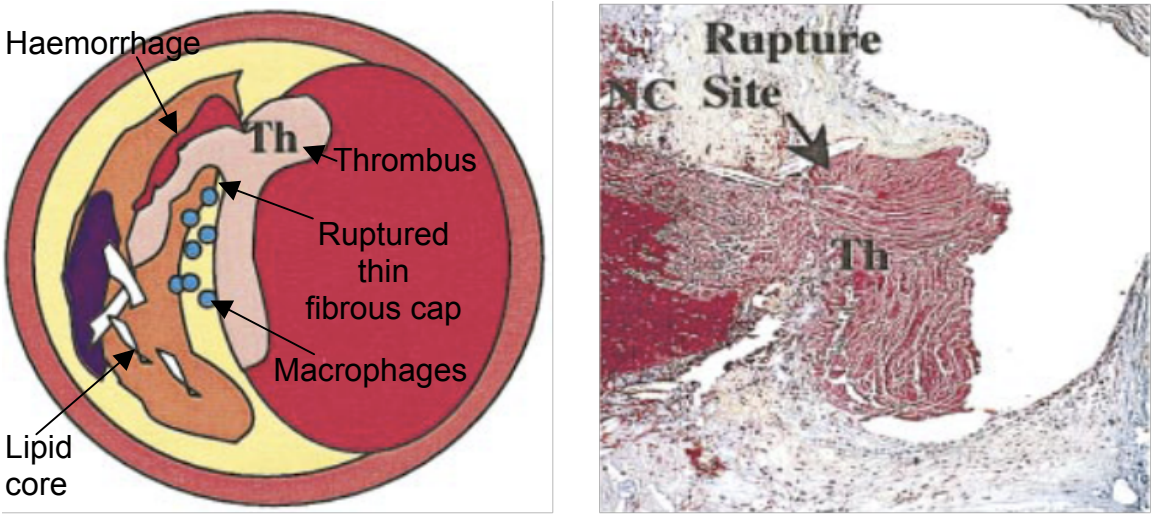

Figure 16. Stary VI lesion: The ruptured thin fibrous cap atheroma. (Figures from Virmani 2000[18])

Plaque erosion

Recent work has shown that fibrous cap erosion (with no direct or continuous contact of thrombus to necrotic core, that is, with an intact cap separating thrombus from core) is associated with thrombus formation and acute clinical sequelae with no evidence of plaque rupture[17, 18, 42, 44, 45]. There is loss of the endothelium and the exposed intima consists of VSMCs, collagen and proteoglycans with varying amounts of infiltrating macrophages and/or T lymphocytes that can precipitate platelet aggregation and thrombus formation (Figure 17). However, the mechanistic processes of erosion is still not understood. The loss of the endothelium and/or part of the fibrous cap may possibly be due to endothelial dysfunction[47, 48], mechanical shear stress or even vasospasm[18]. Tissue factor has been found to be expressed in VSMCs and infiltrating macrophages and present in the extracellular matrix in the cap[43]. However, unless there is active expression of tissue factor it is not obvious that simple denudation of the endothelium and/or part of the fibrous cap will subsequently precipitate platelet aggregation and thrombosis[18]. Plaque erosions have been observed to occur in a variety of lesions with and without a necrotic core; in *thick fibrous cap atheroma*, *pathological intimal thickening*, and possibly in *fibrocalcific plaques* and *calcific nodules*[18, 42]. Its aetiological origins are as yet not clear. Plaque erosion is poorly represented in the Stary schema and is undifferentiated from rupture (it is also classified as Stary VI: complicated lesion with surface defect +/- haematoma +/- thrombosis). In comparison, erosion is more accurately represented in the Virmani schema (Virmani: plaque erosion).

Calcified nodule

This lesion is a rare cause of thrombosis and is described by Virmani et al, to be a lesion with 'fibrous cap disruption and thrombi associated with eruptive, dense, calcified nodules' (Figure 18). It is a recently described entity and little is understood about its origin but it has been proposed by Virmani et al to be associated with healed thin fibrous cap atheromatous plaques[9, 18].

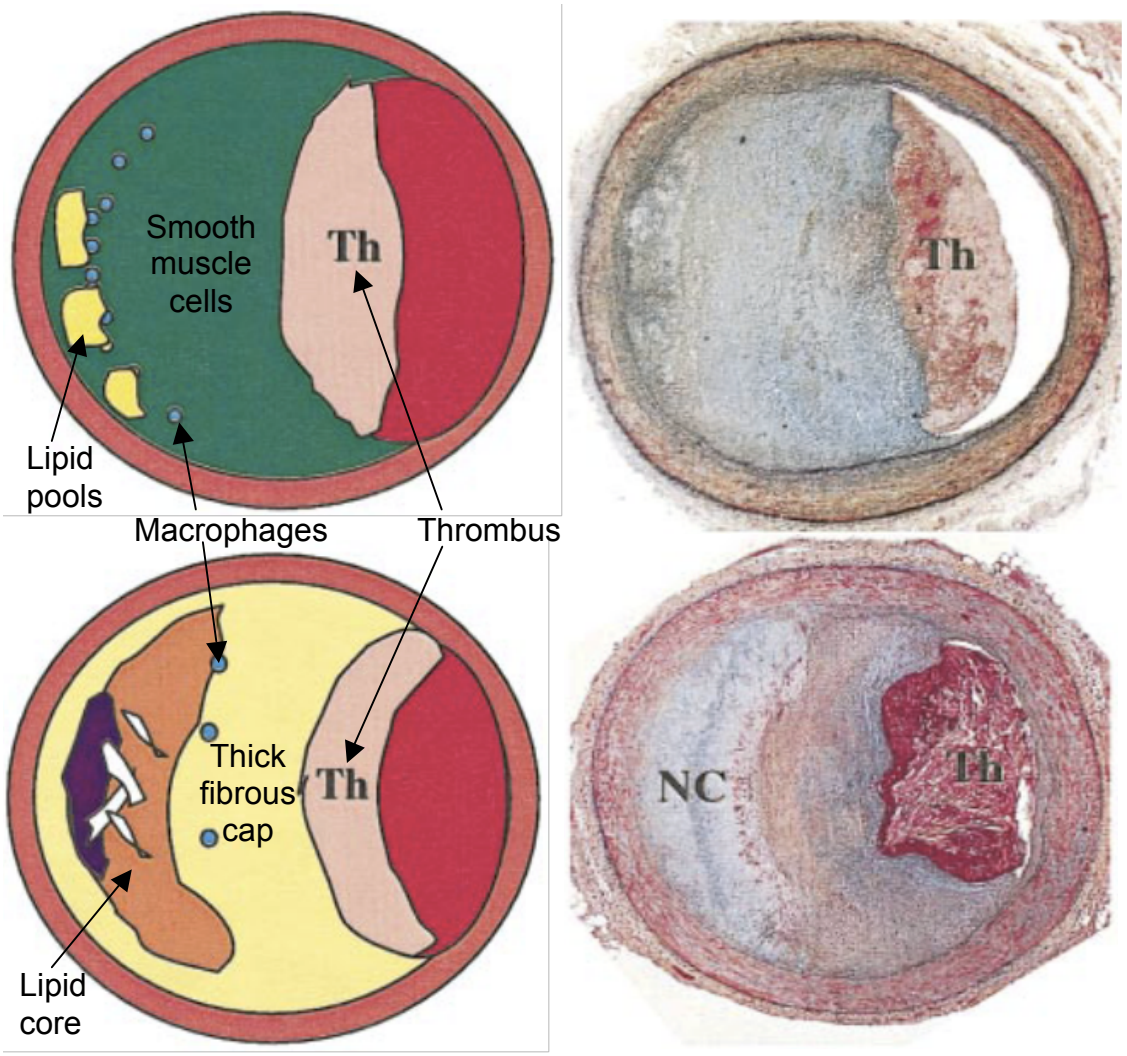

Figure 17. Plaque erosion with thrombus seen with pathological intimal thickening lesion (top pair) and with fibrous cap atheroma (bottom pair). (Figures from Virmani 2000[18])

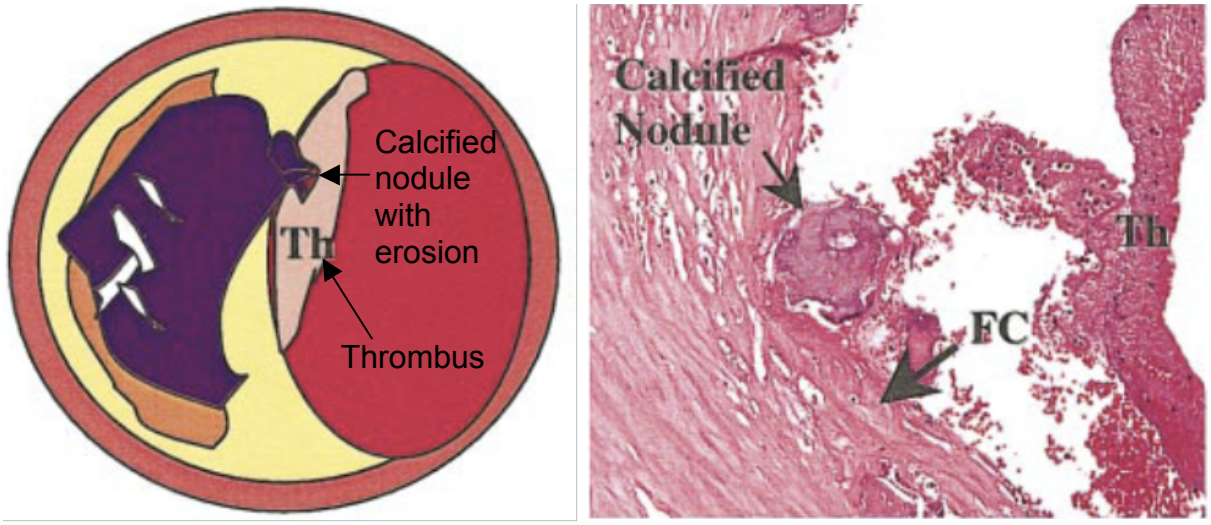

Figure 18. Calcified nodule. (Figures from Virmani 2000[18])

1.2.6 Complex lesions - healing rupture/erosions and rapid lesion growth

After an acute event of plaque rupture or erosion, the disrupted fibrous cap and/or thrombus undergoes organisation and healing. There is migration of VSMCs with the synthesis and deposition of extracellular matrix proteoglycans and collagen. The platelet-thrombus complex is organised and incorporated into the healing-ruptured plaque. This is a dynamic process and the plaque is still highly unstable. The platelet-thrombus plug may destabilise and expose more thrombogenic substrate from within the plaque, or a rupture or erosion may occur at another weakened region of the thin fibrous cap. The recurring events of rupture/erosion and healing has been proposed to be the mechanism accounting for rapid plaque growth and increase in luminal stenosis (in contrast to the slow chronic course of a stable thick fibrous cap atheroma). The resultant complex lesion consists of multiple layers of lipid and necrotic cores separated by healed/healing ruptured fibrous caps with proteoglycan-rich mass or collagen-rich scar (Stary V: fibroatheroma multilayered, or Virmani: healed rupture/erosion[9, 18],Figure 19).

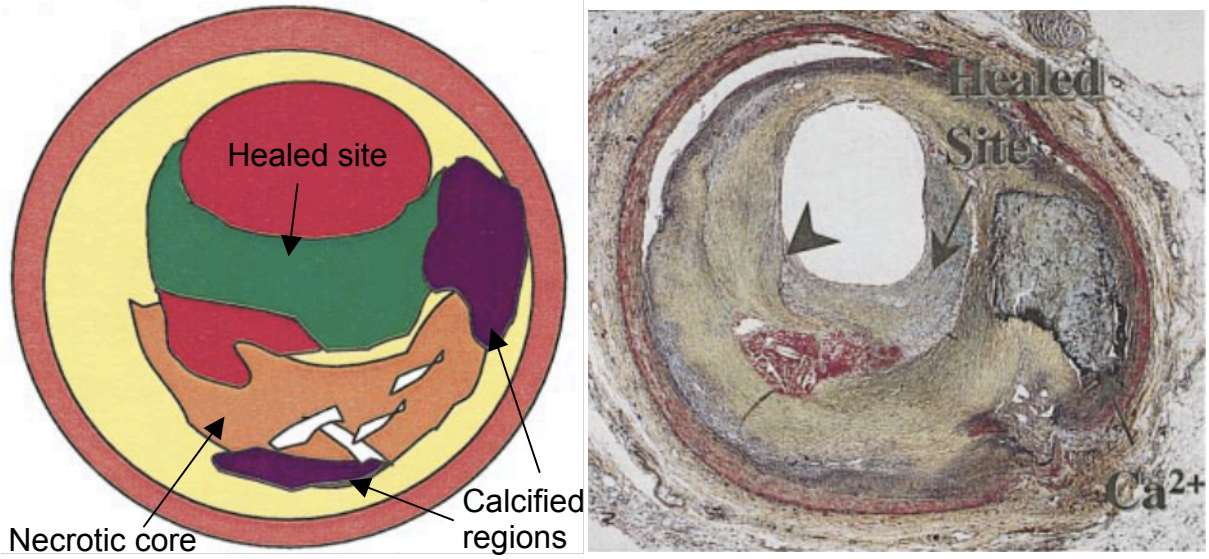

Figure 19. Healed rupture of a thin fibrous cap atheroma. (Figures from Virmani 2000[18])

1.2.7 Advanced lesions with calcified or fibrotic modification: fibrocalcific plaque or fibroatheroma with fibrotic change

Advanced atheromatous lesions can exist with predominant calcific modification of the lipid core (Stary VII: fibroatheroma with calcified core in the schema in Figure 12, or Virmani: fibrocalcific plaque in the schema in Figure 3). These lesions have been described by Virmani et al. as plaques which have thick fibrous caps overlying extensive accumulations of calcium in the intima close to the media with a smaller and sometimes absent lipid-laden necrotic core[18](Figure 20). Advanced lesions with predominant fibrotic changes in the lipid core however have been described by Stary as a VIII: fibroatheroma with fibrotic core (schema in Figure 12). The Virmani schema only allows for the descriptive modification of the Virmani: fibrous cap atheroma (i.e. fibrous cap atheroma with fibrosed core). It is uncertain as to where these lesions fit in the schema of plaque progression. It has been proposed that they are the end stage of the process of plaque rupture and/or erosion with fibrotic healing and calcification [18] or that they principally remain as stable plaques but where calcification or fibrous tissue formation predominates with regression of lipid following lipid reduction treatment[9].

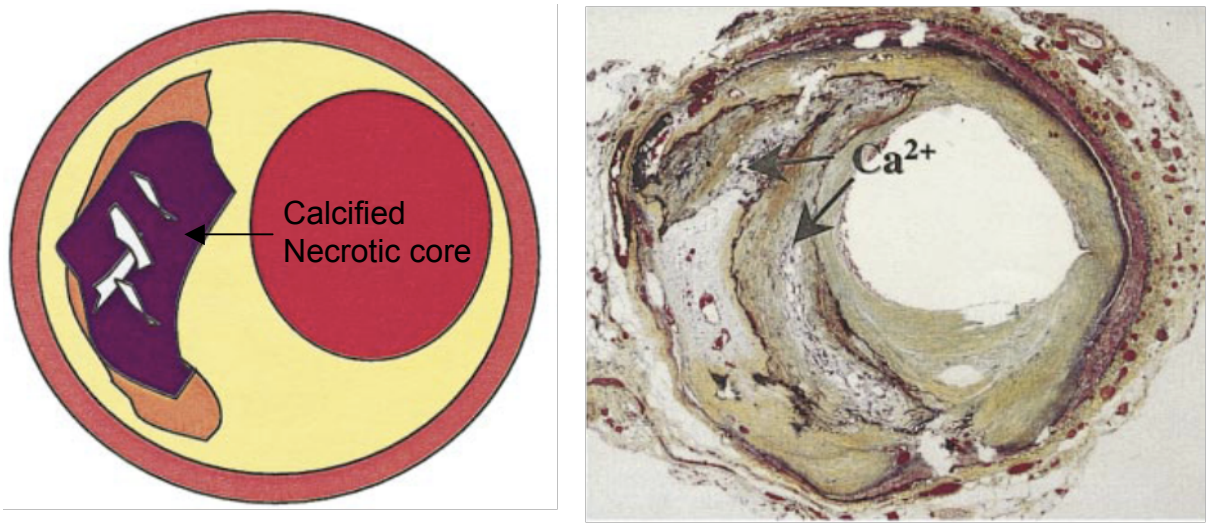

Figure 20. Fibrocalcific plaque. (Figures from Virmani 2000[18])

1.3 The clinical manifestations of atherosclerosis

Atherosclerosis has only been dominantly seen in the latter half of the 20th century with an increase of global life expectancy of about 25 years (this amounts to about 50% increase in longevity in some populations)[49]. This has been attributed to the improvement in socio-economic conditions, disease prevention and healthcare which has lead to a decrease in deaths in infectious diseases and childhood mortality. As a result, there was a shift from a predominance of nutritional deficiencies and infectious diseases, to chronic diseases such as cardiovascular diseases, cancers and diabetes[50, 51].

1.3.1 The stable phenotype and stable plaque

Atherosclerotic plaques are formed from as young as the adolescent years and progress throughout young adult life without any symptoms[9, 35]. Mild atheromata are diffusely distributed throughout the arterial tree. The diffuse nature of atherosclerosis is frequently underestimated even though it is well described by angiography, intravascular ultrasound and at necropsy[9, 52, 53]. It is standard practice to use the proximal 'normal' part of the affected artery as a reference measurement of the normal luminal diameter in the assessment of a stenotic lesion in angiography. However, it is often difficult to estimate the normal luminal diameter as these visually 'normal' segments are likely to have atheroma and are diffusely and mildly narrowed already[54]. Furthermore as the atherosclerotic plaque develops, there is a compensatory progressive increase in the arterial cross-sectional area. This is known as the 'Glagov phenomenon' and is the result of vascular remodelling in the diseased artery. As a result, the atherosclerotic plaque may continue to progressively increase in size with up to 40% cross-sectional area involvement before any appreciable luminal narrowing on angiography[38].

Often the first clinical manifestations of atherosclerosis only present in the later years of adult life after 50 years of age, when these slow growing plaques have increased in size to cause significant narrowing of the vessel lumen[9]. Symptoms often do not become evident until a critical amount of stenosis has developed. It has been demonstrated that coronary blood flow begins to decrease with stenosis greater than 50% in cross-sectional diameter (equivalent to 75% cross-sectional area loss), and decreases rapidly when it exceeds 70% (equivalent to 90% cross-sectional area loss) to cause a restriction in blood flow to the affected regions causing distal tissue ischaemia[55].

The stable phenotype is typified in chronic stable angina, in which the clinical course of exertional symptoms takes a gradual and slow progression over many years tracking the

growth of the stenotic lesion. The thick fibrous cap atheroma and the fibrocalcific plaque is the typical advanced atherosclerotic lesion seen in adults with this stable phenotype [9, 18].

1.3.2 The unstable phenotype and vulnerable plaque

In contrast to stable disease, the main characteristic of the plaque in unstable disease is not the degree of stenosis but the degree of which the plaque is vulnerable to thrombotic occlusion or embolism [17, 18, 42, 46, 56, 57]. In fact, unstable disease is not predominantly caused by atherosclerotic plaques of severe flow-limiting stenosis as was previously believed[18, 42, 52]. It has been observed that about 50% of thrombotic deaths occur from stenoses of less than 50% angiographic cross-sectional diameter (the “50:50 relationship”) [52]. Moreover less than 20% of acute complete thrombotic occlusions occur in lesions of more than 75% luminal diameter narrowing[52]. This is quite a disheartening concept as it would suggest that most acute and potentially catastrophic cardiovascular events would affect the unsuspecting majority of men and women in the industrialised world in a sudden and unpredictable manner such as acute myocardial infarction and ischaemic stroke.

This observation is due to several factors. Large plaques causing severe stenoses are more likely to occlude as a result of a plaque rupture or erosion event as they are associated with a larger thrombus burden in an already significantly reduced vessel lumen. By contrast, in lesions with mild stenoses, a plaque rupture event leading to thrombosis is less likely to occlude the vessel and more likely to occur without any apparent symptoms. However, the mildly stenosed lesions are many times more common, hence the “50:50 relationship”[52, 58, 59]. Furthermore, significant advanced atherosclerotic lesions may have developed in angiographically normal or mildly stenosed vessels without causing any flow limitation or symptoms due to compensatory Glagov vascular remodelling[38], and these advanced lesions may be particularly prone to rupture or erosion. These combination of factors explains why the majority of the cardiovascular events occur without prior symptoms to the unsuspecting many. Thus plaque 'quality' (its propensity to rupture/erode) rather than plaque 'quantity' (its degree of stenosis) is the main determinant of acute unstable manifestations of atherosclerosis.

A definition of the vulnerable plaque has long been a problem that eluded our understanding. It is only relatively recently that we understand that the ruptured thin fibrous cap atheroma accounts for the majority but not all of the fatal thrombotic events. Autopsy studies have shown that about 60-75% of fatal MIs due to coronary thrombosis are caused by plaque rupture. The remainder are mostly caused by plaque erosion of pathological intimal thickening (PIT) lesions and fibrous cap atheromas (FCA) (25-35%)

and rarely by erosion of the calcified nodule (<5%) [17, 18, 57]. An effort to achieve a consensus in the definition of the high-risk, vulnerable and thrombosis prone plaque was made in 2003 in Greece[56]. The principal lesion types which made up the majority of the vulnerable plaques were the TFCA lesion with inflammation, the acute ruptured TFCA and the ruptured TFCA with partial healing that follows. A smaller proportion of vulnerable plaques were from PIT, FCA lesions and calcific nodules with evidence of erosion and adherent thrombus and also the lesions with partially healed erosions.

1.3.3 The vulnerable patient

Plaque vulnerability albeit the main factor influencing the overall clinical consequence is only one factor in the equation. The concept of the vulnerable patient introduced by Naghavi and colleagues further extends our understanding of other factors of blood and myocardial vulnerability which contribute to the determination of clinical events[60, 61].

The thrombogenicity (vulnerability) of the blood is closely correlated to the magnitude of clinical sequelae. Activation of systemic inflammation and disorders of the coagulation/anti-coagulation system resulting in increased activation of the coagulation or the inhibition of the anti-coagulation system have important roles in affecting the magnitude of thrombus formation from a rupture or erosion of the vulnerable plaque. In the event of coronary occlusion the clinical outcome is also affected by the susceptibility (vulnerability) of the myocardium. There is increasing evidence that the autonomic nervous system plays an important role in the genesis of life-threatening arrhythmias in response to acute ischaemia or infarction of the myocardium. Sympathetic hyperactivity predisposes to the generation of ventricular tachyarrhythmias. Vagal activation however confers anti-fibrillatory protection but may also cause significant bradyarrhythmias. The strong afferent stimuli from the infarcting myocardium can also impair the function of the arterial baroreflex leading to haemodynamic instability[61]. Previous ischemic injury as well as underlying cardiac pathology like cardiomyopathy, valvular disorders, electrophysiological and conduction disorders can also adversely affect the outcome of the patient as a result of a myocardial infarction[60, 61].

Although the concept of plaque vulnerability and the vulnerable patient proposed by Naghavi and colleagues addresses coronary disease, it can be easily applied to atherosclerotic disease in any arterial territory. Clearly blood and ischaemic tissue vulnerability play a role in the resultant outcome, but nevertheless, it is the vulnerability of the atherosclerotic plaque that is the predominant factor and trigger to the cascade of acute events.

1.3.4 Identification and treatment of the vulnerable plaque and patient

Most of our emergent strategies in the treatment of atherosclerotic disease such as thrombolysis, angioplasty and stenting, surgical revascularisation and medical therapy only occur after the event of plaque rupture/erosion and subsequent thrombosis. A better strategy would be the identification and targeted treatment of asymptomatic high risk individuals prior to these events; which unfortunately remain a major challenge. Most of our approaches to date in the identification of these individuals involve risk factor screening in primary or secondary prevention. Present strategies in intervention and revascularisation still focuses on the degree of luminal stenosis as a surrogate of future events. Tools to aid us in the early identification of these vulnerable plaques in the vulnerable patient and the timely provision of plaque-stabilising, arterial-remodelling and anti-thrombotic therapies are critical. It has only been in the recent years that we are now focusing on this important issue[60, 61].

Current conventional investigations by angiography are not able to accurately differentiate between stable and unstable plaques[57]. This is because luminal morphology alone does not accurately reflect the actual activity or constitution of the plaque (inflammation, infiltration of macrophages, thin fibrous cap, macrophage and lipid burden)[60]. Novel imaging approaches have been studied to identify the vulnerable lesion such as fluorodeoxyglucose positron emission tomography, intravascular optical coherence tomography, intravascular ultrasound with virtual histology (VH-IVUS) or MRI with superparamagnetic iron oxide or gadolinium fluorine compounds or fibrin-targeted compounds (to determine cell constitution, fibrous cap thickness or lipid core burden)[60]. However these methods are sophisticated, invasive or mainly available in research use only. Currently our understanding of the vulnerable plaque is based on retrospective pathological analyses of arterial occlusion or sudden death. Until we have detailed the natural history of plaques that have been identified as vulnerable, we cannot accurately predict their prognosis[60].

The PROSPECT trial (Providing Regional Observations to Study Predictors of Events in the Coronary Tree) was such a landmark study which gave us the first evidence of the natural history of non-culprit 'asymptomatic' plaques which were studied following intervention on another culprit vessel using VH-IVUS[62]. The results have shown that lesions with a propensity to future cardiac events had features of thin-cap fibroatheroma (HR 3.35 [95% CI of 1.77-6.36]), significant stenoses of minimum luminal area ≤4mm^2 (HR 3.21 [1.61-6.42]) and plaque burden of ≥70% (5.03 [2.51-10.11]). Moreover, most of these lesions had angiographic mild stenoses (30%) at baseline. However this method was not specific enough to identify prospective lesions of future events for potential

intervention as only 18.2% of such lesions with all 3 features at baseline actually developed a cardiac event. Moreover, these results are not easily extrapolated to asymptomatic individuals whom an event has not yet occurred, and prospective invasive follow-up studies in such a population group is not likely to occur, and non-invasive imaging methods and plasma biomarkers would greatly facilitate such future studies.

1.4 Possible mechanistic processes leading to plaque rupture

It stands to reason that the health of the protective fibrous cap is of primary concern in plaque stability. The typical vulnerable plaque has a thin fibrous cap (<65um thick) with sparse VSMCs, heavily infiltrated with macrophages overlying a lipid rich core with necrotic debris and may have intra-plaque haemorrhage and neo-vascularisation[7, 9, 16, 18, 46, 57]. In contrast, the stable plaque has a thick fibrous cap richly populated with VSMCs and a proteoglycan-collagen extracellular matrix, with relatively fewer macrophages surrounding an organised lipid necrotic core which may be undergoing fibro-calcific change and with very few inflammatory cells[9, 16, 18, 57]. Far from being fixed and static, there are dynamic processes involving the fibrous cap and the plaque that influences its propensity to rupture (or erosion) leading to thrombosis and vessel occlusion.

1.4.1 Mechanical forces focus inflammatory processes

The likely regions of mechanical disruption (rupture) of the thin fibrous cap seem to occur at sites of highest shear stress (flow) and wall stress (structural)[63, 64]. This is in contrast to the observation that low shear stress regions (low flow) of a non-laminar flow (turbulent) vessel favour lipid deposition and initiation of atherosclerosis[21, 65, 66]. Biomechanical modelling of circumferential wall stress in ruptured and stable plaques of similar stenoses demonstrated regions of high wall stress at circumferential 'shoulders' where the fibrous cap joins the apparently less diseased walls of the vessel in ruptured plaques[63] (Figure 21). Using computational models examining shear stresses across coronary plaques which have ruptured, mapped by 3-dimensional IVUS, the regions of rupture corresponded to regions of high shear stress of blood flow and concentrated at the proximal longitudinal shoulder of the plaque (Figure 22). These mechanical forces of high shear and wall stress may cause endothelial dysfunction and focus inflammatory, proteolytic or apoptotic processes that weaken the fibrous cap at these rupture prone sites[17, 21, 46].

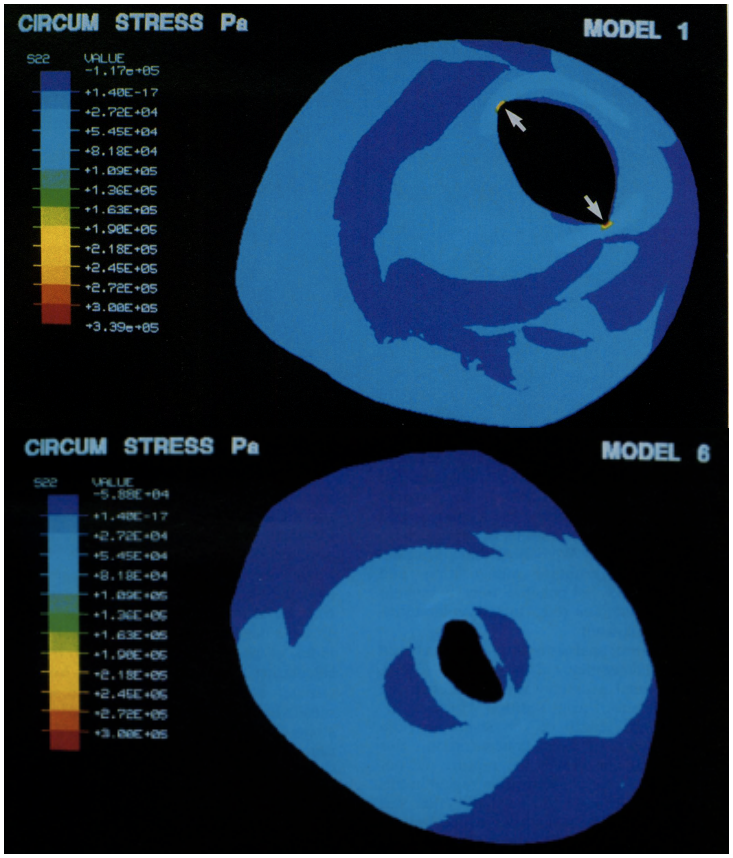

Figure 21. Concentrations of high circumferential wall stress in the shoulder regions (arrows) of a ruptured plaque (top) compared to lower circumferential wall stress in a stable plaque (bottom). Colour gradient of increasing wall stress is shown (red is high). (Figure from Cheng 1993[63]).

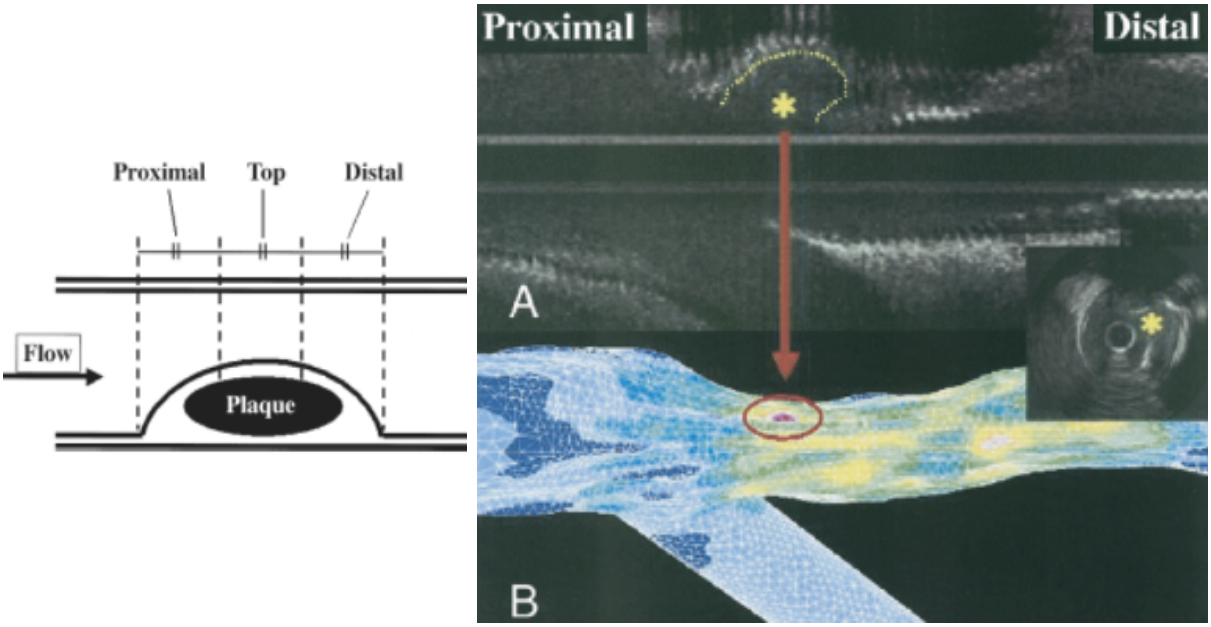

Figure 22. The longitudinal intravascular ultrasound image with plaque rupture observed at the proximal site of the plaque (panel A) corresponding to a localised elevation of shear stress (red, in circle) on the colour mapping of shear stress distribution (assuming smooth surface morphology pre-rupture) (panel B) which has resulted in plaque rupture(*). A diagrammatic longitudinal representation of the artery (left). (Images from Fukumoto et.al. 2008[64]).

1.4.2 Dominant inflammatory processes increase proteolytic activity

This hypothesis proposed by Peter Libby and colleagues is the most extensively described and studied so far to explain plaque rupture. Far from being a fixed structure, the fibrous cap is a metabolically active structure in a dynamic state; where collagen synthesis by VSMCs is balanced against collagen degradation. The critical cumulative effects of inflammatory cytokines drive an increase in expression and activity of proteases and obstruct the activity of proteolytic inhibitors weakening the fibrous cap (Figure 23). The apoptosis of VSMCs ultimately lead to the loss of collagen in the fibrous cap[67-69].

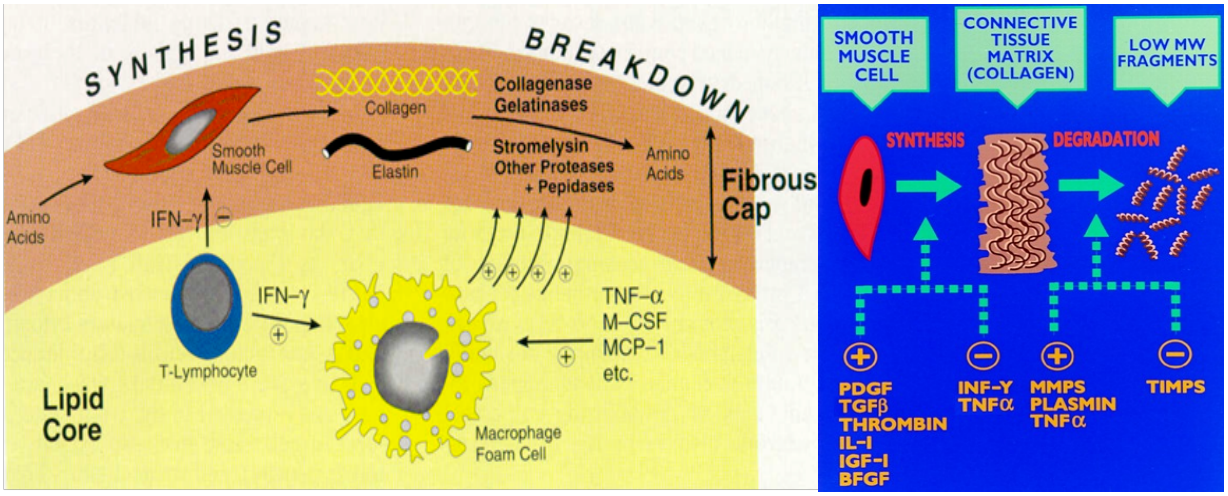

Figure 23. The dynamic state of the fibrous cap influenced by the synthesis of the extracellular matrix by the VSMCs balanced against its breakdown by proteases. (Images from Libby 1995[67]).

Their group and others have found that cytokines such as transforming growth factor-beta (TGF-β) and platelet derived growth factor (PDGF) potently stimulate VSMCs to synthesise the necessary principal collagens (types I and III) that make up the fibrous cap[70]. Contrary to this, they found that interferon-gamma (IFN-γ) inhibits the synthesis of collagens in these VSMCs even under conditions of potent stimulation from TGF-β[70]. IFN-γ, produced by chronically activated T-cells in the plaque[71], not only inhibits the collagen synthesis but also inhibits the proliferation of VSMCs, and may trigger VSMC apoptosis under specific conditions (Figure 23)[70, 72-74].

Interferon-gamma also activates macrophages to produce matrix degrading enzymes of the matrix metalloproteinase (MMP) superfamily[75-77]. Of these, interstitial collagenase (MMP-1; an enzyme specialised in the cleavage of the usually protease-resistant fibrillar collagen that make up the cap), gelatinases (which catalyse the further breakdown of these collagen fragments), and stromelysins are found to be expressed in advanced plaques. Stromelysin is particularly unique in that it is only found in advanced plaques and

may be a key pathway in plaque vulnerability. It inactivates various tissue inhibitors of metallo-proteinases (TIMPs) resulting in the increased activity of numerous MMPs which can degrade a broad range of cap matrix constituents, including the protein backbones of the large proteoglycan macromolecules as well as elastin (another important structural component of the extracellular matrix which gives the cap tensile strength)[75, 77].

These proteases are not synthesised and secreted by the macrophage cells alone. Inflammatory cytokines like interleukin-1(IL-1) or tumour necrosis factor (TNF) synthesised by macrophages and activated T-cells can induce VSMCs to express MMPs like interstitial collagenase, gelatinase B and stomelysin as well[78]. Thus driven by inflammatory cytokines produced by macrophages and T-cells, nearly all the major cell types in the plaque can generate enzymes that degrade the fibrous cap.

It is also observed that of the cathepsin family of enzymes, Cathepsin S and K, are expressed and secreted by VSMCs and macrophages in the plaque and may be stimulated by IL-1β and IFN-γ[79]. These elastolytic enzymes may play a role not only in plaque vulnerability in proteolysis of the elastin fibres in the extracellular matrix, but also in plaque remodelling (Glagov phenomenon) during its growth via its effects on elastin fibres in the arterial medial and adventitial layer.

Endothelial cells can also express proteinases as a result of inflammatory cytokines and oxidised lipoproteins, such as MMP-1 which can then activate MMP-2, a type IV collagenase. Type IV collagen is an important constituent of the sub-endothelial matrix, adhering the endothelial lining to the intimal wall. Its degradation would result in the loss of the integrity of the endothelial lining, promoting desquamative injury to the intima, a possible prelude to plaque erosion[68].

1.4.3 Adaptive immune responses to auto-antigens

The adaptive immune response hypothesis described by Goran Hannson and colleagues propose that adaptive immune responses to specific auto-antigens drive the inflammatory responses to influence the stability or vulnerability of the plaque via a regulatory T-helper cell 'switch'[80]. Although macrophages are the dominant inflammatory cell type, there are significant numbers of T-cells found in plaques as well. The $CD3^+$ $CD4^+$ T helper 1 (Th1) subtype is the majority T-cell found in plaques[71]. Activated Th1 cells secrete IFN-γ, IL-2 and TNF-α and –β, which cause macrophage, VSMC and endothelial cell activation, which in turn release more inflammatory cytokines and proteolytic enzymes[81]. Th1 cell differentiation and activation require IL-12 and osteopontin, also known as early T-lymphocyte activation protein-1 (Eta-1), and they are both expressed by macrophages, VSMCs and endothelial cells in plaques[82, 83]. IFN-γ potently activates macrophages as

does TNF-α. In the context of atherosclerosis, the activation of the Th1 mediated pathway and subsequent macrophage activation leads to very potent pro-inflammatory and pro-atherogenic effects via macrophage TNF-α, IL-1 and IL-6 expression. The release of IL-6 into the circulation will also stimulate the systemic secretion of pentraxins such as C-reactive protein which further escalates a systemic inflammatory response[80, 81, 84, 85].

In contrast, the T-helper 2 cells have responses that antagonise the pro-atherogenic Th1 effects and are athero-protective. The Th2 cells and its cytokines, IL-4, IL-5 and IL-10 have been shown to inhibit inflammatory genes like inducible nitric oxide synthase[86] and cyclo-oxygenase 2[87]. IL-10 knockout atherosclerotic mice have increased lesion development and thrombosis[88]. The Th2 cells and the cytokines they produce are less abundant in advanced end-stage human lesions[81] and may reflect the propensity of these lesions to be vulnerable[80].

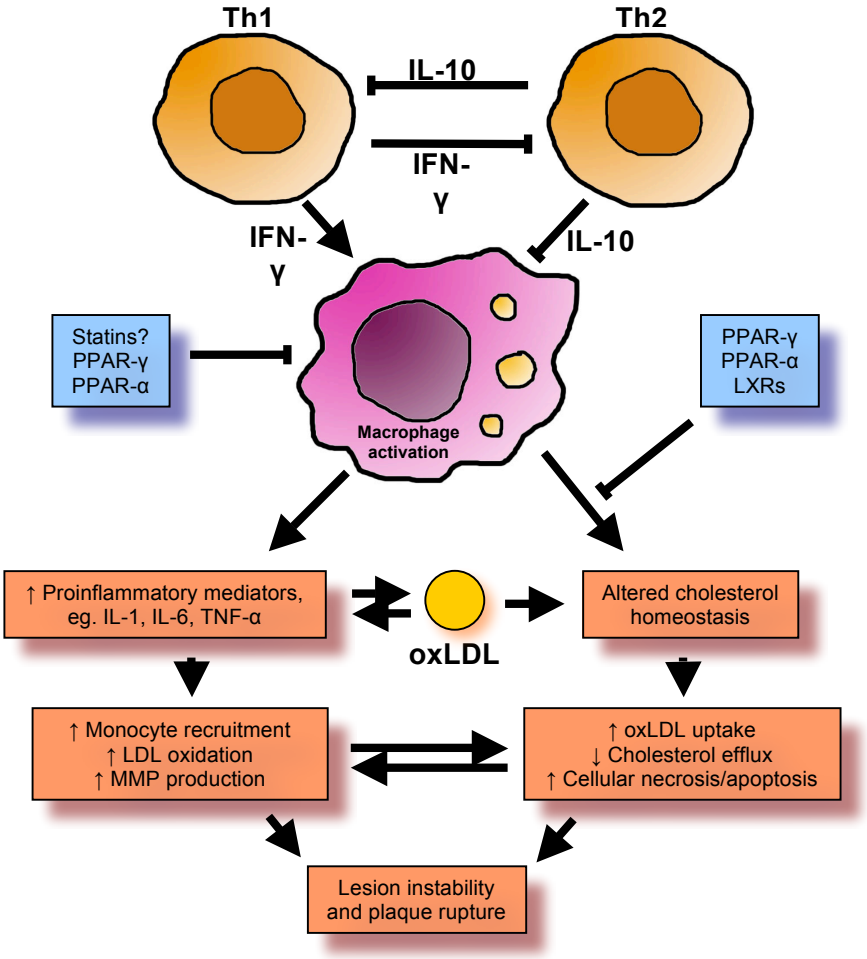

Figure 24. Interactions of macrophages with Th1 and Th2 cells that influence the progression of atherosclerosis (Arrows indicate stimulation, flat-heads indicate inhibition). (Adapted from Li 2002[89]).

The Th1 and Th2 cytokines are cross-regulatory, IL-10 being an inhibitor of the Th1 pathway and IL-12 a Th2 inhibitor, and as such, a dynamic balance of these two cell types

with a dominance of one subset of Th cells could well influence the course of lesion progression to stability or vulnerability[80, 89] (Figure 24).

The T-helper 3 cell (Th3) which produces TGF-β on activation has also been found to be present in the plaque [81, 90]. TGF-β is highly fibrogenic and stimulates collagen synthesis as well as being potently anti-inflammatory[91] and may play a role in plaque stabilisation.

Auto-antigens may be presented on MHC class II molecules to activate specific T-helper cells. Various candidate auto-antigens have been proposed including oxidised LDL, heat shock proteins (HSP) and β2-glycoprotein Ib (β2-GPI). There is evidence that oxidised LDL is an important auto-antigen driving atherosclerosis. Antibodies to oxLDL are found peripherally in the serum and locally in the plaque of both experimental animals and humans[92, 93]. A quarter of the T-cells in human plaques are oxLDL specific[94] and furthermore a subset of peripheral T-cells are activated by oxLDL[95]. Paradoxically lesion progression seems to be inhibited by immunisation to oxLDL[96] as an immune response to extracellular oxLDL may increase the effective clearance of the oxidised moieties of LDL [80]. In contrast, immunisation to HSP60/65 and β2-GPI induced vascular inflammation and progression of atherosclerosis[97-100]. Furthermore HSPs of humans and microbes are structurally and antigenically similar and exhibit molecular mimicry, which may explain the clinical association of infections and atherosclerosis[101].

1.4.4 CD40 and CD40L interaction

The CD40-CD40ligand interaction may play an important role in the activation of the T-cells (Figure 25). CD40 is a co-stimulatory molecule on the cell membrane that is constitutively expressed by B cells, dendritic cells, macrophages and other antigen-presenting cells, which is important in activating the T cell via its CD40 ligand (CD40L). This is normally physiologically important in the T and B cell cooperation in generating antibody responses. However it has been shown that CD40 and CD40L can be induced and expressed in endothelial cells, VSMCs and macrophages by pro-inflammatory cytokine stimulation and IFN-γ[102, 103] and are found to be present on these cells in atherosclerotic lesions. The ligation of CD40 on these cells lead to tissue factor expression in endothelial cells and proteinase secretion in VSMCs and macrophages[103-105]. CD40L knockout animal experiments show inhibition of atherosclerosis suggesting that CD40-CD40L interactions may be an important pathway in atherosclerosis lesion progression[106, 107].

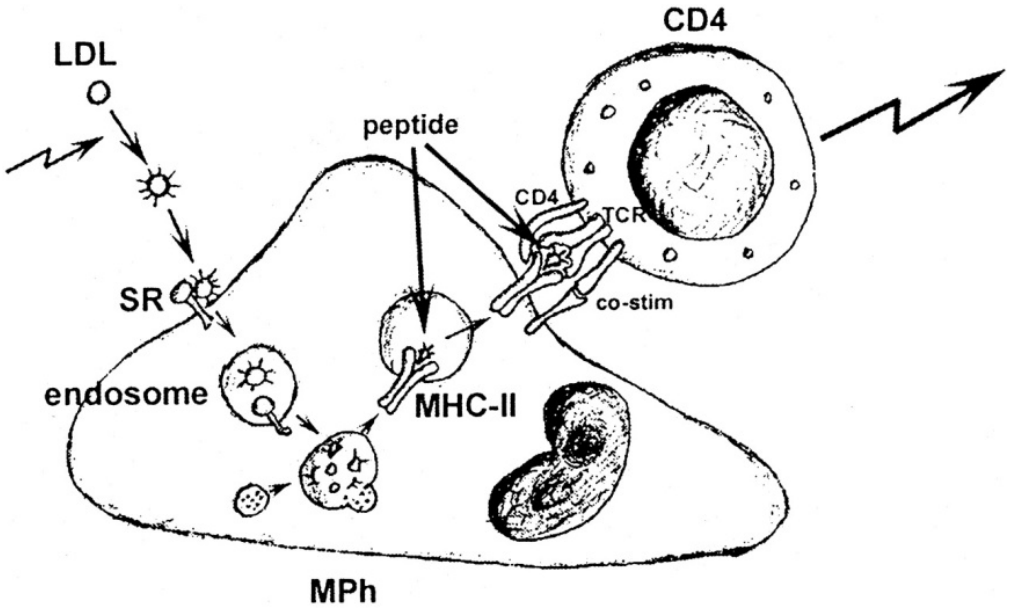

Figure 25. Antigen presentation of modified lipoproteins by macrophages to the CD4 T cell via the presentation of peptide fragments on MHC class II molecules (MHC-II:peptide complex) in the presence of costimulatory factors (marked co-stim in picture) such as CD4, CD40, and B7 molecules. This results in T-cell activation, with proliferation and cytokine secretion. (From Hannson G, ATVB 2001[80])

1.4.5 Role of apoptosis

There is evidence of extensive apoptosis of VMSCs in the cap of advanced atherosclerotic lesions and from VSMCs cultured from plaques[72, 108-110]. These areas of vulnerability with VSMC apoptosis co-localises with regions of increased numbers of macrophages and with regions of macrophage apoptosis[111, 112]. Moreover, VSMC apoptosis is more marked in symptomatic vulnerable plaques compared to asymptomatic stable plaques[113]. These studies imply a direct causal relationship between plaque rupture and apoptosis, suggesting that VSMC apoptosis is possibly triggered by macrophages.

Apoptosis is a highly regulated process which once initiated will continue without further extracellular stimuli. It is determined by complex interactions with the extracellular environment via extrinsic pathway involving membrane-bound death receptors of the tumour necrosis factor-receptor (TNF-R) family, or with intrinsic gene products via the intrinsic pathway dependent on the release of cytochrome-c from mitochondria[114]. This then activates a common pathway cascade of cysteine protease enzymes (caspases) causing programmed cell death[114]. This is different from cellular necrosis with the loss of plasma membrane integrity, cellular fragmentation and release of cellular contents causing inflammation. However, under pathological circumstances where cell energy reserves are reduced, apoptotic cells can be forced to undergo cellular necrotic death instead[115], and may be an important factor in plaque vulnerability.

Various triggers can initiate the apoptotic process in smooth muscle, endothelial or macrophage cells. Endothelial dysfunction due to low shear stress can activate apoptosis via downregulation of anti-apoptotic Bcl-X_L, Bak, anti-apoptotic soluble form of Fas[116] and anti-atherogenic endothelial nitric oxide synthase (eNOS)[117]. Background physiological levels of NO maintained by eNOS has numerous functions from vasodilatation to being atheroprotective by preventing caspase-3 activation and mitochondrial membrane cytochrome-c loss[118-120]. However, excessive pathological levels of NO produced by cytokine-inducible NOS (iNOS) can cause macrophage and endothelial cell apoptosis via both extrinsic and intrinsic pathways[121, 122]. The resultant endothelial defect may be a mechanism of plaque erosion.

VSMC survival is dependent on several constant growth/survival factors such as the persistent cell-matrix interactions of fibronectin from extracellular matrix and cell-cell interactions of the integrin αvβ3[123, 124], vascular endothelial growth factor (VEGF), angiopoietin-1, basic fibroblast growth factor-2 (bFGF-2) and Insulin-like growth factor-1 (IGF-1) signalling [125-127], for the maintenance of the survival pathways. The absence of any of these factors which occur in the vulnerable plaque are a potent inducer of apoptosis in VSMCs.

The major source of oxidative stress is NADPH oxidase[128], regulated by the vasoconstrictor Angiotensin-II[128, 129], and promotes endothelial dysfunction and apoptosis[130]. It creates superoxide (O_2-) the most abundant of the reactive oxygen species which can cause lipid peroxidation (forming oxLDL) as well as react with NO to form peroxynitrite (ONOO-) which can induce ATP depletion and necrosis[131-134]. The OxLDL product itself is a potent inducer of apoptosis in VSMCs mainly via intrinsic apoptotic signalling pathways, and can sensitise extrinsic pathways [135-137]. It can also induce macrophage apoptosis via a mitochondrial pathway [138-140] contributing to the development of the necrotic core.

Macrophages and T-cells are potent inducers of apoptosis via death receptor signalling. T-cells can express death promoting proteins like perforin (which produces membrane damage) and Fas-ligand (Fas-L) [141]. Macrophages can also express Fas-L, secrete TNF-α and MMPs and induce VSMC cell death. Fas-L and TNF-α can induce apoptosis through the extrinsic pathway via the death receptors FasR/CD95 and TNF-R1, but only in combination with the inflammatory cytokines IFN-γ and IL-1β[72]. TNF-α in combination with IFN-γ and IL-1β (pro-inflammatory cytokines synthesised by macrophages) are readily found in the advanced plaque and rapidly induces apoptosis of VSMCs. This reinforces the observation of co-localisation of VSMC apoptosis with regions of high macrophage

content. Similar inflammatory cytokine driven apoptosis of endothelial cells without disruption of the fibrous cap may also explain the events of plaque erosion[142].

1.4.6 Peroxisomal proliferating activating receptors (PPARs)

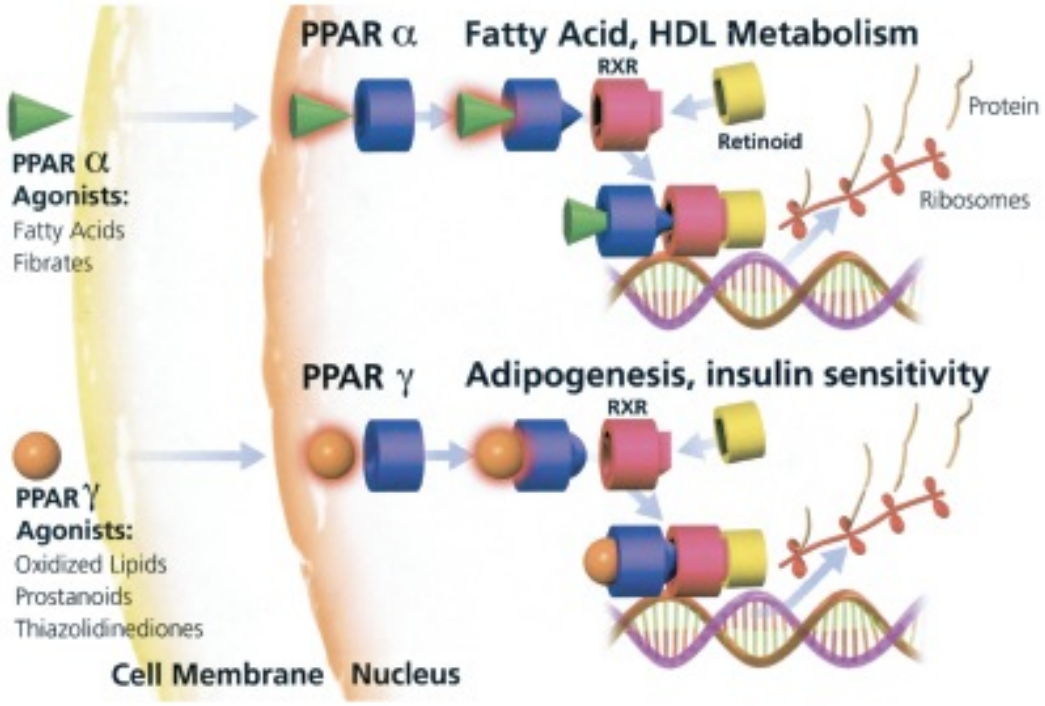

Figure 26. The PPAR pathways (Figure from Libby 2001[68]).

Another interesting pathway may involve the nuclear peroxisomal proliferating activating receptors α and γ (PPAR-α and PPAR-γ) which pair small lipophilic molecules with the nuclear receptor, retinoid X receptor (RXR), forming a transcription factor complex that binds to promoter regions of target genes and regulates their transcription. PPAR-α regulates genes involved in lipoprotein metabolism, increasing the synthesis of apolipoprotein A-1, a major component of HDL, which is potently anti-atherogenic. PPAR-γ regulates genes involved in adipogenesis and insulin sensitivity (Figure 26). PPARs may also individually and separately regulate the expression of other genes that may be involved in plaque progression and vulnerability[68]. The fibrate drug gemfibrozil and polyunsaturated fatty acids, found in high amounts in the Mediterranean diet, bind and activate PPAR-α. Its agonism can limit cytokine-induced inflammation by VCAM-1[143] in endothelial cells and inhibit the expression of tissue factor in monocytes[144, 145]. This may explain the significant reduction in cardiovascular events without a change in LDL levels with gemfibrozil treatment[146] or mediterranean diet[147]. However, under some circumstances, oxidised phospholipids can also augment pro-inflammatory cytokine expression of MCP-1 and IL-8 via the PPAR-α activation[148]. PPAR-γ mutations and

inhibition are responsible for the cardiovascular dysmetabolic syndrome, characterised by insulin resistance, hypertension and dyslipidaemia[149]. The insulin-sensitising thiazolidinediones (glitazones) are PPAR-γ agonists, and can inhibit pro-inflammatory activity in macrophages and VMSCs[150, 151]. However PPAR-γ can also augment endothelial plasminogen activator inhibitor-1 (PAI-1) production enhancing thrombosis, and upregulate the scavenger receptor CD36 expression in macrophages[152]. At present, the overall net effect and importance of the PPAR pathways are still uncertain.

1.4.7 Inflammatory effects of the renin-angiotensin-aldosterone axis

Angiotensin II (AT-II) is a multi-potent pro-inflammatory cytokine, stimulating NADPH oxidase in the synthesis of ROS, IL-6 and MCP-1 production in VSMCs, activating inflammatory pathways in monocytes and VCAM-1 production in endothelial cells via a NFκB pathway and augment PAI-1 expression[153-155]. Furthermore, AT-II drives the production of the mineralocorticoid, aldosterone, which has some pro-inflammatory actions[156]. These findings may explain the clinical benefits seen by ACE inhibitor therapy in the reduction of cardiovascular events independent of the blood pressure lowering effects[157].

1.4.8 The effect of statins

As atherosclerosis is principally a disease of lipid deposition in the arteries, it would make sense to propose that lipid reduction would have a major effect in its abatement. In animal models of atherosclerosis, the lowering of lipid levels by alteration in diet or by inhibition of the synthesis of cholesterol by statins are accompanied by a significant reduction in lesion size and a qualitative benefit in lesion stability with reduced inflammatory cells and decreased inflammatory activation such as reduced VCAM-1, ROS, oxLDL, and MMP expression and activity. Levels of CD40 and CD40-ligand are reduced with a reduction of tissue factor expression and thrombogenicity of the plaque[158-161].

Such dramatic reduction in serum cholesterol achieved in animal studies is not possible by diet control alone in humans. Therefore, 3-hydroxy-3-methylglutaryl co-enzyme A (HMG-CoA) reductase inhibitors, also known as statins, which inhibits the rate-limiting enzyme in cholesterol synthesis, have been used extensively in clinical practice. There is clear clinical evidence that lipid lowering by statin treatment reduces the incidence of coronary events and stroke in a broad spectrum of individuals, but with only a modest reduction in luminal stenosis in contrast to the significant reduction in lesion size seen in animal models. This reduction in cardiovascular risk extends beyond the reduction of serum cholesterol and the small reduction in lesion size[162-166]. This suggests that a

qualitative change in the plaque (its stability) rather than a significant reduction in plaque quantity accounts for the significant reduction of clinical events[68].

As a result, it is proposed that there are other 'pleiotropic' pathways influenced by statins that reduces inflammation and confers plaque stability that is independent of its cholesterol reducing effects. The inhibition of HMG-CoA reductase also reduces the downstream metabolite production of farnesylpyrophosphate and geranylgeranylpyrophosphate which can modify proteins by prenylation of small G proteins involved in intracellular signalling or by induction of Kruppel-like factor-2, a transcription factor that can regulate genes which may have atheroprotective and anti-thrombotic effects[167-171]. Statins have also been shown to upregulate the expression of eNOS[172] and increasing the expression of plasminogen activator and decreasing its inhibitor PAI-1[173] in endothelial cells as well as inhibit tissue factor expression in macrophages[161].

It is important to note that the direct effect of statins on the cellular functions observed in animal and cell culture studies require high concentrations of the drug, at levels beyond those likely to be achieved in clinical use. How relevant these bench observations are to the clinical arena is still questionable. Nevertheless, there are additional effects of statins in reducing inflammation beyond its lipid lowering effects, even though the pathways explaining this is yet uncertain.

1.5 Approaches to the study of plaque rupture.

The current paradigm is that atherosclerosis is a disease initiated by endothelial dysfunction and lipid deposition, driven by progressive accumulation of lipid and its oxidative modification, and the clinical thrombotic events determined by specific immune responses and inflammation. The defence and stability of the plaque rely on the dynamic equilibrium that exists between the protective processes in a 'healthy state' of smooth muscle, endothelial and macrophage cells, against the pro-inflammatory and pro-apoptotic 'destructive state' of these cells. Several hypotheses exist proposing various possible molecular processes and pathways that may lead to plaque rupture. However, we do not know when these inflammatory or immune processes ‘go critical’ as elevated inflammatory activity occur even in early lesions and throughout the progression of the advanced plaque. We do not know which of these pathways have a dominant effect or what the net effect is or even if the dominant pathway has yet to be described. At the present time, the underlying mechanism of plaque rupture is not well understood. The comprehensive

profiling of gene expression in both the VSMCs and macrophages in the stable and unstable plaque will greatly further our insight into the pathological processes involved in plaque rupture.

Level of effect		Effect	"-omic"	Measure/data
Cell	DNA	Genetic influence	Genetics/ Genomics	Single gene mutations SNP polymorphisms Epigenetic modifications Drug responses
	RNA	Gene expression	Transcriptomics/ Genomics	Gene expression profile Transcription and translation factors Gene network/pathways Allelic differential expression Drug responses
	Protein	Protein/enzyme expression	Proteomics	Protein abundance Protein network/pathways Post-translational modifications Protein-protein interactions
		Protein/enzyme activity and metabolites	Metabolomics	Metabolite abundance Drug effects/toxicity
Tissue		Tissue effects	Phenomics	Histology
Organ		Organ effects		Clinical imaging and other clinical investigations
Organism		Organism effects		Clinical events

Table 1. An overview of the different approaches of genetics, transcriptomics, proteomics, metabolomics and phenomics in the study of atherosclerosis (The term 'genomics' is interchangeably applied to the study of genetic polymorphisms and mutations as well as gene expression).

An overview of the various approaches to the interrogation of the cell is shown in Table 1. Genetic approaches, especially with genome-wide association studies, have the potential to identify loci of common polymorphisms of susceptible genes and its regulatory regions involved in plaque rupture, thus providing additional information to help identify likely candidate causal genes. Epigenetic data could give us additional novel information about gene regulation and also identify possible candidate causal genes. Genomic and proteomic data are uniquely able to provide us with comparative functional information of global gene and protein expression, its regulation and active networks. They have the unique ability to potentially identify novel pathways of pathogenic importance. Recent advances in microarray technology provide us the opportunity to simultaneously interrogate the entire transcriptome accurately and reproducibly in an unbiased fashion.

Proteomic approaches however require substantial amounts of biological material, excluding its application in studies involving limited and small clinical samples. Evidently findings from the various methodologies and approaches are complementary in establishing a causal understanding and constantly contribute in a dynamic multi-directional dialogue [174]. In order to be able to combine and analyse such large amounts of "omic" data, advances in bioinformatics, biostatistics and analysis methods are necessary and need to be developed.

1.5.1 Athero-transcriptomics

Cellular gene expression is the most fundamental level at which the genotype gives rise to the phenotype and allows us the ability to study the regulatory gene networks involved in disease states in detail. Previous gene expression (combined with protein expression) studies on human arterial tissue as well as in animal models and cell culture studies that have examined specific hypotheses have suggested that genes governing inflammation and its cytokines, inflammatory cell recruitment and activation, apoptosis, components of the renin-angiotensin system and lipid metabolism, among others, are differentially expressed and regulated in stable and unstable plaques[175-181]). However these studies have been limited by the technical difficulties of interrogating more than a few genes in any one experiment. Thus, the amount of “gene space” that had been searched by such experiments at the time work on this thesis began remained small. The evidence of numerous genes being reported as implicated in plaque rupture suggests that the molecular processes and regulatory gene networks are numerous and complex, and many of these networks are yet undiscovered. Furthermore it is uncertain which networks are dominant in the pathogenesis of plaque rupture.

Over the last 2 decades, the techniques for the evaluation of gene expression have developed from methods that evaluate small numbers of specific single genes (such as Northern blot, fluorescent in-situ hybridisation and quantitative reverse transcription PCR) to high-throughput methods that can identify many hundreds and thousands of genes that differ in expression between experimental samples simultaneously (such as subtractive hybridisation, representational difference analysis, differential display, serial analysis of gene expression and hybridisation to microarrays[182]). These genome-wide gene expression methods allows for the profiling the transcriptome of the cell identifying genes in active expression and their relative abundance. Coupled with advances in bioinformatics and biostatistics, these non-physical maps of the function, hierarchy and interactions of genetic programs can be interpreted to identify genes and their respective networks which may be regulatory in the causation of disease. Such broad-hypotheses experiments uniquely have the potential to show previously unexpected molecular

pathways of possible pathogenic importance. For example, Hilfiker and colleagues showed Angiotensin-II upregulation of CYR61, an angiogenic immediate early gene, in rat VSMCs by a suppression subtractive hybridisation (SSH) PCR method[183]. This gave rise to a novel hypothesis regarding the role of Angiotensin-II in plaque neovascularisation and instability.

There are a variety of methods available for genomic gene expression profiling[182]. Suppression subtractive hybridisation (SSH), representational difference analysis (RDA), differential display (DD) and serial analysis of gene expression (SAGE) have advantages that prior knowledge of the gene sequence or its identity is not needed. SSH, RDA and DD however have limitations in that they are not quantitative methods. Investigation of all potentially differentially expressed genes require high-throughput PCR and sequencing which is time and labour intensive to identify and confirm differential expression on an individual gene basis. Furthermore it is not possible to build a comparative transcriptomic profile of the samples to other experiments as they are normalised to the 'reference state' of the control sample. The SAGE method is however quantitative and cumulative. Accurate quantitative transcript profiles are generated provided that sufficient sequencing is completed. However, like the limitations of the former methods, time and labour intensive high-throughput sequencing efforts are required to identify the SAGE sequence tags. Another potential limitation is the misidentification of TAGs as a result of sequencing or SAGE reference database errors.

1.5.2 Gene expression microarrays

Microarray technology utilises the technique of transcript cDNA hybridisation to corresponding oligonucleotide cDNA anchored onto a platform (such as a glass wafer or slide, or nylon membrane). The main limitations are that it requires the prior knowledge of the sequence of the transcripts, the correct selection of the oligonucleotide sequence representing the genes and it requires highly specialised technology to manufacture. The completion of the Human Genome Project[184] not only provided us with sequence information of the genome but stimulated work on the complete definition of the function of genes on a genome-wide scale (although many remain putative and need further functional characterisation). Coupled with developments in super-high-density oligonucleotide DNA arrays, it has been possible to represent the entire human transcriptome of not only well characterised genes but also including representations of yet uncharacterised hypothetical transcripts potentially worthy for further study. The commercial availability of these high-quality genome-wide gene expression microarrays offers the opportunity to analyse the entire transcriptome simultaneously, with a high degree of accuracy and reproducibility in an unbiased fashion[182, 185, 186].

Gene expression profiling in atherosclerosis has been successfully carried out using microarrays in cell culture systems, in animal models of atherosclerosis, and in human samples. With regard to human atherosclerotic specimens, McCaffrey et al. carried out expression profiling of medial arterial tissue versus fibrous cap overlying atheromatous lesion in carotid endarterectomy specimens using low-density arrays (588 genes) and found a high level of expression of Egr-1 and Egr-1 inducible genes in lesional tissue[187]. Hiltunen and colleagues successfully characterised gene expression in macroscopically normal arteries, fatty streaks and advanced lesions using arrays of over 18,000 genes; 75 genes not previously connected to atherogenesis were found to be upregulated or downregulated in advanced lesions, such as signal mediators Janus kinase 1 (JAK-1) and mitogen-activated protein kinase (MAPK), vascular endothelial growth factor receptor 2 (VEGF-R2) as well as a yet uncharacterised transcript[188]. Faber and colleagues compared expression of 500 genes in histologically characterised whole ruptured and unruptured plaques, and found 2-fold differences in expression in 25 genes. One of these genes coded for perilipin, a phosphoprotein which previously has not been described in atherosclerotic plaques[189]. These studies provided "proof of principle" for the use of microarrays in atherosclerotic tissue samples. However the vast majority of these studies have addressed the issue of atherosclerotic lesion formation and growth, but very few have tried to tackle the question of plaque vulnerability and rupture despite its importance.

1.6 No adequate experimental model for rupture or erosion; human studies necessary.

A variety of animal models of atherosclerosis exist but are at best less than ideal. Rabbits, dogs and rats are generally very resistant to atherosclerosis and develop lipid-rich arterial lesions with some atherosclerotic features if fed extremely high amounts of cholesterol many times higher than that seen in humans. Primates (chimpanzees and monkeys) and pigs on a high cholesterol diet develop a form of atherosclerosis that is very similar to humans. However, the cost of their care is prohibitive, many of the primate species are protected and limited to specific laboratories only[190-192]. Mice only develop atherosclerotic-like lesions with genetic manipulation (ApoE(-/-) or LDLR(-/-) knockout mice). They also have a lipid physiology different to humans where most of their cholesterol is transported in HDL-like particles. However, due to the ease of handling, relatively low cost, wide knowledge base of mouse physiology and its genome, most researchers have preferred to use the mouse model of atherosclerosis[191]. However, the patterns of atheroma in the rabbit, mouse or rat animal models are different to that seen in human disease and are not of the advanced fibrous cap atheroma seen in human adult disease but of the

xanthomatous type. As a result it is difficult to make a distinction between plaque erosion, as defined by endothelial denudation, to fibrous cap rupture[192, 193]. The fact that animal models of plaque instability and rupture require 'heroic' mechanical measures such as balloon or silastic cuff injury to simulate plaque rupture remains a significant problem[191]. There is promise in the Bristol mouse model which develops spontaneous plaque rupture[194] and sudden death. However major limitations still exist as sudden deaths also occur without evidence of a ruptured plaque. Clearly studies on humans as well as animal and cell culture models will help us better understand the pathogenic mechanisms involved in plaque vulnerability. However, no entirely satisfactory animal model of plaque vulnerability currently exists, emphasising the need for gene expression studies using human tissue derived from closely characterised patient populations[191].

1.7 The accurate identification of the phenotype: a multi-domain assessment.

Critical to any attempt to quantify gene expression differences between stable and vulnerable plaques will be the accurate and reliable identification of such plaques. Clearly, symptoms of distal tissue ischaemia represent a key feature in the positive identification of vulnerable plaques; however, many unstable plaques will be asymptomatic[44, 67]. Thus, reliance upon the absence of symptoms alone is inadequate to classify a plaque as stable.

Similarly, although plaque histology is a key feature in the identification of vulnerable plaques[9, 18, 19, 42], the correlation of histological characteristics with clinically important sequelae is imperfect; 50-70% of symptomatic vessels have a ruptured 'culprit' lesion with thrombus (the remainder with plaque erosion, calcific nodule, thromboembolism or of unidentifiable cause) [17, 18, 57]. Moreover, plaque rupture and thrombosis may occur without any symptoms (silent infarction) or rupture/erosion may not necessarily result in thrombosis and occlusion; autopsy studies have shown evidence of old plaque ruptures without infarctions[9, 18, 61].

Invasive and non-invasive imaging assessments of the affected or unaffected artery (e.g. X-ray angiography, computed tomographic (CT) contrast angiography or magnetic resonance (MR) contrast angiography), functional imaging of thrombotic events (e.g. microemboli detection using continuous doppler monitoring) or imaging assessments of end-organ ischaemia or infarction (e.g. radio-isotope perfusion scanning, MR imaging, CT imaging) can provide additional information regarding plaque stability and vulnerability and end-organ events to that derived from histological assessment alone[195-199].

These considerations suggest that in order to accurately identify the phenome and reliably identify stable and vulnerable plaques for subsequent comparative analysis of the stable and vulnerable plaque, assessment in all three of these domains (clinical, histopathological and imaging) will be required.

1.8 Heterogeneity of the plaque: a cell-specific approach.

Previous work on atherosclerosis and plaque rupture using human tissue (and animal models of atherosclerosis) used mostly whole atherosclerotic vessels. The use of whole mount vessels presents many problems. The atherosclerotic plaque is a complex heterogenous tissue that consists of a variety of cell-types which also demonstrate different cellular phenotypes with respect to their location in the tissue (for example, the smooth muscle cells in the cap demonstrate a more synthetic and proliferative type compared to the SMCs in the media which are a more resting and contractile type), as well as acellular regions of calcification, lipid and necrosis. By using an entire atherosclerotic vessel or plaque for gene expression analysis, the approach is effectively pooling the gene expressions of the various cell types in the plaque relative to their cellular abundance. This adds another confounding variable to the analysis. As a result, it is likely that only large significant changes in gene expression are identified and more subtle differences would be masked. Moreover it is necessary that gene expression findings which have been obtained by whole mount tissue be localised to certain cell types by in-situ hybridisation or immunohistochemistry[174]. Very few early genomic studies of atherosclerosis addressed this very important problem of cellular heterogeneity within plaques as no technology was then available to specifically isolate particular cell types from plaques in sufficient number to permit microarray analysis, for which relatively substantial amounts of RNA are required. Other investigators have sought to circumvent this problem by investigating cultured VSMCs derived from atheromatous tissue[200]; while this approach has the benefit of being able to assay stable patterns of gene expression, substantial selection of VSMCs may take place between tissue harvesting and the establishment of stable VSMC cultures. Two relatively recent technical advances, laser microdissection (LMD) and the development of robust and reproducible methods for amplification of small quantities of RNA using T7 polymerase, have now rendered it possible to examine expression profiles in particular cell types using microarrays without the need for an intermediate cell culture step.

1.9 Laser micro-dissection and linear amplification

Laser micro-dissection (LMD) employs UV laser ablation on a thermoplastic membrane which cuts around individual cells and cell groups from either frozen of paraffin-embedded sections[201, 202]. Sections can be quickly immunostained or counterstained to facilitate identification of the cells of interest[203, 204]. LMD, though a relatively recent technique, has already been extensively employed in expression profiling of tumour cells[205-209] and has proved to be of particular value in tissues with complex internal structure, such as the brain, where investigation of single-cell gene expression profiles has been shown to be reliably possible[210, 211]. Stagliano and colleagues applied LMD to healthy human blood vessels and showed its capacity to validate gene expression and identify novel regulated genes in VSMCs[212]. LMD has been used in atherosclerotic tissue in only a few publications to date. Trogan and colleagues carried out LMD to isolate macrophages from lesional tissue in the ApoE knockout mouse, and showed the capacity of the technique, used together with real-time quantitative reverse-transcription PCR (rtPCR) to robustly identify changes in macrophage gene expression in response to lipopolysaccharide injections[203]. Similarly, Langheinrich and colleagues[213], and Zeiffer and colleagues[214], both used LMD in the ApoE knockout mouse to quantitate gene expression changes by rtPCR in macrophages and neointimal VSMCs. In human tissue, Martinet and colleagues used LMD to isolate medial SMCs from carotid endarterectomy and internal mammary arteries[215]. More recently Tuomisto and colleagues used LMD to isolate macrophage-rich shoulder areas from human atherosclerotic specimens and compared the expression of 10,000 clones between these cells and cultured human macrophages using a DNA array[216]. Since the amount of RNA that can be obtained from particular cell subtypes in a single human tissue specimen is insufficient for microarray analysis, Tuomisto and colleagues used linear amplification with T7 polymerase to generate sufficient RNA for microarray analysis. The above papers show the applicability of LMD to both healthy and diseased vascular tissue. To date, LMD has not yet been applied to the study of plaque rupture.

Linear amplification is the second recent technical advance enabling genomic interrogation by microarray of very little biological material obtained from LMD. LMD of individual samples yields RNA in nanogram quantities (typically, 10 to 50 nanograms of total RNA per 1000 microdissected cells), but microarray experiments in general require the loading of 5 to 10 micrograms of labelled cRNA. A variety of approaches have now been shown to provide faithful amplification of RNA extracted from microdissected specimens, mostly involving the production of a double-stranded cDNA (DScDNA) from total RNA and the subsequent use of the DScDNA as template to generate labelled cRNA during an in vitro transcription reaction. Both random PCR amplification and linear

amplification using T7 polymerase (Eberwine method) have been extensively evaluated for sensitivity, reproducibility and reliability, and have been shown to produce no major distortion of gene expression profiles[217-222].

1.10 The major cell-types in the plaque: VSMCs and Macrophages

The two major cell types which play an active role in the stability/instability of the plaque are the VSMCs and the macrophages. The VSMCs synthesise the extracellular matrix components of the protective fibrous cap and its continued existence is crucial to its maintenance. The macrophages have important functions in scavenger activity, lipid metabolism, inflammation and immune modulation. Important cell signalling activity between the two cell types may also influence the stability/instability of the plaque[69].

Two alternative models may be broadly stated regarding the behaviour of macrophages and VSMCs in the genesis of plaque vulnerability. Firstly, it may be that the propensity of a plaque to take on the phenotypic characteristics of vulnerability is principally or even entirely due to the histologically well-documented quantitative differences in the inflammatory cell composition of the plaque. Thus, in vulnerable plaques, the primary characteristic of pathological importance may simply be a greater number of macrophages, the gene expression profile of which is similar to that of macrophages derived from more stable plaques. Alternatively, it may be that stable and unstable plaques are characterised not only by differences in macrophage numbers, but also by differences in macrophage behaviour. Thus, macrophages in unstable plaques may have gene expression profiles that are significantly different from macrophages in stable plaques. If the latter were the case, those genes differentially expressed in macrophages from stable versus unstable plaques would be strong candidates to lie in the pathways causing plaque vulnerability. In a similar fashion, the response of VSMCs to the greater numbers, and possibly different gene expression profile, of plaque macrophages could have both quantitative (a smaller number of VSMCs expressing similar genes in unstable versus stable plaques) and qualitative (different expression profiles of VSMCs derived from unstable and stable plaques) aspects. Histological studies have shown that unstable lesions are characterised by fewer VSMCs in the fibrous cap, but gene expression in VSMCs from stable and unstable plaques has been little studied. Identification of differentially expressed genes in VSMCs from stable and unstable plaques could potentially indicate novel therapeutic targets to prevent plaque instability by “protecting” VSMCs against the actions of inflammatory cells. The above argues in favour of as complete as possible a description of the gene expression patterns in both macrophages

and VSMCs derived from stable and unstable plaques in order to address these questions.

1.11 Three dimensional imaging of gene expression in the plaque

In addition to the quantitative characterisation of gene expression within plaques, spatial descriptions of gene expression in stable and unstable lesions could contribute significantly to our understanding of plaque instability. Hitherto, three dimensional reconstruction of gene expression in atherosclerosis has been difficult to undertake accurately. Novel technology using Optical Projection Tomography, a non-destructive optical microscopy technique, can produce high-resolution 3-dimensional images of whole fixed, intact and unstained biological specimens. Subsequent histological studies as well as gene and protein expression studies can be performed and can allow us to study the expression of any gene of interest in the complex atherosclerotic plaque in three dimensional space[223-225].

1.12 Hypotheses

My research hypotheses are:

1. There are differences in gene expression between stable and unstable plaque VSMCs and macrophages independent of the differences in the quantity of these cell types.
2. These gene expression differences reflect the molecular processes of the various biological pathways that are active. Some of these pathways may be causal in the processes leading to plaque rupture and its regulation may be important in plaque stabilisation.

1.13 Aims

1. To collect and comprehensively characterize samples of atherosclerotic plaques from carotid endarterectomy patients for the study.
2. To accurately identify maximally contrasting samples of stable plaques and unstable plaques for study using multi-domain assessment.
3. To develop a robust and reliable method to isolate high quality RNA in a cell-specific manner from plaque VSMCs and macrophages using LMD.
4. To perform genome-wide expression profiling of the SMC and macrophage transcriptome of stable and unstable plaques.
5. To demonstrate and identify significant gene expression differences between stable and unstable plaques.
6. To identify genes and pathways of biological importance which may be causal in plaque instability for further testing
7. To identify potential therapeutic targets in plaque stabilization strategies or novel biomarkers for the early identification of patients at risk for further testing.
8. To develop the method to study the three dimensional spatial relationship of these differentially expressed genes in the complex atherosclerotic plaque using Optical Projection Tomography.

Chapter 2. Material and methods

2.1 Ethical approval and study execution

Local Research Ethics Committee approval was granted for this study from Newcastle and North Tyneside Local Research Ethics Committees. The study was performed in accordance with the principles of the Declaration of Helsinki and Good Clinical Practice guidelines. Informed consent was obtained pre-operatively from all patients.

2.2 Patient recruitment, consent, clinical data collection

Samples of diseased carotid atheroma were collected from symptomatic and asymptomatic patients undergoing carotid endarterectomy surgery. Samples of normal radial and internal mammary arteries were collected from patients undergoing coronary artery bypass surgery.

2.2.1 Carotid endarterectomy surgery

Rationale

The unique opportunity to study clinical atherosclerotic specimens from both symptomatic and completely asymptomatic individuals was key to the study. Several large multicentre trials have showed benefit in carotid endarterectomy surgery in recently symptomatic patients with symptoms up to 6 months prior to surgery and also in asymptomatic patients with significant carotid artery stenosis compared to optimal medical treatment provided that the peri-operative complication rates were low (<3%)[226-233]. The greatest benefit was realised with earlier surgery in symptomatic patients and with increasing carotid stenosis[230].

The Regional Neurosurgical Centre in Newcastle was able to offer carotid endarterectomy surgery to both symptomatic and asymptomatic patients and was performed by one surgeon, Professor Alexander David Mendelow, Professor of Neurosurgery, who had a low 30-day peri-operative risk of stroke or death (<2%) and was also one of the surgeons in the Medical Research Council Asymptomatic Carotid Surgery Trial[232].

Patient selection: CEA surgery for Symptomatic patients

Atheromatous CEA specimens were obtained from recently symptomatic patients with symptoms of TIA or stroke of the cerebral or retinal territory of the affected carotid artery within 6 months prior to surgery, with carotid luminal stenoses of 50% and greater, without occlusion or sub-occlusion of the artery (NASCET criteria) during their surgery[226-230, 234, 235].

Patient selection: CEA surgery for Asymptomatic patients

Atheromatous CEA specimens were obtained from asymptomatic patients without any symptoms of TIA or stroke of the cerebral or retinal territory of the affected carotid artery or from patients with late symptoms of more than 6 months prior to surgery, with carotid luminal stenoses of 60% and greater, without occlusion or sub-occlusion of the artery (NASCET criteria) during their surgery[231-235].

Patient recruitment and data collection

The patients were routinely seen in pre-admission clinic 1-2 weeks before surgery. They were sent a patient information document about the study in advance and were invited to participate in the "Carotid Atherosclerosis Gene Expression" (CAGE) study at the pre-admission clinic. Informed consent was sought. The patient's symptoms, medical history, medication, risk factor profile, clinical examination and demographics were recorded by direct interview and by review of the medical notes. Based on the clinical history and recorded clinical assessment at the time of the symptoms, the territory of cerebral ischaemia or infarction was established using the Bamford/Oxford stroke classification[236]. Pre-operative laboratory blood results consisting of full blood count, urea and electrolytes, clotting screen and total cholesterol levels were recorded. Results of pre-operative electrocardiograms and cerebral and carotid imaging consisting of CT or MRI of the brain, carotid ultrasound doppler studies and MR, CT or catheter angiography of the carotid arteries and cerebro-vertebral circulation were recorded. The brain and carotid imaging were later reviewed and analysed separately.

2.2.2 Coronary artery bypass surgery

Normal radial and internal mammary artery (IMA) specimens were obtained from patients during routine elective coronary artery bypass surgery (CABG) for chronic stable angina where radial and IMA conduits were planned to be used as bypass grafts. The CABG surgery was performed at the Freeman Road Hospital Cardiothoracic Centre by Professor Stephan Schueler, Consultant Cardiothoracic Surgeon. The patients were given a patient information document and invited to participate in the CAGE study at pre-admission clinic.

Informed consent was sought. The patient's symptoms, medical history, medication, risk factor profile, clinical examination and demographics were recorded by direct interview and by review of the medical notes. Pre-operative laboratory blood results consisting of full blood count, urea and electrolytes, clotting screen and total cholesterol levels were recorded. Results of pre-operative electrocardiograms, cardiac imaging consisting of coronary angiography and cardiac trans-thoracic echocardiography, lung function tests as well as carotid artery doppler ultrasound imaging were recorded.

2.3 Magnetic resonance imaging and angiography

2.3.1 Rationale

Magnetic resonance imaging (MRI) and x-ray computed tomography (CT) of the head, and contrast enhanced magnetic resonance angiography (MRA) of the carotid arteries were performed as standard pre-operative investigative work-up. MRI or CT of the brain were useful in the detection of established cerebral infarction and its territory. MRA of the carotid arteries provide an accurate in-vivo assessment of the carotid lesion prior to endarterectomy surgery with detailed assessment of its location, degree of stenosis and luminal surface morphology. Major carotid plaque surface irregularities have previously been correlated with TIAs and stroke[195-198] and were useful in the identification of high risk lesions.

2.3.2 Imaging

Pre-operative magnetic resonance imaging (MRI) of the brain and 3D gadolinium diethylenetriamine penta-acetic acid (gadolinium-DTPA) contrast-enhanced magnetic resonance angiography (MRA) of the carotid arteries were performed on a 1.5T scanner (Intera, Philips Medical Systems, Netherlands) as routine pre-operative imaging work-up. MRI of the brain was performed using standard hospital head MRI protocols: T2-weighted turbo-spin-echo (TSE) axials, 5mm slices, 20% gap; axial fluid-attenuated inversion recovery (FLAIR) sequence of 5mm slices, 0.9mm resolution, FOV 230mm; T1-weighted TSE coronals 5mm slices with 20% gap; and T2-weighted TSE sagittals 5mm slices with 20% gap. The following parameters were used for the 3-dimensional MR angiography: time of flight (TOF) 3D reconstructed angiogram Fast-Field-Echo (FFE) 150 slices, 0.6mm thick, Time to Echo (TE) 6.9msec, Time to Repetition (TR) 23msec, flip angle 20˚; and contrast enhanced 3D reconstructed angiogram 130 slices, 0.55mm thick, TE 50msec, TR 500 msec, flip angle 40˚, in-plane resolution 0.6mm, 0.2 mg/kg gadolinium-DTPA. The MR

angiographic data was presented as a series of maximum intensity projections obtained every 10 degrees for each imaged extracranial carotid artery.

2.3.3 Image Assessment

The brain imaging by MRI provided evidence of previous cerebral infarction and its territory if present. The Gadolinium-DTPA contrast-enhanced MR angiogram of the carotid artery allowed for the accurate in-vivo image assessment of the plaque as follows:

1) The location of the plaque - common carotid, bifurcation, external or internal carotid artery.

2) Percentage degree of stenosis by NASCET criteria defined as the minimal luminal diameter at point of maximal stenosis in reference to the luminal diameter of a normal segment of internal carotid artery [227-229]. The cases were subsequently classified as falling within one of the following groups of severity: less than 50%, 50-69%, 69-95%, greater than 95% and total occlusions.

3) The plaque surface morphology - irregularities were defined as depressions in the plaque surface extending below the lumen for a distance of at least 1mm. In cases where the irregularities were present, their width and the depth of the irregularities were recorded. The cases were subsequently classified as minor irregularities for depressions of more than 1mm but less than 2mm, and major for depressions of 2mm and more. The proximal and distal edge angles of the irregularities were recorded as well and defined as mild for a <45˚ angle, moderate for 45˚ to 90˚ angle, and severe for an edge of greater than 90˚ angle.

2.4 Transcranial doppler emboli detection

2.4.1 Rationale

The imaging technique of TCD emboli detection had recently been made available to the medical physics department of our surgical unit during the period of this study. Transcranial Doppler monitoring (TCD) of the middle cerebral artery to identify micro-thromboembolic events have been highly correlated with the occurrence of distal ischaemic symptoms[237-240] and plaque ulceration and thrombus[198]. In contrast an absence of microemboli on TCD identifies a patient population at low risk of future ischaemic events[237, 240]. TCD emboli detection monitoring was included as it may provide additional

information regarding plaque instability to that derived from clinical, MRA and histological assessment.

2.4.2 Patient recruitment and consent

Patients were invited to participate in a pre-operative trans-cranial doppler (TCD) emboli detection ultrasound monitoring sub-study. The patients were given a patient information document about the sub-study in addition to the primary study in advance at the pre-admission clinic. An additional consent form was used and informed consent was sought.

2.4.3 TCD recording, analysis and emboli detection

The trans-cranial doppler study was performed at the Medical Physics Department, Newcastle General Hospital during the patient's pre-admission visit. A DWL Multi-dop T2 machine (Compumedics DWL Elektronische Systeme GmbH) with two pulsed wave 2MHz pulsed probes were used to acquire trans-cranial doppler signals of bilateral middle cerebral arteries simultaneously. A Spencer headset fixation device allowed the continuous insonation of both middle cerebral arteries at 45 to 55mm depths at 5-10mm axial widths. Digital recordings were made over a period of 1 hour. A 64-point fast Fourier transform (FFT) was applied with an FFT length of 2ms, overlap of 60% and a high-pass filter set at 100 Hz. Microemboli detection settings were defined according to the criteria recommended in the International Consensus Group on Microemboli Detection[241-243]. They were unidirectional doppler signals, of short duration of <300ms and an amplitude of >8dB above the doppler background. A dual-gate doppler technique was also used to measure separate sample volumes at two depths of 5mm apart in each middle cerebral artery. This allowed the tracking of the moving embolus in different depths of the artery and assisted the differentiation of microemboli from artefact [243, 244]. Both real time and retrospective offline analyses were performed. The positive identification of a high-intensity transient signal (HITS) as a microembolus according to the consensus group criteria and by dual-gate doppler was recorded.

2.5 Specimen collection and Snap-freezing

2.5.1 Snap-freezing - preliminary methodological evaluation

Rationale

I evaluated various methods of snap freezing at the beginning of the study to determine the optimal method of clinical sample preservation. This was important in the maintenance

of histological and biological cell membrane integrity and RNA integrity during laser micro-dissection and RNA extraction. The conventional method of snap-freezing involves the use of liquid nitrogen. Contrary to its reputation as a cryogenic fluid for snap-freezing, liquid nitrogen's efficiency as a coolant is limited by its boiling when in contact with a 'warmer' object (above -196˚C) forming an insulating layer of nitrogen gas, a phenomenon known as the Leidenfrost effect (Johann Gottlob Leidenfrost, A Tract about some qualities of common water, 1756) and may cause non-uniform freezing with macroscopic freeze-fracturing artefacts. I evaluated the various methods of snap-freezing the samples in liquid nitrogen using a solid intermediary (copper plate), a liquid intermediary (isopentane bath) and no intermediary (directly into liquid nitrogen).

Snap-freezing directly in liquid nitrogen

The sample was directly immersed into liquid nitrogen contained in a dewar.

Snap-freezing on a liquid-nitrogen-cooled copper plate

A copper ‘chuck’ in a Pyrex beaker topped up with liquid nitrogen to pre-cool the copper plate was used. The sample was placed directly onto the surface of the liquid-nitrogen-cooled copper plate (Figure 27).

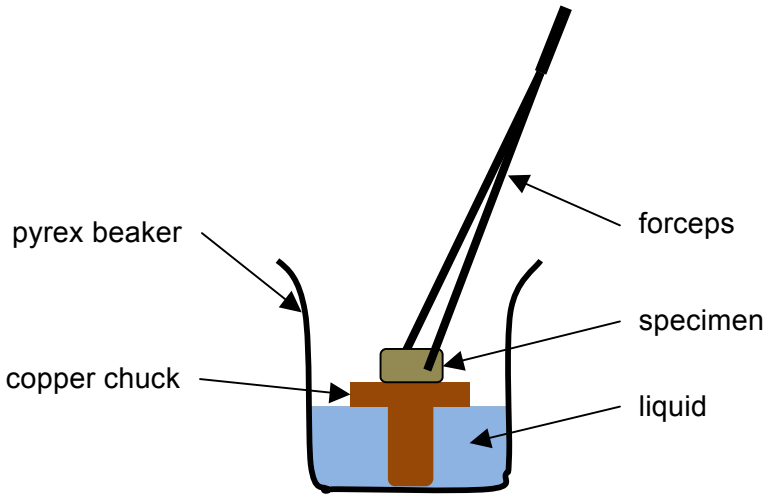

Figure 27. Liquid-nitrogen-cooled copper plate snap-freezing method.

Snap-freezing in liquid-nitrogen-cooled isopentane bath

Isopentane, C_5H_{12}, or 2-methylbutane, is a volatile liquid hydrocarbon at room temperature with a boiling point just above room temperature at 28˚C. When used as a liquid bath cooled in liquid-N_2 it attains a temperature of -160˚C just below its freezing point and was used to freeze the sample within a liquid medium. I used liquid isopentane in a 100ml Pyrex beaker immersed in a dewar of liquid-N_2 and pre-cooled the isopentane to a

temperature just above its freezing point (the isopentane was seen to solidify at the base of the suspended Pyrex beaker and the liquid-N_2 stopped bubbling). The sample was immersed directly into the pre-cooled isopentane (Figure 28).

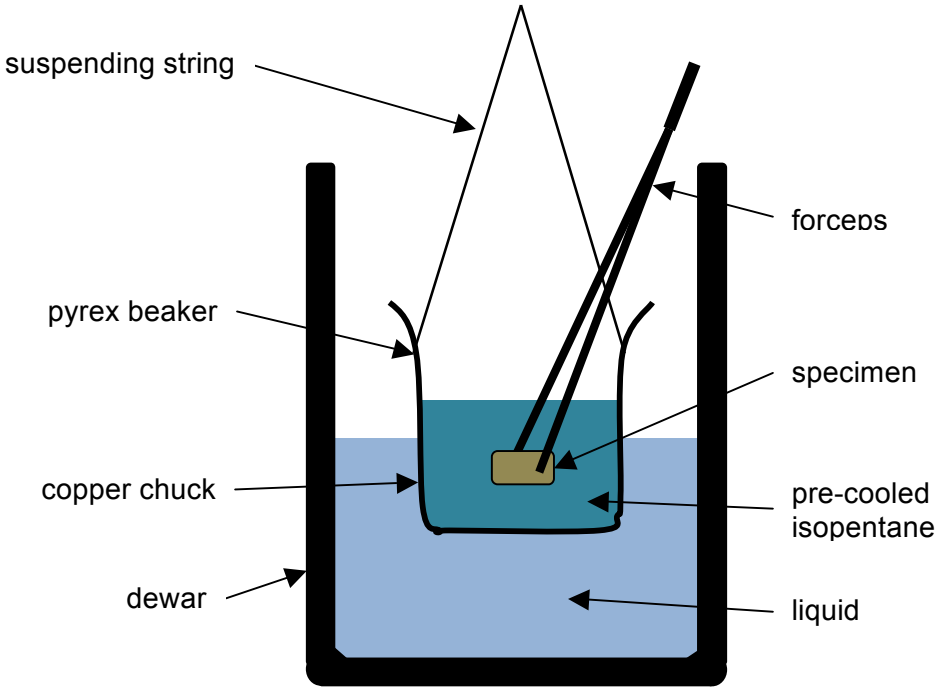

Figure 28. Liquid-nitrogen-cooled isopentane bath snap-freezing method.

2.5.2 CEA surgery and specimens

The carotid endarterectomy surgery was performed under local anaesthetic with dissection and exposure of the carotid artery at the bifurcation. The patient was fully heparinised. The carotid artery was clamped and a longitudinal incision was made to locate the lumen of the artery. If symptoms of cerebral ischaemia occurred a bypass shunt is placed to maintain cerebral perfusion whilst continuing with the endarterectomy surgery. The medial layer was identified and dissected around the diseased atherosclerotic intima and the atherosclerotic plaque was removed in one complete piece '*en-bloc*'. The disease-free media and adventitia of the carotid artery were sutured, de-aired, unclamped and haemostasis was achieved.

The endarterectomised atherosclerotic tissue was immediately processed by me in theatre under sterile conditions to minimise the total ischaemic time to the tissue. The plaque and any apparent site of rupture were identified macroscopically whenever possible, and the endarterectomised specimen was carefully cut transversely using a sterile surgical scalpel into separate 5mm to 6mm long portions. In macroscopically un-ruptured intact plaques the middle part of maximal stenosis was fixed in 10% normal

buffered formalin (NBF) for histopathological analysis later (Figure 29). In macroscopically apparent ruptured plaques part of the site of rupture was fixed in 10% NBF and the other half was snap-frozen. All other distal and proximal segments were immediately snap-frozen using the evaluated method which yielded optimal results; the liquid-nitrogen-cooled isopentane bath method. The freshly dissected samples were orientated and embedded in OCT media (Lamb) mounted in thin plastic disposable 10x10x5mm cryomolds (TissueTek, Bayer) and snap-frozen. The segments were labelled and their orientation documented for histopathological analysis and LMD later. The snap-frozen samples were stored in Nalgene cryogenic containers in a -80˚C freezer. The total ischaemic time (from clamping of the carotid artery to snap-freezing) was recorded.

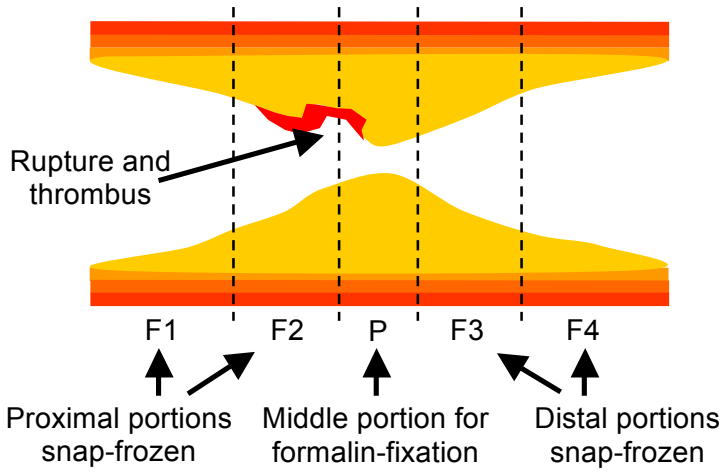

Figure 29. The portions of an endarterectomised carotid atherosclerotic specimen for formalin-fixation and snap-freezing.

2.5.3 CABG surgery and radial and IMA specimens

In CABG surgery, the bypass conduits (grafts) were harvested and prepared prior to cardio-pulmonary bypass and the surgical anastomoses of the grafts. The radial artery and internal mammary artery were commonly used conduits. Excess unused portions were collected and immediately processed by me in theatre under sterile conditions. The atherosclerosis-free radial and IMA specimens were divided into 5-6mm portions, embedded in OCT and snap-frozen and stored in Nalgene cryogenic containers in a -80˚C freezer. The total ischaemic time (from clamping to snap-freezing of the artery) was recorded.

2.6 Sample processing and staining for histological analysis

2.6.1 Formalin fixed paraffin embedded samples

Formalin fixation, decalcification and paraffin embedding

The CEA samples in NBF were processed for histological analysis. They were allowed to fix in NBF for 24 hours, then washed in Tris buffered saline (TBS) and decalcified in EDTA (12.5% Ethylene-diamine-tetra-acetic acid in distilled water, pH 7.4) for 7 days and then washed in tap water for 10 minutes and returned into 10% NBF. Then the specimens were processed and embedded in paraffin wax as follows: the specimens were dehydrated through increasing ethanol gradients of 70%, 80%, 95% and 100%, into chloroform and then into 3 changes of liquid paraffin wax using a conventional tissue processor. The specimens were embedded in paraffin wax in moulds ready for microtome sectioning. These paraffin tissue blocks were then stored at room temperature.

Microtome sectioning, deparaffinisation and rehydration

Microtome cut sections of 5μm thickness were made from both proximal-facing and distal-facing surfaces of the endarterectomised carotid specimens. The cut sections were mounted from a warm water bath (40˚C) onto SuperFrost Plus adhesion-charged microscope slides (Menzel-Glaser) and dried in a 37˚C oven overnight. The slides were deparaffinised through xylene (2 changes, 5 minutes each) and rehydrated through decreasing alcohol gradients; 100%, 95% and 70% (2 changes of 3 minutes each at each stage) and then in TBS.

Histochemical staining

The sections were stained using haematoxylin and eosin (H&E). The rehydrated sections were nuclear stained with haematoxylin for 5 minutes, washed in tap water, differentiated in acid alcohol quickly (2-3 seconds), washed in tap water, blued in Scott's tap water substitute (STWS), washed in tap water, counterstained with eosin (3-4 minutes) and washed in tap water. The slides were then dehydrated through increasing gradients of ethanol (70%, 80%, 95% and 100%) and cleared in Xylene (2 changes, 3 minutes each) and mounted in DPX (Lamb) and coverslipped.

Immunohistochemical staining

Separate sections were immunohistochemically stained using antibodies to smooth muscle actin (SMA) (Dako, mouse monoclonal IgG2a kappa antibody to SMA, clone 1A4) to identify smooth muscle cells using the Vectastain Elite Avidin-Biotin-Complex Antibody Kit (Vector Labs) for mouse monoclonal (PK6102) and counterstained with haematoxylin

and martius-scarlet-blue. The rehydrated sections did not need any antigen retrieval steps. The protocol was as follows: the sections were blocked for endogenous peroxidases in 3% hydrogen peroxide (H_2O_2) in water for 10 minutes. Then washed well in tap water and then in TBS with 0.05% of Tween (TBS-T) (3 minutes). The following steps were performed in a slide incubation tray. The slides were wiped dry around the sections and normal blocking serum was applied (1.5% normal goat serum in TBS) for 20 minutes. The excess serum was wiped off and the primary antibody was applied on the sections (SMA, Dako clone 1A4, 1/200 dilution for 1 hour at room temperature). They were then washed well in TBS-T (2 changes, 3 minutes). The slides were wiped dry around the sections and the biotinylated secondary antibody was applied (Vectastain Elite, 1/200 dilution with 1.5% normal goat serum in TBS) for 30 minutes. Then washed in TBS-T (2 changes, 3 minutes each), wiped dry around the sections, and the Avidin-Biotin Complex solution was applied (Vectastain Elite, 1/50 Reagent A and 1/50 Reagent B in TBS) for 30 minutes. They were washed in TBS-T (2 changes, 3 minutes each). The following steps were performed in a designated area for Di-amino-benzidine (DAB). Freshly prepared and filtered DAB solution was applied (Sigmafast DAB peroxidase substrate tablet sets, D4418) onto the sections. They were allowed to stain brown over 7 minutes. The sections were washed in tap water for 10 minutes. The nuclei were counterstained with Celestin Blue for 5 minutes, washed in tap water, then in Haematoxylin for 5 minutes, washed in tap water, differentiated quickly in acid alcohol (2-3 seconds), washed in tap water, blued in Scott's tap water substitute (STWS) and washed in tap water. Then the sections were stained with 0.5% martius yellow (2 minutes), washed in tap water, stained with 1% brilliant crystal scarlet (5-10 minutes), washed in tap water, differentiated with 1% phosphotungstic acid (up to 1 minute), the acid was left on and 0.5% soluble aniline blue was applied for 3 minutes. The sections were then washed, dehydrated through increasing gradients of ethanol (70%, 80%, 95% and 100%) and cleared in Xylene (2 changes, 3 minutes each) and then mounted in DPX (Lamb) and coverslipped.

2.6.2 Snap-frozen samples

Cryosectioning, acetone fixation and rehydration

The snap frozen specimens were also processed for histology and analysis. As these snap frozen samples were to be used for laser micro-dissection (LMD) and RNA extraction later, an RNAse-free environment and method were employed. The frozen samples were thawed from storage at -80˚C to between -20˚C to -25˚C gradually in the cryostat over 30 minutes. The OCT embedded snap-frozen tissue blocks were mounted onto RNase-free treated 25mm wide cork disks (Lamb), allowing the frozen blocks to be mounted on and off the cryostat chuck without thawing the base of the specimen. The

snap frozen specimens were cryosectioned at 10µm thickness on the Leica CM3050 cryostat and mounted onto SuperFrost Plus adhesion-charged microscope slides (Menzel-Glaser). The mounted sections were fixed in acetone for 1 minute at room temperature and allowed to air-dry thoroughly. The sections were then rehydrated in phosphate buffered saline with Tween (PBS-T) for 5 minutes.

Histochemical staining

The sections were stained using haematoxylin and eosin (H&E). The rehydrated sections were nuclear stained with haematoxylin for 2 minutes, washed in PBS-T, differentiated in acid alcohol quickly (2 dips), washed in PBS-T, blued in 0.5% ammonia solution, washed in PBS-T, counterstained with eosin (2 minutes) and washed in PBS-T. The slides were then dehydrated through increasing gradients of ethanol (70%, 80%, 95% and 100%) and cleared in Xylene (2 changes, 3 minutes each) and then mounted in DPX (Lamb) and coverslipped.

Immunohistochemical staining

Separate sections were immunohistochemically stained using antibodies to smooth muscle actin to identify smooth muscle cells (SMA, Dako, mouse monoclonal, clone 1A4) and to CD68 to identify macrophages (Dako, mouse monoclonal, clone PG-M1) using the Vectastain Elite Avidin-Biotin-Complex Antibody Kit (Vector Labs) for mouse monoclonal (PK6102) with nuclear counterstaining with haematoxylin. The rehydrated sections did not need any antigen retrieval method. The sections were blocked for endogenous peroxidases in 3% hydrogen peroxide (H_2O_2) in methanol for 10 minutes. The slides were washed well in PBS-T (3 changes, 3 minutes each). The following steps were performed in a slide incubation tray. The slides were wiped dry around the sections and normal blocking serum was applied (1.5% normal goat serum in PBS) for 20 minutes. The excess serum was wiped off and the primary antibody was applied on the sections (SMA 1/500 for 1hr in RT, CD68 1/125 for 1hr in RT). The slides were washed well in PBS-T (3 changes, 3 minutes). The slides were wiped dry around the sections and the biotinylated secondary antibody was applied (Vectastain Elite, 1/200 dilution with 1.5% normal goat serum in PBS) for 30 minutes. The slides were washed well in PBS-T (3 changes, 3 minutes each), wiped dry around the sections, and the Avidin-Biotin Complex solution (Vectastain Elite, 1/50 Reagent A and 1/50 Reagent B in PBS) was applied for 30 minutes. The slides were washed well in PBS-T (3 changes, 3 minutes each). The following steps were performed in a designated area for Di-amino-benzidine (DAB). Freshly prepared and filtered DAB solution was applied (Sigmafast DAB peroxidase substrate tablet sets, D4418) onto the sections. They were allowed to stain brown over 5 minutes. The sections were washed in PBS-T (3 changes, 3 minutes each). The nuclei

were counterstained with Haematoxylin for 2 minutes, washed in PBS-T, differentiated in acid alcohol quickly (2 dips), washed in PBS-T, blued in 0.5% ammonia solution, and washed in PBS-T again. The slides were then dehydrated through increasing gradients of ethanol (70%, 80%, 95% and 100%) and cleared in Xylene (2 changes, 3 minutes each), mounted in DPX (Lamb) and coverslipped.

2.7 Sample characterisation and selection: the three-domain analysis

2.7.1 Rationale

In order to accurately quantify gene expression differences between stable and unstable plaques, it is crucial that we are able to identify such plaques reliably. We have previously argued the limitations of using singular identifiers of clinical symptoms, histopathology or imaging of the plaque in the classification of these lesions as stable or unstable. In order to accurately and reliably identify unstable and stable lesions, assessment in all three of these domains will be favourable.

2.7.2 Histopathology analysis and selection

The plaque histology is the key feature in the identification of a stable or unstable/ruptured plaque. Histopathological analyses of all the samples were undertaken independently and then by consensus by 2 researchers (KL and Dr. Tuomo Polvikovski, Consultant Histopathologist, Newcastle Hospitals Trust). All samples had their histological features documented and allocated a Virmani classification of atherosclerotic plaque as recommended by the AHA atherosclerosis working group[18].

A histopathologically unstable ruptured plaque is defined as a Virmani classified, “ruptured thin fibrous cap atheroma”; with evidence of a thin fibrous cap with a defect of rupture over a necrotic lipid core, with inflammation, thrombus and haemorrhage.

A histopathologically stable plaque is defined as a Virmani classified, “(thick) fibrous cap atheroma or fibrocalcific lesion”; with evidence of a thick fibrous cap, organised lipid core, with varying degrees of fibrous or calcific changes of the core.

2.7.3 Clinical analysis and selection

Clinically symptomatic patients were designated as patients with ipsilateral symptoms of TIA or stroke within 6 months prior to carotid endarterectomy[228, 230]. The more recent the

clinical event to surgery would correspond with the increased likelihood that the plaque excised would be an acutely ruptured TFCA. For the purposes of this study, I selected clinically symptomatic patients with a more recent clinical event within 3 months prior to surgery.

The clinical criterion for asymptomatic patients selected for carotid endarterectomy surgery was ipsilateral symptoms of TIA or stroke beyond 6 months (in ACAS and ACST they were considered clinically asymptomatic), or no symptoms at all prior to endarterectomy surgery[231-233]. For the purposes of this study, I selected patients without any ipsilateral symptoms at any time.

2.7.4 Imaging analysis and selection

Symptomatic and asymptomatic patients selected for CEA surgery would have already fulfilled the NASCET angiographic/doppler criteria of carotid luminal stenoses of ≥50% and ≥60% respectively, without occlusion or sub-occlusion of the artery[226-235].

The MR images were analysed by 2 researchers independently and then by consensus (KL and Dr. Daniel Birchall, Consultant Radiologist, Newcastle Hospitals Trust). The MRI imaging of the brain provided evidence of large vessel infarction of the brain and its territory. The 3D contrast-enhanced MR angiography which examined plaque surface morphology provided additional information regarding the stability/instability of the plaque.

Those patients classified as “stable” had no MRI evidence of large vessel infarction in the brain and no MR angiographic evidence of major plaque surface irregularities (defined as depressions in the plaque surface extending outside the lumen for a distance of at least 2mm)[195-198]. Those patients classified as “unstable” had evidence of either large vessel brain infarction on MRI of the brain, or plaque surface irregularities on MRA.

2.7.5 Correlation between groups and statistical analysis

Analyses of relationships and correlations between clinical symptoms, radiological imaging characteristics and histopathological classification of the plaques were performed. Two-way correlations between groups and three-way correlation between all domains were made.

Statistical significance between groups with continuous variables were determined using the Student's t-test, and groups with categorical data using the Chi-square test using MiniTab® statistical analysis software. Tests of significance of categorical data in a 2x3 contingency table were performed using the Chi-square test of independence for k

groups. Complex 3-way contingency table tests for significance was performed using a 3-way log-linear analysis (http://faculty.vassar.edu/lowry/VassarStats.html). The log-linear analysis is an extension of the 2-way contingency table chi-square analysis where the conditional relationships between 2 or more discrete categorical variables are analysed by weighted natural logarithms of the cell frequencies within a contingency table. This allows for comparisons of multiple variables in which the derived chi-square values are linear, allowing for more complex analyses. The test statistic, G^2 is distributed approximately as chi-square and its associated null hypothesis can be estimated through reference to the appropriate sampling distribution of chi-square as defined by its degrees of freedom[245].

2.7.6 Three-domain analysis and final sample selection

From the bank of collected specimens, we selected maximally contrasting unstable versus stable samples for further study by RNA profiling. Using the three-domain enrichment criteria we selected for the highest ranking stable versus the highest ranking unstable samples based on their histological, radiological and clinical criteria. The histological criteria of a stable plaque or unstable/ruptured plaque is mandatory. The selected stable samples fulfilled all 3 domain criteria: histologically, a thick fibrous cap atheroma or fibro-calcific lesion; clinically no symptoms attributable to stroke or TIA at any time; and radiologically, no major irregularity of surface morphology on MRA or evidence of a previous infarction on MRI brain scan. Conversely, the selected unstable samples fulfilled all 3 domain criteria: histologically a ruptured thin fibrous cap atheroma; clinically with a recent stroke or TIA within 3 months and radiologically, with or without major surface irregularity on MRA and previous infarction on MRI brain scan. This combined three-domain approach is outlined in Figure 30.

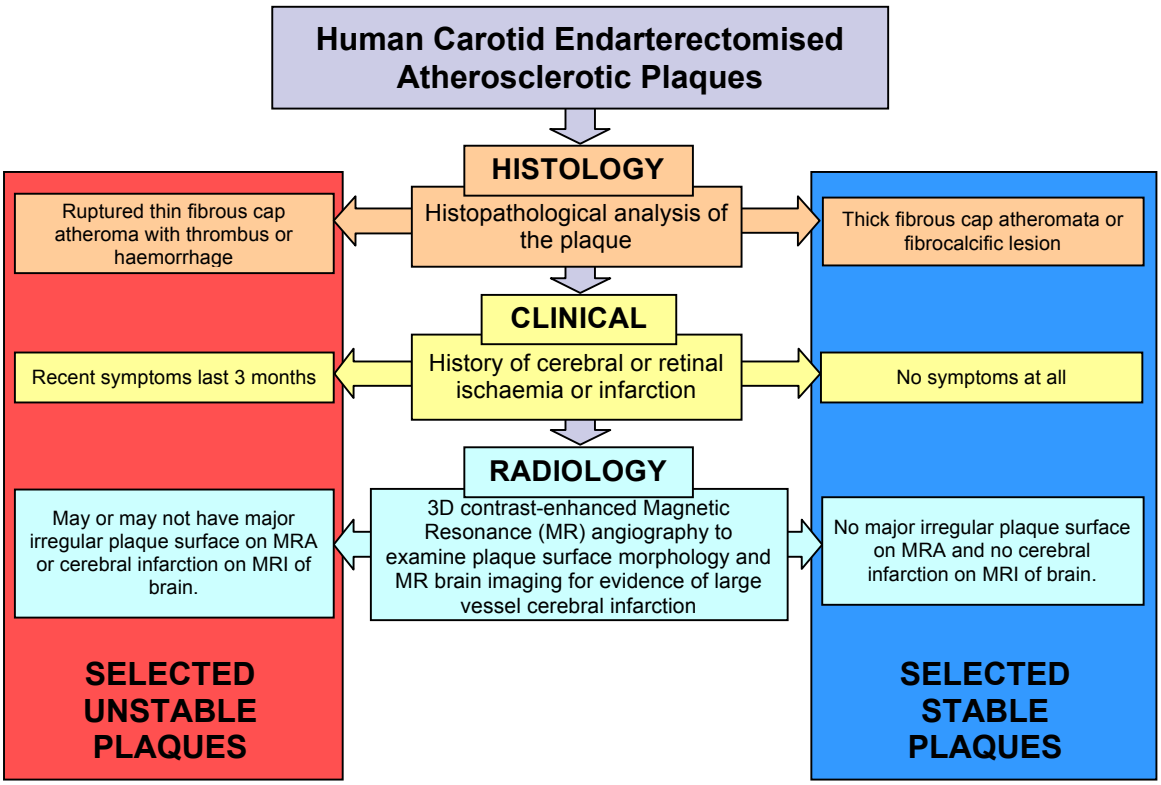

Figure 30. Three domain characterisation of the samples and the respective criteria for the selection of stable and unstable samples for gene expression profiling.

2.7.7 Trans-cranial doppler emboli detection

I also assessed the contribution of a fourth criterion of no ipsilateral microemboli detected during an hour's TCD monitoring period for the stable group and conversely, one or more microembolic events in an hour of monitoring for the unstable group in the selection of stable and unstable lesions.

2.8 RNA extraction method

2.8.1 Rationale

Although a variety of RNA extraction methods are available, an optimal method has not been determined for the extraction from very small amounts of LMDed tissue. Linear amplification of RNA is sensitive to RNA degradation. As a result, paramount to the successful amplification of mRNA for microarray, it was necessary for me to systematically evaluate and develop an optimal method of isolating high quality RNA in high yield from the atherosclerotic plaque.

2.8.2 RNA extraction from whole tissue

Trizol Phenol-Chloroform extraction

Firstly I confirmed the RNA quality of snap-frozen whole tissues. Snap-frozen cryosections of normal arterial tissue and carotid endarterectomised tissue were used. General considerations for RNA work were applied. Whole cryosections of 10µm thickness of varying amounts were collected still frozen into pre-cooled 2mL RNase-free eppendorf tubes in the -20˚C cryostat. One mL of Trizol reagent containing β-Mercaptoethanol (β-ME) was added and vortexed at high speed in room temperature immediately and then homogenised using the IKA T-25 rotor-stator homogeniser (Cole-Palmer, UK). RNA was extracted from the homogenised samples using the Phenol-Chloroform method using Trizol (Invitrogen, UK) according to the manufacturer's standard protocol. The extracted RNA was resuspended in RNase-free water (Qiagen) and stored in a -80˚C freezer.

RNeasy silica-column extraction

I also evaluated the silica-column extraction method for RNA extractions from small amounts of tissue (~1mg) in the work-up to the very small amounts of tissue isolated by LMD (~20µg). Whole cryosections were homogenised by high-speed vortexing for 30 seconds in the RLT lysis buffer. RNA was extracted using RNeasy Mini (tissues of 5-30mg) and Micro (tissues less than 5mg) kits (Qiagen, UK) according to the manufacturers' standard protocols.

2.8.3 RNA extraction from Laser Micro-Dissection

Materials, preparation and LMD

Snap-frozen cryosections of normal arterial tissue and carotid endarterectomised tissue were used. They were unstained cryosections fixed in 95% ethanol and processed for LMD using the modified Leica 95% Ethanol protocol with substitution of the xylene clearing steps with additional 100% Ethanol clearing (described in the next section).

Evaluation of various RNA extraction kits

I evaluated several methods of RNA extraction including the chloroform-phenol extraction and several silica-based column extraction methods from LMDed samples. Several RNA extraction kits were evaluated using the manufacturers' standard protocols to determine the method which yielded the highest quality and quantity of RNA from LMD. The kits evaluated were:

- Trizol-reagent Phenol-Chloroform RNA extraction (Invitrogen, UK)

- RNeasy Micro silica-column RNA extraction (Qiagen, UK)
- PicoPure silica-column RNA extraction (Arcturus, UK)
- NanoPrep silica-column RNA extraction (Stratagene, UK)
- RNAqueous Micro silica-column RNA extraction (Ambion, UK)

Further optimisation of RNA extraction method

I assessed the utility of Proteinase-K and DNase-I digestion, the use of carrier RNA, the homogenisation methods, protein-rich tissue protocols, lipid-rich tissue protocols and tested several modifications of the RNA extraction protocols of the silica-based column extraction method to increase the yield and quality of the RNA extracted.

DNase-I digestion for DNA elimination

The silica-based column extraction methods were evaluated with and without on-column DNase-I digestion using RNase-free DNase (Qiagen, UK) according to the respective manufacturers' protocol.

Proteinase-K digestion for protein-rich or fibrous tissue

The RNeasy Micro kit (Qiagen, UK) was used with Proteinase-K (Qiagen, UK) using the manufacturer's protocol for 'total RNA isolation from Fibrous Tissues' was evaluated. This protocol was useful for the extraction of RNA from highly fibrous and protein rich tissues such as heart, muscle and skin.

Trizol-Column hybrid method for lipid rich tissue

High amounts of lipid may interfere with the extraction of RNA from the tissues. I evaluated the method of RNA isolation from lipid rich tissues using Trizol-reagent (Invitrogen, UK) for the separation of lipid from RNA, followed by RNeasy Micro (Qiagen, UK) column RNA isolation and purification. This was performed using the 'RNeasy Lipid Tissue protocol for total RNA isolation from adipose tissue, brain and other fatty animal tissues' from Qiagen.

Homogenisation of fibrous tissues

Different homgenisation methods were tested to ensure that satisfactory homogenisation of fibrous tissue was achieved for RNA extraction. The methods evaluated were:

- ***High speed vortexing:*** the samples were vortexed on high speed for 5 minutes in the lysis buffer.
- ***Fine gauge needle passage:*** the samples were passaged through the fine gauge (23G) needle in a 1 ml syringe a total of 50 times.

- ***Sonication:*** the samples were sonicated at 20,000 Hertz at medium to high amplitude of 1 second pulses for 3 times.

Use of Carrier RNA

During the isolation of RNA from very small amounts of tissue of 10-20µg, typical amounts from LMD, the extracted RNA may preferentially adhere to the plastic surfaces of the materials used in its extraction such as the pipette tips and eppendorf tubes. The use of carrier RNA may minimise such losses. In the RNA extractions of LMD material, 20ng of carrier RNA (5µL of a 4ng/µL working solution) was added to the lysis buffer prior to homogenisation of the LMD cells by high speed vortexing. The carrier RNA used was poly-A RNA (Qiagen, UK) which did not interfere with subsequent RT-PCR, even when oligo-dT was used as a primer for reverse transcription (oligo-dT in the reverse transcription reactions were in such large amounts that the carrier RNA amounts are insignificant in comparison).

Low retention polymer plastics for RNA extraction

In order to minimise RNA loss by RNA adhesion to the plastics used for RNA work, RNase-free Neptune aerosol barrier pipette tips and Neptune microcentrifuge tubes (Radleys, UK) made with low retention polymer for ultra low sample adhesion were used.

Effect of Lysis Buffer volume to RNA yield

I evaluated the effect of the difference in volume of RLT lysis buffer used in the RNA extraction of LMD material using the RNeasy Micro kit (Qiagen, UK) following retrospective observations of reduced RNA yields using larger amounts of pooled lysis buffer in the LMD extractions.

Double elution step to increase extracted RNA concentration

The linear amplification reactions of RNA, necessary for generating enough cRNA for the microarray experiments, require a minimal amount of high quality RNA as starting material in a maximum volume of 3µL. Therefore a high enough concentration of RNA is required. In order to achieve this from the small volumes of RNA extracted from LMD material and without a significant reduction of the overall yield of RNA extracted, I evaluated a modification of the RNeasy Micro protocol to use the minimum volume of RNase-free water (Qiagen) for elution to fully hydrate the silica-based column (14µL) and ran the elute through twice, generating a resultant 11-12µL of higher concentration RNA.

2.8.4 The optimal RNA extraction protocol

I have developed an optimal RNA extraction protocol using the Qiagen RNeasy Micro kit with DNaseI treatment and further modifications to the standard protocol as follows: After LMD, 75ul of Buffer RLT with β-ME with 20ng of carrier RNA (5μL of a 4ng/μL solution) was pipetted onto the cap with the micro-dissectates. The micro-tube was closed carefully, spun down and then vortexed at high speed for 30s, then spun down again to achieve homogenization and lysis of the LMDed cells and then stored in -70˚C. Each LMD session consisted of about 10 cryosections with about 5,000-10,000 cells isolated. LMDs of several sessions of the same cell-type from the same region and lesion were pooled together for RNA extraction to achieve higher concentrations and yields. RNA extraction with on-column DNase-I treatment was performed according to the manufacturer's instructions with the final re-suspension of RNA performed using 14μL of RNase-free water with a repeat elution. The resultant 12μL of isolated and purified total-RNA was stored in a -80˚C freezer until needed.

2.9 RNA quantity and quality measurement

2.9.1 RNA evaluation by Agilent Bioanalyser RNA LabChip

RNA quantity and quality was assessed by micro-capillary electrophoresis using the Agilent Bioanalyser 2100 RNA LabChip (Agilent Technologies, UK) following the manufacturer's standard protocol. The RNA PicoChip was used for very small concentrations of RNA of 200 to 5000pg/μL, and the RNA NanoChip was used for concentrations of RNA of 5 to 500ng/μL. The RNA was qualitatively reported by electropherogram, fluorescence graph and ribosomal 28S/18S ratios. A quantitative measurement of the RNA was also reported. High quality RNA samples were defined by 28S/18S ratios >1.5 and baselines with low background degradation noise.

Towards the end of the study, the bioanalyser software had been updated to incorporate a RNA Integrity Number (RIN) in RNA quality assessment (RIN of 6 to 10 - intact RNA, 3-6 partially degraded RNA, <3 severely degraded RNA[246]). The high quality samples described prior to the RIN assessments were equivalent to RIN values of 6 and above.

2.9.2 RNA evaluation by Nanodrop

RNA quantity and purity were assessed by ultraviolet (UV) absorbance at 230nm, 260nm and 280nm wavelengths on the Nanodrop ND-3000 Spectrophotometer (NanoDrop

Technologies, USA) using 1μL of solution. The samples were mixed well by vortexing or pipetting, and denatured at 70˚C for 2 minutes and quenched at 4˚C and kept on ice prior to the measurements. The measurements were performed in duplicate or in triplicate.

OD260 readings of 1 was equivalent to 40mg/mL of RNA. The OD260:OD280 ratios ≥ 2 would represent high RNA purity from protein, phenol, salts or DNA contamination. The OD260:OD230 ratios of ≥ 1.8 would indicate high RNA purity from carbohydrate and phenol contamination.

2.9.3 RNA quantification by RiboGreen

RNA quantification was also performed by fluorescence-based quantification using the Quant-iT RiboGreen RNA kit (Invitrogen, USA) using the Fluoroskan Ascent FL microplate fluorometer (Thermo Scientific, UK) following the manufacturers' standard protocols.

2.9.4 Electrophoresis and visualisation of RNA

The RNA purity and quality from RNA extraction and purification, and the fragmentation of cRNA prior microarray hybridisation were evaluated using agarose gel electrophoresis. Extracted total RNA was denatured at 70˚C for 2 minutes and then quenched at 4˚C and kept on ice prior to loading onto the gel. 1.5% agarose gels were made using 1.5g of SeaKem LE Agarose powder (Cambrex, USA) in 100mL of 1xTAE, containing 5μL of 25mM ethidium bromide. 1.5μL of Orange G loading dye (Sigma-Aldrich, UK) was added to 3μL of RNA sample. The samples were loaded alongside 5μL of GeneRuler 100bp DNA Ladder (Fermentas, Germany) for size reference. Electrophoresis was carried out between electrodes 30cm apart for 30 minutes at 160V in 1xTAE buffer. Gels were visualised using a GeneGenius bioimaging system (SynGene, Synoptics Ltd, UK) and photographed using GeneSnap image acquisition software (SynGene, Synoptics Ltd, UK).

2.10 Laser Micro-Dissection method

2.10.1 Rationale

Different LMD protocols are available based on a variety of LMD platforms and for different applications on varying tissue types and biology. As there is limited experience of LMD on the atherosclerotic plaque and LMD has not yet been applied to the study of plaque rupture, an optimised or validated LMD protocol has not been established. I evaluated the manufacturer's RNA LMD protocols and identified its limitations. It was

necessary to optimise the protocol in its application to the atherosclerotic plaque and in particular to plaque rupture.

2.10.1 Original Leica LMD protocols

The original Leica LMD protocols had several recommended methods for the processing of snap-frozen specimens for LMD and RNA extraction and were evaluated using snap-frozen IMA specimens. Cryosections of 10μm thickness were mounted on RNase-free Leica PET-membrane slides with clear identification of the muscular medial layer without the need of staining. The initial LMD trials were performed without staining, eliminating the potential effects of staining on the degradation of RNA during these tests.

Leica no-fixation protocol

The cryosections on Leica PET-membrane slides were air-dried for 30 minutes in room temperature (no-fixation), then rehydrated in DEPC-treated ddH_2O for 3 minutes, stained with haematoxylin for 1 minute (omitted), washed in DEPC-ddH_20, and then thoroughly dried in a 37˚c oven for 30mins and then taken for LMD.

Leica 95% Ethanol fixation protocol

The cryosections on Leica PET-membrane slides were allowed to air-dry for 5-10 minutes in room temperature. They were then fixed in 95% Ethanol for 1 minute, then rehydrated in DEPC-ddH_2O for 3 minutes. Then they were stained in haematoxylin for 1 minute (omitted), washed in DEPC-ddH_2O for 1 minute, blued in Ammonia water 0.25%, washed in DEPC-ddH_2O for 1 minute, then stained with Eosin for 1 minute (omitted), washed in DEPC-ddH_2O for 1 minute, then dehydrated in increasing ethanol gradients of 75%, 95%, 100% and 100% for 30 seconds each, then cleared in xylene twice for 20 seconds each. The sections were allowed to air-dry and then taken to LMD.

Leica Acetone fixation protocol

The protocol was the same as the ethanol fixation protocol except that the cryosections on Leica PET-membrane slides were allowed to air-dry for 5-10 minutes in room temperature, then fixed in acetone for 5 minutes, then the acetone was air-dried off for 3 minutes, and then rehydrated in DEPC-ddH_2O for 3 minutes. The staining and dehydration steps were the same as the 95% Ethanol fixation method, and the slides were taken to LMD.

2.10.2 Optimisation of the LMD process

The original Leica LMD protocols did not work for our more fragile and fat/cholesterol rich sections resulting in severe histological artefact, section loss and failure to LMD. We systematically evaluated alternative methods of LMD section fixation, staining and processing to develop an optimised LMD protocol which was reproducible, reliable and robust. An overview of the various steps tested in the LMD protocol is shown in Figure 31.

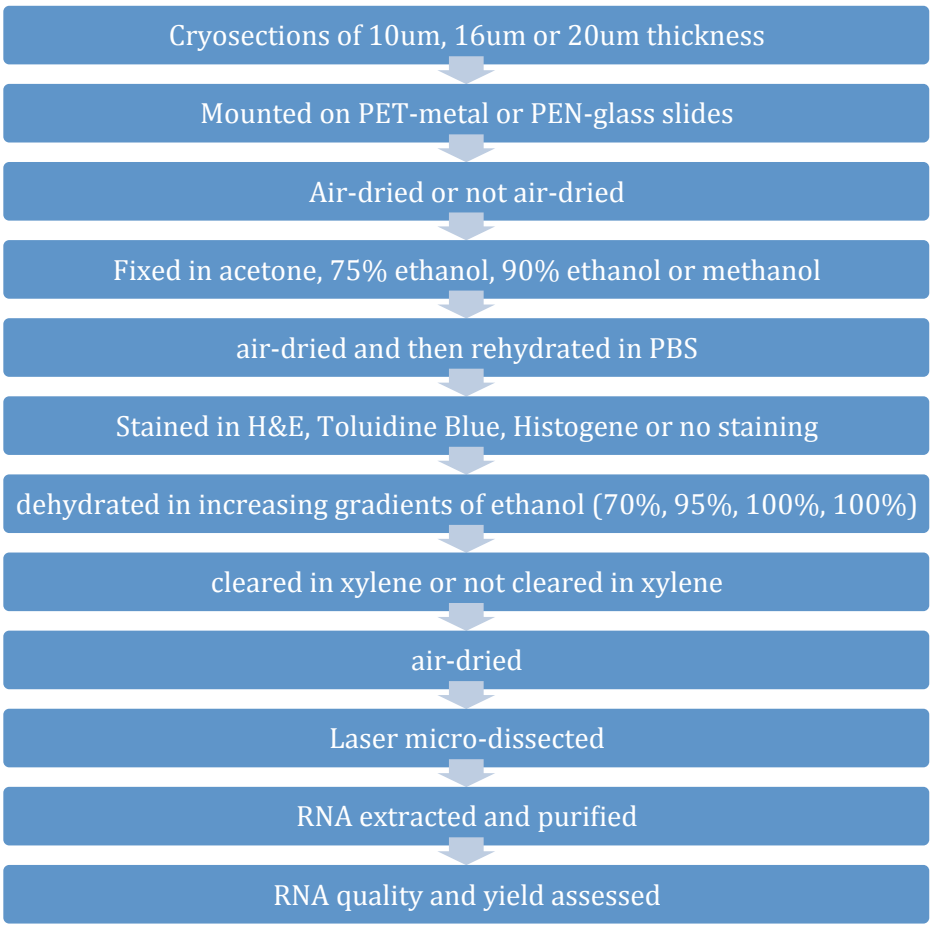

Figure 31. Overview of steps involved and optimised in snap-frozen specimen cryosectioning, fixation, staining, processing and LMD.

LMD cryosection thickness

Varying cryosection thickness of 8um, 10um, 16um and 20um may affect the adequate fixation, staining and LMD of the sections as well as RNA quality. This was evaluated.

LMD thermoplastic membrane slides

Two different types of LMD slides were in use at the time. Leica thermoplastic polyethylene naphthalate (PEN) membrane mounted on glass slides and Leica thermoplastic polyethylene terephthalate (PET) membrane mounted on metal frames, rendered RNase-free, were evaluated. The cryosections were mounted and melted on

using heat transference from the fingers and kept cool at -20˚C in the cryostat until all the sections required are mounted on the slide before fixation.

Rendering Leica Thermoplastic membrane slides RNase-free

The Leica thermoplastic membrane slides made of polyethylene naphthalate (PEN) mounted on glass slides or polyethylene terephthalate (PET) mounted on metal slides were pre-treated to render them RNase-free. They were immersed in RNase AWAY (VWR) in a 50ml falcon tube for 10seconds, then rinsed thoroughly in DEPC-ddH_2O in 50ml falcon tubes (3 changes, 3 minutes each), then oven dried in an RNase AWAY treated slide box. The slides were kept sealed in the slide boxes until needed. They were then UV irradiated (256nm wavelength) for 15 minutes prior to use.

Air-drying versus no drying

Air-drying the cryosections prior to fixation may help the samples to adhere to the membrane. However, air-drying freshly cryosectioned plaque in room temperature may expose the contents to endogenous RNases prior to fixation. We evaluated this.

LMD section fixation

The literature at the time showed success with various fixation techniques for RNA LMD work on other tissue types. This included fixation with 70% Ethanol, 90% Ethanol, Acetone, Acetone-Ethanol and Methanol[247]. RNA extraction of 3% paraformaldehyde (PFA) or 10% normal buffered formalin (NBF) fixed tissue or paraffin embedded tissue had demonstrated poor results in previous studies[247, 248]. We evaluated and assessed the optimal method of fixation and processing for our tissue using fixation methods of: 75% Ethanol for 1 minute, 90% Ethanol for 1 minute, Acetone for 1 minute then air-dried, or Methanol for 1 minute then air-dried. They were then rehydrated in PBS ready for staining.

LMD section histochemical staining

A variety of histochemical staining methods have been used and reported in the LMD of other different tissue types for RNA work[249]. Different histochemical stains were used for histological differentiation depending on the tissue studied. We evaluated the histochemical staining of our tissue by Haematoxylin and Eosin, Haematoxylin only, Toluidine Blue, HistoGene (Arcturus) and none.

LMD section dehydration and xylene clearance

The stained and washed sections were then taken through a series of increasing alcohol gradients (70%, 95%, 100%, 100%) for 30 seconds each. Thereafter we assessed if

clearance of bound water by immersion in xylene for 30 seconds was required or not. Following which, the slides were air-dried thoroughly and taken directly for LMD.

Laser Micro-Dissection

Small cellular regions of intima and media from the samples were laser micro-dissected using the Leica AS LMD platform using the x4 objective. A highly accurate confocal laser cuts the membrane around the region of interest and the inert membrane containing the selection of cells falls by electrostatic force into the collection cap directly under the membrane. Highly cellular regions were selected for this exercise and necrotic or acellular regions were avoided.

RNA extraction and evaluation outcomes

We assessed the LMD-prepared sections for tissue artefact and adherence, histological detail, quality and staining, and ease of laser micro-dissection. RNA was extracted using the optimised RNeasy Micro silica-based column extraction method with DNase-I treatment. The RNA quality and yield was assessed using the Agilent Bioanalyser PicoChip.

2.10.3 The optimal LMD protocol

I have developed a highly optimised and validated RNA LMD protocol as follows: The solutions for fixation and processing were prepared beforehand in 50ml RNase-free Falcon tubes held on a rack in a large ice box at 4˚C. General considerations for RNA work were applied. The -70˚C stored sealed LMD slide-mailers were thawed in a -20˚C cryostat (over 30 minutes). The LMD slides were removed from the sealed slide-mailers in a cryostat at -20°C in a frozen state.

The LMD slides were then thawed and processed serially one at a time. The LMD slide was thawed and air-dried in room temperature (RT) in a closed desiccant tray (RNase-free slide tray with silica gel desiccants) for 1 minute. This allowed thawing and air-drying without water condensation on the sections. Then fixed in 75% Ethanol in a 50ml falcon tube (which fits one slide at a time) on ice for 2 minutes, rehydrated and washed well (gentle dipping x5) in DEPC-water on ice for 30 seconds, stained with Haematoxylin solution in RT for 20 seconds, then washed well (gentle dipping x5) in DEPC-water on ice for 30 seconds, then into 0.5% Ammonia on ice for 10 seconds, and were next taken through a gradient of Ethanols at 75%, 95%, 100% on ice for 30 seconds each and finally in Ethanol 100% in RT for 1 min to ensure proper dehydration and clearing of water from the sections. Excess Ethanol was wiped off the slides using kimwipes and air-dried in a closed desiccant tray for 2 minutes. The slides were transferred and kept in a RNase-free

slide container without desiccants in RT and taken for LMD. The haematoxylin-stained LMD sections showed clear cellular and nuclear detail for the LMD of these regions performed using the Leica AS LMD platform on the x4 objective.

2.11 Validation of RNA stability and integrity from LMD

2.11.1 RNA stability during the LMD process

In order to validate the stability of the RNA of the processed sections for LMD, we extracted RNA from LMD of IMA and CEA specimens of fresh cryosectioned 'unprocessed' frozen tissue, optimised protocol processed LMDed sections performed without delay and optimised protocol processed LMD sections left at room temperature for 6 hours prior to LMD. RNA was extracted using the optimised RNeasy Micro method with DNase-I treatment and RNA yield and quality was assessed using the Agilent Bioanalyser PicoChip.

2.11.2 Integrity of the extracted RNA from LMD

The integrity of the extracted RNA from LMD was assessed by the reverse transcription of mRNA from its poly-A tail using oligo-dT primers followed by the PCR amplification of a region of the mRNA located 500 to 800bp from the 3' poly(A) tail. Degraded RNA would have fragmented mRNA and would not reverse transcribe past the region of truncation and would yield poor PCR products.

Design of GAPDH Primers

Primers specific to the GAPDH mRNA (Genbank: M33197 transcript) of 1268bp in length were designed for the middle portion of the mRNA at a region 692bp to 477bp from the 3' poly(A) tail, yielding a 216bp product. The forward primer was designed from the end of exon 7 to the beginning of exon 8, allowing the primer to be specific for mRNA and not DNA. Using the NCBI Basic Local Alignment Search Tool (BLAST), the primer sequences were specific to human GAPDH mRNA, producing a PCR product of 216bp. The primers were synthesised commercially by MWG.

GAPDH Forward Primer: 5'-GACTCATGACCACAGTCCATG-3'

GAPDH Reverse Primer: 5'-GGTCCACCACTGACACGTTG-3'

Reverse Transcription and PCR

The RNA was reverse transcribed into cDNA using Superscript III First-Strand synthesis system for RT-PCR kit, primed by oligo-d(T) according to the manufacturer's protocols. The optimal PCR conditions for the GAPDH primers were determined on HTO Control Human DNA using Taq polymerase (Bioline) 1 unit with 1x buffer, 0.2mM dNTP, 0.2mM Forward GAPDH primer, 0.2mM Reverse GAPDH primer, varying concentrations of $MgCl_2$ (1mM, 1.5mM and 2mM) in 20µL reactions under these conditions; initial denaturation at 95˚C for 5 minutes, then 35 PCR cycles of denaturation at 95˚C for 30 seconds, a gradient of annealing temperatures (from 50˚C to 70˚C) for 30 seconds, extending at 72˚C for 30 seconds, and upon completion to maintain at 4˚C. The best result was achieved at an annealing temperature of 62˚C with 2mM of $MgCl_2$ in the PCR reactions. The products were visualised by 1.5% agarose gel electrophoresis with ethidium bromide.

2.12 LMD cryosectioning & Scout section histopathological analysis

The selected stable and unstable specimens for gene expression profiling were processed for LMD to isolate cell-pure regions of macrophages and VSMCs. The cryosections were histopathologically analysed in advance to identify the regions of interest for LMD. In order to do this, a strategy of immunohistochemically stained scout sections at every 100µm intervals to identify cellularly pure regions of macrophages and VSMCs for LMD was devised.

2.12.1 Cryosectioning for LMD and scout sections

The cryosections for LMD were mounted onto the pre-cooled (-20˚C in the cryostat) and RNase-free rendered Leica LMD PET membrane slides (Optivision UK). The cryosections were melted onto the thermoplastic membrane using heat transference from the thumb. The mounted slides remained in the cryostat at -20˚C to -25˚C. The slides were stored in sealed pre-cooled RNase-free rendered ‘5-slide mailers’ (Lamb) at -70˚C until they were used for LMD.

At intervals of every 10 sections for LMD, 3 ‘scout’ cryosections were mounted onto charged glass slides (SuperFrost Plus, BDH) for histochemical and immunohistochemical staining.

2.12.2 Immunohistochemical staining of Scout sections

The Scout sections were immediately fixed in acetone for 1min, air-dried then stored in sealed '5-slide mailers' (Lamb) in a -20°C freezer until ready for ICC staining performed in batches. The slides were histochemically stained with H&E, and immunohistochemically stained for smooth muscle actin (SMA to identify the VSMCs) and CD68 (to identify macrophages).

2.12.3 Scout section histopathological analysis and identification of regions of interest for LMD

Detailed histopathological analyses of the scout cryosections were performed. The regions of interest were: 1) macrophages underlying the thick fibrous cap of the stable lesion, 2) macrophages underlying (and maybe infiltrating) the thin fibrous cap of the unstable lesion adjacent to the defect/rupture of the cap, 3) VSMCs of the thick fibrous cap of the stable lesion, 4) VSMCs of the thin fibrous cap of the unstable lesion adjacent to the defect/rupture of the cap. Care was taken to LMD macrophage regions of cell-enriched regions (and cell-pure whenever possible) of macrophages without infiltration of smooth muscle cell or other inflammatory cell types. The converse was also true for the VSMCs; the LMD of cell-enriched and whenever possible cell-pure regions of VSMCs without infiltration of macrophage or other inflammatory cell types.

2.13 RNA amplification and Microarray

The LMD of 10,000 cells would typically yield about 20ng of total-RNA from VSMCs and about 40ng from macrophages. These amounts were not sufficient for hybridisation to a microarray which requires several micrograms of RNA. The linear amplification of RNA was necessary to generate larger amounts of RNA for use in microarray experiments whilst preserving the relative transcript abundance for transcriptomic profiling.

2.13.1 RNA amplification

We used the Affymetrix GeneChip® Two Cycle Target Labelling and Control Reagents Kit with the recommended modifications to the protocol for smaller starting amounts for RNA amplification developed by Affymetrix in the GeneChip® Eukaryotic Small Sample Target Labelling Assay Version II[250] (Figure 32). This validated and optimised protocol was designed to linearly amplify limited and small amounts of starting material of 10 to 100ng (typical yields from LMD) using a T7-oligo-dT primed RNA polymerase in-vitro

transcription (IVT) developed from the original Eberwine method[221]. Comprehensive Quality Control Assessment (QCA) measures were built into the system to maintain and ensure a high quality, robust and reproducible experimental result was generated for each sample.

Starting amounts of 15ng to 60ng of total RNA of high quality and of a concentration of >5ng/μL was used. The Affymetrix Poly-A Amplification Controls were added with the starting material at the beginning. The protocol is summarised in Figure 32. The first strand cDNA synthesis was performed using the T7 Oligo dT primer and SuperScript II reverse transcriptase, and the second strand cDNA was synthesised using DNA polymerase I. The generated double-stranded cDNA was incubated with Ambion's MEGAscript T7 RNA polymerase for 16 hours for the first cycle of in-vitro-transcription amplification. The generated cRNA was purified using RNeasy Mini columns (Qiagen). The purified cRNA was eluted in 13μL of RNase-free water which we modified to generate higher concentrations of eluted cRNA in a smaller eluting volume in order to use almost all the generated first cycle cRNA for the second cycle of IVT. Furthermore we needed only 1-2μL of cRNA for quantitation analysis using the Fluoroskan Ascent microplate fluorometer (Thermo Scientific) and the NanoDrop 3000 (Thermo Scientific).

All of the remaining purified cRNA of about 9μL in volume was used for the second cycle IVT reactions. The first strand cDNA was synthesised using random primers and SuperScript II, followed by second strand cDNA synthesis with the T7 Oligo Promoter Primer and DNA polymerase I. The double-stranded DNA was cleaned up by ethanol precipitation, and then incubated using the ENZO BioArray HighYield RNA Transcript Labelling Kit for the second cycle of IVT amplification using the T7 RNA polymerase with biotin-labelled ribonucleotides. The generated cRNA was purified using the RNeasy Mini columns and eluted in 30ul of RNase-free water. The cRNA was quantified using the Fluoroskan Ascent microplate fluorometer and NanoDrop ND-3000 to assess if a sufficient final amount was generated for microarray.

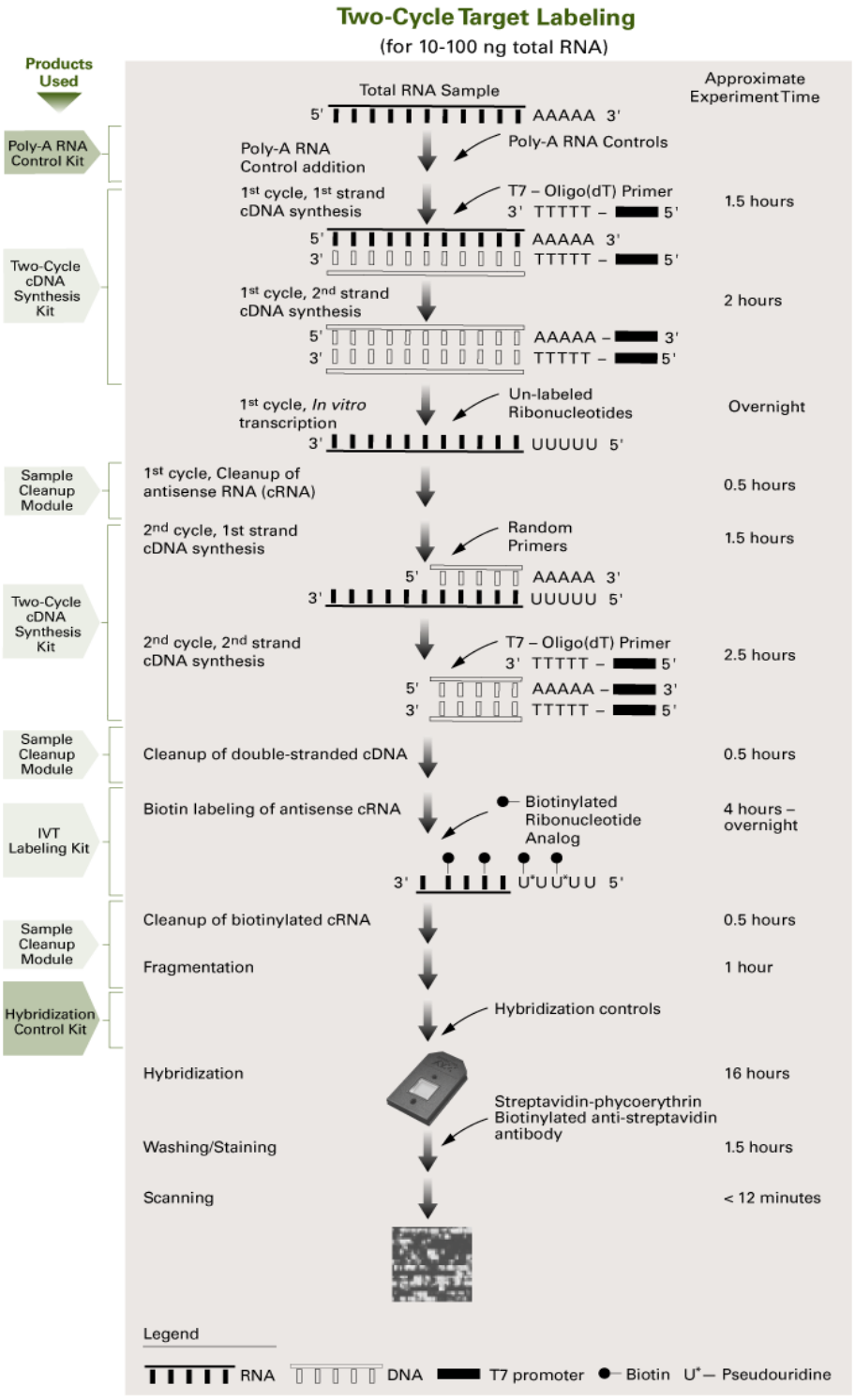

Figure 32. Schematic representation of the 2-cycle linear amplification reaction with generation of biotin-labelled amplified cRNA, followed by its fragmentation, hybridisation to the array, then the washing, staining and scanning of the microarray. (Figure from Affymetrix:Technote[250])

2.13.2 Linear amplification 3' bias and Affymetrix microarray design

The 2-cycle IVT linear amplification generates amplified cRNA products of shorter length than the whole mRNA transcript with a 3' bias due to the oligo-dT priming in the 1st IVT amplification cycle and the random priming in the 2nd cycle[218, 250]. As a result, high 3'/5' ratios are typical of 2 cycle IVT amplifications. The Affymetrix microarrays were designed to address this inherent 3' bias of linear amplification and have their probesets designed within 600bp of the 3' end of the transcripts to minimise this effect. However, the linear amplification reactions are sensitive to mild to moderate degrees of RNA degradation, as truncated mRNA transcripts will not successfully amplify or worse, are amplified with a significant 3' bias with an inaccurate representation of transcript abundance. As a result, only high quality RNA was used for linear amplification to generate enough cRNA for hybridisation to microarrays, defined by 28S/18S ratios of ≥1.6 with a clean baseline on the Bioanalyser electropherogram profile, which is equivalent to a RIN value of >6 representing intact RNA.

2.13.3 Microarray hybridization

The cRNA was fragmented and hybridised to the microarray using the manufacturer's standard protocol[251]. Twenty micrograms of biotin labelled cRNA from each sample was fragmented. One microlitre aliquots of unpurified cRNA and purified cRNA and 2µL of fragmented cRNA were run on a 1.5% agarose gel electrophoresis with a 100bp ladder to confirm the purification and fragmentation of the cRNA into 35-200nt fragments. The fragmented labelled cRNA and the Hybridisation Controls were added into the Eukaryotic Hybridisation Cocktail and then incubated onto the array. The hybridised array was then washed and stained with streptavidin-phycoerythrin on the automated GeneChip® Fluidics Station 450 using the manufacturer's set washing protocols optimised specifically to the different types of arrays. The robotic Fluidic Station ensured a high degree of reproducibility between the arrays. The washed and stained arrays were then scanned on the Affymetrix 3000 GeneChip® Scanner using the GeneChip® Operating System (GCOS) generating raw gene expression data.

2.13.4 Affymetrix Test3 microarray

Five microliters of fragmented labelled cRNA was hybridised to the Affymetrix Test3 array (Test Chip). The Test Chip contained probesets which assessed sample quality and amplification performance as well as array performance and hybridisation kinetics

(including the washing and staining of the array) and were part of the QCA measures of performance and quality.

2.13.5 Affymetrix HG-U133 plus 2.0 GeneChip microarray

Only cRNA with satisfactory QCA measures was then hybridised to the Affymetrix HG-U133 plus 2.0 GeneChip genome-wide microarray. This ensured a high quality microarray experiment was performed and generated reliable, reproducible results. The Affymetrix Human Genome U133 Plus 2.0 Array is a single microarray containing over 1,300,000 unique oligonucleotide features (probesets) covering over 47,000 transcripts and variants of well characterised human genes. This is a comprehensive representation of the human transcriptome and enabled the genome-wide interrogation of expression analysis in one experiment.

2.14 Microarray data analysis

2.14.1 Microarray data analysis software

Dataset generation, reporting and analysis software

The microarray GeneChip processed and unprocessed (raw) signal intensity results and quality control measures were reported using the Affymetrix GeneChip Operating System (GCOS) software version 1.3 (Affymetrix, USA) for analysis. The datasets were imported into GeneSpring (version 7.3.1), an advanced visualisation and analysis software for genomic expression data by Silicon Genetics (Agilent Technologies, USA) for further analyses.

Importing datasets and meta-data

Meta-data of the samples consisting of the clinical data of clinical, radiological and histological analyses, and the laboratory data of LMD, RNA and array variables were also imported into GeneSpring for multivariate analyses and the subsequent reporting of the microarray data. The meta-data was compliant to the 'Minimum Information About a Microarray Experiment' (MIAME) standards of microarray data reporting[252].

Genome build and annotation

The Affymetrix HG-U133 plus 2.0 pre-annotated genome probeset template was used and the probeset gene annotations were updated using the GenBank gene identifiers from the EntrezGene, Unigene and GenBank databases of the National Institute of Health's (NIH)

National Centre for Biotechnology Information (NCBI) using the GeneSpider data-mining program on GeneSpring

2.14.2 Affymetrix probeset design and transcript present/absent detection

The Affymetrix GeneChip oligonucleotide array is a single channel (one colour) signal array. The signal strength of each probe spot was represented by a numerical value. The Affymetrix probes occur in pairs; as perfect match (PM) and mismatch (MM) probe-pairs. The mismatch probe had a single nucleotide mismatch in its 25-nucleotide oligomer probe to detect the presence/absence of gene expression and in the estimation of background noise. Each transcript probeset was made of 11 probe-pairs, with over 54,000 probesets in the Affymetrix HG-U133plus 2.0 array, resulting in over 1,300,000 raw signal data which require processing and analysis from each GeneChip array[253, 254].

We used the Affymetrix detection algorithm to assign a Present, Marginal or Absent call in the detection each probeset [251, 255]. As a result, the GeneChip arrays were able to have highly specific transcript detection with high detection sensitivity and were able to detect transcript abundances as low as 1:100,000[253, 254].

2.14.3 Background correction, signal quantification, probeset summarisation and normalisation

The correction for background noise, accurate signal quantification and summarisation of each probeset (from the 11 probe-pairs) and correction for systematic experimental variation between arrays (by array normalisation) were necessary for accurate and reliable comparative gene expression analyses. Although various methods were available there was no consensus agreement as to which optimal. Therefore I performed a comparative assessment of the various methods on our datasets. The methods evaluated were:

Affymetrix GCOS determined probeset signal intensity and normalisation

These were the default algorithms of signal quantification and background correction designed by Affymetrix and built into the GeneChip Operating System (GCOS). In Essentially, each probe-pair signal was corrected for background noise and the probeset signal was determined by the biweight means of the 11 probe-pairs using the One-Step Tukey's Biweight Estimate which yields a reproducible weighted mean which was insensitive to outliers[255]. The GCOS determined probeset signal intensities were $\log_2$ transformed and global median array normalisation was performed by dividing the log

transformed probeset signal values by the median (50th percentile) probeset signal value of each array on GeneSpring[256, 257] which produces a normalisation of similar medians across the arrays.

RMA determined probe-set signal intensity and normalisation

The Robust Multi-array Average (RMA) method was motivated following detailed modelling of the array kinetics of the Affymetrix GeneChip with improvements in background correction, normalisation and probeset summarisation to calculate a more accurate and precise signal intensity[258] and was performed on GeneSpring[257]. In summary, a non-linear and modelled background correction was performed, then the individual probe-pair background corrected signal intensities were normalised using quantile normalisation[259] resulting with the global signal values of each array to have a similar distribution of median and inter-quartile ranges whilst preserving individual probe relative transcript abundance and rank within each array. Finally the signal intensities of the probesets were derived from the 11 probes using median polishing, a robust model fitting technique that protects against outlier probes[259].

GC-RMA determined probe-set signal intensity and normalisation

The GC-RMA (Robust Multi-array Average with GC-content background correction) was the result of further optimisation of the model of GeneChip array kinetics. It shared identical quantile normalisation and median polishing of probeset summarisation as in RMA. However, the probe-level signal intensity estimation and background correction was more accurately determined by modelled nucleotide binding affinity based on probe sequence information (based on hybridisation theory predicting stronger hybridisation of G/C pairs due to its three hydrogen bonds compared to the A/T pair which formed two. In contrast, the U and C labelled bases in the amplified cRNA were observed to impede binding)[260-262]. This was performed on GeneSpring[257].

Descriptive statistics

Exploratory descriptive statistical methods were used to examine the distribution, variance, and linearity of the gene expression data in evaluation of the effects of probe-level processing (background correction, quantification and summarisation) and global normalisation on the data.

Box-plots: medians and distribution of global array signal intensities

The distribution and variation of the data before and after normalisation were assessed using inter-quartile box-plots[256-258]. This enabled the graphical assessment of per-chip

global normalisation on the uniformity of the median and the distribution of signal intensities of the arrays in the experiment.

MA-plots: linearity and variance of normalised log ratios

The log ratio of relative abundance as described earlier (M, on the y-axis, the $\log_2$ of the ratio of the probeset signal intensity divided by its median) was plotted against the probeset intensity of averaged abundance (A, on the x-axis, the mean of the probeset signal values across the arrays in the experiment) in a scatter plot called the MA plot[256-258]. The MA-plots revealed the intensity dependency of the log ratios, its distribution of variance and the linearity of the log ratios.

2.14.4 Macrophage Expression Profile Correlation

To explore the relationship between the expression profiles of our data and from other human tissue and cell types we obtained whole genome profiles using Affymetrix arrays from the NCBI Gene Expression Omnibus (GEO) repository (www.ncbi.nlm.nih.gov/geo/). These included data from a panel of 79 different cell and tissue types[263] (n=158), from adipocytes[264] (n=24) and from 4 separate macrophage experiments[265-268] (n=106). Exploratory and unsupervised cluster analyses were performed and the relationships were visualised by Condition Tree clustering (using Spearman correlation as the similarity measure and confidence levels were assessed using 100 bootstraps), and Principal Component Analysis (PCA) .

A list of genes differentially expressed during macrophage activation by chemokines (CCL2 and CXCL1), low density lipoprotein (LDL, oxLDL and mmLDL) as well as by a combination of CXCL4 with oxLDL was obtained from the paper by Cho et al (3815 genes)[265]. The expression profiles of the micro-dissected specimens for this subset of genes were compared with those repository samples of blood cell origin[263] as well as activated and unactivated macrophages[265-268] to explore the relationship of our samples to these cell sub-types.

2.14.5 Unsupervised exploratory clustering

The similarity (and dis-similarity/separation) of the samples due to their gene expression profiles were assessed using 2 different methods; condition tree dendrograms and principal components analysis on GeneSpring[256, 257]. Entire array datasets were used without any pre-filtering of the probesets and were therefore performed without supervision. This allows the observation for any clustering of the samples as a result of differences in their gene expression profiles without prior classification of the samples.

The spontaneous clustering seen may be analysed for correlation to the disease phenotype studied (ruptured vs stable plaques) or other potential confounding biological factors or technical variations.

Principal components analysis

PCA allows the reduction of the complexity of the genome-wide transcriptomic dataset of all the samples by identifying a number of principal components which define most of the variability in the data. Although PCA does not ignore covariances and correlations, it concentrates on variances in the variables to maximally separate the samples [257, 269]. It uses similarity measures (by standard correlation) to compare the transcript signal intensities (as expression vectors) to the 3 major principal components which caused most of the variation seen between the samples (as weighted vectors). The samples are plotted to the 3 major principal components in the x, y and z-axes. This facilitated the observation of similarity and dissimilarity between the samples based on their gene expression profiles in 3-dimensional gene expression space.

Condition tree dendrograms

Using a different method to PCA, the condition tree dendrograms (CTD) uses similarity measures (by Pearson or Spearman correlation) comparing the transcript signal intensities between the samples in a step-wise manner, clustering samples of similar gene expression profiles into branches and organises them into mock phylogenetic trees.

The classification of organisms into phylogenetic trees is a central concept in biology. Organisms sharing similar properties were clustered together and the location of the branch demonstrated how similar the organisms were. This concept was applied in microarray analysis in the classification of conditions (i.e. each sample was a yet unclassified condition), and these mock phylogenetic trees were referred to as condition trees[256, 257].

The condition tree dendrograms of all the samples were performed by measures of similarity of the normalised probeset signal intensity values using Pearson and Spearman correlation. The condition tree was determined from the calculation of the correlation of each condition/sample with every other sample being analysed. The samples of highest correlation were paired and the probeset expression values were averaged. The correlation of this new composite gene expression profile was then calculated to the other samples and the process was repeated until all the samples have been paired[257]. The distance of the branches reflect the similarity of the pairs to each other and the clustering of the samples by these similarity measures were visualised in the condition tree dendrogram.

Outlier samples and sample QC

These descriptive statistical measures and exploratory cluster analysis were also used to identify significant outlier samples for further examination, exclusion or reconciliation These measures were part of the microarray sample QC process.

2.14.6 Statistical analysis

Probeset pre-filtering

Prior to comparative statistical analysis of the 2 groups, probesets of genes which were not expressed and Affymetrix control genes were removed from analysis. Their inclusion in the analysis would contribute to the error of multiple testing. This included the probesets which were flagged Absent using the Affymetrix present/marginal/absent call algorithm and the non-human Affymetrix spiked-in control probesets (n=62). The stringency/leniency of the overall proportion of absent called probesets were examined.

Comparison/Inference Statistics and Multiple Test Error

The inferential statistical analysis was performed on GeneSpring. The pre-filtered probesets were analysed using a 1-way ANOVA parametric test with the assumption of equal variances of log-expression ratios in both groups. Multiple test correction was performed using the Benjamini and Hochberg method with a false discovery rate of 10% which was appropriate for the purposes of gene discovery. Ranked gene lists based on degree of differential expression measured in the ratio of fold change were made.

Power Calculations

With respect to power calculations, the number of replicates necessary to achieve specified power in microarray experiments was relatively little explored in the statistical literature. The methods that have been suggested require data regarding the between-sample variability in expression of particular genes [270-273]. The between-sample variability would be higher in human samples in comparison to in-bred animal samples. The number of replicates required also depends on the desired fold change cut-off, the percentage power of detection and the chosen type 1 error rate of significance (p-value). Wei and colleagues have calculated from gene expression data in human specimens that 5 biological replicates would have 90% power to detect genes with four-fold expression differences with a type 1 error rate of 0.01[270]. Thus, five replicates seemed statistically reasonable and was comparable with the numbers studied in previous publications in atherosclerosis[186-189, 200, 216].

2.14.7 Data-mining and Annotation of the Genelist

The gene annotations which were previously updated using the GenBank gene identifiers from the EntrezGene, Unigene and GenBank databases using GeneSpider in GeneSpring (described in chapter 2.14.1) were also checked using the Affymetrix NetAffx™ Analysis Centre, a web-based data-mining portal (www.affymetrix.com/analysis/index.affx), using the Affymetrix probeset IDs to confirm the probeset gene identities.

Further details of the individual genes were manually mined by web-links to Entrez Gene, GeneCards, Ensembl, OMIM and PubMed from GeneSpring. Comparisons to publicly available expression data were performed in GeneSpring by web-links to databases in GEO (Gene Expression Omnibus) at NCBI and ArrayExpress at EBI, to observe the expression of the gene of interest in similar tissue, cell type or disease process.

2.14.8 Functional bioinformatic analysis

Complex bioinformatic analyses were performed using cluster, classification and genome ontology approaches. Bioinformatic analyses according to gene networks and pathways were also performed. Significant genes, networks and pathways were identified for further testing.

The BiNGO plug-in (Biological Network Gene Ontology tool) for the open-source Java platform Cytoscape[274] was used to identify significantly over-represented Gene Ontology Biological Processes among the differentially expressed genes. Unique Locuslink (LOC) identifiers of the genes were mapped to the GO database in BiNGO. The significance of over-representation was calculated using the hypergeometric test with Benjamini and Hochberg's multiple testing correction at a false discovery rate of 10%. Biological processes represented by ≤3 genes were excluded.

We used WebGestalt[275] (WEB-based Gene SeT AnaLysis Toolkit) to identify among the pathways in the Kyoto Encyclopaedia of Genes and Genomes (KEGG) database those that were significantly over-represented among the set of differentially expressed genes. Unique EntrezGene identifiers of the genes were mapped to the KEGG database using WebGestalt. The significance of over-representation was calculated using the hypergeometric test. Pathways containing ≤3 genes were excluded.

2.15 Real-time PCR quantitation of target genes

The microarray findings were the result of multiple stages of sample and RNA handling, amplification and microarray data manipulation. The appropriate validation of these findings was important in the confirmation of my results. This was performed using quantitative real-time PCR (qRTPCR), a highly sensitive and accurate method of quantifying transcript abundance. However, as very small amounts of starting material from LMD was used, our starting amounts of total-RNA in each qRTPCR reaction were in picograms and not nanograms. This required some evaluation and optimisation. Following optimisation, the validation of differentially expressed genes was carried out in two stages. I first performed the technical validation of the microarray data by the qRTPCR gene expression quantitation of the 12 statistically significant genes of highest fold-difference from the unamplified RNA of the 11 LMD CEA samples in the microarray experiment. Second, I replicated the findings of the microarray experiment (biological validation) in a larger number of stable and unstable ruptured plaques to a total number of 25 samples. This involved the identification of additional stable and unstable carotid samples identified using the 3-domain enrichment criteria, LMD and RNA extraction, and the measurement of gene expression using qRTPCR.

2.15.1 Preliminary methodological optimisation

Evaluation of reverse transcription method- priming and RT enzymes

The reverse transcription (RT) step must produce cDNA of high yield and quality to generate the maximal amount of starting material for qRTPCR. We evaluated RT primed by oligo-dT (dT) or random hexamer (rH). We also evaluated 4 different RT enzymes; SuperScript III RT from Invitrogen, Sensiscript RT from Qiagen, cDNA archive kit RT from Applied Biosystems and ImProm-2 RT from Promega, using the manufacturer's standard protocols. One nanogram of total-RNA isolated from HeLa cell culture (Invitrogen), LMDed internal mammary artery (IMA) VSMCs and LMDed carotid endarterectomy (CEA) plaque macrophage cells were used for RT. Reactions with no RNA template and no RT enzyme were used as negative controls. 'Housekeeping' genes were quantified using Qiagen's QuantiTect GlobeGene Primer Assays. High expression transcripts of GAPDH (Hs_GAPDH_1_SG), and of low expression MYST2 (Hs_MYST2_1_SG) were quantified from very small amounts of cDNA template (generated from 100pg and 10pg of total-RNA) by qRTPCR using SYBR-green (Qiagen QuantiTect) and performed on the ABI 7900HT platform using 20µl reaction volumes in 384 well plates and in duplicates, performed according to the manufacturers' protocols. The qRTPCR protocol was as follows: HotStarTaq activation at 95°C for 15mins, PCR cycles of 94°C denaturation for

15s, 55°C annealing for 30s, 72°C extension for 30s for up to 55cycles, then dissociation-melting curve analysis of 95°C for 30s, 60°C for 30s with slow ramp to 95°C at 2C/s, then the products were held at 4°C. PCR products were also checked by 1.5% agarose gel electrophoresis with a 50bp DNA ladder.

Evaluation of qRTPCR method- different chemistries

Three qRTPCR chemistries were evaluated for high reproducibility, accuracy and sensitivity in the detection of low abundance transcripts. We evaluated the Platinum qPCR Master Mix by Invitrogen with Taqman Validated Primer and FAM-Probes, the Taqman Universal PCR Master Mix by Applied Biosystems with Taqman Validated Primer and Fam-Probes and the SYBR-green Quantitect Master Mix by Qiagen with Qiagen Globegene Validated Primers. cDNA was generated from random hexamer primed SuperScript III reverse transcribed RNA from HeLa cell culture and LMDed macrophages from the carotid plaque. High expression GAPDH and low expression MYST2 'housekeeping' genes were quantified in a dilution series and performed in quadruplicate on the ABI 7900HT platform using 20µl reaction volumes in 384 well plates. The Qiagen QuantiTect qRTPCR chemistry using Qiagen's GlobeGene primers was described earlier. The Invitrogen Platinum and ABI Taqman qRTPCR chemistries were performed according to the manufacturers' instructions using Taqman Primer-Probes for GAPDH (HS00266705_g1) and MYST2 (HS00272972_m1) from Applied Biosystems using the qPCR protocol as follows: UNG enzyme incubation for 50°C for 2mins, Taq polymerase enzyme activation at 95°C for 10mins, PCR cycles of 95°C denaturation for 15s then 60°C annealing/extension for 1min for up to 45 PCR cycles, and held at 4°C.

Evaluation of the use of carrier RNA

I evaluated the utility of carrier RNA in the qRTPCR of small amounts of RNA/DNA in its potential benefit in reduction of non-specific adhesion to plastics and degradation by nucleases. I used low adhesion plastics to minimise this effect but carrier RNA may have additional benefit. Furthermore DNA and RNA at low concentrations are vulnerable to nucleases. The nuclease catalysed degradation of target transcripts may be reduced by competition of the carrier RNA for these nucleases.

Poly-A carrier RNA (Qiagen, UK) was added into the mastermix to achieve a final concentration of 1ng/µl in a final qRTPCR reaction volume of 20µl per well. Quantitative real time PCR by Taqman qPCR using 5 Taqman Primer-Probes for LEP, ASPN, ECM2, PDGFD and FCGR3AB (details in Table 2) of dilution series of total-RNA from IMA tissue was performed with and without the use of carrier RNA in triplicate. I assessed whether the use of carrier RNA had any observable benefit in the reduction of the variability of the

replicates and the precision of measurement to the regression line especially at low template concentrations.

Taqman primer and probe design and selection

The Taqman primers and probes were selected from pre-designed, optimised and validated Taqman probe and primer sets (based on 5' nuclease chemistry) from the Taqman Gene Expression Assays library (Applied Biosystems). The criteria for selection were that the primer-probe sets were manufacturer validated and designed to anneal to sequences in exons on both sides of an intron and the amplified regions spanned exon/exon boundaries of the mRNA transcript. This enabled the selection of highly specific primer-probe sets of high qRTPCR efficiency which also differentiated between mRNA and potential contaminating genomic DNA. The primer-probe sets selected are listed in Table 2.

Gene Symbol	Gene Name	EntrezGene ID	Taqman Probe ID
PPIA	Peptydylprolyl Isomerase A (Cyclophillin A)	5478	HS99999904_m1
SDHA	Succinate Dehydrogenase Complex Subunit A	6389	HS00188166_m1
GAPDH	Glyceraldehyde 3-phosphate dehydrogenase	2597	HS00266705_g1
MYST2	MYST histone acetyltransferase 2	11143	HS00272972_m1
GUSB	Glucuronidase, beta	2990	HS99999908_m1
TBP	TATA box binding protein	6908	HS00427620_m1
TUBB	Tubulin, beta polypeptide	203068	HS00742828_s1
FABP4	Fatty Acid Binding Protein 4	2167	HS00609791_m1
PPBP	Pro-Platelet Binding Protein 4	5473	HS00234077_m1
PACAP	Pro-Apoptotic Caspase Adaptor Protein	51237	HS00414907_m1
FCGR3AB	Fc Fragment of IgG, low affinity IIIA & IIIB Receptor (CD16a&b)	2214/2215	HS00275547_m1
LEP	Leptin	3952	HS00174877_m1
CD38	CD38 antigen (p45)	952	HS00277045_m1
PDGFD	Platelet Derived Growth Factor D	80310	HS00228671_m1
ECM2	Extracellular Matrix Protein 2	1842	HS00154821_m1
RGS5	Regulation of G-Protein Signalling 5	8490	HS00186212_m1
OGN	Osteoglycin	4969	HS00247901_m1
SFRP2	Secreted Frizzled-Related Protein 2	6423	HS00293258_m1
ASPN	Asporin	54829	HS00214395_m1

Table 2. Taqman Gene Expression Assay Probeset details.

Evaluation of primer-probe qRTPCR efficiency

An assessment of the efficiencies of qRTPCR of the individual primer-probe sets were performed using standard curves of a dilution series of template cDNA from the RT of total-RNA of LMDed IMA VSMCs and performed in triplicate. By incorporating qRTPCR efficiency corrections, a more accurate qRTPCR quantitation of transcript abundance was possible.

Assessment of minimal detection threshold

In order to validate the confidence in the quantitation of low abundance transcripts especially from very small starting amounts of total RNA, we performed qRTPCR using further dilution series of template cDNA from IMA VSMCs, down to very small amounts of 2pg equivalent of total RNA in triplicate to determine the minimum detectable threshold. This was defined as the highest mean Ct with a low variance (triplicate Ct range ≤1) and was within 0.5 Ct from the regression line.

Optimised Taqman qRTPCR experimental protocol

Real-time quantitative PCR was performed on the Taqman ABI7900HT platform using 384 well plates. A total reaction volume of 20ul per well was used. This comprised of 1µl of Primer (x20 concentration), 10µl of Taqman Universal PCR Master Mix (x2 concentration) and 9µl aliquot of diluted sample cDNA equivalent to 500pg of starting total-RNA. The Taqman Gene Expression Assay Probesets used is shown in Table 2. The diluted sample cDNA was made of reverse transcribed sample cDNA diluted in RNase-free water (Qiagen) with 20ng of poly(A) RNA (final concentration of 1ng/µl in each qRTPCR reaction, from Qiagen) as carrier nucleic acid. Samples were run in triplicate. Negative template controls were run on every plate. Reference cDNA from IMA VSMC samples were run on every plate to assess inter-plate variability and for inter-plate calibration. The PCR conditions were as follows: initial UNG activation for 50°C for 2mins, AmpliTaq activation at 95°C for 10mins, PCR cycles of 95°C denaturation for 15s then 60°C annealing/extension for 1min for up to 45 PCR cycles, and held at 4°C on completion.

2.15.2 Reference gene selection and assessment

The relative quantitation (RQ) of transcript abundance is performed by the quantitation of target gene transcript abundance to a reference 'housekeeping' control gene which is universally expressed by the tissue/cell type in a constant and unchanging fashion. This allows the accurate quantitation of transcript abundance to an internal control. However, non-changing reference genes vary depending on the tissue or cell type as well as the biology or disease state in question. Previously used unvalidated reference control genes

may have been unreliably used nor can they be universally applied from another tissue/cell type or disease state[276]. To address this, we selected a panel of stable non-changing candidate control genes from the microarray experiment and evaluated them further to identify the most stable reference control genes specific to my study; in plaque macrophages and in the stable/ruptured plaque.

A compilation of 115 potential reference control genes was made from the Affymetrix 100 endogenous control genes mask (www.affymetrix.com/analysis/index.affx) and from well known commercially available control genes from Qiagen GeneGlobe and Taqman Primer-Probes which were represented on the HG-U133plus2 microarray. The top 7 genes that demonstrated the least variability in the GCRMA normalised microarray data were selected for further testing by qRTPCR.

In order to identify the most stable reference control genes in our study population we used the method described by Vandesompele et al using the geNorm analysis software[276]. In summary, the expression stability was evaluated and a gene-stability measure (M) based on the average pairwise variation between a particular gene and all the other genes studied was generated. High expression stability is indicated by a low M value as an estimate of combined variation of the individual gene.

2.15.3 Analysis of qRTPCR data, efficiency correction, normalisation and calibration

The Ct values were calculated using the ABI Prism 7900HT Sequence Detection System (SDS) Software 2.2 with the Ct threshold set at 0.20 and automatic baseline detection. The Ct values were exported into QBase version 1.3.4 for analysis[277]. QBase is a program written in Visual Basic for Applications (VBA) code in Microsoft Excel for the management and automated analysis of real-time quantitative PCR data which allowed for the accurate quantitation of transcript abundance by employing a delta-Ct relative quantitation model (RQ) with PCR efficiency correction and multiple reference gene normalisation and inter-plate calibration. The PCR efficiencies were calculated using the SDS 2.2 software from standard curves determined from serial dilutions of template cDNA. We used PPIA and SDHA as our 2 reference control genes which we had validated earlier.

2.15.4 Quantitative real-time PCR - Technical validation of microarray findings

The unamplified total-RNA from the LMD of plaque macrophages from the 11 samples used originally for the microarray experiment was reverse transcribed to cDNA by rH

primers using SS3 RT (Invitrogen). The quantitation of transcript abundance by qRTPCR was performed using the Taqman primer-probes and qRTPCR chemistry (Applied Biosystems) on the ABI7900HT platform using optimisations of carrier RNA, amplification efficiency correction, multiple reference gene normalisation and inter-plate calibration and performed in triplicate. The log-transformed qRTPCR results and the microarray GCRMA normalised results were compared and the linear correlation was determined by the Pearson correlation coefficient.

2.15.5 Increasing the sample size - Biological validation by qRTPCR

Sample selection

Our findings were then biologically cross-validated by real-time PCR for the same 12 genes that had been the subject of the technical validation. A total of 25 samples (13 stable and 12 unstable) were studied. Eleven samples had been processed and studied in the microarray experiment. A further 14 samples (7 stable and 7 ruptured samples) were identified by the enrichment criteria in the 3 domains.

Laser micro-dissection and RNA isolation

These samples were cryosectioned, immunostained and histologically analysed for LMD. The plaque macrophages were LMDed, RNA was isolated and its quantity and quality assessed using the Agilent Bioanalyser 2100. At this point in time, the bioanalyser software had been updated to incorporate a RNA Integrity Number (RIN) in RNA quality assessment (RIN of 6 to 10 - intact RNA, 3-6 partially degraded RNA, <3 severely degraded RNA[246]). The details of the additional 14 samples processed were shown in Table 3.

Three samples had degraded total RNA with RIN values of 2.9 to 3.3. The other 10 samples had good RNA quality and one with mild degradation. The 3 samples with degraded RNA profiles would previously not have passed quality measures for oligo-dT primed RNA polymerase amplification. However, as my qRTPCR assays were random hexamer primed and the PCR products were short (100bp) and very specific (using Taqman Primer-Probes and designed to span inter-exonic regions), they were not prone to failure of quantitation typically seen in oligo(dT) primed qRTPCR as a result of mRNA transcript degradation and truncation near the poly(A) tail. I was still able to accurately quantify transcript abundance in the presence of mild to moderate RNA degradation and demonstrated successful qRTPCR reactions with expected Ct measurements with

minimal variability of the replicates and were similar to the other samples of good RNA quality (shown in Table 4).

Sample	Histology	RNA quality	RIN	No of cells LMDed	RNA isolated (ng)
CEA22	RupTFCA	Good quality	6.8	15000	117.4
CEA23	RupTFCA	Good quality	6.8	10500	87.7
CEA113	RupTFCA	Good quality	7.2	3000	15.5
CEA68	RupTFCA	Mod-Severe degradation	2.9	9500	190.8
CEA42	RupTFCA	Good quality	6.3	7500	59.3
CEA114	RupTFCA	Mild degradation	4.5	5500	38.1
CEA107	RupTFCA	Good quality	5.9	13600	551
CEA64	StableFCL	Good quality	5.8	10200	98.7
CEA92	StableFCL	Good quality	5.8	8500	49.1
CEA88	StableFCA	Mod-Severe degradation	3.3	11500	87.1
CEA112	StableFCA	Mod-Severe degradation	3.3	20200	74.6
CEA44	StableFCA	Good quality	5.6	12000	235.3
CEA117	StableFCA	Good quality	6.8	2600	27.2
CEA84	StableFCA	Good quality	6.5	1860	10.1

Table 3. The 14 CEA samples LMDed and RNA extracted for further study.

		PPIA		SDHA	
Sample	RNA RIN	mean Ct	SD	mean Ct	SD
CEA 68	2.9	28.4	0.04	33.2	0.17
CEA 88	3.3	28.5	0.03	33.2	0.16
CEA 112	3.3	28.3	0.04	33.2	0.09
CEA 114	4.5	28.7	0.01	33.5	0.02
CEA 64	5.8	28.9	0.04	34.4	0.14
CEA 23	6.8	28.6	0.07	33.4	0.13

Table 4. Quantitative RTPCR results of the samples with degraded RNA (CEA68, 88 and 112), mild degradation of RNA (CEA114) and samples with good quality RNA (CEA64 and 22), demonstrating the tolerance of our qRTPCR assay to RNA degradation. The variance of the replicates is quantified by the standard deviation (SD).

Relative quantitation analysis and cluster analysis

The gene expression was analysed on unamplified RNA using the Taqman platform. The results from all the 25 samples were then analysed for differences in gene expression between stable and ruptured plaque macrophages using ANOVA. A two-tailed p-value <0.05 was accepted as significant. This larger sample group twelve-gene expression profile was then mapped to 3-dimensional gene expression space using Principal Components Analysis on GeneSpring to demonstrate the relative separation (and clustering) of the samples.

2.16 Immunohistochemistry of target proteins

The protein products of Leptin and FABP4 of the PPAR-Adipocytokine signalling pathway were then studied by immunohistochemistry to confirm the differential protein expression and their spatial distribution in the atherosclerotic plaque. Preliminary optimisation work was necessary to develop the IHC staining protocols of the antibodies to these proteins on the snap-frozen acetone-fixed and paraffin-embedded formalin-fixed sections of atherosclerotic plaque.

2.16.1 Immunohistochemistry optimisation work

Tissue selection, sectioning and processing

FFPE and snap-frozen specimens of atherosclerotic plaques were used for the optimisation work. Small bowel intestinal tissue and breast adenocarcinoma FFPE specimens were used as positive control tissues for Leptin and FABP4. Lung tissue FFPE specimens were used as negative control tissues. Microtome sections of 5μm thickness were made from the FFPE specimens and cryosections of 10μm thickness were made from the snap-frozen specimens and processed as previously described for IHC. The sections were H&E and immuno-stained using antibodies to FABP4 and Leptin.

FABP4 and Leptin antibodies tested

Commercially available and previously reported antibodies to FABP4 and Leptin proteins were used[278, 279]. Two rabbit polyclonal antibodies to FABP4 (Abcam, ab13979 and ab75808) and another two antibodies to Leptin; a mouse monoclonal antibody from Abcam (ab20115) and a rabbit polyclonal antibody from Santa Cruz (A20:sc842) were evaluated.

Antigen retrieval methods evaluated

Various antigen retrieval methods were evaluated to expose the protein epitopes masked by the tissue fixation process from FFPE sections. Heat induced epitope recovery (HIER) methods by microwave oven, pressure cooker or heated water bath, and enzyme digestion epitope recovery methods by trypsin digestion using conventional protocols[280] were evaluated. FFPE sections with no pre-treatment were used as baseline controls. The snap-frozen sections did not require pre-treatment.

Microwave oven: The deparaffinised and rehydrated slides were immersed in citrate buffer solution pH6 in a plastic coplin jar and heated in a microwave oven (850w) at full power for 5 minutes for 2 cycles. The solution was kept topped up. The slides were then

allowed to cool down to room temperature[280]. The Dako Target Retrieval Solution (cat#1699) at pH 9.8 was also tested.

Pressure cooker: The slides were immersed in citrate buffer solution pH6 in a pressure cooker and heated until maximum pressure and maintained at full pressure for 1 to 3 minutes and were then allowed to cool down to room temperature[280]. An alternative EDTA buffer solution at pH 8 was also tested.

Heated water bath: The slides were immersed in citrate buffer solution pH 6 in a water bath at 95°C for 5 minutes for 2 cycles. The solution was kept topped up and not allowed to boil. They were then allowed to cool down in the buffer to room temperature[280, 281].

Tripsin digestion: The sections were covered with Trypsin 0.05% in calcium chloride 0.1% at pH 7.8 and incubated at room temperature for 10 minutes[280].

Antibody dilution and incubation optimisation and immunohistochemical staining

The FFPE processed sections and the snap-frozen acetone-fixed sections were processed for immunohistochemistry using the Vectastain Elite Avidin-Biotin-Complex Antibody Kit (Vector Labs) , visualised using DAB and counterstained with haematoxylin. The antibody dilutions and incubation times were also optimised to yield the best signal to background staining.

2.16.2 Immunohistochemical work of atherosclerotic plaques

Snap-frozen and FFPE samples of stable and ruptured atherosclerotic plaques were processed. The sections were immunohistochemically stained in sequential order for H&E, SMA, Leptin, CD68, Leptin, CD68, FABP4, CD68, FABP4, and the last serial section as a negative ICC control (no primary antibody applied), using the optimised antigen retrieval and antibody incubation protocols developed followed by the standard immunohistochemistry protocol using the Vectastain Elite kit, visualised using DAB and counterstained with haematoxylin. Small bowel intestinal and breast adenocarcinoma FFPE tissue sections were used as positive control tissues. Lung FFPE tissue sections were used as negative control tissues.

Leptin optimised ICC protocol

FFPE sections: Leptin antibody, sc842, with a 95C water bath for 5 minutes of 2 cycles using a Citrate buffer pH6 with an antibody dilution of 1/75 for 1 hour incubation at room temperature.

Frozen sections: Leptin antibody, ab20115 at 1/2000 dilution for 1 hour incubation at room temperature.

FABP4 optimised ICC protocol

FFPE sections: FABP4 antibody, ab13979, with the pressure cooker method at 1 minute maximum pressure using a Citrate buffer pH6 with an antibody dilution of 1/500 for 1 hour incubation at room temperature.

Frozen sections: FABP4 antibody ab75808 at 1/100 dilution for 1 hour incubation at room temperature.

2.16.3 Semi-quantitative immunohistochemical analysis

Digitised images of FFPE immunostained sections processed as described above were captured (though a x5 and x20 objective) using a Zeiss Axiovision system. Macrophage cells were identified using CD68 immunostaining. The signal intensities of SMA, CD68, FABP4 and Leptin were semi-quantitatively estimated by observer ranking of signal intensity to a reference template; a value of 0 for no detectable staining, 1 for weak staining, 2 for moderate staining and 3 for heavy/strong staining. The regions analysed included the macrophages under the thin fibrous caps of ruptured TFCA lesions and under the thick fibrous caps of stable FCA/FCL plaques as well as the macrophages in the base of the lipid cores in these lesions. Differences in protein expression were determined using ANOVA. A two-tailed p-value of <0.05 was accepted as significant.

2.16.4 Quantitative immunohistochemical analysis

The digitised images of the FFPE immunostained sections were analysed using Image-Pro Plus (v6, Media Cybernetics, UK). Macrophage cells were identified using CD68 immunostaining and a template mask of CD68 positive regions was created and used for the detection of FABP4 and Leptin signal intensity in these regions in the adjacent serial sections. Duplicate slides were performed for each antibody. Negative control slides were used for background signal correction. CD68 was used as the reference control protein and assumed to be of constant and uniform expression in the macrophages throughout the specimens. FABP4 to CD68 and Leptin to CD68 signal intensity ratios were generated and compared in the macrophages under the thinned fibrous cap and at the base of the lipid core of ruptured TFCA plaques, and analysed for differences in protein expression using ANOVA. A two-tailed p-value <0.05 was accepted as significant.

2.17 Optical Projection Tomography of the atherosclerotic plaque

2.17.1 Rationale and introduction

In addition to the quantitative characterisation of gene expression within plaques, spatial descriptions of gene expression in stable and unstable lesions could contribute significantly to our understanding of plaque instability. Hitherto, three dimensional reconstruction of gene expression in vascular tissue has been difficult to undertake accurately. I have demonstrated the complexity of the atherosclerotic plaque in its heterogenous constitution of various cell-types as well as multiple lesion types in overlay. Novel technology using optical projection tomography allows us to demonstrate gene expression of several genes onto a scaffold of the complex atherosclerotic plaque in three dimensional space[223-225].

Optical projection tomography (OPT) is a rapid, non-destructive optical microscopy technique which can produce high-resolution 3-dimensional images of whole fixed, intact and unstained biological specimens with a thickness of up to 15mm[224, 225]. Subsequent histological studies as well as gene and protein expression studies can be performed. The anatomical, structural and gene/protein expression features can then be mapped to the 3D digital OPT model and then viewed and analysed in 3D and in any plane or projection. It has been successfully used to study 3D gene expression in complex biological tissues like the developing brain of the human embryo[223] and an example illustrating this is shown in Figure 33. It has not yet been applied to the study of adult vascular tissue or the complex atherosclerotic plaque.

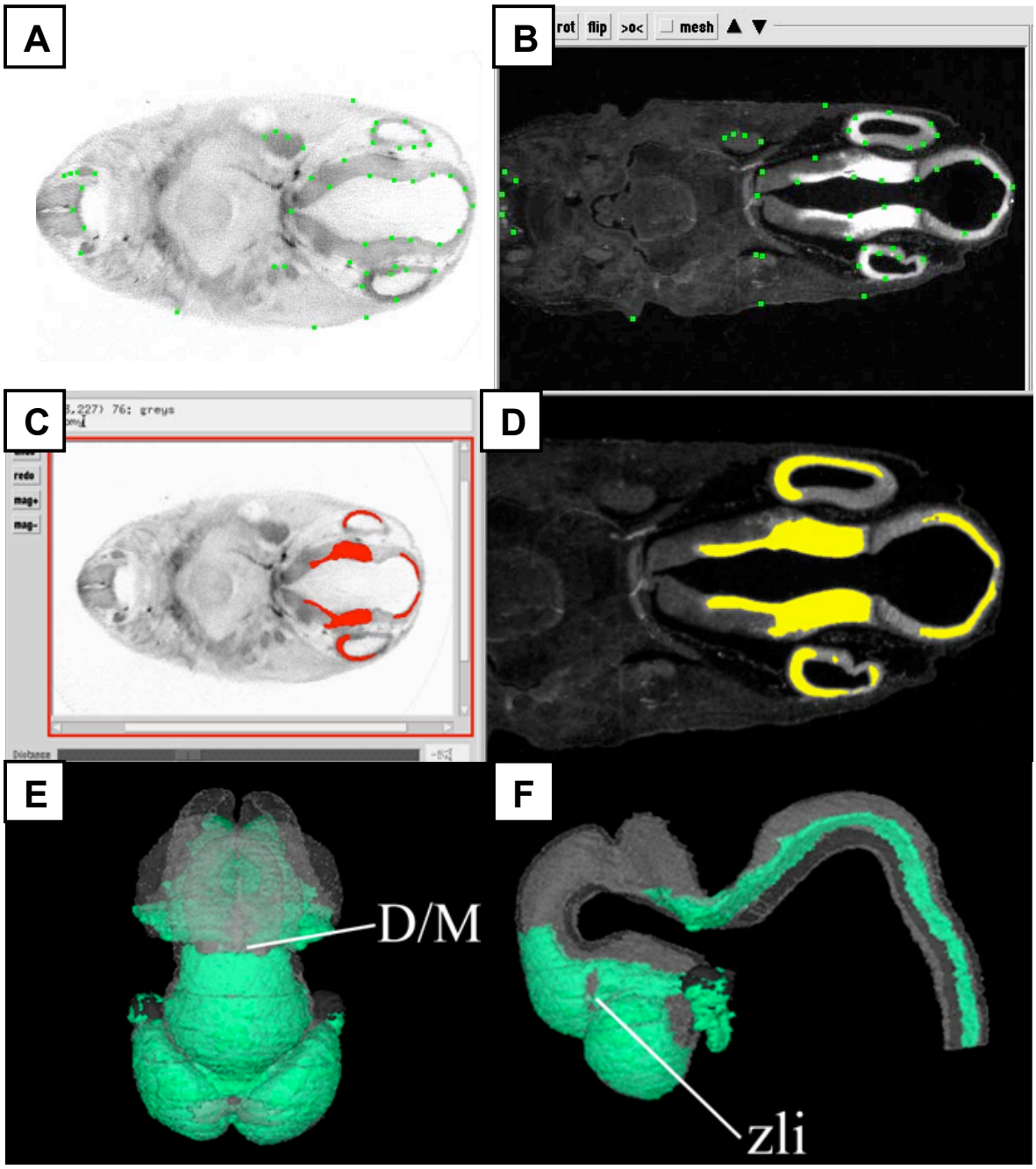

Figure 33. An example of 3D gene expression mapping of PAX6 in a developing embryonic human brain using optical projection tomography. Tissue In-Situ Hybridisation (TISH) section data to the OPT model are shown (panels A to D). The digitised TISH section (A) was transformed to the equivalent section in the OPT model (B). The thresholded gene expression signal (C) was mapped onto the OPT section (D) using the same transformation. Panel E and F shows a surface rendered model of the 3D expression pattern of PAX6 (in green) in frontal and lateral views. In these 2 views, separate gene expression domains in the forebrain and hindbrain were seen. For reference the neural tube has been rendered dark pale grey and the eye dark grey. The absence of PAX6 expression in the diencephalons/midbrain (D/M) boundary, in the zona limitans intrathalamica (zli), the forebrain alar-basal boundary and the striatopallidal boundary in the basal telencaphalon were seen by viewing the 3D model at various angles which were not appreciated in the standard 2D TISH sections. An mpeg movie of the PAX6 expression domain is demonstrated on the enclosed CD as **Movie1**. (Pictures and movie courtesy of Susan Lindsay, Human Development Group, Institute of Human Genetics, Newcastle-upon-Tyne.)

2.17.2 The OPT protocol for vascular and atherosclerotic tissue

Specimen fixation and decalcification

I have performed the preliminary work to establish the protocols for OPT analysis of normal vascular tissue and on diseased calcified atherosclerotic tissue. The whole undissected specimen is fixed in fresh 4% paraformaldehyde in DEPC-treated phosphate buffered saline (PBS) for 12 to 16 hours. The specimen is then immersed in 50mls of neutral ethylene-diamine-tetra-acetic acid (EDTA) decalcifying solution in a falcon tube with gentle agitation on a shaker over 1 week at room temperature, changing the solution twice each day. The EDTA decalcifying solution is prepared as so: add 62.5g of EDTA to 437.5mls of DEPC-H_2O (the solution is cloudy) and add 6.25g of NaOH pellets to neutralise to a pH of 7 (solution will become clear).

OPT

After a week of decalcification, the sample is washed in DEPC-treated PBS and then embedded in 1% low melting point agarose, dehydrated in a graded series of methanol and cleared using a mixture of benzyl alcohol and benzyl benzoate (1:2 part BABB mixture, which renders the agarose and sample transparent).

The transparent specimen is then scanned on the OPT microscope platform by rotating the specimen, supported in a transparent cylinder of agarose gel, through 360 degrees in angular steps of 0.9 degrees around a single axis while holding it in position for imaging. A digital image of the static specimen is taken at each of the 400 rotated positions. Images are obtained by detecting the paraformaldehyde-fixed specimen's autofluorescence using a wideband fluorescin isothiocyanate (FITC) filter with excitation at 465-500nm and emission from 515-560nm. The images were then assembled to recreate the 3D shape of the specimen using modified back-projection tomography algorithms, and high-resolution digital representations of physical microtome sections through the specimen in any plane can be produced[225].

Post-OPT processing, histology and expression studies

After OPT scanning the sample was rehydrated in a decreasing graded series of methanol and then removed from the agarose block by incubation in 0.29M sucrose solution at 55°C. The sample was then processed for paraffin wax embedding and 5µm microtome sections were cut. The serial sections were mounted on separate Histobond glass slides such that every 20th section was mounted together in series on the same glass slide (Figure 34). This strategy allowed me to perform up to 20 separate histochemical,

immunohistochemical protein expression or in-situ hybridisation gene expression studies at regular 100μm intervals throughout the entire specimen.

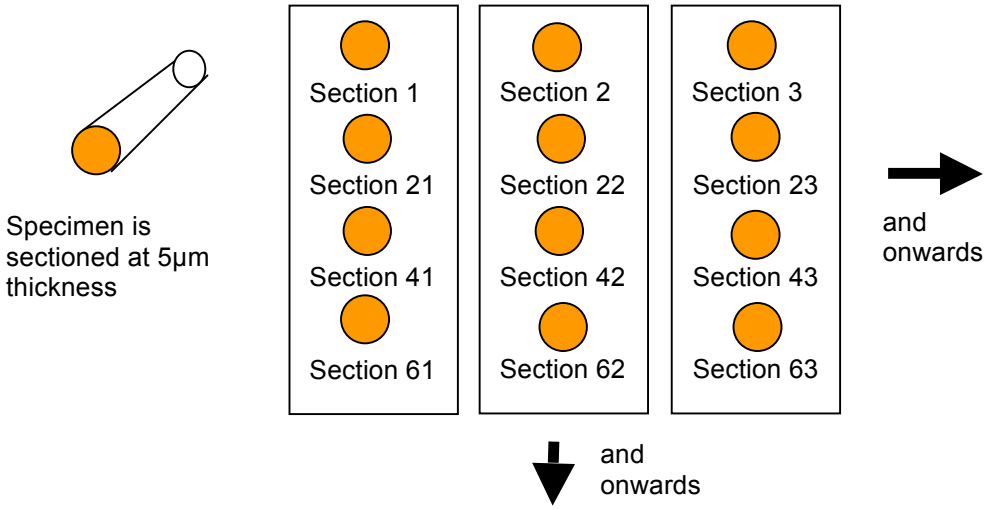

Figure 34. Method for mounting sections on slides for histochemistry, immunohistochemistry or in-situ hybridisation staining for OPT.

Histology, protein and gene expression mapping

Images of histological, protein or gene expression stained sections were captured through a x2.5 objective using the Zeiss Axiovision system. A modified warping interface of the MAPaint software[223, 224], was used to match each stained, physical section to the corresponding digital OPT section. Correspondences between the physical (source) section and the digital (target) images were identified and manually tie-pointed, which enabled the source image to be transformed into the shape of the target section, and the image transformation saved. The interface uses interactive thresholding to extract the expression signal from the source image and then applies the image transformation to map this signal into the space of the 3D OPT model. This was carried out for the sections through the entire specimen until the full 3D expression pattern was built up for the specimen.

Chapter 3. The clinical and pathological characterisation of patients

3.1 Overview

In order to study the differences in gene expression between stable and vulnerable advanced atherosclerotic plaques, we need to be able to identify these lesions accurately and reliably, whilst preserving the in-vivo transcriptomic expression and RNA quality in the cells. We collected human carotid atheromatous plaques at the time of the patient's endarterectomy surgery with immediate processing and snap-freezing of the samples. Detailed clinical information was collected as well as radiological investigations and histopathological analyses of the lesions. The samples were fully characterised and information from all three clinical, radiological and histopathological domains were analysed and compared, and then used in the identification and selection of stable and vulnerable plaques for gene expression studies.

3.2 Patient recruitment and Sample collection

3.2.1 Samples from patients during Carotid Endarterectomy Surgery

Over a three year period, patients undergoing elective carotid endarterectomy surgery were invited to participate in the Carotid Atherosclerosis Gene Expression (CAGE) study. A total of 118 atherosclerotic CEA specimens were collected from 118 CEA operations of 110 patients; 8 had bilateral carotid endarterectomies performed at separate admissions during this time period and both endarterectomies were collected. All the patients had complete clinical, radiological and histological workup and the samples were fully characterised.

Of the 118 CEA samples, 4 samples were used entirely for Optical Projection Tomography work and the remaining 114 samples were processed for LMD, microarray and gene expression work. The samples were snap-frozen in the surgical theatres with a mean total ischaemic time of 15 minutes (95%CI of 13.5-16.5 minutes). The total ischaemic time was calculated from the clamping of the carotid artery to the snap-freezing of the specimen in isopentane-liquid nitrogen bath. All 114 samples were successfully extracted, dissected into 5mm portions and snap-frozen.

3.2.2 Samples from patients during Coronary Artery Bypass Surgery

A total of 13 normal internal mammary arteries and 3 normal radial arteries were collected from 13 patients undergoing coronary artery bypass graft surgery. Two internal mammary arteries and 1 radial artery were used for Optical Projection Tomography work, and the remaining 11 internal mammary and 2 radial arteries were snap frozen and used as normal artery controls for LMD gene expression work.

3.3 Clinical Data

3.3.1 Clinical symptoms

Clinical data were collected for all the 118 specimens. Seventy four samples were from patients with previous symptoms of TIAs or CVAs of the territory supplied by the carotid artery which was operated on (ipsilateral symptoms). Forty one samples were from patients without any symptoms at all referable to the territory supplied by the carotid artery which was operated on (true asymptomatics). Three samples were from patients with ambiguous clinical histories who were deemed clinically 'unclassified'. Of the 74 samples from patients with previous symptoms, 39 had symptoms within 6 months (recent symptomatics) and 35 had their last symptom more than 6 months prior to surgery (late symptomatics) (see Figure 35).

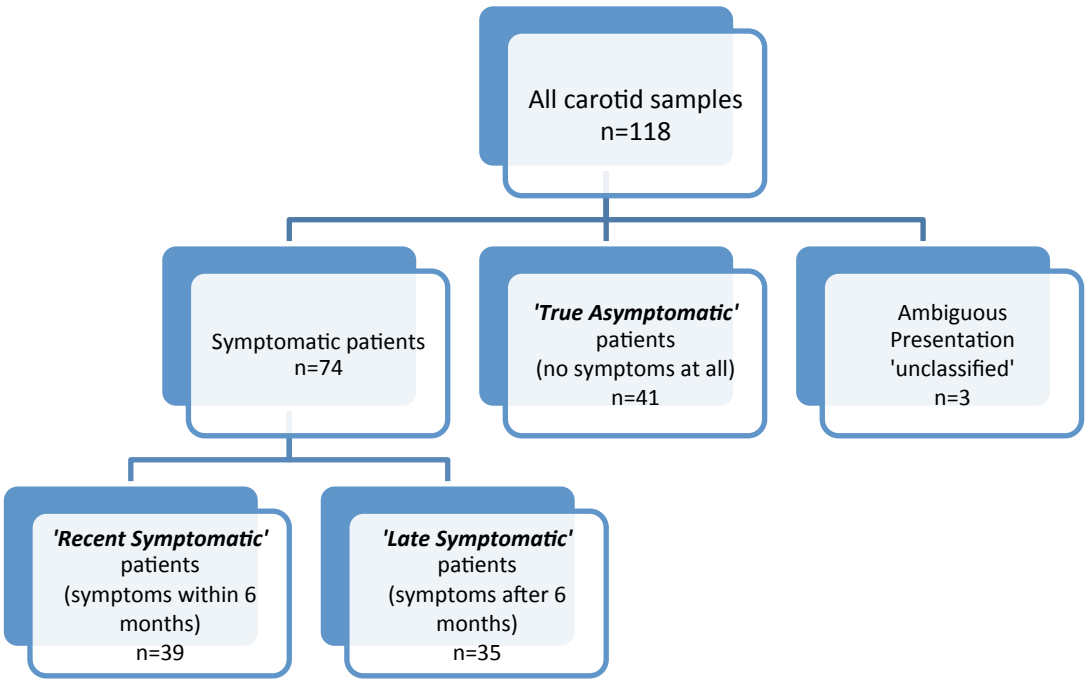

Figure 35. Flowchart of Carotid endarterectomy specimens collected from clinically symptomatic and asymptomatic patients.

Of the symptomatic patients, the 'recent symptomatics' presented early and had their CEA surgery at a median time of 60 days from their TIA or stroke. In comparison, the 'late symptomatics' had a median time of 1 year from their last TIA or stroke. They were older (69.6 years compared to 65.5 years, p=0.05) and suffered more strokes than TIAs alone compared to the 'recent symptomatics' (60% strokes compared to 36% strokes, p=0.002) (see Table 5).

More than half (53%) of all the symptomatic patients had their CEA surgery within 6 months from their last ischaemic event (Figure 36). Nearly a third (32%) received their CEA surgery within 3 months and would have gained the most significant benefit from CEA surgery[230]. The patients with previous ischaemic symptoms of 6 months and more (47%) were referred and accepted for CEA as 'asymptomatic' patients, according to the criteria established by ACST/ACAS.

Bin	*Frequency*	*Cumulative %*
30	13	17.57%
60	7	27.03%
90	4	32.43%
120	6	40.54%
150	5	47.30%
180	4	52.70%
210	7	62.16%
240	2	64.86%
270	4	70.27%
300	3	74.32%
330	1	75.68%
360	4	81.08%
390	0	81.08%
420	0	81.08%
450	1	82.43%
480	0	82.43%
510	0	82.43%
540	0	82.43%
570	1	83.78%
600	1	85.14%
More	11	100.00%

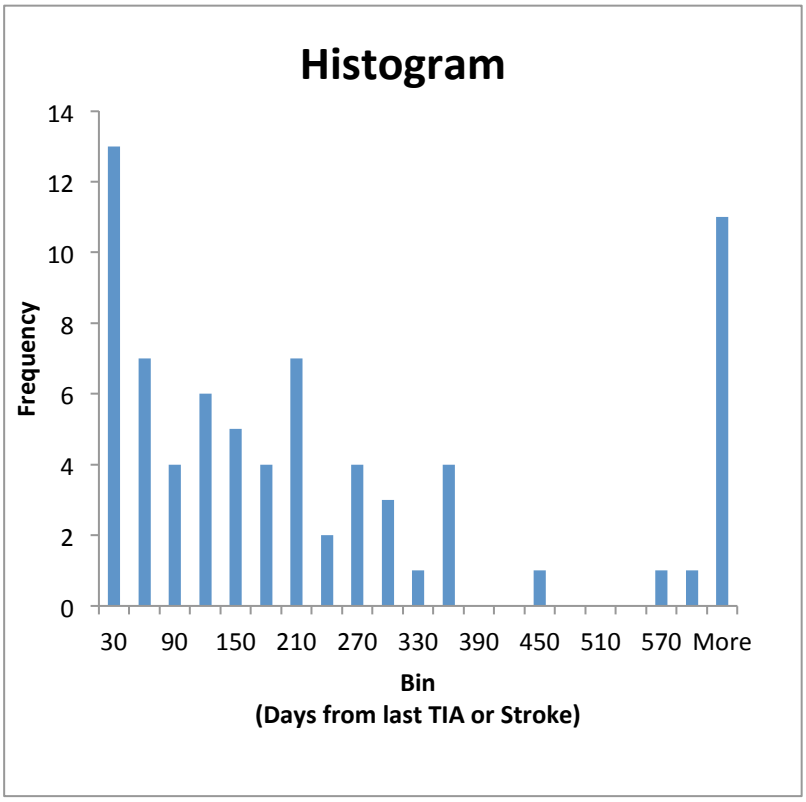

Figure 36. Histogram of all the symptomatic patients distributed according to the time of their last event of TIA or stroke prior to surgery (in 30 day bins).

In the group of 41 'true asymptomatic' patients, about half were discovered following investigation and treatment for symptoms of TIAs or stroke in the territories supplied by the contralateral carotid or vertebro-basilar arteries. Five had bilateral severe stenoses and had already received endarterectomy surgery of the symptomatic side, 4 had occluded carotid disease of the symptomatic side (and were thus without an indication for

CEA surgery of the symptomatic side) and the remaining 11 had mild stenotic lesions of the carotid artery (<50%) of the symptomatic side and not indicated for symptomatic CEA surgery. The other half of 'true asymptomatic' patients were incidental diagnoses of asymptomatic severe carotid stenoses following auscultation of a carotid bruit on medical examination (n=17), during investigative work-up for coronary artery bypass surgery (n=3) and vascular imaging for a cerebral haemorrhage (n=1).

3.3.2 Demographics

There was an equal spread of patients in the 3 clinical groups (Table 5). The mean age of all patients receiving carotid endarterectomy surgery was 67.7 years (95% CI: 65.4 to 69.5 years). There were no significant differences in sex or body mass index (BMI = weight(in kg) / height(in m)^2) between the two symptomatic and asymptomatic groups. The mean BMI for all CEA patients was 26.9 which was in the WHO overweight category. However, the late symptomatic patients were significantly older (by 4.1 years) and were more likely to have had a CVA compared to the recent symptomatic patients who were more likely to have TIAs. A possible explanation is that increased age and presentation with stroke rather than TIA may have led to a delayed referral for carotid endarterectomy surgery. This may be due to the patient requiring a longer recovery period after their stroke, indecision about surgery or an initial preference for conservative medical management.

3.3.3 Vascular Risk Factor Profile

A large majority of all CEA patients were previous or current smokers (73%). A large proportion of patients were still smoking at the time of their CEA surgery (31%). The other 2 major risk factors observed were hypertension (84%) and hypercholesterolaemia (86%). Forty one percent of patients had concurrent coronary artery disease, 9% had peripheral artery disease but we did not have any patients with severe renal impairment (creatinine >200 µmol/L or on regular haemodialysis). Twenty seven percent had a positive family history of premature coronary artery or cerebrovascular disease (events in 1st degree family members, <55 years in men, <60 years in women) and 23% had diabetes mellitus. There were no significant differences seen in any of the risk factors across the 3 clinical groups.

	Recent Symptomatics (last symptom within 6 months)	Late Symptomatics (last symptom after 6 months)	True Asymptomatics (no symptoms at all)	p-val
Total number	39	35	41	
Age (mean, 95%CI)	65.5 (62.4-68.6)	69.6 (67.1-72.1)	68.1 (66.0-70.3)	0.05
Sex (M/F in %)	M(59%), F(41%)	M(46%), F(54%)	M(63%), F(37%)	ns
Height (in m) (mean,95%CI)	1.68 (1.64-1.71)	1.63 (1.60-1.67)	1.67 (1.64-1.70)	ns
Weight (in kg) (mean, 95%CI)	75.4 (69.0-81.9)	72.0 (67.6-76.5)	73.5 (69.3-77.6)	ns
BMI (mean, 95%CI)	26.9 (24.7-29.2)	26.9 (25.6-28.2)	26.1 (25.1-27.1)	ns
Symptoms:				
LastSymp (median in days)	60	360	0	
TIAs only (n,%)	25 (64%)	14 (40%)	0	0.0381
CVAs (n,%)	14 (36%)	21 (60%)	0	
Other Territory TIAs or CVAs (n,%)	6 (15%)	10 (29%)	21 (51%)	0.002
Risk Factor Profile:				
Smoking - never	18.4%	24.2%	29.3%	
- ex	44.7%	45.5%	39.0%	ns
- current	36.8%	30.3%	31.7%	
FHx of premCAD/CVD	37.8%	26.5%	17.5%	ns
Diabetes	20.5%	30.3%	21.1%	ns
Treated HTN	82.1%	88.6%	85.4%	ns
Treated Hypercholesterolaemia	89.7%	80.0%	87.8%	ns
Renal Failure, Cr>200	0.0%	0.0%	0.0%	ns
AF or pAF	0.0%	5.7%	5% (n=2)	ns
Ischaemic Heart Disease	43.6%	28.6%	48.8%	ns
Peripheral Vascular Disease	0.0%	8.6%	19.5%	ns
Medication:				
Antiplatelets - Aspirin	87.2%	88.6%	85.0%	ns
- Dipyridamole	25.6%	37.1%	25.0%	ns
- Clopidogrel	25.6%	14.3%	7.5% (n=3)	ns
Warfarin	2.6% (n=1)	0.0%	2.5% (n=1)	ns
Statin treatment	86.8%	77.1%	87.8%	ns
ACEi/ARB	66.7%	68.6%	62.5%	ns
Diuretic	30.8%	40.0%	25.0%	ns
Bblocker	23.1%	31.4%	42.5%	ns
CCB	25.6%	42.9%	35.0%	ns
Other antianginal	15.4%	14.3%	30.0%	ns
Other Antihypertensive	2.6%	5.7%	2.5%	ns
Metformin	12.8%	8.6%	12.5%	ns
Other oral hypoglycaemic	2.6%	20.0%	10.0%	ns
Insulin	5.1%	2.9%	0.0%	ns
Lab and bedside investigations:				
Haemoglobin (g/dL)	13.6 (13.2-14.1)	13.2 (12.8-13.6)	13.7 (13.2-14.2)	ns
Creatinine (µmol/L)	105.8 (96.6-115.0)	104.1 (97.1-111.1)	97.1 (92.3-101.8)	ns
Random blood glucose (mmol/L)	6.5 (5.8-7.2)	6.9 (5.9-8.0)	6.0(5.5-6.5)	ns
Random cholesterol (mmol/L)	5.00 (4.50-5.51)	4.87 (4.54-5.20)	4.55 (4.24-4.86)	ns
BP (systole) (mmHg)	44 (137-152)	144 (138-150)	141 (134-148)	ns
BP (diastole) (mmHg)	76 (73-79)	75 (72-78)	77 (73-80)	ns
Rhythm on ECG	SR (100%)	SR (100%)	SR(95%) AF(n=1),Paced(n=1)	ns

Table 5. CEA specimens in their clinical groups with clinical and demographic data, risk factor profile, medication, blood pressure, ECG and laboratory results (Demographic data, blood results and blood pressure presented as the mean value with 95% CI in parentheses).

3.4 Radiological Data

3.4.1 Carotid plaque surface morphology and stenosis severity

The 118 endarterectomy operations were performed on 110 patients (8 patients had bilateral CEA surgery during this study and had the same radiological imaging study). There were carotid angiography data of both carotids available from all 110 patients for the assessment of carotid lesion stenosis severity and surface morphology (surface irregularity). A total of 220 carotid artery angiograms were available for analysis. Almost all of the carotid angiograms were performed by MR angiography (96 patients). However 10 patients had CT angiography and 4 patients had catheter angiography with digital subtraction due to limited/poor imaging results with initial MR angiography requiring an alternative imaging modality or due to patient preference or inability to tolerate the MR head scan because of claustrophobia.

From the 220 carotid artery angiograms, 120 had a smooth luminal surface, 29 had evidence of a mild plaque surface irregularity (depression defect of luminal surface of more than 1mm but less than 2mm in depth), and 62 had evidence of a significant plaque surface irregularity (depression defect of luminal surface of more than 2mm in depth) on carotid artery angiogram. Seven angiograms revealed occluded carotid arteries and 2 were of limited quality that plaque surface assessment was not accurate (but stenosis severity assessment was acceptable).

Fifty two carotid arteries had mild stenoses of less than 50% (according to the NASCET criteria of stenosis assessment), 23 arteries had stenoses from 50-69%, 133 arteries had stenoses of 70-98% and 12 arteries had stenoses of >98% (subtotally or totally occluded).

3.4.2 Radiological evidence of cerebral infarction

Of the 110 patients, there were brain imaging data available for 106 patients; MRI head scans from 95 patients and CT head scans from 11 patients, for the assessment of evidence of large vessel cerebral infarction and evidence of small vessel disease. Four patients did not have available brain imaging data for assessment. Their head scans were performed in foreign hospitals with typed reports but the images were not available for analysis. Of the 106 patients, there was radiological evidence of large vessel cerebral infarction in 43 patients (2 had radiological evidence of cerebral infarction in both hemispheres) and evidence of diffuse small vessel disease in 66 patients.

3.5 Histopathological classification of atherosclerotic lesions: a hybrid amalgamated classification schemata

I initially intended to use the Virmani schema for the histopathological classification of the lesions in our study. However, in the course of the work I realised the limitations of using either the Virmani or the Stary classification system exclusively. Clearly a unified amalgamation of the two schemes would allow for the comprehensive and detailed histopathological classification of the various lesion sub-types with clear differentiation of the stable and unstable plaque. In this work, I have designed and utilised a hybrid schemata and classification system incorporating the linear numerical progression of the plaque described by Stary with the morphologically descriptive classification of the plaque by Virmani, incorporating both plaque rupture, erosion and the calcified nodule, and with a clearer description of pathological intimal thickening and further described and classified the 'fibrous lesion'. This schema is shown in Figure 37. The detailed descriptions of the lesion classifications used in this study with references to both Virmani and Stary lesion class types are shown in Table 6.

Both the Stary and Virmani classification schemes were in agreement in the description of the non-atherosclerotic intimal lesions of intimal thickening and the subsequent development of intimal xanthoma. However, the morphological description of the lesion with pathological intimal thickening which was observed by Virmani et al. and in our work was not represented in the Stary classification. It is a poorly defined entity and is often described as a pathologically advanced Stary III Intermediate lesion[18] and was considered an early stage lesion, benign and not associated with thrombosis or clinical sequelae. In our study, we had numerous lesions demonstrating pathological intimal thickening in the proximal and distal mildly stenosed portions of a severely stenosed advanced plaque which were indistinguishable from a Stary III Intermediate lesion. However, we also had 7 plaques of severe stenoses (from 65 to 95% diameter stenosis) with predominant pathological intimal thickening at the sites of maximal stenosis. We had difficulty in distinguishing PIT from Intimal Xanthoma (of a Stary III Intermediate lesion).). For the purposes of this study, we differentiated Intimal Xanthoma (i.e. of a Stary III Intermediate lesion) with minimal luminal narrowing (due to Glagov remodelling), from the PIT lesion with evidence of luminal encroachment and may range from mild to severe stenosis.

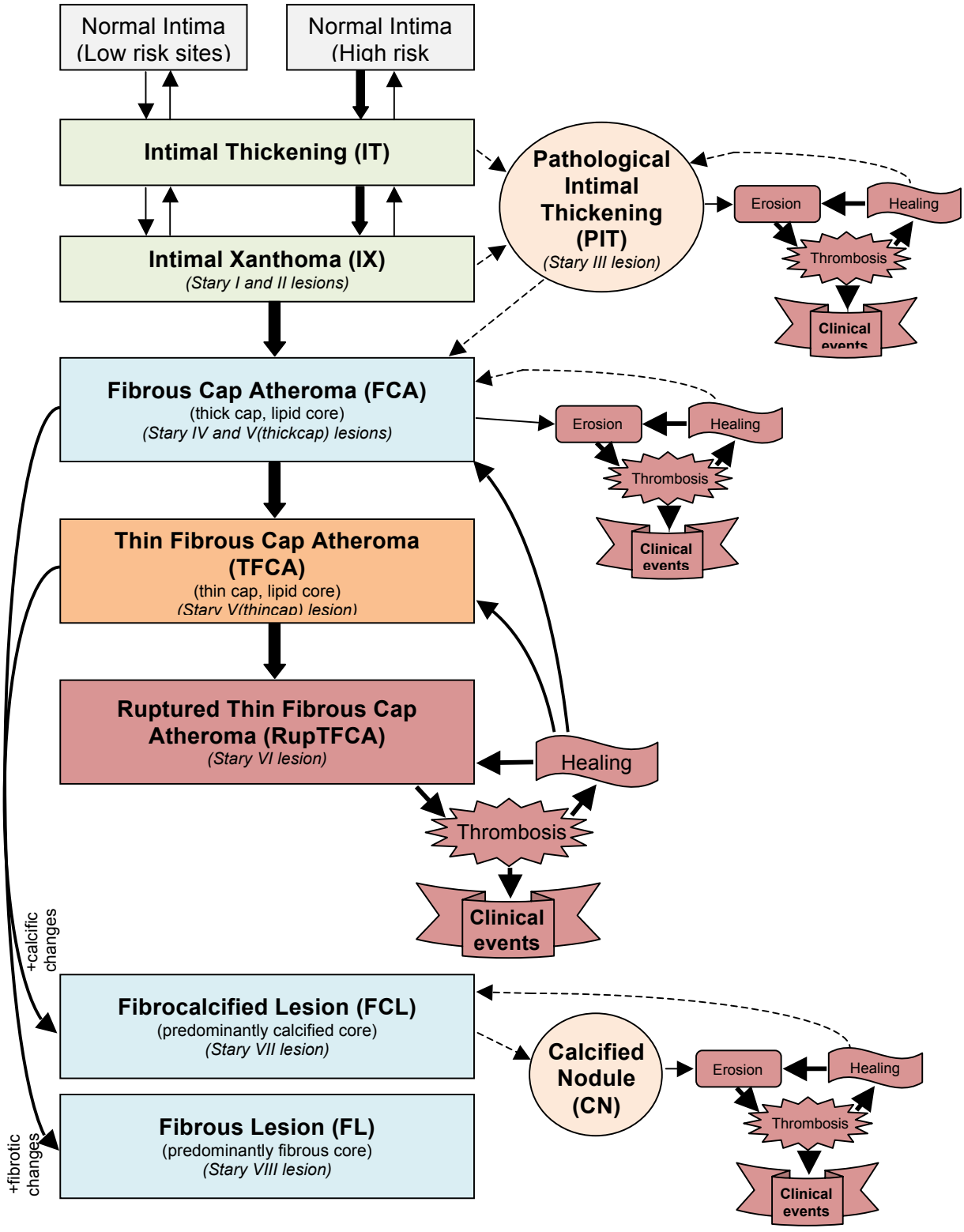

Figure 37. The hybrid schemata of atherosclerotic plaque progression used in our study. (Bold arrows denote well established relationships and thicker arrows denotes higher propensity in progression. Dashed arrows reflect as yet putative relationships. Red boxes are unstable lesions associated with thrombus. Orange and tan boxes are vulnerable (pre-rupture/erosion) lesions without thrombus. Blue boxes are stable lesions. Green boxes are early pre-atherosclerotic lesions.)

Hybrid/combined Classification	Virmani Classification	Stary Classification (with numerical grading)	Morphological Description	Thrombosis
Non-atherosclerotic intimal lesions				
Intimal thickening (IT)	Intimal thickening	Adaptive intimal thickening	Diffuse or focal thickening of the intima by the accumulation of SMCs. There is an absence of lipid or macrophage foam cells.	Absent
Intimal xanthoma (IX)	Intimal xanthoma	I: Initial lesion II: Fatty streak III: Intermediate lesion	Diffuse or focal thickening of the intima with accumulation of SMCs, extracellular lipid and macrophage foam cells (intracellular lipid). There is no necrotic core or fibrous cap and **there is usually no discernable luminal narrowing**. Such lesions may regress at low susceptibility sites.	Absent
Progressive atherosclerotic lesions				
Pathological intimal thickening (PIT)	Pathological intimal thickening	*(undescribed)* *(more advanced version of a type III: Intermediate lesion)*	Intimal thickening with diffuse SMCs in a proteoglycan-rich matrix with areas of accumulation of extracellular lipid but no evidence of a necrotic core. Macrophages and inflammatory cells are scattered throughout the lesion and ***may vary in amount. The degree of luminal stenosis may vary from mild to severe. There is no distinct fibrous cap.*** (may have evidence of a healed rupture or erosion)	Absent
PIT +erosion	PIT with erosion	*(undescribed)*	Luminal thrombosis, plaque is the same as above.	Thrombus mostly mural and infrequently occlusive
Fibrous cap atheroma (FCA)	Fibrous cap atheroma	IV: Atheroma V: Fibroatheroma + thick cap	Well formed lipid necrotic core (region of accumulated extracellular lipid, acellular with evidence of cellular debris) with an overlying fibrous cap of organised layers of SMCs in a proteoglycan-collagen matrix. The thickness of the fibrous cap is at least 65μm. (may have evidence of a healed rupture or erosion)	Absent
FCA +erosion	FCA with erosion	*(undescribed)*	Luminal thrombosis, plaque is the same as above. There is no communication of thrombus with the necrotic core.	Thrombus mostly mural and infrequently occlusive
Thin fibrous cap atheroma (TFCA)	Thin fibrous cap atheroma	V: Fibroatheroma + thin cap	A fibrous cap atheroma with a thin fibrous cap infiltrated by macrophages and inflammatory cells with underlying necrotic core. There are rare SMCs. The fibrous cap is less than 65μm (at least focally) thick.	Absent (may contain intra-plaque haemorrhage or fibrin)
Ruptured TFCA (RupTFCA)	Plaque rupture	VI: Complicated lesion with rupture +/- thrombosis or haemorrhage	A disruption of the fibrous cap with luminal thrombus in communication with the underlying necrotic core. Usually occurs at the weakened and thinned cap of a TFCA. Intraplaque haemorrhage is often present.	Thrombus usually occlusive*
Fibrocalcific plaque/lesion (FCL)	Fibrocalcific plaque	VII: Fibroatheroma with predominant calcific change	A collagen-rich plaque usually with significant stenosis containing large areas of predominant calcification of the core and other regions of the plaque with few inflammatory cells. A necrotic core may still be present. There is a distinct overlying thick fibrous cap (at least 65μm) with SMCs of varying amounts. (May have evidence of a healed rupture or erosion)	Absent

Fibrous lesion (FL)	*(undescribed)*	VIII: Fibro-atheroma with predominant fibrous change	A collagen-rich plaque usually with significant stenosis containing large areas of predominant fibrous changes of the core and other regions of the plaque with few inflammatory cells. A necrotic core may still be present. There is a distinct overlying thick fibrous cap (at least 65μm) with SMCs of varying amounts. (may have evidence of a healed rupture or erosion)	Absent
Calcified nodule (CN)	Calcified nodule	*(undescribed)*	Eruptive nodular calcification with underlying fibrocalcific plaque. ***The calcific nodule is extruding out into the lumen often covered with only a layer of endothelium or an acellular thin fibrous cap.*** (may have evidence of a healed rupture or erosion)	Absent
CN +erosion	CN with erosion	(undescribed)	Luminal thrombosis, plaque is the same as above.	Thrombus usually non-occlusive

Additional descriptive lesion codes used:
+Rupture
+Erosion
+Thrombus
+Haemorrhage
+Healing rupture/erosion
+Minor foci of calcification
(*note: Thrombus seen in a RupTFCA is usually occlusive in the coronary arteries but non-occlusive and thromboembolic in the carotid arteries due to the difference in vessel size (3-4mm diameter vs 5-6mm diameter).

Table 6. The hybrid schemata amalgamating the AHA (Virmani) atherosclerotic lesion classification with reference to the original Stary lesion type. In bold were the additional descriptions to aid differentiation of the lesion types.

The description of the fibrous cap atheroma was similar in both systems. The fibrocalcified plaque was identical to the Stary VII: Fibroatheroma with predominant calcific change. Plaque rupture was identical to the Stary VI: Complicated fibroatheroma with rupture. However, the vulnerable thin fibrous cap atheroma described as a significant entity by Virmani representing a key stage of plaque vulnerability prior to plaque rupture was not categorically represented in the Stary system. Neither were the descriptions of plaque erosion with evidence of thrombosis seen in the fibrous cap atheroma, the fibrocalcified plaque or in pathological intimal thickening. The calcified nodule with or without evidence of erosion or thrombus was also without representation in the original Stary classification system. On the other hand, the Stary VIII: fibroatheroma with predominant fibrous change lesion was not represented in the Virmani system. These lesion types were all observed and appropriately classified and represented in our work using the amalgamated schemata and classification system. In preference to a morphological descriptive classification of the lesion by Virmani and for the purpose of this study, we have called the fibrous cap atheroma with predominant fibrous change of the core (Stary VIII lesion) the 'fibrous lesion'.

I had some difficulty in distinguishing the PIT lesion from the lesion with advanced atheromatous plaque with predominant fibrous change- the fibrous lesion. In these lesions the necrotic lipid core had undergone fibrotic change and was not as apparent. However, a distinct but acellular old fibrous cap was apparent in the fibrous lesion but not in the PIT lesion. In comparison, the PIT lesion had diffuse scattered SMCs, proteoglycan matrix and macrophages scattered within the lesion without the organised layers seen in a distinct fibrous cap. These descriptions were used to differentiate the PIT and fibrous lesions.

It was occasionally difficult to differentiate FCA from FCL using the general definitions by Stary and Virmani. The description of the Fibrocalcified plaque by Virmani was of "a collagen-rich plaque with significant stenosis containing large areas of calcification with few inflammatory cells; a necrotic core may be present". It was the degree of calcification and hypocellularity that would differentiate a FCA from a FCL lesion, and the two lesions may be quite similar otherwise. In our study, calcification was seen in almost all the plaques in a wide variation in degree of calcification. For the purpose of this study, the lesion remains as an FCA if the calcific changes seen were mild (about a third or less) with an additional label of 'minor foci of calcification seen'. The lesion was classified as FCL if the calcification occupied more than a third of the plaque.

I have found in the utility of an amalgamated hybrid schemata and classification system, I was able to address the specific limitations which I have encountered in the application of either the Stary or Virmani classification systems. All the lesion types were represented, observed and appropriately classified in our study.

3.6 Histological Data

Of the 118 endarterectomy specimens collected, there were 114 specimens with available histological analysis. Four specimens were used entirely for OPT work and were not available for histological analysis.

3.6.1 Heterogeneity of the plaque

There was significant heterogeneity of the atherosclerotic plaque seen in each individual endarterectomy specimen. From the serial sections taken every 5mm throughout the endarterectomy specimen, heterogeneity of lesion histopathological classification was observed throughout the length of the endarterectomy specimen. At the peripheral mildly stenosed portions of the lesion (in the distal and proximal ends of the CEA specimen) intimal thickening, xanthoma or pathological intimal thickening lesions were often seen. Lesion progression was observed such that the middle portions of the lesion with the most severe stenosis and a larger plaque burden contained the more advanced atherosclerotic lesion types of fibrous cap atheroma, thin fibrous cap atheroma, ruptured TFCA, fibrocalcified lesions and fibrous lesions (Figure 38). Heterogeneity of lesion types was observed in the transverse sections of the CEA specimens as well. Different lesion types were observed in the same transverse section of the plaque, occurring adjacent or overlying each other in the diseased intimal wall of the artery forming a multi-layered complex lesion (Figure 38). A majority of specimens (64%) had 2 or more different atherosclerotic lesion grades seen within each complex atherosclerotic plaque; 45% had two, 17% had three, 2% had four different lesion types.

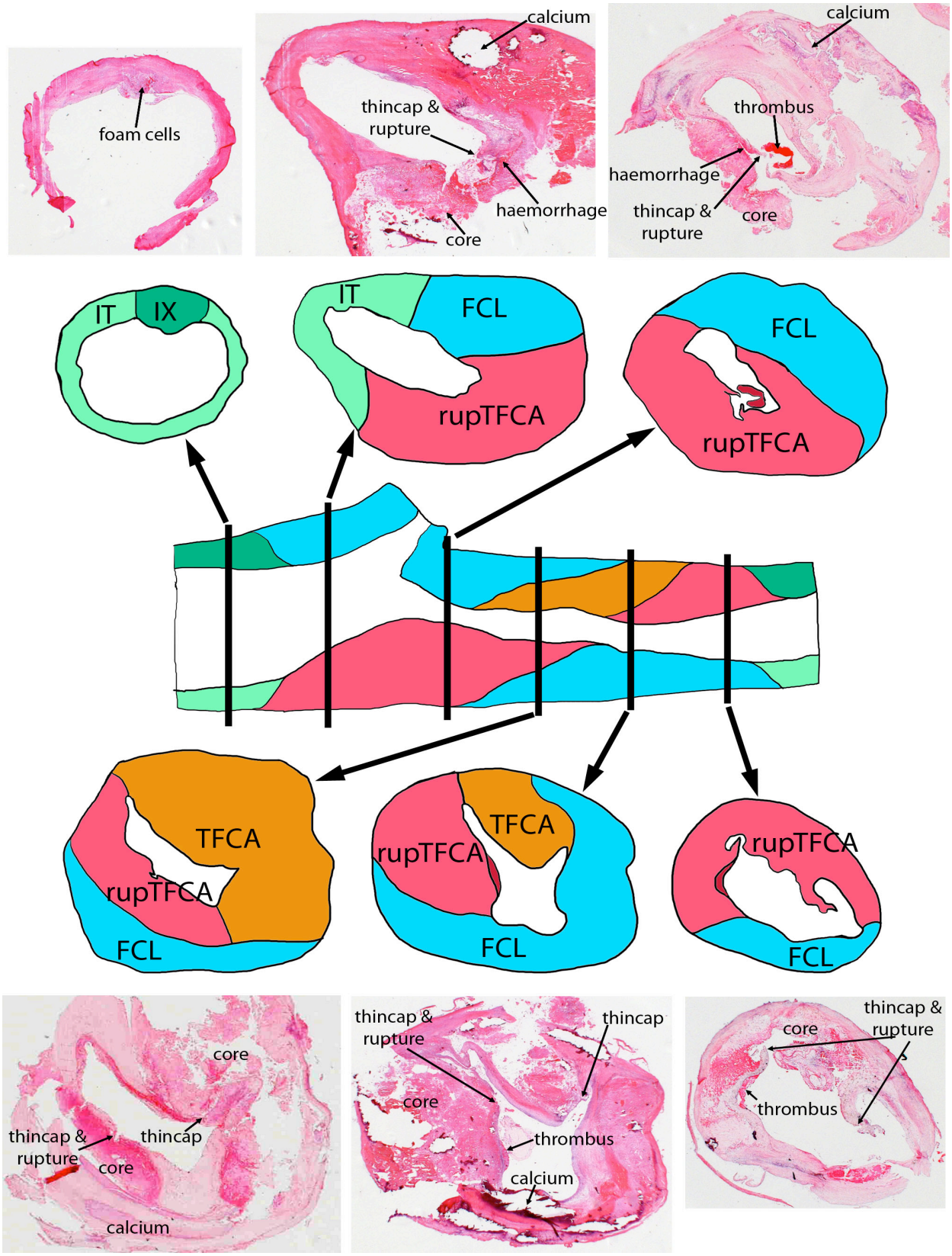

Figure 38. The complex atherosclerotic plaque seen, consisting of multiple lesion types adjacent and overlying each other in longitudinal section (middle) and in multiple transverse sections (top and bottom) in the diseased carotid artery.

3.6.2 Lesions types associated with thrombi

The predominant lesion type for each specimen is reported in Table 7. Of the 114 endarterectomy specimens, there were 24 specimens with lesion types associated with thrombi; 16 were ruptured thin fibrous cap atheromas, 3 were erosions and 5 were calcified nodules. Almost all (96%) of these specimens were from patients with a previous stroke or TIA; 88% had recent events within 6 months from surgery. Seventy two percent had major surface irregularity (of >2mm depression depth) seen on MR angiography.

All of the specimens with ruptured thin fibrous cap atheroma had an obvious defect/rupture of the thin fibrous cap with haemorrhage and thrombus (Figure 39), except for one specimen where the thrombus was physically removed by the surgeon during the endarterectomy procedure. The 3 plaques with erosions had thrombus overlying a thick fibrous cap atheroma (n=1) and fibrocalcified lesions (n=2) without a clear disruption of the cap in continuation to the lipid or fibrocalcified core. All the calcified nodules were from severely calcified fibrocalcified lesions. Although there were no visible thrombus seen on histology with the calcified nodules they were all from patients with recent symptoms of stroke or TIA within 6 months.

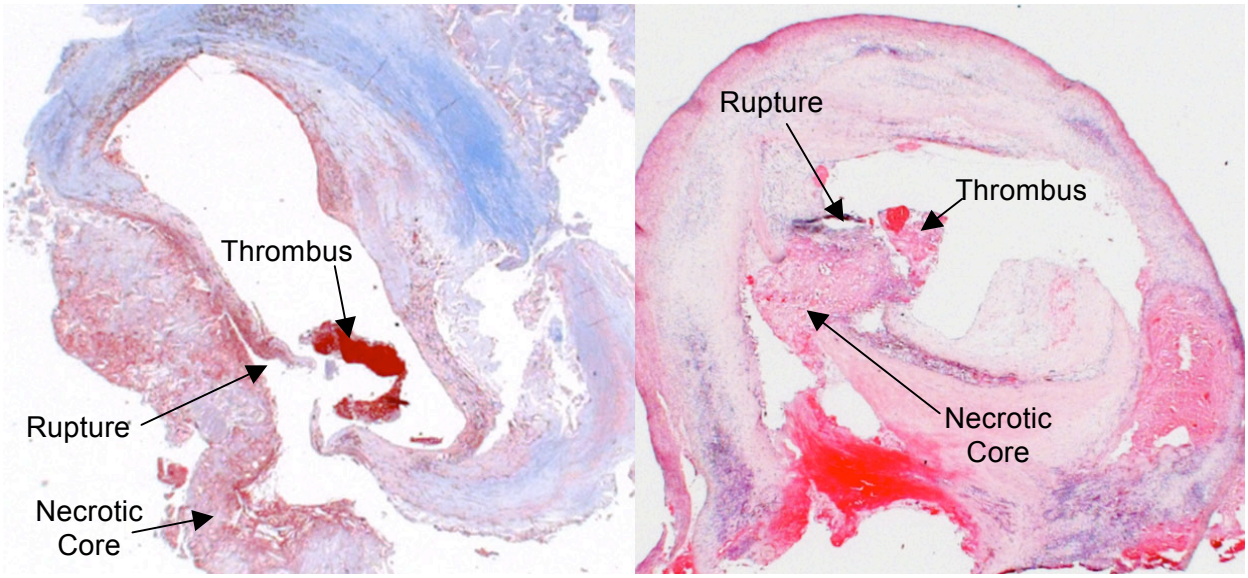

Figure 39. Photomicrographs of ruptured thin fibrous cap atheromas with thrombus.

		Unstable lesions associated with thrombi			Vulnerable lesions		Stable lesions		
		Ruptured Thin Fibrous Cap Atheroma	Plaque Erosion	Calcified Nodule	Healing old ruptured plaques	Thin Fibrous Cap Atheroma	Fibrous Cap Atheroma	Fibro-calcified Plaque	Pathological Intimal Thickening
Total number		16	3	5	8	6	25	44	7
% of all specimens		14%	3%	4%	7%	5%	22%	39%	6%
Symptoms	**Recent Symptoms**	75%*	100%	100%	13%	17%	20%	16%	71%
	Late Symptoms	13%	0	0	25%	50%	36%	34%	14%
	Truly Asymptomatic	6%	0	0	63%	33%	44%	48%*	0%*
Age (mean in years, 95%CI)		65 (60-70)	59 (25-93)	69 (63-76)	74 (69-78)	73 (65-100)	69 (66-72)	68 (66-70)	62 (54-71)
Risk Factor Profile	**Smoking (current or previous)**	68.8%	100.0%	80.0%	87.5%	66.7%	56.0%	77.3%	71.4%
	FHX of premature CAD/CVD	31.3%	33.3%	40.0%	12.5%	0.0%	24.0%	27.3%	42.9%
	Diabetes	18.8%	0.0%	20.0%	12.5%	0.0%	28.0%	20.5%	42.9%
	Hypertension -treated	81.3%	66.7%	100.0%	75.0%	66.7%	88.0%	88.6%	85.7%
	Hypercholesterolaemia -treated	81.3%	66.7%	100.0%	75.0%	66.7%	88.0%	88.6%	85.7%
	Ischaemic Heart Disease	18.8%	66.7%	80.0%	25.0%	50.0%	44.0%	18.2%	57.1%
	Peripheral Vascular Disease	6.3%	0.0%	0.0%	50.0%	0.0%	4.0%	4.5%	0.0%
Stenosis (mean in %, 95%CI)		84% (78-90)	93% (76-99)	92% (80-99)	91% (82-99)	90% (77-99)	91% (86-95)	88% (84-91)	77% (68-87)
Plaque Surface Irregularity	**Major**	68.8%	100.0%	80.0%	75.0%	33.3%	32.0%	20.5%	42.9%
	Mild	25.0%	0.0%	0.0%	12.5%	16.7%	28.0%	25.0%	0.0%
	Smooth	6.3%	0.0%	20.0%	12.5%	50.0%	40.0%	54.5%	57.1%
Fresh thrombus seen on histology		93.80%	100%	0%	0%	0%	0%	0%	0%

Table 7. Breakdown of the predominant lesion types in the CAGE study to symptoms, risk factor profile, plaque stenosis and surface irregularity on MR angiography. (*note: 3 samples had indeterminate clinical symptoms and were clinically unclassified, as a result the percentages of these 3 groups do not total to 100%)

3.6.3 Stable lesions

Seventy six specimens had stable lesion types of fibrous cap atheroma (FCA, 22%), fibrocalcified plaque/lesion (FCL, 39%) and pathological intimal thickening (PIT, 6%) without any evidence of erosion or rupture or thrombus. Three quarters of stable lesions had no major plaque surface irregularity on MR angiography.

The fibrous cap atheromas and fibrocalcified plaques had thick fibrous caps with varying degrees of smooth muscle cellularity. About half (52%) of the fibrocalcified lesions were hypocellular with very few smooth muscle cells in their fibrous caps and very few macrophages in their fibrous and calcified cores. 30% of the fibrocalcified plaques were severely calcified with calcification of more than half of the former necrotic lipid core. Photomicrographs of stable FCA and FCL plaques are shown in Figure 40 and Figure 41. The variability in the amounts of VSMCs populating the fibrous cap is demonstrated in Figure 40.

The majority of the fibrous cap atheroma and fibrocalcified plaques were from patients without any symptoms (true asymptomatics) or with prior symptoms of more than 6 months (late symptomatics); 80% of FCAs and 82% of FCLs. However, an interesting and unexpected observation was that 71% of lesions with pathological intimal thickening were from patients with recent symptoms within 6 months (Table 7). There were no obvious differences between the groups in demographics, risk factor profile, degree of stenosis or plaque surface irregularity to account for this. Photomicrographs of the PIT lesion is shown in Figure 42.

Although the numbers of lesions with PIT were small (n=7), it was possible to perform a 3x2 contingency table of the 3 expected stable lesion types and of recent symptoms to old/no symptoms, in a Chi-Square test of independence in k groups (Table 8). One fibrocalcified plaque and one pathological intimal thickening lesion were from patients with indeterminate symptoms but their symptoms were longer than 6 months prior to surgery and could be included in the analysis in the combined late symptomatic/asymptomatic group. The contingency table Chi-Square test was feasible within the acceptable parameters (no expected frequencies was below 1 or any expected frequency was less than 5 in more than 20% of the cells). This produced a Chi-square statistic of 10.84, with 2 degrees of freedom, and a Pearson p-value of 0.0044. Applying a Yates' correction for continuity to improve the accuracy of the null-condition sampling distribution of the chi-square especially in low sample numbers yielded a corrected Chi-Square statistic of 7.803 and a Yates' corrected p-value of 0.02 which was still significant. This suggests a significant association between lesions with pathological intimal thickening and recent

cerebro-embolic symptoms. The relatively recently described PIT lesion may not be as stable a lesion as we had thought.

	Fibrous cap atheroma	Fibrocalcified plaque	Pathological Intimal Thickening	Total
Recent symptoms (within 6 months)	5	7	5	17
Late symptoms (>6 months) or no symptoms at all	20	37	2	59
Total	25	44	7	76

Chi-square=10.84, DoF=2, p=0.0044

Table 8. 3x2 Contingency Table comparing the 3 groups of stable lesion types to recent symptoms.

3.6.4 Vulnerable lesions

There were 14 specimens with predominant vulnerable lesion types. Eight of them were plaques with evidence of previous rupture of the fibrous cap with healing, demonstrating major plaque surface irregularity on MR angiography (Table 7) where 4 had organising residual thrombus with endothelialisation. Of the 8 healing plaques, 3 were still thin fibrous cap atheromas and 5 had undergone fibrocalcification of the core to form fibrocalcified plaques. The remaining 6 of the 14 vulnerable lesions were thin fibrous cap atheroma without any evidence of rupture or thrombosis (Figure 44). Half of the 14 specimens were from patients with previous symptoms of stroke or TIA, only 14% had recent symptoms. Interestingly, 60% of the healing ruptured plaques did not cause any prior symptoms to those patients nor were there any radiological evidence of cerebral infarction on their brain scans, even though 2 of them clearly had evidence of old thrombus with endothelialisation and incorporation into the healing plaque.

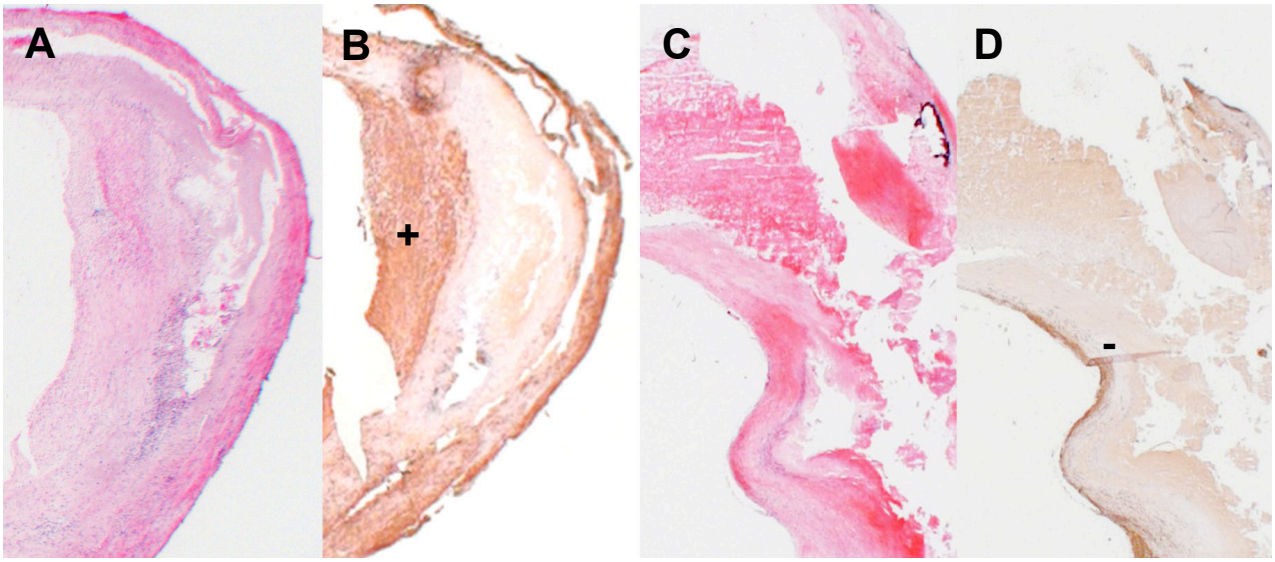

Figure 40. Photomicrographs of stable thick fibrous cap atheroma. Two different specimens were stained with H&E in panels A & C, and immunostained with SMA to identify VSMCs in panels B & D. The difference in cellularity of the thick fibrous cap with more VSMCs(+) and less VSMCs(-) is demonstrated.

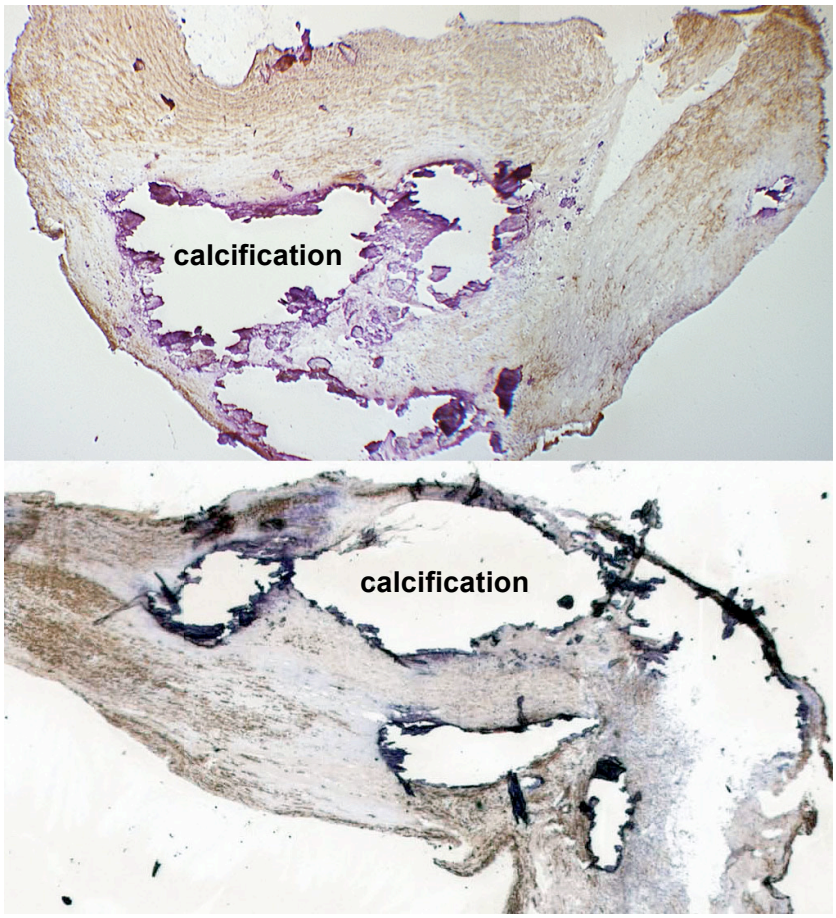

Figure 41. Photomicrographs of stable fibrocalcified lesions. Immunostaining with SMA identifies VSMCs in the fibrous cap (stained brown) and severe calcification of the former necrotic core is seen.

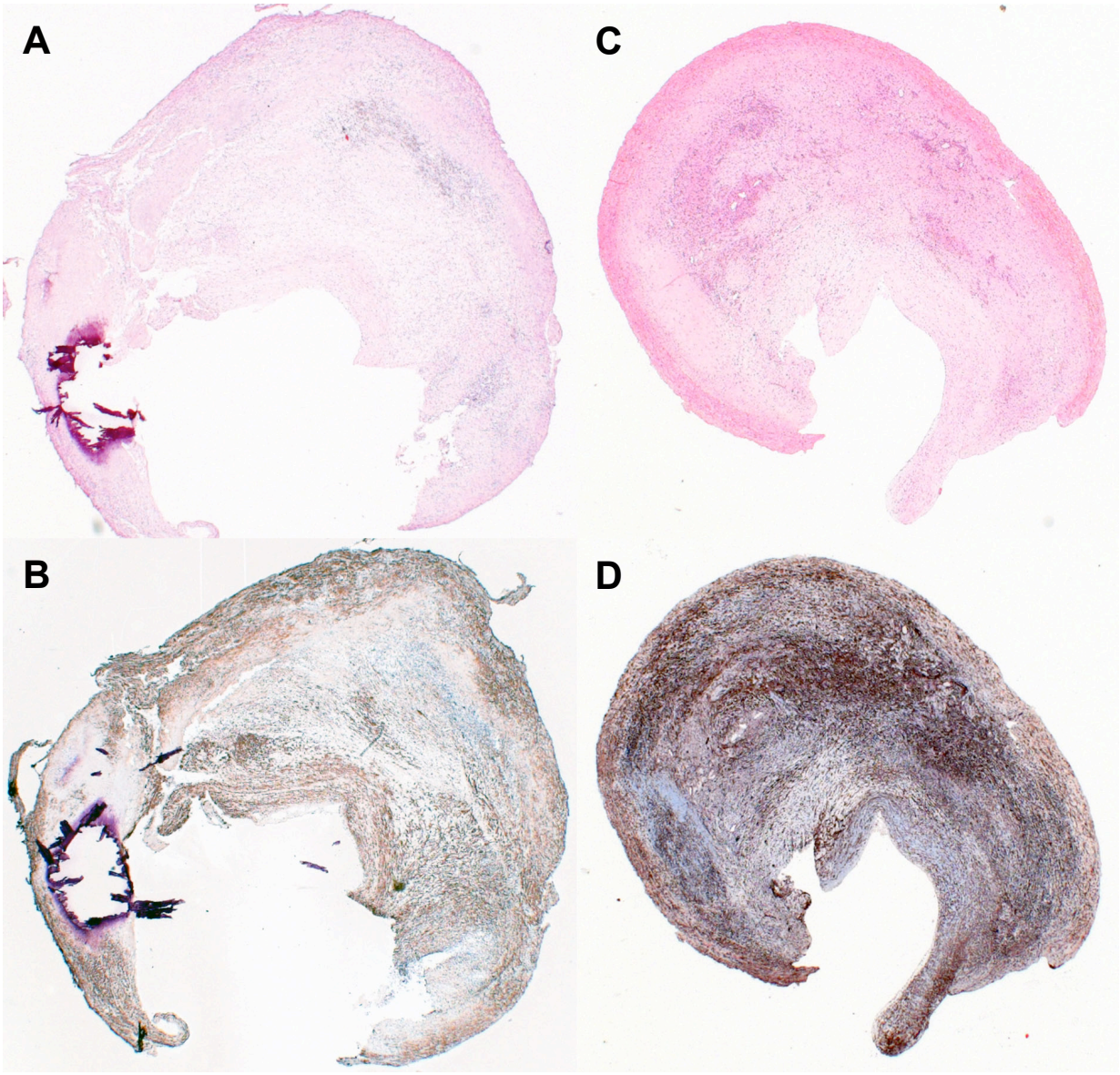

Figure 42. Photomicrographs of pathological intimal thickening lesions. Two separate specimens with PIT stained with H&E (top panels A & C) and immunostained with SMA to identify VSMCs (bottom panels B & D) shows the high cellularity of these lesions with VSMCs with pockets of macrophages and extracellular lipid but without an organised lipid or necrotic core making it difficult to identify/differentiate a fibrous cap. There is significant luminal encroachment.

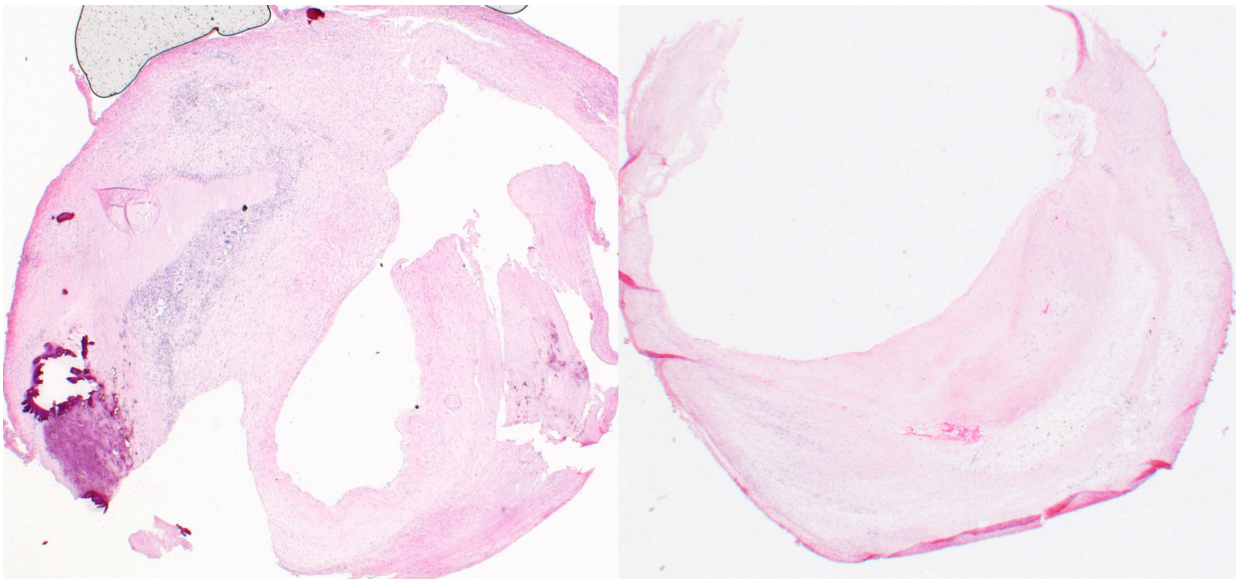

Figure 43. Photomicrographs of fibrous lesions.

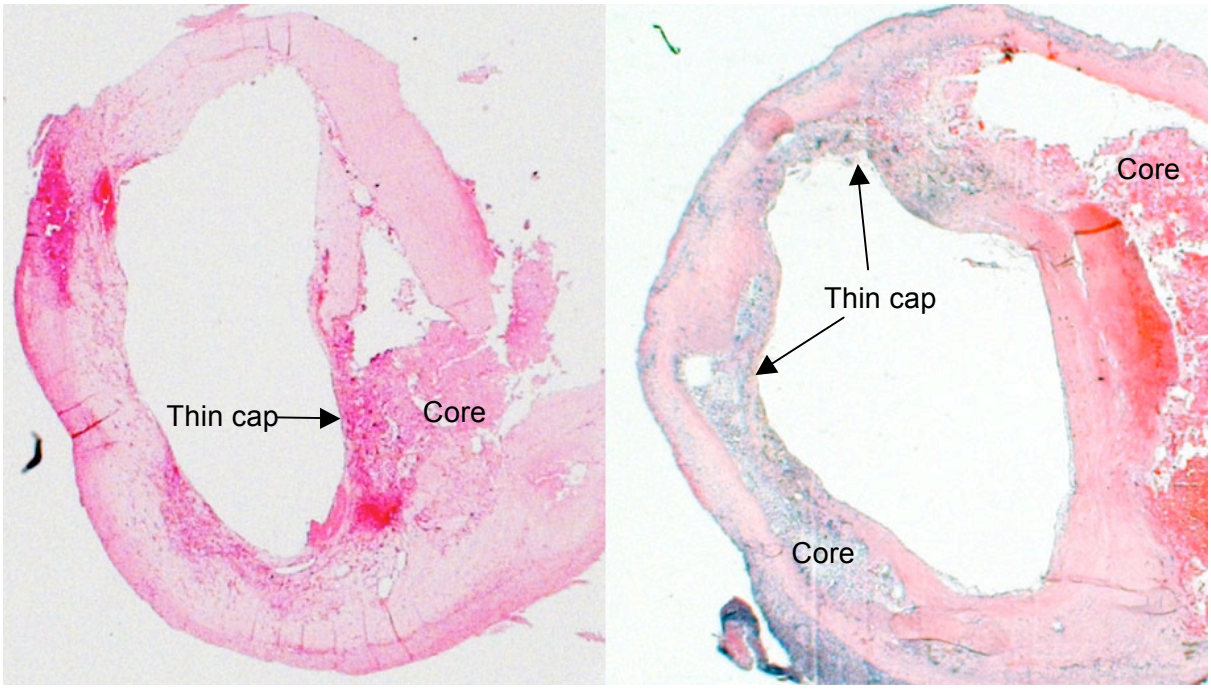

Figure 44. Photomicrographs of vulnerable thin fibrous cap atheroma.

3.7 Transcranial doppler emboli detection

Over a period of 1 year, I introduced transcranial doppler emboli detection in the assessment of the carotid plaque. I recruited 12 patients from the 42 patients available during that time. Thirty patients were unsuccessfully recruited due to technician, researcher or machine unavailability (70%), patient unavailability (20%) or patient refusal (10%).

TCD emboli detection ultrasound scanning was performed on the 12 patients. Three of the patients (25%) were successfully scanned with doppler ultrasound data of both middle cerebral arteries. Three patients (25%) had partial success with successful insonation with doppler ultrasound data of one of the two middle cerebral arteries only, the other middle cerebral artery was difficult to insonate. Six patients (50%) had failed scans where both middle cerebral arteries were difficult to insonate. The difficulties in detecting and maintaining a doppler ultrasound signal were due to increased temporal bone thickness and increased arterial convolution in the elderly, which may reflect the limitations of this technique.

Trans-cranial doppler results were available from the successful insonation of 9 of 24 middle cerebral arteries from the 12 patients. The data is presented in Table 9. There were 3 positive scans for micro-emboli, 2 of which fulfilled both the Consensus Group Criteria for micro-emboli detection and dual-gate doppler criteria and in one the Consensus Group Criteria was fulfilled but we were not able to maintain a reasonable second-gate doppler signal for dual-gate doppler analysis. The remaining 6 successful insonations were negative for micro-emboli; 4 had high intensity transient signals (HITS) of low amplitude or of long duration and undetected in the second gate and were identified as signal artefacts, and 2 had no HITS at all during the hour of recording.

From the 3 positive results for embolic phenomenon detected in the middle cerebral artery, 2 had recent symptoms of stroke within the last 6 months and one was clinically completely asymptomatic. They were high grade stenotic lesions (85-98%) and 2 had major plaque surface irregularities on MR angiography. The 2 recently symptomatic patients had plaque histology of a calcified nodule (a lesion type associated with thrombi) and pathological intimal thickening (a lesion type which our data suggests has an association with clinical events). The large number of emboli positive HITS in the completely asymptomatic patient was initially an unexpected finding. However, independent analysis of the plaque histology revealed an unstable lesion type of an acutely ruptured thin fibrous cap atheroma with evidence of fresh thrombus and haemorrhage.

TCD evidence of micro-emboli	TCD doppler data	Sex	Age	Symptoms	% MRA Stenosis	MRA Surface Irregularity	Cerebral infarction on scan	Plaque histology
Positive	72 HITS (majority of them >80% micro-emboli positive)	F	61	None	98	Major	No	RupTFCA
Positive	20 micro-emboli positive HITS	F	74	Symp <6months	95	Major	No	CN
Positive*	4 HITS (>8dB transient signals but second gate tracking poor signal)	M	65	Symp <6months	85	No	No	PIT
Negative	1 artefact events	M	63	None	60	No	Not Available	FCL
Negative	2 artefact events	M	79	None	70	Mild	No	FCL
Negative	2 artefact events	M	65	None	30	Major	No	N/A
Negative	30 artefact events (prev CEA)	M	65	None since CEA	Previous CEA	Previous CEA	No	N/A
Negative	No events (prev RCEA)	M	65	None since CEA	Previous CEA	Previous CEA	Yes (Prev CEA)	N/A
Negative	No events	M	65	None	40	No	No	N/A

All the 6 negative TCD scans for micro-emboli did not have any clinical events affecting the respective cerebral territory; 2 had previous CEA surgery of the related (ipsilateral) carotid artery and had no further clinical events since.

There was poor recruitment of patients for TCD scans mainly due to resource limitations and limited success in scanning due to technical limitations. As a result, this modality although promising, was only successfully applied to a small minority of samples and was of limited use in the characterisation of the stability/instability of the plaques collected in this study. After the pilot period over a year I decided to stop performing further TCD scans.

3.8 Correlation between Clinical, Radiological and Histological Findings

3.8.1 Symptoms and Surface irregularity

A total of 208 carotid angiogram surface morphology results were correlated to clinical symptoms out of the 220 angiogram results available. Twelve angiogram results were excluded from the analysis; 2 angiograms were of limited quality and thus were not possible for accurate plaque surface analysis, 3 had indeterminate clinical symptoms and were clinically 'unclassified' and 7 had occluded carotid arteries.

Sixty percent of symptomatic patients demonstrated plaque surface irregularity on carotid angiography performed mainly by MR angiography. Two-thirds had severe irregularity of plaque surface (greater than 2mm depression defect) and a third had mild surface irregularity (1-2mm depression defect). In comparison, only 30% of asymptomatic patients demonstrated any irregularity of plaque surface (of 1mm and greater depression defect).

I compared the 3 clinical groups of recent symptomatic patients, late symptomatic patients and true asymptomatic patients to the 3 grades of plaque surface irregularity of no irregularity (smooth), mild (1-2mm depression) and severe irregularity (>2mm depression) and observed a significant association with a Pearson p-value of 0.0016 (Table 10). A 2x2 comparison of the presence/absence of any symptoms against the presence/absence of any surface irregularity (>1mm depression) produced an association of higher significance with a Pearson p-value of 0.000033 (Table 11).

		Symptoms?			
		Recent Symptomatic patients	Late Symptomatic patients	True Asymptomatic patients	Total
Surface Irregularity?	Severe	18	19	24	61
	Mild	8	10	11	29
	Smooth	17	21	80	118
	Total	43	50	115	208

Chi-square = 17.45, DoF=4, p=0.0016

Table 10. Contingency table (3x3) comparing symptoms to the grades of plaque surface irregularity (see text for details) (DoF; degrees of freedom).

		Symptoms?		
		Yes	No	Total
Surface Irregularity?	Yes	55	35	90
	No	38	80	118
	Total	93	115	208

Chi-square= 17.26, DoF=1, p=0.000033

Table 11. Contingency table (2x2) comparing the presence of any prior symptoms to the presence of any surface irregularity of more than 1mm depth.

3.8.2 Symptoms and Radiological evidence of infarction

Of the 106 patients with available head scan data for analysis, we compared the clinical symptoms of these patients to any evidence of large vessel cerebral infarction of the corresponding anterior circulation territories supplied by the relevant carotid artery. Of the total of 212 datasets available, 210 datasets were analysed. Two datasets were excluded with indeterminate clinical symptoms and were clinically 'unclassified'.

Unsurprisingly, I found significant association of evidence of cerebral infarction to symptoms of stroke or TIA (Table 12) with a Pearson p-value of $<1x10^{-9}$. Forty two percent of patients with symptoms had corresponding radiological evidence of cerebral infarction of the respective cerebral territory supplied by the relevant carotid artery. Of the patients who present with a clinical presentation of a stroke, 56% had radiological evidence confirming this on their brain scan. However, more interestingly, of the patients with TIAs only, 28% demonstrated evidence of cerebral infarction on their brain scan with their transient presentation of symptoms and by definition with no residual deficit.

Furthermore, 4% of asymptomatic patients demonstrated evidence of cerebral infarction on their brain scan. These findings demonstrate the limitations on the reliance of symptoms alone and that a proportion of cerebral infarctions occur with no clinically detectable residual defect and some occur silently.

		Symptoms?			
		CVAs	TIAs	None	Total
Radiological evidence of infarction?	Yes	28	13	4	45
	No	22	34	109	165
	Total	50	47	113	210

Chi-square= 58.05, DoF=2, $p<1x10^{-9}$

Table 12. Contingency table (2x3) comparing of presence of previous symptoms of TIA or stroke to evidence of cerebral infarction on brain imaging.

3.8.3 Surface irregularity and Stenosis severity

Of the 220 carotid angiogram results available for analysis, 211 were analysed in correlation of plaque surface irregularity to stenosis severity. Nine angiogram results were excluded; 2 were of limited quality for accurate plaque surface analysis and 7 had completely occluded carotid arteries with an absence of luminal contrast to demonstrate plaque surface morphology.

Presented in a 2x4 contingency table, plaque surface irregularity (>1mm depression) was present in 12% of the stenoses of <50% group, in 26% of the stenoses of 50-69% group, in 60% of the stenoses of 70-95% group and in 53% of the stenoses of >95% group (Table 13). I found a significant association with a Pearson $p=9x10^{-8}$.

		Severity of stenosis				
		<50%	50-69%	70-95%	96-99%	Total
Plaque surface irregularity?	Yes	6	6	54	25	91
	No	45	17	36	22	120
	Total	51	23	90	47	211

Chi-square=35.562, DoF=3, $p=9x10^{-8}$

Table 13. Contingency table (2x4) comparing the degree of stenosis to the presence of any plaque surface irregularity (>1mm depression).

3.8.4 Symptoms and Stenosis severity

From the total 220 angiogram results in the assessment of stenosis severity, 216 results were used in the correlation to clinical symptoms. Four results were excluded with indeterminate clinical symptoms and were clinically 'unclassified'.

In a comparison of any prior symptoms to stenosis severity, I found that 19% had prior symptoms in the <50% stenosis group, 18% of the 50-69% stenosis group, 64% of the 70-95% stenosis group and 52% of the >95% stenosis and occluded artery group. There was a strong association with a Pearson p-value of 2.3×10^{-7} (Table 14).

		Severity of stenosis				
		<50%	50-69%	70-95%	96-99%	Total
Symptoms?	Yes	10	4	56	28	98
	No	42	18	32	26	118
	Total	52	22	88	54	216

Chi-square=33.66, DoF=3, $p=2.3 \times 10^{-7}$

Table 14. Contingency table (2x4) comparing the degree of stenosis to the presence of any prior symptoms of TIA or stroke.

3.8.5 Symptoms and histology

Of the total 118 specimens, there were 114 samples with full histological analysis with lesion classification (four samples were used for OPT work). All these samples had clinical symptom classifications except for 3 which had indeterminate symptoms. A fibrocalcified plaque and a pathological intimal thickening lesion were from patients with indeterminate symptoms but their symptoms were longer than 6 months prior to surgery and could be included in the analysis in the combined late symptomatic/asymptomatic group. A ruptured thin fibrous cap atheroma had indeterminate symptoms within 3 months and had to remain 'unclassified' and was excluded from the analysis.

I examined if the histological lesion seen correlated to recent clinical symptoms. I compared the histological groups of 'unstable lesions associated with thrombi', 'vulnerable lesions' and 'stable lesions' to recent clinical symptoms (Table 15) and found an association with a Pearson p-value of 2×10^{-8} demonstrating a strong correlation of symptoms to histological findings. Most of the unstable lesion-types associated with thrombi (87%) had recent symptoms. In comparison, 14% of vulnerable lesion-types and 22% of stable lesion-types had recent symptoms. Just over half (51%) of the patients with

recent symptoms had unstable lesion-types associated with thrombi, and 80% of patients with late symptoms or no symptoms at all had stable lesion-types.

	Unstable lesion-types associated with thrombi (RupTFCA, plaque erosion, calcified nodule)	Vulnerable lesion-types (Healing oldRupTFCA, TFCA)	Stable lesion-types (FCA, FCL, PIT)	total
Recent symptoms (<6months)	20	2	17	39
Late symptoms (>6months) or no symptoms	3	12	59	74
total	23	14	76	113

Chi-square=35.48, DoF=2, $p=2x10^{-8}$

Table 15. Contingency table (2x3) comparing histological lesion type to recent symptoms.

The PIT lesion was included in the stable lesion group in the analysis because of my original hypothesis that it was a stable lesion type. In light of my observations that the PIT lesion was behaving as an outlier (and was more similar to the unstable lesion), the next analysis was performed excluding the 7 PIT lesions (Table 16). I observed a more significant relationship between symptoms and histology with a Pearson p-value of $<1x10^{-8}$.

	Unstable lesions associated with thrombi (RupTFCA, plaque erosion, calcified nodule)	Vulnerable lesions (Healing oldRupTFCA, TFCA)	Stable lesions (FCA, FCL)	total
Recent symptoms (<6months)	20	2	12	34
Late symptoms (>6months) or no symptoms	3	12	57	72
total	23	14	69	106

Chi-square=40.66, DoF=2, $p=1x10^{-8}$

Table 16. Contingency table (3x2) comparing histological lesion type to recent symptoms, excluding the 7 PIT lesions.

A alternative comparison of true asymptomatic patients and patients with any prior symptoms to the histological lesion groups (Table 17), still yielded a significant but less impressive result with a Pearson p-value of 0.0016. Most of the true asymptomatic patients (80%) had stable lesions, but only 31% of symptomatic patients had unstable lesions on histology. This was due to a significant number of patients with late symptoms found with stable lesions (n=25, 35%) included in the symptomatic group seen with plaque healing and stabilisation.

		Unstable lesion-types associated with thrombi (RupTFCA, plaque erosion, calcified nodule)	Vulnerable lesion-types (Healing oldRupTFCA, TFCA)	Stable lesion-types (FCA, FCL, PIT)	total
Symptoms?	Yes	22	7	42	71
	No	1	7	32	40
total		23	14	74	111

Chi-square=12.87, DoF=2, p=0.0016

Table 17. Contingency table (2x3) comparing histological lesion type to presence (or absence) of symptoms. (Note: the 3 patients with indeterminate symptoms were excluded from the analysis.)

3.8.6 Surface irregularity and histology

There were 114 carotid angiograms with corresponding histological data available for analysis. One of the angiograms was of limited quality for plaque surface morphology analysis and was excluded from the correlation analysis.

I compared the histological lesion groups of 'unstable lesions associated with thrombi', 'vulnerable lesions' and 'stable lesions' to the presence (or absence) of any plaque surface irregularity (depressions of >1mm in depth) on angiography. I found a significant association of plaque surface irregularity seen on MR angiography with histology (Table 18) with a Pearson p-value of 0.0012. Nearly all (91%) of unstable lesions of ruptured thin fibrous cap atheroma, plaque erosion or calcified nodule were associated with plaque surface irregularity on angiography. The majority (71%) of the vulnerable lesions of healing old ruptured plaques and thin fibrous cap atheroma had surface irregularities. Within the histological stable lesions group (fibrous cap atheroma, fibrocalcified plaque and pathological intimal thickening) there was an equal division of half with surface irregularity and half without. Most of the lesions without any surface irregularity on angiography were stable lesions (86%). In comparison, surface irregularity seen on angiography is less discerning of the lesion type; 30% were in the histological unstable lesion group, 14% were in the vulnerable lesion group and 55% were in the stable lesion group.

		Unstable lesions associated with thrombi (Ruptured thin fibrous cap atheroma, plaque erosion, calcified nodule)	Vulnerable lesions (Healing old ruptured plaques, thin fibrous cap atheroma)	Stable lesions (Fibrous cap atheroma, fibrocalcified plaques, pathological intimal thickening)	total
Plaque surface irregularity?	Yes	21	10	38	69
	No	2	4	38	44
total		23	14	76	113

Chi-square=13.39, DoF=2, p=0.0012

Table 18. Contingency table (2x3) comparing histological lesion type to the presence of plaque surface irregularity detected using MR angiography.

3.8.7 Correlation in 3 domains: Symptoms, Surface irregularity and Histology

I have demonstrated the correlation of clinical symptoms to plaque surface irregularity, surface irregularity to histology, and histology to clinical symptoms in various 2-way comparisons. In my efforts to identify the most likely unstable lesion of an acutely ruptured thin fibrous cap atheroma and the most likely stable lesion of a thick fibrous cap atheroma or fibrocalcified plaque, I proposed a 3 domain analysis in the selection of these lesions. This is based on the hypothesis that although a single domain of plaque characterisation (such as the presence of symptoms) is useful it is not perfect, as we have observed in the 2-way comparisons, and therefore a 3 domain analysis and selection would be a powerful method in the selection of maximally contrasting unstable and stable lesions. The 3-way interaction can be assessed using a 3-way log-linear model, a Chi-Square based analysis of a 2x2x2 table of cross-categorised frequency data.

3-way correlation using the log-linear 2x2x2 model

Of the 118 specimens, 4 were used for OPT work, 3 had indeterminate symptoms and were clinical 'unclassified' and 1 had limited image quality for plaque surface morphology analysis and were excluded. There were 110 specimen datasets with complete clinical, radiological and histological data available for analysis.

I have combined the lesion types in the 'unstable lesions associated with thrombi' and the 'vulnerable lesions' as an 'unstable and vulnerable lesion types' group in comparison with the 'stable lesion types' group for the histology categories. The 'unstable and vulnerable lesion types' include ruptured thin fibrous cap atheroma, plaque erosion, calcified nodule, thin fibrous cap atheroma and healing ruptured plaques. The 'stable lesion types' include fibrous cap atheroma, fibrocalcified plaque and pathological intimal thickening. The clinical categories were the presence or the absence of symptoms of stroke or TIA. The imaging categories were the presence or absence of plaque surface irregularity on angiography.

The 2-way interactions of histology to surface irregularities, histology to symptoms and surface irregularities to symptoms were determined (Table 19). The Pearson chi-square p-values were significant in all the 3 comparisons at $p=0.0012$, $p=0.032$ and $p=0.019$ respectively.

The 2x2x2 frequency data required for the computation of the log-linear 2x2x2 analysis were generated (Table 20). The 3-way log-linear analysis performed with 4 degrees of freedom produced a G2 statistic of 20.66, corresponding to a $p<0.0005$. The 3 domains of clinical symptoms, radiological evidence of surface irregularity and histological findings

have significant correlation to each other which was increased in 3-way interaction. This supports my approach utilising the 3 domains in the analysis and selection of maximally contrasting unstable and stable lesions.

		Plaque surface irregularity?		
		Yes	No	total
Histology lesion type?	Unstable and vulnerable lesion types	30	6	36
	Stable lesion types	38	36	74
	total	68	42	110

Chi-square statistic = 10.5, Pearson's p = 0.0012

		Clinical Symptoms?		
		Yes	No	total
Histology lesion type	Unstable and vulnerable lesion types	28	8	36
	Stable lesion types	42	32	74
	total	70	40	110

Chi-square statistic = 4.63, Pearson's p = 0.032

		Symptoms?		
		Yes	No	total
Plaque surface irregularity	Yes	49	19	68
	No	21	21	42
	total	70	40	110

Chi-square statistic = 5.46, Pearson's p = 0.019

Table 19. The 2-way interaction tables across the 3 conditions of clinical symptoms, angiographic plaque surface irregularity and histological lesion type. The Chi-square statistic with 1 degree of freedom and the Pearson's p-value were computed.

Condition A1:'Unstable and Vulnerable lesion types on histology' (RupTFCA, Erosion, CN, TFCA, healing RupTFCA)

		Condition C: Clinical Symptoms?		
		Yes	No	total
Condition B: Angiographic plaque surface irregularity?	Yes	23	7	30
	No	5	1	6
	total	28	8	36

Condition A2:'Stable lesion types on histology' (FCA, FCL, PIT)

		Condition C: Clinical Symptoms?		
		Yes	No	total
Condition B: Angiographic plaque surface irregularity?	Yes	26	12	38
	No	16	20	36
	total	42	32	74

log-linear analysis:

degrees of freedom [ABC] = 4

G^2 [ABC] = 20.66

$p<0.0005$

Table 20. The 2x2x2 cross-categorised frequency data input for the computation of the 3-way log-linear analysis of Clinical symptoms, Angiographic plaque surface irregularity and Histological lesion types. Frequency data of the presence or absence of symptoms (Condition A) to surface irregularity (Condition B) that exists in 'unstable and vulnerable lesion types' (Condition C1) were generated on the left and in 'stable lesion types' (Condition C2) on the right. The log-linear analysis statistic, G^2, is distributed approximately as Chi-Square and its value would correspond quite closely to the Chi-Square statistic.

3.9 Three domain analysis, Sample usage and Selection

3.9.1 Selection of the unstable plaque: the ruptured thin fibrous cap atheroma

A Venn diagram of the 3 domain analysis for the selection of the unstable recently symptomatic (within 90 days) ruptured thin fibrous cap atheroma (RupTFCA) is presented in Figure 45. The utility of the radiological criteria of major surface irregularity was preferential in the selection and would not exclude the specimens from selection. Fifteen RupTFCA samples were ranked according to their characteristics in the 3 domains. The Venn diagram demonstrates the selection of the unstable ruptured plaque by rank order of:

Rank 1: RupTFCA with major surface irregularity and symptoms <90 days (n=6).
Rank 2: RupTFCA without major surface irregularity and symptoms <90 days (n=2).
Rank 3: RupTFCA with major surface irregularity and symptoms >90 days (n=4).
Rank 4: RupTFCA without major surface irregularity and symptoms >90 days (n=3).

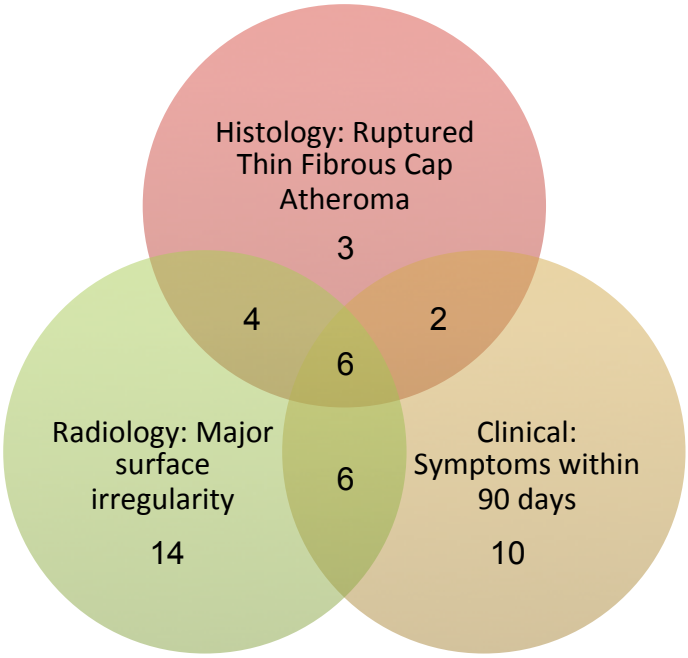

Figure 45. Venn diagram of the selection of the symptomatic unstable ruptured plaque for gene expression analysis using the criteria in 3 domains.

The selected samples were processed and cryosectioned for LMD. Of the top ranked group of 6 samples, 4 samples were successfully taken through to LMD and RNA isolation, and two were not; one was too fragmented for LMD and the other did not demonstrate RupTFCA on deeper cryosectioning into the snap-frozen blocks. All the

second and third ranked samples were successfully processed through to LMD. All of the fourth ranked samples were successfully processed except one sample which RupTFCA was not demonstrated on deeper cryosectioning into the snap-frozen blocks.

The top ranked unstable ruptured thin fibrous cap atheromas were preferentially selected for microarray gene expression profiling. The remaining samples were used for the qRTPCR gene expression validation work later. The clinical, radiological and histological characteristics of these specimens are detailed in Table 21.

3.9.2 Selection of the stable plaque : the fibrous cap atheroma and fibrocalcified plaque

The relative distribution of the samples which have passed the respective clinical, radiological and histological criteria for the stable plaque are shown in the Venn diagram in Figure 46. There were 14 specimens which have passed all 3 domain criteria and were ranked first in the selection for the Stable Plaque. The second rank of selection if required would be from the samples with histology of a stable FCA or FCL and were true asymptomatics but with surface irregularity on MRA (n=3).

The snap-frozen specimens with thick fibrous cap atheroma or thick fibrous cap fibrocalcified plaques were processed and cryosectioned for LMD. Of the first rank samples, 11 were successfully taken through LMD and RNA isolation. The other 3 specimens were not suitable; one was hypocellular (with very few macrophages or VSMCs) and 2 had histology consistent with pathological intimal thickening on deeper cryosectioning. Of the second rank samples, 1 was successfully taken through LMD and RNA isolation. The other 2 samples were not suitable; one which although was asymptomatic had evidence of cerebral infarction on the head scan and the other sample had histology consistent with pathological intimal thickening on deeper cryosectioning.

The top ranked samples stable thick fibrous cap atheroma or thick fibrous cap fibrocalcified plaques were preferentially selected for microarray gene expression profiling. The remaining samples were used for the gene expression validation work after. The clinical, radiological and histological characteristics of these specimens are detailed in Table 22. Details of the initial test sample used for LMD and microarray, with histology of stable fibrocalcified plaque but had prior symptoms more than a year ago, is included in the table.

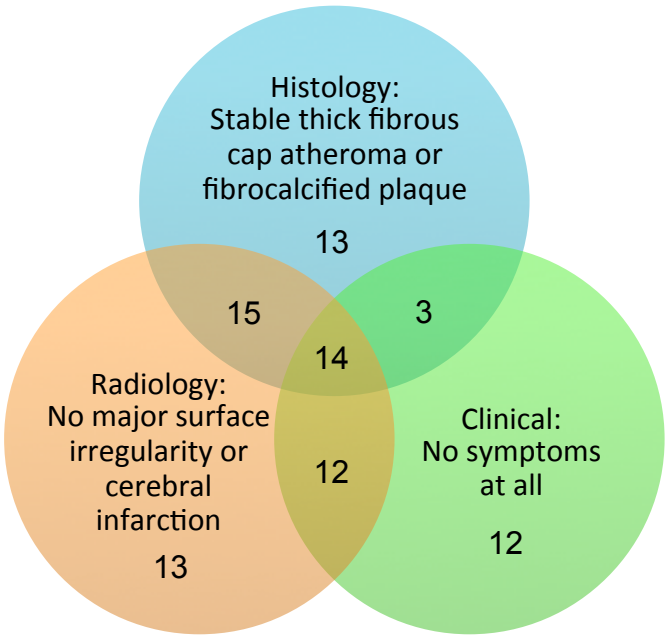

Figure 46. Venn diagram of the selection of the asymptomatic stable plaque for gene expression analysis using the criteria in 3 domains.

CEA code	Age	Sex	Clinical					Radiology			Histology			Purpose	
			Clinical Symptom Group	TIA	CVA	Clinical Diagnosis	Days from last event	Stenosis %	Surface Irregularity	Cerebral infarction	Lesion Type	Thrombus	Haemorrhage	Micro-array	Valid-ation
CEA17	67	M	SYMP≤90	no	Yes	Partial Anterior Circulation Infarction	30	90	Major	no	Ruptured thin fibrous cap atheroma	Yes	Yes	✓	✓
CEA100	73	F	SYMP≤90	no	Yes	Partial Anterior Circulation Infarction	35	75	Major	Yes	Ruptured thin fibrous cap atheroma	Yes	Yes	✓	✓
CEA33	63	M	SYMP≤90	Yes	no	Amaurosis Fugax	3	70	Major	no	Ruptured thin fibrous cap atheroma	Yes	Yes	✓	✓
CEA35	53	M	SYMP≤90	Yes	no	Partial Anterior Circulation TIA	28	70	Major	no	Ruptured thin fibrous cap atheroma	Yes	Yes	✓	✓
CEA57	74	F	SYMP≤180	Yes	no	Amaurosis Fugax	180	95	Major	no	Ruptured thin fibrous cap atheroma	Yes	Yes	✓	✓
CEA113	54	M	SYMP≤90	Yes	no	Amaurosis Fugax and Partial Anterior Circulation Infarction	28	80	Mild	Yes	Ruptured thin fibrous cap atheroma	Yes	Yes		✓
CEA107	62	M	SYMP≤90	no	Yes	Partial Retinal Infarction	49	98	Major	no	Ruptured thin fibrous cap atheroma	Yes	Yes		✓
CEA114	72	M	SYMP≤90	no	Yes	Amaurosis Fugax and Partial Anterior Circulation Infarction	90	90	Major	Not avail	Ruptured thin fibrous cap atheroma	Yes	Yes		✓
CEA22	60	M	SYMP≤180	Yes	no	Partial Anterior Circulation TIA	180	95	Mild	no	Ruptured thin fibrous cap atheroma	Yes	Yes		✓
CEA23	77	M	SYMP≤180	no	Yes	Partial Anterior Circulation Infarction	150	65	Major	Yes	Ruptured thin fibrous cap atheroma	Yes	Yes		✓
CEA42	61	F	SYMP>180	no	Yes	Partial Anterior Circulation Infarction	300	80	Smooth	no	Ruptured thin fibrous cap atheroma	Yes	Yes		✓

CEA code	Age	Sex	Clinical	Radiology			Histology				Purpose	
				Stenosis %	Surface irregularity	Cerebral infarction	Lesion type	Thick cap	Core	Inflammation, erosion, rupture	Microarray	Validation
CEA45	68	F	Asymp	95	Smooth	No	Fibrous cap atheroma	Yes	Lipid	No	✓	✓
CEA41	73	M	Asymp	98	Smooth	No	Fibrous cap atheroma	Yes	Lipid	No	✓	✓
CEA25*	58	M	Asymp	90	Mild	No	Fibrous cap atheroma	Yes	Lipid	No	✓	✓
CEA36	67	M	Asymp	75	Smooth	No	Fibrocalcified plaque	Yes	Fibrocalcific	No	✓	✓
CEA81	59	M	Asymp	85	Smooth	No	Fibrocalcified plaque	Yes	Fibrocalcific	No	✓	✓
CEA112	68	M	Asymp	98	Smooth	No	Fibrous cap atheroma	Yes	Lipid	No		✓
CEA84	72	M	Asymp	65	Smooth	Not avail	Fibrous cap atheroma	Yes	Lipid	No		✓
CEA92	67	M	Asymp	90	Smooth	No	Fibrocalcified plaque	Yes	Fibrocalcific	No		✓
CEA88	72	F	Asymp	97	Mild	No	Fibrous cap atheroma	Yes	Lipid	No		✓
CEA117	71	M	Asymp	75	Mild	No	Fibrous cap atheroma	Yes	Lipid	No		✓
CEA64	68	F	Asymp	95	Mild	No	Fibrocalcified plaque	Yes	Fibrocalcific	No		✓
CEA44	73	M	Asymp	60	Major	No	Fibrous cap atheroma	Yes	Lipid	No		✓
CEA14*	45	F	Lacunar Infarction 1 year ago	85	Major	Yes	Fibrous cap atheroma	Yes	Lipid	No	✓	✓

Table 22. Clinical, Radiological and Histological characteristics of the Stable Plaque samples selected for microarray expression profiling and quantitative real-time PCR validation work. (CEA25* and CEA14*- the initial test samples used for LMD and microarray.)

Chapter 4. The isolation and characterisation of cell-specific RNA

4.1 Overview

LMD for gene expression analysis in atherosclerotic tissues is still in its infancy and to date, LMD has not yet been applied to study plaque rupture. A validated LMD protocol specific to our tissue type and biology in question has not been established. Furthermore, an optimal method has not been determined for the extraction from very small amounts of LMDed tissue. Critical to the successful amplification of mRNA for microarray is the isolation of high quality RNA and in sufficient quantity. As a result, it was necessary for me to systematically evaluate and develop optimal methods in sample preparation, LMD and RNA extraction in the isolation of high quality RNA of high yield from the atherosclerotic plaque.

Maximally contrasting stable and ruptured plaques were selected using the validated enrichment criteria in the three-domains described in Chapter 3. The selected specimens were processed for LMD and RNA extraction of cell-pure regions of macrophages and VSMCs using the validated optimal protocols I developed. The typical amounts of RNA isolated from LMD are not sufficient for direct hybridisation to microarrays. High quality RNA was linearly amplified using T7 RNA polymerase to generate sufficient cRNA for hybridisation on the Affymetrix HG-U133plus2 genome-wide microarray. An overview of the various stages involved in the workflow of the specimens is shown in Figure 47 below.

RNA degradation can occur at any stage and is cumulative and may result in a failed experiment if not monitored, or worse, generate a biased transcriptomic profile unrepresentative of the true biological picture. Numerous quality control assessments (QCA) were performed throughout the workflow to monitor RNA quality and experimental performance to ensure a high quality final microarray result (Figure 47). The first confirmation of RNA quality and yield occurs after LMD and RNA extraction, after considerable work, which emphasizes the importance of the optimisation and validation of these upstream processes.

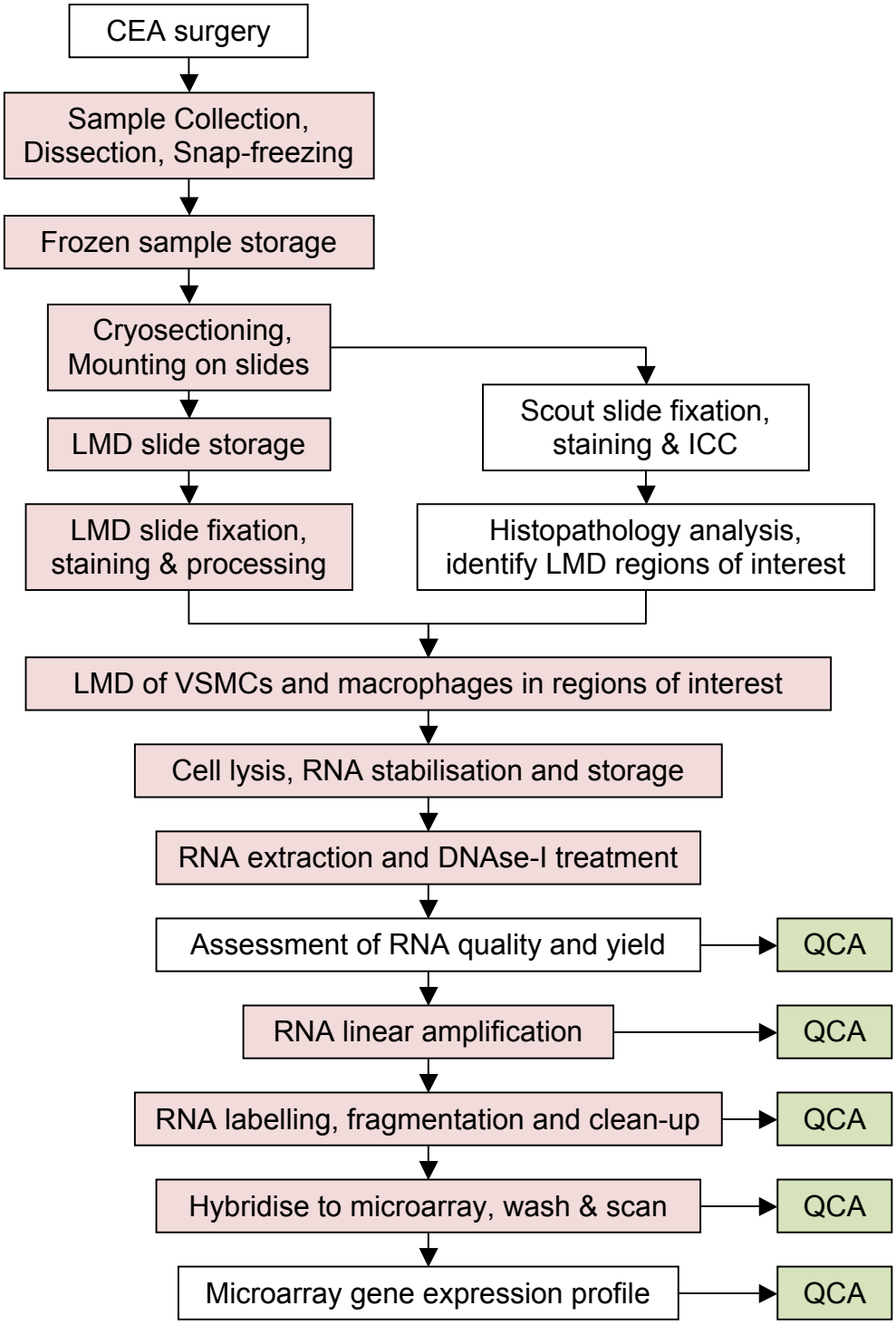

Figure 47. Overview of the steps involved in sample processing leading to Microarray. Highlighted in red are the processes where RNA degradation may occur and in green are the quality control assessments (QCA) of RNA quality and performance through the workflow.

4.2 Evaluation of snap-freezing methods

We evaluated various snap-freezing methods in the preservation of the histology and RNA integrity of the samples. Snap-freezing in liquid-nitrogen-cooled isopentane bath proved to be the most intricate to set up but with the best results. The samples were instantly and uniformly snap-frozen without any macroscopic freeze-fracture artefact seen and cryosectioned well. The histological appearances showed intact and distinct cellular membranes on H&E staining without any apparent microscopic artefacts (Figure 48, panels C&D). In comparison, snap-freezing directly in liquid nitrogen resulted in significant Leidenfrost effect and freeze-fracture cracks in cryoblocks of larger samples such as that of the carotid bulb of the CEA samples but not in the smaller IMA samples. Snap-freezing on a liquid-nitrogen-cooled copper plate froze the samples gradually from the base upwards with macroscopic freeze-fracture artefacts and did not cryosection well. The histology demonstrated loss of cell membrane definition on H&E staining which may be due to slow-freezing artefact with water crystal formation and disruption of cellular membranes (Figure 48, panels A&B). The RNA quality and yield also reflected the histological observations, with optimal results from the liquid-nitrogen-cooled isopentane bath method (described in the next section).

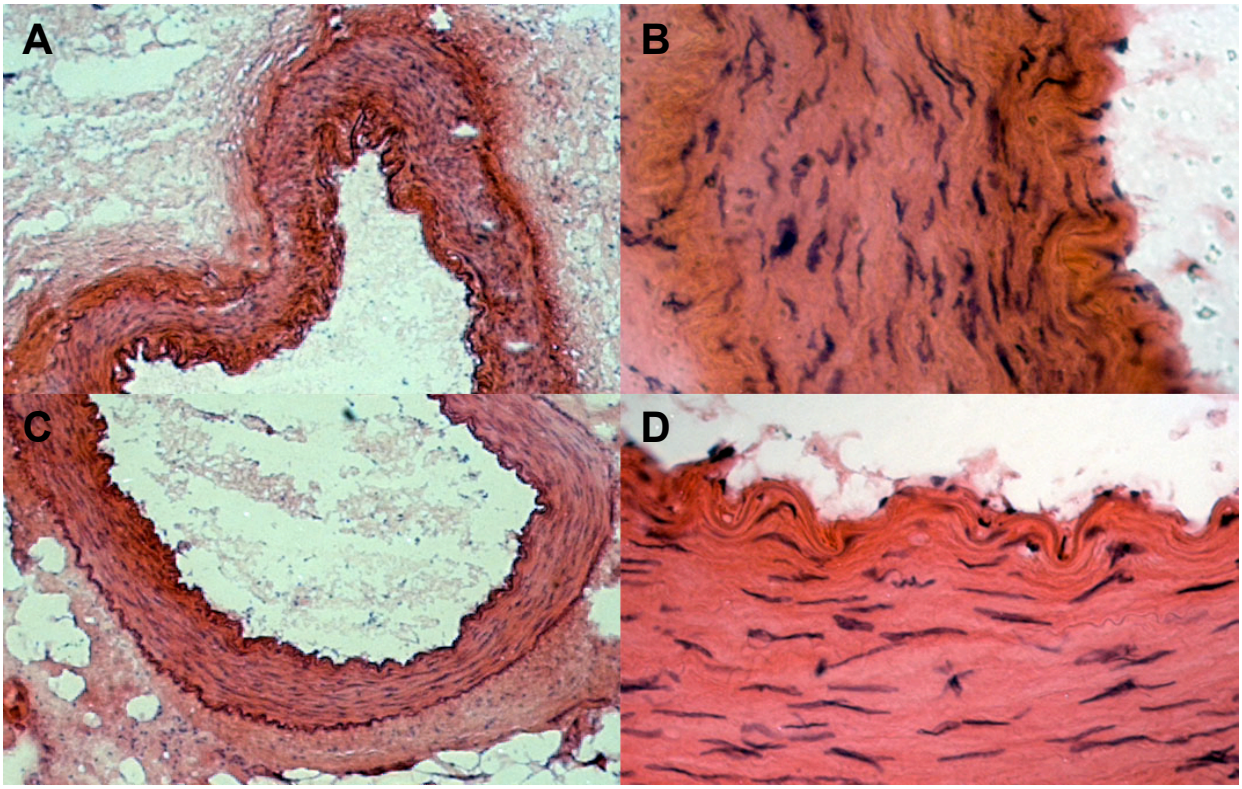

Figure 48. H&E stained cryosections of IMA specimens snap-frozen using the Liquid-N_2-cooled copper plate (A&B) and the Liquid-N_2-cooled isopentane bath (C&D) methods.
(Magnification of x40 in A&C and x100 in B&D)

The histological and RNA results of the different snap-freezing methods are summarised in Table 23. The snap-freezing of the OCT-embedded specimens using liquid-nitrogen-cooled isopentane bath yielded the best results. Subsequent CABG and CEA samples were collected using this method and were all successfully snap-frozen without complication. In our experience, larger sample widths (up to 20x20mm) were still successfully snap-frozen as long as the sample depth (or the narrowest dimension) was 6mm or less.

Method	Macroscopic freeze-fracture?	Cryosectioned well?	Histological detail?	RNA quality?	RNA yield?
Direct immersion in liquid-N_2	Some	-	++	++	++
Liquid-N_2-cooled copper plate	Some	-	+	-	+
Liquid-N_2-cooled isopentane bath	None	+++	+++	+++	+++

Table 23. A summary of the macro- and microscopic characteristics and RNA quality and yield using the different snap-freezing methods.

4.3 Baseline evaluation of RNA quality of snap-frozen specimens

I performed a baseline assessment of RNA quality of the snap-frozen internal mammary artery (IMA) and carotid endarterectomy (CEA) samples by whole tissue RNA extraction in assessment of the optimal snap-freezing methodology as well as validation of the RNA quality of the collected samples.

4.3.1 Baseline RNA extraction from whole tissue IMA specimens

RNA was extracted from small portions of internal mammary artery collected from 4 different patients (IMA1, IMA2, IMA3 and IMA6), weighing 120mg, 450mg, 408mg and 65mg respectively using rotor homogenisation and Trizol-reagent Phenol-Chloroform RNA extraction. The IMA1 sample was snap-frozen using the liquid-nitrogen-cooled copper-plate method, IMA2 by direct immersion in liquid-nitrogen and IMA3 by liquid-nitrogen-cooled isopentane bath. The IMA6 sample was put in normal saline by the surgeon for 2

hours accidentally before snap-freezing in the liquid-nitrogen-cooled isopentane bath and was included as an assessment of RNA degradation.

The RNA yields for IMA1 and IMA2 estimated by UV absorbance optical density (OD) at 260nm using a spectrophotometer were 0.14μg and 0.31μg of total RNA per 1mg of tissue. The RNA analysed on the Agilent Bioanalyser 2100 RNA-Nano-chip reported more conservative estimates of RNA yield for IMA1 and IMA2 (0.08μg and 0.25μg of total RNA per mg of tissue). The RNA yield of IMA3 was 0.4μg per mg of tissue but the RNA yield from IMA6 was very poor at 0.02μg per mg of tissue. The electropherogram and fluorescence graphs showed severe degradation of RNA in IMA6 and moderate degradation of RNA in IMA1. There was almost complete degradation of the 28S ribosomal band and fragmentation of RNA transcripts seen as a diffuse fluorescence of small RNA fragments in the background in both the electropherogram and the fluorescence graph in IMA6 and to a lesser extent in IMA1 (Figure 49). The 28S/18S ribosomal RNA ratios of IMA1 and IMA6 were 0.4 and <0.1 representing severe RNA degradation. In comparison, the RNA of IMA2 and IMA3 were relatively intact, with distinct 28S and 18S Ribosomal bands and a cleaner background in the electropherograms and fluorescence graphs. The 28S/18S ratios of IMA2 and IMA3 were 1.2 and 1.4 representing some RNA degradation (ideally the ratio should be 1.8 to 2). The low molecular weight RNA species of tRNA and 5S ribosomal RNA were also detected, demonstrating its successful extraction by the Trizol Phenol-Chloroform technique.

The liquid-nitrogen-cooled isopentane bath snap-frozen IMA3 sample and the direct liquid-nitrogen immersion snap-frozen IMA2 sample produced the best results in RNA quality and yield with marginally better results in the former. The liquid-nitrogen-cooled copper-plate snap-frozen IMA1 specimen produced moderately degraded RNA and modest yield. The IMA6 specimen which was left in normal saline for 2 hours with no preservation of the RNA from endogenous RNases, explaining the severe degradation of RNA and poor yield.

Expected RNA yields from RNA extractions of mice heart muscle were about 1μg per mg of tissue and yields from vessel walls were lower at 0.5μg per mg of tissue (Qiagen data). Our yield from surgically extracted human vessel wall of 0.31-0.40μg per mg of tissue was within the expected range. The RNA quality was reasonable (with distinct 28S and 18S ribosomal bands and a relatively clean background) but there was evidence of some RNA degradation which may be due to the total ischaemic time of about 20 minutes or more (from the interruption of blood flow to snap-freezing) which the IMA tissues were exposed to during its surgical preparation which was unavoidable.

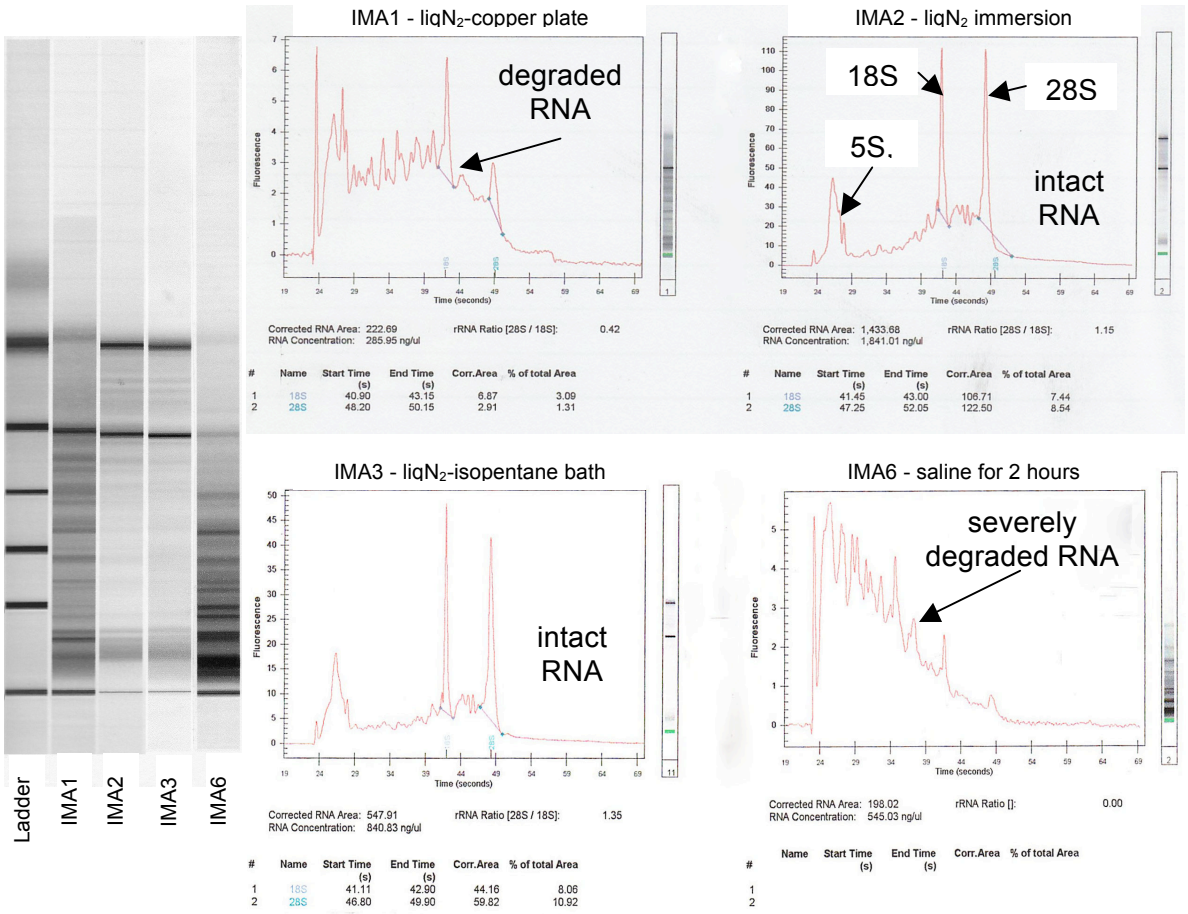

Figure 49. Agilent Bioanalyser electropherogram (left) and fluorescence graphs (right) of total RNA extracted from whole tissue IMA specimens using Trizol.

4.3.2 Baseline RNA extraction from whole tissue CEA specimens

RNA was extracted from small amounts of whole plaques from 3 CEA specimens; CEA06, CEA23, CEA25 weighing 19mg, 30mg and 21mg respectively. This included the fibrous caps, thickened intima and necrotic cores of the atherosclerotic plaques. This was performed using rotor homogenisation and the Trizol-reagent RNA extraction method. The CEA samples were snap-frozen using the liquid-nitrogen-cooled isopentane bath method.

The total RNA isolated was analysed using the Agilent Bioanalyser 2100 RNA Nano-chip (Figure 50). The yields were 0.4µg, 0.36µg and 0.62µg of total RNA per mg of tissue, and were comparable to the yields from the IMA samples. There was evidence of more significant RNA degradation compared to the IMA specimens with poorer 28S/18S ribosomal ratios (of <1.0, 1.2 and <1.0 respectively) with increased background fluorescence of RNA fragmentation and degradation products, despite a shorter total ischemic time of 10 minutes for the CEA specimens. This was however to be expected as the whole tissue of atherosclerotic plaque included necrotic/dead tissue mixed in

combination with other viable and active cells in the heterogenous plaque. I was still able to extract a reasonable yield of total RNA from whole tissue of atherosclerotic plaque.

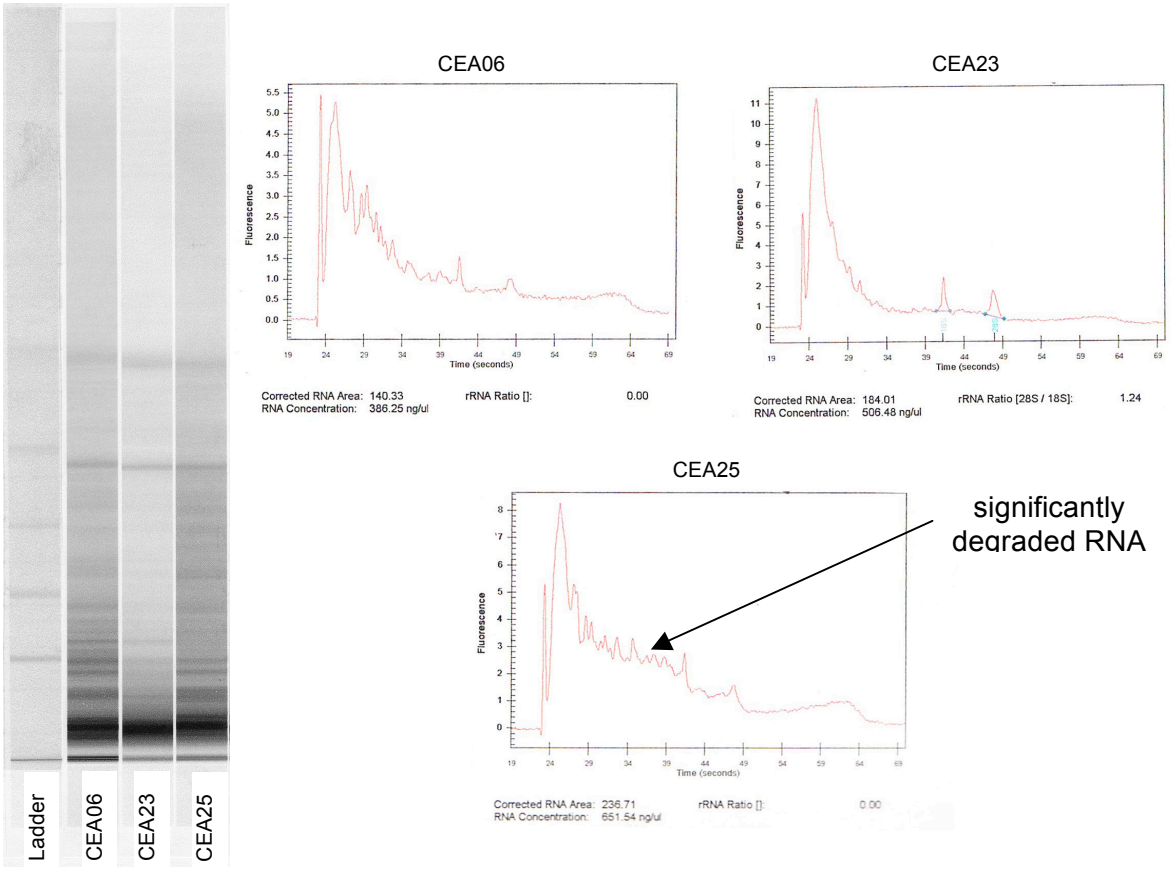

Figure 50. Agilent Bioanalyser Nano-chip electropherogram and Fluorescence graphs of total RNA extracted from whole tissue CEA specimens using Trizol.

4.4 RNA extraction from small amounts of whole tissue

Prior to extracting RNA from LMDed material I demonstrated that I was able to extract RNA from very small amounts of whole tissue. Whole cryosections from IMA samples had RNA extracted using the Trizol-reagent Phenol-Chloroform method with rotor homogenisation and the silica-based column extraction methods using RNeasyMicro (Qiagen) with high-speed vortex homogenisation and were performed in duplicate.

RNA was successfully detected using the Agilent Bioanalyser Pico-chip (Figure 51). The average total RNA yield from Trizol extraction was 65ng of total RNA per 1mg of tissue, 30ng per mg using RNeasyMicro. These were about 10-20% of the yields seen from RNA extraction performed using 10x more tissue. The column extraction methods did not extract the low molecular weight RNA of 5S ribosomal RNA and tRNA and would account for the relative differences seen compared to Trizol. Another contributor may be the inadequate homogenisation of the sections of tissue using high speed vortexing of the

whole tissue in the lysis buffer compared to rotor homogenisation used in the larger tissue amounts. The RNA extracted using RNeasyMicro was of the highest quality with high 28S/18S ratios of 1.6 and 1.9 and a clean background and from as little as 1.5mg of tissue. This demonstrated that I could isolate and detect high quality RNA from a few milligrams of tissue but with a lower expected yield, suggesting that further optimisation of the method was required.

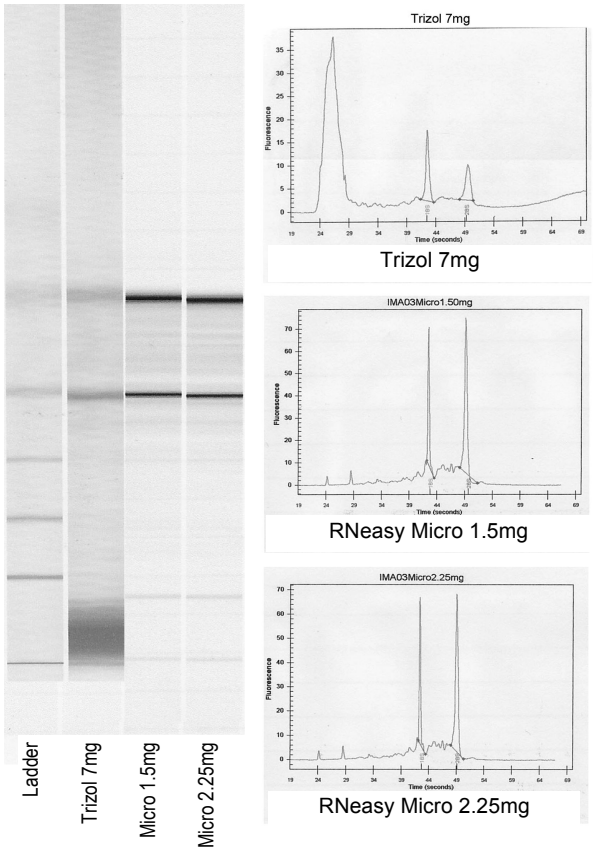

Figure 51. Agilent Bioanalyser Pico-chip electropherogram and fluorescence graphs of RNA extraction from milligrams of snap-frozen IMA tissue using the Trizol Phenol-Chloroform method and the silica-based column extraction methods using RNeasyMicro.

4.5 Optimisation of RNA extraction from very small amounts of LMD tissue

The LMD of 5,000 VSMCs was estimated to be from 12.5 micrograms of material; nearly 100 times less in amount of tissue than that extracted so far. It was important to have an RNA extraction method of the highest yield and quality for downstream RNA amplification and microarray as well as for the accurate assessment of further LMD optimisations. Henceforth, I developed an optimised and reliable method of extracting and detecting RNA from micrograms of LMDed material.

4.5.1 RNA extraction methods and DNase-I digestion

About 5,000 VSMCs were LMDed from unstained 95% ethanol-fixed IMA sections. RNA was extracted from the LMD samples using the Trizol-reagent Phenol-Chloroform method with glycogen carrier, and using the RNA column extraction methods by RNeasyMicro (Qiagen), PicoPure (Arcturus), NanoPrep (Stratagene) and RNAqueousMicro (Ambion), with and without on-column DNase-I digestion. The experiments were performed in duplicate.

The extracted RNA was analysed using the Agilent Bioanalyser Pico-chip (Figure 52). The Trizol extraction isolated a total of 7.3ng of total RNA, approximately 0.58μg of total RNA per mg of tissue. We expected yields of 0.5μg/mg from vascular tissue (Qiagen data). The RNA quality was poor (the 28S/18S ratios were 0.5) but there was no significant DNA contamination. The RNeasyMicro extractions were the most impressive, with the highest yields of 10.8ng (0.86μg/mg) and highest quality RNA (28S/18S ratio of 1.94 with clear ribosomal bands and relatively clean baseline). There was DNA contamination without DNase-I digestion but the ribosomal bands were still clearly seen. The second replicate did not work probably due to the DNA contamination of the columns. The PicoPure extractions had significant RNA degradation (28S/18S ratios of 0.6) with lower yields and DNA contamination. The NanoPrep and RNAqueousMicro extractions failed to extract any RNA.

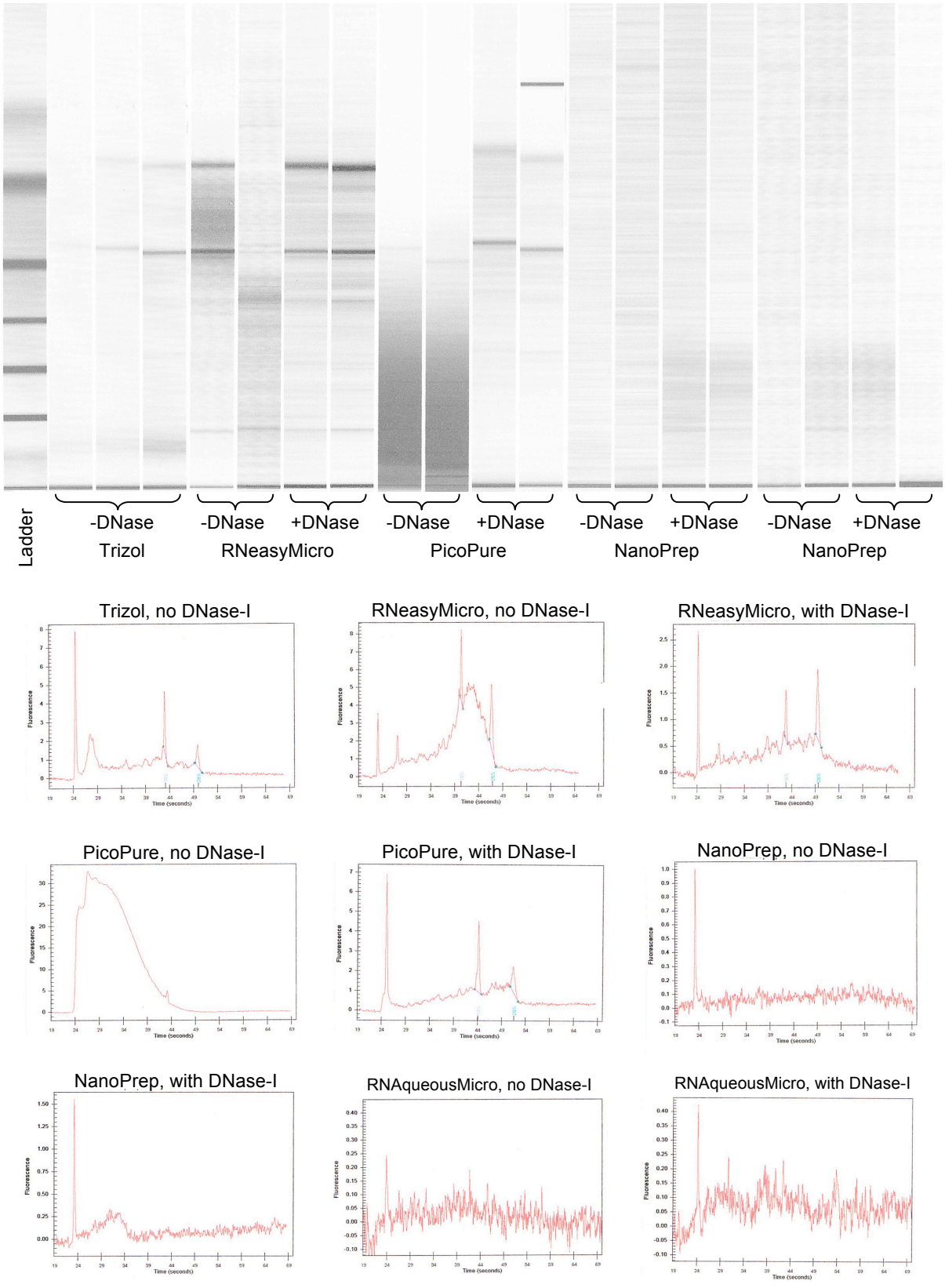

Figure 52. Agilent Bioanalyser Pico-Chip electropherogram and fluorescence graph results of extracted RNA from LMDed smooth muscle cells using Trizol, RNeasyMicro, Picopure, NanoPrep and RNAqueousMicro, with and without DNase-I digestion.

The results, summarised in Table 24, demonstrated that the RNeasyMicro extractions with DNase-I digestion was the most efficient method and produced high quality RNA with high yields and without DNA contamination from as little as an estimated 12.5micrograms of laser micro-dissected tissue.

	Yield (ng of RNA/ 5000 cells)	Yield (µg of RNA/ mg of tissue)	28S/18S ratio	DNA contamination
Trizol, no Dnase-I	7.3	0.58	0.5	no
RNeasyMicro, no DNase-I	*	-	1.55	yes
RNeasyMicro, with DNase-I	10.8	0.86	1.94	no
PicoPure, no Dnase-I	*	-	0	yes
PicoPure, with Dnase-I	6.3	0.52	0.6	no
NanoPrep, no Dnase-I	0	-	0	no
NanoPrep, with Dnase-I	0	-	0	no
RNAqueousMicro, no Dnase-I	0	-	0	no
RNAqueousMicro, with Dnase-I	0	-	0	no

Table 24. Results of the average RNA yield and quality and DNA contamination from LMDed VSMCs using Trizol, RNeasyMicro, Picopure, NanoPrep and RNAqueousMicro, with and without DNase-I digestion. (A 28S/18S ratio of 1.6-2.0 represents high quality RNA. *note: the yields reported here were inaccurate for total RNA as it included nucleic acid from DNA contamination.)

4.5.2 Carrier RNA

I evaluated the use of carrier RNA to minimise the loss of the very small amounts of RNA extracted from LMD due to binding of the RNA to the plastic surfaces. There was no observable difference in the measured yields of total RNA estimated by the Agilent Bioanalyser Pico-chip (similar concentrations were seen, Figure 53). However, in my experimental controls of RNA extractions of only 20ng of carrier RNA with no samples, the Pico-chip Bioanalyser traces only showed a very small low molecular weight band of the carrier RNA with a flat baseline comparable to the Bioanalyser traces of RNase-free water. This suggested that the carrier RNA used was not significantly extracted by the columns. Therefore I continued to use carrier RNA in the RNA extraction of LMD samples as I usually micro-dissected approximately 5,000 to 10,000 cells into each micro-eppendorf tube for RNA extraction.

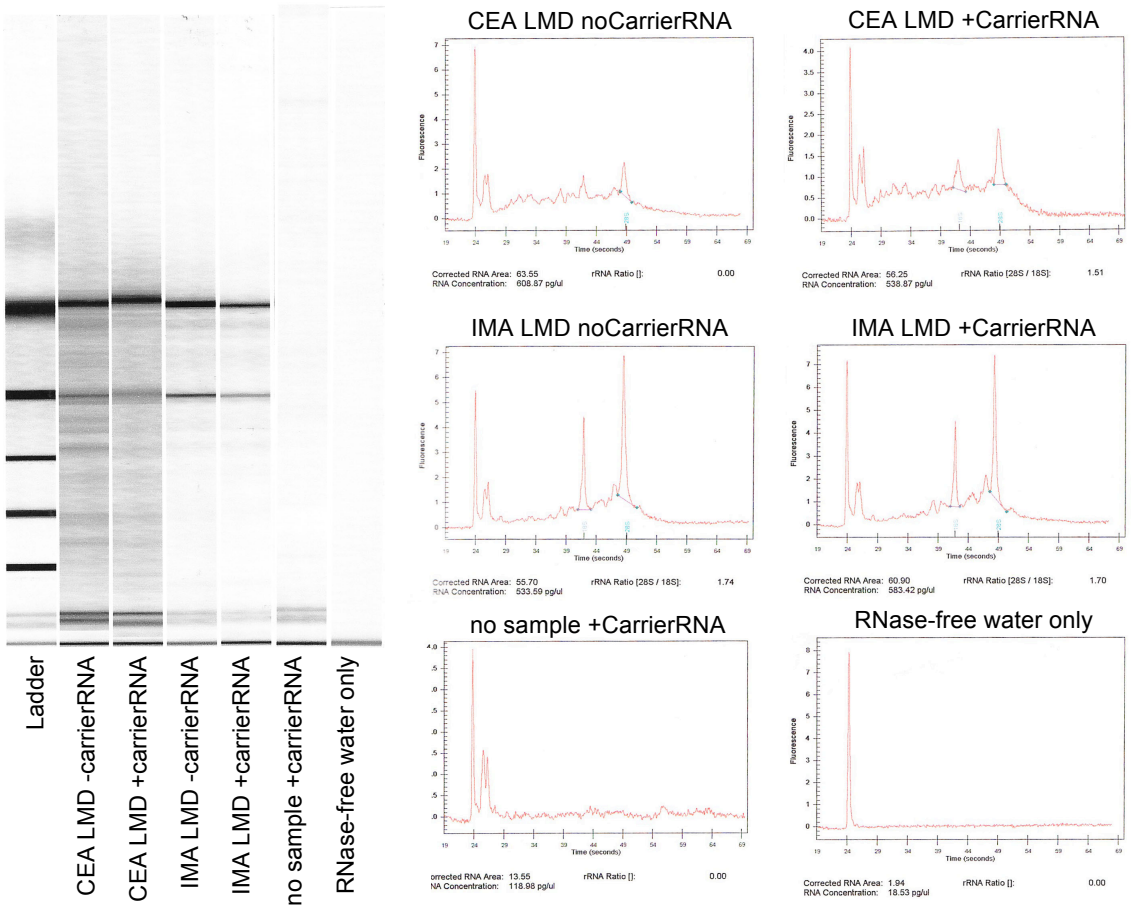

Figure 53. Agilent Bioanalyser Pico-chip results with and without the use of carrier RNA. Experimental control samples of Carrier RNA only and RNase-free water only are also shown.

4.5.3 Increasing the extracted RNA yield: lysis buffer volume

In the later LMD tests on CEA tissue, I used IMA tissue as a positive control of the LMD process. During the course of these experiments, I made a retrospective observation that there was a difference in RNA yields from the LMD of the IMA control sections. I had initially attributed this to random effect. However, it became apparent that this observation may be related to the difference in amount of lysis buffer RLT used. The yields from extractions using less lysis buffer volume were consistently higher and may be due to more efficient binding of the RNA to the silica columns with higher concentration of lysed cells.

To test this hypothesis, I extracted RNA from the LMD of 10,000 VSMCs from IMA tissue using 75µl or 350µl of lysis buffer RLT and performed these in triplicate. The yields from the 75µl lysis buffer extractions were 33ng, 31ng and 41ng. The yields from the 350µl lysis buffer extractions were 16ng, 11ng and 19ng. The increment in yields seen by using

a lower lysis buffer volume when performing LMD of 10,000 cells or less was by a factor of 2.3x. The volume of 75µl of lysis buffer was about sufficient to fully fill the micro-eppendorf cap to capture all the micro-dissectates in the solution, any less lysis buffer may have a detrimental effect. There was a significant benefit of performing the LMD of slides in batches to ensure enough cells were collected in an individual session (of at least more than 10,000 LMDed cells per session if possible). However, there was a risk of RNA degradation as a result of the processed sections remaining in room temperature for longer as a result of this which required further evaluation and was performed later.

4.5.4 Increasing the extracted RNA concentration: double elution

The linear amplification of very small amounts of RNA extracted from LMD, to generate enough amplified cRNA for the microarray experiments, require a reasonable concentration and yield of RNA to work from. By performing a double passage of the minimal amount of 14µl of RNase-free water to fully saturate the extraction columns, I had a final eluate of 11µl with a 10-15% higher concentration compared to a single elution of a final eluate volume of 12µl. There was no appreciable increment of yield but there was an appreciable increment of the concentration of the RNA.

4.5.5 The optimal RNA extraction protocol

From my direct comparison experiments of the various RNA extraction methods available at the time for very small amounts of tissue from LMD, the RNA extraction method with consistently high yields of high quality RNA was the RNeasyMicro (Qiagen) silica-based column extraction method with DNase-I digestion. Further modifications to the protocol included the addition of carrier RNA, using the minimal amount of lysis buffer and a double elution step for maximal RNA extraction of a higher concentration. This was the optimal RNA extraction protocol used for the RNA extraction of LMDed atherosclerotic plaque. The optimal RNA extraction protocol is also described in methods chapter 2.8.4.

4.6 Preliminary Laser micro-dissection trials

The original Leica LMD protocols had several recommended methods of preparing and staining the frozen sections for LMD using air-drying (no-fixation), ethanol fixation and acetone fixation. As the medial layer of VSMCs were clearly seen on the IMA cryosections (Figure 54), these preliminary LMD trials were performed without staining thus omitting its effects on the results of RNA yield and quality.

4.6.1 LMD

The slides processed using the Leica No-Fixation LMD protocol were LMDed without any difficulty and performed in duplicate. However, using the ethanol fixation protocol resulted with desiccation and lifting of the cryosections with the xylene dehydration/clearing stage and LMD was not possible (Figure I). For the purpose of this evaluation, I omitted the xylene clearing step and introduced an additional 100% Ethanol stage of 30 seconds to ensure adequate dehydration/clearing of the sections without desiccation artefact and good section adherence (Figure 54). The sections successfully underwent LMD without any difficulty and were performed in triplicate. Similar problems were seen with the Acetone fixation protocol with xylene dehydration/clearing as well as with its omission, with desiccation artefact and lifting of the cryosections, and LMD was not possible.

Of the samples which were successfully LMDed, 50 microdissections about 50,000μm^2 in area containing about 10,000 medial VSMCs (estimated by the average number of nuclear stains seen on H&E staining of the sections) were made for each (Figure 54).

4.6.2 RNA extraction

RNA was extracted using the PicoPure and RNeasyMicro without proteinase-K or DNase-I digestion and analysed using the Agilent Bioanalyser Pico-chip (Figure 55). The RNA extracted from LMD of VSMCs using the no-fixation LMD protocol was completely degraded. The RNA extracted from the Ethanol-fixation LMD protocol was severely degraded using the PicoPure or RNeasyMicro RNA extraction with evident 28S/18S<1 and fragmented degradation products as well as DNA contamination.

The failure to extract RNA without fixation demonstrated the importance of sample fixation to maintain histological integrity and RNA stability for RNA work as it leaves the sample vulnerable to RNases. However, it was disappointing that the Leica Ethanol fixation protocol produced poor quality RNA. The ethanol fixation protocol had been used for LMD and RT-PCR experiments of arterial vessels reported in three recent publications at that time[203, 212, 216]. However, they did not utilise the Agilent Bioanalyser to assess RNA quality

or integrity. High RNA quality was critical to the successful linear amplification reactions required to generate sufficient cRNA for microarray. As the amplification reactions were primed from the poly(A) tail, any significant degradation of mRNA would lead to unsuccessful amplification of the mRNA past the point of truncation. Although we were able to isolate an average yield of 8.4ng of total-RNA from 10,000 LMDed VMSCs using RNeasyMicro, the RNA was too degraded to be used.

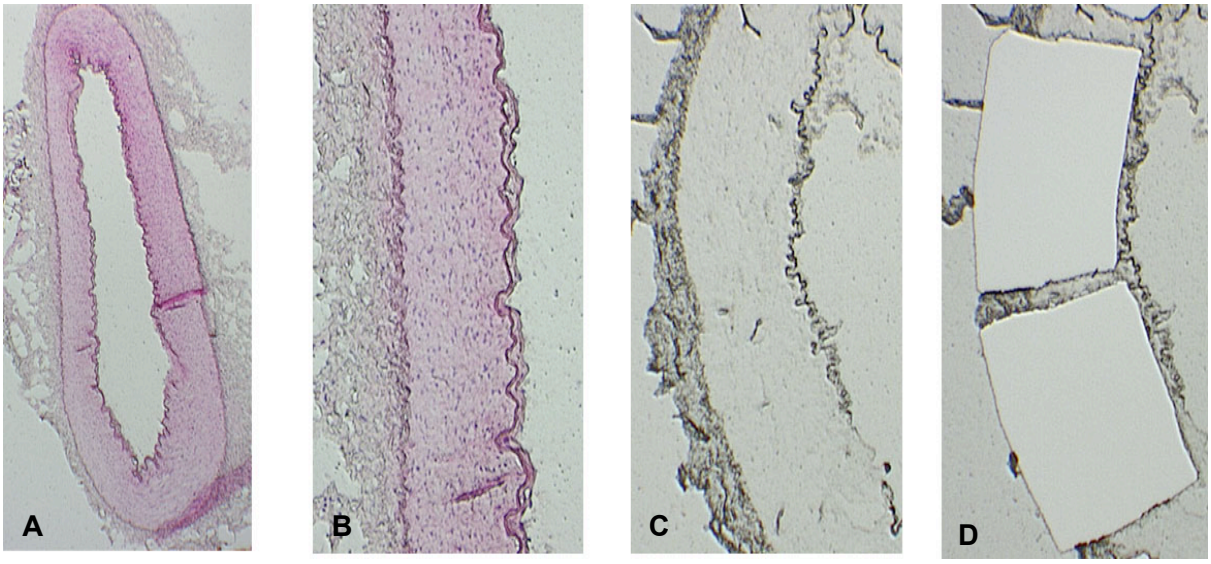

Figure 54. IMA cryosections used for the LMD tests (fixed with 95% Ethanol and without xylene clearing). A&B: H&E stained IMA section of 10µm thickness at 10x magnification and 40x magnification. C&D: IMA sections without staining on a LMD PET-membrane slide at 40x magnification before LMD and after LMD.

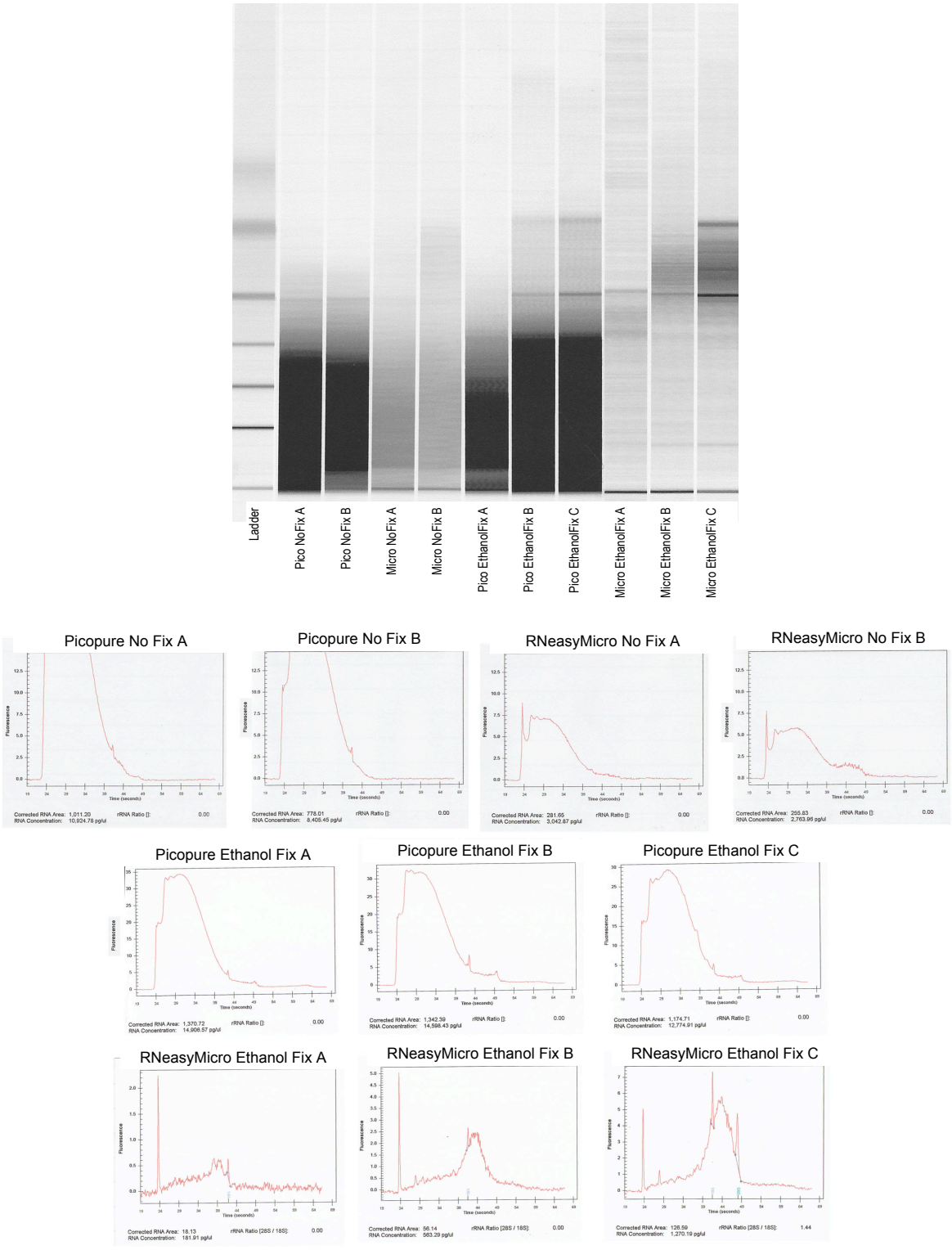

Figure 55. Agilent Bioanalyser results of RNA extracted from the initial LMD trials of VSMCs LMDed from IMA cryosections using the original Leica no-fixation (in duplicate, A&B) and ethanol fixation protocols (in triplicate, A,B&C) and RNeasyMicro and PicoPure RNA extraction methods.

4.7 Optimisation of the LMD process

The difficulty in extracting high quality RNA would be greater in the atherosclerotic plaque with a necrotic core and significant amounts of extracellular RNases. Therefore further optimisation to develop a robust protocol of sample preparation, fixation, staining and processing to produce an adequately prepared section for LMD which was RNA stable with the successful extraction of high quality RNA was critical. I have systematically evaluated and optimised the various stages/factors in the LMD process which could affect RNA integrity and the mechanics of LMD.

4.7.1 Cryosection thickness and OCT embedding media

Different cryosection thickness were tested. I found that cryosections of 10μm thickness were optimal in the overall balance of producing intact sections with minimal artefact, with good section adherence to the LMD thermoplastic membrane and LMDed well. Any excess OCT surrounding the specimens was trimmed off for cryosectioning as residual OCT interfered with the ability of the laser to cut successfully.

4.7.2 LMD membrane slides and air-drying

I found that air-drying of 10 minutes according to the original Leica protocols was detrimental to the integrity of the RNA. I evaluated the effects of a shorter period of air-drying of only 1 minute in room temperature as well as the use of the Leica LMD glass slides and metal slides. The results of a comparative experiment of LMDed VSMCs from IMA cryosections fixed using 90% ethanol without staining or xylene clearing are tabulated in Table 25.

	LMD membrane glass slides		LMD membrane metal slides	
	Air-dried	Not air-dried	Air-dried	Not air-dried
Histological morphology	+++	++	+++	+
Lifting artefact	-	+	-	++
Ease of LMD	+	+	+++	++
RNA quality (28S/18S ratio)	<1	<1	1.3-1.5	1.0
RNA yield (ng/10000cells)	3ng	4.4ng	11ng	7.2ng

Table 25. Comparison of LMD membrane glass slides vs. metal slides, and air-drying versus no air-drying of the mounted cryosections on the slides.

I had found that the glass-membrane slides frequently had trapped water in between the thermoplastic membrane and the glass slide causing difficulty in LMD and may explain the poor RNA yield and quality due to uninhibited RNase activity in an aqueous environment . These issues were not observed with the metal-membrane slides which cut well and generated better quality and yields of RNA. Air drying resulted in better adhesion and histological morphology of the sections. The use of membrane-metal slides and 1 minute of air-drying produced the best results and were incorporated into the LMD protocol.

4.7.3 Fixation and histochemical staining

I evaluated different methods of fixation using 90% ethanol, 75% Ethanol, Acetone and methanol for 1 minute and histochemical staining using toluidine blue, HistoGene stain (Arcturus) and Haematoxylin & Eosin staining. Acetone and methanol fixation resulted in poorer RNA quality and yield with significant lifting artefact with acetone fixation and difficulty in LMD (Figure 56). The histogene stain did not stain the nuclei well and cellular differentiation was poor (Figure 57). Both histogene and toluidine blue stained samples had poor RNA quality and yield. I have found that 75% ethanol fixation with H&E staining to produce the best results with high quality and yields of RNA, good section adhesion and removal of OCT and LMDed well, with good histological detail (Table 26). I later found that staining with haematoxylin alone provided sufficient histological detail and eosin staining was unnecessary.

	75% Ethanol			90% Ethanol			Acetone			Methanol		
	H&E	Tol Blue	Histo -gene	H&E	Tol Blue	Histo -gene	H&E	Tol Blue	Histo -gene	H&E	Tol Blue	Histo -gene
Histological detail	+++	++	+	+++	++	+	+++	++	+	+++	++	+
Lifting artefact	-	-	-	-	-	-	++	++	++	-	-	-
Ease of LMD	+++	+++	+++	++	++	++	-	-	-	+	+	+
RNA quality (28S/18S ratio)	2.0	<1	<1	1.9	<1	1.3	1.8	<1	1.3	<1	<1	<1
RNA yield (ng/10000 cells)	10	2	2.5	14	2	1.3	10	1	1.8	9	1.7	2

Table 26. Results of the different methods of fixation and histochemical staining.

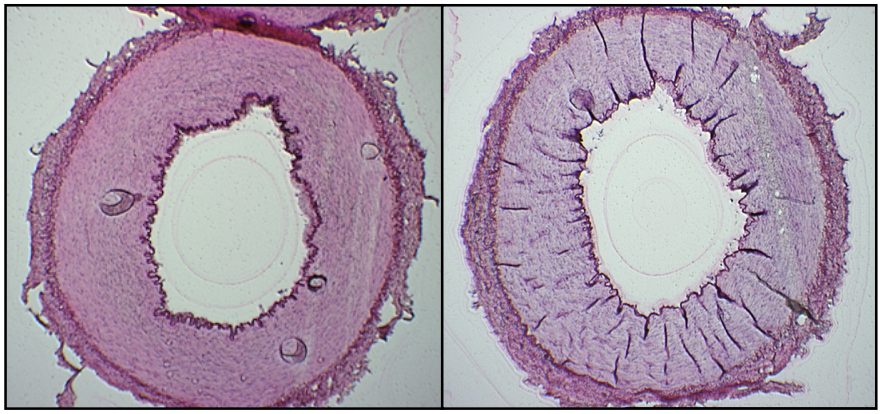

Figure 56. The lifting artefact and 'rucking' of the section fixed in acetone (right causing significant difficulty in LMD) compared to 75% ethanol fixation (left).

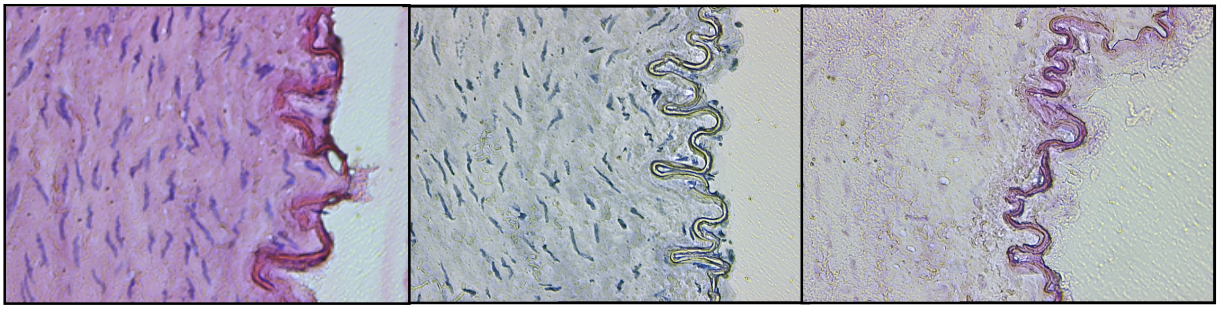

Figure 57. Histochemical staining with (from the left) haematoxylin and eosin, toluidine blue and HistoGene stains of 90% ethanol-fixed IMA cryosections demonstrating the differentiation of cellular detail by the different stains.

4.7.4 Xylene clearing

The xylene stages caused significant lifting of the sections and desiccation artefact causing poor histological definition and unsuccessful LMD (Figure 58). I have omitted the xylene stages in order to preserve histological integrity and for successful LMD. Instead, I have substituted this with a 100% ethanol stage and ensured that the sections were thoroughly air-dried in an RNase-free enclosed slide rack with packets of silica gel hygroscopic desiccants to ensure adequate clearance of water from the fixed and stained LMD sections.

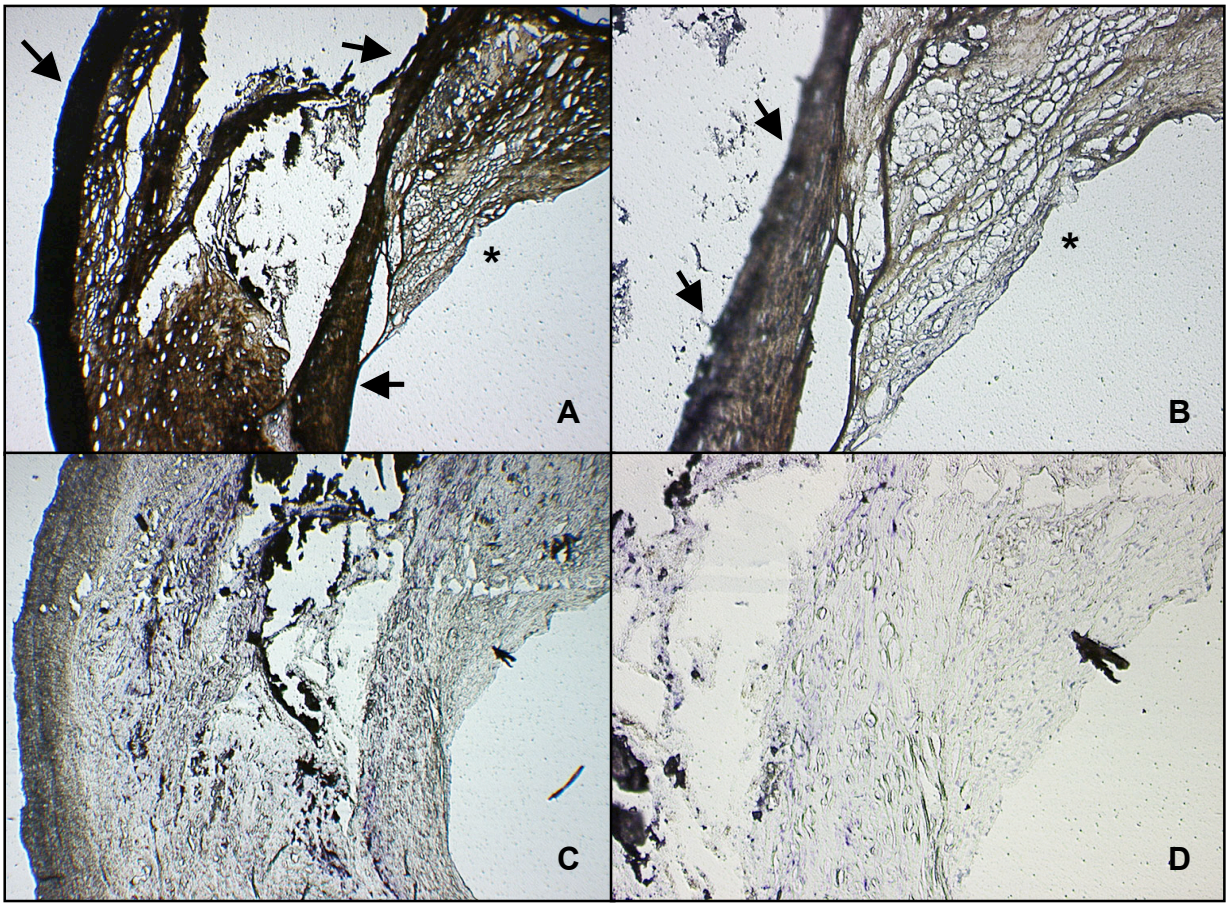

Figure 58. Effect of xylene clearing on atherosclerotic plaque frozen tissue sections on LMD PET-membrane slides (A&B) compared to prolonged 100% ethanol dehydration and clearing (C&D). x40 magnification on the left and x100 on the right. Desiccation artefact (asterisks) and lifting (arrows) is seen with xylene.

4.7.5 Further modifications

From our observations thus far, the diseased atheromatous CEA tissue were more fragile and prone to RNA degradation compared to normal vascular tissue. This was possibly due to the biological milieu of necrotic processes evident in the necrotic lipid core which was likely to be rich in RNases and ROS[282]. Several factors which minimised RNase and chemical activity were the adequate fixation of the sections, keeping the temperature of the sections low therefore inhibiting enzymatic activity, minimising the length of exposure to the aqueous stages, the adequate dehydration of the sections and specific inhibitors of RNases.

I made the following changes to the LMD protocol. The initial and aqueous stages of the protocol were performed on ice. After the freshly mounted cryosections were heat-adhered to the membrane slides they were allowed to air-dry for 1 minute in a desiccant chamber on ice and then fixed in 75% ethanol for 2 minutes, washed, stained in haematoxylin, and dehydrated in increasing ethanol gradients on ice. The final 100%

ethanol step was performed at room temperature and increased to a minute to ensure the adequate removal of water. Then the slides were air-dried thoroughly in an enclosed desiccant slide chamber for 2 minutes in room temperature, and were taken up for LMD immediately in an enclosed slide holder in room temperature.

I had also tried the use of RNAlater solution which stabilises the RNA and inhibits RNases. However, I found that the specimens failed to embed well in OCT and did not cryosection well as a result of fixation/immersion in the RNAlater solution and was not suitable for our purposes.

4.7.6 Testing the proposed modifications

Four CEA specimens were LMDed using the proposed modifications to the LMD protocol. The SMA and CD68 immuno-stained scout sections guided the LMD of the cap VSMCs and the core macrophages. Figure 59 shows the Agilent Bioanalyser Pico-chip results of the RNA extracted using the optimised RNeasyMicro protocol. The RNA extracted from macrophages surrounding the necrotic cores of fixed and stained CEA atheromatous plaque were consistently of high yield and high quality. However, the VSMCs laser micro-dissected from the fibrous caps were all of poor quality with evidence of severe RNA degradation despite good numbers of VSMCs in the thick fibrous cap.

At this stage, I had a working optimised LMD and RNA extraction protocol for the isolation of high quality and yield of RNA from the macrophage cells of the CEA atherosclerotic plaque. However, more evaluation work was necessary to further optimise the protocol for RNA extraction of VSMCs from the fibrous cap.

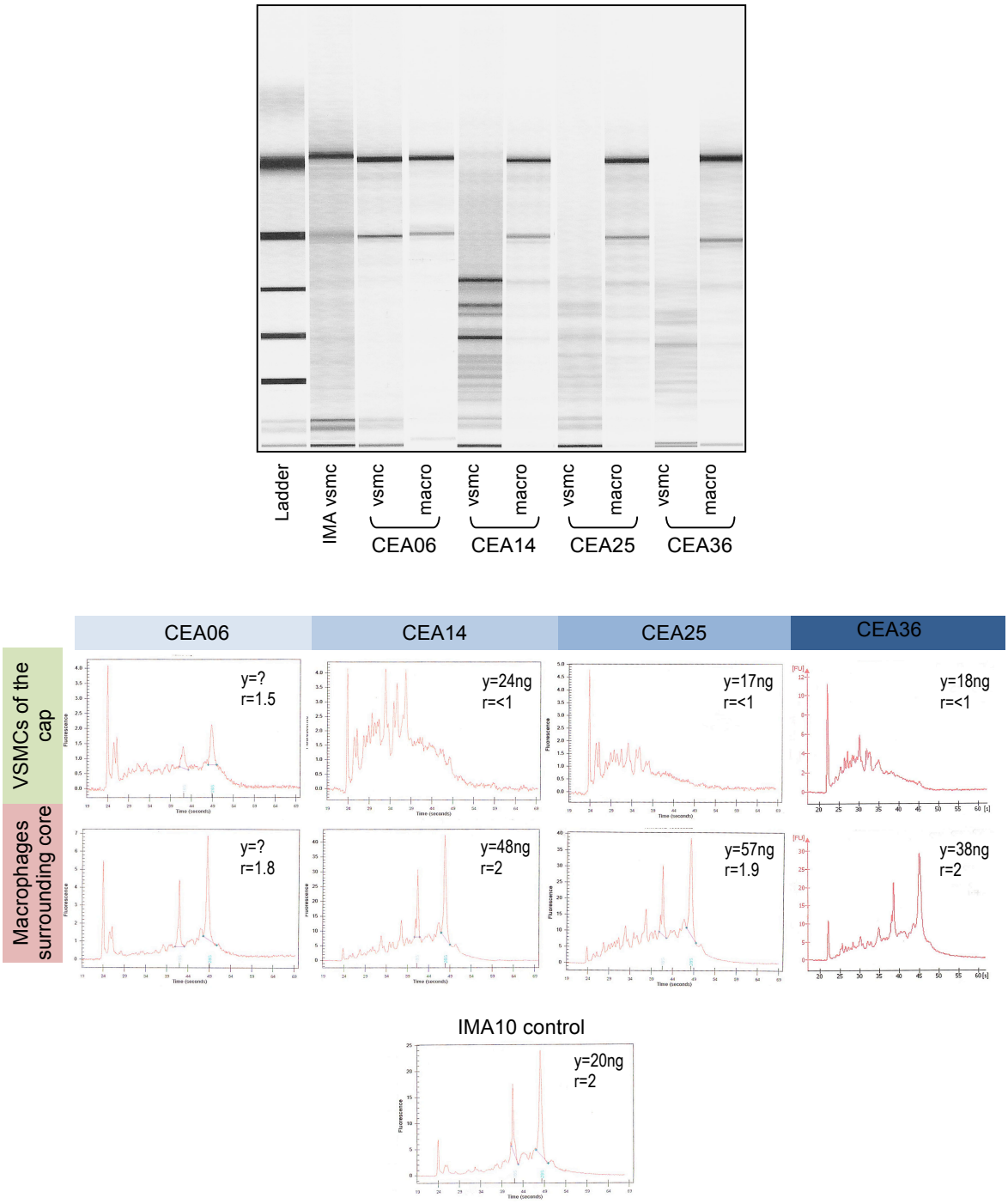

Figure 59. The Bioanalyser Pico-chip results of the RNA extracted from LMD of VSMCs and Macrophages from 75% ethanol fixed and haematoxylin stained CEA specimens using the highly optimised LMD protocol. (y=yields in ng/10,000cells, r=28S/18S ratios, no cell count for CEA06 and cannot estimate yield).

4.7.7 Further evaluation of LMD of VSMCs in the fibrous cap

I proceeded to test different methods of homogenisation using high-speed vortexing, fine-gauge needle-syringing and high-frequency sonication of fibrous tissues as well as RNA extraction methods for protein-rich tissues using proteinase-K digestion or lipid-rich tissues using Trizol with silica-column extraction. There was no significant improvement in the quality or quantity of extracted RNA from the fibrous caps of the atherosclerotic plaque but instead the RNA extracted was of poorer quality and yield.

RNA extraction of VSMCs in the fibrous cap: a conclusion

There was no advantage in using specialised protocols for protein or lipid rich tissues or additional homogenisation in the RNA extraction from VSMCs in the fibrous cap. None of these steps may be advised. It would seem a reasonable conclusion that the RNA extraction from the fibrous cap of the atheromatous plaques was as optimal as could be achieved by LMD using the technology available presently and its yield was within expected ranges. Instead the degraded quality of RNA seen may be a true reflection of the biological condition of the cells in the cap. Henceforth I continued in my work to LMD and extract RNA from the fibrous cap using the final optimised LMD and RNA protocols developed despite the degraded quality of the RNA extracted.

4.7.8 The optimal RNA LMD protocol

The final optimised LMD protocol incorporated the cumulative work performed on normal arteries from IMA and radial artery and on atherosclerotic plaques from CEA surgery. The changes made from the original Leica RNA LMD protocol for our purpose and tissue type were significant and included: the use of Leica LMD PET-membrane slides, unfixed and aqueous stages of the process were performed on ice, brief air-drying for 1 minute before fixation in desiccant chamber, fixation with 75% ethanol for 2 minutes, haematoxylin staining alone, a longer final 100% ethanol clearing stage for 1 minute, the thorough air-drying in a desiccant chamber at room temperature for 2 minutes and the omission of the xylene clearing stages. The optimal RNA LMD protocol is also described in methods chapter 2.10.3.

4.8 The stability and integrity of RNA extracted from LMD

4.8.1 Stability of RNA of the processed LMD sections

There was a hypothetical risk of RNA degradation as a result of the sections remaining in room temperature awaiting LMD and RNA stabilisation in the RNase-inactivating guanidine-isothiocyanate RLT lysis buffer. Moreover, the microdissections of the same specimen from several slides were collected together for RNA extractions to maximise the RNA yield and concentration. It was important to validate the stability of the RNA of the processed cryosections on the LMD membrane slides and their susceptibility to RNA degradation.

Radial artery cryosections were processed for LMD and one slide was immediately LMDed and the other was remained at room temperature for 7 hours before LMD. This was performed in duplicate. A CEA sample was similarly processed but was left at room temperature for 5 hours. The extracted RNA quality and yield from the LMD slides left in room temperature for 5 to 7 hours prior to LMD were not significantly different from the slides processed immediately (Figure 60), confirming that the final optimised LMD protocol produced fixed and stained sections which were RNA stable for LMD.

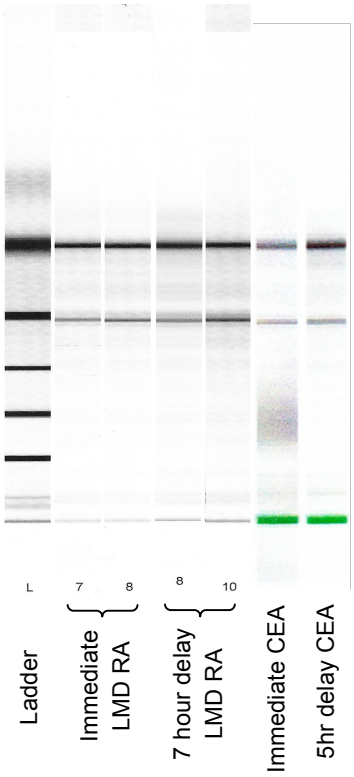

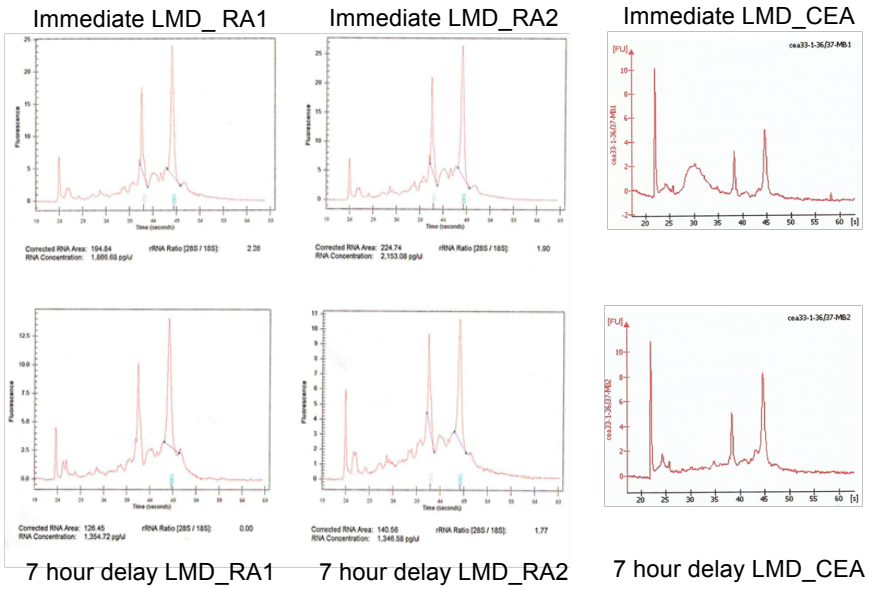

	IMA VSMCs		CEA Macro	
	immediate	7hr delay	immediate	5hr delay
RNA quantity	24ng	18ng	66ng	90ng
RNA 28S/18S ratio	1.9	1.9	2.0	2.0

Figure 60. Assessment of RNA stability of the processed LMD sections demonstrating the stability of the RNA on the LMD membrane slides.

4.8.2 Preservation of RNA integrity

The integrity of the RNA was assessed by oligo-dT primed reverse transcription followed by the PCR amplification of GAPDH mRNA at a region 692bp to 477bp away from the poly-A tail, producing a PCR product of 216bp. Intact mRNA would successfully reverse transcribe the length of the mRNA and generate a good PCR product whereas degraded RNA would not. The RNA extracted from IMA VSMCs and CEA macrophages produced PCR products of 216bp (Figure 61). These results confirmed the preservation of the integrity of the RNA extracted using the optimised LMD and RNA protocols from IMA and CEA specimens.

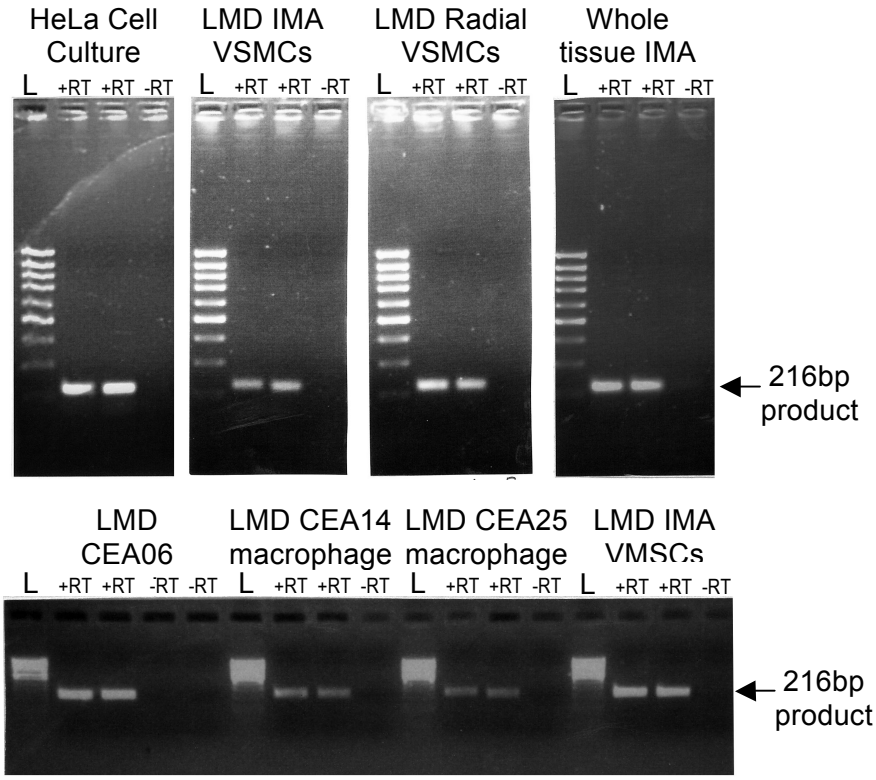

Figure 61. Agarose gel electrophoresis of the oligo-dT primed RT-PCR of GAPDH mRNA demonstrating the preservation of the integrity of the extracted RNA. (L, 100bp ladder; +RT, with reverse transcriptase; -RT, without reverse transcriptase as negative control).

4.9 LMD of the stable and ruptured atherosclerotic plaques

I proceeded with the LMD of the selected maximally contrasting stable and ruptured plaques. I compared: 1) the gene expression profiles of VSMCs in thick fibrous caps of stable plaques versus VSMCs in thin fibrous caps of ruptured plaques, and 2) the expression profiles of macrophages under the thick fibrous caps and overlying the boundary of the necrotic cores of stable plaques to macrophages under the thin fibrous caps and overlying the boundary of the necrotic cores of ruptured plaques.

4.9.1 Scout section histological analysis and identification of VSMC and Macrophage regions for LMD

Scout sections and LMD of the Stable Plaque

The thick fibrous caps containing VSMCs overlying the necrotic core of FCA and FCL stable plaques were identified by SMA immunostaining and LMDed (Figure 62, panels B&F). CD68 immunostaining identified the macrophage cell type for LMD. The region of CD68 immunostaining occupied the same regions of immunostaining by leukocyte common antigen (LCA which identifies any inflammatory cell type) confirming the macrophage as the predominant inflammatory cell-type in the plaque (Figure 62, panel C&D). The regions selected for the LMD were foamy macrophages (macrophage cells engorged with lipid) at the boundary between the necrotic core and the thick protective fibrous cap (Figure 62, panel D&F). The center of the core with necrotic debris and extracellular lipid was avoided.

Regions with mixed cellularity, containing both VSMC and macrophage cell-types were avoided in order to obtain LMD isolation of mostly the same cell type (cellularly pure or enriched). The regions LMDed containing VSMCs in the fibrous caps did not have any significant staining with LCA or CD68 confirming a cell-pure LMD of VSMCs with minimal inflammatory cells (<10%). This was also confirmed by histological analysis of the H&E slides by the histological identification of the spindle-like smooth muscle cells in organised layers in the fibrous cap without any infiltration by granular lipid laden macrophage foam cells or other inflammatory cells. Conversely, the regions LMDed containing macrophage cells did not have any significant staining with SMA and with confluent staining of CD68 confirming a cell-pure LMD of macrophages with minimal infiltration of VSMCs. This was also confirmed by histological analysis of the H&E slides. Occasionally it was not possible to have regions with no SMA uptake at all in the LMD of the macrophages. This was seen more so in stable plaques. Nevertheless, the estimated proportion of infiltration of VSMCs to macrophage cells in these regions by cell count was less than 10%.

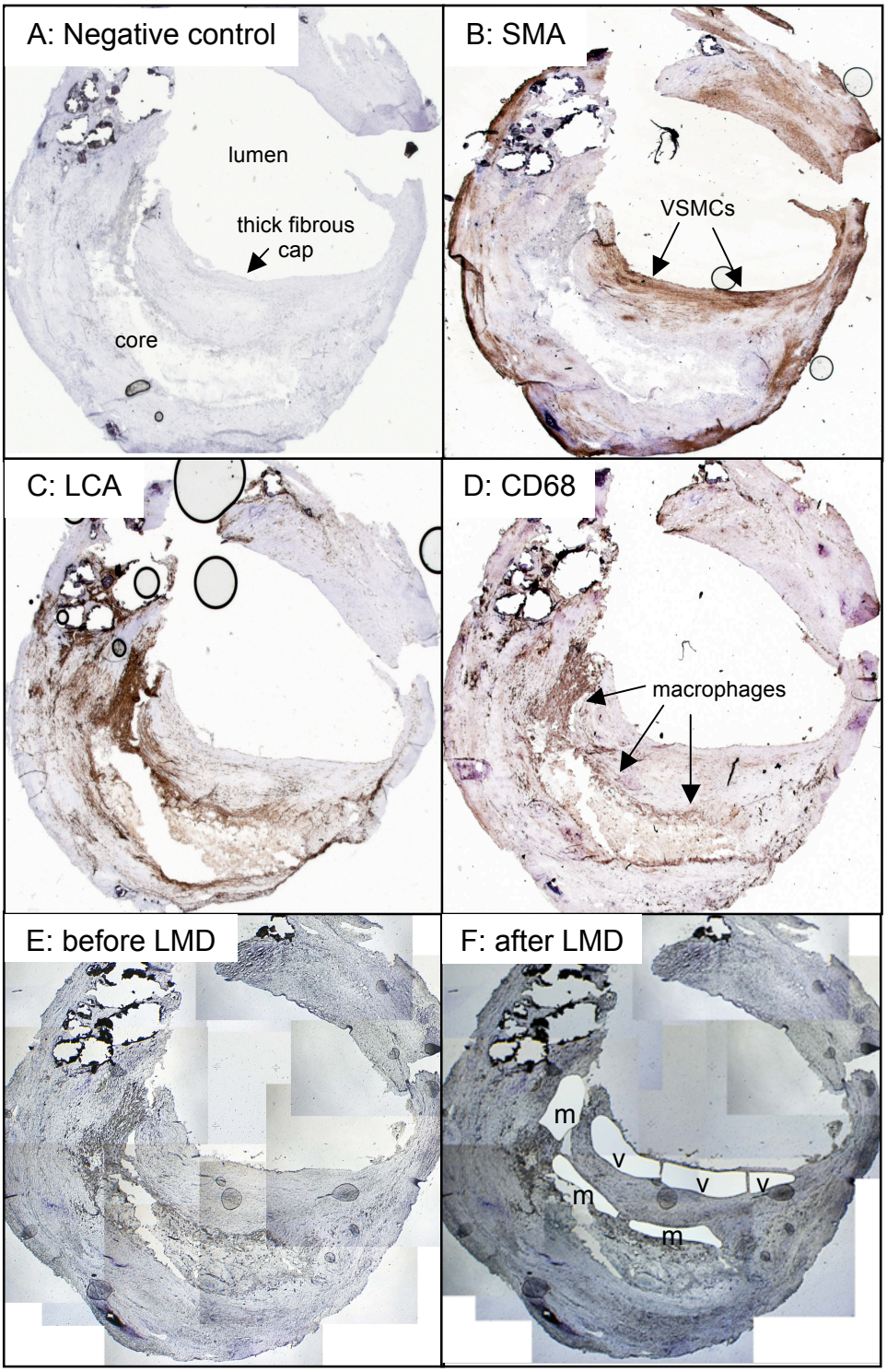

Figure 62. Scout and LMD cryosections of a stable thick fibrous cap atheromatous plaque.

Scout sections and LMD of the Ruptured Plaque

The thin fibrous cap and the region of rupture with adherent thrombus over exposed necrotic core (and occasionally with extrusion of core contents) and haemorrhage were identified (Figure 63, panel A). VSMCs confirmed by SMA staining in the fibrous caps adjacent to the site of rupture overlying the necrotic core were identified and LMDed (Figure 63, panel B&D). The macrophage regions selected for the LMD were the foamy macrophages identified by confluent CD68 immunostaining at the boundary between the necrotic core and the thin fibrous cap adjacent to the site of rupture. The center of the core with necrotic debris, extracellular lipid, haemorrhage or thrombus were avoided (Figure 63, panel C&D).

Similar to the stable plaques, regions with mixed cellularity were avoided. This was achieved in all of the LMD of macrophage specific regions as there was very little staining of SMA near the necrotic cores of ruptured TFCAs.

In contrast to stable plaques, the LMD of VSMCs from the fibrous caps of ruptured plaques were less successful. The majority of thin fibrous caps adjacent to the site of rupture had hardly any VSMCs. Two samples had mostly acellular fibrous caps (CEA33 and CEA57, Table 27 and Figure 64). Another lesion had adjacent fibrous caps with SMA staining but were heavily infiltrated by macrophages (CEA17, Table 27 and Figure 65) and the LMD of VSMCs without macrophage cell contamination was not possible. Individual cell by cell LMD rather than regional LMD was possible but this would not generate enough starting RNA for linear amplification and was not feasible. Of the 5 ruptured plaques selected for LMD and microarray, only 2 plaques had regions of VSMCs in the adjacent cap that were suitable for LMD but in limited numbers (Table 27).

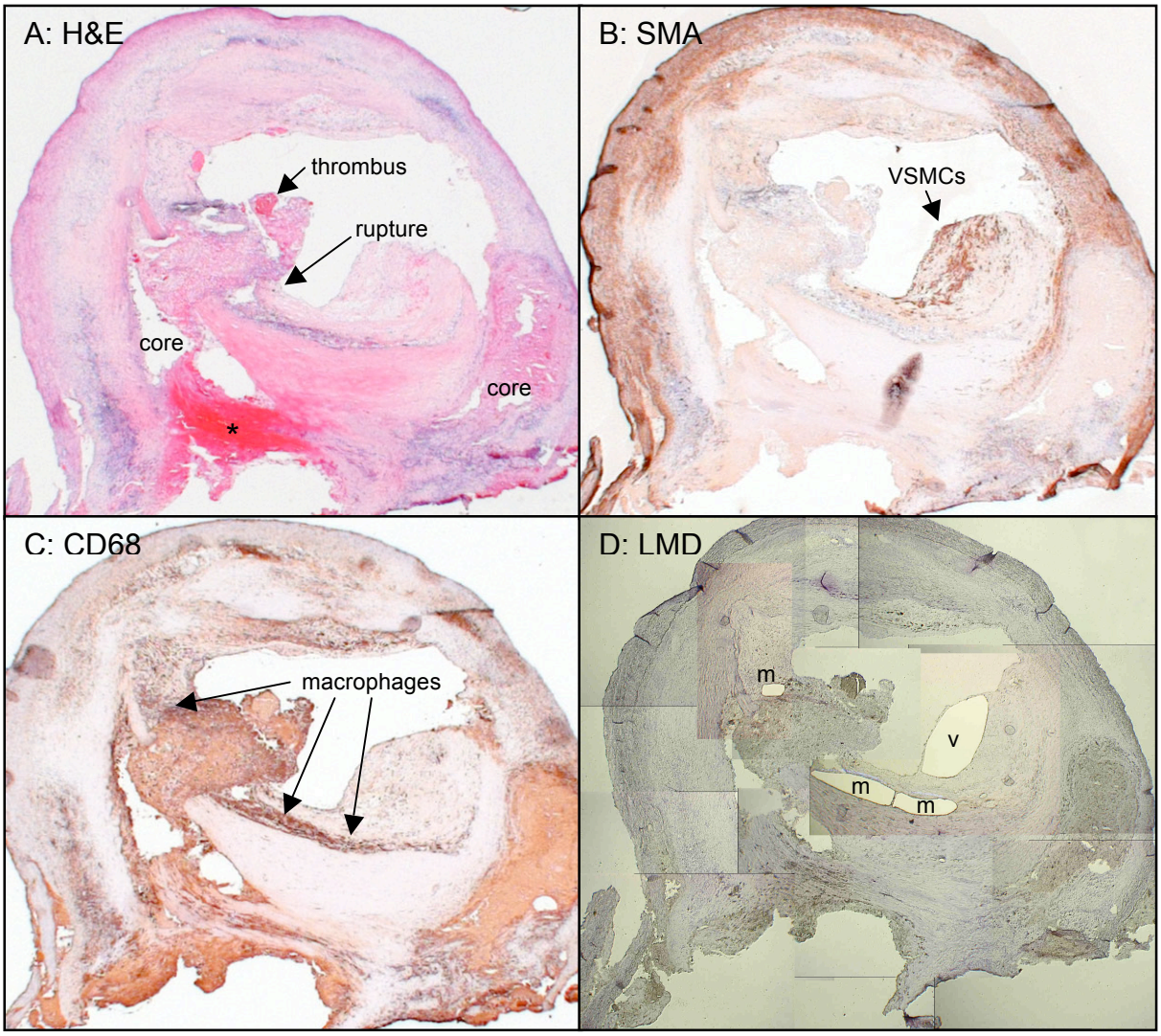

Figure 63. Frozen sections of CEA35 showing a ruptured thin fibrous cap atheroma with extrusion of the core contents and thrombus over the exposed core.(*intra-plaque haemorrhage).

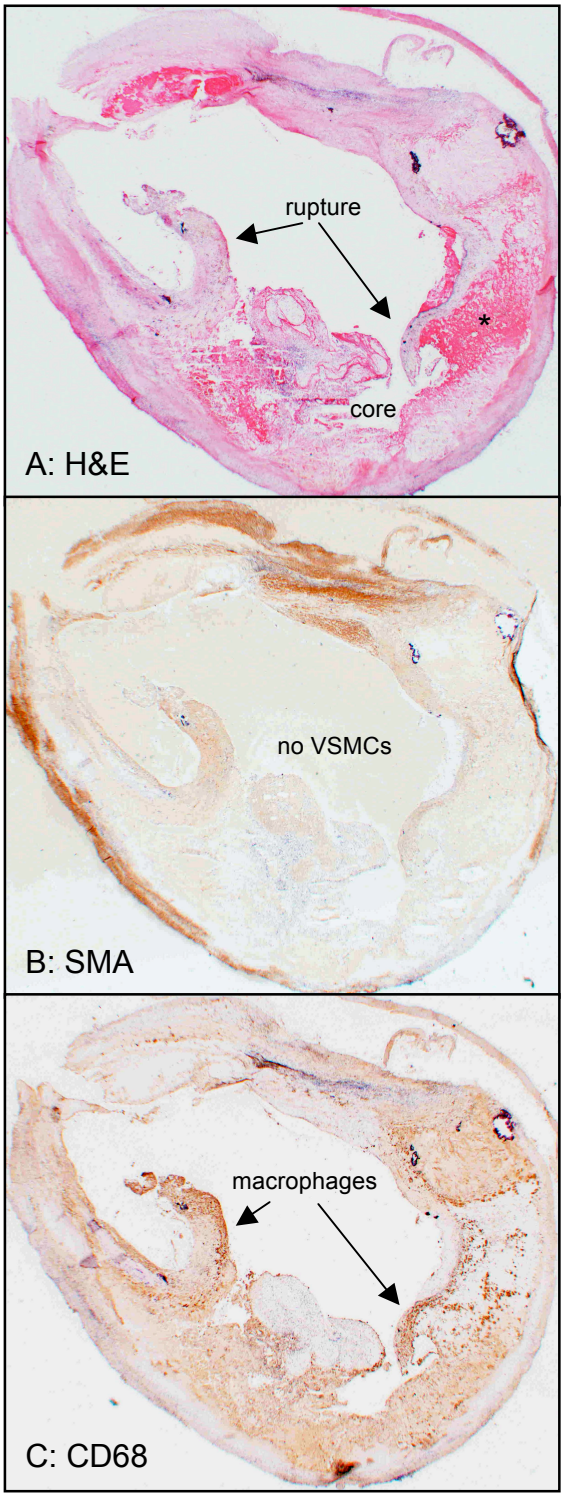

Figure 64. Frozen scout sections of CEA33 showing a ruptured thin fibrous cap atheroma with very little VSMCs in the fibrous cap for LMD. (*intra-plaque haemorrhage).

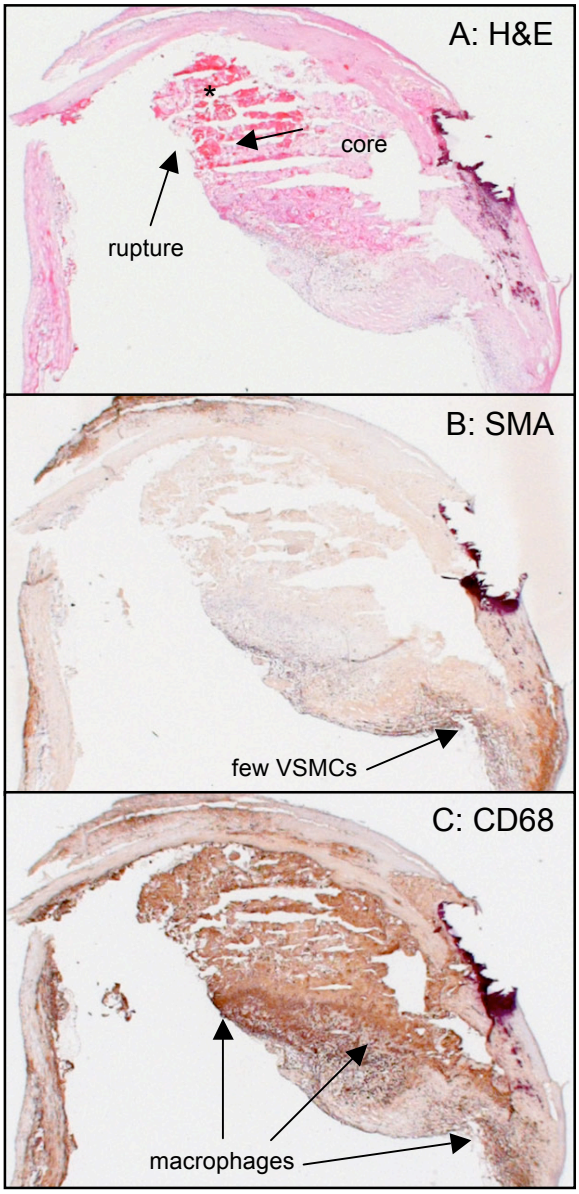

Figure 65. Frozen scout sections of CEA17 showing a ruptured thin fibrous cap atheroma with some VSMCs in the cap which were infiltrated with macrophages.

4.9.2 RNA extraction of VSMCs in the fibrous cap

The results of the fibrous cap VSMC LMD and RNA extraction is shown in Table 27 with the Bioanalyser results in Figure 66. The RNA extracted from the IMA VSMCs as positive controls of LMD were of expected yields (20 to 24ng per 10,000 cells) and high quality (28S/18S ratios of 1.8-2, with clean baselines). The RNA extracted from the VSMCs in the fibrous caps had RNA profiles of severe degradation. There were no visible ribosomal bands with evidence of low molecular weight fragments of degraded RNA seen in the baseline (Figure 66). Only CEA17 had an RNA profile of good quality but this was due to the LMD of a region of mixed cellularity; the fibrous cap was infiltrated with macrophages, about 60% were VSMCs and 40% were macrophage foam cells (CEA 17$^{(1)}$:Figure 66, Table 27). An attempt was made to improve the LMD by locating a part of the lesion with an intact fibrous cap without significant macrophage infiltration by performing more cryosections deeper into the tissue cryoblock (and therefore further away from the ruptured atheromatous plaque) (CEA17redo$^{(4)}$:Table 27) but the fibrous cap (although now quite thick and well populated with VSMCs) was still significantly infiltrated with macrophage foam cells (estimated 80% VSMCs: 20% macrophages by ICC identification and cell count).

The yields of the RNA extracted were also poor. The average yield was 8.9ng per 10,000 VSMCs LMDed from the fibrous caps. This was 2.5x less than the estimated yield of RNA extracted from the LMD of VSMCs of the IMA specimens (22ng per 10,000 cells). Of the 10 LMD and RNA extractions performed, the total yields from 8 of them were too low for RNA amplification (<20ng).

The total yields of RNA could be increased by the LMD of more cells. This was only possible in the stable plaques with enough VSMCs in the cap. A stable plaque specimen, CEA41, which failed to generate enough RNA on the first attempt at the LMD of 10,000 cells, had another attempt (CEA41redo:Table 27) with the LMD of 31,000 cells to generate 44ng of RNA. The only 2 samples with yields of more than 40ng were from stable plaques. Although this was just enough for RNA amplification using high quality RNA, it was not so for degraded RNA. Assuming that there may be at least 10% of intact mRNA in a degraded RNA sample, I would need an amount of at least 10 times more. The oligo-dT primed RNA amplification is sensitive to RNA degradation. The linear amplification of poor quality starting mRNA will produce low yields of cRNA with very high 3' bias further affecting the relative quantification of transcript abundance in gene expression profiling[217, 218, 283]. As the RNA extracted from these 2 samples were severely degraded and too low in yield to amplify and without sufficient VSMC RNA from ruptured samples to compare to, we did not proceed with RNA amplification.

We concluded that it was not possible to perform the LMD work to compare the transcriptomic profiles of the VSMCs of the fibrous caps in the stable and ruptured atherosclerotic lesions using microarray with the current technology available. We decided to store the small and limited quantities of extracted VSMC RNA and the few remaining processed but uncut VSMC LMD slides in the freezers of the Neurovascular Unit tissue bank (CAGE study) for future use but not to proceed further with analyses of VSMC RNA in this thesis.

CEA code	3-Domain selection	Plaque Histology	LMD of VSMCs in fibrous cap done?	VSMCs LMDed (est. # of cells)	RNA nett yield (ng)	RNA yield (ng/10000 cells)	RNA quality-28S/18S	RNA quality-baseline
CEA14	Test Sample	Fibrocalcified plaque	Yes	4500	11	24.4	<1	severely degraded
CEA25	Test Sample Stable Plaque	Fibrous cap atheroma	Yes	3500	6.6	18.9	<1	severely degraded
CEA36	Stable Plaque	Fibrocalcified plaque	Yes	109100	53.5	4.9	<1	severely degraded
CEA41	Stable Plaque	Fibrous cap atheroma	Yes	10000	10.8	10.8	<1	severely degraded
CEA45	Stable Plaque	Fibrous cap atheroma	No (stored)	-	-	-	-	-
CEA81	Stable Plaque	Fibrocalcified plaque	No (stored)	-	-	-	-	-
CEA17	Ruptured Plaque	Ruptured thin fibrous cap atheroma	Yes[(1)]	3000	14.3	47.7	1.9[(1)]	good[(1)]
CEA33	Ruptured Plaque	Ruptured thin fibrous cap atheroma	Yes[(2)]	4800	13	27.1	<1	severely degraded
CEA35	Ruptured Plaque	Ruptured thin fibrous cap atheroma	Yes	13500	16.9	12.5	<1	severely degraded
CEA57	Ruptured Plaque	Ruptured thin fibrous cap atheroma	No[(3)]	-	-	-	-	-
CEA100	Ruptured Plaque	Ruptured thin fibrous cap atheroma	No (stored)	-	-	-	-	-
CEA41 redo	Stable Plaque	Fibrous cap atheroma	Yes	31000	44	14.2	<1	severely degraded
CEA17 redo	Ruptured Plaque	Ruptured thin fibrous cap atheroma	Yes[(4)]	4000	2.3	5.8	1.8[(4)]	good[(4)]
CEA35 redo	Ruptured Plaque	Ruptured thin fibrous cap atheroma	Yes	38400	16.7	4.3	<1	severely degraded

Table 27. VSMC LMD and RNA yield and quality from stable and ruptured samples.
CEA17[(1)]: LMD of a region of mixed cellularity (60% VSMCs: 40% macrophages), CEA33[(2)]: LMD of VSMCs not over the necrotic core of the ruptured plaque but over an intimal xanthoma adjacent to the plaque, CEA57[(3)]: No VSMCs seen in the acellular fibrous cap, CEA17redo[(4)]: Further LMD of deeper cryosections but the fibrous cap was still of mixed cellularity (80% VSMCs: 20% macrophages).

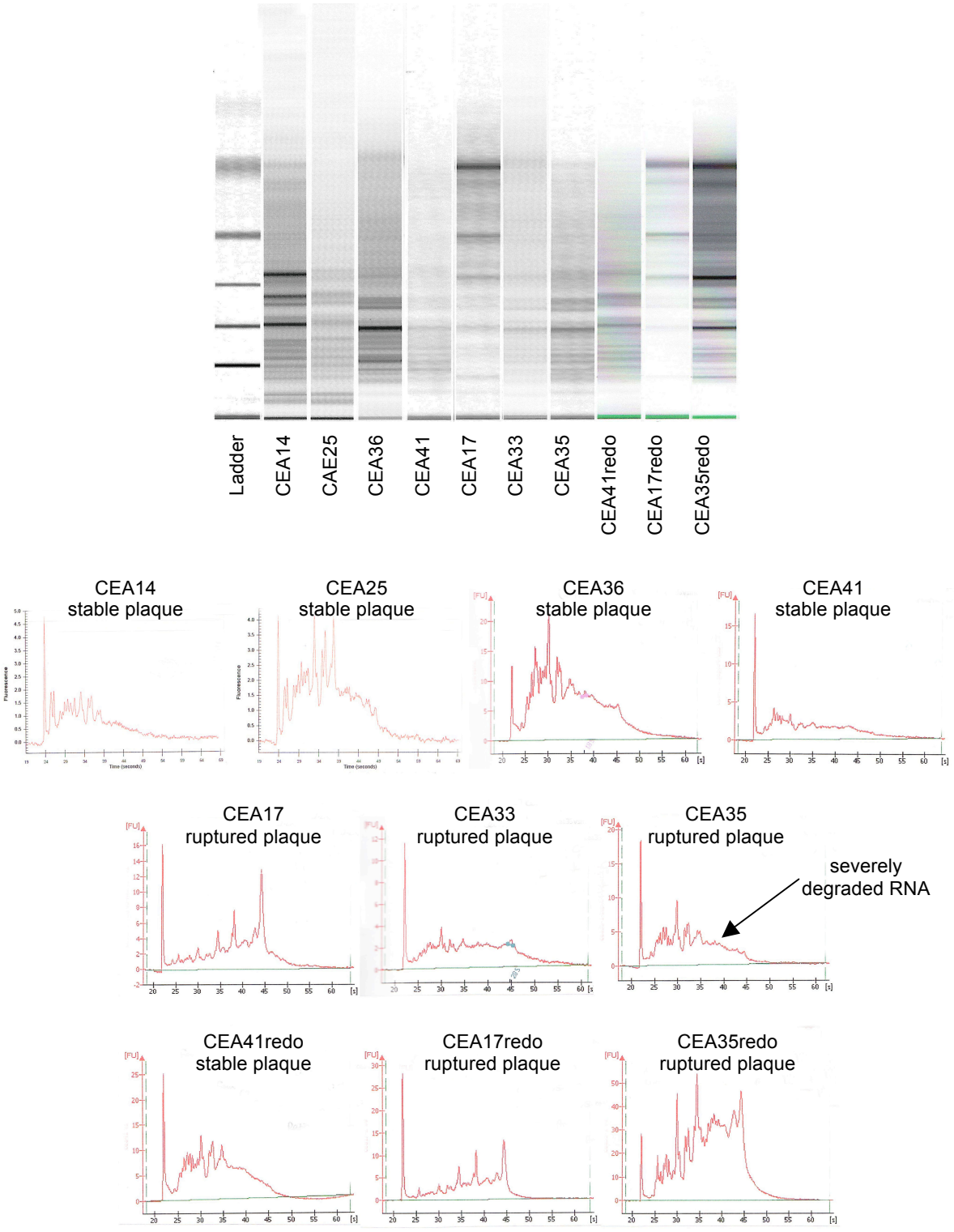

Figure 66. Agilent Bioanalyser Pico-chip results of RNA extracted from the LMD of VSMCs in the fibrous caps of stable and ruptured atherosclerotic plaques showing severely degraded RNA.

4.9.3 RNA extraction of Macrophages under the fibrous cap

The results of the LMDed plaque macrophages and the RNA yields and quality are shown in Table B with the Bioanalyser results in Figure 67. The same IMA VSMC LMD positive controls were used as with the plaque VSMC extractions. The RNA extracted from the LMD of the macrophages from the atherosclerotic plaques was of sufficient amounts from all samples for RNA amplification. There was a high average yield from the LMD of macrophages from the atherosclerotic plaque of 44.7ng from 10,000 macrophage cells (95% CI of 35 to 55ng).

The RNA extracted was of high quality with an average ribosomal 28S/18S ratio of 1.75 (95% CI of 1.45 to 2.0) and with a clean baseline in all the samples except for 3 samples. These 3 samples demonstrated some evidence of RNA degradation by an abnormal raised baseline on the florescence graphs which is consistent with low molecular weight products of RNA degradation (CEA33 & 35) or DNA/protein contamination (CEA33 & 36). Only one of the three had a low ribosomal 28S/18S ratio (CEA35 had the lowest ratio of all the RNA extracted at 1), the ratios were preserved in the other 2 samples (CEA33 & 36 had ratios measured at 2). Retrospective histological examination revealed that apoptotic/necrotic macrophage regions in the necrotic core were LMDed and is described in the next section. The LMD and RNA extraction of these 3 CEA specimens were repeated avoiding these regions resulting in high quality RNA of high yield for amplification and microarray (Table 28).

The Bioanalyser RIN measurements were only introduced later in the study and were not available at this stage of my experiments. However, the Bioanalyser electropherogram profiles of the samples used for amplification and microarray were of high quality and were similar to RIN scores of 6 and above. There were no significant differences in RNA yields (ng/10,000cells) or quality (28S/18S) between the stable and ruptured plaques ($p=0.83$ and $p=0.86$). The measurements of RNA yield and quality suggest that the macrophage cells in both the stable and ruptured plaques had similar degrees of transcriptomic activity (they were not quiescent in the stable plaques and activated in the ruptured plaques). The differences in transcriptome profiles would therefore reflect the different activity of genes or pathways between the two groups. Moreover the RNA was of similar quality between the two groups which minimises any bias to gene expression measurements resulting from RNA degradation.

CEA code	3-Domain selection	Plaque Histology	Macro-phage LMD done?	Macro-phages LMDed (# of cells)	RNA nett yield (ng)	RNA yield (ng/10000 cells)	RNA quality-28S/18S	RNA quality-baseline
CEA14	Test Sample	Fibrocalcified plaque	Yes	8600	41.3	48.0	2	Good
CEA25	Test Sample Stable Plaque	Fibrous cap atheroma	Yes	10000	57.5	57.5	1.9	Good
CEA17	Ruptured Plaque	Ruptured thin fibrous cap atheroma	Yes	110200	407	36.9	1.8	Good
CEA41	Stable Plaque	Fibrous cap atheroma	Yes	90000	353.1	39.2	1.7	Good
CEA45	Stable Plaque	Fibrous cap atheroma	Yes	98800	512.6	51.9	1.4	Good
CEA33	Ruptured Plaque	Ruptured thin fibrous cap atheroma	Yes	113650	332.2	29.2	2	Possible degradation
CEA35	Ruptured Plaque	Ruptured thin fibrous cap atheroma	Yes	163000	952	58.4	1	Moderate degradation
CEA36	Stable Plaque	Fibrocalcified plaque	Yes	159000	225.5	14.2	2	Possible degradation
CEA57	Ruptured Plaque	Ruptured thin fibrous cap atheroma	Yes	12000	81.6	68.0	1.9	Good
CEA81	Stable Plaque	Fibrocalcified plaque	Yes	9000	55.8	62.0	1.6	Good
CEA100	Ruptured Plaque	Ruptured thin fibrous cap atheroma	Yes	7000	45.1	64.4	1.6	Good
CEA33 redo	Ruptured Plaque	Ruptured thin fibrous cap atheroma	Yes	48000	152.9	31.9	2	Good
CEA35 redo	Ruptured Plaque	Ruptured thin fibrous cap atheroma	Yes	89200	148.5	16.6	1.7	Good
CEA36 redo	Stable Plaque	Fibrocalcified plaque	Yes	44400	210.1	47.3	1.6	Good

Table 28. Macrophage LMD and RNA yield and quality from stable and ruptured samples.

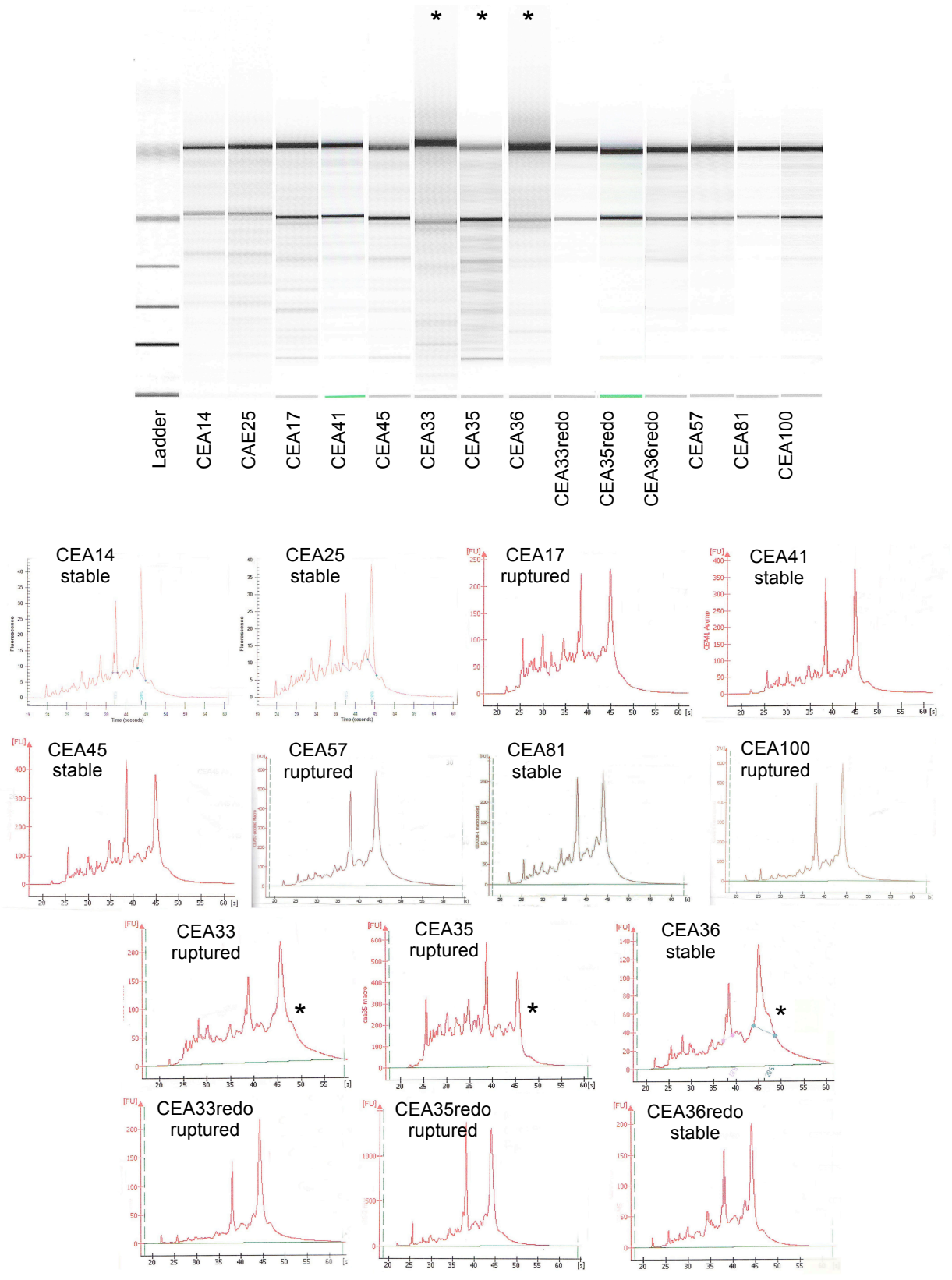

Figure 67. Agilent Bioanalyser Pico-chip results of the RNA extracted from the LMD of macrophages of stable and ruptured atherosclerotic plaques. (*samples with some evidence of RNA degradation, and the same CEA specimens with repeat LMD).

4.9.4 Regions of cellular degradation

Evidence of RNA degradation or DNA/protein contamination was detected in 3 macrophage LMD samples and may inhibit and be detrimental to successful linear RNA amplification. In the retrospective analysis of the regions selected for dissection, it became apparent that some regions LMDed may have contained apoptotic cells bordering areas of necrosis and may contain non-viable cells and degraded RNA. To test this hypothesis, I extracted RNA from focused LMD of these apoptotic regions (seen histologically with indistinct nuclear definition, Figure 68) compared to nearby viable regions of macrophages (with clear and distinct nuclear and cell membrane definition). Good quality RNA was extracted from regions of viable cells. In contrast, I was unable to extract RNA from the apoptotic/necrotic regions despite apparent abundance of cellular nuclei which had indistinct nuclear definition. This may reflect severely degraded RNA in-vivo or the severe degradation of the RNA during the LMD and extraction process which could not be halted. The LMD of these 3 samples was repeated with avoidance of cellular regions with poor nuclear or cellular definition suggesting apoptosis/necrosis and resulted in the successful extraction of high quality RNA (Table 28 and Figure 67: CEA33redo, CEA35redo, CEA36redo).

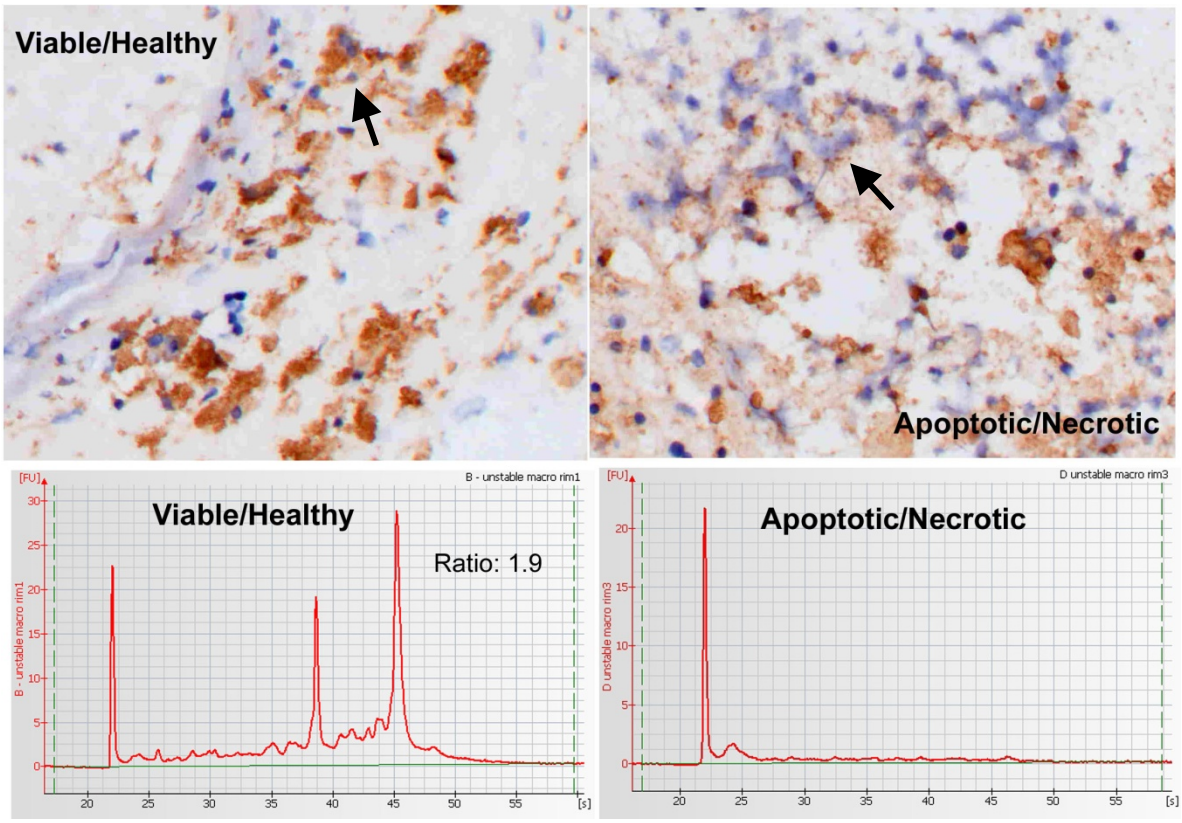

Figure 68. Frozen sections of CEA33 demonstrating apoptotic/necrotic (indistinct nuclei) and healthy viable macrophage cells (clear nuclear definition) in atherosclerotic plaque and the RNA isolated from these regions. CD68 immunostaining with haematoxylin counterstaining of the nuclei.

4.10 RNA amplification and microarray

4.10.1 Batch#1: The initial 2 CEA test samples

The extracted RNA was linearly amplified and hybridised to the Affymetrix test chip and eventually the GeneChip microarray in batches. The RNA from the LMD of the macrophages in the first two CEA test samples was linearly amplified, labelled, fragmented and hybridised to the Affymetrix test chip in our first tests (Batch#1: of CEA14 and CEA25; of which CEA25 was also one of the stable samples selected using the 3-domain criteria).

Linear RNA amplification and cRNA fragmentation

Starting amounts of 20ng of total RNA were used for linear amplification. The first amplification cycle generated 650ng and 312ng of cRNA from CEA14 and CEA25 which was within the expected range. The second cycle of IVT amplification generated 51.6µg and 83.4µg of cRNA which was ample amounts for the microarray experiments.

Twenty micrograms of biotin labelled and purified cRNA from each sample was fragmented and the agarose gel electrophoresis confirmed the adequate fragmentation of the cRNA to sizes of about 35 to 200bp for hybridisation to the microarray (Figure 69).

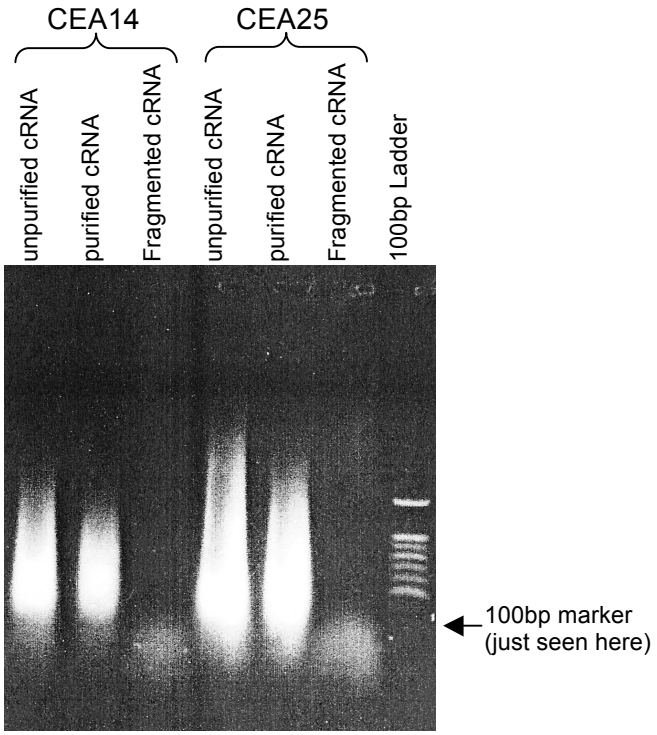

Figure 69. Agarose gel electrophoresis of the amplified cRNA, purified and fragmented, ready for hybridisation to microarray.

Hybridisation to the Test Chip: Quality Control Assessments

Five micrograms of fragmented cRNA was hybridised to the Affymetrix Test3 Array prior to hybridisation to the GeneChip to assess the quality of the amplification, labelling of the generated cRNA and its hybridisation to the microarray (part of the QCA process). The test chip data of the 2 samples are shown in Table 29 (Batch#1) along with the test chip data of the other CEA samples processed later.

Hybridisation and Array QCA

The baseline scanner and array technical quality controls of B2 oligo positive control, background and noise (rawQ) were within operational limits[251]. The hybridisation controls of BioB, BioC, BioD and Cre which were spiked into the hybridisation cocktail and in increasing concentrations were also detected in ascending order of signal strength and were of similar magnitudes between the samples. This confirmed successful hybridisation and operation of the 2 arrays.

Amplification QCA

A marker of the success of the amplification reaction was the generation of more than 40µg of amplified cRNA. Non-human spiked-in poly-A amplification controls of Lys, Phe, Thr and Dap were also used to assess the two cycle IVT RNA amplification reactions and were spiked-in just above the minimum concentrations for detection and in increasing concentrations. The spiked-in controls in the 2 CEA samples were all positively detected in ascending order of detection of signal strength except for Lys. The higher than expected signal intensity of Lys was also observed to in the amplification reactions of all the other CEA samples as well as in the microarray experiments of other groups and may have been due to a wrong concentration of Lys from the manufacturer. The probeset for Trp was a negative control and was not detected. These spiked-in controls confirmed the successful linear amplification of RNA.

Amplification 3' bias

The signal intensities of the 3', M and 5' ends of the spiked-in poly-A controls monitor the 3' amplification bias. A representative assessment of 3' bias was performed using 3'/M ratios, with ratios of less than 3 recommended[251, 255] and should be similar across all the samples. The average 3'/M ratios of the 2 samples were 2.3 and 2.5 which demonstrated amplification without significant bias.

Sample quality QCA

The 3'/M ratios of genes expressed in the native tissue (such as the internal control gene GAPDH) can be used to assess the integrity of the original mRNA (degraded RNA would not successfully reverse transcribe and amplify with a 3' bias). The 3'/M ratios of GAPDH

for the samples were 1.5 and 1.9 and were consistent with the 3'/M ratios of the spike-in amplification controls. This suggests that the RNA of the LMD samples were of high quality and that minimal if any 3' bias was incurred due to mRNA quality.

Percentage present calls

The percentage present calls as a measure of percentage of genes detected as expressed in the array determined using the Affymetrix detection algorithm reflect the sample quality (poor quality samples have low percentage calls) as well as successful array hybridisation. We expect values of 30-35% in the Test3 array from our samples[251, 255] and should be similar across the experiment. Our 2 test samples were 34.9% and 33%, within the expected range.

Global scaling

A global scaling of the array was performed to scale up (or down) the signals of the probesets in the array in normalisation to the other arrays to an arbitrary overall mean fluorescence value of 200 using GCOS. A global scaling factor of <3 reflects the appropriate amount of cRNA was loaded and hybridised with the satisfactory performance of the array[251, 255]. Our 2 samples have optimal values of 1.1 and 0.9 such that very little global scaling was required.

Hybridisation to the Gene Chip

With satisfactory QCA results, the two test samples were hybridised to the Affymetrix genome-wide HG-U133 plus 2.0 GeneChip. Fifteen micrograms of fragmented cRNA was used and both the samples were successfully hybridised to the Gene Chip microarray and scanned, generating our first two genome-wide gene expression profiles of laser micro-dissected atherosclerotic plaque macrophages.

4.10.2 Batch#2: The next 6 CEA samples

Following the successful results from CEA14 and CEA25, the remaining CEA samples were processed in batches. A further 6 samples (CEA17, CEA 33, CEA35, CEA36, CEA41 and CEA45) were amplified and hybridised to the Test Chip array (Batch#2). The LMD details, RNA yield and quality, and Bioanalyser profiles were shown in Table 28 and Figure 67 previously. Three of these samples (CEA33, 35 and 36) had some evidence of RNA degradation observed on their Bioanalyser analyses and repeat LMD was underway. These 3 samples were also amplified and hybridised to the TestChip for further evaluation of the effect of RNA degradation/contamination to amplification and microarray hybridisation. High quality mouse brain total-RNA, which was previously successfully

amplified and hybridised to microarray by another group at the Institute of Human Genetics, was used as a positive control.

The results of the amplification and TestChip QCAs are shown in Table 29 (Batch#2). The RNA amplification reactions generated ample cRNA for microarray hybridisation and the array and hybridisation QCA markers were satisfactory for all the 6 samples and the positive control mouse RNA. Three of the 6 CEA samples had satisfactory amplification and sample QCA measures; CEA17, CEA41 and CEA45, demonstrating that high quality RNA was amplified with little 3' bias and was hybridised successfully onto the TestChip. These 3 samples passed the stringent TestChip QCA measures of sample quality, amplification and array hybridisation performance and were then hybridised to the Affymetrix GeneChip and the results of this is presented later.

Study of the effect of RNA degradation or contamination to amplification

The 3 samples with evidence of some RNA degradation, CEA33, CEA35 and CEA36, demonstrated poor performance in several QCA measures (Table 29). Although ample cRNA was generated, they had high 3'/M ratios of the internal control gene GAPDH from 3.9 to 6.1 (recommended ≤3), high global scale factors of 3 to 3.7 (recommended ≤3) and low percentage of present calls of 26.3% to 28.5% (optimal range 30-35%), suggesting that the starting material had a significant degree of RNA degradation and 3' bias. However, the spiked-in control genes of RNA amplification unexpectedly showed a high average 3'/M ratio of 3.4 to 4.5 as well, suggesting that this was not due to sample mRNA degradation alone but may be due to contaminants in the extracted RNA degrading the spiked-in mRNA controls or inhibiting the amplification reactions. These findings corroborated the histological and RNA extraction findings from non-viable cellularly-degraded regions and demonstrated that subtle evidence of RNA degradation and/or contamination was detrimental to the successful linear and unbiased amplification of RNA for gene expression analysis. As a result, gene expression analyses from linearly amplified poor RNA quality samples should be interpreted with caution.

Batch:		Batch#1		Batch#2						Batch#3					
Sample:	**Control**	**CEA14**	**CEA25**	**CEA17**	**CEA41**	**CEA45**	**CEA33**	**CEA35**	**CEA36**	**CEA33 redo**	**CEA35 redo**	**CEA36 redo**	**CEA57**	**CEA81**	**CEA100**
Plaque type	Mouse	Stable	Stable	Ruptured	Stable	Stable	Ruptured	Ruptured	Stable	Ruptured	Ruptured	Stable	Ruptured	Stable	Ruptured
Starting RNA (ng)	60 ng	20 ng	20 ng	60 ng	60 ng	60 ng	60 ng	60 ng	60 ng	42ng	42ng	57ng	60ng	60ng	60ng
1st cycle cRNA-total yield (ng)	-	650	312	248	455	460.2	347.1	260	221	260	260	198	387	1118	758
2nd cycle cRNA-total yield (µg)	53.4	51.6	83.4	148.5	150.0	143.1	132.0	136.5	123.0	126	75	69	138	69	105
Test Chip QCA measures:															
Scale Factor	0.9	1.1	0.9	0.9	2.5	2.7	3.5	3.0	3.7	1.275	0.912	1.1	0.663	0.682	0.714
B2 Oligo positive control	Present	Present	Present	Present	Present	Present	Present	Present	Present	Present	Present	Present	Present	Present	Present
Background	64.8	53.7	58.2	56.9	57.7	50.2	48.6	48.6	47.4	65.0	101.9	66.2	82.74	98.2	86.6
Noise	2.48	2.44	2.63	2.35	2.03	2.00	1.59	1.81	1.67	2.46	5.75	2.72	3.45	3.64	3.36
Number of Present Calls:	31.40%	34.90%	33.00%	35.60%	30.4%	30.10%	26.30%	27.90%	28.50%	32.10%	31.40%	30.80%	34.00%	33.00%	32.10%
Test Chip Internal Control Genes:															
AFFX-HUMGAPDH/M33197 3'/M Ratio	1.24	1.5	1.9	1.9	2.5	3.3	6.1	3.9	5.5	2.26	2.00	2.20	1.97	1.65	1.86
Test Chip Spike-in Hybridisation Control:															
AFFX-BioB (1.5pM)	42.1	237.4	174.1	56.8	154.3	250.6	313.4	279.2	364.5	90.1	76.2	95.5	61.8	59.3	60.6
AFFX-BioC (5pM)	213.8	546.4	349.7	285.3	662.9	939.8	1266.2	998.9	1394.9	406.2	281.9	408.2	263.3	243.7	238.1
AFFX-BioD (25pM)	840.6	2821.4	2073.0	986.9	2636.7	3164.7	4415.0	3390.0	4424.5	1274.4	1062.2	1154.6	884.5	927.6	886.1
AFFX-Cre (100pM)	2879.6	8834.6	6608.3	3375.8	8574.0	11397.2	16214.4	11683.6	15318.7	5176.5	4403.1	5350.6	3365.4	3090.9	3350.5
Test Chip Spike-in Amplification Control:															
AFFX-Trp (neg control)	0.5	1.2	4.1	0.8	1.7	2.9	3.2	2.5	2.7	0.9	1.9	0.7	0.3	0.6	0.5
AFFX-Lys (1/100000)	147.2	1461.0	896.7	623.8	934.1	1145.8	1689.9	1545.2	1497.7	455.4	278.6	674.1	476.8	351.7	438.2
AFFX-Phe (1/50000)	106.2	999.6	501.4	595.6	790.1	1078.4	1378.1	1258.8	1116.2	441.6	238.0	584.3	422.0	302.1	476.1
AFFX-Thr (1/25000)	226.2	1423.5	870.5	1077.8	886.2	774.2	1241.0	1407.0	1391.5	1046.2	583.7	1522.8	981.2	711.4	841.4
AFFX-Dap (1/7500)	691.3	5726.6	3644.1	3352.1	4579.0	5135.8	7554.3	6646.0	5714.1	3301.8	1884.0	3816.5	2750.6	1611.5	2617.3
Test Chip Spike-in Amplification Control 3'/M Ratio:															
AFFX-Lys (1/100000)	2.4	2.1	2.3	1.7	1.8	2.0	2.6	2.5	2.8	1.87	1.59	2.38	1.86	2.40	2.17
AFFX-Phe (1/50000)	2.2	1.6	1.9	1.5	2.1	2.1	2.4	1.9	2.6	1.58	1.65	1.56	1.43	1.89	1.75
AFFX-Thr (1/25000)	2.8	3.8	3.8	3.5	5.4	6.6	8.1	6.5	9.5	3.25	3.34	3.06	3.57	4.25	3.84
AFFX-Dap (1/7500)	1.8	1.5	2.2	1.8	2.1	2.4	3.0	2.6	3.2	3.28	3.11	2.75	3.40	2.97	3.67
average 3'/M ratios	2.3	2.3	2.5	2.1	2.9	3.3	4.0	3.4	4.5	2.23	2.19	2.33	2.29	2.85	2.59

Table 29. The compiled amplification and TestChip results of the initial test samples (Batch #1) and the subsequent CEA specimens (Batch#2 and Batch#3). Highlighted were the failed QCA markers from the samples with mild-moderate RNA degradation which have amplified with a significant 3'/M bias.

4.10.3 Batch#3: The remaining CEA samples

The remaining samples were processed together as Batch #3. They were amplified from 60ng of starting totalRNA or the highest amount available in 3µl. The yields from first and second cycles of RNA amplification generated ample labelled cRNA (69 to 138µg). The cRNA was fragmented and hybridised to the Affymetrix Test Chip and the results are shown in Table 29.

All the samples amplified well with satisfactory QCA measures of the spiked-in amplification controls, spiked-in hybridisation controls and array QCA measures. The sample internal control gene, GAPDH had 3'/M ratios of 1.65 to 2.26 (recommended <3) confirming the high quality of the RNA samples and the average 3'/M ratios of the spiked-in amplification controls were 2.19 to 2.85 (recommended <3) confirming good amplification reactions. The scale factor and percentage present calls were within expected parameters. All 6 samples were successfully hybridised to the Affymetrix GeneChip.

4.10.4 Hybridisation and scanning of the Affymetrix GeneChip

The amplified cRNA was hybridised to the genome-wide Affymetrix HG-U133 plus 2.0 GeneChip in the 3 batches. The GeneChip has the same QCA measures built-in as the TestChip and are shown in Table 30. The technical QCA measures of the GeneChip array kinetics and hybridisation were satisfactory with B2 oligo positive control, background, noise and detection of the Spiked-in Hybridisation controls within operational ranges. The 'BioB' Hybridisation Control (at a dilution of 1.5 parts per million) was positively detected at the detection threshold of the array and the negative control 'Trp' probeset was undetected across all the arrays, confirming the sensitivity of the array.

The Amplification Control probesets were replicated in the GeneChips and the spiked-in poly-A controls were similar to the TestChip data as expected, as were their 3'/M ratios. The GAPDH internal control gene 3'/M ratios assessed the gamut of sample quality and RNA amplification and labelling reactions, and were replicated in the GeneChip. The GeneChip results were similar to the Test Chip measurements with a range from 1.58 to 3.15, and were less than 2 fold in difference from the highest value to the lowest value and within satisfactory operational limits for the 2 cycle amplification reactions. There was no significant difference in 3'/M ratios between the stable and ruptured groups (p=0.35). The percentage of present calls were satisfactory between 37 to 47% and the scale factors were comparable across the arrays ranging from 1.3 to 2.7.

The samples were all successfully hybridised to the Affymetrix GeneChip with satisfactory QCA measures, generating the complete set of genome-wide macrophage gene expression profiles for transcriptomic analysis from 11 CEA samples. These robust QCA measures although restrictive ensured the high quality and reproducibility of the microarray results and confirmed the technical success of the microarray experiment. The validation of the technical performance of the amplification and microarray experiment was important before embarking on the detailed analyses of the genome-wide transcriptomic datasets.

Sample:	CEA14	CEA25	CEA36 redo	CEA41	CEA45	CEA81	CEA17	CEA33 redo	CEA35 redo	CEA57	CEA100
Batch	1	1	3	2	2	3	2	3	3	3	3
Plaque type	Stable	Stable	Stable	Stable	Stable	Stable	Ruptured	Ruptured	Ruptured	Ruptured	Ruptured
Histology	FCA	FCA	FCL	FCA	FCA	FCL	Rup TFCA	Rup TFCA	Rup TFCA	Rup TFCA	Rup TFCA
GeneChip QCA measures:											
Scale Factor	1.59	1.59	2.40	1.81	2.73	1.32	1.86	1.82	2.29	1.80	1.86
B2 Oligo positive control	Present	Present	Present	Present	Present	Present	Present	Present	Present	Present	Present
Background	47.81	58.82	68.47	56.06	48.71	78.77	55.81	53.76	78.20	67.29	79.17
Noise	2.64	3.42	3.85	2.91	2.39	4.14	3.00	2.86	4.91	3.53	4.65
Present Calls (%)	47.0%	46.6%	44.9%	47.4%	42.7%	42.7%	46.6%	44.8%	36.8%	40.8%	39.5%
GeneChip Internal Control Genes:											
AFFX-HUMGAPDH/ M33197 3'/M Ratio	1.58	1.79	2.28	2.34	3.16	1.59	1.80	2.09	1.88	1.73	1.71
GeneChip Spike-in Hybridisation Control:											
AFFX-BioB (1.5pM)	812.1	782.3	356.5	245.9	305.1	156.5	224	212.1	237.6	188.5	187.2
AFFX-BioC (5pM)	1754.4	1824.3	1378	1106.5	1372	764.2	1201.1	1026.2	1057.5	956.9	936.6
AFFX-BioD (25pM)	8016.9	8014.6	4003.4	3641.6	4391.8	2476.9	4045.9	3395.7	3790.1	2939.6	2802.3
AFFX-Cre (100pM)	19679.4	20186.7	13675.6	9679.2	13089.6	8038.3	10538.1	10600.1	11503	9584.6	9079
GeneChip Spike-in Amplification Control:											
AFFX-Trp (neg control)	8.8	3.5	9.7	3.7	3.9	2.4	1.5	17.6	4.7	2.1	3.1
AFFX-Lys (1/100000)	4810	4388.1	2537.1	1735.3	1723.5	1063.1	3611.2	1327.1	1178.6	1545.2	1735
AFFX-Phe (1/50000)	2307.4	1735.7	1850.5	1131.2	1385.4	850.4	2015.1	965	836.5	1429.5	1876.8
AFFX-Thr (1/25000)	3455.4	3175.6	4831.9	1546.3	962.6	2246.5	4388.6	2633.9	2184.5	3086.8	3164.3
AFFX-Dap (1/7500)	12141.5	12008.2	11382.2	7260.6	7679.9	5979	11651.4	7278.2	7386	8487	8246.2
GeneChip Spike-in Amplification Control 3'/M Ratio:											
AFFX-Lys (1/100000)	2.36	2.48	2.26	2.50	2.32	2.38	1.94	2.25	2.16	2.04	2.49
AFFX-Phe (1/50000)	1.27	1.49	1.23	1.50	1.70	1.16	1.03	1.08	1.20	1.14	1.54
AFFX-Thr (1/25000)	2.98	3.16	2.89	5.37	5.91	3.46	2.83	2.99	2.69	2.99	3.34
AFFX-Dap (1/7500)	1.14	1.85	2.25	1.92	2.46	3.10	1.44	2.42	3.01	2.62	2.88
average 3'/M ratios	2.21	2.38	2.13	3.12	3.31	2.33	1.93	2.11	2.02	2.06	2.46

Table 30. The GeneChip Quality Control Assessment measures of all the macrophage LMD CEA atherosclerotic plaques taken successfully to microarray.

Chapter 5. The analyses of the transcriptome in plaque rupture

5.1 Overview

The microarray experiments generated large datasets of gene expression profiles of the entire transcriptome. This required a complex series of data processing and analysis to be performed in order to identify significant genes and pathways involved in plaque rupture and its validation. An overview of this process is outlined in Figure 70.

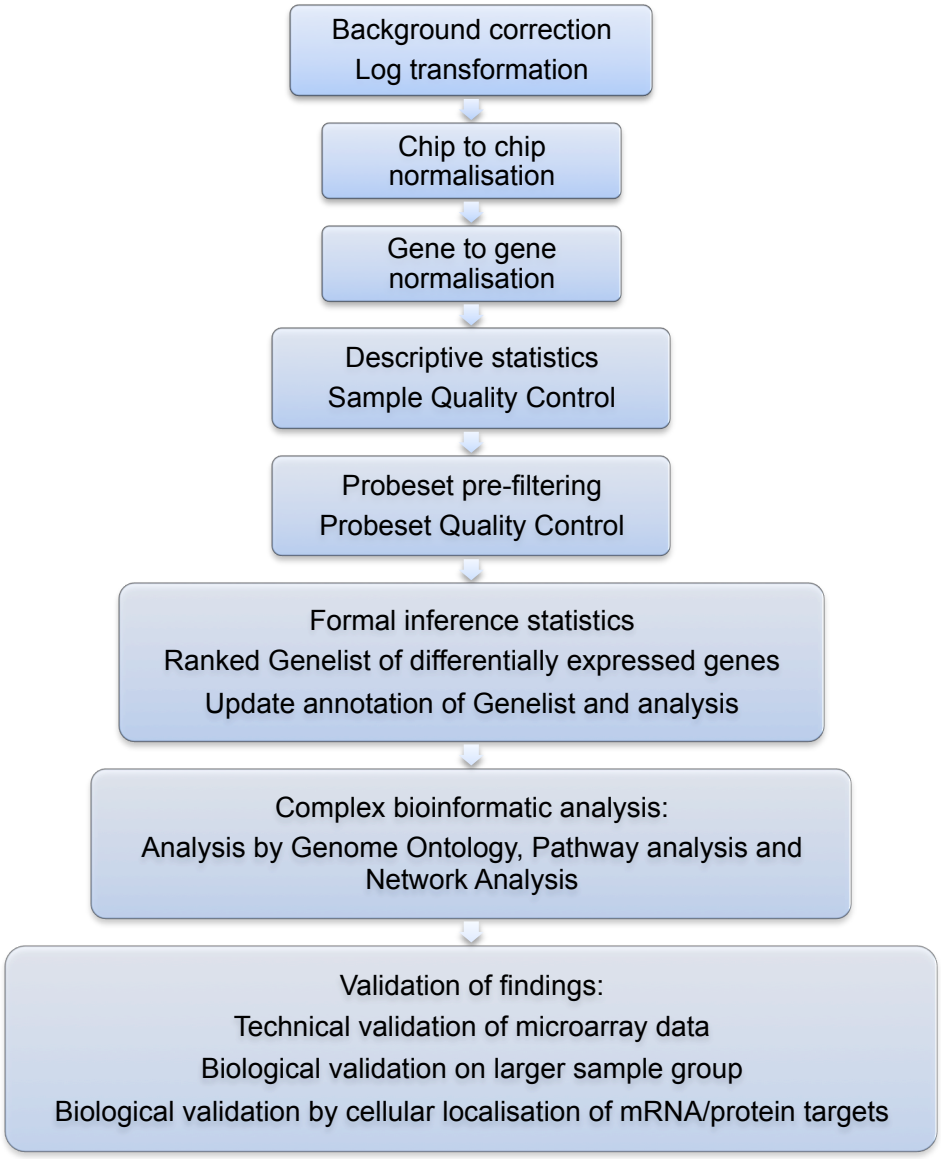

Figure 70. An overview of microarray data analysis leading to the identification of target genes and pathways and the subsequent validation work.

5.2 Background correction, signal quantification, probeset summarisation and normalisation

Prior to the actual analysis and description of the transcriptomic gene expression profiles, the microarray data of raw signal intensities of individual probes were corrected for non-biological systematic errors and noise such that the generated signal intensity values accurately and precisely reflect the true biological transcript abundance. To achieve this, I assessed several methods using GCOS, RMA and GCRMA to achieve the optimal background noise correction, probe signal quantification and probeset summarisation.

5.2.1 Box-plots: medians and distribution of global array signal intensities

An ideal probe-level processing and global normalisation would produce global array probeset signal intensity values which demonstrate a uniform and normal Gaussian distribution across all the arrays in the experiment when $\log_2$ transformed (i.e. with similar median and inter-quartile values). This was visually inspected using box-plots in Figure 71.

I observed a significant degree of variability in the medians between arrays when no normalisation was applied. If comparative gene expression analyses were performed, there would be an artefactual result of 2 fold difference in transcript abundance between CEA45 and CEA81 due to systematic errors of experimental variability and not true biological effect. This was improved by global normalisation procedures in ascending order of increasing uniformity using GCOS, RMA and then GCRMA. GCRMA demonstrated normalised global array signal intensity values of normal Gaussian distribution and with the best uniformity across all the arrays in the experiment.

The box-plots of only probesets with Present or Marginal calls (using the Affymetrix Present/marginal/absent detection algorithm) demonstrate the distribution of the global transcriptome of the array datasets without the background noise and non-specific binding signals generated by the Absent probesets. Overall the distribution of these transcripts were normally distributed (Gaussian) confirming the assumptions necessary for parametric statistical analyses later.

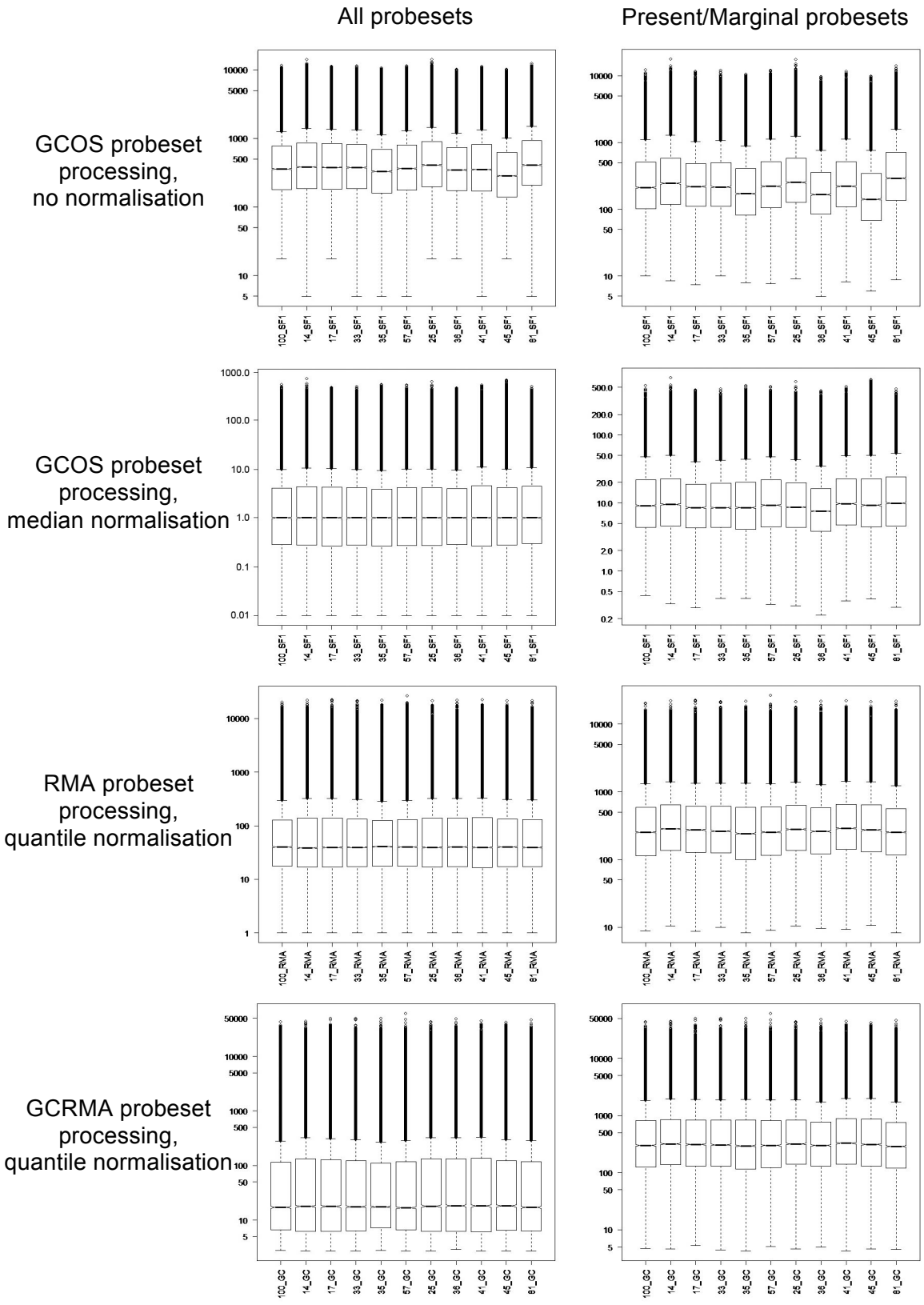

Figure 71. Box-plots of the global probeset signal values of the 11 arrays. The median (50th centile) was marked as the bold line in the middle of the box-plot, with the lower (25th) and upper (75th) quartiles represented by the box. The 95th percentile range was represented by the tabbed lines.

5.2.2 MA-plots: Linearity and variance of normalised log-signal-ratios

By using MA-plots the linearity of the variance of the log-ratios with respect to transcript abundance (low expression transcripts on the left side and high expression transcripts on the right side) could be examined (Figure 72). The ideal normal (Gaussian) distribution of gene expression log-ratios was seen as a linear and symmetrical distribution about the line y=1.

This was particularly revealing of the increased variance of the log-ratios of low expression transcripts (seen as a larger distribution of plots about the x-axis) seen using GCOS due to poorly corrected background noise and non-specific binding. Furthermore, there was a skew in the distribution (non-linear) of log-ratios which was more pronounced without normalisation; with a negative bias in low abundance transcripts and a positive bias in moderate abundance transcripts (marked by arrows in Figure 72).

In comparison, The RMA and GCRMA probe-level processing and normalisation had symmetrical distributions of log-ratios across the transcript abundance spectrum (a symmetrical cigar shape about y=1). This preserved linearity confirmed normal Gaussian distribution in log-ratios which was pertinent for later parametric statistical approaches. The reduced variance of the low and low-medium abundance transcripts compared to GCOS would result in improved precision and detection of differentially expressed genes.

RMA attenuation of biological variance

There was a global reduction of variance of log-ratios seen in the MA-plots for RMA compared to GCRMA (a narrower cigar shape). The global reduction of variance may reflect the attenuation of the true biological variation which we are measuring due to over-aggressive corrections and less accurate modelling[260, 261]. In a comparison of common probesets identified using GCOS, RMA and GCRMA, I have found that the RMA method had the lowest geometric mean of fold change at 3.17 (IQR of 1.96-4.79) demonstrating a significant compression of fold change and attenuation of true biological variation. The GCRMA method had the highest geometric mean of fold change at 4.05 (IQR of 2.16 to 6.69) reflecting the preservation of biological variability. This may be explained by the modelled nucleotide binding affinity based on probe sequence information by GCRMA to more accurately correct for background noise and non-specific binding compared to RMA[260, 261].

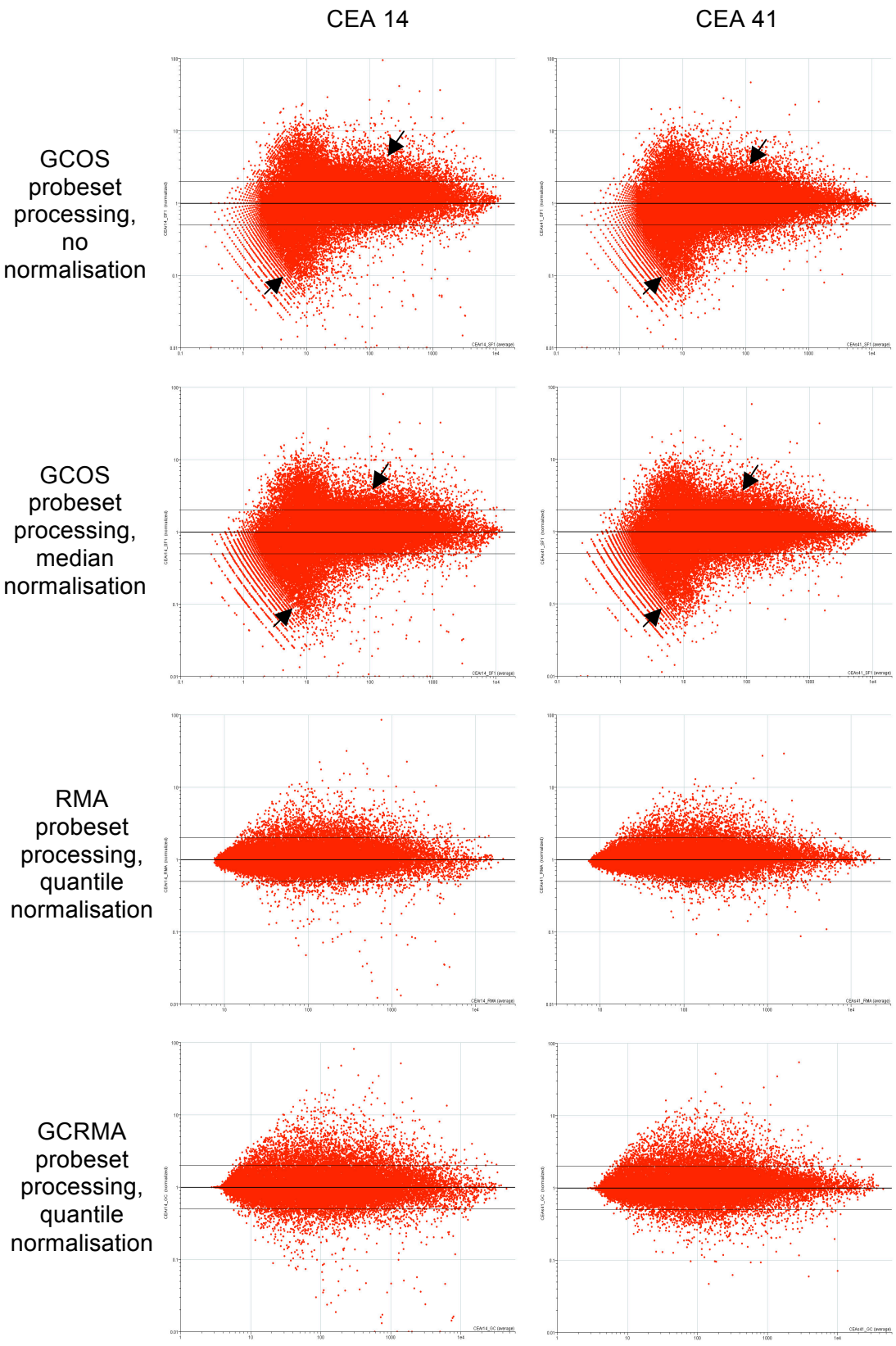

Figure 72. MA-plots of Log-transformed relative abundance ratios; the log-ratio (M), to averaged abundance (A) (MA-plots) of probeset signal intensities. Further details in text.

5.2.3 Evaluation of probe-level processing and normalisation methods, a conclusion

In a summary table of the various probeset processing and normalisation methods with the ranked order of assessment in uniformity of distribution, linearity and variance of the data (Table 31), we showed that GCRMA produced the best results and was used on my microarray dataset. It had optimal global normalisation with uniform median and quartile distribution across the arrays. It demonstrated a linear and normal (Gaussian) distribution of log-ratios with controlled variance of the low expression transcripts and preservation of biological variance and fold difference.

Probeset processing and normalisation method	**Background correction**	**Signal quantification**	**Probeset summarisation**	**Ranked distribution uniformity by Box-plots**	**Ranked Linearity by MA-plots**	**Ranked reduced variance in MA-plots**
GCOS, not normalised	MM-probe	PM signal to background	Tukey's Biweight	4	3	4
GCOS, per-chip median				3	2	3
RMA, per-chip quantile	Modelled optical noise and non-specific binding	PM signal to background	Median Polishing	2	1	2*
GCRMA, per-chip quantile	Modelled optical noise and probe-affinity non-specific binding	probe-affinity modelled PM signal to background	Median Polishing	1	1	1

Table 31. Table showing the various methods of probe-level processing and global normalisation with the ranked order by uniformity of distribution, linearity of log-ratios and low variance (ranked 1 as the best, *RMA with attenuation of measured biological effect).

5.3 Macrophage Expression Profile Correlation

5.3.1 Expression of macrophage specific genes

In order to confirm that I had primarily isolated macrophage cells from LMD, I examined the dataset for the expression of typical macrophage marker genes like CD36, MMP9, MMP12, CD14, MCSFR, cathepsins G,L and H, osteopontin, ApoE and ApoC1, and found them to be expressed in all our samples confirming the presence of macrophage gene expression.

5.3.2 Macrophage gene expression signature

Using a different and unbiased approach in the selection of genes examined, I examined the whole transcriptomic profile of our samples and explored the relationship between our data and the expression profiles of 299 samples from 87 various defined tissue and cell types obtained from the NCBI Gene Expression Omnibus (GEO) repository which included macrophage cell types[263-268]. The comparison of the microarray gene expression signatures by condition tree analysis showed a close relationship between the micro-dissected cells and macrophage cell-lines with a 99% bootstrap confidence level (Figure 73). Importantly, the analysis showed only distant relationships to the profiles of other cell types present in the vessel wall, including smooth muscle cells and T-lymphocytes, with a bootstrap confidence level of 100%. This indicates that substantial enrichment for macrophage-derived RNA was achieved by the LMD protocol.

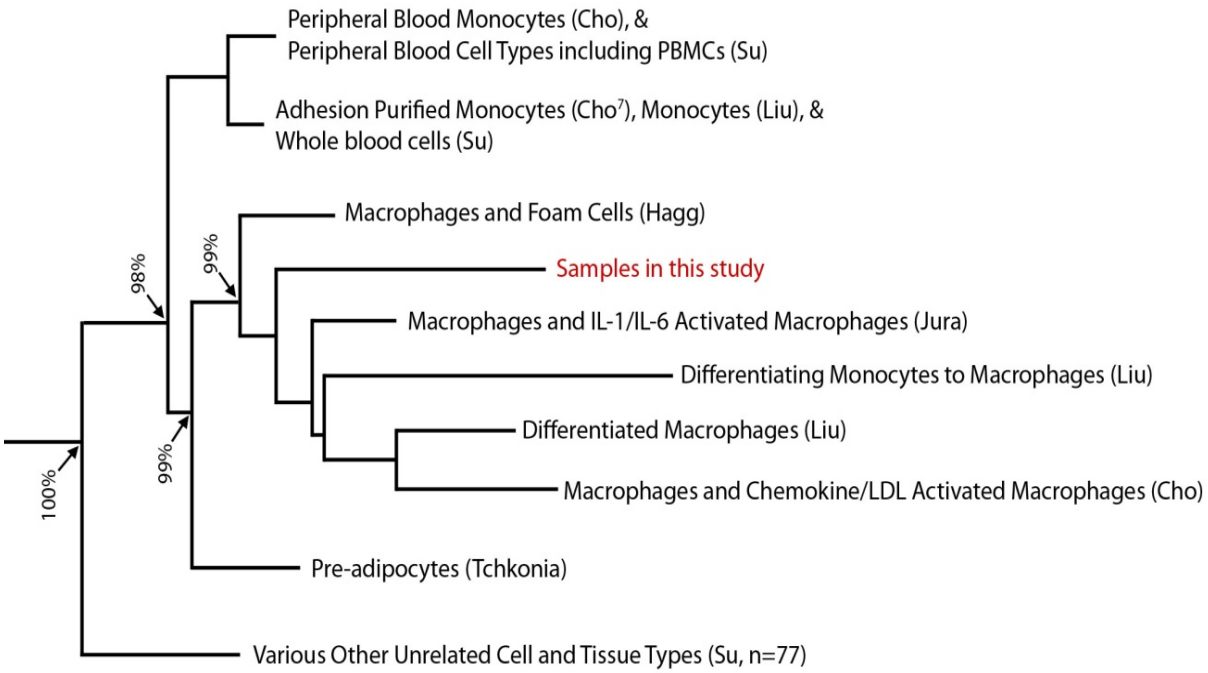

Figure 73. Condition Tree Dendrogram demonstrating the correlation of the genomic expression profiles of the 11 LMD samples in our study to other samples of various types (n=299) using Spearman correlation of the whole array genome-wide gene expression data with bootstrap confidence levels.

5.3.3 Gene expression profile of macrophage activation

I then examined the macrophage gene expression profiles of our samples to other samples of blood cell origin as well as activated and unactivated macrophages. The principal components analysis comparing only the expression of genes previously shown by others to be involved in macrophage activation show that both the stable and ruptured LMD samples overlap and cluster with the activated macrophages studied by others[265-268] (Figure 74, orange clusters). Moreover, they are separate from the expression profiles of unactivated differentiated macrophages[265] (blue clusters), differentiated monocytes and peripheral blood monocytes (PBMCs) from various previous studies[265, 267, 268] (green clusters). They are also distant from the other inflammatory cell types (T-lymphocyte and B-lymphocyte cells, natural killer (NK) cells) and whole peripheral blood cells[263] (green clusters). This demonstrates that the gene expression profiles in our laser micro-dissected samples closely resemble those described in the literature to date for activated macrophages.

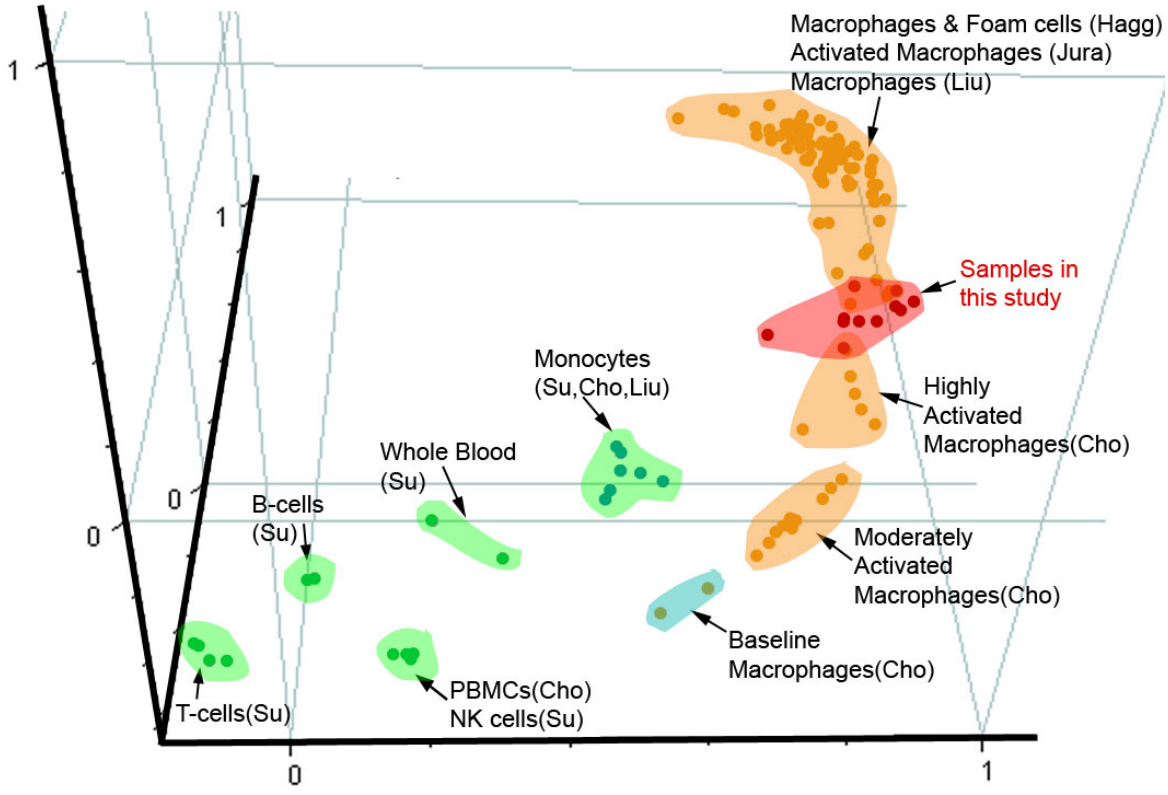

Figure 74. Principal Components Analysis of the LMD samples in this study with samples of blood cell origin and activated/unactivated macrophages using the expression profiles of a subset of genes involved in macrophage activation.

5.4 Unsupervised exploratory clustering

Using the GCRMA normalised datasets, the whole array was analysed to detect for significant clustering of the samples. We used 2 different explorative clustering methods to describe our datasets; by principal components analysis and condition trees. This allowed me to observe the clustering of samples of similar transcriptomic expression profiles and the separation of samples of differing profiles without any assumption of their groups (and were therefore unsupervised). I would expect the major difference in the expression profiles of the LMDed macrophages to be due to the stability/instability of the plaque, as this was the principal comparison in our study. However other factors could have contributed significantly to a difference seen in the expression profiles such as technical variability (variation in LMD, RNA quality, amplification and hybridisation) or other biological differences (such as age, sex, diabetes or hypertension) between the samples.

5.4.1 Principal component analyses

The PCA using the entire array dataset (all probesets) is shown in Figure 75, panel A. The 3 principal components accounted for the majority of the of the overall variance seen in the expression profiles. Using these 3 major principal components, the 11 samples clearly separated into 2 identifiable groups and corresponded to stable or ruptured plaques. The 5 samples comprised of the ruptured group clustered closely together. The 6 samples comprised of the 5 samples of the stable group and the 3-domain unclassified stable plaque of CEA14 was clearly separate from the ruptured group but had greater variance in gene expression space. As the stable samples were histologically more heterogenous compared to the ruptured plaques, this observation was expected. In particular the separation in gene expression space amongst the stable samples correlated to their histology; of thick cap fibrocalcific plaques in CEA36 and 81 and thick fibrous cap atheromas in CEA 14, 25, 41 and 45.

Further analysis by filtering out the probesets which were flagged as absent (using the GCOS absent/marginal/present call algorithm) in all the samples (19,002 probesets were flagged as Absent in all 11 samples) was performed to check that the measured similarity/separation of gene expression profiles were not due to GCRMA resolved signal intensities of absent genes and was shown in Figure 75, panel B. The resultant PCA scatter plot was almost identical to the former PCA scatter plot using all the probesets. The overall variance accounted for by the 3 major principal components were also very similar. This demonstrated that the differential gene expression that caused the maximal separation of the groups were from expressed Present-called genes.

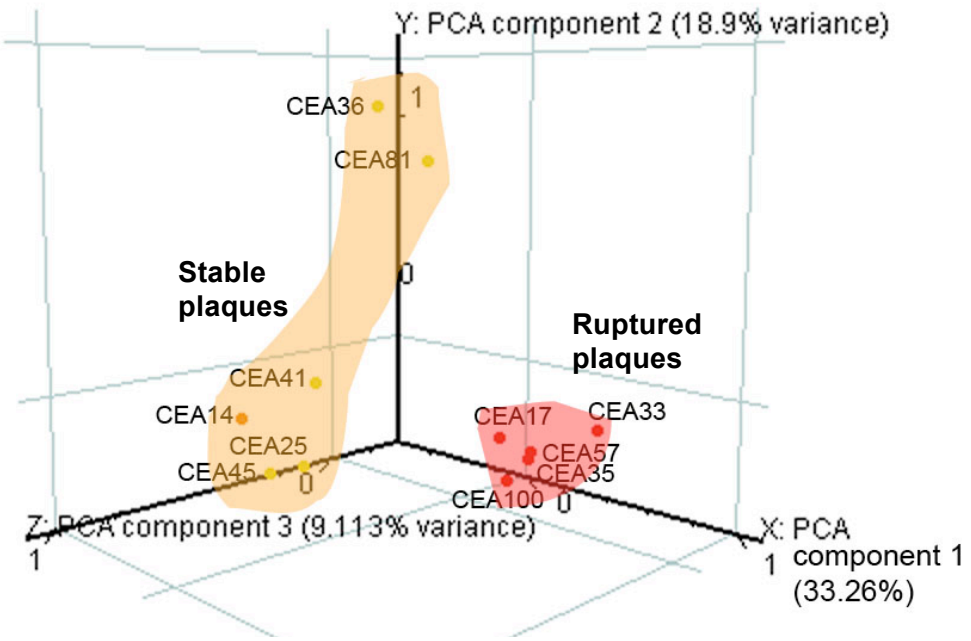

A: Using all probesets

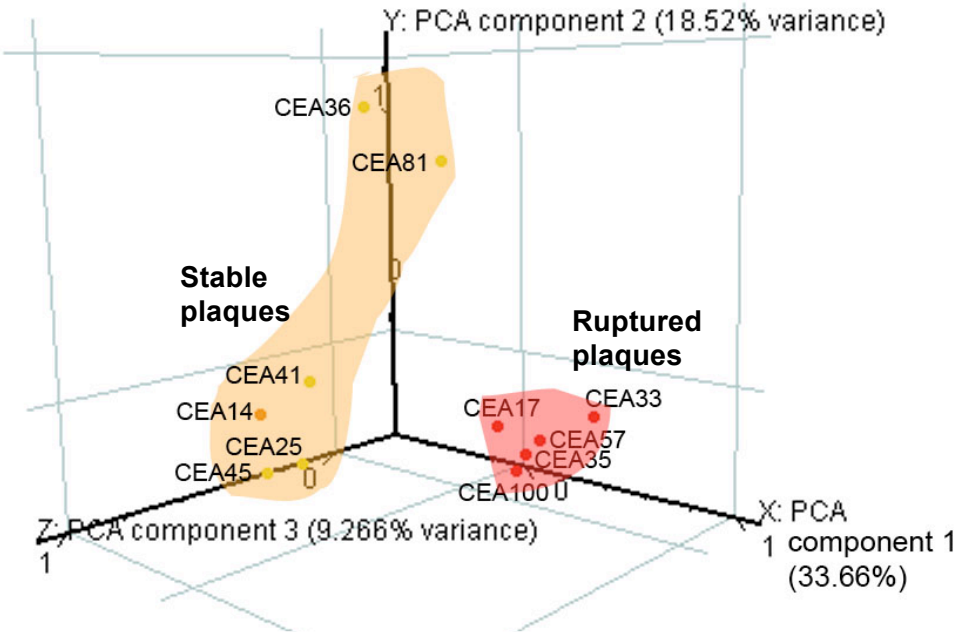

B: With absent probesets removed

Figure 75. Principal component analyses of all the 11 samples of LMDed macrophages from stable and ruptured atherosclerotic plaques plotted by a scatter-plot to the 3 major components. Panel A was the PCA using the entire array probesets and Panel B was the PCA with absent-called probesets removed.

5.4.2 Condition tree dendrograms

The CTD using Pearson correlation on the entire array dataset (all probesets) is shown in Figure 76. panel A. The 11 samples separated into 2 groups in a similar manner to that described using the Principal Components approach. The ruptured plaques had a tight cluster separate from the stable samples. Another tight cluster comprising of the stable FCA plaques, CEA25, 41, 45 and the 3-domain unclassified stable FCA, CEA14 is observed. The other stable FCL plaque samples, CEA36 and 81, were clearly separate in their branching from the ruptured group but did not cluster tightly with the other stable samples demonstrating increased variability in their gene expression profiles.

Without making any assumptions of the Gaussian distribution of the data (which was assumed to be the case by using Pearson correlation) and to address the possibility of extreme signal intensity values (outliers) skewing the measurements, I analysed the data using Spearman correlation, a non-parametric similarity measure, where the signal intensity values were ranked for correlation. The results of the CTD using all the probesets and using Absent-called probesets removed were similar to the that performed using Pearson correlation with some improvement in the clustering of the stable samples (Figure 76, CEA81 and 36 branched closer to the cluster of the other stable samples), confirming the findings using Pearson correlation.

The high similarity measure between the all the samples was 95% using Pearson correlation is representative of a highly uniform cell type isolated (i.e. with low variance). Furthermore, the CTDs performed using absent-called probesets removed showed almost identical results to using all probesets corroborating the observations by PCA, confirming that the clustering was not due to GCRMA resolved signal intensities of absent genes but were from the expressed Present-called genes.

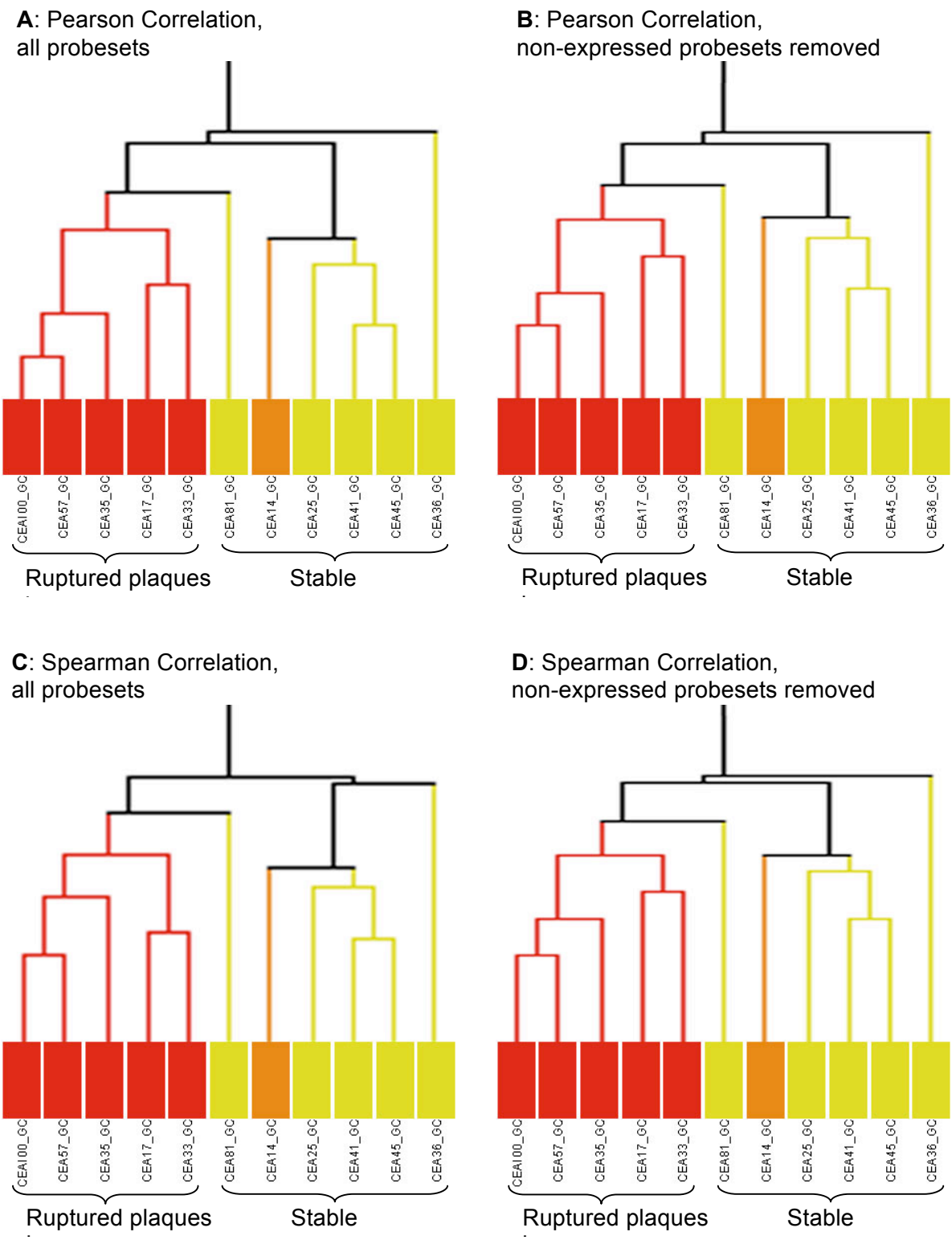

Figure 76. Condition tree dendrograms of all the 11 samples of LMDed macrophages from stable and ruptured atherosclerotic plaques using Pearson Correlation (panels A&B) and using Spearman correlation (panels C&D). Panels A&C were performed using the entire array probesets and Panel B&D were performed with absent-called probesets removed.

5.4.3 Analyses of potential confounding factors

Both methods using PCA and CTD demonstrated the clustering of the samples into the 2 groups of stable and ruptured plaques; with the tight clustering of the 5 ruptured samples (Ruptured cluster) and the clustering of the stable samples as 2 mini-clusters close to each other of the 4 stable samples of thick fibrous cap atheroma (Stable cluster A) and the other 2 stable samples of thick cap fibrocalcific plaques clustering separately (Stable cluster B). Analyses of potential confounding factors and in the identification of outlier samples were also performed using PCA and CTD and were summarised in Table 32 with respect to the clustering observed.

Technical factors contributing to variation

Sources of variation related to the laboratory preparation and processing of the sample were explored. These included LMD and RNA quality, RNA amplification starting amounts and performance in 3'/5' bias, hybridisation batch and array performance (Table 32). No outlier clustering of global gene expression profiles due to such technical sources of variation was observed using PCA or CTD.

Biological factors unrelated to plaque status contributing to variation

Differences in other biological characteristics of the samples such as age, sex, ethnicity, risk factor profile (of diabetes, smoking, hypertension, etc.) or the degree of stenosis severity may contribute to the differences seen in the gene expression profiles in a relatively smaller degree but should not obfuscate the global or major gene expression differences observed due to plaque stability/instability. These variables were examined and no discernable outlier clustering was observed using CTD or PCA (Table 32).

5.4.4 Reclassification and inclusion of CEA14 as a stable sample

CEA14 was an initial test sample processed through to microarray with histological classification of a stable plaque but did not fulfil the other 2 domain criteria; with surface irregularity on MR angiography and old clinical symptoms of a lacunar infarction stroke over a year ago. It was very interesting to observe that CEA14 clustered right in the middle of the stable group of samples in both condition tree and PCA in accordance to its histological classification as a stable thick fibrous cap atheroma. Detailed histological analyses demonstrated that the region of irregularity seen on MR angiography corresponded to a healed stable fibrocalcific plaque 1 cm away from the LMDed frozen sections. The frozen sections which were processed for LMD and microarray were from a separate stable thick fibrous cap atheromatous lesion. There was no evidence of rupture

or erosion. Based on these arguments, CEA14 was classified as a stable sample and was included in the subsequent microarray data analysis.

5.4.5 Unsupervised clustering, a conclusion

By using two different unsupervised clustering methods I have found that the samples clearly separate and cluster into stable and ruptured groups. There was no clustering of global gene expression profiles observed due to technical sources of variation or from potentially confounding biological factors unrelated to plaque status. The clustering observed was due to specific differences in the gene expression profiles of these samples due to their phenotype of a stable or ruptured plaque. This supports my hypothesis that there are differences in the macrophage gene expression patterns between stable and ruptured plaques (and not just a difference in their number) which influence the biological processes leading to plaque rupture. The successful identification of these genes of differential expression can help the identification of biological pathways and gene networks involved in plaque rupture.

Sample	CEA14	CEA25	CEA41	CEA45	CEA36	CEA81	CEA17	CEA33	CEA35	CEA57	CEA100
PCA and CTD cluster	StableA	StableA	StableA	StableA	StableB	StableB	Ruptured	Ruptured	Ruptured	Ruptured	Ruptured
Histology of the lesion	FCA	FCA	FCA	FCA	FCL	FCL	RupTFCA	RupTFCA	RupTFCA	RupTFCA	RupTFCA
3-Domain classification	Unclassified	Stable	Stable	Stable	Stable	Stable	Ruptured	Ruptured	Ruptured	Ruptured	Ruptured
Total ischaemic time (minutes)	10	14	15	28	13	21	10	9	13	12	19
RNA yield from LMD (ng/10000cells)	48.0	57.5	39.2	51.9	47.3	62.0	36.9	31.9	16.6	68.0	64.4
RNA quality- 28S/18S ratio	2	1.9	1.7	1.4	1.6	1.6	1.8	2	1.7	1.9	1.6
RNA amplification starting material (ng)	20 ng	20 ng	60 ng	60 ng	57ng	60ng	60 ng	42ng	42ng	60ng	60ng
RNA amplification cRNA yield (g)	51.6	83.4	150.0	143.1	69	69	148.5	126	75	138	105
AffyQC-Scale Factor	1.59	1.587	1.81	2.732	2.404	1.322	1.862	1.824	2.292	1.802	1.857
AffyQC-% Present Calls	47	46.6	47.4	42.7	44.9	42.7	46.6	44.8	36.8	40.8	39.5
AffyQC-GAPDH3'/M' Ratio	1.58	1.79	2.34	3.16	2.28	1.59	1.8	2.09	1.88	1.73	1.71
RNA amplification & hybridisation batch	1	1	2	2	3	3	2	3	3	3	3
Age	45	58	73	68	67	59	67	63	53	74	73
Sex	female	male	male	female	male	male	male	male	male	female	female
Ethnicity	Caucasian	Caucasian	Caucasian	Caucasian	Caucasian	Caucasian	Caucasian	Caucasian	Caucasian	Asian	Caucasian
Clinical Symptoms	LACI	None	None	None	None	None	PACI	AFugax	PACI	AFugax	PACI
Time since symptoms prior to surgery (days)	360	0	0	0	0	0	30	3	28	180	35
Smoker	yes	no	no	no	ex	no	ex	ex	ex	no	yes
Treated hypercholesterolaemia	yes	yes	yes	yes	yes	yes	no	yes	yes	yes	yes
Treated hypertension	yes	no	yes	yes	yes	yes	yes	yes	no	no	yes
Diabetes	no	no	no	no	NIDDM	no	no	no	no	no	NIDDM
Family history of premature CAD/CVD	yes	no	no	no	no	no	yes	yes	yes	no	no
Ischaemic heart disease	no	yes	yes	yes	yes	no	no	yes	no	no	no
Radiology- Degree of Stenosis	85	90	98	95	75	85	90	70	70	95	60
Radiology- Surface Morphology	Irregular	Mild irreg	Smooth	Smooth	Smooth	Smooth	Irregular	Irregular	Irregular	Irregular	Irregular

5.4.6 Comparison between groups (Inference statistics)

Pre-filtering of non-expressed probesets

Prior to formal inferential statistical analysis, probesets of transcripts which were not expressed were removed from analysis. Including these probesets in the formal inferential statistical tests would significantly increase the number of statistical tests performed and contribute to the error of multiple testing. The non-human Affymetrix spiked-in control probesets (n=62) were removed. I chose to be only moderately stringent in the pre-filtering of probesets and removed only probesets flagged Absent in ≥6 of the 11 samples (n=29,080 probesets removed) (the remaining probesets were flagged Present in ≥5 of the 11 samples). This allowed the inclusion of genes which were expressed in one group but were not expressed in the other group.

Comparison statistics and multiple test error

The resultant pre-filtered GCRMA normalised probesets (n=25,538) were statistically analysed using a one-way ANOVA parametric test with the variances in both groups assumed to be similar. In an ANOVA analysis without multiple test correction, a p-value cut-off of p≤0.05 identified 5,554 probesets to be significant. However a substantial number of the probesets identified would have been identified by chance due to the multiple testing of over 25,000 probesets. A lower p-value cut-off could be used to identify a genelist of statistically significant probesets; using p-value cut-off of p≤0.005 identified 1,243 probesets. However, the p-value would have little meaning in the interpretation of significance due to the confounding issue of multiple testing (a p-value of ≤0.05 does not actually predict a probability of 5% of the genes identified occurring by chance).

We corrected for the error of multiple testing using the Benjamini and Hochberg method which estimates a false discovery rate (FDR). We used a FDR cut-off of 10% which was appropriate for the purpose of gene discovery (as the genes identified were to be tested in a larger number of samples subsequently). A total of 1,187 probesets which represent 914 known genes were identified to be statistically significant and differentially expressed between stable and ruptured plaques, from which about 119 probesets were expected to have passed the restriction by chance (FDR of 10%).

5.4.7 Examination of the Genelist ranked by expression fold difference

Data-mining check of accuracy of gene annotation

The accuracy of the previously updated probeset gene descriptions and annotations from the NIH databases of EntrezGene, Genbank and Unigene using the probeset Genbank

identifiers by the GeneSpyder program on GeneSpring were compared to the Affymetrix database on NetAffx[284] using the Affymetrix unique probeset IDs. This database is updated by Affymetrix every quarterly to the most recent nucleotide, protein and functional biological data available and the probeset sequences are also updated to ensure the accurate match to the gene identifiers. There was 100% concordance of the gene name and annotation of the 1,187 probesets using both methods.

Examination of Genelist by fold change

The 1,187 differentially expressed probesets were ranked by relative fold difference in expression (fold change) of the geometric mean of signal strength of the ruptured samples to the stable samples. Three hundred and thirty two probesets were of 4 fold relative differential expression and higher, and 717 probesets were of 2 fold or greater expression. The statistically significant genelist of 1,187 probesets was graphically represented in a line graph of the relative expression of the probesets in the ruptured and stable groups in Figure 77. The relative expression of the probesets in each sample were also graphically represented in a heatmap and the twenty genes showing the highest differences in fold change between ruptured and stable samples were listed in Figure 78.

The 15 highest fold difference probesets which were up-regulated in the ruptured group compared to the stable group are shown in Table 33. Twelve probesets mapped to 10 known unique and well characterised genes and 3 probesets represented variations of the immunoglobulin kappa variable proteins (IGKV). We found genes involved in lipid processing and signalling (FABP4, Leptin), apoptosis genes (PACAP, CD38), inflammation and oxidation (HMOX1, DHRS9), immune response genes (PPBP, FCGR3A/B, IGJL3) and cell adhesion (CD300A) amongst the 10 highly ranked genes upregulated in the ruptured plaque. FABP4 was the highest differentially expressed gene in the ruptured samples compared to the stable samples.

The top 15 probesets of highest fold difference which were up-regulated in the stable group compared to the ruptured group are also listed in Table 34. Fourteen probesets mapped to 13 known unique and well characterised genes and 1 probeset represented a hypothetical protein-coding transcript similar to the FIBIN gene associated with pectoral fin bud initiation in zebrafish. Of the known genes identified, genes for proteins in the extracellular matrix and cell adhesion (ASPN, OGN, ITGBL1, COL21A1, ECM2, COL8A1, PCDH10), WNT signalling (SFRP2), G-protein signalling (RGS5, FNDC1), ion transport (KCNT2) and oxidation process (FMO2) were highly expressed in the stable plaque.

The complete list of the 1,187 significantly up- and down-regulated probesets from the microarray analysis available as a tab-delimited file in the enclosed CD.

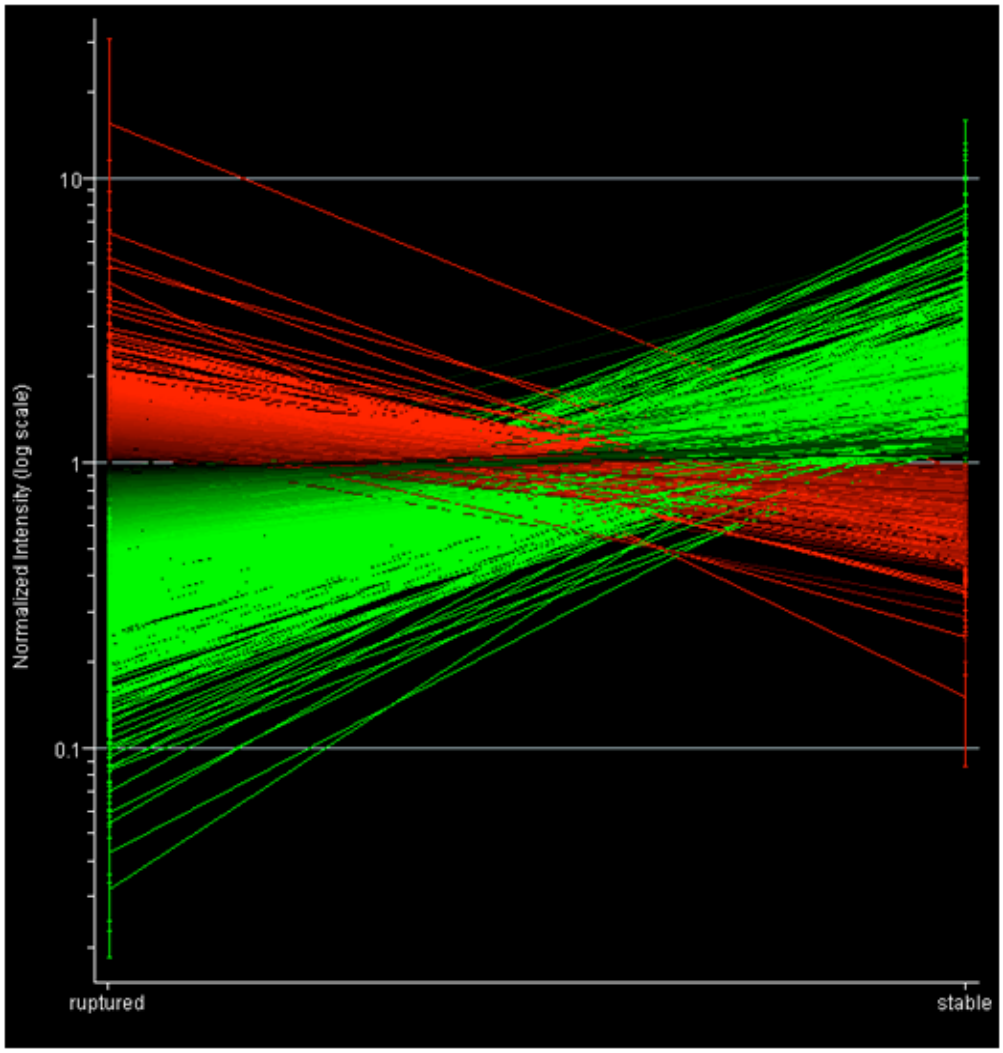

Figure 77. The relative difference in transcript expression between ruptured and stable groups of the 1,187 statistically significant probesets are represented here on a logarithmic scale. The geometric means of the signal intensity ratios with standard error bars are shown. Red represents high expression in the ruptured group relative to the stable group, and vice-versa in green.

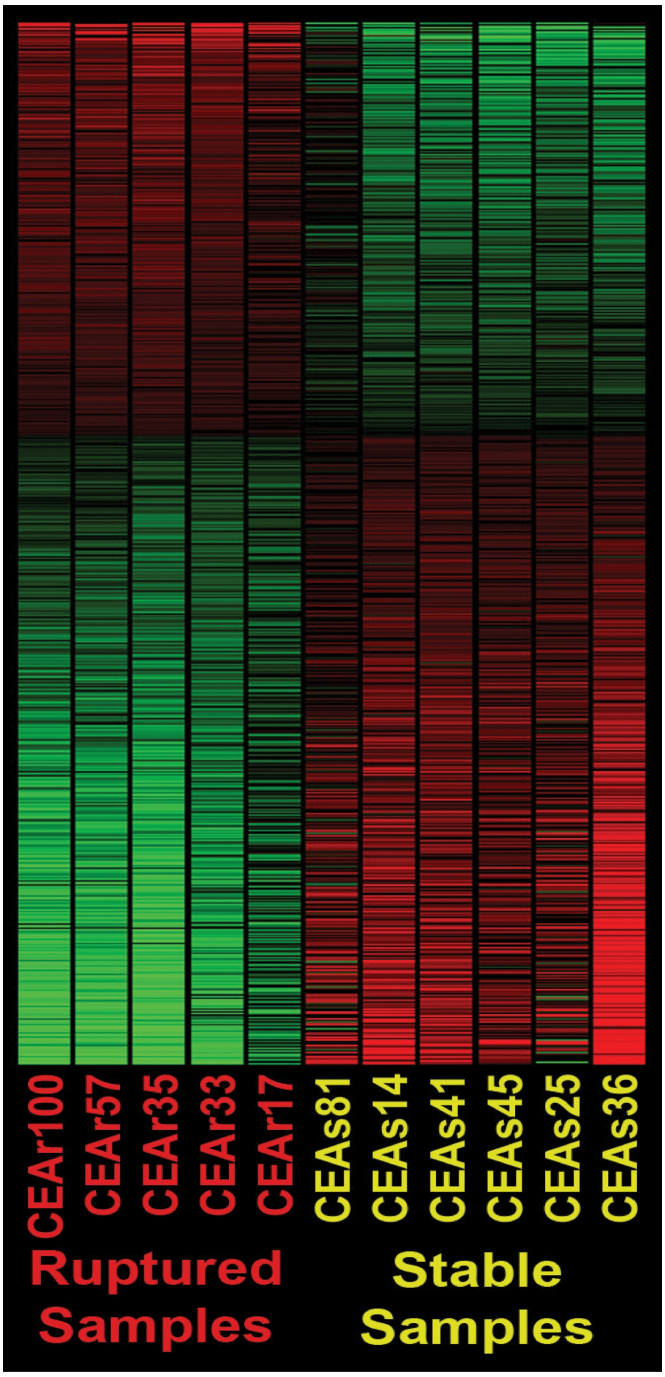

Figure 78. A heatmap of the statistically significant differentially expressed probesets ranked by fold difference which graphically represents the relative expression of the probesets in each sample. Topmost were probesets of highest fold difference in expression in ruptured to stable samples and the bottom vice-versa. Red represents over-expression, green represents under-expression referenced to the ruptured samples.

Affymetrix Probeset ID	False Discovery Rate (%)	Fold Change	Gene Symbol	Gene Name	Gene description	Gene type	Entrez Gene ID	KEGG Pathways	Gene Ontology Biological Processes
203980_at	0.0717	28.11	FABP4	Fatty acid binding protein 4	A cytosolic lipid chaperone in macrophages. Involved in regulating macrophage endoplasmic reticulum (ER) stress.	protein coding	2167	PPAR signalling pathway	cholesterol homeostasis, cytokine production, lipid metabolic process, negative regulation of protein kinase activity, positive regulation of inflammatory response
214146_s_at	0.0749	16.96	PPBP	Pro-platelet basic protein (chemokine (C-X-C motif) ligand 7)	This growth factor is a potent chemo-attractant and activator of neutrophils. It stimulates various cellular processes including DNA synthesis, mitosis, glycolysis, intracellular cAMP accumulation, prostaglandin E2 secretion, and synthesis of hyaluronic acid and sulfated glycosaminoglycan	protein coding	5473	Chemokine signalling pathway, Cytokine-cytokine receptor interaction	chemotaxis, defence response, immune response, platelet activation and degranulation
223565_at	0.0826	12.79	PACAP	proapoptotic caspase adaptor protein	PACAP interacts with caspases inducing apoptosis.	protein coding	51237	-	apoptosis, positive regulation of immunoglobulin biosynthetic process
221286_s_at	0.0871	12.3	PACAP	proapoptotic caspase adaptor protein	PACAP interacts with caspases inducing apoptosis.	protein coding	51237	-	apoptosis, positive regulation of immunoglobulin biosynthetic process
204006_s_at	0.0692	7.552	FCGR3A, FCGR3B	Fc fragment of IgG, low affinity IIIa, receptor (CD16a), Fc fragment of IgG, low affinity	FCGR3-related sequence is a determinant of macrophage overactivity in rats. Low copy numbers of FCGR3B in humans was associated with glomerulonephritis in the autoimmune disorder systemic lupus erythematosus.	protein coding	2214/ 2215	NK mediated cytotoxicity, osteoclast differentiation, phagosome, SLE, Fc□R-	immune response

Affymetrix Probeset ID	False Discovery Rate (%)	Fold Change	Gene Symbol	Gene Name	Gene description	Gene type	Entrez Gene ID	KEGG Pathways	Gene Ontology Biological Processes
205692_s_at	0.0463	6.876	CD38	CD38 antigen (p45)	CD38 is a novel multifunctional ectoenzyme widely expressed in cells and tissues especially in leukocytes. CD38 also functions in cell adhesion, signal transduction and calcium signalling.	protein coding	952	calcium signalling pathway, haematopoetic cell lineage, nicotinate and nicotinamide metabolism	B cell receptor signalling pathway, induction of apoptosis, signal transduction, response to IL-1
207092_at	0.0711	6.608	LEP	leptin	This gene encodes a protein which plays a major role in the regulation of body weight. This protein, which acts through the leptin receptor, can inhibit food intake and regulate energy expenditure to maintain constancy of the adipose mass. It also has several endocrine functions, is involved in the regulation of immune and inflammatory responses, hematopoiesis, angiogenesis and wound healing. Mutations in this gene and/or its regulatory regions cause severe obesity with hypogonadism and atherosclerosis. This gene has been linked to type 2 diabetes mellitus development.	protein coding	3952	Adipocytokine signalling pathway, cytokine-cytokine receptor interaction, Jak-STAT signalling pathway	cholesterol and lipid metabolic process, signal transduction
211644_x_at	0.0927	6.211	IGKC, LOC642113, LOC647478, LOC651505, LOC651961, IGK@, IGKC, IGKV3-20, IGKV3D-11, IGKV3D-15	Immunoglobulin kappa variable 1-5	Encodes for variations of immunoglobulin kappa	protein coding	3514, 642113, 647478, 651505, 651961	-	immune response
203665_at	0.0812	6.022	HMOX1	heme oxygenase (decycling) 1	Heme oxygenase, an essential enzyme in heme catabolism, cleaves heme to form biliverdin, which is subsequently converted to bilirubin by biliverdin reductase, and	protein coding	3162	Heme degradation, porphyrin metabolism	heme oxidation, angiogenesis, negative regulation of smooth muscle cell proliferation,

Affymetrix Probeset ID	False Discovery Rate (%)	Fold Change	Gene Symbol	Gene Name	Gene description	Gene type	Entrez Gene ID	KEGG Pathways	Gene Ontology Biological Processes
					carbon monoxide, a putative neurotransmitter. Heme oxygenase activity is induced by its substrate heme and by various non-heme substances. Heme oxygenase occurs as 2 isozymes, an inducible heme oxygenase-1 and a constitutive heme oxygenase-2.				
216207_x_at	0.0864	5.972	IGKV1D-13, LOC649876, IGKC, IGKV1-5, LOC100130100, LOC647506, LOC650405, LOC652493, LOC652694	Immunoglobulin kappa variable 1D-13	Encodes for variations of immunoglobulin kappa	protein coding	28902, 649876, 100130100, 28299, 3514, 647506, 650405, 652493, 652694	-	immune response
223952_x_at	0.0694	5.907	DHRS9	dehydrogenase/reductase (SDR family) member 9	This gene transcript and protein expression is upregulated by retinoic acid in human tracheobronchial epithelial cells, resulting in enchanced retinol metabolism.	protein coding	10170	Metabolic pathways, retinol metabolism	oxidation-reduction process
224009_x_at	0.072	5.448	DHRS9	dehydrogenase/reductase (SDR family) member 9	This gene transcript and protein expression is upregulated by retinoic acid in human tracheobronchial epithelial cells, resulting in enchanced retinol metabolism.	protein coding	10170	Metabolic pathways, retinol metabolism	oxidation-reduction process
211798_x_at	0.0874	5.416	IGLJ3	immunoglobulin lambda joining 3	This gene encodes for the immunoglobulin lambda light chains, the antigen recognition molecules of B cells	protein coding	28831	-	immune response
217078_s_at	0.0943	5.257	CD300A	CD300A antigen	A membrane bound antigen present on monocytes, dendritic cells, neutrophils and some T and B lymphocytes. May have a cellular activation function.	protein coding	11314	-	cell adhesion

Table 33. Table summarising the top 15 probesets of highest relative expression in ruptured samples compared to stable samples which mapped to 10 known unique and well characterised genes (highest expression in ruptured plaques from the top of the table).

Affymetrix Probeset ID	False Discovery Rate (%)	Fold Change	Gene Symbol	Gene Name	Gene description	Gene type	Entrez Gene ID	KEGG Pathways	Gene Ontology Biological Processes
226930_at	0.0475	0.0434	FNDC1	Fibronectin type III domain containing 1	This encodes for a protein which functions as an activator of G protein signalling. It was found to be induced in response to rat ventricular ischaemia to promote G protein signalling.	protein coding	84624	-	-
1556329_a_at	0.0905	0.0423	PCDH10	Protocadherin 10	Protocadherins form a subfamily of calcium-dependent cell-cell adhesion molecules in the cadherin superfamily. Protocadherin-10 belongs to a subclass of protocadherins that share a highly conserved 17-amino acid cytoplasmic motif	protein coding	57575	-	cell adhesion
219304_s_at	0.0981	0.0403	PDGFD	platelet derived growth factor D	Members of the PDGF family, such as PDGFD, are disulfide-bonded dimeric proteins involved in developmental and physiologic processes, as well as in cancer, fibrotic diseases, and arteriosclerosis. It induces macrophage recruitment, increased interstitital pressure and increased pericyte/smooth muscle cell proliferation and inhibition of vascular leakiness.	protein coding	80310	Focal adhesion, Gap junction, regulation of actin cytoskeleton	positive regulation of cell division, regulation of peptydyl-tyrosine phosphorylation
228268_at	0.0618	0.0371	FMO2	Flavin containing monooxygenase 2	The flavin-containing monooxygenases are NADPH-dependent flavoenzymes that catalyze the oxidation of heteroatom centers in numerous drugs and xenobiotics.	protein coding	2327	Drug metabolism - cytochrome p450	NADP metabolic process, oxygen and reactive oxygen species metabolic process
226237_at	0.0692	0.0366	COL8A1	Collagen, type VIII, alpha 1	This gene encodes one of the two alpha chains of type VIII collagen.	protein coding	1295	-	angiogenesis, cell adhesion
226769_at	0.0475	0.036	LOC387758; FIBIN	fin bud initiation factor homolog (zebrafish)	This gene encodes for a hypothetical protein which is not yet well characterised in humans. It has been shown to be involved in pectoral fin bud initiation in zebrafish.	protein coding	387758	-	-

Affymetrix Probeset ID	False Discovery Rate (%)	Fold Change	Gene Symbol	Gene Name	Gene description	Gene type	Entrez Gene ID	KEGG Pathways	Gene Ontology Biological Processes
234103_at	0.0475	0.0322	KCNT2	Potassium channel, subfamily T, member 2	Encodes for a transmembrane potassium channel protein	protein coding	343450	-	ion transport
206101_at	0.0531	0.0321	ECM2	extracellular matrix protein 2, female organ and adipocyte specific	Encoded for extracellular matrix protein 2, sharing extensive similarity with known ECM proteins.	protein coding	1842	-	extracellular matrix
209071_s_at	0.0907	0.0306	RGS5	regulator of G-protein signalling 5	This gene encodes a member of the regulators of G protein signalling (RGS) family. The RGS proteins are signal transduction molecules which are involved in the regulation of heterotrimeric G proteins by acting as GTPase activators. This gene is a hypoxia-inducible factor-1 dependent, hypoxia-induced gene which is involved in the induction of endothelial apoptosis. This gene is also one of three genes on chromosome 1q contributing to elevated blood pressure. Alternatively spliced transcript variants encoding different isoforms have been identified.	protein coding	8490	-	regulation of G-protein coupled receptor protein signalling pathway
1557080_s_at	0.0475	0.0291	ITGBL1	Integrin, beta-like 1 (with EGF-like repeat domains)	This encodes a 494-amino acid protein with beta-integrin EGF-like repeat domains, and widely expressed in many tissues but readily detectable in aorta only.	protein coding	9358	-	cell adhesion, cell-matrix adhesion, integrin-mediated signalling pathway
208096_s_at	0.0475	0.027	COL21A1	collagen, type XXI, alpha 1	COL21A1 belongs to the family of fibril-associated collagens with an interrupted triple helix (FACIT collagens). FACIT collagens bind to the surface of collagen fibrils and link them with other matrix molecules. It is localised to tissues containing type 1 collagen and may serve to maintain the integrity of the ECM.	protein coding	81578	-	cell adhesion

Affymetrix Probeset ID	False Discovery Rate (%)	Fold Change	Gene Symbol	Gene Name	Gene description	Gene type	Entrez Gene ID	KEGG Pathways	Gene Ontology Biological Processes
214927_at	0.0475	0.0269	ITGBL1	Integrin, beta-like 1 (with EGF-like repeat domains)	This encodes a 494-amino acid protein with beta-integrin EGF-like repeat domains, and widely expressed in many tissues but readily detectable in aorta only.	protein coding	9358	-	cell adhesion, cell-matrix adhesion, integrin-mediated signalling pathway
222722_at	0.0971	0.0228	OGN	Osteoglycin (osteoinductive factor, mimecan)	This gene encodes a protein which induces ectopic bone formation in conjunction with transforming growth factor beta. This protein is a small proteoglycan which contains tandem leucine-rich repeats (LRR).	protein coding	4969	-	-
223122_s_at	0.0765	0.0185	SFRP2	secreted frizzled-related protein 2	Members of the 'frizzled' (FZ) transmembrane protein family are receptors for Wnt family members, cysteine-rich glycosylated ligands implicated in a variety of cellular processes, including control of cell polarity and malignant transformation. The secreted frizzled-related proteins (SFRPs) appear to act as soluble modulators of Wnt signalling by competing with membrane-bound frizzled receptors for the binding of secreted Wnt ligands.	protein coding	6423	Wnt signalling pathway	Wnt receptor signalling, cell death, cell differentiation, cell-cell signalling, collagen fibril organisation, negative regulation of apoptosis
219087_at	0.0475	0.0108	ASPN	asporin (LRR class 1)	This gene encodes an extracellular matrix protein that is a member of the small leucine-rich proteoglycan family, binds collagen and calcium and may induce collagen mineralisation. High expression in cartilage, aorta, uterus and heart.	protein coding	54829	-	bone mineralisation, negative regulation of TGF beta receptor signalling pathway, extracellular matrix

Table 34. Table summarising the top 15 probesets of highest relative expression in stable samples compared to ruptured samples which mapped to 13 known unique genes and 1 gene encoding for a hypothetical protein (highest expression in stable plaques from the bottom of the table).

5.4.8 Functional bioinformatic analysis

We examined the list of 1,187 statistically significant probesets which represented 914 unique genes which were differentially expressed, for dominant and significant biological process themes and biological pathways. The representation of these biological themes and pathways in the genelist were statistically analysed and then ranked for further examination.

Gene Ontology biological process analysis

We used the Biological Networks Gene Ontology tool (BiNGO)[274] in Cytoscape[285] to map the 914 unique genes to Genome Ontology (GO) database using Locuslink identifiers, of which 509 unique genes had GO annotations for analysis. The results are listed in Table 35. The GO biological process groups have overlapping genes amongst the categories and some categories which were identified belong to parent groups. As a result the sum of the percentage of genes in each group do not add up with all the groups. I have organised the GO biological process categories in organic layout to aid the visualisation of the relationships between the groups in Figure 79. We have found that genes involved in cell signalling (with sub-categories- cell communication, 206 genes, $p=3.4x10^{-9}$ and signal transduction, 156 genes, $p=3.6x10^{-5}$), cell adhesion (with 61 genes, $p=8.1x10^{-11}$), protein phosphorylation (with sub-categories of phosphorus/phosphate metabolism, 63 genes, $p=3.01x10^{-5}$, protein amino acid phosphorylation, 45 genes, $p=5.28x10^{-4}$, and phosphorylation, 51 genes, $p=5.28x10^{-4}$) and actin cytoskeleton and cell motility processes (with sub-category of cell organisation and biogenesis, 91 genes, $p=5.36x10^{-3}$) were very significantly represented in our genelist, even after multiple test correction set at an FDR of 10%. A large proportion of the genes represented from our genelist were significantly identified in these biological processes. This suggests that the biological activity of these processes in the macrophages may be important in determining the stability or instability of the plaque.

Further differentiation of these processes which were active in the stable or ruptured plaque were made. Of the 470 probesets which were upregulated in the ruptured plaque, we observed that the active biological processes involved were: cell communication (35% of the probesets, of which the majority consists of signal transduction 31%), protein or cellular localisation/transport (30%), cellular response to stimulus (23%, which consists of defense response 15%, immune response 14%, stress response 13%), phosphate and phosphorous metabolism (11%) and lipid metabolism (10%). In the stable plaque, of the 717 probesets which were upregulated, we found that biological processes which were active were: cell communication (40%, in particular signal transduction 27% and cell

adhesion 16%) and cell development (24% of the probesets, consisting of collagen, vessel development, bone remodelling and ossification genes). We can therefore demonstrate that there are different programmes of biological activity in the stable and ruptured plaque macrophages.

GO-ID	p-value	p-value (with MTC)	Genes in Category	% of genes in List	Total genes in Category	Description
7154	3.36E-09	1.71E-06	206	40.50%	3346	cell communication
7165	3.59E-05	5.22E-03	156	30.60%	2695	signal transduction
16043	4.21E-05	5.36E-03	91	17.90%	1395	cell organization and biogenesis
6793	1.18E-07	3.01E-05	63	12.40%	730	phosphorus metabolism
6796	1.18E-07	3.01E-05	63	12.40%	730	phosphate metabolism
7242	4.55E-04	3.86E-02	63	12.40%	948	intracellular signalling cascade
7155	8.10E-11	8.25E-08	61	12.00%	577	cell adhesion
16310	3.11E-06	5.28E-04	51	10.00%	599	phosphorylation
6468	3.03E-06	5.28E-04	45	8.80%	501	protein amino acid phosphorylation
8104	4.43E-04	3.86E-02	44	8.60%	598	protein localization
15031	2.71E-04	3.07E-02	43	8.40%	567	protein transport
45184	5.25E-04	4.11E-02	43	8.40%	585	establishment of protein localization
46907	1.86E-03	8.05E-02	42	8.30%	605	intracellular transport
51649	2.10E-03	8.56E-02	42	8.30%	609	establishment of cellular localization
51641	2.44E-03	9.57E-02	42	8.30%	614	cellular localization
6886	9.04E-04	5.76E-02	31	6.10%	390	intracellular protein transport
9966	1.13E-03	6.37E-02	18	3.50%	184	regulation of signal transduction
7167	9.86E-04	5.91E-02	17	3.30%	167	enzyme linked receptor protein signalling pathway
30029	4.55E-04	3.86E-02	16	3.10%	142	actin filament-based process
30036	1.70E-03	8.05E-02	14	2.80%	131	actin cytoskeleton organization & biogenesis
16055	5.65E-04	4.11E-02	12	2.40%	91	Wnt receptor signalling pathway
31589	1.37E-03	6.97E-02	9	1.80%	62	cell-substrate adhesion
7160	1.37E-03	6.97E-02	9	1.80%	62	cell-matrix adhesion

Table 35. The biological processes of the differentially expressed genes identified.

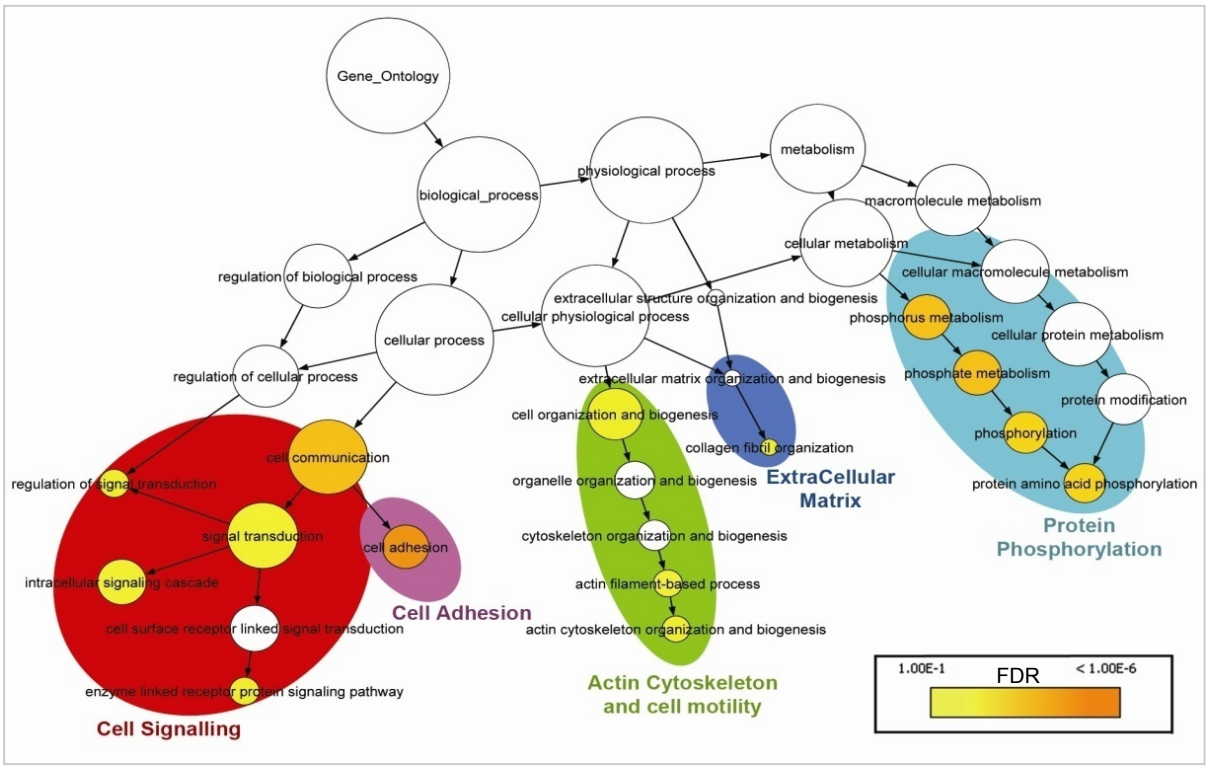

Figure 79. Gene Ontology Analysis of the differentially expressed statistically significant genelist from microarray analysis. Significantly over-represented biological processes, demonstrated in an organic layout, were coloured from yellow to orange by its degree of significance of representation. The parent GO terms were also shown to clarify functional relationships (in white). Background coloured ovals were added to highlight the significant themes.

Biological pathways are not as well described in the Genome Ontology database as they are in the KEGG database. Nevertheless, 2 pathways were identified; the Wnt receptor signalling pathway and the enzyme linked receptor protein signalling pathway, which were both upregulated in the stable plaque.

Pathway Analysis using KEGG

Pathway analysis was performed on the set of statistically significant differentially expressed genes using WebGestalt[4], a web-based gene set analysis toolkit, to identify significantly over-represented pathways in the Kyoto Encyclopaedia of Genes and Genomes database (KEGG, a resource of well annotated and characterised biological pathways) which may be of potential causative importance in plaque rupture.

Thirteen KEGG pathways were significantly differentially expressed at $p<0.0025$ (Table 36). After adjustments for multiple testing error (Bonferroni), the 13 pathways were still significant with an adjusted p-value of <0.05. Eight of these pathways were chiefly up-regulated in stable samples, Four had a balanced configuration, and one, the

PPAR/Adipocytokine signalling pathway, was chiefly up-regulated in ruptured when compared to stable samples ($p=5.4x10^{-7}$).

The PPAR/Adipocytokine pathway was the fourth most significantly differentially expressed KEGG pathway, after Focal Adhesion ($p=1.3x10^{-10}$), Adherens Junction ($p=1.4x10^{-10}$), and Actin Cytoskeleton ($p=2.6x10^{-9}$) pathways, which were more highly expressed in stable samples. The PPAR/Adipocytokine pathway was also the only significant cell signalling (signal transduction) pathway upregulated in ruptured plaques. The TGF-beta ($p=3.60x10^{-4}$) and Wnt signalling pathways ($p=1.59x10^{-3}$)were the only significant cell signalling pathways upregulated in stable plaques. The other 2 cell signalling pathways were of balanced configuration between stable and unstable plaques (Insulin signalling and T-cell receptor signalling).

Upregulated signalling pathway in ruptured plaques: the PPAR/Adipocytokine Signalling Pathway

The PPAR/Adipocytokine Signalling Pathway, which incorporates FABP4 and Leptin, was the most strongly up-regulated KEGG pathway in ruptured samples ($p=5.5x10^{-7}$). Fifteen genes were identified to be significantly differentially expressed between stable and unstable plaques, of which eleven genes were up-regulated in the ruptured plaque. The PPAR/Adipocytokine Signalling Pathway with the 15 significantly identified genes highlighted in red is shown in Figure 80 and Figure 81. The details of the 15 genes with the reported false discovery rate and fold change from the microarray data of 11 samples is shown in Table 37. FABP4 and Leptin are key genes in the PPAR/adipocytokine signalling pathway; these genes were individually amongst the most differentially expressed statistically significant genes in the ruptured plaques compared to the stable plaques (FABP4: 28.1fold over-expressed; Leptin: 6.6 fold over-expressed; Table 37). These results suggest that the PPAR/Adipocytokine signalling pathway is the most significantly up-regulated gene network in the process of plaque rupture and may potentially play a causative role.

Upregulated signalling pathway in stable plaques: TGF-beta signalling pathway and Wnt signalling pathway

The TGF-beta signalling pathway (9 genes, $p=3.60x10^{-4}$, Figure 83) and the Wnt signalling pathway (11 genes, $p=1.56x10^{-3}$, Figure 82) were the only 2 signal transduction pathways which were upregulated in the stable plaques. Eight out of the nine genes in our genelist were upregulated in the stable plaque in the TGF-beta signalling pathway and all nine genes are highlighted in Figure 83. All the eleven genes in our genelist were upregulated in stable plaque macrophages in the Wnt signalling pathway and are highlighted in Figure 82. This pathway was also identified independently using the GO

biological process terms to be significant. Moreover, the SFRP2 gene, which encodes for one of the component proteins in the Wnt signalling pathway was also independently identified as one of the top ranking genes of high expression in the stable group. These findings show that the TGF-beta and the Wnt signalling pathways are both upregulated in the stable plaque and may have a causal role in plaque stabilisation.

KEGG Parent Node	KEGG Pathway	Observed no. of genes in genelist	Total no. of genes in pathway	P-value	Group with majority genes up-regulated (no. of genes)
Cell Communication	Focal adhesion	25	203	1.30×10^{-10}	Stable(22)
Cell Communication	Adherens junction	16	78	1.41×10^{-10}	Stable(13)
Cell Motility	Regulation of actin cytoskeleton	24	217	2.62×10^{-9}	Stable(16)
Signal Transduction	PPAR/Adipocytokine signalling Pathway	15	121	5.45×10^{-7}	Ruptured(11)
Signalling Molecules and Interaction	ECM-receptor interaction	11	85	1.12×10^{-5}	Stable(11)
Cell Communication	Tight junction	13	135	4.36×10^{-5}	Stable(10)
Signalling Molecules and Interaction	Cytokine-cytokine receptor interaction	19	263	4.89×10^{-5}	Balanced (11 ruptured)
Signal Transduction	Insulin signalling pathway	12	138	2.11×10^{-4}	Balanced (7 stable)
Signal Transduction	TGF-beta signalling pathway	9	87	3.60×10^{-4}	Stable(8)
Signalling Molecules and Interaction	Cell adhesion molecules	11	133	5.61×10^{-4}	Stable(7)
Signal Transduction	Wnt signalling pathway	11	152	1.56×10^{-3}	Stable(11)
Immune system	NK cell mediated cytotoxicity	10	135	2.09×10^{-3}	Balanced (6 ruptured)
Signal Transduction	T cell receptor signalling pathway	8	94	2.44×10^{-3}	Balanced (4)

Table 36. The list of statistically significant KEGG Pathways identified using WebGestalt.

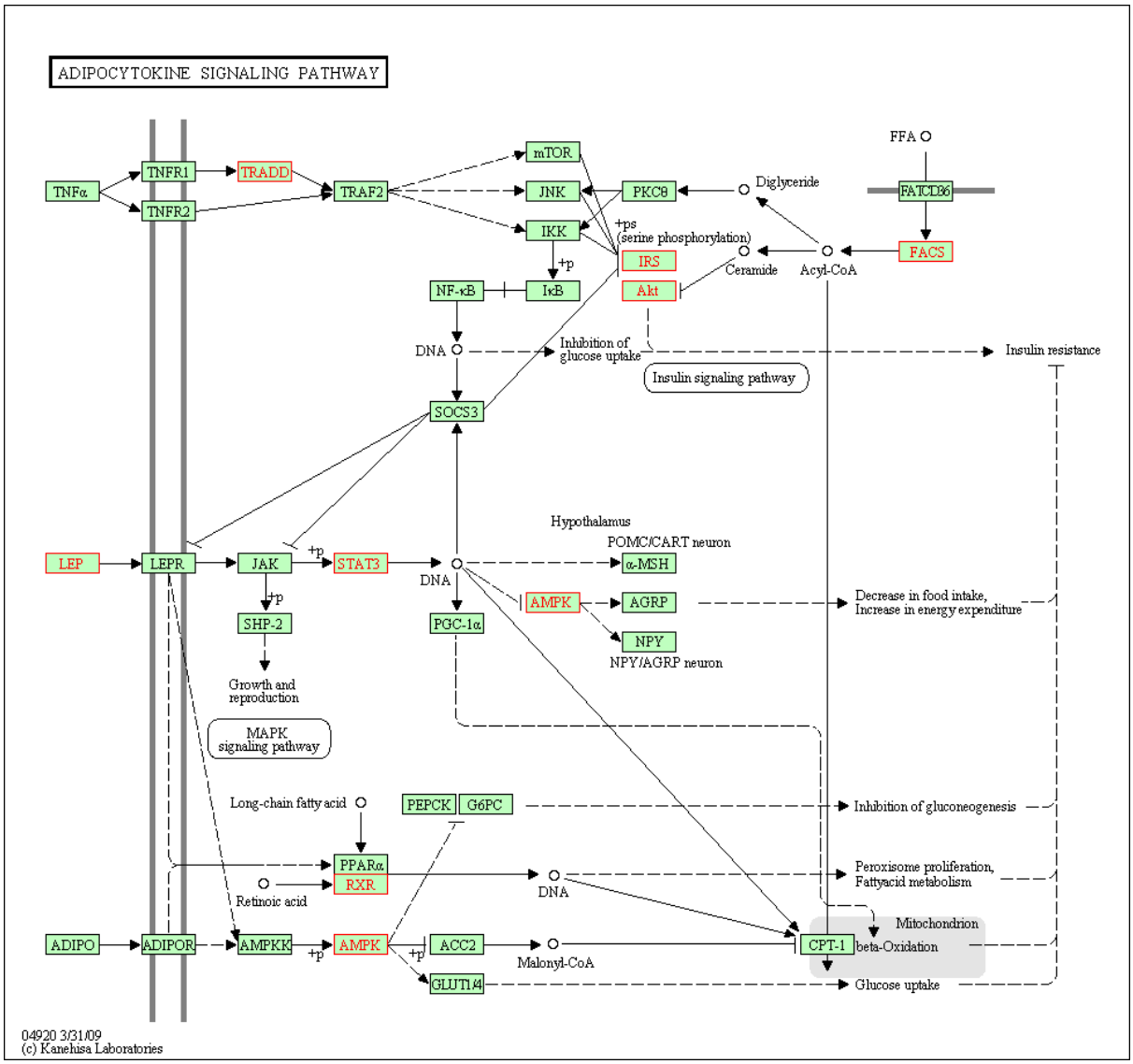

Figure 80. The Adipocytokine component of the PPAR/Adipocytokine Signalling Pathway with the significantly identified differentially expressed genes highlighted in red.

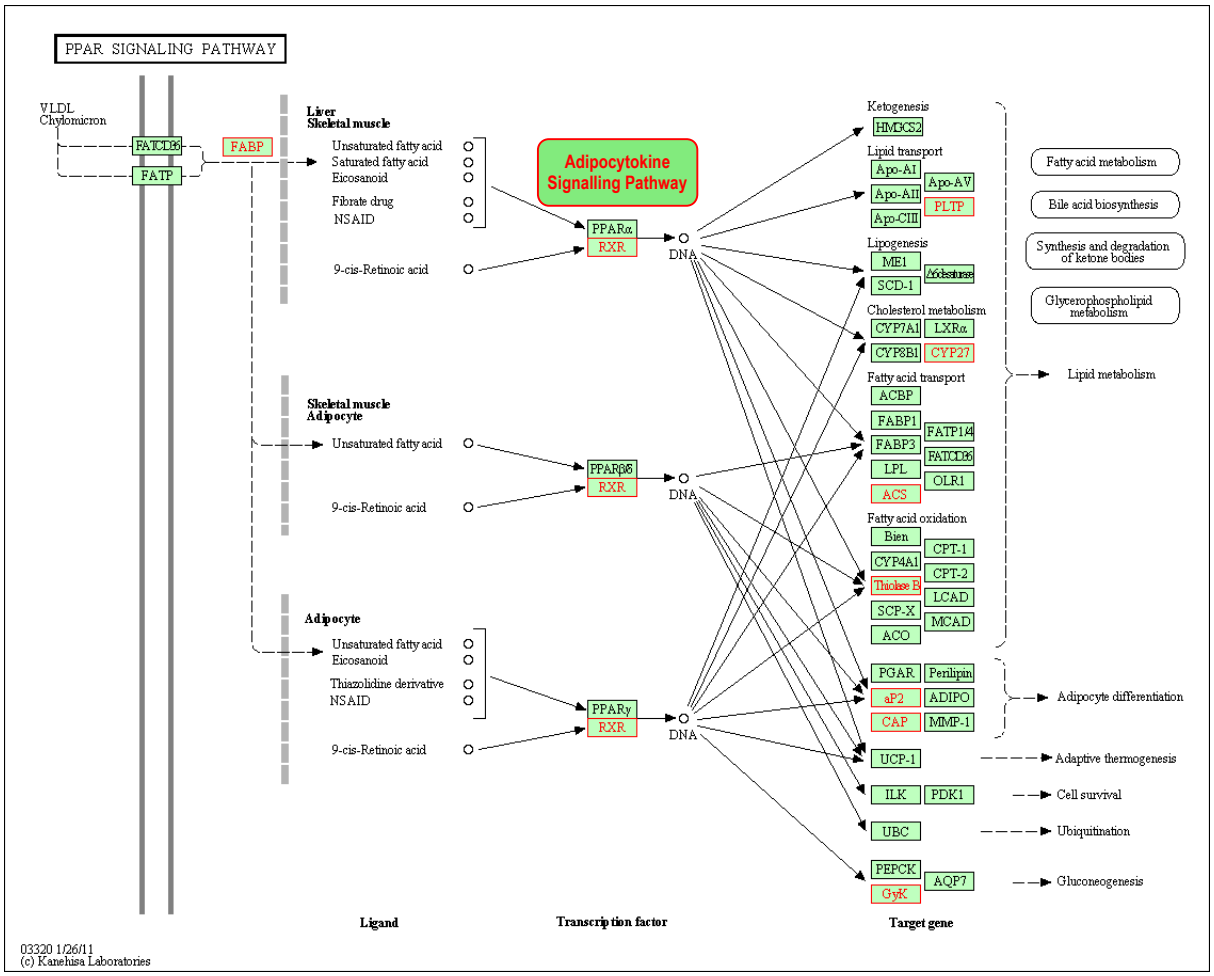

Figure 81. The PPAR component of the PPAR/Adipocytokine Signalling Pathway with the significantly identified differentially expressed genes highlighted in red.

Gene Name	Gene Symbol	Entrez-Gene ID	Regulation	False Discovery Rate	Fold Change
Fatty acid binding protein 4, adipocyte/macrophage	FABP4	2167	Up-regulated	0.072	28.1
Leptin	LEP	3952	Up-regulated	0.071	6.61
Acyl-CoA synthetase long-chain family member 1	ACSL1	2180	Up-regulated	0.067	3.02
Cytochrome P450, family 27, subfamily A, polypeptide 1	CYP27A1	1593	Up-regulated	0.094	2.96
Phospholipid transfer protein	PLTP	5360	Up-regulated	0.093	2.93
Glycerol kinase	GK	2710	Up-regulated	0.084	2.16
Retinoid X receptor, alpha	RXRA	6256	Up-regulated	0.060	2.14
Signal transducer and activator of transcription 3 (acute-phase response factor)	STAT3	6774	Up-regulated	0.077	2.10
Acyl-CoA synthetase long-chain family member 5	ACSL5	51703	Up-regulated	0.069	1.80
TNFRSF1A-associated via death domain	TRADD	8717	Up-regulated	0.089	1.55
Acetyl-Coenzyme A acyltransferase 1	ACAA1	30	Up-regulated	0.062	1.44
Protein kinase, AMP-activated, alpha 1 catalytic subunit	PRKAA1	5562	Down-regulated	0.056	1/1.63
V-AKT murine thymoma viral oncogene homolog 3 (protein kinase B, gamma)	AKT3	10000	Down-regulated	0.067	1/2.70
Insulin receptor substrate 1	IRS1	3667	Down-regulated	0.072	1/5.49
Sorbin and SH3 domain containing 1	SORBS1	10580	Down-regulated	0.075	1/10.9

Table 37. Differentially regulated genes in the PPAR/Adipocytokine Signalling Pathway (FDR<10%).

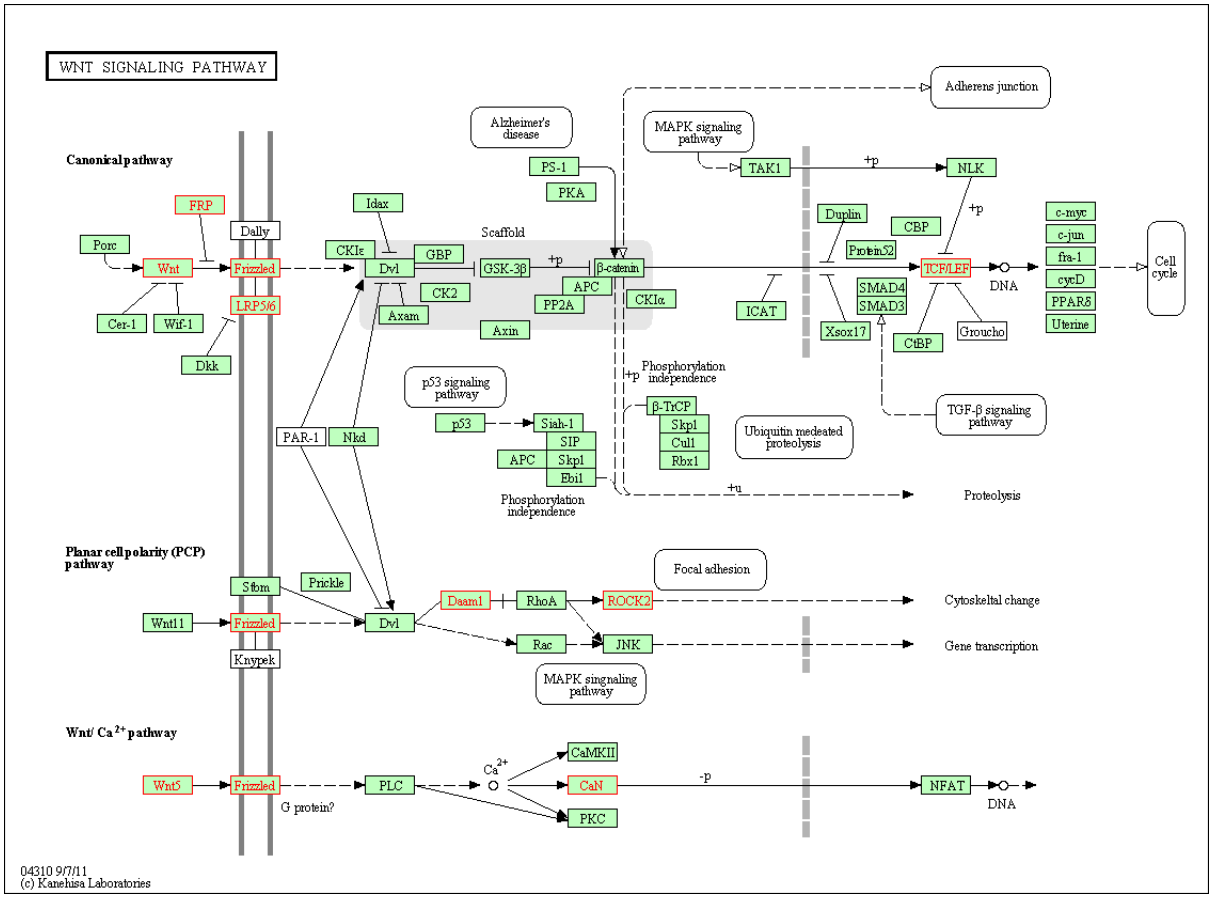

Figure 82. The Wnt signalling pathway with the significantly identified differentially expressed genes highlighted in red (and were all upregulated in the stable plaque)

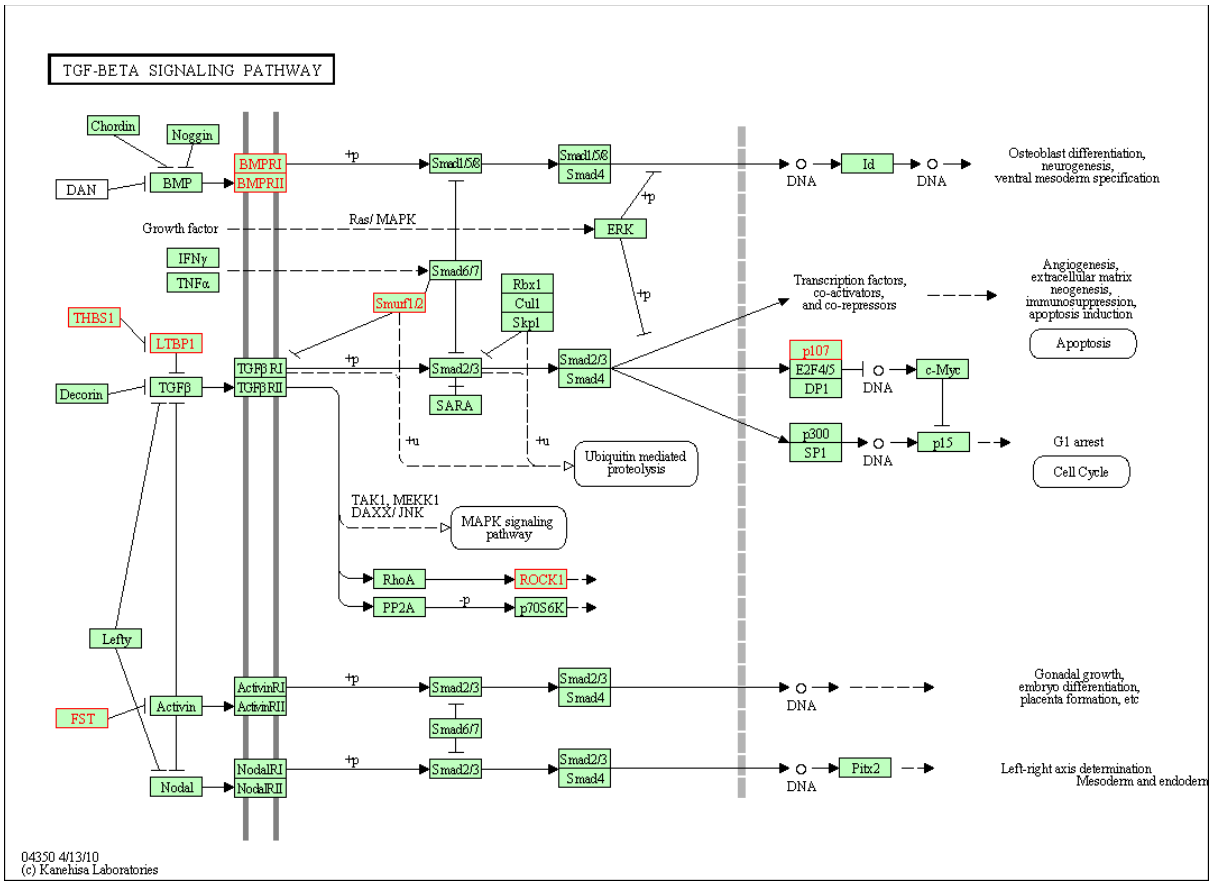

Figure 83. The TGF-beta signalling pathway with the significantly identified differentially expressed genes highlighted in red (and were mostly upregulated in the stable plaque)

5.5 Gene expression validation work

As the microarray findings were the result of RNA amplification, hybridisation and microarray data processing, the appropriate validation was necessary to confirm the microarray results. This was performed using qRT-PCR. Standard qRTPCR reactions often use starting amounts of >2ng of total-RNA. As we were using RNA from LMD our starting amounts were in the sub-nanogram range, some evaluation and optimisation of RT and qRT-PCR was necessary.

5.5.1 Preliminary evaluation and optimisation of RT and qRT-PCR work

Evaluation of different Reverse Transcriptases and priming

We evaluated reverse transcription using oligo-dT (dT) or random hexamer (rH) priming and assessed 4 different RT enzymes to generate the maximal amount of high quality starting cDNA for qRTPCR. The priming of the RT reaction using rH consistently generated a higher yield of cDNA template compared to dT priming and is demonstrated in the qRTPCR amplification plots in Figure 84 showing rH-primed RT generating higher yields (left shift in amplification curve, lower Ct). Random hexamer priming also eliminates the 3' bias of the generated cDNA associated with oligo-dT priming and is more representative of the actual mRNA abundance. Of the 4 RTs compared, SuperScript III and cDNA archive kit generated larger amounts of cDNA compared to Sensiscript, and ImProm2 had a large number of failed reactions particularly with the lower expression transcript MYST2 (Figure 85). Superscript III was also the most sensitive RT to detect small amounts of cDNA and also was the most consistent in reporting the delta CTs between the 100pg and 10pg cDNA templates.

We demonstrated significant variation in the efficiency of reverse transcription using different RT enzymes and priming. The SuperScript III RT kit from Invitrogen using random hexamer primers, generated the highest yield of cDNA template with the most consistent, reproducible and accurate qRTPCR results and was used in our experiments.

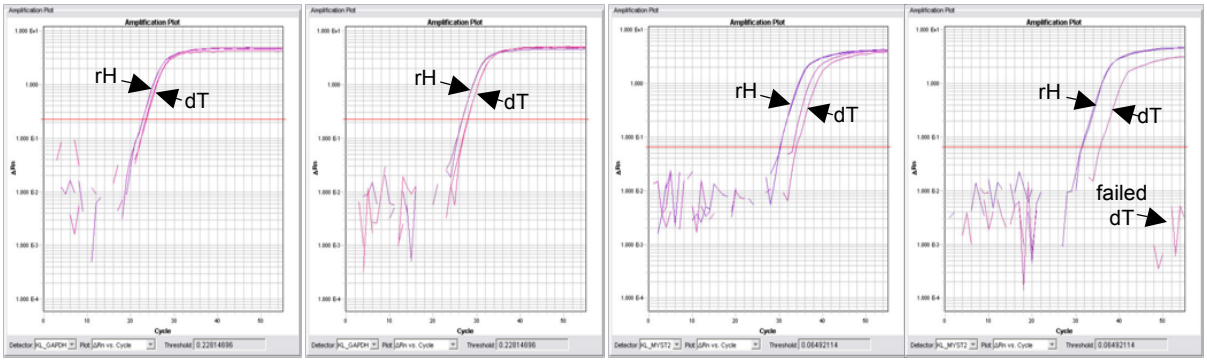

GAPDH_rH, HeLa_100pg GAPDH_rH, CEA_100pg MYST2_rH, HeLa_100pg MYST2_rH, CEA_100pg

Figure 84. qRTPCR amplification plots comparing random hexamer and oligo-dT primed RT using Superscript III.

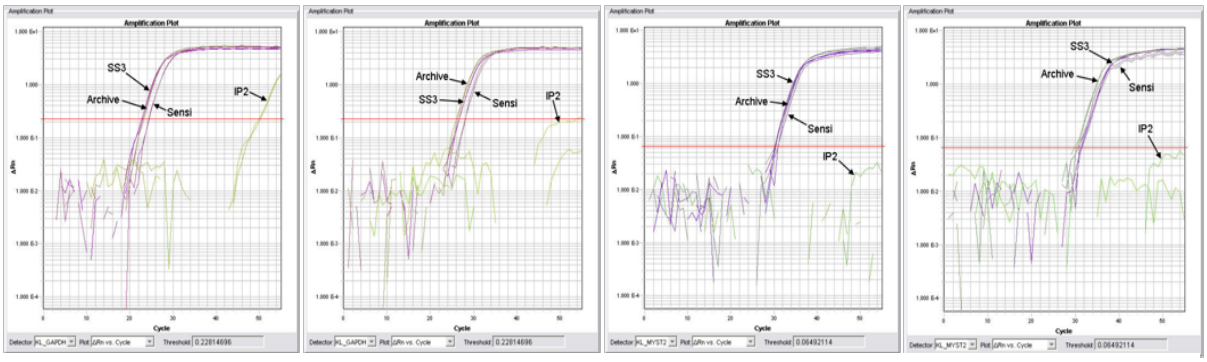

GAPDH_rH, HeLa_100pg GAPDH_rH, CEA_100pg MYST2_rH, HeLa_100pg MYST2_rH, CEA_100pg

Figure 85. qRTPCR amplification plots comparing yields from the 4 reverse transcriptases: SS3; SuperScript III, Archive; cDNA archive, Sensi; Sensiscript, IP2; ImProm-2.

Evaluation of different qRTPCR methods

The comparison matrix of the 3 qRTPCR chemistries; the Invitrogen Platinum qPCR, the Applied Biosystems Taqman PCR and Qiagen SYBR-green Quantitect PCR, is shown in Figure 86. The Taqman-PCR with Taqman-PrimerProbe chemistry was the best performing qRTPCR chemistry. It was the most precise and reproducible with the least variation in replicates and the highest R^2 correlation of 0.988 and 0.975, compared to the Invitrogen-qPCR with Taqman-PrimerProbe chemistry (R^2 of 0.945 and 0.964) and the Qiagen-SYBRgreen-PCR with Globegene-Primers chemistry (R^2 of 0.917 and 0.861). It was the most sensitive and was able to quantify the low expression MYST2 transcript down to 10pg of template total-RNA. It was subsequently used in our experiments.

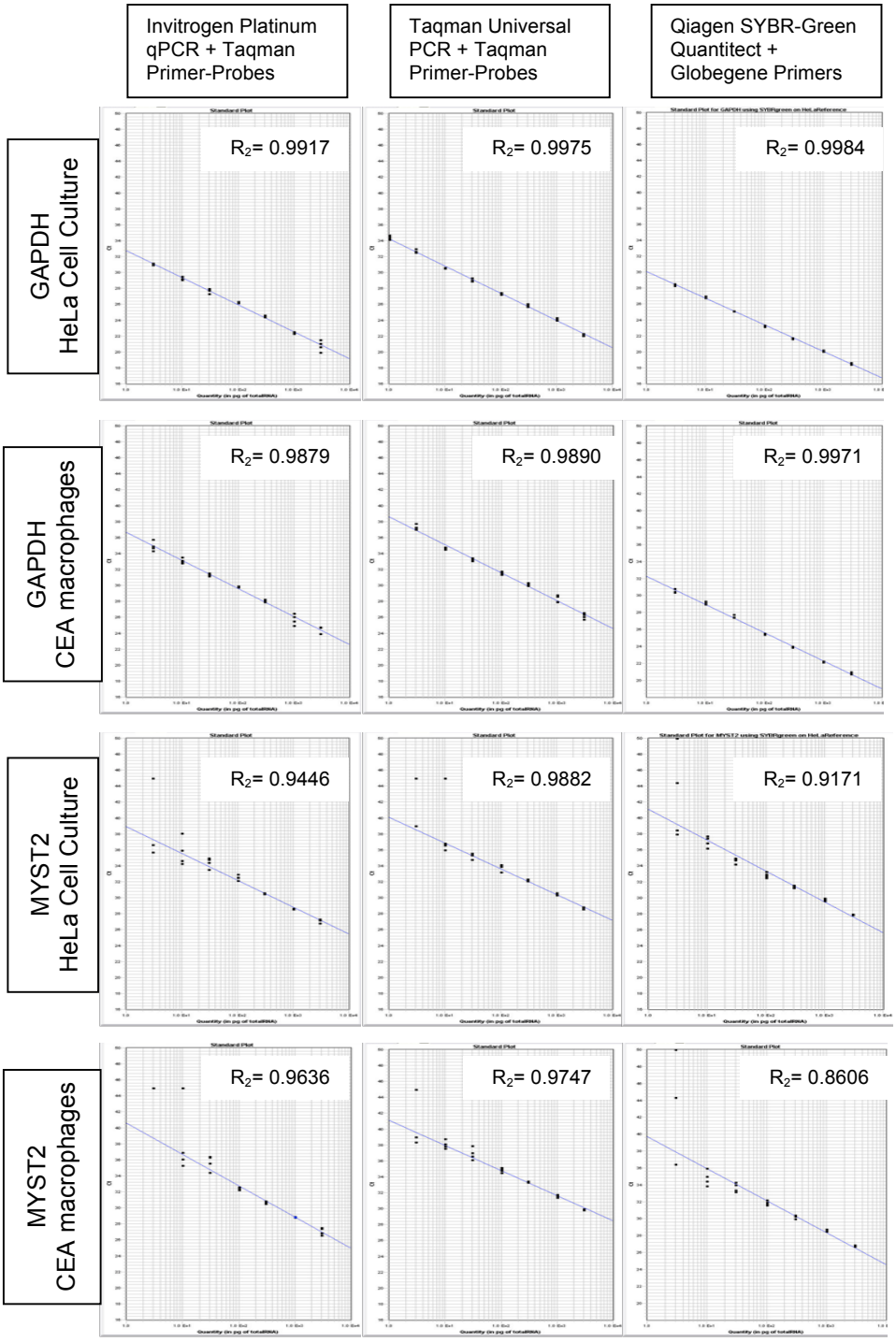

Figure 86. Comparison matrix of the 3 different qRTPCR chemistries using standard curve dilution series of cDNA from total-RNA from HeLa cell cultures and LMDed CEA macrophages. The abundance of high expression GAPDH and low expression MYST2 transcripts were quantified in quadruplicate.

Evaluation of the use of carrier RNA

I assessed if carrier RNA may be advantageous in the successful quantitation of low transcript abundances from small amounts of starting material by reducing the non-specific binding of nucleic acids to the plastics used in the preparation and reactions. I found a reduction in the variability of replicates especially at low template concentrations with an increased R^2 correlation to the regression line with the use of carrier RNA and the calculated PCR efficiencies were also improved as a result of improved precision and accuracy at low template concentrations, in 4 of the 5 genes tested (Figure 87 and Table 38). More importantly there was no significant inhibition of qRTPCR. As a result, carrier RNA (at 1ng/µl) was used in our subsequent experiments.

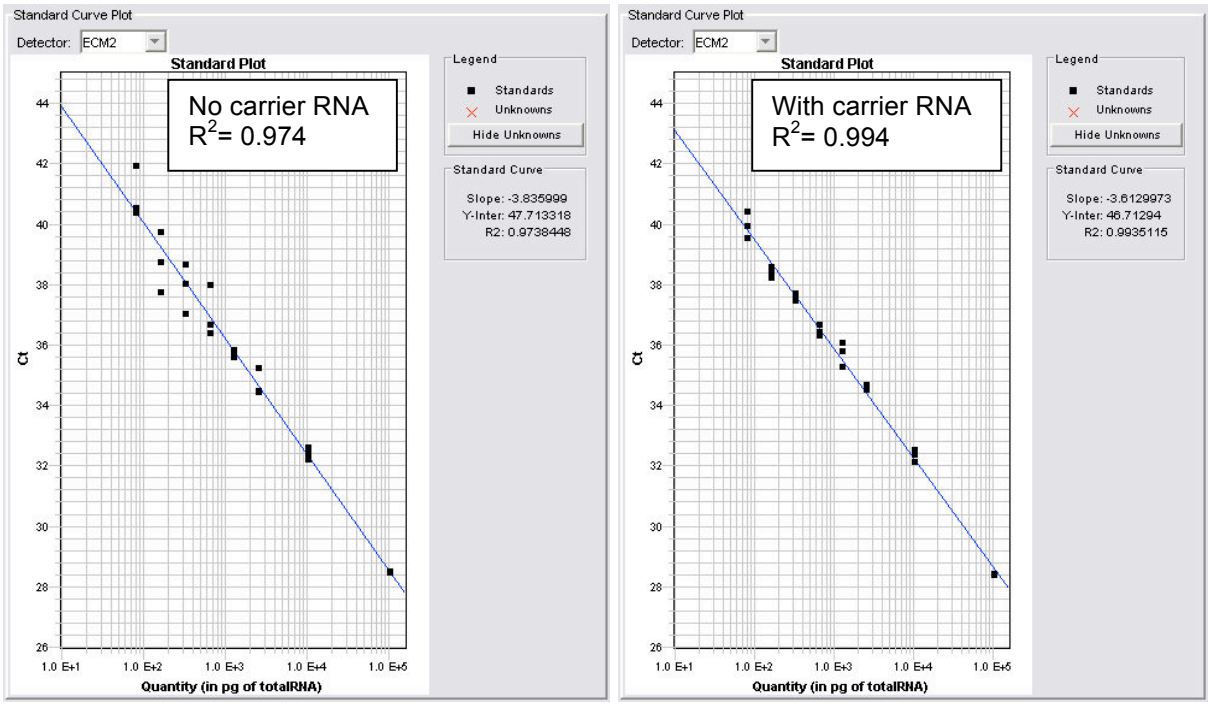

Figure 87. An example of a standard curve of a cDNA dilution series of the ECM2 transcript, demonstrating reduced variability with carrier RNA (right) compared to without (left).

	R^2 correlation		Efficiency of qRTPCR	
Gene	no carrier RNA	with carrier RNA	no carrier RNA	with carrier RNA
LEP	0.96759	0.9746	93.1%	94.5%
ASPN	0.97493	0.98701	94.2%	94.5%
ECM2	0.97384	0.99351	82.4%	88.9%
PDGFD	0.98156	0.98645	88.2%	91.6%
FCGR3AB	0.98752	0.9631	92.0%	89.9%

Table 38. R^2 correlation and calculated efficiency of qRTPCR with and without carrier RNA.

Taqman Primer-Probe PCR amplification efficiency and minimum detection threshold

The qRTPCR efficiencies of all the Taqman primer-probes and their validated minimum detectable thresholds are listed in Table 39. There was high amplification efficiencies of >90% for almost all the Taqman validated primer-probes used except for 2 primer-probesets; GUSB (89%) and TUBB (82%). The accurate quantitation of transcript abundance was possible by applying individual amplification efficiency corrections.

Probe	Purpose	Efficiency	SD of Efficiency	Minimum detection threshold (Ct)
GAPDH	Reference Candidate	96.87%	0.94%	39
MYST2	Reference Candidate	99.99%	3.48%	39
GUSB	Reference Candidate	89.17%	2.62%	39.5
TBP	Reference Candidate	92.05%	2.44%	40
TUBB	Reference Candidate	81.68%	1.84%	40
PPIA	Reference Gene	97.22%	1.23%	39.2
SDHA	Reference Gene	90.04%	1.62%	40.2
FABP4	Target Gene	95.27%	0.96%	39
PPBP	Target Gene	92.77%	3.38%	40.1
PACAP	Target Gene	92.53%	1.96%	40.2
FCGR3AB	Target Gene	90.06%	2.16%	40.2
LEP	Target Gene	92.01%	4.34%	39.2
CD38	Target Gene	99.78%	1.95%	39.6
ECM2	Target Gene	90.18%	2.24%	40
RGS5	Target Gene	93.68%	1.75%	39.4
PDGFD	Target Gene	91.46%	2.82%	40.1
OGN	Target Gene	91.64%	1.85%	39.5
ASPN	Target Gene	91.34%	1.90%	40
SFRP2	Target Gene	91.84%	1.00%	39.5

Table 39. The PCR efficiencies of the Taqman Primer Probes used and their minimum detection thresholds. SD, standard deviation.

Ranging experiments to determine adequate starting amounts of cDNA

A ranging test experiment two microarray samples with ample total RNA isolated was performed to determine the minimum amounts of sample cDNA required per reaction for the successful quantitation of transcript abundance above the minimal detectable limits by qRTPCR (Table 40). I was able to quantify microarray signals of high expression (1000-10000), medium expression (100-1000) and in all except for one of the low expression microarray signals (5-100) using 500pg of starting material. The lowest microarray signals across the other microarray samples were in the 5-10 region which I could quantify at a Ct of 39. The qRTPCR assays were able to detect transcripts of low abundance to a Ct of 39 to 40 but not reliably beyond a Ct of 40. Therefore qRTPCR reactions which failed detection or had a Ct measured beyond 40, had a ceiling Ct of 40 set (the minimum detection threshold). I was able to confirm that the starting amounts equivalent to 500pg of total-RNA was adequate for the quantitation of the target transcripts of interest and that there was sufficient remaining unamplified total RNA for the qRTPCR experiments.

	CEA35		CEA81	
	Unnormalised MA signal	500pg qRTPCR Ct	Unnormalised MA signal	500pg qRTPCR Ct
SDHA	665	33.52	578	33.31
FABP4	1,996	30.21	12	38.08
PPBP	103	not done	6	39.38
PACAP	116	35.48	127	34.61
FCGR3AB	686	27.94	46	28.94
LEP	680	33.40	34	37.60
CD38	76	35.40	14	35.13
ECM2	13	39.19	852	36.19
RGS5	13	36.53	493	31.93
PDGFD	10	39.56	215	36.42
OGN	6	39.14	864	32.80
ASPN	10	not detected	2,061	32.85
SFRP2	6	39.81	2,376	30.90

Table 40. A ranging test experiment of CEA35 (a ruptured sample) and CEA81 (a stable sample) using 500pg equivalent of total RNA in each qRTPCR reaction.

5.5.2 Multiple reference control genes selection and assessment

As validated reference control genes for LMDed macrophages in plaque rupture has not yet been determined, I proceeded to determine the most stable control genes for my study. From the panel of 115 compiled candidate reference control genes, a reasonable empirical number of genes were selected for further testing; seven genes that demonstrated the least variability in the normalised microarray data of the 11 LMDed plaque macrophage samples were identified (listed in Table 39 as reference candidate genes).

The stability of these candidate reference control genes was further evaluated by qRTPCR using the method described by Vandesompele and colleagues[276] to generate a gene-stability measure (M). The M values calculated by geNorm are shown in ranked order in Table 41. All the 7 shortlisted genes reached M values well below the default limit of 1.5 suggested by Vandesompele, ratifying the initial method of selection using the least variable genes in the microarray data. However, GAPDH, a commonly used reference control gene in previous qRTPCR studies in atherosclerosis, was observed to be the second worst performing control gene in my evaluation. After stepwise exclusion of the least stable genes from bottom to top in Table 41, PPIA and SDHA were found to be the two most stable reference genes. A minimum of 2 reference control genes were required to minimise the single reference control gene error[276]. When PPIA and SDHA were used in combination, they demonstrated very high expression stability with a paired M gene-stability measure of 0.143.

In order to assess the significance of more reference control genes contributing to overall expression stability, a pair-wise variation analysis was performed (Figure 88)[276]. The addition of a third reference control gene to the minimum two (the next ranked gene, TUBB, shown Figure 88 as $V_{2/3}$) generated a pairwise variation of 0.085. This had a low variation (of less than the 0.15 limit determined by Vandesompele) suggesting that the additional third gene had little added advantage in expression stability and had no significant effect in the calculation of a reliable normalisation factor. Consequently the 2 genes, PPIA and SDHA, were used as the reference control genes for relative quantitation.

Ranking	Gene	M value
1	PPIA	0.335
2	SDHA	0.360
3	TUBB	0.389
4	TBP	0.410
5	MYST2	0.500
6	GAPDH	0.534
7	GUSB	0.603
Best combination of 2 genes	PPIA and SDHA	0.143

Table 41. Expression stability of the candidate reference genes calculated by the M-statistic, and ranked from the most stable at the top. Low M values indicate high expression stability.

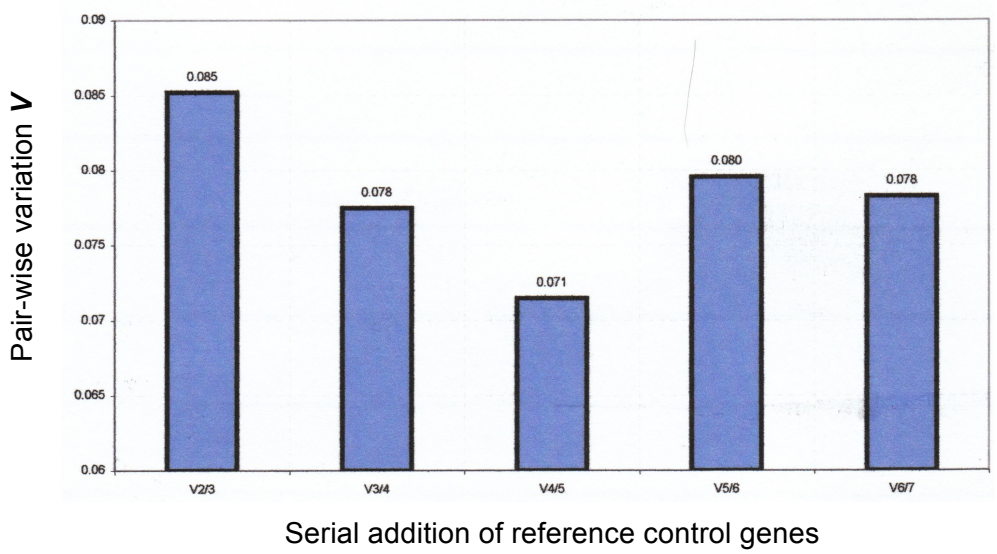

Figure 88. Pair-wise variation analysis of the serial inclusion of additional reference control genes in the determination of the optimal number of control genes for normalisation.

5.5.3 Technical validation of microarray results by qRTPCR

The real-time quantitative PCR assays of the 12 statistically significant genes with the highest fold change using the unamplified total-RNA from micro-dissection were compared to the microarray results of the same 11 samples. The scatter plot of all the quantitative data points of the qRTPCR data (in relative quantitation) to the microarray data (in signal intensity) is shown in Figure 89. The 'best fit' regression line had a slope of 1.07 demonstrating near to a 1 to 1 relationship in the quantitation of transcript abundance by microarray compared to qRTPCR. There was a high correlation between expression levels determined from microarray (linear-amplified) and from qRTPCR (unamplified) with a Pearson correlation coefficient of 0.94. These findings provide technical validation of the microarray results using a second quantitative RNA measurement methodology.

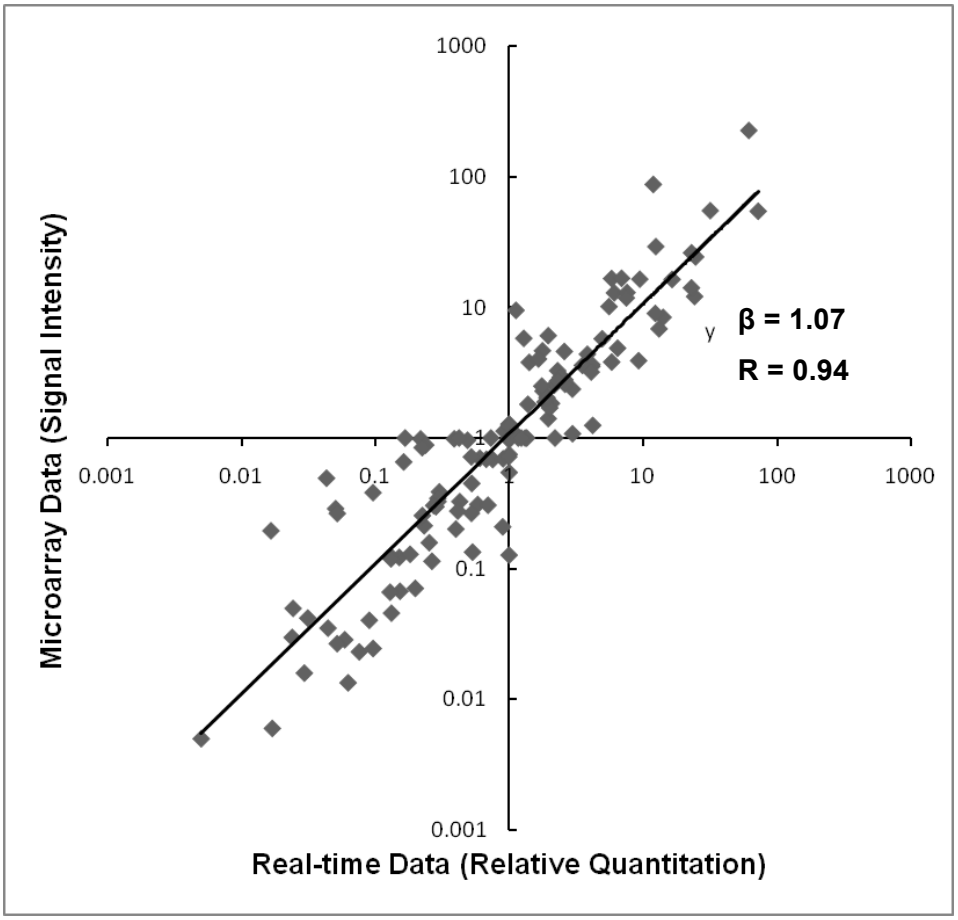

Figure 89. Validation of the microarray data by Real-time quantitative PCR. The gene expression quantitation by real-time PCR of the unamplified RNA is plotted against the linear-amplified microarray results demonstrating a 1:1 linear relationship and high correlation.

5.5.4 Biological validation by qRTPCR - testing on a larger sample size

Description of Samples

The microarray findings were then biologically cross-validated using a larger total number of 25 samples (13 stable and 12 ruptured). Their summary demographics are shown in Table 42. Histological evidence of a ruptured thin fibrous cap atheromatous plaque was present in all twelve samples designated Ruptured; among the thirteen samples designated Stable, 9 were thick fibrous cap atheroma and 4 were fibro-calcific plaques, with no evidence of plaque rupture. The detailed clinical, radiological and histopathological descriptions of the samples studied were reported in Table 21 and Table 22 in Chapter 3.

	Ruptured samples	Stable samples	p-value
No of samples (males)	12 (8)	13 (9)	ns
Mean Age (SD)	65.9 (8.3)	66.2 (8.0)	ns
Median time from Last Event in days (IQR)	42 (30-180)	n/a	-
Mean Maximal luminal diameter stenosis on MR angiogram (SD)	82.3% (11.1)	85.2%(12.8)	ns
Smoking (present or previous)	67%	62%	ns
Hypercholesterolemia	83%	100%	ns
Hypertension	83%	69%	ns
Diabetes	25%	23%	ns
Ischemic Heart Disease	8%	54%	0.002
Medication: Aspirin/Clopidogrel	100%	92%	ns
Medication: Statin	83%	100%	ns
Medication: ACEi/ARB	67%	69%	ns
Medication: Metformin	17%	23%	ns

Table 42. Demographics of patients included in unstable and stable sample groups and the corresponding significance between groups (SD- standard deviation, IQR- inter-quartile range, ns- not significant).

Relative quantitation

Expression of the 12 genes was assessed in the additional 14 samples, selected and processed in an identical fashion, by real-time PCR. In the combined set of 25 samples (12 ruptured and 13 stable) there was significant evidence of differential expression (at $p<0.05$) for 11 out of the 12 genes tested (Figure 90). These results are broadly in accordance with the FDR of 10% that we specified in the analyses of the microarray data. The degree of fold change were also broadly similar in rank to that seen in the microarray experiment.

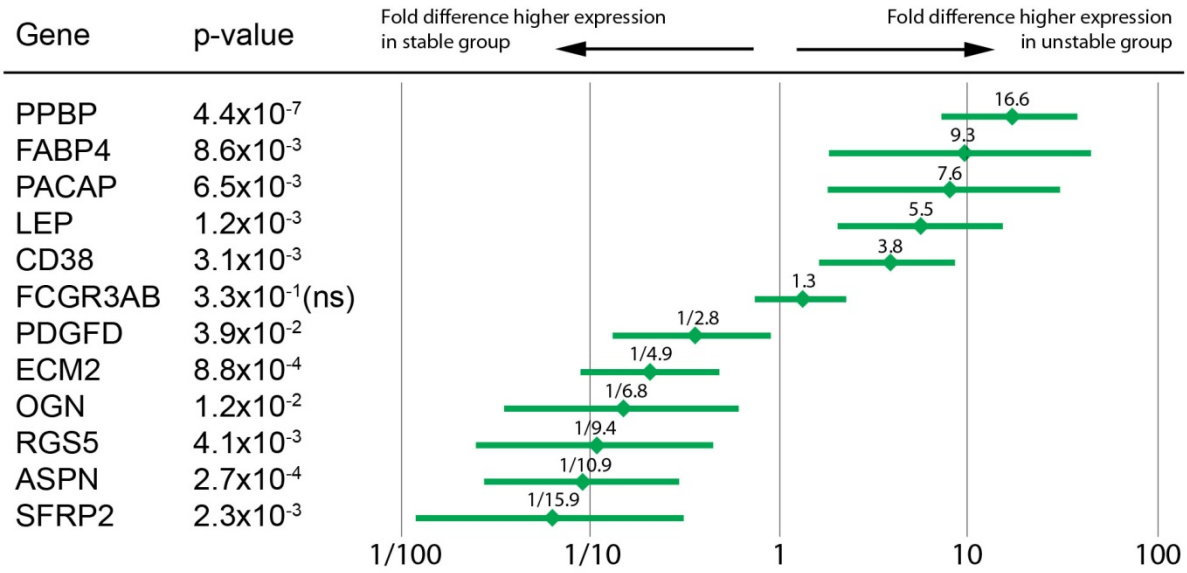

Figure 90. The quantitative Real-Time PCR results of the 12 top ranking statistically significant genes tested on a larger total sample number of 25 (12 unstable and 13 stable). The fold difference with the 95% confidence intervals and the ANOVA p-values are shown.

Cluster analysis

This larger sample group twelve-gene expression profile was then mapped to 3-dimensional gene expression space using Principal Components Analysis on GeneSpring to demonstrate the relative separation (and clustering) of the samples. Principal Components Analysis using the real-time PCR data based on the expression of these 12 genes revealed a separation of the 25 samples along an “axis of stability” in gene expression space (Figure 91). This demonstrated the variation in gene expression profiles of these 'top' 12 genes in the separation of the samples into highly unstable ruptured samples with multiple previous events of TIA/CVA at one end of the spectrum, then unstable ruptured samples with a single previous event of TIA/CVA, and asymptomatic stable FCL/FCA plaques on the other end of the spectrum.

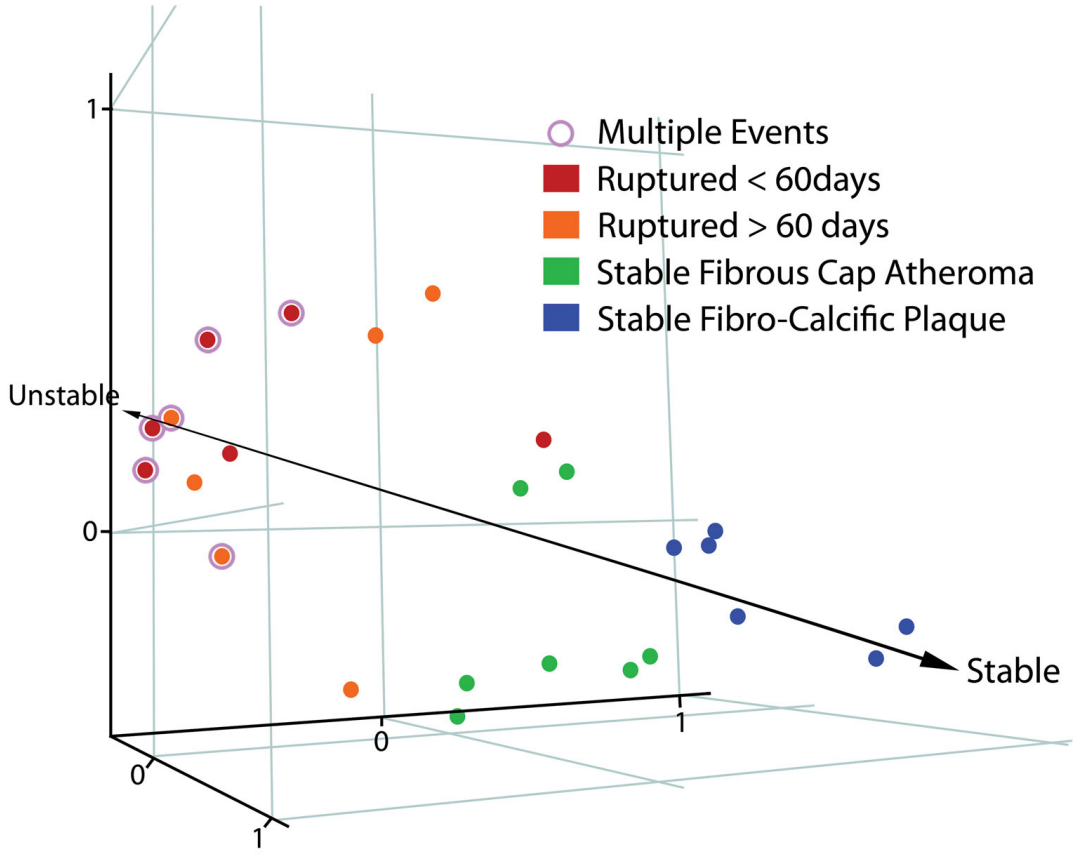

Figure 91. The relative clustering and separation of the 25 samples in gene expression space using Principal Components Analysis on all the genes tested in qRTPCR.

Chapter 6. Expression imaging in the stable and unstable plaque

6.1 An overview

The protein products of Leptin and FABP4 of the PPAR-Adipocytokine signalling pathway were studied by immunohistochemistry to confirm differential protein expression and their spatial distribution in the atherosclerotic plaque. Leptin and FABP4 were the differentially regulated key component genes involved in the most significantly upregulated pathway in unstable plaques compared to stable plaques, and were also amongst the top ranking in differential expression of the statistically significant genes identified, accordingly these were the two genes prioritised for immunohistochemical study. Time constraints precluded the performance of IHC for all the genes we had identified as differentially regulated.

6.2 Immunohistochemistry of target proteins

6.2.1 Preliminary antibody optimisation work

FFPE sections

The direct incubation of the antibodies on the FFPE sections without pre-treatment resulted in weak protein staining with significant background staining due to the masking of protein epitopes by the tissue fixation process in FFPE specimens. Various antigen retrieval methods to unmask the protein epitopes were evaluated and the results are summarised in Table 43.

The best results for Leptin were achieved using the antibody from Santa Cruz, sc842, with a 95C water bath for 5 minutes of 2 cycles using a Citrate buffer pH6 with an antibody dilution of 1/75 for 1 hour incubation at room temperature, with strong positive staining with minimal background staining. The best results for FABP were achieved using the Abcam antibody, ab13979, with the pressure cooker method at 1 minute maximum pressure using a Citrate buffer pH6 with an antibody dilution of 1/500 for 1 hour incubation at room temperature, with strong positive staining and with minimal non-specific background staining. This high signal to noise ratio was essential for the semi-quantitative immunohistochemistry analysis downstream.

Antigen Retrieval method	Buffer Solution	Leptin sc842								Leptin ab20115								FABP4 ab13979								FABP4 ab75808							
		Atheroma Macrophage		Intestinal Adipocytes		Breast Adeno-Carcinoma		Lung Parenchyma		Atheroma Macrophage		Intestinal Adipocytes		Breast Adeno-Carcinoma		Lung Parenchyma		Atheroma Macrophage		Intestinal Adipocytes		Breast Adeno-Carcinoma		Lung Parenchyma		Atheroma Macrophage		Intestinal Adipocytes		Breast Adeno-Carcinoma		Lung Parenchyma	
No pre-treatment	-	S	b	S	b	S	b	S	b	SS	bb	S	bb					S	b	SS	b	SS	b	S	b	-	b	S	b				
Trypsin digestion	Calcium chloride									S	bb	S	bb					-	-	-	-					-	-	-	-				
Microwave heating	Citrate pH 6	S	-	S	-	S	-	-	-	SS	b	-	b	-	b	-	b																
	Dako pH 9.8	SS	bb	SS	bb	S	b	S	b	SSS	bb	SS	bb					#	#	#	#	#	#	#	#	#	#	#	#	#	#	#	#
Pressure cooker heating	Citrate pH 6	SS	-	S	-	S	-	-	-	SS	-	-	-					SS	-	SS	-	SS	-	-	-	SS	-	S	b	-	-	-	-
	EDTA pH 8									SSS	bb	-	b					S	-	SS	b	SS	b	-	-	SS	b	S	b	S	b	-	b
Water bath heating	Citrate pH 6	SSS	-	SS	-	SS	-	-	-																								

Frozen sections

The snap-frozen sections were rapidly fixed in Acetone, then rehydrated and did not require antigen retrieval pre-treatment. The best results were obtained from the Leptin antibody, ab20115 at 1/2000 dilution for 1 hour incubation at room temperature, and from the FABP4 antibody, ab75808 at 1/100 dilution for 1 hour incubation at room temperature.

6.2.2 FABP4 and Leptin protein expression in the plaque

Samples

FFPE sections and snap-frozen cryosections were made from the endarterectomised carotid atherosclerotic plaques of stable and ruptured samples which were previously selected using the 3-domain criteria for stability/instability. These were the same samples studied in the microarray and quantitative real time PCR experiments. Of the total of 25 samples previously studied, 16 samples (8 stable and 8 ruptured) had sufficient remaining material for immunohistochemistry and were processed.

Snap-frozen and paraffin-embedded section immunohistochemistry

Frozen section examples of a thick fibrous cap atheroma with a thick muscular cap well populated with VSMCs (identified by SMA immuno-staining) and a ruptured thin fibrous cap atheroma with a thin and interrupted rim of VSMCs are shown in Figure 92. Formalin-fixed paraffin-embedded sections of a ruptured thin fibrous cap atheroma and of a stable thick fibrous cap atheroma are shown in Figure 93 and Figure 94 respectively. The extensive necrotic core containing macrophages identified by CD68 immuno-staining is demonstrated in the ruptured plaque and a smaller organised necrotic core is seen in the stable plaque. There was co-localisation of Leptin and FABP4 immuno-staining with CD68, representing the expression of the Leptin and FABP4 proteins in the macrophages of the atherosclerotic plaque, particularly in the macrophages in the boundary just under the fibrous cap and above the lipid core. There was little uptake of Leptin or FABP4 immunostaining in the VSMCs of the thick fibrous cap in the stable plaque or in the thin rim of VSMCs in the residual fibrous cap in the ruptured plaque. I observed that the macrophages under the respective caps demonstrated greater staining of Leptin and FABP4 compared to the macrophages in the middle or at the base of the necrotic cores. There was also weaker staining of both Leptin and FABP4 in the stable samples in contrast to heavier staining in the ruptured samples. The frozen sections demonstrated some sectioning artefact as a result of the cryosectioning of the ruptured plaque (marked by * in Figure 92).

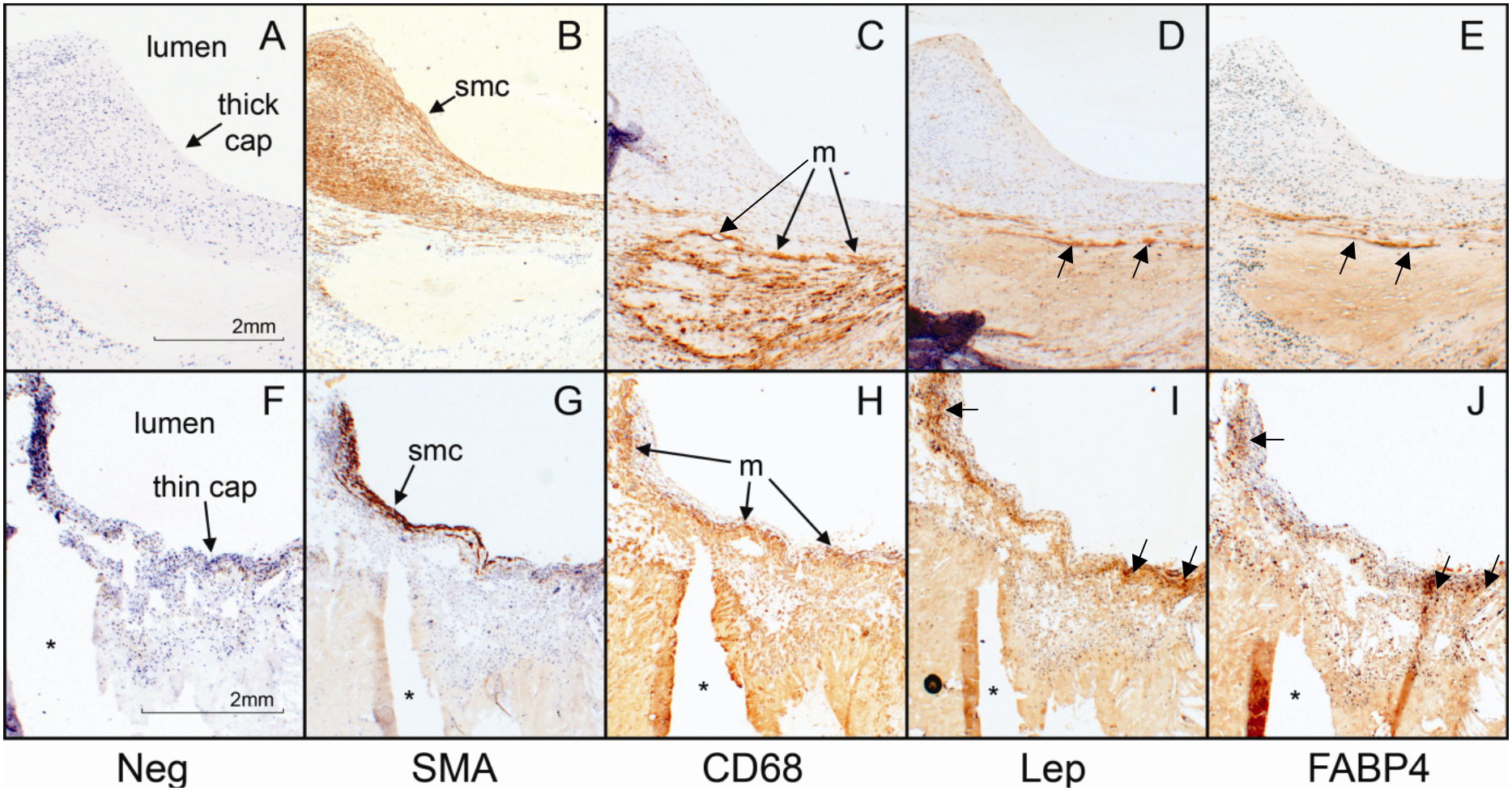
lumen
A
thick
cap
2mm
B
smc
C
m
D
E
F
lumen
thin cap
2mm
G
smc
H
m
I
J
Neg
SMA
CD68
Lep
FABP4

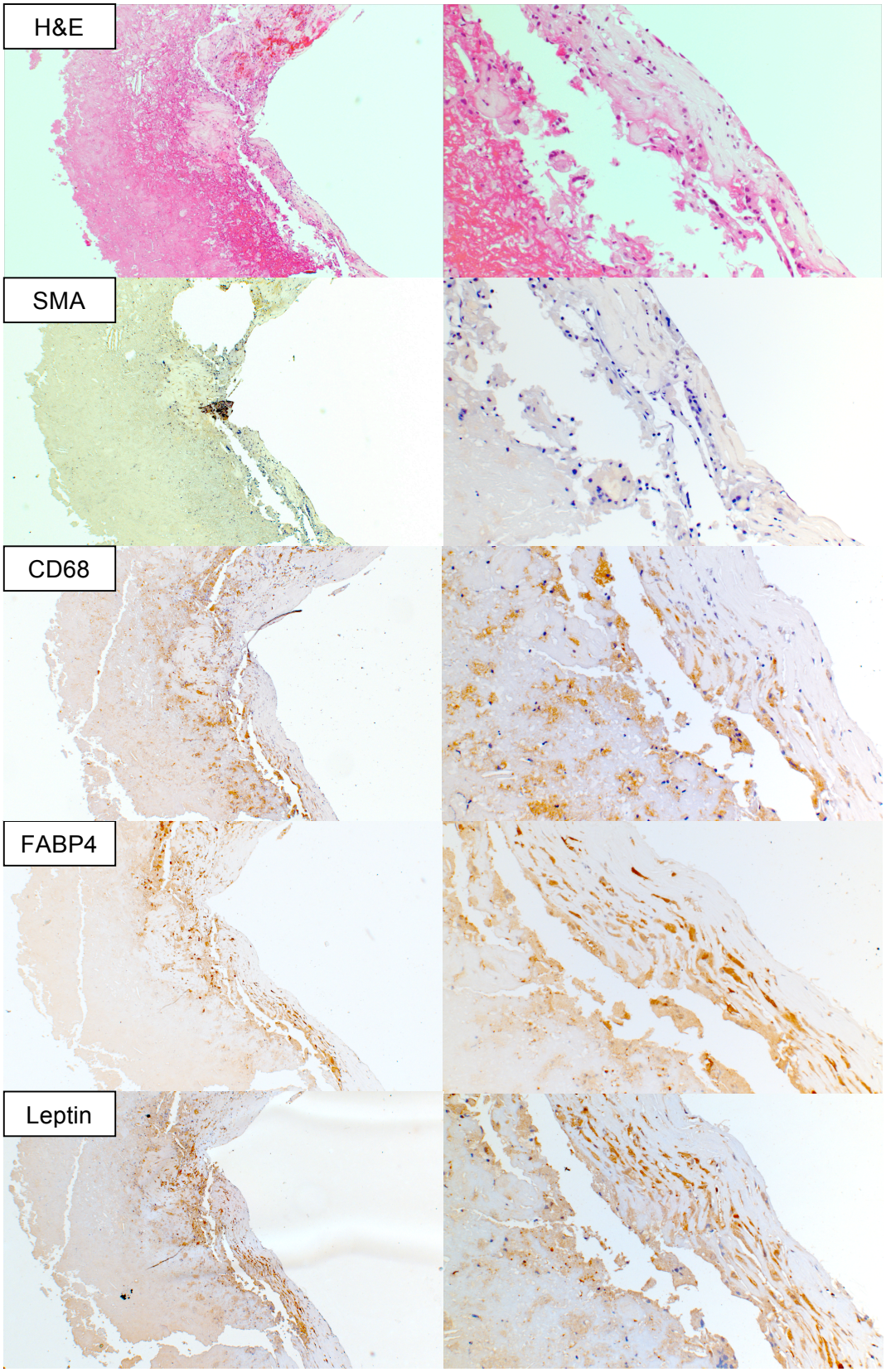

Figure 93. FFPE immuno-stained sections of an unstable ruptured thin fibrous cap atheroma (5x magnification on the left and 20x magnification on the right). Colocalisation of Leptin and FABP4 immunostaining with CD68 with heavy staining is seen.

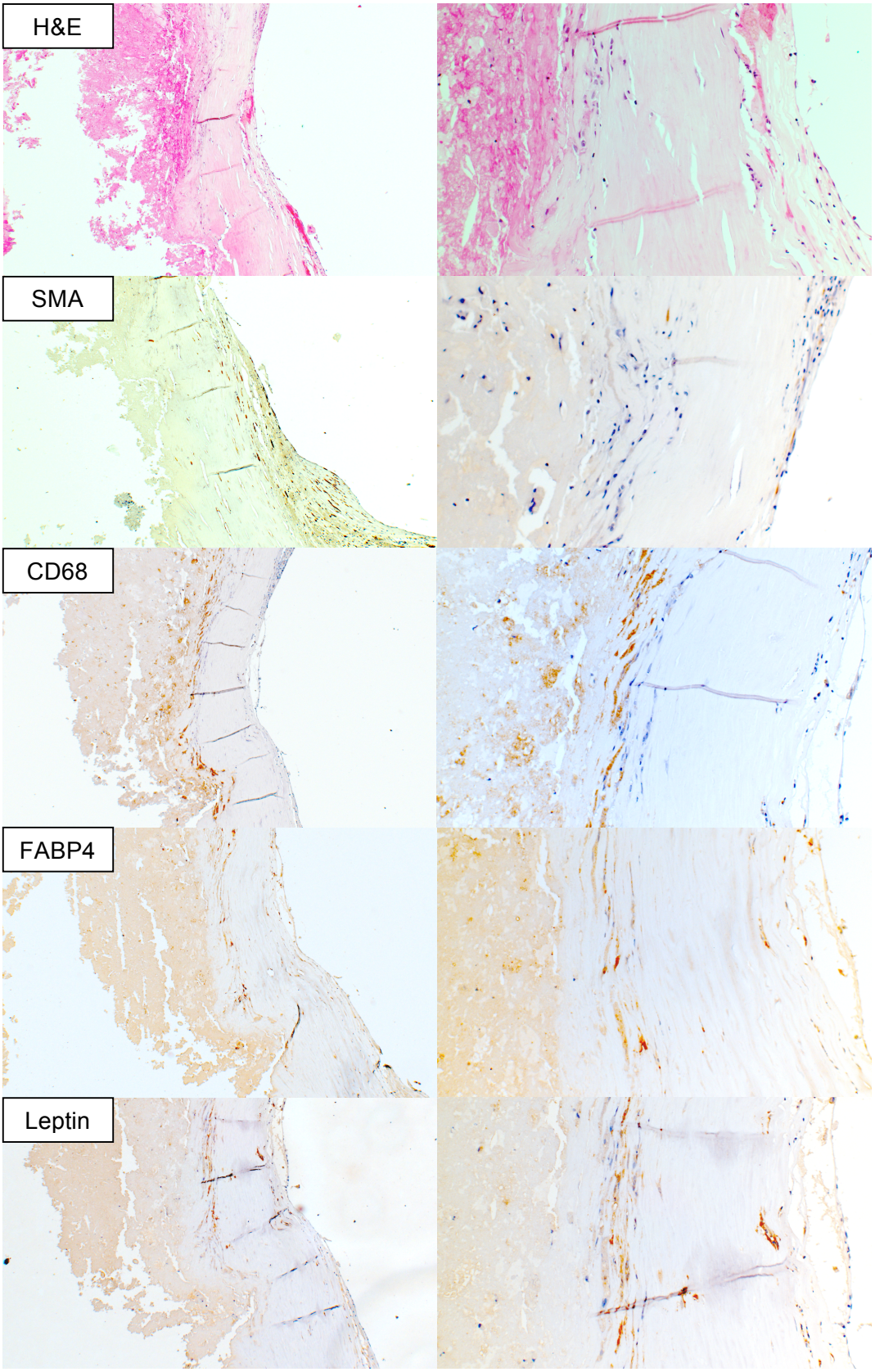

Figure 94. FFPE immuno-stained sections of a stable thick fibrous cap atheroma (5x magnification on the left and 20x magnification on the right). Colocalisation of Leptin and FABP4 immunostaining with CD68 with less heavy staining is seen.

The snap-frozen and FFPE section immunohistochemistry studies of Leptin and FABP4 confirm their protein expression in plaque macrophages with their increased expression in ruptured plaques. There was heterogeneity in the expression of these proteins in the macrophages within the plaque with a predominance of expression in the macrophages under the fibrous cap which lends further support to their causal role in plaque rupture.

6.2.3 Semi-quantitative Immunohistochemistry analysis

The protein expression studied by immunohistochemical staining of the paraffin-embedded formalin-fixed tissue sections of the 8 stable and 8 ruptured atherosclerotic plaques were semi-quantitatively measured by ranking of observed staining intensity. All 16 lesions were immuno-stained and analysed. However, 3 of the 8 stable lesions showed a change in lesion classification from FCA or FCL to pathological intimal thickening on deeper sectioning of the specimen and could not be analysed. All of the remaining ruptured TFCA lesions did not demonstrate histological evidence of rupture but were analysed as the sections were TFCA lesions adjacent and near to the site of rupture. No discernable immuno-staining was given a value of 0, weak stain of 1, moderate stain of 2 and heavy/strong stain with a value of 3. The mean values with the standard deviations in parentheses are summarised in Table 44.

	SMA	CD68	FABP4	LEP	FABP4 less CD68	LEP less CD68
Ruptured TFCA macrophages under cap	0.1 (±0.2)	1.6 (±0.5)	1.4 (±0.7)	1.1 (±0.7)	-0.25 (±0.8)	-0.56 (±0.5)
Ruptured TFCA macrophages at base	0.1 (±0.2) *p=0.55*	1 (±0.5) *p=0.02*	0.3 (±0.4) *p=0.002*	0.1 (±0.2) *p=0.002*	-0.69 (±0.6) *p=0.22*	-0.88 (±0.6) *p=0.27*
Stable FCA/FCL macrophages under cap	1.2 (±0.4) *p=4.1x10^{-5}*	1.7 (±1.2) *p=0.88*	0.4 (±0.2) *p=0.01*	0.7 (±0.8) *p=0.41*	-1.30 (±1.2) *p=0.07*	-1.00 (±0.6) *p=0.18*

Table 44. The semi-quantitative analysis of protein immunohistochemical staining of SMA, CD68, Leptin and FABP4 in the macrophages of stable and unstable ruptured plaques (see text for details) (the p-values are the comparisons with the ruptured TFCA macrophages).

FABP4 and Leptin staining under the thin fibrous cap compared to the base of the atheroma

I was able to demonstrate that there was significant difference in protein expression of FABP 4 and Leptin in macrophages under the thin fibrous cap of ruptured plaques compared to the macrophages under the lipid core (FABP4 1.4 vs 0.3, p=0.002, and Leptin 1.1 vs 0.1, p=0.002). However, there was also a lesser difference in macrophage cell density reflected by the difference in CD68 staining (1.6 vs 1.0, p=0.02) which may contribute to the differences in the overall FABP4 and Leptin staining observed. In an attempt to address this, FABP4 and Leptin staining intensities were compared relative to CD68 (the 2 far right columns) in a semi-quantitative manner. A negative value denotes

comparatively weaker staining to CD68. There was a mild difference in rank category of staining relative to CD68 but with a wide variation and were not significant as a result (p=0.22 and 0.27).

FABP4 and Leptin staining under the thin fibrous cap of ruptured plaques compared to the thick fibrous cap of stable plaques

In a comparison between macrophages under the thin fibrous caps of unstable plaques and under the thick fibrous caps of stable lesions, I observed that there was also a significant difference in FABP4 staining (1.4 vs 0.4, p=0.01) but not in Leptin staining (1.1 vs 0.7, p=0.41) due to the larger variation of staining intensity seen with Leptin in the stable plaque macrophages. In comparison, the mean CD68 staining was similar between the lesion types but with greater variation in the stable plaques as expected. By performing paired corrections to CD68 staining as before, I found a larger difference with of FABP4 staining (-0.25 vs -1.30, p=0.07) and Leptin staining (-0.56 vs -1, p=0.18) relative to CD68, with the greater staining in the ruptured plaque macrophages, but were not statistically significant due to the larger variation seen using a semi-quantitative approach and the limited sample numbers used.

6.2.4 Quantitative immunohistochemistry pilot data

The staining intensity of FABP4 and Leptin was quantitatively measured relative to CD68 using the Image-Pro Plus software (Media Cybernetics, UK). A preliminary and limited comparison of 4 ruptured TFCA lesions were analysed and the immuno-staining intensities of FABP4 and Leptin in macrophages under the thin fibrous caps were compared to those located at the base of the lipid cores of the lesions. Initial attempts at using black and white images for quantitative immunohistochemistry proved difficult due to the nuclear counter-staining by haematoxylin, and as a result, three colour analysis (RGB) was used. The FABP4:CD68 and Leptin:CD68 staining intensity ratios in the 3 colour channels with the standard deviation of the ratios in parentheses are reported in Table 45. There was no observable advantage in the use of separate colour channels in the isolation of the DAB immunostaining signals of FABP4 and Leptin from the haematoxylin nuclear counter-stain. I was not able to detect any significant difference in protein expression in any colour channel used for FABP4 or Leptin between macrophages under the thin fibrous cap and at the base of the lipid core in ruptured TFCA lesions in this pilot work.

Antibody & colour detection channel	Mean cap macrophage FABP4:CD68 ratio	Mean base macrophage FABP4:CD68 ratio	p-val
FABP4-Red	0.24 (±0.24)	0.21 (±0.20)	ns
FABP4-Green	0.46 (±0.29)	0.37 (±0.20)	ns
FABP4-Blue	0.61 (±0.37)	0.72 (±0.24)	ns
FABP4-RGB	0.42 (±0.30)	0.43 (±0.20)	ns
Leptin-Red	0.38 (±0.34)	0.32 (±0.32)	ns
Leptin-Green	0.61 (±0.57)	0.56 (±0.70)	ns
Leptin-Blue	0.88 (±0.78)	1.13 (±1.76)	ns
Leptin-RBG	0.62 (±0.56)	0.67 (±0.92)	ns

Table 45. The FABP4 to CD68 and Leptin to CD68 signal intensity ratios in the 3 colour detection channels. The mean of the ratios with the SD in parentheses are reported.

These were preliminary findings limited to only 4 ruptured TFCA lesions and were incomplete. However, this pilot data has demonstrated several issues regarding the quantitative immunohistochemistry methodology in its application to serial immuno-stained sections. A confounding issue was that the cells in the serial sections analysed were not the same macrophage cells nor were they in the same position, but were adjacent macrophage cells in close proximity. This meant that it was impossible to use a precise immuno-stain mask to identify the specific positions to detect the Leptin or FABP4 signal in serial sections (unlike double immunostaining experiments), as subtle positional changes, cracks or irregularities in the tissue blocks prohibited this. As a result, the regions sampled had to be significantly expanded to include regions without immunostaining to cover the common regions across several serial sections and was less precise. This also meant that significant background signal staining was picked up as a result of haematoxylin counterstaining which accounted for as much as 40% of the detected signal. There was a wide variation in the measured signal intensities of the replicates. This may in part be explained by the imprecise sampling and increased background noise as well as random experimental variation in immuno-staining intensity of different slides. I have also observed significant variation in the measured signal of CD68, which was used as a reference control of macrophage protein expression; its mean signal intensity was 35.4 across the experiment but there was a large variation in signal intensity across the slides (SD of 22.7 and ranged from 4.2 to 84.7).

Due to constraints on time, the quantitative immunohistological analyses of all the 8 ruptured TFCA and 5 stable FCA/FCL lesions have not yet been performed and potentially significant differences between macrophages under the thin fibrous caps of ruptured TFCAs and the thick fibrous caps of stable FCA/FCL lesions have not yet been determined. The work pilot work was limited to only 4 ruptured TFCA lesions but was useful to highlight several technical issues in the methodology of quantitative immunohistochemistry; whereby double immuno-fluorescence staining methods may be advantageous.

6.3 Optical Projection Tomography of the atherosclerotic plaque

I have performed the preliminary work to establish the protocols for OPT analysis of normal vascular tissue and in carotid atherosclerotic tissue. Figure 95 shows the generated 3D OPT reconstructions from FITC auto-fluorescence scanning of a normal radial artery. In panel A the 3D reconstructed external lateral view of the artery is seen. A barrel view of the lumen of the artery seen from the reconstructed digital transverse section of the artery is seen in panel B. Panel C shows a digitally reconstructed longitudinal section of the artery demonstrating the 3D view of the lumen along this cut. Panel D shows a 20μm thick longitudinal digitally reconstructed section of the artery, demonstrating a small branch artery originating from the radial artery. Panel E shows the same branch artery from a 20μm thick digitally reconstructed transverse section. In the enclosed CD, mpeg movies of a lateral view of the radial artery (**Movie 2**), of the 'digital' longitudinally sectioned artery (**Movie 3**) and a 'fly-through' movie reconstructed from 'digital' sections of the radial artery demonstrating the origin or the small branch artery (**Movie 4**) can be seen.

Figure 96 shows the OPT reconstructed images of an atherosclerotic plaque from carotid endarterectomy surgery with its corresponding MR angiogram. Panel A shows a frontal 3D reconstruction with the longitudinal surgical incision (marked 's') seen. Panel B shows a longitudinal digital section with a 3D view of the atheromatous common carotid artery at its bifurcation with the lipid core (marked 'c') clearly seen. Panel C shows a digital transverse section across the atheromatous lesion in the internal carotid artery demonstrating the lipid cores (marked 'c') with a 3D view into the stenotic lumen. Panel D shows a series of digital transverse sections down the carotid whole mount demonstrating the complex atheromatous burden in the common carotid artery (CCA) at the bottom to its bifurcation in the middle and the internal and external carotid arteries at the top (ICA/ECA). The surgical incision can also be seen (marked 's'). Panel E and F are paired

panels of an OPT digitally reconstructed longitudinal 20μm thick section (left) and a corresponding digital section from the pre-operative 3D contrast MR angiogram (right), demonstrating the preservation of the in-vivo anatomy by OPT with higher resolution 3D imaging of the lesion. Mpeg movies of the OPT reconstructions of the lateral view of the carotid artery (**Movie 5**), the 'digital' longitudinally sectioned atheromatous common carotid artery at its bifurcation (**Movie 6**), the 'digital' transverse sectioned atheromatous artery demonstrating luminal encroachment in the internal carotid artery (**Movie 7**) and a 'fly-through' movie reconstructed from 'digital' transverse' sections of the carotid artery (**Movie 8**) is shown in the enclosed CD.

Histochemical, protein and gene expression staining of the stable and ruptured complex atherosclerotic plaque can be mapped to the OPT digital reconstructions generated. This may enable histological, anatomical/structural and gene/protein expression analyses to be performed in any view and plane in 3D. Time constraints have precluded the gene and protein expression study of FABP4 and Leptin using OPT and this would be a focus for future study. Importantly, I have laid out the methodological roadmap for the three dimensional study any gene or protein in the atherosclerotic plaque using OPT.

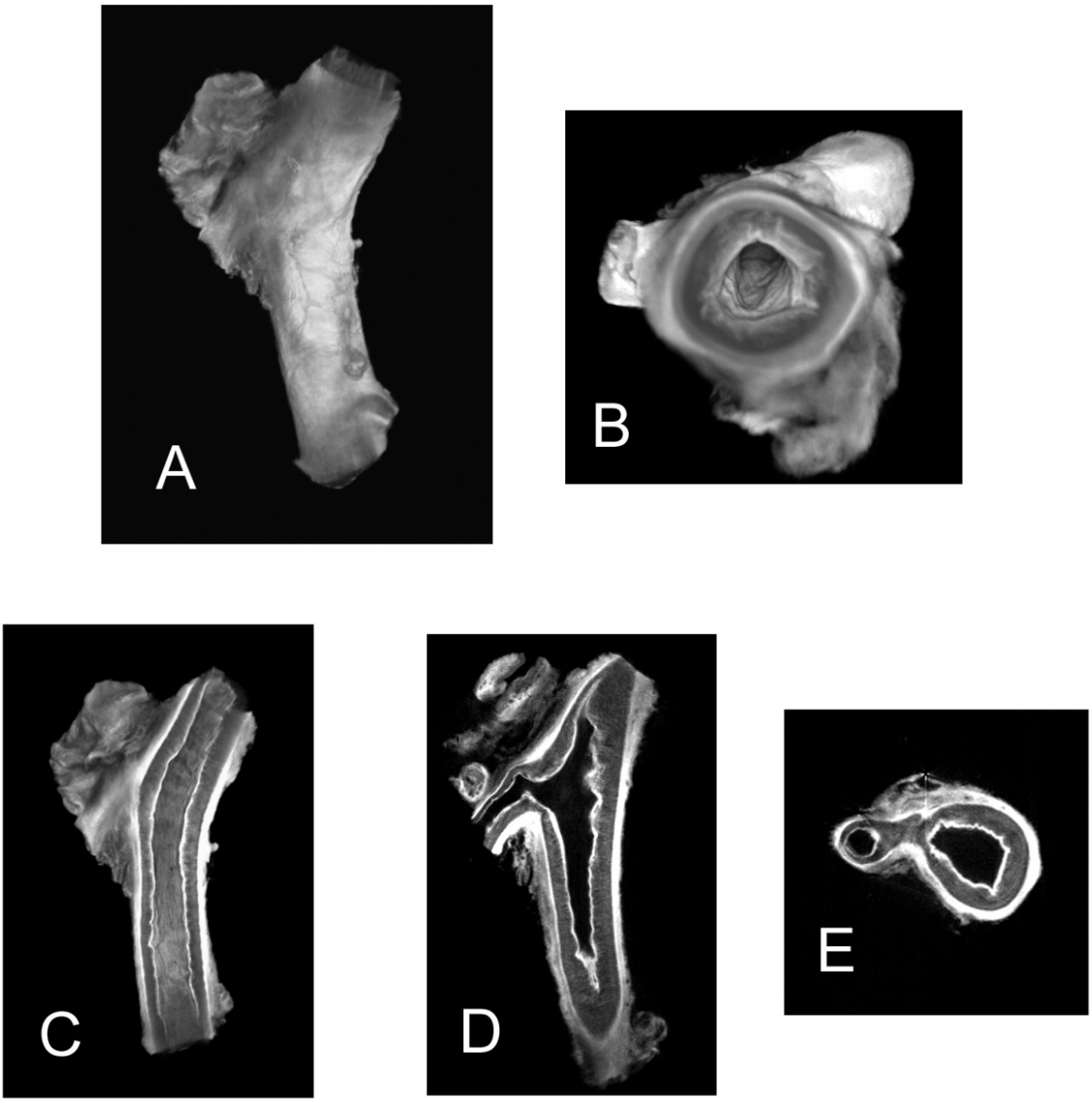

Figure 95. Optical Projection Tomography 3D reconstructions of a FITC scanned whole and intact normal radial artery. 'Digital' sections are made by computer reconstructions using the raw 3D scanned data. Various digital views of the whole mount artery can be demonstrated (see text).

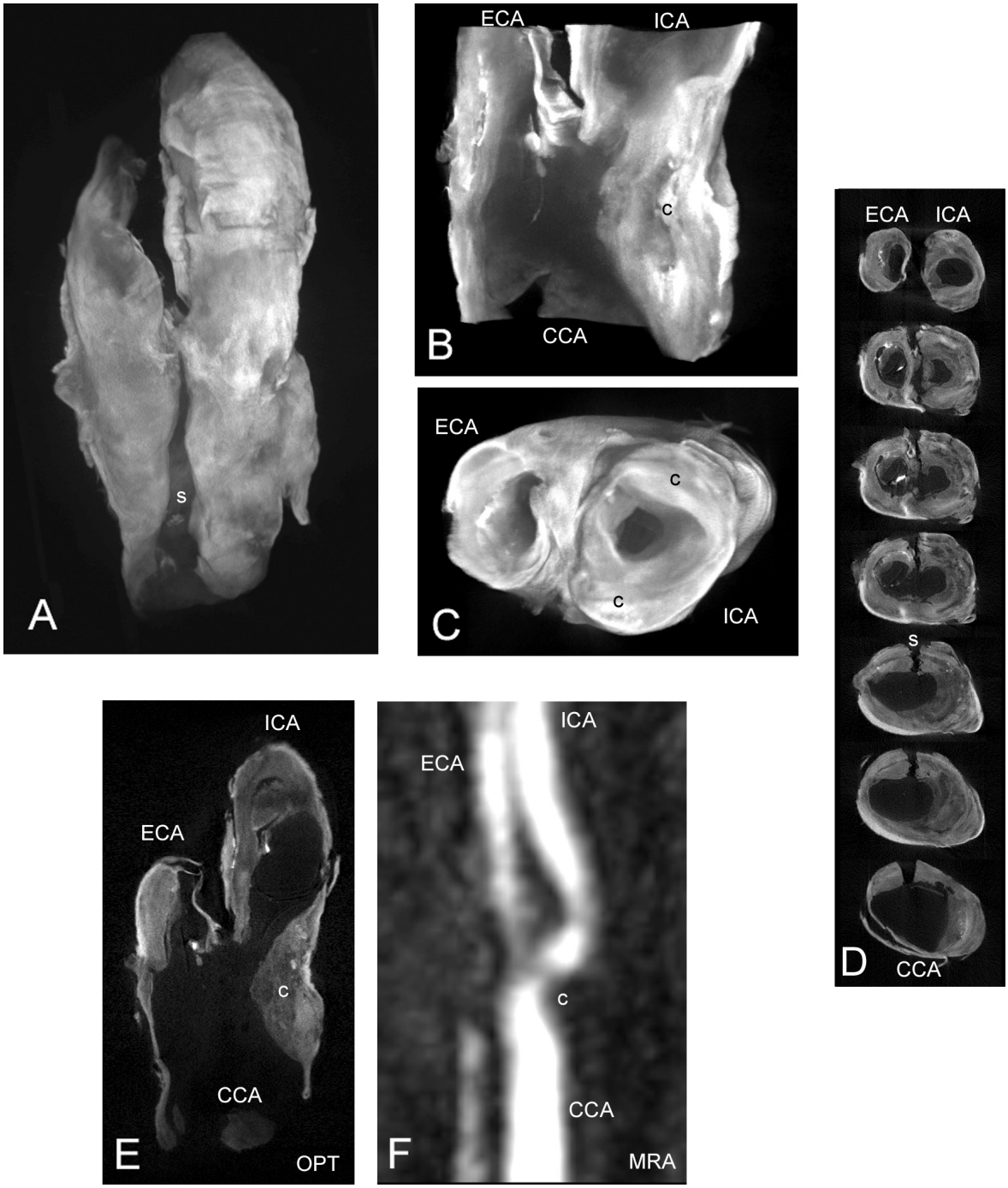

Figure 96. Optical Projection Tomography 3D reconstructions of a scanned whole mount atherosclerotic carotid artery removed at carotid endarterectomy. Various digital reconstructed sections and views are demonstrated (see text).

Chapter 7. Discussion

In this work, I have demonstrated significant differences in the gene expression profiles between macrophage-rich regions derived from stable and unstable atheromatous plaques. Genome-wide expression profiles in stable and unstable samples spontaneously clustered into groups entirely congruent with their clinical designation. This indicates that in addition to the well-established differences in the degree of macrophage infiltration into unstable and stable lesions, there are also important differences in the molecular signature of the plaque macrophages. Nine hundred and fourteen genes were differentially expressed between the unstable and stable sample groups; some of these may have causal relationships with plaque rupture. Leptin and FABP4, which both have functions linking lipid metabolism to inflammation, were among the most differentially expressed genes, with 5.5 (95% CI 2.1-14.4) fold and 9.3 (95% CI 1.9 - 46.7) fold overexpression respectively in unstable relative to stable samples. Moreover, the adipocytokine/PPARG signalling pathway incorporating both FABP4 and leptin was the most strongly up-regulated KEGG pathway in unstable samples ($p=5.5 \times 10^{-7}$). Comparison of expression profiles from laser micro-dissected samples with publicly available expression profiles from a variety of cell types showed a close correspondence between our samples and activated macrophages, indicating that I had largely been successful in isolating macrophage-specific mRNA. The microarray results were validated using qRTPCR on the unamplified RNA from the same 11 samples with a high degree of correlation (R=0.94) and a 1:1 relationship in degree of magnitude of expression difference, in high confidence in the interpretation of the microarray results. The microarray findings were then further successfully cross-validated in a larger sample size of 25. Amongst the genes which passed qRTPCR cross-validation were FABP4 (9.3 fold, $p=8.6 \times 10^{-3}$) and Leptin (5.5 fold, $p=1.2 \times 10^{-3}$). These cell-specific data from clinical samples show the importance of genes in the PPAR-Adipocytokine signalling pathway linking lipid metabolism to inflammation in plaque instability, and importantly confirm the data from mouse models suggesting that modifying the expression or action of these genes in plaque macrophages may have therapeutic potential.

The specific and differential protein expressions of FABP4 and Leptin in plaque macrophages were confirmed by immunohistochemistry on the stable and ruptured plaque sections. The differential protein expression of FABP4 and Leptin in the plaque macrophages in the ruptured plaque and its preponderance to macrophages under the thin fibrous cap supports the hypothesis of a causal role of these proteins and the PPAR-Adipocytokine signalling pathway in plaque rupture. I have also developed the Optical Projection Tomography protocols for vascular and atherosclerotic tissue and generated 3

dimensional OPT reconstructions of normal arteries and of advanced atherosclerotic plaques for 3D gene or protein expression studies.

7.1 Clinical and pathological characterisation of the plaque

The clinical and pathological characterisation of the plaque in the 3 domains were performed in this study primarily to accurately identify the stable and unstable plaques for gene expression study. However in doing so, several interesting observations were made, in particular, the significant association of PIT lesions with clinical symptoms and the high degree of correlation between the domains.

7.1.1 The PIT lesion and plaque erosion

Interestingly the plaques with evidence of thrombus overlying an erosion in our study were from a FCA and two from FCLs. These sources of erosion have been previously described by Virmani and colleagues[18, 42]. I did not find any thrombus overlying the 5 calcified nodule lesions or the 7 PIT lesions which have previously been described as lesions to be associated with thrombi[18]. However almost all of these lesions were from patients with recent symptoms (<6 months) in our study, supporting the association of these lesion types to erosive thrombus and clinical events. In a recent study of sudden coronary death by Tavora and colleagues, of the deaths associated with thrombi, 80% were due to plaque rupture and the remaining 20% were due to plaque erosion[286]. The 4:1 ratio of rupture to erosion was similarly seen in our study. Moreover, they observed 70% of erosions occur overlying atheromatous lesions and 30% over PIT lesions. This supports my observations of erosion and thrombus seen mostly over FCA and FCL lesions.

The PIT lesion was described as a 'preatheromatous' intermediate lesion (Stary III lesion) and of presumed aetiological origin from xanthomatous change of intimal thickening lesions[17, 18, 42]. It is a commonly observed atherosclerotic lesion type and an infrequent cause of plaque erosion[286]. Moreover I did not find any thrombi overlying these lesions in my study cohort and the histological analyses were performed independently and blinded from the clinical phenotype. On this basis, I initially classified the PIT lesion similar to the other lesions which were more commonly associated with plaque erosion and thrombosis such as the FCA and FCL lesions, as a stable plaque type. It became apparent on the examination of these lesions in relation to clinical symptoms, a significant association of the PIT lesion to recent symptoms (<6 months) and of the FCA and FCL lesions to late or no symptoms (p=0.004). My observations lends further support to the understanding that the PIT lesion is not a stable lesion but is associated with clinical sequelae of plaque

erosion and thrombosis due to some "as-yet-unidentified" property worthy of further study. In a speculative manner, the PIT lesion can be described as a pre-erosion lesion type analogous to the TFCA lesion as a pre-cursor lesion to plaque rupture.

7.1.2 Plaque surface morphology as an independent predictor of clinical events

The 2-way comparisons between clinical, radiological and histology of the atherosclerotic plaques from CEA surgery have demonstrated significant correlations between the measured variables in our study. I have shown a significant correlation between the previous stroke or TIA and any surface irregularity (p=0.00003). This relationship has also been reported in the ECST and NASCET studies but with a lower level of significance (p=0.01). The higher significance in correlation in our study may be explained by a selected population of patients in our study performed post-event and a more sensitive imaging modality to detect plaque surface irregularities (3D MRA vs 2D catheter angiography). The close correlation of symptoms and surface irregularity may be explained by the increased prevalence of surface irregularity with increasing degree of stenosis which I observed ($p=9x10^{-8}$). Furthermore, it is well established that the increase in carotid stenosis is a strong predictor of future stroke events and is and one of the major determinants in the decision for CEA surgery[226, 227, 231, 232]. Unsurprisingly a strong correlation between stenosis grade and symptoms was seen in our dataset ($p=2.3x10^{-7}$). It was therefore uncertain if surface irregularity was independent of stenosis grade in the prediction of clinical events. From the analyses of the ECST and NASCET data, it was found that although angiographic surface irregularity increased in frequency with increasing degree of stenosis, surface irregularity remained an independent predictor of future stroke or TIA at all degrees of stenosis and this relationship was still evident beyond 2 years of follow-up. Post-hoc sub-group analyses of our study population according to stenosis severity showed a similar trend but statistical significance was not reached due to the small sample numbers in the sub-groups (data not shown). This is further corroborated by macroscopic examinations of plaque surface of 1,252 CEA specimens by Park and colleagues, who found a higher incidence of plaque surface irregularity in symptomatic than in asymptomatic patients[287]. These observations suggest that plaque surface irregularity is a highly significant independent risk factor for clinical sequelae and is similar in importance to the degree of stenosis in the identification of clinically significant carotid disease (i.e. the high risk plaque).

7.1.3 Detailed plaque surface morphology using 3-dimensional MR imaging

Previous studies using 2-dimensional imaging modalities have limited ability to resolve plaque surface morphology and have obscured such a relationship as a result. For example, conventional catheter angiography, being a 2-dimensional imaging technique has poor diagnostic accuracy for the detection of plaque morphology with poor agreement between angiography and pathological observation of plaque ulceration[288, 289]. It was acknowledged in the ECST study that the true association of plaque irregularity and stroke risk may have been significantly underestimated as a result of this[290]. The ability to detect plaque surface irregularity is greatly improved by using 3-dimensional imaging techniques such as 3D contrast-enhanced MRA, due to its ability to image atheromatous vessels in any specified plane.

In a study using high-resolution ex-vivo 3D MR imaging of 100 gadolinium-doped CEA specimens, Troyer and colleagues reported a good correlation of surface irregularities to symptoms of stroke or TIA (p=0.01). They found the correlation strongest when comparing major irregularities (>2mm depression defect) to mild or no irregularity of plaque surface (1-2mm depression defect and smooth surface). In comparison, I found the strongest correlation when comparing any irregularity (1mm or more depression defect) versus no significant irregularity (p=0.00003). Analyses of my data using major irregularities (>2mm) versus mild irregularities or none (<2mm) will still yield a significant but lesser correlation (p=0.0029). My study differed in that I was performing in-vivo MR assessments with an in-plane resolution of 0.6mm. Troyer's ex-vivo experiment with custom MR coils had an in-plane resolution of 0.2 mm. It is possible that some 1mm depression defects may have been underestimated using our modality and some mild depression defects of 1-2mm detected on our MR imaging may in fact be greater reflecting the limitations of in-vivo clinical imaging. Several in-vivo studies have since reported the successful identification of ruptured fibrous caps with significant association with clinical events[195, 197]. However, these studies used a complex protocol in the determination of plaque constituents which is prohibitive in daily clinical application. Our study used a simple rapid 3D reconstruction protocol in assessment of surface morphology and stenosis severity which we were able to demonstrate similar success in correlation to clinical events, validating its utility in identifying plaques of clinical significance.

7.1.4 Correlations between histology, clinical symptoms and radiographic plaque surface irregularity

Several studies have described the histological characteristics of surface ulceration and plaque rupture with clinical events and cerebral micro-emboli[198, 291]. However there were also contradicting reports which failed to demonstrate an association of histological findings of plaque rupture, thrombosis or intraplaque haemorrhage to symptoms[292]. In my work, I have found a strong association between plaque histopathological lesion sub-type to clinical symptoms of stroke and TIA ($p=2x10^{-8}$). This was in part due to the use of an amalgamated classification schema which satisfactorily differentiates between plaque rupture, erosion and the various vulnerable and stable sub-types allowing for a more detailed analysis in histological correlation to the clinical symptoms and radiographic evidence of plaque surface irregularity. Previous histological studies had focused mainly on plaque rupture[198, 291, 292] but we now appreciate that although 60-65% of thrombosis events occur as a result of plaque rupture, 20-35% of thrombosis events are the result of plaque erosion[18, 42].

My observations and arguments of the close and independent correlations seen in 2-way analyses between symptoms, plaque surface irregularity and histology would suggest that their associations were synergistic and summative when all 3 criteria were used together. However, in order to perform the multi-way correlation, I needed to simplify the 2-way correlations to a standard 2x2 Chi-Square. These sub-group divisions were required to remain the same in 3-way analysis and were not always optimal in 2-way analysis. Furthermore, only half of the data which I had analysed previously in surface irregularity to clinical symptoms were used in the 3-way analysis as the other half of the data did not have a carotid endarterectomy and thus no histological data to analyse. Despite these various restrictions the independent 2-way analyses were still statistically significant (at $p=0.0012$, $p=0.032$ and $p=0.019$) and the 3-way log-linear analysis yielded a greater and significant correlation with $p<0.0005$. This supports and validates our methodology of using criteria in all 3 domains in the selection of the stable/unstable plaque.

7.1.5 Sample characterisation and selection

One of the critical issues of previous microarray gene expression studies in atherosclerosis was the limited characterisation of the samples studied and the lack of detailed clinical and demographic information about the sample donors. Most did not classify the plaque histology to well known histological classifications using either the Stary or Virmani criteria. Only 2 studies had detailed histological characterisation of human samples reported[188, 216]. A summary of these previous studies is shown in Table 46

and Table 47 in section 7.3.9 in this chapter. The lack of detailed characterisation of samples limited the interpretation and comparison of microarray data particularly in the study of plaque rupture. For example, Vemuganti and colleagues compared lesions from symptomatic to asymptomatic patients without reporting the histological classification of the lesions, but on the contrary they were described to be of similar histological constitution between the symptomatic/asymptomatic samples, confounding the interpretation of their findings[293].

The reliable and accurate identification of the unstable and stable plaque is critical in the expression profiling of these lesions. I have demonstrated the limitations of a single variable such as the presence or absence of symptoms in the identification of the unstable and stable plaque. The perfect single discriminator in the identification of the unstable/stable lesion is elusive and as yet unknown. Despite this the few studies investigating plaque vulnerability have relied on the presence or absence of symptoms alone[293-296] or the macroscopic appearances[297] or histological evidence of plaque rupture[189] alone in their selection of samples for study.

By using validated criteria in the 3 independent strong predictors of plaque stability/instability in the ranking and selection of lesions, I was able to identify maximally contrasting unstable and stable lesions. The enrichment criteria were designed to be highly selective and specific in the identification of these lesions. As a result I would expect only small numbers of samples would be selected and a large proportion would fall short of the selection and would be left unused. Although the number of samples studied by microarray in my study were relatively small (n=11), I was confident in the accurate identification of the stable and unstable lesions studied and the cell-specific nature of the isolation of the macrophages and the resultant microarray results. Selection from the extremes of a distribution is a frequently employed method of increasing the power of studies comparing genetic factors among human subjects. Furthermore, I have also designed a second stage of validation on a larger sample group (n=25) by qRTPCR to confirm the biological reproducibility of our findings. This approach is novel and no study to date has used such a comprehensive multi-modality approach in the identification of the stable and unstable plaque for gene expression study.

7.2 Isolation and characterisation of cell-specific RNA

7.2.1 The atherosclerotic plaque: an unstable tissue susceptible to RNA damage

The total RNA which I had extracted from whole atheromatous tissue yielded variable results in RNA quality. This was not entirely surprising as a mix of viable/healthy and non-viable/apoptotic cells as well as dead/necrotic cellular debris were collectively homogenised in the RNA extraction. These observations were supported by similar findings in previous gene expression work using whole tissues; Martinet and colleagues[282] reported significant variability in RNA quality ranging from almost intact RNA to strongly degraded despite snap-freezing immediately in liquid-nitrogen. This was more marked in advanced atherosclerotic plaques compared to normal tissue or earlier lesions. They demonstrated that additional RNA damage independent of RNAse activity can occur due to oxidative stress in the ROS-enriched environment of the plaque. Furthermore the iron deposited by intra-plaque haemorrhage may itself chemically cleave RNA[282]. These observations recommend that whole tissue RNA extraction from atherosclerotic plaques is undesirable and further supports our approach using LMD for the accurate isolation of specific cells in the plaque for gene expression analysis.

In a study by Lee and colleagues[298], they demonstrated that variation in RNA degradation was seen in different tissue types (gut tissue was the most prone to RNA degradation and CNS tissue was the most protected) as well as between post-mortem donors (due to differences in cause of death). Furthermore, progressive delay in RNA stabilisation by late snap-freezing for as little as three hours led to a significant loss in yield and quality[298]. This mirrors my observation of marked RNA degradation seen in inadequate snap-freezing (by pre-cooled copper plate) or its delay. These findings suggest that the advanced atherosclerotic plaque is an unstable tissue-type prone to RNA degradation, highlighting the importance of optimal specimen snap-freezing to protect the cells and RNA from additional damage. The inherent challenges of working with such 'unstable' tissue prone to RNA degradation explained the further optimisations required to generate high quality RNA from LMD of CEA specimens which were not necessary for the LMD of normal vessels.

7.2.2 Confounding RNA effects due to tissue ischaemia

The human tissues used in our study were from clinically stable patients at elective surgery. These 'living' tissues were collected immediately at the time of surgery in theatre. As a result, the total ischaemic time of the CEA specimens was short with a mean of 15

minutes (95%CI of 13.5-16.5 minutes). However, pprevious studies in atherosclerosis have used a variety of arterial tissues collected at varying times of tissue ischaemia and even after death. Diseased and normal arteries extracted at the time of vascular surgery[187, 189, 200, 215, 293-297, 299-302], at the time of transplant organ harvesting after early donor death or from the explanted heart of the transplant recipient[188, 200, 300, 302-305] and also postmortem tissue from 'fast' autopsy (collected within 24 hours of death)[216, 306] have been used in gene expression analysis (Table 46 and Table 47). This was mainly due to the lack of available tissue to study from the same source; for instance, early carotid lesions were only available from autopsy but ruptured carotid plaques were hardly available from this source. In order to overcome this, different arterial beds and/or different sources have been used and compared, introducing an added level of variability to (and possibly obscure) the results. In addition to the effects of RNA degradation, the transcriptomic changes which occur as a result of tissue ischaemia and death may alter the expression profile significantly. In a study comparing the gene expression profiles of whole advanced atherosclerotic plaques collected from autopsy and from surgery, Sluimer and colleagues have found that 3% of all the genes expressed in atherosclerotic tissue were statistically significantly differentially expressed even after multiple testing[307] caused by tissue ischaemia/death. In comparison, our study identified 4.6% of the genes expressed to be significantly differentially expressed in a comparison of 'living' macrophages in the stable and ruptured plaque, suggesting that a significant amount of genes are affected by tissue ischaemia/death, confounding the results generated from previous studies using such tissue. Genes involved in cell growth, nucleic acid metabolism and signal transduction to be mainly affected as well as cell adhesion, stress response, cell death, immune response and lipid metabolism genes were influenced by tissue ischaemia/death[307], which are also of interest in atherosclerosis. These arguments recommended the rapid snap-freezing of samples during collection with minimal delay from the time of tissue ischaemia to capture an accurate in-vivo transcriptomic profile of the plaque.

7.2.3 RNA damage is inherent in the atherosclerotic plaque

I have also found some variability in the RNA extracted from LMDed macrophages reflective of that seen in whole tissue RNA extraction. By retrospective analysis I identified celullarly degraded regions with poor histological nuclear definition of apoptotic or necrotic macrophage cells which have contributed to the extraction of degraded quality RNA to be avoided during LMD. Macrophage cell apoptosis in the plaque has previously been reported[111]. However, RNA degradation was also persistently seen in the VSMCs of the fibrous caps of advanced atherosclerotic plaques in both stable and ruptured lesions. Similar observations of increased RNA degradation in advanced atherosclerotic plaques

and increasingly so in highly inflamed and/or ruptured plaques were reported by Martinet and colleagues[282, 308]. However, by using whole tissues, they found it difficult to find a potential link between structural features of the plaque and RNA degradation[282]. My observations were more precisely focused to specific regions and cell-types in the plaque using LMD. I have found that RNA degradation was not limited to macrophages in inflamed ruptured plaques but was also seen in macrophages in stable fibrous cap atheromas.

The RNA damage observed in the atherosclerotic plaque can be caused not only by indigenous RNases but also by oxidative stress and intraplaque haemorrhage followed by iron deposition. Inflammation plays a major role in atherosclerosis with increased oxidative stress and production of reactive oxygen species which may in turn damage a wide variety of cellular components, including lipids, proteins and nucleic acids[67, 69, 309]. Oxidative DNA damage by ROS in the atherosclerotic plaque has been described[310] but its effect on RNA less so. Oxidative base damage of RNA is detrimental to its function and is frequently overlooked as it is more difficult to detect[308]. RNA oxidative damage have been detected in the cellular cytoplasm of macrophages, VMSCs and endothelial cells in thin fibrous cap atheroma immunohistochemically using a monoclonal antibody which recognises the 8-oxo-2'-deoxyguanosine residue; the marker for nucleic acid oxidative damage[282, 309, 310]. Furthermore, RNA is susceptible to free radical attack with almost complete degradation of total RNA with H_2O_2 and other free radical donors in-vitro[282]. Intraplaque haemorrhage, a common histological finding in advanced atherosclerotic plaques[9, 18], results in the deposition of large amounts of iron in the plaque. Free Fe(II) ions have been shown to cleave RNA in the absence of ROS in-vitro at 37°C and may also be implicated in RNA damage in the plaque.

I made an unexpected finding during the evaluation of the linear amplification of the moderately degraded RNA extracted from macrophage CD68 positive regions which also included these cellularly degraded and possibly apoptotic macrophages. If the poor RNA amplification was due only to poor RNA quality of the starting material, the amplification of 'perfect' spiked-in mRNA would not be influenced. However, the spiked-in amplification controls amplified with a significantly higher 3'/M and 3'/5' bias, suggesting that specific factors were present in the extracted material which may be degrading the spiked-in mRNA or inhibiting the amplification reactions. It is possible that factors such as RNases, ROS or Fe(II) ions from these necrotic/non-viable regions of the plaque were contaminating the extracted RNA.

These arguments suggest that RNA appears to be a major target of oxidative damage in the atherosclerotic plaque and is at present poorly understood. Further research is

required to get a better understanding of the role of RNA damage in atherosclerosis and plaque rupture.

7.2.4 Poor quality RNA extracted from VSMCs reflective of biological condition

I have consistently found that the quality of the RNA extracted from LMDed VSMCs of both the thick fibrous caps of stable plaques and of adjacent fibrous caps in ruptured plaques to be of poor quality even though of reasonable yield. I was uncertain if this was due to methodological limitations of extracting high quality RNA or reflective of the true biology of the fibrous caps. Only two previous microarray experiments have tried to isolate VSMCs in the fibrous cap of the plaque by macro-dissection using a scalpel and the isolated RNA was directly hybridised to microarrays without amplification[187, 302]. Two other studies used LMD to isolate intimal VSMCs from adjacent non-atheromatous vessel and medial VSMCs in the periphery of the lesion (but not VSMCs from the fibrous caps) for linear amplification and microarray profiling[215, 216]. Another 3 studies have used LMD to isolate RNA from VSMCs in pre-atheromatous intimal thickening lesions but not advanced plaques for RT-PCR[213, 214, 311]. However none of these studies assessed or reported the quality of the RNA extracted despite its importance. Although I have demonstrated that RNA of high quality and yield can be isolated from non-atherosclerotic medial VSMCs, to date no study has reported the successful use of LMD to isolate high quality RNA from VSMCs in the fibrous caps of advanced atheromatous lesions for RNA amplification and microarray.

The degraded RNA profiles of the VSMCs in the fibrous cap may be explained by the evidence of cellular senescence and apoptosis in the VMSCs. The VSMCs derived from atherosclerotic thickened intima proliferate more slowly, undergo earlier senescence and demonstrate higher levels of apoptosis in-vitro compared to VSMCs derived from the media[110]. VSMCs have been shown to express apoptotic markers including BAX, which are not present in pre-atheromatous intimal thickening of vessels, and are primed for cell death to occur with additional trigger signals present in advanced atherosclerotic plaques[312, 313]. Cellular apoptosis have been observed in both VSMCs and macrophages in the plaque and peak in advanced lesions[314]. In an animal model with selective induction of VSMC apoptosis, Clarke and colleagues have demonstrated that VSMC apoptosis in normal vessels were surprisingly resilient and demonstrated highly efficient clearance of apoptotic bodies. In contrast, VSMC apoptosis alone in atherosclerotic plaques was sufficient to induce multiple features of vulnerability to rupture such as fibrous cap thinning and increased apoptotic debris, necrotic core and inflammation[315]. The above findings may explain the degraded RNA isolated despite using highly optimised methods of LMD

and RNA extraction and is reflective of the biological condition of the VSMCs in the fibrous cap of the plaque.

7.2.5 Uniform cellular content

A critical factor in the design of the microarray experiment is the uniformity of the samples being compared with respect to the question being asked. Previous large-scale gene expression studies in atherosclerosis and in plaque rupture have mostly used whole vessel segments which made the interpretation of the findings difficult due to the cellular heterogeneity of the plaque (Table 46 and Table 47). The observed difference in gene expression may be a result of the differences seen in cellular composition between samples rather than a difference in gene expression of specific sub-populations of cells in the plaque. In order to address this issue, three different methods have been used to isolate uniform cell-type specific populations from the plaque; by macro-dissection, micro-dissection and cell culture.

Macro-dissection of the components of the atherosclerotic plaque (VSMC rich fibrous cap, media and non-atherosclerotic intima) was used in 2 previous studies[187, 302]. However this method was limited by the imprecise dissection of uniform cell-types especially from cellularly complex heterogenous regions of the plaque.

Techniques to culture pure cell-types after isolation from the vessel wall (as well as differentiated blood isolates) have also been previously employed[174, 185]. However, the major limitation of these methods were the inadvertent transcriptomic shift of gene expression profiles that would have occurred by in vitro cultures and would not be representative of the true biological situation. As a result, cell culture models of disease conditions were best suited in their role to test hypotheses and specific pathways[185].

Laser micro-dissection methods such as that employed in our study have the ability to isolate uniform cell-type regions for gene expression analysis with high precision. It has only been used in three previous human studies in atherosclerosis for large scale gene expression profiling- by Tuomisto and colleagues to study macrophage profiles in advanced atherosclerotic plaques compared to normal intima[216], by Volger and colleagues to study endothelial cell profiles in early versus advanced stage plaques[316], and by Martinet and colleagues to profile medial VSMCs in carotid endarterectomy samples[215]. LMD has not yet been applied to study plaque rupture. Tuomisto and colleagues used LMD to isolate macrophage-rich shoulder regions of stable atherosclerotic plaques and from VSMC-rich intima from adjacent diffuse intimal thickening regions from the same carotid endarterectomy sample. A second comparison was also made from expression profiling of PMA-stimulated vs unstimulated THP-1 derived macrophage cell cultures.

Although this study sought to identify gene expression changes from macrophages in atherosclerosis and not specifically to address plaque rupture, it did demonstrate similar dominant GO biological process themes of cell signalling and communication, cell structure and motility, and metabolism processes in the macrophages as that seen in our study; supporting our more focused observations of macrophage activity in plaque rupture.

7.2.6 Optimisation of the LMD and RNA technique

As only a few studies had applied LMD to atherosclerotic tissues at the start of our study[203, 212, 213, 215, 216] mainly as proof of principle and using varying protocols on different LMD platforms, a validated LMD protocol for gene expression studies on atherosclerotic tissue did not exist at the time. Since then another 4 studies have reported the use of LMD in atherosclerosis using other different protocols as well[214, 311, 316, 317]. I found that the original Leica RNA LMD protocol performed poorly on our tissues, particularly on the unstable advanced atherosclerotic plaque. As a result, I made significant modifications to achieve optimal results for CEA atherosclerotic tissue and vascular tissue LMD and also demonstrated that the RNA was stable on the prepared LMD sections. The optimisations of the LMD technique had to be made in parallel with the optimisations in the RNA extraction method adding another level of complexity.

Various fixatives have been used in the preparation of cryosections for LMD. In an evaluation study of the effects of fixation on RNA extraction from LMD tested on mouse liver tissue by Goldsworthy and colleagues[247], good results with high RNA yields were found using precipitive fixatives such as 70% Ethanol and produced better histological morphology corroborating our findings. Cross-linking fixatives such as 3% paraformaldehyde or 10% normal-buffered-formalin and paraffin embedding have produced the worst results in RNA yield and quality[247, 248]. Yet despite this 4% PFA and formalin have been used in previous LMD studies in atherosclerosis and without any assessment of RNA quality[214, 215, 316].

I found significant variation in RNA yield and quality with different histochemical stains. This was similarly observed by Okuducu and colleagues[249]. Other groups, in an effort to circumvent the problems with unoptimised histochemical staining, have sacrificed histological clarity and did not use any histochemical staining for their LMD[311, 316]. I demonstrated that with adequate fixation using the optimal LMD protocol developed, staining with haematoxylin did not cause any significant RNA degradation and produced similar results in RNA quality and yield compared to no staining.

Most of the LMD studies performed on atherosclerotic tissue have used silica-based RNA extraction kits[212, 214-216, 311, 317]. However, I found significant variability between the different silica-based extraction kits from different manufacturers, with variable success and a wide range in the efficiency of RNA extraction with the best results from the RNeasyMicro kit from Qiagen, highlighting the importance of the proper evaluation of these kits prior to its use.

7.2.7 Validation of RNA quality

A significant variability of the quality and quantity of the extracted RNA was encountered using whole tissue as well as in the variation (or poor optimisation) of LMD and RNA methodology. Despite being an important quality measure, RNA quality was checked in very few previous large-scale gene expression studies in atherosclerosis and actually reported in only two[294, 297] (Table 46 and Table 47). For example, in a study using samples of coronary plaque collected by therapeutic intracoronary directional cutting atherectomy[294], 19 of the 27 samples collected had significant RNA degradation and they were limited to the profiling of the remaining 8 samples of reasonable RNA quality only. In a study demonstrating the proof of principle of RNA extraction from LMD of VSMCs from normal arterial tissue[212], I was able to compare the Bioanalyser RNA electropherograms from my LMD extractions to that reported by them, demonstrating that the RNA isolated in my study is of higher quality, further ratifying that I have developed an optimal LMD and RNA extraction method.

7.2.8 Small sample amounts and linear amplification

Previous microarray studies in atherosclerosis isolated small amounts of RNA from limited amounts of tissue. As a result, it was necessary to pool individual samples to generate enough material for the experiment[187-189, 215, 216, 302]. This was evidently so in animal studies of atherosclerosis due to the limited tissue harvested from each animal[185]. The problem with this approach was that individual expression data necessary to describe the intrinsic variation of the samples was lost, preventing downstream statistical analysis of significance. Moreover so in laser micro-dissection (as well as in macro-dissection) was the isolation of relatively very small amounts of cells and RNA which was insufficient for microarray. In order to generate enough RNA without pooling, linear amplification methods employing T7 RNA polymerase have been employed. There had been various reports regarding the variability and reproducibility of amplification methods[318, 319]. However, further optimisations in the methodology have resulted in high accuracy and reproducibility. The Affymetrix microarray and its 2-cycle linear amplification protocol is a highly optimised and validated platform capable of producing robust and reliable large-

scale gene expression data[218, 250, 320]. High replicate correlation was seen from 2-cycle amplification of 10ng (r^2 of 0.96 to 0.98) and 100ng (r^2 of 0.98 to 0.99) of total-RNA demonstrating good reproducibility[250, 321]. Furthermore, the linear relationship of relative transcript abundance is also maintained[250] mirroring the results of the technical validation of our microarray results using qRTPCR. This is mostly due to the numerous QCA measures of quality and performance built into the system. In the only LMD study of atherosclerosis which have reported their QC parameters for microarray, Paul and colleagues have LMDed macrophages from atherosclerotic lesions in a mouse model of disease. In comparison, they had higher global scaling factors of an average of 3.5 (our average was 1.9) and GAPDH 3'/5' ratios of an average of 39.0 (our ratio was 6.82). This was surprising considering that they were using animal models of atherosclerosis and had greater control of experimental conditions and sample quality compared to that typically seen in clinical specimens. This demonstrated the high sample quality and amplification performance of our microarray study.

7.3 Analyses of the transcriptome in plaque rupture

7.3.1 LMDed cells had expression profiles of activated macrophages

Although I have endeavoured to isolate principally macrophages from the ruptured and stable plaques and avoided VSMCs (immuno-stained with SMA) and other cell types (not immuno-stained with CD68) using LMD, there remained the possibility of some contribution from these other cell types to the overall gene expression profiles. By comparing our samples with the gene expression profiles of 87 other human cell and tissue types, I have observed that our samples clustered with macrophage cell lines and separated from VSMCs, T and B-cells and other unrelated cell types, confirming that I have been largely successful in isolating macrophages from the atherosclerotic plaque. The clustering using sub-profiles generated using macrophage-specific genes showed our samples clustered with activated and differentiated macrophage cell lines and separated from other inflammatory and haematopoietic cell types found in the plaque, suggesting that the our population of LMDed macrophages from the plaque were mostly activated and differentiated macrophages.

This approach to verify cell uniformity and the isolation of specific cell types has not previously been used in microarray studies of atherosclerosis. The approaches used thus far involved the confirmation of the expression of a panel of macrophage specific genes like CD68, MMPs, macrophage colony stimulating factor receptor and cathepsins[216, 297]. Our data demonstrated the positive expression of these known macrophage genes.

However, these approaches would be affected by reporting bias in the selection of the genes to be tested. Moreover the absence in expression of some of the genes may reflect the underlying biology being studied rather than the failure of isolation of the correct cell type. On the contrary, the expression of genes known in other cell types may reflect yet undetermined expression in the cell type under interrogation. By using the whole transcriptome to generate the expression profiles, I had the unique ability to analyse the data in an unbiased and unsupervised manner in the determination of such relationships. Furthermore, these genomic analyses allowed us to measure the confidence in the observed clustering and separation using permutative statistical methods such as bootstrap analysis. This enabled us to demonstrate that our LMDed cells were principally from activated macrophages with a high confidence of 98% and were not from other cell types with a confidence of nearly 100%.

7.3.2 Unsupervised clustering confirmed ruptured and stable groups

I used two different methods of exploratory cluster analysis to describe and explore the dominant relationships in the gene expression profiles between the samples. The samples spontaneously separated into 2 groups clearly; as stable and ruptured plaques, which demonstrated the dominant gene expression differences seen were due to this relationship. As I have validated that I have isolated principally macrophage cells from the genomic expression profiles, this confirmed my hypothesis that differences in gene expression exist between the sub-population of macrophages under the fibrous caps of the stable and ruptured plaque rather than just a difference in the proportions of cell types which influence biological processes that may confer instability/stability to the plaque.

Such exploratory clustering methods performed prior to the pre-filtering of the datasets and inferential statistical analyses have the unique ability to describe dominant relationships in gene expression profiles between the samples without prior assumptions about the samples and allows for the examination of these relationships in an unbiased and unsupervised manner. Correlation to the principal categories of the study question can be made but moreover potential confounding relationships which may mask the biological gene expression differences of interest may also be observed. Despite the importance of exploring these relationships in genome-wide microarray experiments which are performed for hypothesis generation, these approaches have only been used in one previous microarray experiment in atherosclerosis. In a microarray study using whole atherosclerotic plaque tissue from macroscopically smooth (stable) and ulcerated (unstable) intimal surfaces of the plaque, Papaspyridopulos and colleagues[297] revealed dominant gene expression effects due to inter-individual differences using exploratory clustering methods by PCA, which may mask the smaller differences of gene expression

due to the principal comparison of plaque type (stable or unstable). There was a high intrinsic variance across the samples in their experiment which may be due to the cellular heterogeneity from using whole plaque tissue.

The microarray data also demonstrated low background and non-specific binding noise (the clustering observed was identical after removal of probesets which were absent which is the major contributor to the background noise in the experiment). There was also a high degree of sample homogeneity in the genome-wide expression profiles of our samples (the similarity measure using Pearson correlation across all the arrays using condition trees was 95%). A high similarity measure of ≥95% would be expected in uniform cell culture experiments and a measure of 90-95% from homogenous human tissue samples. Similarity measures of less than 85% were frequently observed from cellularly heterogenous human tissue samples (personal communication, Dr Ewan Hunter, GeneSpring, Agilent Technologies). The higher the similarity of the genome-wide profiles of the samples would reflect a lower intrinsic variance in the sample population enabling the increased resolution of gene expression changes due to the biology in question. The high similarity measure of our experiment comparable to cell culture experiments is ascribed to the uniform macrophage cell-type isolated using LMD in our study. The combination of low background noise and high similarity across our samples facilitated the clear clustering of our samples and the identification of statistically significant genes of differential expression.

I have also detected an increased heterogeneity in the expression profiles of the stable plaque which correlated to the differences in histological lesion classification of stable thick fibrous cap atheromata and stable thick fibrous cap fibrocalcific plaque. The main difference between these plaques were increased calcification of the lipid core and reduced cellularity seen in the fibrocalcific plaque. Although the numbers of samples involved were too small (4vs2) for any reasonable comparative statistical analysis, the PCA and CTD data would suggest that there were interesting differences in macrophage gene expression of these sub-groups which are worthy of further investigation.

7.3.3 Identification of genes of significant differential expression and regulated pathways

I have identified just under a thousand genes of differential expression with statistical significance even after correction for the error of multiple testing. The resultant genelist represents the complex differential expression profiles between stable and ruptured plaque macrophages and require more exploration and organisation to simplify its

contents further in order to gain insight into the differences in the biological activity of the macrophage in plaque rupture.

This could be simply done by ranking the genelist by the magnitude of gene expression fold-difference in relative transcript abundance using the assumption that the genes with large magnitudes in difference are likely to play major roles. Using this approach, I have identified a smaller set of 30 probesets (15 most highly ranked of higher expression in ruptured plaques and the other 15 of the most highly ranked in expression in stable plaques) which mapped to 23 known genes and 1 hypothetical protein-coding transcript. This is similar in approach to using a Volcano plot to rank and identify genes of interest for further examination[255, 322] and I have used this in the selection of 12 target genes of interest in the validation of the microarray data by qRTPCR. However, the main limitation of this method is that genes demonstrating a smaller magnitude of gene expression which may affect a significant biological effect were not identified and missed (especially if its role of action is at a critical part of a biological pathway, acting as a promoter or trigger to a cascade of activity)[322].

More complex approaches using bioinformatic techniques to analyse a genelist may be used which circumvents such issues. I used techniques to enrich the biological annotation and to look for associations between the genes to identify dominant biological gene and protein networks in the genelist. I also employed statistical methods to calculate the probability that the genes from a pathway or classification were differentially expressed as would be expected by chance, and also applied corrections for multiple testing error, increasing the confidence in our observations. By performing such bioinformatic analyses using the Genome Ontology database of biological process terms and the KEGG database of well curated biological pathways, I was able to identify biological processes and pathways which were differentially regulated with statistical confidence, and drew further insight into the biology of the macrophage in plaque stability/instability.

7.3.4 Cell signalling pathways are significantly regulated in plaque stability/instability

I found that the vast majority of the genes regulated in macrophages in both the stable and ruptured plaques were cell communication genes (40.5% of all differentially expressed genes with GO classification) and in particular signal transduction genes (30.6%). This majority was still observed when only the 470 probesets upregulated in the ruptured plaque were examined (35% and 31%) or when the 717 probesets upregulated in the stable plaque were examined (40% and 27%). This demonstrated that the majority of the differential expression of the genes between stable and ruptured plaques were

accounted for by cell signalling processes and different pathways were upregulated in the stable plaque and the unstable plaque. This was observed in the results of the pathway analysis; 11 of the 13 identified KEGG categories or pathways were in KEGG parent nodes of signal transduction (n=5), cell communication (n=3) and signalling molecules and interaction (n=3). And of the signalling pathways, the PPAR/Adipocytokine signalling pathway was the most significant and upregulated in the ruptured plaque and the TGF-beta signalling pathway and Wnt signalling pathway were upregulated in the stable plaque. This is of particular interest as it is possible that these pathways may play a causal role in macrophages in determining the stability or instability of the plaque.

7.3.5 Activated, scavenging and phagocytic phenotype in unstable plaque macrophages

I also found that the ruptured plaque macrophages had upregulation of genes involved in protein and cellular localisation (30% of the probesets upregulated in the ruptured plaque with GO annotations) with the biological sub-process terms of intra-cellular transport, vesicle-mediated transport, protein transport, golgi apparatus to endoplasmic reticulum vesicle transport, secretory and endocytotic processes significantly identified. Moreover, lipid metabolic processes were also significantly upregulated (10%). This is in keeping with the increased endocytosis of oxidised LDL via scavenger receptors and CD36[23, 34] and the increased lipid processing of the large lipid burden seen in the ruptured plaque[9, 18]. Consistent with this were the higher expression of scavenger receptors found in our genelist; scavenger receptor B1 (3.5 fold, p=0.01) and scavenger receptor B2 (1.4 fold, p=0.03). CD36 was of higher expression in the ruptured plaque as well (4 fold, p=0.04) but was not significant after multiple test correction. The upregulation of genes involved in the transport and secretion of various enzymes observed is further supported by the upregulation of genes involved in protein modification and phosphorylation (11%) and in defense, immune and stress responses (13 to 15%) reported. These findings are consistent with a highly activated, lipid engorged, phagocytic and secretory macrophage type in the unstable ruptured plaque.

7.3.6 Synthetic, migratory and remodeling phenotype in stable plaque macrophages

In the stable plaque macrophages, I found a subset of cell communication genes which were upregulated exclusive of the signal transduction sub-group, in cell adhesion (16%). These genes were similarly observed in the KEGG cell communication sub-groups of focal adhesion ($p=1.30x10^{-10}$), adherens junction ($p=1.41x10^{-10}$) and tight junction

($p=4.36x10^{-5}$). These KEGG groups are closely inter-related with common genes in two or more groups and all the three groups have common pathways to the KEGG pathway of cell motility and regulation of the actin cytoskeleton which was also identified to be significantly upregulated in stable plaques ($p=2.62x10^{-9}$). It is plausible that the macrophage phenotype in the stable plaque exhibit increased cellular motility and migration as focal adhesions are required for the structural and signalling communications between the cellular actin cytoskeleton and the extracellular matrix. Motile cells have dynamically changing focal adhesions, which are constantly being assembled at the leading edge and disassembled at the trailing edge[323]. This also explains the significant representation of the extracellular-matrix and receptor interaction KEGG group ($p=1.12x10^{-5}$) as the extracellular matrix interacts with the actin cytoskeleton involving the integrins[323]. There is increasing evidence that macrophage motility and its ability to emigrate from the atherosclerotic plaque is important in the regression of atherosclerosis by moving lipids, necrotic material and cells to regional lymph nodes[324, 325]. These findings suggest that the ability of the plaque macrophage to mobilise and emigrate may be important in maintaining the stability of the plaque.

The GO biological process of cell development were also significantly represented in the stable plaque macrophages with sub-groups in muscle, skeletal and bone development/remodelling identified along with extracellular matrix genes such as collagen, laminin, fibronectin and thrombospondin. This was initially interpreted as VSMC contamination from the LMD of the stable plaque. However, when I analysed the genelist to look for differential gene expression of a panel of VSMC marker genes which was previously used in a LMD study[316], of the 13 genes specific to VSMCs none were in our genelist except for one; vinculin. Vinculin is an actin filament binding protein involved in cell-matrix and cell-cell adhesion with a role in cell adhesion and migration. It is not specific to VSMCs and is expressed in various tissues and are found particularly in the podosomes of human macrophages[326]. This would suggest that these observations were not from VMSCs. On further study, it became apparent that these specific ECM subtypes were also expressed and secreted in macrophages[327]. Laminins, which are major components of basement membranes, specifically laminin γ1 and β1 were found to be upregulated in stable plaque macrophages in our data. The synthesis and secretion of laminin γ1, β1 and α4 have been found in macrophages/monocytes and played a major role in chemokine-induced migration of these cells[328, 329]. Fibronectin is also synthesised and secreted by macrophages to promote macromolecule opsonisation, adhesion to other ECM proteins and macrophage migration[330, 331]. Thrombospondin has also been shown to be secreted by macrophages and aid the binding of cell-cell and cell-matrix with fibrinogen, fibronectin, laminin, collagen and integrins[332]. The most interesting observation was that a variety of types of collagen were upregulated in the LMDed macrophages in

stable plaques in our study. The ECM collagen in the atherosclerotic plaque is known to be mostly derived from VSMCs and the macrophages are known to secrete metalloproteinases capable of degrading collagen[67, 69]. Little known is that macrophages can also synthesise ECM components such as fibronectin as well as the whole gamut of collagen types[333]. More specifically, human macrophages in the atherosclerotic plaque have been shown to secrete collagen VIII (COL8A1 was significantly expressed in stable plaques in our genelist as well), but decreased upon stimulation with LPS and IFNγ with the increased secretion of MMP1[334]. This demonstrated a switch of the macrophage from a collagen-producing to a degradative phenotype. Furthermore, I also found upregulated biological process sub-groups in biomineral formation, bone remodelling and ossification in the stable samples, suggesting calcification processes were upregulated in the stable plaques compared to the unstable plaques. All these findings would suggest that genes involved in the synthesis of extracellular matrix, calcification and remodelling were dominant in the stable plaque macrophages. Although there is evidence of ECM synthetic activity in macrophages as described above, double immunostaining or sequential immunostaining-in-situ-hybridisation techniques[330, 331] will be useful to confirm the specific differential expression of these ECM sub-types in stable plaque macrophages as well as VSMCs.

The organisation and description of the genes of differential expression allowed us to gain further insight into the activity in the plaque macrophage cell. The above observations and arguments suggest that the biological activity of the macrophage in the unstable plaque is very different than that in the stable plaque and almost polar opposites; of an activated, scavenging and phagocytic macrophage phenotype in the unstable plaque compared to a synthetic, migratory and remodelling phenotype in the stable plaque.

7.3.7 FABP4, Leptin and the PPAR-Adipocytokine signalling pathway

The PPAR/Adipocytokine signalling pathway is responsible for lipid metabolism and lipid-mediated processes with various metabolic and inflammatory effects, linking obesity, inflammation, hypertension, dyslipidaemia, insulin resistance, diabetes and atherosclerosis together, comprising the 'metabolic syndrome'[335]. The adipocytokines, namely leptin, resistin, adiponectin, TNFα and visfatin, are key trigger molecules which regulate the pathway via its respective membrane receptors with various metabolic and vascular effects. Fatty acid binding proteins (FABPs) are small intracellular proteins which bind free fatty acids to transcription factors of the peroxisome proliferator-activated receptor (PPAR) family and coordinate lipid responses in cells and regulate metabolic and inflammatory pathways. The PPAR/Adipocytokine signalling pathway and its key upstream components, FABP4 and Leptin were amongst the highest ranked upregulated

genes and the most significant upregulated signalling pathway in the ruptured plaque macrophage and is of specific interest as it may play a causal role in plaque instability.

Leptin

Leptin is the principal adipocytokine, which is mainly produced by adipocytes, and has central effects as a satiety signal to feeding centres in the hypothalamus (brain-gut axis). Accordingly, plasma levels are higher in obese persons. Recent studies have demonstrated that leptin has other important peripheral actions: for example, it is produced during inflammation, and can modulate the innate and adaptive immune responses[336, 337]. A variety of potential actions of leptin in the pathogenesis of atherosclerosis have been proposed - leptin promotes endothelial dysfunction, smooth muscle cell proliferation, platelet aggregation and the production of inflammatory cytokines. The leptin receptor is expressed in a wide range of tissue-types and as a result these peripheral effects are widespread[336, 337].

More recently other sources of Leptin have been reported; Leptin has been found to be synthesised and secreted gastric wall, vascular cells, placenta, ovary, skeletal muscle and liver [337]. Numerous studies have examined the direct effects of leptin on macrophages but leptin expression in macrophages itself is not well described. Only one publication had reported increased leptin immunoreactivity of alveolar macrophages was seen in COPD patients who smoked using immunocytochemistry[338]. Leptin was clearly expressed in our macrophage-rich areas. Using the publicly available microarray data of the gene expression profiles from 79 different tissues which I used in the macrophage expression signature analysis (GDS596 from GEO)[263] I found similar Leptin expression between peripheral blood monocytes and adipocytes (signals of 35 and 27 respectively). In comparison smooth muscle cells had low expression (signal of 4). Examination of other Affymetrix microarray expression profiles of monocyte, macrophage and stimulated macrophage cell cultures from the GEO microarray repository (GDS3203, GDS3203) also demonstrated Leptin expression with probeset signal strengths of 400 to 550, similar to our ranges. My analysis of publicly available microarray data have confirmed that others had also observed leptin to be expressed in macrophages.

Macrophages in human atherosclerotic plaques express the leptin receptor[339] and the downstream effects of Leptin mainly activated via the JAK/STAT pathway with translocation of STAT 1, 3, or 5 [336, 337] to the nucleus and activation of transcription. I found both STAT3 (2.1 fold) and STAT5 (1.7 fold) significantly upregulated in ruptured plaque macrophages in our genelist. Leptin downregulates the expression of PPARG in macrophages *in vitro*, an effect it has in common with FABP4[340], and it acts as a potent macrophage chemoattractant[341]. It also induces the release of other cytokines such as

TNFα, IL6, CCL2 and VEGF in monocytes and macrophages and promotes the proliferation and differentiation of monocytes to macrophages[337]. Leptin also has immuno-modulating effects on T-cells inducing the switch to Th1 cells with the cytokine production of TNFα, IFNγ and IL2 which further activates the surrounding macrophages[342]. Leptin has effects on macrophage lipid accumulation that are of potential importance in atherosclerosis: macrophages treated with leptin form cytoplasmic lipid bodies and synthesise the inflammatory eicosanoid leukotriene B4[343]. Macrophages from mice deficient in leptin (*ob/ob*) have a reduced capacity to accumulate cholesterol compared with wild type cells[344]. Moreover, an uncommon polymorphism in the leptin gene has been associated with carotid intima-medial thickness, a marker of atherosclerosis, in man[345].

Although these previous studies have investigated the consequences of the exogenous application of leptin to macrophages demonstrating its pro-atherogenic effects, none has explored the potential importance of autocrine/paracrine signalling by macrophage-derived leptin. Our results therefore suggest such signalling may promote intracellular lipid accumulation and inflammatory mediator production that predispose to plaque instability. The differences I observed in the expression of downstream signalling molecules in the leptin pathway such as RXR-alpha, STAT3, IRS, and Akt, reinforce the suggestion that this pathway is activated when plaques become unstable.

Li and colleagues have demonstrated that the pro-inflammatory cytokine production and proliferation of VSMCs caused by Leptin can be attenuated by metformin in cell culture studies[346]. Thiazolidinediones bind to PPARγ and can inhibit leptin expression[347]. These approaches to attenuate the pro-inflammatory effects of Leptin and down-regulate the adipocytokine pathway may have potential benefit in plaque stabilisation. Further experiments using mouse knockout models of atherosclerosis may demonstrate the attenuation of atherosclerotic progression using these drugs but the potential benefits of plaque stabilisation may not be realised as a good animal model of plaque rupture is still lacking.

Patients at high cardiovascular risk typically have high circulating levels of plasma leptin[348], which could also contribute to this process; however, differential levels of circulating leptin among our study participants would not confound our results. The relative importance of circulating leptin and macrophage-derived leptin in plaque instability cannot be quantified from our experiments; transplantation experiments using *ob/ob* mouse bone marrow would be of considerable interest in this regard.

FABP4

Fatty-acid binding protein 4 (FABP4; or adipocyte/macrophage fatty acid binding protein) was the gene most strongly differentially expressed in the ruptured plaque in our microarray experiment (28.1 fold). FABP4 is one of a family of at least nine lipid chaperones which co-ordinate lipid responses in cells affecting metabolic and inflammatory pathways[349]. The exact biological functions of the FABPs remain unknown. FABP4 is the family member expressed in adipocytes, macrophages and dendritic cells. In the macrophage, FABP4 attenuates cholesterol efflux via its inhibitory effect on the peroxisome proliferator-activated receptor gamma (PPARG) – liver X receptor-alpha (LXRa) – ATP binding cassette A1 (ABCA1) pathway[350]. PPARα and PPARγ are both expressed significantly in atherosclerotic plaque macrophages[351]. FABP4 also regulates inflammatory responses via the inhibitor of kappa-B kinase (IKK)/JNK pathway[350], and may be a key signalling molecule in the development of endoplasmic reticulum stress[349]. Mice that are double knockout for Apolipoprotein E (APOE) and FABP4 are protected from atherosclerosis compared to the APOE knockout alone[352, 353]; bone marrow transplantation studies have shown that this atheroprotective effect is mainly due to the absence of FABP4 in macrophages[353].

FABP4 is expressed in macrophages on differentiation from monocytes, and following activation with a number of different species *in vitro*[349, 353]. FABP4 expression in macrophages has been shown to be suppressed *in vitro* by the administration of statins[354], and macrophages from FABP4 knockout animals produce lower amounts of the cytokines TNF-alpha, interleukin 1-beta, interleukin-6 and monocyte chemoattractant protein-1[350]. A genetic polymorphism in the FABP4 promoter region results in diminished FABP4 expression in adipose tissue, and has been associated with reduced risk of diabetes and cardiovascular disease in man[355]. Furuhashi and colleagues have shown that chemical inhibition of FABP4 using the small molecule inhibitor BMS309403 in the APOE knockout mouse markedly reduced atheroma, and in particular macrophage foam cell formation[356]. In adipocyte cell cultures, the seed extract of Irvingia Gabonensis inhibited adipogenesis with the down-regulation of PPARγ and Leptin protein expression and upregulation of Adiponectin protein expression[357].

Macrophage expression of FABP4 has been shown by others, using multiple approaches, to be important in the development of atherosclerosis; our data in clinical specimens extends the phenotypic range of FABP4 involvement in disease to plaque instability. Inhibitors of FABP4 are potential therapeutic targets for plaque stabilisation but its assessment in animal models may be of limited scope as plaque rupture at present cannot be closely modelled in knockout mice. Future studies will be necessary to identify whether the up-regulation of FABP4 and leptin expression in unstable plaque

macrophages is driven by one or other of the two genes, or by an as yet unidentified genetic or epigenetic factor. Although there have been important recent insights regarding the mechanisms whereby FABP4 influences the atherosclerotic process, the local role of leptin remains little studied and requires further investigation.

7.3.8 Other target genes and pathways

The KEGG pathways of Wnt and TGF-beta signalling were less significantly differentially expressed in our samples than was the PPARG/Adipocytokine pathway. These pathways were both downregulated rather than upregulated in unstable samples, suggesting that they were less likely to reflect causal processes of plaque rupture but conversely may be associated with plaque stabilisation. The T-helper 3 cell (Th3) which produces TGF-β on activation has been found to be present in the plaque [81, 90]. TGF-β is highly fibrogenic and stimulates collagen synthesis as well as being potently anti-inflammatory[91] and may play a role in plaque stabilisation. A systematic analysis of the involvement of the Wnt pathways in atherosclerosis has not been performed. There has been no description of its involvement in plaque rupture. There is some evidence of the involvement of Wnt pathways in regulation of endothelial dysfunction and VSMC proliferation and migration, but it is not yet described in macrophages in atherosclerosis[358]. The systematic future investigation of the differentially expressed genes in these pathways would be of substantial interest.

7.3.9 Previous large-scale gene expression studies of atherosclerosis and plaque rupture

Most studies compared atheromatous with normal vessels

A substantial number of previous studies have quantified gene expression in human atherosclerosis using microarrays and other approaches (summarised in Table 46 and Table 47). Most have compared atheromatous with normal vessels (Table 46). These studies demonstrated recurrent themes in the profiling of gene expression of the advanced atherosclerotic plaque and have identified genes involved in inflammation, immune response, protein degradation (matrix degradation), apoptosis, cell proliferation and lipid processing. As the comparisons were mainly of whole tissues of diseased atherosclerotic plaque comprised mostly of macrophages, inflammatory cells, and lipid rich necrotic cores, to normal undiseased vessels comprised mostly of VSMCs, these observations reflected the activity of biological processes of the dominant cell type(s) profiled. While such comparisons are clearly of great interest, they are not specific for the

stage in the disease process that causes the majority of the acute morbidity and mortality of atherosclerosis, that is, plaque rupture.

Fewer studies compared stable with unstable plaques

Fewer previous studies have addressed plaque vulnerability and have been conducted on whole stable and unstable plaques (6 studies, Table 47)[189, 293-297]. While this approach has the potential to yield somewhat greater specificity for the pathophysiological process of plaque rupture, the results could still be significantly confounded by the differences in cell composition between stable and unstable lesions. Indeed, genes that would be consistent with the quantity of macrophages present in a lesion (for example inflammatory mediators, matrix metalloproteinases, pro-apoptotic factors) have been consistently reported as differentially expressed in such studies of whole stable and unstable plaques. There has been no study to date addressing plaque rupture using laser micro-dissection to isolate a uniform cell type for comparison and our study is novel in this approach.

Limited statistical significance

Half of the previous human studies in atherosclerosis and plaque rupture have not employed statistical measures but only ranked the magnitude of differential expression based on fold change (10 studies, Table 46) because their study design hindered such comparisons (e.g. pooling of the samples, small sample numbers, large intrinsic variance of samples due profiling whole tissues and imprecise sample phenotyping). This method has its advantages in its simplicity but it fails to demonstrate the statistical significance/confidence and reproducibility of the data.

The other 10 studies (Table 46 and Table 47) which have applied comparison statistical methods in their analysis had a limited ability to identify genes of differential expression due to the higher intrinsic variability from profiling whole tissue samples, and as a result it was frequently not possible to apply a correction for the error of multiple testing. Of the 20 studies, only 6 studies attempted to apply MTC to their results. Two studies failed to find final significance using MTC. They were both studies of plaque rupture using clinically phenotyped whole tissue samples. Only 4 studies of atherosclerosis have successfully utilised MTC in their analysis. None of the 6 studies in plaque rupture had multiple testing corrections performed and the number of genes identified to be significantly differentially expressed ranged from 6 to 289. In comparison our study identified 5,554 probesets of $p<0.05$ without MTC and 1,187 probesets with MTC using a FDR of 10% due to our cell specific approach, accurate sample phenotyping, optimisation of experimental processes and adequate sample numbers in our study.

Study	Sample Comparisons	Profiling method (no of probesets/ genes studied)	Donor details	Donor tissue	Principal Cell type	Cell/tissue isolation	RNA quality assessment	Sample data			Data analysis					Validation		Public Repository
								Donor Data	Clinical Data	Histological Classificatn	Samples pooled	Comparison Statistics	Multiple Test Correction	Gene Ontology	Pathway Analysis	RNA Validation	Protein Validation	
Tyson, 2002	Atherosclerosis	RDA (N/A)	Sx/ED/Tx	Multiple arteries	Mixed	Whole tissue	✖	✓	✖	✓	✖	N/A	N/A	✖	✖	✓	✓	✖
McCaffrey, 2000	Atherosclerosis	Microarray (588)	Sx (1hr delay)	Carotid artery	VSMC	Macrodissctn	Yes, not reported	✖	✖	✖	✓	✖	✖	✖	✖	✓	✓	✖
Zohlnhofer, 2001	Restenosis	Microarray (2435)	PCI/Sx/Tx	Multiple arteries	Mixed	Whole tissue	✖	✓	✓	✖	✖	✓	✖	✖	✖	✓	✓	✖
Hiltunen, 2002	Atherosclerosis	Microarray (18376)	Tx/ED	Multiple arteries	Mixed	Whole tissue	✖	✓	✖	✓	✓	✖	✖	✓	✖	✓	✓	✖
Martinet, 2002	Apoptosis	Nylon array (205)	Sx (immediate)	Carotid & IMA	Mixed/ VSMC	Whole tissue	✖	✓	✖	✖	✓	✖	✖	✖	✖	✓	✓	✖
Woodside, 2003	Apoptosis	Nylon array (205)	Sx (?delay)	Carotid artery	Mixed	Whole tissue	✖	✖	✖	✖	✖	✖	✖	✖	✖	✓	✖	✖
Archacki, 2003	Atherosclerosis	Microarray (12000)	Tx/ED	Coronary artery	Mixed	Whole tissue	Yes, not reported	✓	✖	✓	✖	✓	✖	other	✖	✓	✓	?
Tuomisto, 2003	Atherosclerosis	Microarray (6000)	Tx/ED/PM	Multiple arteries	Macro, VSMC	LMD and cell culture	✖	✓	✖	✓	✓	✖	✖	✓	✖	✓	✖	✖
Seo, 2004	Atherosclerosis	Microarray (12558)	PM	Aorta	Mixed	Whole tissue	Yes, not reported	✓	✖	✖	✖	class cluster	✖	✓	✖	✖	✖	✖
King, 2005	Atherosclerosis	Microarray (22000)	Tx/ED	Coronary artery	Mixed	Whole tissue	Yes, not reported	✓	✓	✓	✖	✓	✓	✓	✓	✖	✓	✖
Tabibiazar, 2005	Atherosclerosis	Microarray (22000)	Tx/ED	Coronary artery	Mixed	Whole tissue	Yes, not reported	✓	✖	✓	✖	✓	✓	✓	✓	✖	✖	✓
Adams, 2006	Atherosclerosis	Microarray (21000)	Sx/ED	Carotid artery	VSMC/ Mixed	WholeTissue Macrodissctn	✖	✓	✖	✓	✓	✓	✓	✖	✖	✖	✓	✖
Volger,	Atherosclerosis	Microarray	PM	Multiple	Endo-	LMD	✖	✓	✓	✓	✖	✓	✓	✖	✓	✖	✓	✖

Study	Sample Comparisons (no of samples)	Profiling Method (no of probesets/ genes studied)	Donor collection and delay?	Donor tissue	Principal Cell type	Cell/tissue isolation	RNA quality assessment	Sample data			Data analysis					Validation		Public Repository
								Donor Data	Clinical Data	Histological Classificatn	Samples pooled	Comparison Statistics	Multiple Test Correction	Gene Ontology	Pathway Analysis	RNA Validation	Protein Validation	
Randi, 2003	Symptoms of unstable angina (4vs4)	Nylon-array (482)	PCI (immediate)	Coronary artery	Mixed	Whole tissue	Yes, reported	✗	✓	✗	✗	✓	✗	✗	✗	✗	✗	✗
Vemuganti, 2005	Symptoms of stroke (6vs4)	Microarray (44860)	Surgery (?delay)	Carotid artery	Mixed	Whole tissue	✗	✓	✓	✗	✗	✓	✗	other	✗	✓	✗	✗
Dahl, 2007	Symptoms of stroke (4vs4)	Microarray (14500)	Surgery (immediate)	Carotid artery	Mixed	Whole tissue	✗	✓	✓	✗	✗	✓	✗*	✗	✗	✓	✓	✗
Ijas, 2006	Symptoms of stroke (4vs4)	Microarray (12600)	Surgery (?delay)	Carotid artery	Mixed	Whole tissue	✗	✓	✓	✗	✗	✗	✗*	other	✗*	✓	✓	✓
Papaspyr, 2006	Macroscopic plaque defect (4vs7#)	Microarray (44860)	Surgery (immediate)	Carotid artery	Mixed	Whole tissue	Yes, reported	✓	✗	✗	✗	✓	✗	✗	✗	✓	✓	✗
Faber, 2001	Histological plaque rupture (3vs3)	SSH (N/A)	Surgery (immediate)	Multiple arteries	Mixed	Whole tissue	✗	✓	✗	✓	✓	✗	N/A	✗	✗	✓	✓	✗

Table 47. Large scale human gene expression studies of plaque vulnerability (notes: ✗* attempted but unsuccessful; # multiple sampling from same specimen, PCI-percutaneous coronary intervention).

Sample sizes representative of its intrinsic variance

The sample size of 5 ruptured vs 6 stable samples profiled by microarray in our study, although relatively small in number as a result of the highly selective and accurate identification of stable/unstable samples using the 3 domain approach, was the largest number of samples profiled in comparison to previous studies of plaque rupture (Table 47). Previous power calculations performed by Wei and colleagues have recommended that 5 biological replicates would have 90% power to detect genes with 4-fold expression differences with a type 1 error rate of 0.01[270], and these numbers were comparable to the sample numbers studied in previous microarray experiments. However, these calculations were based on human gene expression data with a relatively high degree of background variability. Significant efforts were made in my study to minimise the intrinsic variance of the samples, such as accurate sample phenotyping, uniform cell type, high sample quality and experimental performance and an internally optimised and validated wet-lab and in-silico experimental protocol. I have demonstrated that I had genomic macrophage profiles of high similarity of 95% across our samples using CTD, closely approximating that of uniform human cell culture experiments. Furthermore, I was successful in identifying the largest set of genes of differential expression with statistical significance and multiple testing corrections compared to previous microarray studies in plaque rupture. I further strengthened the confidence in our microarray results by cross-validation experiments on a larger sample set in confirmation of the microarray findings. Although the sample numbers were relatively small in this study and it was unlikely that I have identified all the genes involved in plaque rupture, there was significant confidence in the microarray results and in the genes which I have identified in this study. These findings demonstrate that I was generally successful in my approach and study design.

Higher level analyses

It was not possible to perform higher level pathway analysis successfully in the previous studies in plaque rupture. For example, Ijas and colleagues[296] in their study of comparing whole symptomatic vs asymptomatic plaques applied their genelist to KEGG pathways and were not able to identify any pathways of significance. Only 3 studies in atherosclerosis applied pathway analysis in their data analysis successfully. They were successful in doing so by profiling large numbers of samples to address the high intrinsic variance observed using whole tissue samples[304, 305] or by the application of LMD for cell-specific profiling of endothelial cells[316]. There has been no microarray studies in plaque rupture which has successfully applied such higher level analyses successfully; our study was the first to be able to do so.

Accurate phenotyping of samples

Of the studies of plaque vulnerability, 3 studies used only the clinical symptoms of stroke to phenotype the samples as symptomatic or asymptomatic[293, 295, 296] which as I have demonstrated in my study, using the clinical phenotype alone was imprecise in the identification of the unstable/stable plaque. Features of plaque instability such as fibrous cap rupture or erosion with thrombosis and haemorrhage occur in both symptomatic and asymptomatic patients which may confound the findings have been well described[291, 359]. This was also observed in the histological analyses of the samples profiled by Ijas and colleagues[296]; three of the asymptomatic samples had evidence of plaque ulceration and two of the symptomatic samples had no evidence of ulceration or rupture. Moreover histological analysis was not performed in one study[295] limiting the interpretation of the data. In the study by Vemuganti and colleagues[293], the symptomatic and asymptomatic plaques studied were reported to have similar histological characteristics. Indeed, their findings were the most different in comparison to any of the other studies; they identified 289 transcripts only (from a 44k array; less than 0.7% of all the genes) which had a difference in expression ($p<0.05$ without MTC) which the majority (71%) were genes involved in cell proliferation and neoplastic processes. These findings underscores the importance of the accurate phenotyping of the samples in the identification of the stable and unstable lesions for gene expression study.

Similarity/differences in findings

These studies using whole tissue approaches to plaque rupture have not, in general, identified the genes yielded by our more cell-specific approach although, as might be expected, our results resemble those of previous studies to a degree. For example, Papaspyridonos and colleagues' study[297] of paired comparisons of whole tissue disrupted versus stable regions of the same carotid sample identified 170 differentially expressed genes, of which 33 were also identified to be differentially expressed in our study. Of the 170 genes, 130 were also expressed in our samples but were not identified to be differentially expressed by our cut-offs of statistical significance, using our more cell specific approach. However Papaspyridonos' study made multiple comparisons from the same plaque/individual; from 3 plaques from separate patients, rather than generating a pairwise comparison of 3 stable regions by 3 disrupted regions for analysis, a total of 11 samples were analysed (comprised of 4 stable regions and 7 disrupted regions) which falsified the assumption of independence of the samples. Furthermore the exploratory clustering revealed greater variation in gene expression from each separate patient compared to that of stable/disrupted regions of the plaque, masking the latter. This limited their analysis to intra-plaque comparisons rather than inter-plaque comparisons.

No previous study in plaque rupture or in atherosclerosis has identified the upregulation of the PPAR/adipocytokine signalling pathway that we describe. In the study by Dahl and colleagues[295] comparing symptomatic stroke patients with asymptomatic patients, both FABP4 and Leptin were in the their statistically significant genelist of 136 genes ($p<0.05$ but without MTC), supporting our findings. FABP4 was the highest in rank of fold change in differential expression (20 fold higher expression in symptomatic plaques) in their study. Our microarray data had a slightly higher fold difference of 28 using our cell-specific approach. Unfortunately they were not able to perform pathway analyses with the small number of genes identified; as a result they were unable to further specify and identify relevant pathways of significance from their results.

7.3.10 Microarray study design

In two influential reviews by Bijnens and Daemen[185], and Tuomisto and Yla-Herttuala[174], many critical issues in the design, methodology, analysis and interpretation of large scale gene expression studies in atherosclerosis were identified. This included a lack of detailed clinical and demographic information about sample donors and sample selection, the heterogeneity of sample donor tissue-type (carotid, aortic or radial, etc), sample collection (surgical or post-mortem) and the profiling of non-uniform cellular content. Many studies profiled pooled samples rather than individual specimens. The problem with this approach was that individual expression data necessary to describe the intrinsic variation of the samples was lost, preventing downstream statistical analysis of significance. They also recommended the use of appropriate statistical methodology including multiple testing correction, the employment of pathway-based analytical approaches and the validation of microarray findings by alternative methods and in replicate samples. Furthermore there has been a lack of the public availability of the microarray datasets which prohibits the further comparative analyses and in-silico experiments between studies. These various issues are summarised in Table 46 and Table 47, and discussed in the relevant sections earlier. Although these reviews were published at the time of the completion of my microarray experiments, my PhD study had successfully addressed and complied with all these important microarray design, methodology and data analysis issues.

7.3.11 Transcript abundance quantitation in validation

I found significant variation in efficiency of the qRTPCR chemistries and particularly in the reverse transcription reactions using different enzymes from separate manufacturers. The variation in efficiency of RT and the high efficiency of SSIII were also observed by others[360] corroborating my findings and more importantly emphasised the importance of my preliminary evaluation and optimisation work.

I then used a different method of priming of reverse transcription by using random hexamers in my qRTPCR work compared to the oligo-dT priming used in the linear amplification to generate the microarray results. This was performed to address the 3' bias and shorter amplified RNA product generated as a result of oligo-dT primed linear amplification which may cause biased microarray results when using conventional microarrays which were not designed to address this[361]. Kockx and colleagues also found significant difference in the quantitation of housekeeping genes between dT and rH-primed qRTPCR demonstrating the increased variation seen with dT-priming due to degradation and cleavage of mRNA transcripts[282]. Random hexamer priming is not susceptible to mild to moderate RNA degradation unlike oligo-dT priming. I demonstrated that rH-primed qRTPCR was able to quantitate transcript abundances with high precision (a low SD) and accuracy (similar Ct to other samples) in samples with evidence of partial RNA degradation. Furthermore the oligo-dT linearly amplified microarray results closely correlated with the rH-primed qRTPCR results (R=0.94) with a 1:1 relationship in magnitude of fold difference measured, demonstrating that the microarray results were not affected by any amplification bias or RNA degradation. By addressing the potential issues described above I have increased the robustness of my validation work lending further confidence in the interpretation of the microarray results.

7.3.12 The selection of stable reference control genes

The accurate relative quantitation of transcript abundance by qRTPCR is frequently performed by normalisation to an internal control gene. GAPDH, β-actin, 18S and 28S rRNA genes have been commonly used as single control genes in previous studies in atherosclerosis. However, numerous studies have demonstrated that these 'housekeeping genes' can have significantly variable expression[276, 362-364]. Previous conventional normalisation strategies using single control genes have been demonstrated to lead to erroneous normalisation of the results by up to 3 fold in 25% of cases[276] and in some cases as variable as 7 to 23 fold[365]. An internal control gene which is universally expressed, with a constant level of expression across all tissues, cells, experimental treatments and study designs does not exist[276, 362-364, 366]. The careful evaluation for control genes of stable expression according to the cell/tissue and disease/biology being studied and the use of two or more control genes are necessary for the accurate quantitation of transcript abundance[276].

The evaluation or the use of multiple control genes in atherosclerosis has not previously been established. About two thirds of previous microarray studies in atherosclerosis have validated their microarray results semi-quantitatively by RTPCR or quantitatively by real-time quantitative PCR and have only used a single control gene in normalisation. Only

one previous study used two control genes, similar to my approach[297]. However, as that study used whole plaque tissue, its results could not be extrapolated to our macrophage focused approach. Previous atherosclerosis studies commonly used GAPDH, β-actin, β2-microglobulin and ribosomal 18S as control genes which have since been demonstrated by others to be significantly variable in their expression[365, 366]. In my shortlisting of candidate control genes from the microarray data, β-actin failed selection due to its high variability. And GAPDH was the second most variable control gene from our panel of 7 candidates, mirroring the observations of others[365, 366]. In our evaluation, PPIA and SDHA were the control genes of most stable expression in plaque macrophages from stable and unstable lesions. This not only enabled accurate gene expression quantification in our study, but the methodological insights gained would be useful to future work in this field.

7.3.13 The biological validation of target genes of interest

In the biological cross-validation, the 14 additional samples studied were of lower rank in selection using the 3 domain enrichment criteria and were not as maximally contrasting samples of stable and unstable plaques as the 11 samples used in microarray. As a result, the fold change of the target genes tested on the total 25 samples were less in magnitude compared to the microarray results, but remained broadly similar in rank and statistically significant. This biological cross-validation performed on a larger and phenotypically more heterogenous cohort of stable and unstable lesions is a robust confirmation of our microarray results reflecting the wider clinical spectrum of stable and unstable plaque seen in 'real-world' settings.

The qRTPCR gene expression profiles examined in more detail using explorative unsupervised clustering by principal components analysis, revealed an interesting separation of the samples along an axis in three dimensional gene expression space. There was clustering of the samples according to a spectrum of clinical and histological characterisation of instability/stability; from the highly unstable recurrently symptomatic ruptured plaques, then the moderately unstable less acutely ruptured plaques, to the stable FCA and FCL plaques. This demonstrated differences in the programmed molecular processes and cellular activity/behaviour of the macrophages in these different sub-groups conferring stability or instability worthy of further study. Future microarray transcriptomic analysis of intermediate sub-groups such as the TFCA lesion type would be of significant interest.

7.4 Expression imaging in the stable and unstable plaque

7.4.1 Heterogeneity in protein expression of FABP4 and Leptin

Following the biological validation of gene expression of FABP4 and Leptin, I then confirmed the protein expression of Leptin and FABP4 in plaque macrophages and its increased protein expression in ruptured plaque macrophages compared to stable plaques. However, I also observed significant heterogeneity in the expression of these proteins from the macrophages within the lesion. In particular, the macrophages under the fibrous caps predominantly expressed Leptin and FABP4 in high amounts but less so in the macrophages within the lipid core, in the base or in the scattered or infiltrating macrophages outside of the lesion. This would suggest different sub-populations of macrophages, each with different dominant cellular programs or signalling, co-exist within the complex atherosclerotic plaque. There is some evidence from previous work in atherosclerosis of variation in protein expression from macrophages in the plaque suggesting that sub-populations of macrophages exist within the plaque. Dahl and colleagues found that Visfatin, another adipocytokine, was found to be only expressed in plaque macrophages within the lipid core but not by macrophages outside the core or adjacent to the lesion[295]. Further sub-populations of macrophages were also seen within the same lipid core by Ijas and colleagues[296]; they found that CD163, a macrophage marker of immune regulation and activation, was not expressed by all of the macrophages in the lesion but only in specific clusters of macrophages.

This is not surprising as the macrophage cell is capable of a wide range of biological functions ranging from its principal scavenging functions, its role in host defence and phagocytosis, its activity in immune/inflammatory modulation and response, its ability in chemotaxis and emigration, as well as its synthetic/secretory functions[367]. Although speculative, it may be that macrophages within the lipid core have a predominant role in oxidised lipid and necrotic debris scavenging and phagocytosis, macrophages infiltrating the fibrous cap and shoulder regions may have a dominant migratory phenotype, and macrophages under the stable thick fibrous cap or the vulnerable thin fibrous cap may play an important role in the maintenance of stability or promoting signalling and enzymatic cascades involved in the instability of the fibrous cap and consequent plaque rupture. The variation and preponderance of the protein expression of Leptin and FABP4, which are key upstream signalling proteins in the PPAR-Adipocytokine signalling pathway with pro-inflammatory, pro-atherosclerotic and lipid engorging effects, in the macrophages under the fibrous cap further supports our hypothesis of their potential causative role in plaque rupture.

7.4.2 Quantitative immunohistochemistry

I have initially demonstrated a difference in FABP4 and Leptin staining intensities between the macrophages under the thick and thin fibrous caps of stable and unstable plaques as well as a difference between the macrophages under the thin cap and the base of the lipid core in the same ruptured plaque. However these observations may have been due to the differences in macrophage numbers between the plaques as was observed by a lesser difference in CD68 staining. A semi-quantitative analysis with a correction for CD68 staining demonstrated a difference which did not quite achieve statistical significance. This may have been due to the lack of accuracy in the semi-quantitative method in the estimation of staining intensity and the small sample numbers (8vs5). Moreover, as the same samples were also used for LMD and gene expression work, the remaining tissues analysed for IHC were a considerable distance away from the region of interest, particularly in the ruptured plaques. I found that these lesions were of a more stable profile or a different lesion altogether. Of the 25 samples only 13 had suitable FFPE sections approximating the lesion type studied by gene expression. This may have resulted in a diluted difference in protein expression.

I have attempted to address the limitations of the semi-quantitative method by performing a more detailed and accurate quantitative protein expression analysis using Image-Pro Plus. However, in my pilot data of 4 unstable plaques comparing the signal intensities of FABP4 and Leptin of the macrophages under the thin cap to those at the base of the lipid core of the same lesions, I was not able to demonstrate a difference in signal intensity ratio to CD68. This was partly due to several methodological issues which had limited our ability to detect and quantify any differences. Firstly, there was significant contribution from background staining noise as a result of haematoxylin nuclear counterstaining. Next, there was a wide variability in signal intensities measured in replicates. Furthermore, a larger region was quantified due cell to cell variations seen in serial section comparison analysis and resulted in imprecise sampling with confounding higher background noise. I have also observed a significant variation of CD68 protein expression which I have used a protein expression reference control. This may be due to the technical variability in immuno-staining due to variations of epitope recovery, primary and secondary antibody incubation and to a shorter time of DAB staining[368, 369]. As CD68 epitope is localised to lysosomes and phagosomes in the macrophage cell, regulation in its phagocytic activity may result in variation in its protein expression (with higher CD68 expression in unstable vs stable)[370, 371]. CD68 had 2-fold higher expression in ruptured samples compared to stable samples in our microarray dataset (p=0.03 without MTC, not significant with MTC) and demonstrated differential expression with macrophage differentiation and activation by oxLDL[265]. It is possible that CD68 protein expression is not constant across

macrophages in the stable/unstable plaque and may not be a suitable protein expression reference control. Despite this, CD68 may still be satisfactorily used to detect the location/regions of macrophage cells to create an accurate template mask for signal quantitation of FABP4 and Leptin. In order to do this the same cells and section must be analysed. By using double immunohistochemical or immunofluorescence staining methods and avoiding haematoxylin nuclear counterstaining, it is possible to accurately and precisely isolate Leptin and FABP4 protein signal staining with low background noise and in the same cells expressing CD68. Although these preliminary findings were limited to only 4 samples and incomplete, they have provided important methodological insight for future quantitative immunohistochemistry protein expression studies in plaque rupture.

7.4.3 Three dimensional imaging of gene and protein expression in the atherosclerotic plaque

I have demonstrated the complex nature of the atherosclerotic plaque in its heterogeneity of cell constituents as well as the multiple lesion sub-types adjacent to and overlying each other in the plaque. I have also demonstrated complex and variable gene and protein expression in the various sub-populations of macrophages in the plaque. The limitations of the 2D transverse sections sampled at different regions in the plaque had previously made the interpretation of gene and protein expression difficult. Further detailed 3 dimensional gene or protein expression analysis of the entire plaque to aid the interpretation and analysis in any plane or virtual section would be of significant interest. Analysis and correlation of 3D gene and protein expression in reference to the cell constituents, plaque anatomy, lesion histology, flow dynamics and wall stress can be performed. By using Optical Projection Tomography, I have successfully generated 3D digital reconstructions of the radial artery and the atherosclerotic plaque for in-situ hybridisation gene expression and immunohistochemistry protein expression experiments. I have established the protocols for 3D Optical Projection Tomography analysis and have laid out the methodological roadmap for three dimensional study of any gene and protein the atherosclerotic plaque using OPT.

7.5 Limitations of the study

However, this study has certain methodological limitations. I was not able to fully explore the utility of TCD in the detection of unstable and stable plaques in my study due to the difficulties encountered in recruiting and performing TCD examinations. The recently completed Asymptomatic Carotid Emboli Study (ACES) reported an annual absolute risk of stroke of 3.62% in patients with embolic signals compared to 0.7% in those without[199], which supports the utility of TCD emboli detection in the functional assessment of plaque stability/instability and in the risk stratification of asymptomatic plaques for aggressive antiplatelet therapy and/or urgent CEA surgery. However as the authors point out, the availability of the technique is limited and its training is time consuming, limiting the widespread application of this technique, which mirrors our experience as well.

The laser micro-dissection approach we describe is technically challenging, and was therefore performed on only a limited number of samples. It was only feasible to LMD regions of uniform cellular types to isolate sufficient total-RNA without significant contamination of other cell types. Although I have sought to minimise the contamination of VSMCs in our macrophage LMD (<10% in the stable plaques), and our comparisons with publicly available sequence from macrophages clearly indicate the largely macrophage origin of our RNA, I cannot exclude a degree of contamination from other cell types intimately associated with the macrophage in the atheromatous plaque. This also hinders us from the study of other lesion types of greater cellular mix such as the PIT lesion and the LMD of other cell-types like T-cells or neutrophils, as I would need to isolate 25,000-40,000 cells to generate sufficient RNA of about 6-7ng/μl for amplification using the present technology. Future technological advancements in the successful and robust amplification from a few nanograms of starting material would be of great benefit and will make cell-by-cell LMD possible.

Although I applied an improved probe-level processing algorithm and normalisation using GCRMA, resulting in reduced variance and improved precision and accuracy, genes with only small fold changes between stable and unstable plaques would most likely not have been detected after the application of a multiple testing correction. The signal to noise ratio is made worse with RNA amplification. The relatively small sample size also limits the precision with which I can quantify the expression differences observed, as reflected by quite wide confidence intervals around the point estimates of fold change.

Another limitation of a microarray approach is the reliance on the design and quality of the array in its manufacturing process and technical quality, and it the representation of the genes studied. In our case, as yet uncharacterised probesets and genes are unlikely to be

represented our array. This is not a limitation with other approaches such as suppression subtractive hybridisation (SSH) or representational difference analysis (RDA). However these methods have their own limitations as they only identify genes of differential expression but the quantitation and statistical analysis of transcript abundance is not possible. With the advancements in microarray technology and its manufacturing process, high quality microarrays of high sensitivity, accuracy and precision can be produced. The high quality Affymetrix microarrays used in our study manufactured using photolithography methods fulfil many of these attributes.

7.6 Causality and future work

Expression differences between stable and unstable plaques do not alone imply causality, since our approach cannot distinguish expression differences occurring as a cause or consequence of plaque instability. Associations described in genetic-epidemiological studies between polymorphisms in the genes I have identified and disease endpoints would substantially reinforce the evidence in favour of causality, since these associations could not be confounded by the subsequent development of disease. Such associations with atherosclerosis related endpoints have been described for both leptin (with carotid intima-medial thickness) and FABP4 (with cardiovascular and diabetes risk). More generally, investigation of haplotype-tagging single nucleotide polymorphisms or rare sequence variants in some of the other genes I have found to be differentially expressed would be of interest. These could provide further evidence in favour of causal associations where specific pharmacological inhibitors or gene knockout animals are not available. In the case of FABP4, evidence from mouse models has shown that administration of a pharmacological FABP4 inhibitor is protective from atherosclerosis[356], adding further support to the idea that FABP4 plays a causal role in plaque instability. It is possible that FABP4 has a role in regulating leptin expression in macrophages; investigation of this possibility using the recently described specific FABP4 inhibitor would be of interest. There is some information regarding the regulation of macrophage leptin by metformin and thiazolidinodiones, as well as the regulatory effects on PPARγ, leptin and adipokinin by the seed extract of Irvingia Gabonensis, but these early findings are limited to cell culture studies and animal models of their regulatory effect has not yet been performed. Such future work would be of interest.

7.7 Conclusion

There are differences in gene expression signatures in macrophages from stable and unstable plaques which are independent of the differences in cellular constitution between them. There are genes and pathways which were statistically significant in differential expression between stable and unstable plaques, some of which may be causal in plaque vulnerability. Components of the PPARG/Adipocytokine signalling pathway and more specifically, its key regulating proteins FABP4 and Leptin are significantly upregulated in ruptured plaques and may play a role in plaque destabilisation leading on to rupture. Our results suggest that therapeutic efforts to downregulate the PPARG/Adipocytokine signalling pathway involving FABP4 and leptin may be a useful plaque stabilization strategy.

Conflicts of Interest

There are no conflicts of interest.

Sources of Funding

The work was funded by a Wellcome Clinical Research Training Fellowship awarded to KL.

References

1. Scarborough P, Bhatnagar P, Wickramasinghe K, Smolina K, Mitchell C, Rayner M. Coronary heart disease statistics. BHF: London; 2010.

2. Colyer WR, Jr., Cooper CJ. Cardiovascular morbidity and mortality and renal artery stenosis. *Progress in cardiovascular diseases.* 2009;52(3):238-242.

3. Aslam F, Haque A, Foody J, Lee LV. Peripheral arterial disease: current perspectives and new trends in management. *Southern medical journal.* 2009;102(11):1141-1149.

4. Poredos P, Jug B. The prevalence of peripheral arterial disease in high risk subjects and coronary or cerebrovascular patients. *Angiology.* 2007;58(3):309-315.

5. Steg PG, Bhatt DL, Wilson PW, D'Agostino R, Sr., Ohman EM, Rother J, Liau CS, Hirsch AT, Mas JL, Ikeda Y, Pencina MJ, Goto S. One-year cardiovascular event rates in outpatients with atherothrombosis. *Jama.* 2007;297(11):1197-1206.

6. *Collins English dictionary*. 4th ed. Glasgow: HarperCollins Publishers; 2000.

7. Davies MJ. Anatomic features in victims of sudden coronary death. Coronary artery pathology. *Circulation.* 1992;85(1 Suppl):I19-24.

8. Libby P, Ridker PM, Maseri A. Inflammation and Atherosclerosis. *Circulation.* 2002;105(9):1135-1143.

9. Stary HC, Chandler AB, Dinsmore RE, Fuster V, Glagov S, Insull W, Jr, Rosenfeld ME, Schwartz CJ, Wagner WD, Wissler RW. A Definition of Advanced Types of Atherosclerotic Lesions and a Histological Classification of Atherosclerosis : A Report From the Committee on Vascular Lesions of the Council on Arteriosclerosis, American Heart Association. *Circulation.* 1995;92(5):1355-1374.

10. Larner AJ. Caleb Hillier Parry (1755-1822): clinician, scientist, friend of Edward Jenner (1749-1823). *Journal of medical biography.* 2005;13(4):189-194.

11. Virchow R. *Cellular Pathology Based on Physiological and Pathological Histology*. Birmingham: Ala: Classics of Medicine Library; 1858.

12. Aschoff L. Die arteriosklerose. *Mediz Klinik.* 1930;Suppl 1:1-20.

13. Badimon L, Badimon JJ, Penny W, Webster MW, Chesebro JH, Fuster V. Endothelium and atherosclerosis. *J Hypertens Suppl.* 1992;10(2):S43-50.

14. Falk E, Fernandez-Ortiz A. Role of thrombosis in atherosclerosis and its complications. *Am J Cardiol.* 1995;75(6):3B-11B.

15. Ross R. The pathogenesis of atherosclerosis: a perspective for the 1990s. *Nature.* 1993;362(6423):801-809.

16. Stary HC, Chandler AB, Glagov S, Guyton JR, Insull W, Jr., Rosenfeld ME, Schaffer SA, Schwartz CJ, Wagner WD, Wissler RW. A definition of initial, fatty streak, and intermediate lesions of atherosclerosis. A report from the Committee on Vascular Lesions of the Council on Arteriosclerosis, American Heart Association. *Circulation.* 1994;89(5):2462-2478.

17. van der Wal AC, Becker AE, van der Loos CM, Das PK. Site of intimal rupture or erosion of thrombosed coronary atherosclerotic plaques is characterized by an inflammatory process irrespective of the dominant plaque morphology. *Circulation.* 1994;89(1):36-44.

18. Virmani R, Kolodgie FD, Burke AP, Farb A, Schwartz SM. Lessons from sudden coronary death: a comprehensive morphological classification scheme for atherosclerotic lesions. *Arterioscler Thromb Vasc Biol.* 2000;20(5):1262-1275.

19. Stary HC. Natural history and histological classification of atherosclerotic lesions: an update. *Arterioscler Thromb Vasc Biol.* 2000;20(5):1177-1178.

20. Lusis AJ. Atherosclerosis. *Nature.* 2000;407(6801):233-241.

21. Gimbrone MA, Jr. Vascular endothelium, hemodynamic forces, and atherogenesis. *The American journal of pathology.* 1999;155(1):1-5.

22. Boren J, Olin K, Lee I, Chait A, Wight TN, Innerarity TL. Identification of the principal proteoglycan-binding site in LDL. A single-point mutation in apo-B100 severely affects proteoglycan interaction without affecting LDL receptor binding. *The Journal of clinical investigation.* 1998;101(12):2658-2664.
23. Podrez EA, Febbraio M, Sheibani N, Schmitt D, Silverstein RL, Hajjar DP, Cohen PA, Frazier WA, Hoff HF, Hazen SL. Macrophage scavenger receptor CD36 is the major receptor for LDL modified by monocyte-generated reactive nitrogen species. *The Journal of clinical investigation.* 2000;105(8):1095-1108.
24. Goldstein JL, Ho YK, Basu SK, Brown MS. Binding site on macrophages that mediates uptake and degradation of acetylated low density lipoprotein, producing massive cholesterol deposition. *Proceedings of the National Academy of Sciences of the United States of America.* 1979;76(1):333-337.
25. Hegele RA. Paraoxonase genes and disease. *Annals of medicine.* 1999;31(3):217-224.
26. Dong ZM, Chapman SM, Brown AA, Frenette PS, Hynes RO, Wagner DD. The combined role of P- and E-selectins in atherosclerosis. *The Journal of clinical investigation.* 1998;102(1):145-152.
27. Collins RG, Velji R, Guevara NV, Hicks MJ, Chan L, Beaudet AL. P-Selectin or intercellular adhesion molecule (ICAM)-1 deficiency substantially protects against atherosclerosis in apolipoprotein E-deficient mice. *J Exp Med.* 2000;191(1):189-194.
28. Shih PT, Brennan ML, Vora DK, Territo MC, Strahl D, Elices MJ, Lusis AJ, Berliner JA. Blocking very late antigen-4 integrin decreases leukocyte entry and fatty streak formation in mice fed an atherogenic diet. *Circulation research.* 1999;84(3):345-351.
29. Gu L, Okada Y, Clinton SK, Gerard C, Sukhova GK, Libby P, Rollins BJ. Absence of monocyte chemoattractant protein-1 reduces atherosclerosis in low density lipoprotein receptor-deficient mice. *Molecular cell.* 1998;2(2):275-281.
30. Boring L, Gosling J, Cleary M, Charo IF. Decreased lesion formation in CCR2-/- mice reveals a role for chemokines in the initiation of atherosclerosis. *Nature.* 1998;394(6696):894-897.
31. Smith JD, Trogan E, Ginsberg M, Grigaux C, Tian J, Miyata M. Decreased atherosclerosis in mice deficient in both macrophage colony-stimulating factor (op) and apolipoprotein E. *Proceedings of the National Academy of Sciences of the United States of America.* 1995;92(18):8264-8268.
32. Marathe S, Kuriakose G, Williams KJ, Tabas I. Sphingomyelinase, an enzyme implicated in atherogenesis, is present in atherosclerotic lesions and binds to specific components of the subendothelial extracellular matrix. *Arterioscler Thromb Vasc Biol.* 1999;19(11):2648-2658.
33. Ivandic B, Castellani LW, Wang XP, Qiao JH, Mehrabian M, Navab M, Fogelman AM, Grass DS, Swanson ME, de Beer MC, de Beer F, Lusis AJ. Role of group II secretory phospholipase A2 in atherosclerosis: 1. Increased atherogenesis and altered lipoproteins in transgenic mice expressing group IIa phospholipase A2. *Arterioscler Thromb Vasc Biol.* 1999;19(5):1284-1290.
34. Suzuki H, Kurihara Y, Takeya M, Kamada N, Kataoka M, Jishage K, Ueda O, Sakaguchi H, Higashi T, Suzuki T, Takashima Y, Kawabe Y, Cynshi O, Wada Y, Honda M, Kurihara H, Aburatani H, Doi T, Matsumoto A, Azuma S, Noda T, Toyoda Y, Itakura H, Yazaki Y, Kodama T, et al. A role for macrophage scavenger receptors in atherosclerosis and susceptibility to infection. *Nature.* 1997;386(6622):292-296.
35. Velican D, Velican C. Atherosclerotic involvement of the coronary arteries of adolescents and young adults. *Atherosclerosis.* 1980;36(4):449-460.
36. Armstrong ML, Heistad DD, Megan MB, Lopez JA, Harrison DG. Reversibility of atherosclerosis. *Cardiovascular clinics.* 1990;20(3):113-126.
37. Strong JP, Malcom GT, McMahan CA, Tracy RE, Newman WP, 3rd, Herderick EE, Cornhill JF. Prevalence and extent of atherosclerosis in adolescents and young

adults: implications for prevention from the Pathobiological Determinants of Atherosclerosis in Youth Study. *Jama.* 1999;281(8):727-735.

38. Glagov S, Weisenberg E, Zarins CK, Stankunavicius R, Kolettis GJ. Compensatory enlargement of human atherosclerotic coronary arteries. *N Engl J Med.* 1987;316(22):1371-1375.

39. Schwartz SM, deBlois D, O'Brien ER. The intima. Soil for atherosclerosis and restenosis. *Circulation research.* 1995;77(3):445-465.

40. Shanahan CM, Weissberg PL. Smooth muscle cell phenotypes in atherosclerotic lesions. *Current opinion in lipidology.* 1999;10(6):507-513.

41. Stary HC. Atherosclerosis image library, http://www.atherosclerosis-image-library.at.

42. Farb A, Burke AP, Tang AL, Liang TY, Mannan P, Smialek J, Virmani R. Coronary plaque erosion without rupture into a lipid core. A frequent cause of coronary thrombosis in sudden coronary death. *Circulation.* 1996;93(7):1354-1363.

43. Wilcox JN, Smith KM, Schwartz SM, Gordon D. Localization of tissue factor in the normal vessel wall and in the atherosclerotic plaque. *Proceedings of the National Academy of Sciences of the United States of America.* 1989;86(8):2839-2843.

44. Davies MJ. A macro and micro view of coronary vascular insult in ischemic heart disease. *Circulation.* 1990;82(3 Suppl):II38-46.

45. Burke AP, Farb A, Malcom GT, Liang YH, Smialek J, Virmani R. Coronary risk factors and plaque morphology in men with coronary disease who died suddenly. *N Engl J Med.* 1997;336(18):1276-1282.

46. Davies MJ, Thomas AC. Plaque fissuring--the cause of acute myocardial infarction, sudden ischaemic death, and crescendo angina. *Br Heart J.* 1985;53(4):363-373.

47. Kolpakov V, Polishchuk R, Bannykh S, Rekhter M, Solovjev P, Romanov Y, Tararak E, Antonov A, Mironov A. Atherosclerosis-prone branch regions in human aorta: microarchitecture and cell composition of intima. *Atherosclerosis.* 1996;122(2):173-189.

48. Pittilo RM, Bull HA, Gulati S, Rowles PM, Blow CM, Machin SJ, Woolf N. Nicotine and cigarette smoking: effects on the ultrastructure of aortic endothelium. *International journal of experimental pathology.* 1990;71(4):573-586.

49. Yusuf S, Ounpuu S. Tackling the growing global burden of atherosclerotic cardiovascular diseases. *Eur J Cardiovasc Prev Rehabil.* 2003;10(4):236-239.

50. Yusuf S, Reddy S, Ounpuu S, Anand S. Global burden of cardiovascular diseases: part I: general considerations, the epidemiologic transition, risk factors, and impact of urbanization. *Circulation.* 2001;104(22):2746-2753.

51. Yusuf S, Reddy S, Ounpuu S, Anand S. Global burden of cardiovascular diseases: Part II: variations in cardiovascular disease by specific ethnic groups and geographic regions and prevention strategies. *Circulation.* 2001;104(23):2855-2864.

52. Fishbein MC, Siegel RJ. How big are coronary atherosclerotic plaques that rupture? *Circulation.* 1996;94(10):2662-2666.

53. Nissen SE, Gurley JC, Grines CL, Booth DC, McClure R, Berk M, Fischer C, DeMaria AN. Intravascular ultrasound assessment of lumen size and wall morphology in normal subjects and patients with coronary artery disease. *Circulation.* 1991;84(3):1087-1099.

54. Mann JM, Davies MJ. Assessment of the severity of coronary artery disease at postmortem examination. Are the measurements clinically valid? *Br Heart J.* 1995;74(5):528-530.

55. Gould KL, Lipscomb K. Effects of coronary stenoses on coronary flow reserve and resistance. *Am J Cardiol.* 1974;34(1):48-55.

56. Schaar JA, Muller JE, Falk E, Virmani R, Fuster V, Serruys PW, Colombo A, Stefanadis C, Ward Casscells S, Moreno PR, Maseri A, van der Steen AF. Terminology for high-risk and vulnerable coronary artery plaques. Report of a meeting on the vulnerable plaque, June 17 and 18, 2003, Santorini, Greece. *European heart journal.* 2004;25(12):1077-1082.

57. de Feyter PJ, Ozaki Y, Baptista J, Escaned J, Di Mario C, de Jaegere PP, Serruys PW, Roelandt JR. Ischemia-related lesion characteristics in patients with stable or unstable angina. A study with intracoronary angioscopy and ultrasound. *Circulation.* 1995;92(6):1408-1413.

58. Ellis S, Alderman E, Cain K, Fisher L, Sanders W, Bourassa M. Prediction of risk of anterior myocardial infarction by lesion severity and measurement method of stenoses in the left anterior descending coronary distribution: a CASS Registry Study. *Journal of the American College of Cardiology.* 1988;11(5):908-916.

59. Moise A, Lesperance J, Theroux P, Taeymans Y, Goulet C, Bourassa MG. Clinical and angiographic predictors of new total coronary occlusion in coronary artery disease: analysis of 313 nonoperated patients. *Am J Cardiol.* 1984;54(10):1176-1181.

60. Naghavi M, Libby P, Falk E, Casscells SW, Litovsky S, Rumberger J, Badimon JJ, Stefanadis C, Moreno P, Pasterkamp G, Fayad Z, Stone PH, Waxman S, Raggi P, Madjid M, Zarrabi A, Burke A, Yuan C, Fitzgerald PJ, Siscovick DS, de Korte CL, Aikawa M, Juhani Airaksinen KE, Assmann G, Becker CR, Chesebro JH, Farb A, Galis ZS, Jackson C, Jang I-K, Koenig W, Lodder RA, March K, Demirovic J, Navab M, Priori SG, Rekhter MD, Bahr R, Grundy SM, Mehran R, Colombo A, Boerwinkle E, Ballantyne C, Insull W, Jr, Schwartz RS, Vogel R, Serruys PW, Hansson GK, Faxon DP, Kaul S, Drexler H, Greenland P, Muller JE, Virmani R, Ridker PM, Zipes DP, Shah PK, Willerson JT. From Vulnerable Plaque to Vulnerable Patient: A Call for New Definitions and Risk Assessment Strategies: Part I. *Circulation.* 2003;108(14):1664-1672.

61. Naghavi M, Libby P, Falk E, Casscells SW, Litovsky S, Rumberger J, Badimon JJ, Stefanadis C, Moreno P, Pasterkamp G, Fayad Z, Stone PH, Waxman S, Raggi P, Madjid M, Zarrabi A, Burke A, Yuan C, Fitzgerald PJ, Siscovick DS, de Korte CL, Aikawa M, Airaksinen KE, Assmann G, Becker CR, Chesebro JH, Farb A, Galis ZS, Jackson C, Jang IK, Koenig W, Lodder RA, March K, Demirovic J, Navab M, Priori SG, Rekhter MD, Bahr R, Grundy SM, Mehran R, Colombo A, Boerwinkle E, Ballantyne C, Insull W, Jr., Schwartz RS, Vogel R, Serruys PW, Hansson GK, Faxon DP, Kaul S, Drexler H, Greenland P, Muller JE, Virmani R, Ridker PM, Zipes DP, Shah PK, Willerson JT. From vulnerable plaque to vulnerable patient: a call for new definitions and risk assessment strategies: Part II. *Circulation.* 2003;108(15):1772-1778.

62. Stone GW, Maehara A, Lansky AJ, de Bruyne B, Cristea E, Mintz GS, Mehran R, McPherson J, Farhat N, Marso SP, Parise H, Templin B, White R, Zhang Z, Serruys PW. A prospective natural-history study of coronary atherosclerosis. *N Engl J Med.* 2011;364(3):226-235.

63. Cheng GC, Loree HM, Kamm RD, Fishbein MC, Lee RT. Distribution of circumferential stress in ruptured and stable atherosclerotic lesions. A structural analysis with histopathological correlation. *Circulation.* 1993;87(4):1179-1187.

64. Fukumoto Y, Hiro T, Fujii T, Hashimoto G, Fujimura T, Yamada J, Okamura T, Matsuzaki M. Localized elevation of shear stress is related to coronary plaque rupture: a 3-dimensional intravascular ultrasound study with in-vivo color mapping of shear stress distribution. *Journal of the American College of Cardiology.* 2008;51(6):645-650.

65. Ku DN, Giddens DP, Zarins CK, Glagov S. Pulsatile flow and atherosclerosis in the human carotid bifurcation. Positive correlation between plaque location and low oscillating shear stress. *Arteriosclerosis (Dallas, Tex.* 1985;5(3):293-302.

66. Asakura T, Karino T. Flow patterns and spatial distribution of atherosclerotic lesions in human coronary arteries. *Circulation research.* 1990;66(4):1045-1066.

67. Libby P. Molecular bases of the acute coronary syndromes. *Circulation.* 1995;91(11):2844-2850.

68. Libby P. Current concepts of the pathogenesis of the acute coronary syndromes. *Circulation.* 2001;104(3):365-372.

69. Libby P. Molecular and cellular mechanisms of the thrombotic complications of atherosclerosis. *Journal of lipid research.* 2009;50 Suppl:S352-357.

70. Amento EP, Ehsani N, Palmer H, Libby P. Cytokines and growth factors positively and negatively regulate interstitial collagen gene expression in human vascular smooth muscle cells. *Arterioscler Thromb.* 1991;11(5):1223-1230.
71. Hansson GK, Holm J, Jonasson L. Detection of activated T lymphocytes in the human atherosclerotic plaque. *The American journal of pathology.* 1989;135(1):169-175.
72. Geng YJ, Henderson LE, Levesque EB, Muszynski M, Libby P. Fas is expressed in human atherosclerotic intima and promotes apoptosis of cytokine-primed human vascular smooth muscle cells. *Arterioscler Thromb Vasc Biol.* 1997;17(10):2200-2208.
73. Hansson GK, Jonasson L, Holm J, Clowes MM, Clowes AW. Gamma-interferon regulates vascular smooth muscle proliferation and Ia antigen expression in vivo and in vitro. *Circulation research.* 1988;63(4):712-719.
74. Warner SJ, Friedman GB, Libby P. Immune interferon inhibits proliferation and induces 2'-5'-oligoadenylate synthetase gene expression in human vascular smooth muscle cells. *The Journal of clinical investigation.* 1989;83(4):1174-1182.
75. Galis Z, Sukhova G, Kranzhofer R, Clark S, Libby P. Macrophage Foam Cells from Experimental Atheroma Constitutively Produce Matrix-Degrading Proteinases. *PNAS.* 1995;92(2):402-406.
76. Galis ZS, Sukhova GK, Lark MW, Libby P. Increased expression of matrix metalloproteinases and matrix degrading activity in vulnerable regions of human atherosclerotic plaques. *The Journal of clinical investigation.* 1994;94(6):2493-2503.
77. Henney AM, Wakeley PR, Davies MJ, Foster K, Hembry R, Murphy G, Humphries S. Localization of stromelysin gene expression in atherosclerotic plaques by in situ hybridization. *Proceedings of the National Academy of Sciences of the United States of America.* 1991;88(18):8154-8158.
78. Galis ZS, Muszynski M, Sukhova GK, Simon-Morrissey E, Unemori EN, Lark MW, Amento E, Libby P. Cytokine-stimulated human vascular smooth muscle cells synthesize a complement of enzymes required for extracellular matrix digestion. *Circulation research.* 1994;75(1):181-189.
79. Sukhova GK, Shi GP, Simon DI, Chapman HA, Libby P. Expression of the elastolytic cathepsins S and K in human atheroma and regulation of their production in smooth muscle cells. *The Journal of clinical investigation.* 1998;102(3):576-583.
80. Hansson GK. Immune Mechanisms in Atherosclerosis. *Arterioscler Thromb Vasc Biol.* 2001;21(12):1876-1890.
81. Frostegard J, Ulfgren AK, Nyberg P, Hedin U, Swedenborg J, Andersson U, Hansson GK. Cytokine expression in advanced human atherosclerotic plaques: dominance of pro-inflammatory (Th1) and macrophage-stimulating cytokines. *Atherosclerosis.* 1999;145(1):33-43.
82. Uyemura K, Demer LL, Castle SC, Jullien D, Berliner JA, Gately MK, Warrier RR, Pham N, Fogelman AM, Modlin RL. Cross-regulatory roles of interleukin (IL)-12 and IL-10 in atherosclerosis. *The Journal of clinical investigation.* 1996;97(9):2130-2138.
83. Ashkar S, Weber GF, Panoutsakopoulou V, Sanchirico ME, Jansson M, Zawaideh S, Rittling SR, Denhardt DT, Glimcher MJ, Cantor H. Eta-1 (osteopontin): an early component of type-1 (cell-mediated) immunity. *Science.* 2000;287(5454):860-864.
84. Loppnow H, Libby P. Proliferating or interleukin 1-activated human vascular smooth muscle cells secrete copious interleukin 6. *The Journal of clinical investigation.* 1990;85(3):731-738.
85. Seino Y, Ikeda U, Ikeda M, Yamamoto K, Misawa Y, Hasegawa T, Kano S, Shimada K. Interleukin 6 gene transcripts are expressed in human atherosclerotic lesions. *Cytokine.* 1994;6(1):87-91.
86. Bogdan C, Vodovotz Y, Paik J, Xie QW, Nathan C. Mechanism of suppression of nitric oxide synthase expression by interleukin-4 in primary mouse macrophages. *Journal of leukocyte biology.* 1994;55(2):227-233.

87. Mehindate K, al-Daccak R, Aoudjit F, Damdoumi F, Fortier M, Borgeat P, Mourad W. Interleukin-4, transforming growth factor beta 1, and dexamethasone inhibit superantigen-induced prostaglandin E2-dependent collagenase gene expression through their action on cyclooxygenase-2 and cytosolic phospholipase A2. *Laboratory investigation; a journal of technical methods and pathology.* 1996;75(4):529-538.

88. Pinderski Oslund LJ, Hedrick CC, Olvera T, Hagenbaugh A, Territo M, Berliner JA, Fyfe AI. Interleukin-10 blocks atherosclerotic events in vitro and in vivo. *Arterioscler Thromb Vasc Biol.* 1999;19(12):2847-2853.

89. Li AC, Glass CK. The macrophage foam cell as a target for therapeutic intervention. *Nat Med.* 2002;8(11):1235-1242.

90. McCaffrey TA, Du B, Consigli S, Szabo P, Bray PJ, Hartner L, Weksler BB, Sanborn TA, Bergman G, Bush HL, Jr. Genomic instability in the type II TGF-beta1 receptor gene in atherosclerotic and restenotic vascular cells. *The Journal of clinical investigation.* 1997;100(9):2182-2188.

91. Kulkarni AB, Huh CG, Becker D, Geiser A, Lyght M, Flanders KC, Roberts AB, Sporn MB, Ward JM, Karlsson S. Transforming growth factor beta 1 null mutation in mice causes excessive inflammatory response and early death. *Proceedings of the National Academy of Sciences of the United States of America.* 1993;90(2):770-774.

92. Salonen JT, Yla-Herttuala S, Yamamoto R, Butler S, Korpela H, Salonen R, Nyyssonen K, Palinski W, Witztum JL. Autoantibody against oxidised LDL and progression of carotid atherosclerosis. *Lancet.* 1992;339(8798):883-887.

93. Yla-Herttuala S, Palinski W, Butler SW, Picard S, Steinberg D, Witztum JL. Rabbit and human atherosclerotic lesions contain IgG that recognizes epitopes of oxidized LDL. *Arterioscler Thromb.* 1994;14(1):32-40.

94. Stemme S, Faber B, Holm J, Wiklund O, Witztum JL, Hansson GK. T lymphocytes from human atherosclerotic plaques recognize oxidized low density lipoprotein. *Proceedings of the National Academy of Sciences of the United States of America.* 1995;92(9):3893-3897.

95. Frostegard J, Wu R, Giscombe R, Holm G, Lefvert AK, Nilsson J. Induction of T-cell activation by oxidized low density lipoprotein. *Arterioscler Thromb.* 1992;12(4):461-467.

96. Zhou X, Caligiuri G, Hamsten A, Lefvert AK, Hansson GK. LDL immunization induces T-cell-dependent antibody formation and protection against atherosclerosis. *Arterioscler Thromb Vasc Biol.* 2001;21(1):108-114.

97. Xu Q, Dietrich H, Steiner HJ, Gown AM, Schoel B, Mikuz G, Kaufmann SH, Wick G. Induction of arteriosclerosis in normocholesterolemic rabbits by immunization with heat shock protein 65. *Arterioscler Thromb.* 1992;12(7):789-799.

98. George J, Shoenfeld Y, Afek A, Gilburd B, Keren P, Shaish A, Kopolovic J, Wick G, Harats D. Enhanced fatty streak formation in C57BL/6J mice by immunization with heat shock protein-65. *Arterioscler Thromb Vasc Biol.* 1999;19(3):505-510.

99. George J, Afek A, Gilburd B, Blank M, Levy Y, Aron-Maor A, Levkovitz H, Shaish A, Goldberg I, Kopolovic J, Harats D, Shoenfeld Y. Induction of early atherosclerosis in LDL-receptor-deficient mice immunized with beta2-glycoprotein I. *Circulation.* 1998;98(11):1108-1115.

100. George J, Harats D, Gilburd B, Afek A, Shaish A, Kopolovic J, Shoenfeld Y. Adoptive transfer of beta(2)-glycoprotein I-reactive lymphocytes enhances early atherosclerosis in LDL receptor-deficient mice. *Circulation.* 2000;102(15):1822-1827.

101. Mayr M, Metzler B, Kiechl S, Willeit J, Schett G, Xu Q, Wick G. Endothelial cytotoxicity mediated by serum antibodies to heat shock proteins of Escherichia coli and Chlamydia pneumoniae: immune reactions to heat shock proteins as a possible link between infection and atherosclerosis. *Circulation.* 1999;99(12):1560-1566.

102. Karmann K, Hughes CC, Schechner J, Fanslow WC, Pober JS. CD40 on human endothelial cells: inducibility by cytokines and functional regulation of adhesion

molecule expression. *Proceedings of the National Academy of Sciences of the United States of America.* 1995;92(10):4342-4346.
103. Mach F, Schonbeck U, Bonnefoy JY, Pober JS, Libby P. Activation of monocyte/macrophage functions related to acute atheroma complication by ligation of CD40: induction of collagenase, stromelysin, and tissue factor. *Circulation.* 1997;96(2):396-399.
104. Schonbeck U, Mach F, Sukhova GK, Murphy C, Bonnefoy JY, Fabunmi RP, Libby P. Regulation of matrix metalloproteinase expression in human vascular smooth muscle cells by T lymphocytes: a role for CD40 signaling in plaque rupture? *Circulation research.* 1997;81(3):448-454.
105. Schonbeck U, Mach F, Sukhova GK, Atkinson E, Levesque E, Herman M, Graber P, Basset P, Libby P. Expression of stromelysin-3 in atherosclerotic lesions: regulation via CD40-CD40 ligand signaling in vitro and in vivo. *J Exp Med.* 1999;189(5):843-853.
106. Mach F, Schonbeck U, Sukhova GK, Atkinson E, Libby P. Reduction of atherosclerosis in mice by inhibition of CD40 signalling. *Nature.* 1998;394(6689):200-203.
107. Lutgens E, Gorelik L, Daemen MJ, de Muinck ED, Grewal IS, Koteliansky VE, Flavell RA. Requirement for CD154 in the progression of atherosclerosis. *Nat Med.* 1999;5(11):1313-1316.
108. Han DK, Haudenschild CC, Hong MK, Tinkle BT, Leon MB, Liau G. Evidence for apoptosis in human atherogenesis and in a rat vascular injury model. *The American journal of pathology.* 1995;147(2):267-277.
109. Clarke M, Bennett M. Defining the role of vascular smooth muscle cell apoptosis in atherosclerosis. *Cell cycle (Georgetown, Tex.* 2006;5(20):2329-2331.
110. Bennett MR, Evan GI, Schwartz SM. Apoptosis of human vascular smooth muscle cells derived from normal vessels and coronary atherosclerotic plaques. *The Journal of clinical investigation.* 1995;95(5):2266-2274.
111. Kolodgie FD, Narula J, Burke AP, Haider N, Farb A, Hui-Liang Y, Smialek J, Virmani R. Localization of apoptotic macrophages at the site of plaque rupture in sudden coronary death. *The American journal of pathology.* 2000;157(4):1259-1268.
112. Bennett MR. Apoptosis of vascular smooth muscle cells in vascular remodelling and atherosclerotic plaque rupture. *Cardiovasc Res.* 1999;41(2):361-368.
113. Dhume AS, Soundararajan K, Hunter WJ, 3rd, Agrawal DK. Comparison of vascular smooth muscle cell apoptosis and fibrous cap morphology in symptomatic and asymptomatic carotid artery disease. *Annals of vascular surgery.* 2003;17(1):1-8.
114. Stoneman VE, Bennett MR. Role of apoptosis in atherosclerosis and its therapeutic implications. *Clin Sci (Lond).* 2004;107(4):343-354.
115. Leist M, Single B, Castoldi AF, Kuhnle S, Nicotera P. Intracellular adenosine triphosphate (ATP) concentration: a switch in the decision between apoptosis and necrosis. *J Exp Med.* 1997;185(8):1481-1486.
116. Bartling B, Tostlebe H, Darmer D, Holtz J, Silber RE, Morawietz H. Shear stress-dependent expression of apoptosis-regulating genes in endothelial cells. *Biochemical and biophysical research communications.* 2000;278(3):740-746.
117. Ignarro LJ, Napoli C. Novel features of nitric oxide, endothelial nitric oxide synthase, and atherosclerosis. *Current diabetes reports.* 2005;5(1):17-23.
118. Dimmeler S, Haendeler J, Galle J, Zeiher AM. Oxidized low-density lipoprotein induces apoptosis of human endothelial cells by activation of CPP32-like proteases. A mechanistic clue to the 'response to injury' hypothesis. *Circulation.* 1997;95(7):1760-1763.
119. Kim YM, Bombeck CA, Billiar TR. Nitric oxide as a bifunctional regulator of apoptosis. *Circulation research.* 1999;84(3):253-256.
120. Brookes PS, Salinas EP, Darley-Usmar K, Eiserich JP, Freeman BA, Darley-Usmar VM, Anderson PG. Concentration-dependent effects of nitric oxide on

mitochondrial permeability transition and cytochrome c release. *The Journal of biological chemistry.* 2000;275(27):20474-20479.

121. Buttery LD, Springall DR, Chester AH, Evans TJ, Standfield EN, Parums DV, Yacoub MH, Polak JM. Inducible nitric oxide synthase is present within human atherosclerotic lesions and promotes the formation and activity of peroxynitrite. *Laboratory investigation; a journal of technical methods and pathology.* 1996;75(1):77-85.

122. Chung HT, Pae HO, Choi BM, Billiar TR, Kim YM. Nitric oxide as a bioregulator of apoptosis. *Biochemical and biophysical research communications.* 2001;282(5):1075-1079.

123. Mason CA, Chang P, Fallery C, Rabinovitch M. Nitric oxide mediates LC-3-dependent regulation of fibronectin in ductus arteriosus intimal cushion formation. *Faseb J.* 1999;13(11):1423-1434.

124. Coleman KR, Braden GA, Willingham MC, Sane DC. Vitaxin, a humanized monoclonal antibody to the vitronectin receptor (alphavbeta3), reduces neointimal hyperplasia and total vessel area after balloon injury in hypercholesterolemic rabbits. *Circulation research.* 1999;84(11):1268-1276.

125. Karsan A, Yee E, Poirier GG, Zhou P, Craig R, Harlan JM. Fibroblast growth factor-2 inhibits endothelial cell apoptosis by Bcl-2-dependent and independent mechanisms. *The American journal of pathology.* 1997;151(6):1775-1784.

126. Zachary I, Mathur A, Yla-Herttuala S, Martin J. Vascular protection: A novel nonangiogenic cardiovascular role for vascular endothelial growth factor. *Arterioscler Thromb Vasc Biol.* 2000;20(6):1512-1520.

127. Patel VA, Zhang QJ, Siddle K, Soos MA, Goddard M, Weissberg PL, Bennett MR. Defect in insulin-like growth factor-1 survival mechanism in atherosclerotic plaque-derived vascular smooth muscle cells is mediated by reduced surface binding and signaling. *Circulation research.* 2001;88(9):895-902.

128. Griendling KK, Sorescu D, Ushio-Fukai M. NAD(P)H oxidase: role in cardiovascular biology and disease. *Circulation research.* 2000;86(5):494-501.

129. Harrison DG, Cai H, Landmesser U, Griendling KK. Interactions of angiotensin II with NAD(P)H oxidase, oxidant stress and cardiovascular disease. *J Renin Angiotensin Aldosterone Syst.* 2003;4(2):51-61.

130. Schmidt-Ott KM, Kagiyama S, Phillips MI. The multiple actions of angiotensin II in atherosclerosis. *Regul Pept.* 2000;93(1-3):65-77.

131. Betteridge DJ. What is oxidative stress? *Metabolism.* 2000;49(2 Suppl 1):3-8.

132. Kojda G, Harrison D. Interactions between NO and reactive oxygen species: pathophysiological importance in atherosclerosis, hypertension, diabetes and heart failure. *Cardiovasc Res.* 1999;43(3):562-571.

133. Napoli C, de Nigris F, Palinski W. Multiple role of reactive oxygen species in the arterial wall. *J Cell Biochem.* 2001;82(4):674-682.

134. Radi R, Beckman JS, Bush KM, Freeman BA. Peroxynitrite-induced membrane lipid peroxidation: the cytotoxic potential of superoxide and nitric oxide. *Arch Biochem Biophys.* 1991;288(2):481-487.

135. Napoli C, Quehenberger O, De Nigris F, Abete P, Glass CK, Palinski W. Mildly oxidized low density lipoprotein activates multiple apoptotic signaling pathways in human coronary cells. *Faseb J.* 2000;14(13):1996-2007.

136. Rusinol AE, Thewke D, Liu J, Freeman N, Panini SR, Sinensky MS. AKT/protein kinase B regulation of BCL family members during oxysterol-induced apoptosis. *The Journal of biological chemistry.* 2004;279(2):1392-1399.

137. Aviram M. Review of human studies on oxidative damage and antioxidant protection related to cardiovascular diseases. *Free Radic Res.* 2000;33 Suppl:S85-97.

138. Salvayre R, Auge N, Benoist H, Negre-Salvayre A. Oxidized low-density lipoprotein-induced apoptosis. *Biochimica et biophysica acta.* 2002;1585(2-3):213-221.

139. Yao PM, Tabas I. Free cholesterol loading of macrophages is associated with widespread mitochondrial dysfunction and activation of the mitochondrial

apoptosis pathway. *The Journal of biological chemistry.* 2001;276(45):42468-42476.

140. Asmis R, Begley JG. Oxidized LDL promotes peroxide-mediated mitochondrial dysfunction and cell death in human macrophages: a caspase-3-independent pathway. *Circulation research.* 2003;92(1):e20-29.

141. Henderson EL, Geng YJ, Sukhova GK, Whittemore AD, Knox J, Libby P. Death of smooth muscle cells and expression of mediators of apoptosis by T lymphocytes in human abdominal aortic aneurysms. *Circulation.* 1999;99(1):96-104.

142. Slowik MR, Min W, Ardito T, Karsan A, Kashgarian M, Pober JS. Evidence that tumor necrosis factor triggers apoptosis in human endothelial cells by interleukin-1-converting enzyme-like protease-dependent and -independent pathways. *Laboratory investigation; a journal of technical methods and pathology.* 1997;77(3):257-267.

143. Marx N, Sukhova GK, Collins T, Libby P, Plutzky J. PPARalpha activators inhibit cytokine-induced vascular cell adhesion molecule-1 expression in human endothelial cells. *Circulation.* 1999;99(24):3125-3131.

144. Marx N, Mackman N, Schonbeck U, Yilmaz N, Hombach V, Libby P, Plutzky J. PPARalpha activators inhibit tissue factor expression and activity in human monocytes. *Circulation.* 2001;103(2):213-219.

145. Neve BP, Corseaux D, Chinetti G, Zawadzki C, Fruchart JC, Duriez P, Staels B, Jude B. PPARalpha agonists inhibit tissue factor expression in human monocytes and macrophages. *Circulation.* 2001;103(2):207-212.

146. Rubins HB, Robins SJ, Collins D, Fye CL, Anderson JW, Elam MB, Faas FH, Linares E, Schaefer EJ, Schectman G, Wilt TJ, Wittes J. Gemfibrozil for the secondary prevention of coronary heart disease in men with low levels of high-density lipoprotein cholesterol. Veterans Affairs High-Density Lipoprotein Cholesterol Intervention Trial Study Group. *N Engl J Med.* 1999;341(6):410-418.

147. de Lorgeril M, Salen P, Martin JL, Monjaud I, Delaye J, Mamelle N. Mediterranean diet, traditional risk factors, and the rate of cardiovascular complications after myocardial infarction: final report of the Lyon Diet Heart Study. *Circulation.* 1999;99(6):779-785.

148. Lee H, Shi W, Tontonoz P, Wang S, Subbanagounder G, Hedrick CC, Hama S, Borromeo C, Evans RM, Berliner JA, Nagy L. Role for peroxisome proliferator-activated receptor alpha in oxidized phospholipid-induced synthesis of monocyte chemotactic protein-1 and interleukin-8 by endothelial cells. *Circulation research.* 2000;87(6):516-521.

149. Barroso I, Gurnell M, Crowley VE, Agostini M, Schwabe JW, Soos MA, Maslen GL, Williams TD, Lewis H, Schafer AJ, Chatterjee VK, O'Rahilly S. Dominant negative mutations in human PPARgamma associated with severe insulin resistance, diabetes mellitus and hypertension. *Nature.* 1999;402(6764):880-883.

150. Ricote M, Huang J, Fajas L, Li A, Welch J, Najib J, Witztum JL, Auwerx J, Palinski W, Glass CK. Expression of the peroxisome proliferator-activated receptor gamma (PPARgamma) in human atherosclerosis and regulation in macrophages by colony stimulating factors and oxidized low density lipoprotein. *Proceedings of the National Academy of Sciences of the United States of America.* 1998;95(13):7614-7619.

151. Jiang C, Ting AT, Seed B. PPAR-gamma agonists inhibit production of monocyte inflammatory cytokines. *Nature.* 1998;391(6662):82-86.

152. Tontonoz P, Nagy L, Alvarez JG, Thomazy VA, Evans RM. PPARgamma promotes monocyte/macrophage differentiation and uptake of oxidized LDL. *Cell.* 1998;93(2):241-252.

153. Han Y, Runge MS, Brasier AR. Angiotensin II induces interleukin-6 transcription in vascular smooth muscle cells through pleiotropic activation of nuclear factor-kappa B transcription factors. *Circulation research.* 1999;84(6):695-703.

154. Hernandez-Presa M, Bustos C, Ortego M, Tunon J, Renedo G, Ruiz-Ortega M, Egido J. Angiotensin-converting enzyme inhibition prevents arterial nuclear factor-kappa B activation, monocyte chemoattractant protein-1 expression, and

macrophage infiltration in a rabbit model of early accelerated atherosclerosis. *Circulation.* 1997;95(6):1532-1541.

155. Kranzhofer R, Browatzki M, Schmidt J, Kubler W. Angiotensin II activates the proinflammatory transcription factor nuclear factor-kappaB in human monocytes. *Biochemical and biophysical research communications.* 1999;257(3):826-828.

156. Rocha R, Stier CT, Jr., Kifor I, Ochoa-Maya MR, Rennke HG, Williams GH, Adler GK. Aldosterone: a mediator of myocardial necrosis and renal arteriopathy. *Endocrinology.* 2000;141(10):3871-3878.

157. Yusuf S, Sleight P, Pogue J, Bosch J, Davies R, Dagenais G. Effects of an angiotensin-converting-enzyme inhibitor, ramipril, on cardiovascular events in high-risk patients. The Heart Outcomes Prevention Evaluation Study Investigators. *N Engl J Med.* 2000;342(3):145-153.

158. Aikawa M, Rabkin E, Okada Y, Voglic SJ, Clinton SK, Brinckerhoff CE, Sukhova GK, Libby P. Lipid lowering by diet reduces matrix metalloproteinase activity and increases collagen content of rabbit atheroma: a potential mechanism of lesion stabilization. *Circulation.* 1998;97(24):2433-2444.

159. Aikawa M, Sugiyama S, Hill CC, Voglic SJ, Rabkin E, Fukumoto Y, Schoen FJ, Witztum JL, Libby P. Lipid lowering reduces oxidative stress and endothelial cell activation in rabbit atheroma. *Circulation.* 2002;106(11):1390-1396.

160. Aikawa M, Rabkin E, Sugiyama S, Voglic SJ, Fukumoto Y, Furukawa Y, Shiomi M, Schoen FJ, Libby P. An HMG-CoA reductase inhibitor, cerivastatin, suppresses growth of macrophages expressing matrix metalloproteinases and tissue factor in vivo and in vitro. *Circulation.* 2001;103(2):276-283.

161. Colli S, Eligini S, Lalli M, Camera M, Paoletti R, Tremoli E. Vastatins inhibit tissue factor in cultured human macrophages. A novel mechanism of protection against atherothrombosis. *Arterioscler Thromb Vasc Biol.* 1997;17(2):265-272.

162. MRC/BHF Heart Protection Study of cholesterol lowering with simvastatin in 20,536 high-risk individuals: a randomised placebo-controlled trial. *Lancet.* 2002;360(9326):7-22.

163. Ridker PM, Rifai N, Pfeffer MA, Sacks F, Braunwald E. Long-term effects of pravastatin on plasma concentration of C-reactive protein. The Cholesterol and Recurrent Events (CARE) Investigators. *Circulation.* 1999;100(3):230-235.

164. Ridker PM, Cannon CP, Morrow D, Rifai N, Rose LM, McCabe CH, Pfeffer MA, Braunwald E. C-reactive protein levels and outcomes after statin therapy. *N Engl J Med.* 2005;352(1):20-28.

165. Ridker PM, Rifai N, Clearfield M, Downs JR, Weis SE, Miles JS, Gotto AM, Jr. Measurement of C-reactive protein for the targeting of statin therapy in the primary prevention of acute coronary events. *N Engl J Med.* 2001;344(26):1959-1965.

166. Ridker PM, Danielson E, Fonseca FA, Genest J, Gotto AM, Jr., Kastelein JJ, Koenig W, Libby P, Lorenzatti AJ, MacFadyen JG, Nordestgaard BG, Shepherd J, Willerson JT, Glynn RJ. Rosuvastatin to prevent vascular events in men and women with elevated C-reactive protein. *N Engl J Med.* 2008;359(21):2195-2207.

167. Arslan F, Pasterkamp G, de Kleijn DP. Unraveling pleiotropic effects of statins: bit by bit, a slow case with perspective. *Circulation research.* 2008;103(4):334-336.

168. Libby P, Aikawa M, Jain MK. Vascular endothelium and atherosclerosis. *Handbook of experimental pharmacology.* 2006(176 Pt 2):285-306.

169. Ray KK, Cannon CP. Early time to benefit with intensive statin treatment: could it be the pleiotropic effects? *Am J Cardiol.* 2005;96(5A):54F-60F.

170. Schonbeck U, Libby P. Inflammation, immunity, and HMG-CoA reductase inhibitors: statins as antiinflammatory agents? *Circulation.* 2004;109(21 Suppl 1):II18-26.

171. Wang CY, Liu PY, Liao JK. Pleiotropic effects of statin therapy: molecular mechanisms and clinical results. *Trends in molecular medicine.* 2008;14(1):37-44.

172. Endres M, Laufs U, Huang Z, Nakamura T, Huang P, Moskowitz MA, Liao JK. Stroke protection by 3-hydroxy-3-methylglutaryl (HMG)-CoA reductase inhibitors mediated by endothelial nitric oxide synthase. *Proceedings of the National Academy of Sciences of the United States of America.* 1998;95(15):8880-8885.

173. Bourcier T, Libby P. HMG CoA reductase inhibitors reduce plasminogen activator inhibitor-1 expression by human vascular smooth muscle and endothelial cells. *Arterioscler Thromb Vasc Biol.* 2000;20(2):556-562.
174. Tuomisto TT, Binder BR, Yla-Herttuala S. Genetics, genomics and proteomics in atherosclerosis research. *Annals of medicine.* 2005;37(5):323-332.
175. Brasier AR, Recinos A, 3rd, Eledrisi MS. Vascular inflammation and the renin-angiotensin system. *Arterioscler Thromb Vasc Biol.* 2002;22(8):1257-1266.
176. Dechend R, Fiebler A, Lindschau C, Bischoff H, Muller D, Park JK, Dietz R, Haller H, Luft FC. Modulating angiotensin II-induced inflammation by HMG Co-A reductase inhibition. *Am J Hypertens.* 2001;14(6 Pt 2):55S-61S.
177. Fabunmi RP, Sukhova GK, Sugiyama S, Libby P. Expression of tissue inhibitor of metalloproteinases-3 in human atheroma and regulation in lesion-associated cells: a potential protective mechanism in plaque stability. *Circulation research.* 1998;83(3):270-278.
178. Gerdes N, Sukhova GK, Libby P, Reynolds RS, Young JL, Schonbeck U. Expression of interleukin (IL)-18 and functional IL-18 receptor on human vascular endothelial cells, smooth muscle cells, and macrophages: implications for atherogenesis. *J Exp Med.* 2002;195(2):245-257.
179. Mallat Z, Corbaz A, Scoazec A, Besnard S, Leseche G, Chvatchko Y, Tedgui A. Expression of interleukin-18 in human atherosclerotic plaques and relation to plaque instability. *Circulation.* 2001;104(14):1598-1603.
180. Mallat Z, Heymes C, Ohan J, Faggin E, Leseche G, Tedgui A. Expression of interleukin-10 in advanced human atherosclerotic plaques: relation to inducible nitric oxide synthase expression and cell death. *Arterioscler Thromb Vasc Biol.* 1999;19(3):611-616.
181. Schieffer B, Schieffer E, Hilfiker-Kleiner D, Hilfiker A, Kovanen PT, Kaartinen M, Nussberger J, Harringer W, Drexler H. Expression of angiotensin II and interleukin 6 in human coronary atherosclerotic plaques: potential implications for inflammation and plaque instability. *Circulation.* 2000;101(12):1372-1378.
182. Moody DE. Genomics techniques: An overview of methods for the study of gene expression. *J. Anim Sci.* 2001;79(E-Suppl):E128-135.
183. Hilfiker A, Hilfiker-Kleiner D, Fuchs M, Kaminski K, Lichtenberg A, Rothkotter HJ, Schieffer B, Drexler H. Expression of CYR61, an angiogenic immediate early gene, in arteriosclerosis and its regulation by angiotensin II. *Circulation.* 2002;106(2):254-260.
184. Lander ES, Linton LM, Birren B, Nusbaum C, Zody MC, Baldwin J, Devon K, Dewar K, Doyle M, FitzHugh W, Funke R, Gage D, Harris K, Heaford A, Howland J, Kann L, Lehoczky J, LeVine R, McEwan P, McKernan K, Meldrim J, Mesirov JP, Miranda C, Morris W, Naylor J, Raymond C, Rosetti M, Santos R, Sheridan A, Sougnez C, Stange-Thomann N, Stojanovic N, Subramanian A, Wyman D, Rogers J, Sulston J, Ainscough R, Beck S, Bentley D, Burton J, Clee C, Carter N, Coulson A, Deadman R, Deloukas P, Dunham A, Dunham I, Durbin R, French L, Grafham D, Gregory S, Hubbard T, Humphray S, Hunt A, Jones M, Lloyd C, McMurray A, Matthews L, Mercer S, Milne S, Mullikin JC, Mungall A, Plumb R, Ross M, Shownkeen R, Sims S, Waterston RH, Wilson RK, Hillier LW, McPherson JD, Marra MA, Mardis ER, Fulton LA, Chinwalla AT, Pepin KH, Gish WR, Chissoe SL, Wendl MC, Delehaunty KD, Miner TL, Delehaunty A, Kramer JB, Cook LL, Fulton RS, Johnson DL, Minx PJ, Clifton SW, Hawkins T, Branscomb E, Predki P, Richardson P, Wenning S, Slezak T, Doggett N, Cheng JF, Olsen A, Lucas S, Elkin C, Uberbacher E, Frazier M, Gibbs RA, Muzny DM, Scherer SE, Bouck JB, Sodergren EJ, Worley KC, Rives CM, Gorrell JH, Metzker ML, Naylor SL, Kucherlapati RS, Nelson DL, Weinstock GM, Sakaki Y, Fujiyama A, Hattori M, Yada T, Toyoda A, Itoh T, Kawagoe C, Watanabe H, Totoki Y, Taylor T, Weissenbach J, Heilig R, Saurin W, Artiguenave F, Brottier P, Bruls T, Pelletier E, Robert C, Wincker P, Smith DR, Doucette-Stamm L, Rubenfield M, Weinstock K, Lee HM, Dubois J, Rosenthal A, Platzer M, Nyakatura G, Taudien S, Rump A, Yang H, Yu J, Wang J, Huang G, Gu J, Hood L, Rowen L, Madan A, Qin S, Davis

RW, Federspiel NA, Abola AP, Proctor MJ, Myers RM, Schmutz J, Dickson M, Grimwood J, Cox DR, Olson MV, Kaul R, Raymond C, Shimizu N, Kawasaki K, Minoshima S, Evans GA, Athanasiou M, Schultz R, Roe BA, Chen F, Pan H, Ramser J, Lehrach H, Reinhardt R, McCombie WR, de la Bastide M, Dedhia N, Blocker H, Hornischer K, Nordsiek G, Agarwala R, Aravind L, Bailey JA, Bateman A, Batzoglou S, Birney E, Bork P, Brown DG, Burge CB, Cerutti L, Chen HC, Church D, Clamp M, Copley RR, Doerks T, Eddy SR, Eichler EE, Furey TS, Galagan J, Gilbert JG, Harmon C, Hayashizaki Y, Haussler D, Hermjakob H, Hokamp K, Jang W, Johnson LS, Jones TA, Kasif S, Kaspryzk A, Kennedy S, Kent WJ, Kitts P, Koonin EV, Korf I, Kulp D, Lancet D, Lowe TM, McLysaght A, Mikkelsen T, Moran JV, Mulder N, Pollara VJ, Ponting CP, Schuler G, Schultz J, Slater G, Smit AF, Stupka E, Szustakowski J, Thierry-Mieg D, Thierry-Mieg J, Wagner L, Wallis J, Wheeler R, Williams A, Wolf YI, Wolfe KH, Yang SP, Yeh RF, Collins F, Guyer MS, Peterson J, Felsenfeld A, Wetterstrand KA, Patrinos A, Morgan MJ, de Jong P, Catanese JJ, Osoegawa K, Shizuya H, Choi S, Chen YJ. Initial sequencing and analysis of the human genome. *Nature.* 2001;409(6822):860-921.

185. Bijnens AP, Lutgens E, Ayoubi T, Kuiper J, Horrevoets AJ, Daemen MJ. Genome-wide expression studies of atherosclerosis: critical issues in methodology, analysis, interpretation of transcriptomics data. *Arterioscler Thromb Vasc Biol.* 2006;26(6):1226-1235.

186. Hiltunen MO, Niemi M, Yla-Herttuala S. Functional genomics and DNA array techniques in atherosclerosis research. *Current opinion in lipidology.* 1999;10(6):515-519.

187. McCaffrey TA, Fu C, Du B, Eksinar S, Kent KC, Bush H, Jr., Kreiger K, Rosengart T, Cybulsky MI, Silverman ES, Collins T. High-level expression of Egr-1 and Egr-1-inducible genes in mouse and human atherosclerosis. *The Journal of clinical investigation.* 2000;105(5):653-662.

188. Hiltunen MO, Tuomisto TT, Niemi M, Brasen JH, Rissanen TT, Toronen P, Vajanto I, Yla-Herttuala S. Changes in gene expression in atherosclerotic plaques analyzed using DNA array. *Atherosclerosis.* 2002;165(1):23-32.

189. Faber BC, Cleutjens KB, Niessen RL, Aarts PL, Boon W, Greenberg AS, Kitslaar PJ, Tordoir JH, Daemen MJ. Identification of genes potentially involved in rupture of human atherosclerotic plaques. *Circulation research.* 2001;89(6):547-554.

190. Badimon L. Atherosclerosis and thrombosis: lessons from animal models. *Thrombosis and haemostasis.* 2001;86(1):356-365.

191. Cullen P, Baetta R, Bellosta S, Bernini F, Chinetti G, Cignarella A, von Eckardstein A, Exley A, Goddard M, Hofker M, Hurt-Camejo E, Kanters E, Kovanen P, Lorkowski S, McPheat W, Pentikainen M, Rauterberg J, Ritchie A, Staels B, Weitkamp B, de Winther M, for the MAFAPS Consortium. Rupture of the Atherosclerotic Plaque: Does a Good Animal Model Exist? *Arterioscler Thromb Vasc Biol.* 2003;23(4):535-542.

192. Getz GS. When is atherosclerosis not atherosclerosis? *Arterioscler Thromb Vasc Biol.* 2000;20(6):1694.

193. Calara F, Silvestre M, Casanada F, Yuan N, Napoli C, Palinski W. Spontaneous plaque rupture and secondary thrombosis in apolipoprotein E-deficient and LDL receptor-deficient mice. *The Journal of pathology.* 2001;195(2):257-263.

194. Williams H, Johnson JL, Carson KG, Jackson CL. Characteristics of intact and ruptured atherosclerotic plaques in brachiocephalic arteries of apolipoprotein E knockout mice. *Arterioscler Thromb Vasc Biol.* 2002;22(5):788-792.

195. Takaya N, Yuan C, Chu B, Saam T, Underhill H, Cai J, Tran N, Polissar NL, Isaac C, Ferguson MS, Garden GA, Cramer SC, Maravilla KR, Hashimoto B, Hatsukami TS. Association between carotid plaque characteristics and subsequent ischemic cerebrovascular events: a prospective assessment with MRI--initial results. *Stroke; a journal of cerebral circulation.* 2006;37(3):818-823.

196. Troyer A, Saloner D, Pan XM, Velez P, Rapp JH. Major carotid plaque surface irregularities correlate with neurologic symptoms. *J Vasc Surg.* 2002;35(4):741-747.
197. Yuan C, Zhang S-x, Polissar NL, Echelard D, Ortiz G, Davis JW, Ellington E, Ferguson MS, Hatsukami TS. Identification of Fibrous Cap Rupture With Magnetic Resonance Imaging Is Highly Associated With Recent Transient Ischemic Attack or Stroke. *Circulation.* 2002;105(2):181-185.
198. Sitzer M, Muller W, Siebler M, Hort W, Kniemeyer HW, Jancke L, Steinmetz H. Plaque ulceration and lumen thrombus are the main sources of cerebral microemboli in high-grade internal carotid artery stenosis. *Stroke; a journal of cerebral circulation.* 1995;26(7):1231-1233.
199. Markus HS, King A, Shipley M, Topakian R, Cullinane M, Reihill S, Bornstein NM, Schaafsma A. Asymptomatic embolisation for prediction of stroke in the Asymptomatic Carotid Emboli Study (ACES): a prospective observational study. *Lancet neurology.* 2010;9(7):663-671.
200. Tyson KL, Weissberg PL, Shanahan CM. Heterogeneity of gene expression in human atheroma unmasked using cDNA representational difference analysis. *Physiological genomics.* 2002;9(2):121-130.
201. Curran S, McKay JA, McLeod HL, Murray GI. Laser capture microscopy. *Mol Pathol.* 2000;53(2):64-68.
202. Hergenhahn M, Kenzelmann M, Grone HJ. Laser-controlled microdissection of tissues opens a window of new opportunities. *Pathol Res Pract.* 2003;199(6):419-423.
203. Trogan E, Choudhury RP, Dansky HM, Rong JX, Breslow JL, Fisher EA. Laser capture microdissection analysis of gene expression in macrophages from atherosclerotic lesions of apolipoprotein E-deficient mice. *Proceedings of the National Academy of Sciences of the United States of America.* 2002;99(4):2234-2239.
204. Fend F, Emmert-Buck MR, Chuaqui R, Cole K, Lee J, Liotta LA, Raffeld M. Immuno-LCM: laser capture microdissection of immunostained frozen sections for mRNA analysis. *The American journal of pathology.* 1999;154(1):61-66.
205. Luzzi V, Holtschlag V, Watson MA. Expression profiling of ductal carcinoma in situ by laser capture microdissection and high-density oligonucleotide arrays. *The American journal of pathology.* 2001;158(6):2005-2010.
206. Alevizos I, Mahadevappa M, Zhang X, Ohyama H, Kohno Y, Posner M, Gallagher GT, Varvares M, Cohen D, Kim D, Kent R, Donoff RB, Todd R, Yung CM, Warrington JA, Wong DT. Oral cancer in vivo gene expression profiling assisted by laser capture microdissection and microarray analysis. *Oncogene.* 2001;20(43):6196-6204.
207. Kitahara O, Furukawa Y, Tanaka T, Kihara C, Ono K, Yanagawa R, Nita ME, Takagi T, Nakamura Y, Tsunoda T. Alterations of gene expression during colorectal carcinogenesis revealed by cDNA microarrays after laser-capture microdissection of tumor tissues and normal epithelia. *Cancer Res.* 2001;61(9):3544-3549.
208. Leethanakul C, Patel V, Gillespie J, Shillitoe E, Kellman RM, Ensley JF, Limwongse V, Emmert-Buck MR, Krizman DB, Gutkind JS. Gene expression profiles in squamous cell carcinomas of the oral cavity: use of laser capture microdissection for the construction and analysis of stage-specific cDNA libraries. *Oral Oncol.* 2000;36(5):474-483.
209. Yim SH, Ward JM, Dragan Y, Yamada A, Scacheri PC, Kimura S, Gonzalez FJ. Microarray analysis using amplified mRNA from laser capture microdissection of microscopic hepatocellular precancerous lesions and frozen hepatocellular carcinomas reveals unique and consistent gene expression profiles. *Toxicol Pathol.* 2003;31(3):295-303.
210. Luo L, Salunga RC, Guo H, Bittner A, Joy KC, Galindo JE, Xiao H, Rogers KE, Wan JS, Jackson MR, Erlander MG. Gene expression profiles of laser-captured adjacent neuronal subtypes. *Nat Med.* 1999;5(1):117-122.

211. Zhan G, Shaheen F, Mackiewicz M, Fenik P, Veasey SC. Single cell laser dissection with molecular beacon polymerase chain reaction identifies 2A as the predominant serotonin receptor subtype in hypoglossal motoneurons. *Neuroscience.* 2002;113(1):145-154.
212. Stagliano NE, Carpino AJ, Ross JS, Donovan M. Vascular gene discovery using laser capture microdissection of human blood vessels and quantitative PCR. *Ann N Y Acad Sci.* 2001;947:344-349.
213. Langheinrich AC, Braun-Dullaeus RC, Walker G, Jeide I, Schilling R, Tammoscheit K, Dreyer T, Fink L, Bohle RM, Haberbosch W. Effects of 3-deazaadenosine on homocysteine and atherosclerosis in apolipoprotein E-deficient mice. *Atherosclerosis.* 2003;171(2):181-192.
214. Zeiffer U, Schober A, Lietz M, Liehn EA, Erl W, Emans N, Yan ZQ, Weber C. Neointimal smooth muscle cells display a proinflammatory phenotype resulting in increased leukocyte recruitment mediated by P-selectin and chemokines. *Circulation research.* 2004;94(6):776-784.
215. Martinet W, Schrijvers DM, De Meyer GR, Thielemans J, Knaapen MW, Herman AG, Kockx MM. Gene expression profiling of apoptosis-related genes in human atherosclerosis: upregulation of death-associated protein kinase. *Arterioscler Thromb Vasc Biol.* 2002;22(12):2023-2029.
216. Tuomisto TT, Korkeela A, Rutanen J, Viita H, Brasen JH, Riekkinen MS, Rissanen TT, Karkola K, Kiraly Z, Kolble K, Yla-Herttuala S. Gene expression in macrophage-rich inflammatory cell infiltrates in human atherosclerotic lesions as studied by laser microdissection and DNA array: overexpression of HMG-CoA reductase, colony stimulating factor receptors, CD11A/CD18 integrins, and interleukin receptors. *Arterioscler Thromb Vasc Biol.* 2003;23(12):2235-2240.
217. Kenzelmann M, Klaren R, Hergenhahn M, Bonrouhi M, Grone HJ, Schmid W, Schutz G. High-accuracy amplification of nanogram total RNA amounts for gene profiling. *Genomics.* 2004;83(4):550-558.
218. Klur S, Toy K, Williams MP, Certa U. Evaluation of procedures for amplification of small-size samples for hybridization on microarrays. *Genomics.* 2004;83(3):508-517.
219. Wang E, Miller LD, Ohnmacht GA, Liu ET, Marincola FM. High-fidelity mRNA amplification for gene profiling. *Nature biotechnology.* 2000;18(4):457-459.
220. Zhao H, Hastie T, Whitfield ML, Borresen-Dale AL, Jeffrey SS. Optimization and evaluation of T7 based RNA linear amplification protocols for cDNA microarray analysis. *BMC genomics.* 2002;3(1):31.
221. Eberwine J, Yeh H, Miyashiro K, Cao Y, Nair S, Finnell R, Zettel M, Coleman P. Analysis of gene expression in single live neurons. *Proceedings of the National Academy of Sciences of the United States of America.* 1992;89(7):3010-3014.
222. Van Gelder RN, von Zastrow ME, Yool A, Dement WC, Barchas JD, Eberwine JH. Amplified RNA synthesized from limited quantities of heterogeneous cDNA. *Proceedings of the National Academy of Sciences of the United States of America.* 1990;87(5):1663-1667.
223. Kerwin J, Scott M, Sharpe J, Puelles L, Robson SC, Martinez-de-la-Torre M, Ferran JL, Feng G, Baldock R, Strachan T, Davidson D, Lindsay S. 3 dimensional modelling of early human brain development using optical projection tomography. *BMC Neurosci.* 2004;5(1):27.
224. Sharpe J. Optical projection tomography as a new tool for studying embryo anatomy. *J Anat.* 2003;202(2):175-181.
225. Sharpe J, Ahlgren U, Perry P, Hill B, Ross A, Hecksher-Sorensen J, Baldock R, Davidson D. Optical projection tomography as a tool for 3D microscopy and gene expression studies. *Science.* 2002;296(5567):541-545.
226. Randomised trial of endarterectomy for recently symptomatic carotid stenosis: final results of the MRC European Carotid Surgery Trial (ECST). *Lancet.* 1998;351(9113):1379-1387.

227. Beneficial effect of carotid endarterectomy in symptomatic patients with high-grade carotid stenosis. North American Symptomatic Carotid Endarterectomy Trial Collaborators. *N Engl J Med.* 1991;325(7):445-453.
228. Barnett HJ, Taylor DW, Eliasziw M, Fox AJ, Ferguson GG, Haynes RB, Rankin RN, Clagett GP, Hachinski VC, Sackett DL, Thorpe KE, Meldrum HE, Spence JD. Benefit of carotid endarterectomy in patients with symptomatic moderate or severe stenosis. North American Symptomatic Carotid Endarterectomy Trial Collaborators. *N Engl J Med.* 1998;339(20):1415-1425.
229. Barnett HJ, Warlow CP. Carotid endarterectomy and the measurement of stenosis. *Stroke; a journal of cerebral circulation.* 1993;24(9):1281-1284.
230. Rothwell PM, Eliasziw M, Gutnikov SA, Warlow CP, Barnett HJ. Endarterectomy for symptomatic carotid stenosis in relation to clinical subgroups and timing of surgery. *Lancet.* 2004;363(9413):915-924.
231. Endarterectomy for asymptomatic carotid artery stenosis. Executive Committee for the Asymptomatic Carotid Atherosclerosis Study. *Jama.* 1995;273(18):1421-1428.
232. Halliday A, Mansfield A, Marro J, Peto C, Peto R, Potter J, Thomas D. Prevention of disabling and fatal strokes by successful carotid endarterectomy in patients without recent neurological symptoms: randomised controlled trial. *Lancet.* 2004;363(9420):1491-1502.
233. Rothwell PM, Goldstein LB. Carotid endarterectomy for asymptomatic carotid stenosis: asymptomatic carotid surgery trial. *Stroke; a journal of cerebral circulation.* 2004;35(10):2425-2427.
234. Rothwell PM, Eliasziw M, Gutnikov SA, Fox AJ, Taylor DW, Mayberg MR, Warlow CP, Barnett HJ. Analysis of pooled data from the randomised controlled trials of endarterectomy for symptomatic carotid stenosis. *Lancet.* 2003;361(9352):107-116.
235. Rothwell PM, Warlow CP. Low risk of ischemic stroke in patients with reduced internal carotid artery lumen diameter distal to severe symptomatic carotid stenosis: cerebral protection due to low poststenotic flow? On behalf of the European Carotid Surgery Trialists' Collaborative Group. *Stroke; a journal of cerebral circulation.* 2000;31(3):622-630.
236. Bamford J, Sandercock P, Dennis M, Burn J, Warlow C. Classification and natural history of clinically identifiable subtypes of cerebral infarction. *Lancet.* 1991;337(8756):1521-1526.
237. King A, Markus HS. Doppler embolic signals in cerebrovascular disease and prediction of stroke risk: a systematic review and meta-analysis. *Stroke; a journal of cerebral circulation.* 2009;40(12):3711-3717.
238. Molloy J, Markus HS. Asymptomatic embolization predicts stroke and TIA risk in patients with carotid artery stenosis. *Stroke; a journal of cerebral circulation.* 1999;30(7):1440-1443.
239. Siebler M, Nachtmann A, Sitzer M, Rose G, Kleinschmidt A, Rademacher J, Steinmetz H. Cerebral microembolism and the risk of ischemia in asymptomatic high-grade internal carotid artery stenosis. *Stroke; a journal of cerebral circulation.* 1995;26(11):2184-2186.
240. Spence JD, Tamayo A, Lownie SP, Ng WP, Ferguson GG. Absence of microemboli on transcranial Doppler identifies low-risk patients with asymptomatic carotid stenosis. *Stroke; a journal of cerebral circulation.* 2005;36(11):2373-2378.
241. Basic identification criteria of Doppler microembolic signals. Consensus Committee of the Ninth International Cerebral Hemodynamic Symposium. *Stroke; a journal of cerebral circulation.* 1995;26(6):1123.
242. Markus HS, Ackerstaff R, Babikian V, Bladin C, Droste D, Grosset D, Levi C, Russell D, Siebler M, Tegeler C. Intercenter agreement in reading Doppler embolic signals. A multicenter international study. *Stroke; a journal of cerebral circulation.* 1997;28(7):1307-1310.
243. Ringelstein EB, Droste DW, Babikian VL, Evans DH, Grosset DG, Kaps M, Markus HS, Russell D, Siebler M. Consensus on microembolus detection by TCD.

International Consensus Group on Microembolus Detection. *Stroke; a journal of cerebral circulation.* 1998;29(3):725-729.
244. Brucher R, Russell D. Automatic online embolus detection and artifact rejection with the first multifrequency transcranial Doppler. *Stroke; a journal of cerebral circulation.* 2002;33(8):1969-1974.
245. Agresti A. *An introduction to categorical data analysis.* New York, USA: John Wiley & Sons, Inc.; 1996.
246. Mueller O, Lightfoot S, Schroeder A. RNA Integrity Number (RIN) - Standardization of RNA quality Control: a Application Technical Note. 2004:1-7.
247. Goldsworthy SM, Stockton PS, Trempus CS, Foley JF, Maronpot RR. Effects of fixation on RNA extraction and amplification from laser capture microdissected tissue. *Molecular carcinogenesis.* 1999;25(2):86-91.
248. Shibutani M, Uneyama C, Miyazaki K, Toyoda K, Hirose M. Methacarn fixation: a novel tool for analysis of gene expressions in paraffin-embedded tissue specimens. *Laboratory investigation; a journal of technical methods and pathology.* 2000;80(2):199-208.
249. Okuducu AF, Janzen V, Hahne JC, Ko Y, Wernert N. Influence of histochemical stains on quantitative gene expression analysis after laser-assisted microdissection. *International journal of molecular medicine.* 2003;11(4):449-453.
250. Affymetrix. Technical Note: GeneChip Eukaryotic Small Sample Target Labelling Assay Version II;No. 701265 Rev. 2.
251. Affymetrix. GeneChip Expression Analysis, Technical manual;No. 701045 Rev. 4.
252. Brazma A, Hingamp P, Quackenbush J, Sherlock G, Spellman P, Stoeckert C, Aach J, Ansorge W, Ball CA, Causton HC, Gaasterland T, Glenisson P, Holstege FC, Kim IF, Markowitz V, Matese JC, Parkinson H, Robinson A, Sarkans U, Schulze-Kremer S, Stewart J, Taylor R, Vilo J, Vingron M. Minimum information about a microarray experiment (MIAME)-toward standards for microarray data. *Nature genetics.* 2001;29(4):365-371.
253. Affymetrix. Technical Note: Design and performance of the GeneChip Human Genome U133 Plus 2.0 and Human Genome U133A 2.0 Arrays;No. 701483 Rev. 2.
254. Affymetrix. Data Sheet: GeneChip Human Genome U133 Arrays;No. 701484 Rev. 5.
255. Affymetrix. GeneChip Expression Analysis, Data analysis fundamentals;No. 701190 Rev. 4.
256. Tuimala J, Laine MM. *DNA Microarray Data Analysis*. Helsinki, Finland: CSC - Scientific Computing Ltd.; 2003.
257. SiliconGenetics. *GeneSpring User Manual Version 7.0*; 2004.
258. Irizarry RA, Hobbs B, Collin F, Beazer-Barclay YD, Antonellis KJ, Scherf U, Speed TP. Exploration, normalization, and summaries of high density oligonucleotide array probe level data. *Biostatistics (Oxford, England).* 2003;4(2):249-264.
259. Bolstad BM, Irizarry RA, Astrand M, Speed TP. A comparison of normalization methods for high density oligonucleotide array data based on variance and bias. *Bioinformatics (Oxford, England).* 2003;19(2):185-193.
260. Wu Z, Irizarry RA. Stochastic models inspired by hybridization theory for short oligonucleotide arrays. *J Comput Biol.* 2005;12(6):882-893.
261. Wu Z, Irizarry RA, Gentleman R, Murillo FM, Spencer F. A Model Based Background Adjustment for Oligonucleotide Expression Arrays. *Johns Hopkins University, Dept. of Biostatistics Working Papers.* 2004;(http://www.bepress.com/jhubiostat/paper1).
262. Wu Z, Irizarry RA. Preprocessing of oligonucleotide array data. *Nature biotechnology.* 2004;22(6):656-658; author reply 658.
263. Su AI, Wiltshire T, Batalov S, Lapp H, Ching KA, Block D, Zhang J, Soden R, Hayakawa M, Kreiman G, Cooke MP, Walker JR, Hogenesch JB. A gene atlas of the mouse and human protein-encoding transcriptomes. *Proceedings of the National Academy of Sciences of the United States of America.* 2004;101(16):6062-6067.

264. Tchkonia T, Lenburg M, Thomou T, Giorgadze N, Frampton G, Pirtskhalava T, Cartwright A, Cartwright M, Flanagan J, Karagiannides I, Gerry N, Forse RA, Tchoukalova Y, Jensen MD, Pothoulakis C, Kirkland JL. Identification of depot-specific human fat cell progenitors through distinct expression profiles and developmental gene patterns. *Am J Physiol Endocrinol Metab.* 2007;292(1):E298-307.

265. Cho HJ, Shashkin P, Gleissner CA, Dunson D, Jain N, Lee JK, Miller Y, Ley K. Induction of dendritic cell-like phenotype in macrophages during foam cell formation. *Physiological genomics.* 2007;29(2):149-160.

266. Hagg DA, Jernas M, Wiklund O, Thelle DS, Fagerberg B, Eriksson P, Hamsten A, Olsson B, Carlsson B, Carlsson LM, Svensson PA. Expression profiling of macrophages from subjects with atherosclerosis to identify novel susceptibility genes. *International journal of molecular medicine.* 2008;21(6):697-704.

267. Jura J, Wegrzyn P, Korostynski M, Guzik K, Oczko-Wojciechowska M, Jarzab M, Kowalska M, Piechota M, Przewlocki R, Koj A. Identification of interleukin-1 and interleukin-6-responsive genes in human monocyte-derived macrophages using microarrays. *Biochimica et biophysica acta.* 2008;1779(6-7):383-389.

268. Liu H, Shi B, Huang CC, Eksarko P, Pope RM. Transcriptional diversity during monocyte to macrophage differentiation. *Immunology letters.* 2008;117(1):70-80.

269. Joliffe IT. *Principal Component Analysis*. 2 ed: Springer; 2002.

270. Wei C, Li J, Bumgarner RE. Sample size for detecting differentially expressed genes in microarray experiments. *BMC genomics.* 2004;5(1):87.

271. Pan W, Lin J, Le CT. How many replicates of arrays are required to detect gene expression changes in microarray experiments? A mixture model approach. *Genome Biol.* 2002;3(5):research0022.

272. Lee ML, Whitmore GA. Power and sample size for DNA microarray studies. *Stat Med.* 2002;21(23):3543-3570.

273. Lee ML, Kuo FC, Whitmore GA, Sklar J. Importance of replication in microarray gene expression studies: statistical methods and evidence from repetitive cDNA hybridizations. *Proceedings of the National Academy of Sciences of the United States of America.* 2000;97(18):9834-9839.

274. Maere S, Heymans K, Kuiper M. BiNGO: a Cytoscape plugin to assess overrepresentation of gene ontology categories in biological networks. *Bioinformatics (Oxford, England).* 2005;21(16):3448-3449.

275. Zhang B, Kirov S, Snoddy J. WebGestalt: an integrated system for exploring gene sets in various biological contexts. *Nucleic acids research.* 2005;33(Web Server issue):W741-748.

276. Vandesompele J, De Preter K, Pattyn F, Poppe B, Van Roy N, De Paepe A, Speleman F. Accurate normalization of real-time quantitative RT-PCR data by geometric averaging of multiple internal control genes. *Genome Biol.* 2002;3(7):RESEARCH0034.

277. Hellemans J, Mortier G, De Paepe A, Speleman F, Vandesompele J. qBase relative quantification framework and software for management and automated analysis of real-time quantitative PCR data. *Genome Biol.* 2007;8(2):R19.

278. Zhao L, Shen ZX, Luo HS, Shen L. Possible involvement of leptin and leptin receptor in developing gastric adenocarcinoma. *World J Gastroenterol.* 2005;11(48):7666-7670.

279. Elmasri H, Karaaslan C, Teper Y, Ghelfi E, Weng M, Ince TA, Kozakewich H, Bischoff J, Cataltepe S. Fatty acid binding protein 4 is a target of VEGF and a regulator of cell proliferation in endothelial cells. *Faseb J.* 2009;23(11):3865-3873.

280. Hayat MA. *Microscopy, immunohistochemistry, and antigen retrieval methods: for light and electron microscopy*: Kluwer Academic / Plenum Publishers, New York; 2002.

281. Formalin-fixed Paraffin-embedded Tissue Section Antigen Retrieval Method by 95°C heat treatment. *Santa Cruz Biotechnology Inc.* Available at: http://www.scbt.com/protocol_immunoperoxidase_cell_staining.html.

282. Martinet W, De Meyer GR, Herman AG, Kockx MM. RNA damage in human atherosclerosis: pathophysiological significance and implications for gene expression studies. *RNA biology.* 2005;2(1):4-7.
283. Naderi A, Ahmed AA, Barbosa-Morais NL, Aparicio S, Brenton JD, Caldas C. Expression microarray reproducibility is improved by optimising purification steps in RNA amplification and labelling. *BMC genomics.* 2004;5(1):9.
284. Affymetrix. Netaffx, the Affymetrix web-based data-mining portal. Available at: http://www.affymetrix.com/analysis/index.affx.
285. Shannon P, Markiel A, Ozier O, Baliga NS, Wang JT, Ramage D, Amin N, Schwikowski B, Ideker T. Cytoscape: a software environment for integrated models of biomolecular interaction networks. *Genome research.* 2003;13(11):2498-2504.
286. Tavora F, Cresswell N, Li L, Ripple M, Fowler D, Burke A. Sudden coronary death caused by pathologic intimal thickening without atheromatous plaque formation. *Cardiovasc Pathol.* 2011;20(1):51-57.
287. Park AE, McCarthy WJ, Pearce WH, Matsumura JS, Yao JS. Carotid plaque morphology correlates with presenting symptomatology. *J Vasc Surg.* 1998;27(5):872-878; discussion 878-879.
288. Estol C, Claasen D, Hirsch W, Wechsler L, Moossy J. Correlative angiographic and pathologic findings in the diagnosis of ulcerated plaques in the carotid artery. *Archives of neurology.* 1991;48(7):692-694.
289. Streifler JY, Eliasziw M, Fox AJ, Benavente OR, Hachinski VC, Ferguson GG, Barnett HJ. Angiographic detection of carotid plaque ulceration. Comparison with surgical observations in a multicenter study. North American Symptomatic Carotid Endarterectomy Trial. *Stroke; a journal of cerebral circulation.* 1994;25(6):1130-1132.
290. Rothwell PM, Gibson R, Warlow CP. Interrelation between plaque surface morphology and degree of stenosis on carotid angiograms and the risk of ischemic stroke in patients with symptomatic carotid stenosis. On behalf of the European Carotid Surgery Trialists' Collaborative Group. *Stroke; a journal of cerebral circulation.* 2000;31(3):615-621.
291. Golledge J, Greenhalgh RM, Davies AH. The symptomatic carotid plaque. *Stroke; a journal of cerebral circulation.* 2000;31(3):774-781.
292. Milei J, Parodi JC, Ferreira M, Barrone A, Grana DR, Matturri L. Atherosclerotic plaque rupture and intraplaque hemorrhage do not correlate with symptoms in carotid artery stenosis. *J Vasc Surg.* 2003;38(6):1241-1247.
293. Vemuganti R, Dempsey RJ. Carotid atherosclerotic plaques from symptomatic stroke patients share the molecular fingerprints to develop in a neoplastic fashion: a microarray analysis study. *Neuroscience.* 2005;131(2):359-374.
294. Randi AM, Biguzzi E, Falciani F, Merlini P, Blakemore S, Bramucci E, Lucreziotti S, Lennon M, Faioni EM, Ardissino D, Mannucci PM. Identification of differentially expressed genes in coronary atherosclerotic plaques from patients with stable or unstable angina by cDNA array analysis. *J Thromb Haemost.* 2003;1(4):829-835.
295. Dahl TB, Yndestad A, Skjelland M, Oie E, Dahl A, Michelsen A, Damas JK, Tunheim SH, Ueland T, Smith C, Bendz B, Tonstad S, Gullestad L, Froland SS, Krohg-Sorensen K, Russell D, Aukrust P, Halvorsen B. Increased expression of visfatin in macrophages of human unstable carotid and coronary atherosclerosis: possible role in inflammation and plaque destabilization. *Circulation.* 2007;115(8):972-980.
296. Ijas P, Nuotio K, Saksi J, Soinne L, Saimanen E, Karjalainen-Lindsberg ML, Salonen O, Sarna S, Tuimala J, Kovanen PT, Kaste M, Lindsberg PJ. Microarray analysis reveals overexpression of CD163 and HO-1 in symptomatic carotid plaques. *Arterioscler Thromb Vasc Biol.* 2007;27(1):154-160.
297. Papaspyridonos M, Smith A, Burnand KG, Taylor P, Padayachee S, Suckling KE, James CH, Greaves DR, Patel L. Novel candidate genes in unstable areas of human atherosclerotic plaques. *Arterioscler Thromb Vasc Biol.* 2006;26(8):1837-1844.

298. Lee J, Hever A, Willhite D, Zlotnik A, Hevezi P. Effects of RNA degradation on gene expression analysis of human postmortem tissues. *Faseb J.* 2005;19(10):1356-1358.
299. Woodside KJ, Hernandez A, Smith FW, Xue XY, Hu M, Daller JA, Hunter GC. Differential gene expression in primary and recurrent carotid stenosis. *Biochemical and biophysical research communications.* 2003;302(3):509-514.
300. Zohlnhofer D, Klein CA, Richter T, Brandl R, Murr A, Nuhrenberg T, Schomig A, Baeuerle PA, Neumann FJ. Gene expression profiling of human stent-induced neointima by cDNA array analysis of microscopic specimens retrieved by helix cutter atherectomy: Detection of FK506-binding protein 12 upregulation. *Circulation.* 2001;103(10):1396-1402.
301. Hagg DA, Olson FJ, Kjelldahl J, Jernas M, Thelle DS, Carlsson LM, Fagerberg B, Svensson PA. Expression of chemokine (C-C motif) ligand 18 in human macrophages and atherosclerotic plaques. *Atherosclerosis.* 2009;204(2):e15-20.
302. Adams LD, Geary RL, Li J, Rossini A, Schwartz SM. Expression profiling identifies smooth muscle cell diversity within human intima and plaque fibrous cap: loss of RGS5 distinguishes the cap. *Arterioscler Thromb Vasc Biol.* 2006;26(2):319-325.
303. Archacki SR, Angheloiu G, Tian XL, Tan FL, DiPaola N, Shen GQ, Moravec C, Ellis S, Topol EJ, Wang Q. Identification of new genes differentially expressed in coronary artery disease by expression profiling. *Physiological genomics.* 2003;15(1):65-74.
304. King JY, Ferrara R, Tabibiazar R, Spin JM, Chen MM, Kuchinsky A, Vailaya A, Kincaid R, Tsalenko A, Deng DX, Connolly A, Zhang P, Yang E, Watt C, Yakhini Z, Ben-Dor A, Adler A, Bruhn L, Tsao P, Quertermous T, Ashley EA. Pathway analysis of coronary atherosclerosis. *Physiological genomics.* 2005;23(1):103-118.
305. Tabibiazar R, Wagner RA, Ashley EA, King JY, Ferrara R, Spin JM, Sanan DA, Narasimhan B, Tibshirani R, Tsao PS, Efron B, Quertermous T. Signature patterns of gene expression in mouse atherosclerosis and their correlation to human coronary disease. *Physiological genomics.* 2005;22(2):213-226.
306. Seo D, Wang T, Dressman H, Herderick EE, Iversen ES, Dong C, Vata K, Milano CA, Rigat F, Pittman J, Nevins JR, West M, Goldschmidt-Clermont PJ. Gene expression phenotypes of atherosclerosis. *Arterioscler Thromb Vasc Biol.* 2004;24(10):1922-1927.
307. Sluimer JC, Kisters N, Cleutjens KB, Volger OL, Horrevoets AJ, van den Akker LH, Bijnens AP, Daemen MJ. Dead or alive: gene expression profiles of advanced atherosclerotic plaques from autopsy and surgery. *Physiological genomics.* 2007;30(3):335-341.
308. Martinet W, de Meyer GR, Herman AG, Kockx MM. Reactive oxygen species induce RNA damage in human atherosclerosis. *European journal of clinical investigation.* 2004;34(5):323-327.
309. Toyokuni S. Reactive oxygen species-induced molecular damage and its application in pathology. *Pathology international.* 1999;49(2):91-102.
310. Martinet W, Knaapen MW, De Meyer GR, Herman AG, Kockx MM. Elevated levels of oxidative DNA damage and DNA repair enzymes in human atherosclerotic plaques. *Circulation.* 2002;106(8):927-932.
311. Stolle K, Weitkamp B, Rauterberg J, Lorkowski S, Cullen P. Laser microdissection-based analysis of mRNA expression in human coronary arteries with intimal thickening. *J Histochem Cytochem.* 2004;52(11):1511-1518.
312. Kockx MM, De Meyer GR, Buyssens N, Knaapen MW, Bult H, Herman AG. Cell composition, replication, and apoptosis in atherosclerotic plaques after 6 months of cholesterol withdrawal. *Circulation research.* 1998;83(4):378-387.
313. Kockx MM, De Meyer GR, Muhring J, Jacob W, Bult H, Herman AG. Apoptosis and related proteins in different stages of human atherosclerotic plaques. *Circulation.* 1998;97(23):2307-2315.
314. Lutgens E, de Muinck ED, Kitslaar PJ, Tordoir JH, Wellens HJ, Daemen MJ. Biphasic pattern of cell turnover characterizes the progression from fatty streaks to ruptured human atherosclerotic plaques. *Cardiovasc Res.* 1999;41(2):473-479.

315. Clarke MC, Figg N, Maguire JJ, Davenport AP, Goddard M, Littlewood TD, Bennett MR. Apoptosis of vascular smooth muscle cells induces features of plaque vulnerability in atherosclerosis. *Nat Med.* 2006;12(9):1075-1080.
316. Volger OL, Fledderus JO, Kisters N, Fontijn RD, Moerland PD, Kuiper J, van Berkel TJ, Bijnens AP, Daemen MJ, Pannekoek H, Horrevoets AJ. Distinctive expression of chemokines and transforming growth factor-beta signaling in human arterial endothelium during atherosclerosis. *The American journal of pathology.* 2007;171(1):326-337.
317. Paul A, Yechoor V, Raja R, Li L, Chan L. Microarray gene profiling of laser-captured cells: a new tool to study atherosclerosis in mice. *Atherosclerosis.* 2008;200(2):257-263.
318. Polacek DC, Passerini AG, Shi C, Francesco NM, Manduchi E, Grant GR, Powell S, Bischof H, Winkler H, Stoeckert CJ, Jr., Davies PF. Fidelity and enhanced sensitivity of differential transcription profiles following linear amplification of nanogram amounts of endothelial mRNA. *Physiological genomics.* 2003;13(2):147-156.
319. Schneider J, Buness A, Huber W, Volz J, Kioschis P, Hafner M, Poustka A, Sultmann H. Systematic analysis of T7 RNA polymerase based in vitro linear RNA amplification for use in microarray experiments. *BMC genomics.* 2004;5(1):29.
320. Luzzi V, Mahadevappa M, Raja R, Warrington JA, Watson MA. Accurate and reproducible gene expression profiles from laser capture microdissection, transcript amplification, and high density oligonucleotide microarray analysis. *J Mol Diagn.* 2003;5(1):9-14.
321. Wilson CL, Pepper SD, Hey Y, Miller CJ. Amplification protocols introduce systematic but reproducible errors into gene expression studies. *BioTechniques.* 2004;36(3):498-506.
322. Chen JJ, Wang SJ, Tsai CA, Lin CJ. Selection of differentially expressed genes in microarray data analysis. *The pharmacogenomics journal.* 2007;7(3):212-220.
323. Zamir E, Geiger B. Molecular complexity and dynamics of cell-matrix adhesions. *Journal of cell science.* 2001;114(Pt 20):3583-3590.
324. Francis AA, Pierce GN. An integrated approach for the mechanisms responsible for atherosclerotic plaque regression. *Experimental and clinical cardiology.*16(3):77-86.
325. Williams KJ, Feig JE, Fisher EA. Cellular and molecular mechanisms for rapid regression of atherosclerosis: from bench top to potentially achievable clinical goal. *Current opinion in lipidology.* 2007;18(4):443-450.
326. Linder S, Hufner K, Wintergerst U, Aepfelbacher M. Microtubule-dependent formation of podosomal adhesion structures in primary human macrophages. *Journal of cell science.* 2000;113 Pt 23:4165-4176.
327. Nathan CF. Secretory products of macrophages. *The Journal of clinical investigation.* 1987;79(2):319-326.
328. Wicha MS, Huard TK. Macrophages express cell surface laminin. *Experimental cell research.* 1983;143(2):475-479.
329. Pedraza C, Geberhiwot T, Ingerpuu S, Assefa D, Wondimu Z, Kortesmaa J, Tryggvason K, Virtanen I, Patarroyo M. Monocytic cells synthesize, adhere to, and migrate on laminin-8 (alpha 4 beta 1 gamma 1). *J Immunol.* 2000;165(10):5831-5838.
330. Villiger B, Kelley DG, Engleman W, Kuhn C, 3rd, McDonald JA. Human alveolar macrophage fibronectin: synthesis, secretion, and ultrastructural localization during gelatin-coated latex particle binding. *The Journal of cell biology.* 1981;90(3):711-720.
331. Liptay MJ, Parks WC, Mecham RP, Roby J, Kaiser LR, Cooper JD, Botney MD. Neointimal macrophages colocalize with extracellular matrix gene expression in human atherosclerotic pulmonary arteries. *The Journal of clinical investigation.* 1993;91(2):588-594.
332. Jaffe EA, Ruggiero JT, Falcone DJ. Monocytes and macrophages synthesize and secrete thrombospondin. *Blood.* 1985;65(1):79-84.

333. Schnoor M, Cullen P, Lorkowski J, Stolle K, Robenek H, Troyer D, Rauterberg J, Lorkowski S. Production of type VI collagen by human macrophages: a new dimension in macrophage functional heterogeneity. *J Immunol.* 2008;180(8):5707-5719.
334. Weitkamp B, Cullen P, Plenz G, Robenek H, Rauterberg J. Human macrophages synthesize type VIII collagen in vitro and in the atherosclerotic plaque. *Faseb J.* 1999;13(11):1445-1457.
335. Weiss R, Dziura J, Burgert TS, Tamborlane WV, Taksali SE, Yeckel CW, Allen K, Lopes M, Savoye M, Morrison J, Sherwin RS, Caprio S. Obesity and the metabolic syndrome in children and adolescents. *N Engl J Med.* 2004;350(23):2362-2374.
336. Yang R, Barouch LA. Leptin signaling and obesity: cardiovascular consequences. *Circulation research.* 2007;101(6):545-559.
337. Guzik TJ, Mangalat D, Korbut R. Adipocytokines - novel link between inflammation and vascular function? *J Physiol Pharmacol.* 2006;57(4):505-528.
338. Vernooy JH, Drummen NE, van Suylen RJ, Cloots RH, Moller GM, Bracke KR, Zuyderduyn S, Dentener MA, Brusselle GG, Hiemstra PS, Wouters EF. Enhanced pulmonary leptin expression in patients with severe COPD and asymptomatic smokers. *Thorax.* 2009;64(1):26-32.
339. Schroeter MR, Schneiderman J, Schumann B, Gluckermann R, Grimmas P, Buchwald AB, Tirilomis T, Schondube FA, Konstantinides SV, Schafer K. Expression of the leptin receptor in different types of vascular lesions. *Histochemistry and cell biology.* 2007;128(4):323-333.
340. Cabrero A, Cubero M, Llaverias G, Alegret M, Sanchez R, Laguna JC, Vazquez-Carrera M. Leptin down-regulates peroxisome proliferator-activated receptor gamma (PPAR-gamma) mRNA levels in primary human monocyte-derived macrophages. *Molecular and cellular biochemistry.* 2005;275(1-2):173-179.
341. Gruen ML, Hao M, Piston DW, Hasty AH. Leptin requires canonical migratory signaling pathways for induction of monocyte and macrophage chemotaxis. *Am J Physiol Cell Physiol.* 2007;293(5):C1481-1488.
342. Lord GM, Matarese G, Howard JK, Baker RJ, Bloom SR, Lechler RI. Leptin modulates the T-cell immune response and reverses starvation-induced immunosuppression. *Nature.* 1998;394(6696):897-901.
343. Maya-Monteiro CM, Almeida PE, D'Avila H, Martins AS, Rezende AP, Castro-Faria-Neto H, Bozza PT. Leptin induces macrophage lipid body formation by a phosphatidylinositol 3-kinase- and mammalian target of rapamycin-dependent mechanism. *The Journal of biological chemistry.* 2008;283(4):2203-2210.
344. Kjerrulf M, Berke Z, Aspegren A, Umaerus M, Nilsson T, Svensson L, Hurt-Camejo E. Reduced cholesterol accumulation by leptin deficient (ob/ob) mouse macrophages. *Inflamm Res.* 2006;55(7):300-309.
345. Gaukrodger N, Mayosi BM, Imrie H, Avery P, Baker M, Connell JM, Watkins H, Farrall M, Keavney B. A rare variant of the leptin gene has large effects on blood pressure and carotid intima-medial thickness: a study of 1428 individuals in 248 families. *Journal of medical genetics.* 2005;42(6):474-478.
346. Li L, Mamputu JC, Wiernsperger N, Renier G. Signaling pathways involved in human vascular smooth muscle cell proliferation and matrix metalloproteinase-2 expression induced by leptin: inhibitory effect of metformin. *Diabetes.* 2005;54(7):2227-2234.
347. Kallen CB, Lazar MA. Antidiabetic thiazolidinediones inhibit leptin (ob) gene expression in 3T3-L1 adipocytes. *Proceedings of the National Academy of Sciences of the United States of America.* 1996;93(12):5793-5796.
348. Wolk R, Berger P, Lennon RJ, Brilakis ES, Johnson BD, Somers VK. Plasma leptin and prognosis in patients with established coronary atherosclerosis 10.1016/j.jacc.2004.07.050. *Journal of the American College of Cardiology.* 2004;44(9):1819-1824.
349. Furuhashi M, Hotamisligil GS. Fatty acid-binding proteins: role in metabolic diseases and potential as drug targets. *Nat Rev Drug Discov.* 2008;7(6):489-503.

350. Makowski L, Brittingham KC, Reynolds JM, Suttles J, Hotamisligil GS. The fatty acid-binding protein, aP2, coordinates macrophage cholesterol trafficking and inflammatory activity. Macrophage expression of aP2 impacts peroxisome proliferator-activated receptor gamma and IkappaB kinase activities. *The Journal of biological chemistry.* 2005;280(13):12888-12895.
351. Sueyoshi S, Mitsumata M, Kusumi Y, Niihashi M, Esumi M, Yamada T, Sakurai I. Increased expression of peroxisome proliferator-activated receptor (PPAR)-alpha and PPAR-gamma in human atherosclerosis. *Pathol Res Pract.* 2010;206(7):429-438.
352. Boord JB, Maeda K, Makowski L, Babaev VR, Fazio S, Linton MF, Hotamisligil GS. Adipocyte fatty acid-binding protein, aP2, alters late atherosclerotic lesion formation in severe hypercholesterolemia. *Arterioscler Thromb Vasc Biol.* 2002;22(10):1686-1691.
353. Makowski L, Boord JB, Maeda K, Babaev VR, Uysal KT, Morgan MA, Parker RA, Suttles J, Fazio S, Hotamisligil GS, Linton MF. Lack of macrophage fatty-acid-binding protein aP2 protects mice deficient in apolipoprotein E against atherosclerosis. *Nat Med.* 2001;7(6):699-705.
354. Llaverias G, Noe V, Penuelas S, Vazquez-Carrera M, Sanchez RM, Laguna JC, Ciudad CJ, Alegret M. Atorvastatin reduces CD68, FABP4, and HBP expression in oxLDL-treated human macrophages. *Biochemical and biophysical research communications.* 2004;318(1):265-274.
355. Tuncman G, Erbay E, Hom X, De Vivo I, Campos H, Rimm EB, Hotamisligil GS. A genetic variant at the fatty acid-binding protein aP2 locus reduces the risk for hypertriglyceridemia, type 2 diabetes, and cardiovascular disease. *Proceedings of the National Academy of Sciences of the United States of America.* 2006;103(18):6970-6975.
356. Furuhashi M, Tuncman G, Gorgun CZ, Makowski L, Atsumi G, Vaillancourt E, Kono K, Babaev VR, Fazio S, Linton MF, Sulsky R, Robl JA, Parker RA, Hotamisligil GS. Treatment of diabetes and atherosclerosis by inhibiting fatty-acid-binding protein aP2. *Nature.* 2007;447(7147):959-965.
357. Oben JE, Ngondi JL, Blum K. Inhibition of Irvingia gabonensis seed extract (OB131) on adipogenesis as mediated via down regulation of the PPARgamma and leptin genes and up-regulation of the adiponectin gene. *Lipids in health and disease.* 2008;7:44.
358. Tsaousi A, Mill C, George SJ. The Wnt pathways in vascular disease: lessons from vascular development. *Current opinion in lipidology.* 2011;22(5):350-357.
359. Golledge J, Cuming R, Ellis M, Davies AH, Greenhalgh RM. Carotid plaque characteristics and presenting symptom. *The British journal of surgery.* 1997;84(12):1697-1701.
360. Stahlberg A, Kubista M, Pfaffl M. Comparison of reverse transcriptases in gene expression analysis. *Clinical chemistry.* 2004;50(9):1678-1680.
361. Spiess AN, Mueller N, Ivell R. Amplified RNA degradation in T7-amplification methods results in biased microarray hybridizations. *BMC genomics.* 2003;4(1):44.
362. Thellin O, Zorzi W, Lakaye B, De Borman B, Coumans B, Hennen G, Grisar T, Igout A, Heinen E. Housekeeping genes as internal standards: use and limits. *Journal of biotechnology.* 1999;75(2-3):291-295.
363. Andersen CL, Jensen JL, Orntoft TF. Normalization of real-time quantitative reverse transcription-PCR data: a model-based variance estimation approach to identify genes suited for normalization, applied to bladder and colon cancer data sets. *Cancer Res.* 2004;64(15):5245-5250.
364. Suzuki T, Higgins PJ, Crawford DR. Control selection for RNA quantitation. *BioTechniques.* 2000;29(2):332-337.
365. Warrington JA, Nair A, Mahadevappa M, Tsyganskaya M. Comparison of human adult and fetal expression and identification of 535 housekeeping/maintenance genes. *Physiol. Genomics.* 2000;2(3):143-147.
366. Hsiao LL, Dangond F, Yoshida T, Hong R, Jensen RV, Misra J, Dillon W, Lee KF, Clark KE, Haverty P, Weng Z, Mutter GL, Frosch MP, MacDonald ME, Milford EL,

Crum CP, Bueno R, Pratt RE, Mahadevappa M, Warrington JA, Stephanopoulos G, Stephanopoulos G, Gullans SR. A compendium of gene expression in normal human tissues. *Physiological genomics.* 2001;7(2):97-104.

367. Burke B, Lewis CE. *The macrophage*. 2nd ed. Oxford ; New York: Oxford University Press; 2002.

368. Matkowskyj KA, Schonfeld D, Benya RV. Quantitative immunohistochemistry by measuring cumulative signal strength using commercially available software photoshop and matlab. *J Histochem Cytochem.* 2000;48(2):303-312.

369. Cregger M, Berger AJ, Rimm DL. Immunohistochemistry and quantitative analysis of protein expression. *Archives of pathology & laboratory medicine.* 2006;130(7):1026-1030.

370. Saito N, Pulford KA, Breton-Gorius J, Masse JM, Mason DY, Cramer EM. Ultrastructural localization of the CD68 macrophage-associated antigen in human blood neutrophils and monocytes. *The American journal of pathology.* 1991;139(5):1053-1059.

371. Pulford KA, Sipos A, Cordell JL, Stross WP, Mason DY. Distribution of the CD68 macrophage/myeloid associated antigen. *International immunology.* 1990;2(10):973-980.